

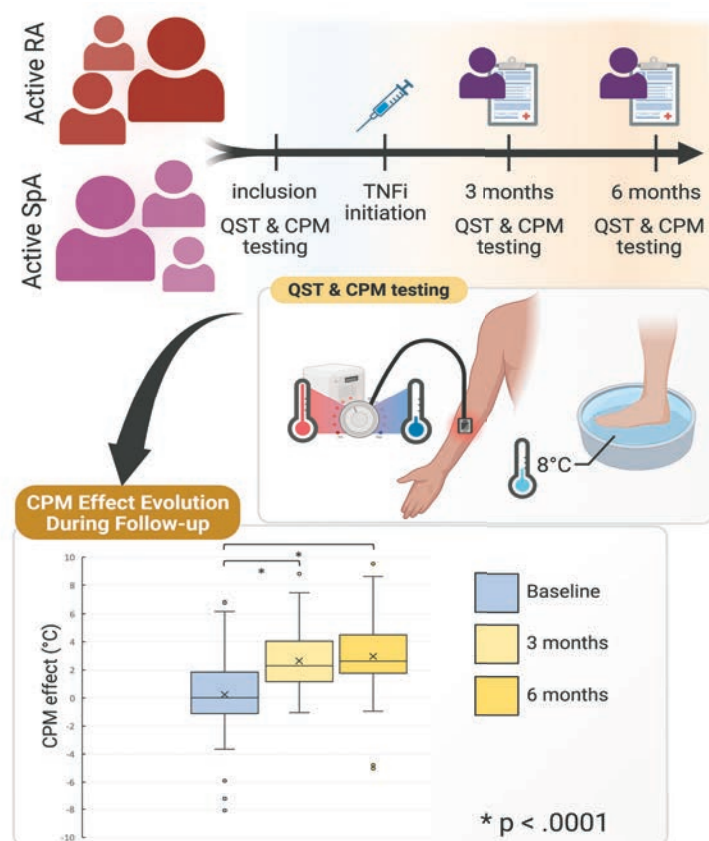
Clinical Connections

Changes in Descending Pain Modulation During Anti-TNF Therapy in RA and SpA

Trouvin et al, *Arthritis Rheumatol.* 2025;77:658–663

CORRESPONDENCE

Anne-Priscille Trouvin, MD, PhD: annepriscille.trouvin@aphp.fr



SUMMARY

The RAPID study investigated changes in descending pain inhibitory controls in patients with active rheumatoid arthritis (RA) or spondyloarthritis (SpA). Patients with active disease, naïve to biological DMARD and initiating TNF inhibitor (TNFi) treatment, were included. They were followed for six months after the initiation of the TNFi. At each follow-up visit, descending inhibitory controls were assessed using conditioned pain modulation (CPM). The CPM effect was evaluated by measuring the change in heat pain threshold (°C) before and after an intense painful stimulus. This intense stimulus is used to activate the descending inhibitory controls. The CPM effect is calculated as the difference between the heat pain threshold after stimulation (T^2) and before stimulation (T^1). A positive CPM effect ($T^2 > T^1$) indicates activation of the descending pain inhibitory pathways. A CPM effect close to zero or negative indicates a lack of inhibitory control.

In patients, the CPM effect significantly improved from $0.25 \pm 2.57^\circ\text{C}$ (before anti-TNF) to $2.96 \pm 2.50^\circ\text{C}$ after six months of TNFi treatment. Results suggest that in active inflammatory rheumatic diseases, the descending inhibitory controls of pain, which are impaired when the disease is active, are improved after TNFi treatment.

KEY POINTS

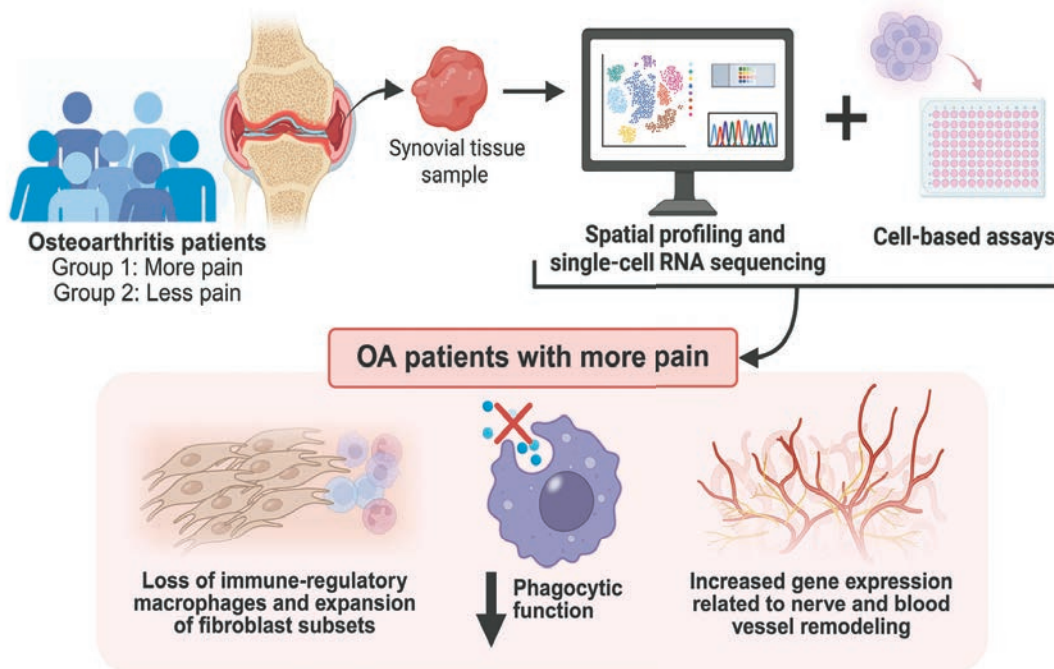
- Central sensitization has been proposed as a mechanism of persistent pain in chronic inflammatory rheumatism, and patients with active disease may have impaired descending pain modulation.
- When anti-TNF treatment is initiated, impaired descending pain modulation is restored more effectively in patients without residual pain.
- Patients with residual pain who receive treatment might have persistent impaired pain modulation, and changing the bDMARD might not be the best option.

Association of Synovial Innate Immune Exhaustion With Worse Pain in Knee OA

Philpott, et al. *Arthritis Rheumatol.* 2025;77:664–676

CORRESPONDENCE

C. Thomas Appleton, MD, PhD: tom.appleton@sjhc.london.on.ca



KEY POINTS

- Interactions between innate immune cells and synovial fibroblasts may play key roles in determining pain outcomes in OA.
- Neurovascular remodeling in synovial tissue likely underlies worsening of OA-related pain.
- Treatment of innate immune cell exhaustion should be investigated as a strategy to improve OA pain outcomes.

SUMMARY

Poorly controlled pain remains a major clinical challenge in the management of knee osteoarthritis (OA). Worse pain is linked to synovitis in OA, which involves infiltration of innate immune cells into the synovial tissue. However, the role of innate immune regulatory cells in pain is unknown. Philpott et al aimed to identify subsets of synovial cells and their pathophysiologic mechanisms in patients with worse OA-related pain. They used combined spatial transcriptomics/proteomics and single-cell RNA sequencing analyses to profile synovial tissue from patients with knee OA.

Results showed that patients with worse pain had tissue signs of blood vessel dysfunction. Worse pain was associated with macrophage exhaustion, characterized by impaired phagocytic function, a reduction in the number of immune-regulatory macrophages, and expansion of fibroblast subtypes. In addition, synovial cells from patients with worse pain demonstrated increased expression of pathways related to nerve and blood vessel remodeling and increased neuronal stress. The findings suggest that synovial cell subsets play differing roles in OA-related pain. Since the synovium is critical for maintaining joint health and homeostasis, innate immune cell exhaustion may be a novel treatment target for preventing the progression of pain and joint failure in OA.

Topical Mupirocin Targets *Staphylococcus* Species in CLE Lesions

Researchers have previously shown that *Staphylococcus aureus*, a dynamic colonizer of 30% of the U.S. population, promotes systemic lupus erythematosus (SLE)-like autoimmune inflammation. The links between SLE and *S. aureus* have been suggested for more than a decade, with some evidence indicating that ongoing colonization may provide exposure to *S. aureus* inflammatory triggers. Researchers have also found that *S. aureus* is associated with type I interferon (IFN) production.

In this issue, Abernathy-Close et al (p. 705) report that topical mupirocin treatment decreased lesional *Staphylococcus* and correlated with decreased IFN signaling, inflammatory gene expression, and barrier dysfunction.

The study included 12 patients randomized to receive a week of topical treatment with either 2% mupirocin or petroleum jelly vehicle on a single, accessible cutaneous lupus erythematosus (CLE) lesion. While mupirocin decreased the lesional *Staphylococcus* burden, the relative abundance of other bacterial genera colonizing CLE lesions was unaltered by mupirocin treatment. Microbial profiling of nasal swabs demonstrated that topical skin application of mupirocin to CLE lesions also resulted in a significant decrease of *Staphylococcus* carriage in the nares.

After topical mupirocin treatment, the investigators identified 173 differentially expressed genes in CLE lesions. Mupirocin treatment, but not vehicle control, decreased

the expression of genes involved in IFN signaling. Mupirocin treatment also up-regulated the expression of key skin barrier pathways and down-regulated pathways involved in skin mitosis and cell division. The Type I IFN-related gene changes in skin treated with mupirocin correlated with decreased monocytes and activated dendritic cells.

The authors conclude that a topical antibiotic could reduce *Staphylococcus* colonization and decrease lupus skin inflammation and type I IFN responses. A medication targeting *S. aureus* on the skin may thus benefit CLE as a primary treatment or adjunct therapy. They call for more research to better understand the CLE lesional factors influencing colonization by staphylococcal species.

Journal Club

A monthly feature designed to facilitate discussion on research methods in rheumatology.

Association of Therapies for Axial Spondyloarthritis on the Risk of Hip and Spine Fractures

Driscoll et al, *Arthritis Rheumatol.* 2025;77:577–685

Among people with axial spondyloarthritis (axSpA), risk of vertebral fracture is doubled, and risk of non-vertebral fracture is increased by 10%. This increased risk is thought to be due to local bone remodeling in the spine and systemic inflammation. While TNF inhibitors (TNFi) are effective at controlling axSpA symptoms, their effects on fracture risk are not known. To address this knowledge gap, Driscoll et al assessed the impact of TNFi and nonbiologic conventional synthetic disease-modifying antirheumatic drugs (csDMARDs) on hip and spine fractures in patients with axSpA, relative to patients receiving nonsteroidal anti-inflammatory drugs (NSAIDs).

This study applied a nested case-control study design to data on adults with axSpA from the Merative MarketScan Database (2006–2021). A case-control design was chosen because of the relative rarity of the outcome (hip or spine fracture) and to allow use of all fracture cases in the data set. Hip and spine fractures were defined by ICD-9 or ICD-10 diagnosis or procedure codes. For each patient with fracture (cases), up to 10 controls without fracture were selected. Medication exposure (TNFi, csDMARDs, NSAIDs [referent], or none) was assessed hierarchically for association with risk of hip or spine fracture using unconditional logistic regression

with confounder adjustment. The study included 1,229 patients with fracture and 12,290 controls. Individuals receiving TNFi had 29% lower odds of fracture compared to those receiving NSAIDs (odds ratio [OR] 0.71, 95% confidence interval [CI] 0.59–0.85), accounting for age, sex, and diagnosis year. Results were similar in the fully adjusted model (OR 0.75, 95% CI 0.62–0.91) and when stratified by sex.

Questions

1. What are the strengths and weaknesses of using claims data to study risk of fractures? Would such a study have been feasible using other types of data (e.g., electronic health records, registry)?
2. How did the choice of the referent group (NSAIDs) impact interpretation of the results? How might results have changed if the referent group was no medication?
3. How might confounding by indication affect the results of this study? What if individuals with more severe axSpA were more likely to be treated with a TNFi? What if more frail individuals were less likely to be treated with a TNFi?

In this Issue

Highlights from this issue of *A&R* | By Lara C. Pullen, PhD

Disturbed Spatial WNT Activation May Be a Driver in Systemic Sclerosis Pathology

Research has shown that in human adult healthy skin, the activation of WNT/ β -catenin signaling is spatially distinct, with increased activation of

p. 740 WNT/ β -catenin signaling in the papillary dermis compared with that seen in the reticular dermis. Unfortunately, this spatial difference has been difficult to study because rodent skin models do not sufficiently reflect the human papillary skin structure.

In this issue, Fakhouri et al (p. 740)

report an association of the “reticularized” skin phenotype in systemic sclerosis (SSc) with a profound loss of physiologic spatial WNT/ β -catenin activation. They are the first to report that the perturbations in the physiologic gradient of WNT/ β -catenin in SSc correspond with anatomic changes of the papillary and reticular dermis, as well as changes in the spatial distribution of specific fibroblast subsets.

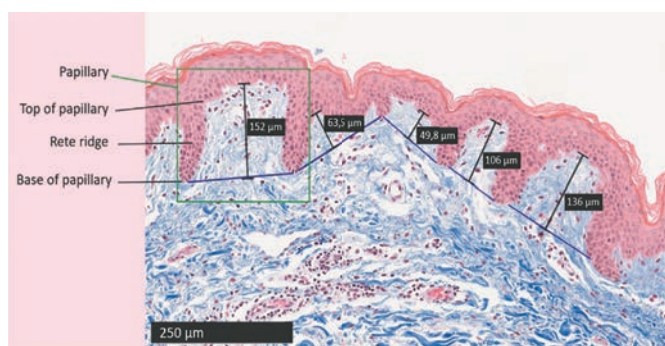


Figure 1. Visualization of papillary measurements.

The investigators found that SSc skin showed decreases in papillae number, area, and height compared with healthy controls and hypertrophic scars. Moreover, the expression of papillary/reticular marker genes shifted toward a reticular expression profile in SSc. When looking at the level of previously defined fibroblast populations, researchers found the increase of reticular marker genes to

be particularly pronounced in the PI16+ and SFRP4+ populations.

Mechanistically, the team found that, in healthy skin, the expression of the WNT/ β -catenin target *AXIN2* and the number of fibroblasts with nuclear β -catenin staining pattern was increased in the papillary compared with the reticular dermis. This polarization was lost in SSc with a two-fold increase in β -catenin-positive fibroblasts and *AXIN2*-expressing fibroblasts throughout the dermis. Moreover,

they identified an enrichment of genes related to WNT/ β -catenin regulation in the PI16+ population that relocated from the reticular to the papillary dermis in SSc. In discussing the implications of their findings for future therapeutic approaches, the authors propose that rescuing the spatial WNT/ β -catenin activation might help restore physiologic skin organization in patients with fibrosing disorders.

New Data Suggest a Path Toward Precision Medicine for Lupus Nephritis

Monocytes play a fundamental biologic role in lupus nephritis (LN) and immune complex glomerulonephritis and drive several pathways leading to kidney inflammation. The

p. 696 infiltration of monocytes in glomeruli affected by LN is a CD40–CD40L-mediated process, after which the monocytes mediate glomerular inflammation by patrolling and engaging other effectors, such as neutrophils, thereby leading to further tissue injury. Twenty years ago, researchers demonstrated the requirement for CD40–CD40L in delayed-type hypersensitivity crescentic

glomerulonephritis, thereby identifying CD40 as a potential therapeutic target in humans.

Rheumatologists and nephrologists searching for an ideal LN regimen have turned their attention to CD40 to identify new therapies and subgroups of patients who would better respond to specific therapeutic regimens, thereby moving toward a more personalized, patient-centered approach. A phase 2 trial tested different doses of the anti-CD40 monoclonal antibody BI 655064 as an add-on therapy to the standard of care in patients with active LN and a post hoc analysis showed a potential benefit of the higher tested doses.

In this issue, Uzzo et al (p. 696) used a novel, reliable statistical approach to investigate the predictive role of histologic features on renal outcome in patients enrolled in the BI655064 phase II trial.

The researchers found that if glomerular monocytes were present in LN kidney biopsy samples, high-dose treatment with anti-CD40 monoclonal antibody improved the reduction of proteinuria at 52 weeks and led to a higher complete renal response than if monocytes were absent. They found that histology could be used to identify patients most likely to respond to BI 655064.

Topical Mupirocin Targets *Staphylococcus* Species in CLE Lesions

Researchers have previously shown that *Staphylococcus aureus*, a dynamic colonizer of 30% of the U.S. population, promotes systemic lupus erythematosus (SLE)-like autoimmune inflammation. The links between

p. 705

SLE and *S. aureus* have been suggested for more than a decade, with some evidence indicating that ongoing colonization may provide exposure to *S. aureus* inflammatory triggers. Researchers have also found that *S. aureus* is associated with type I interferon (IFN) production.

In this issue, Abernathy-Close et al (p. 705) report that topical mupirocin treatment decreased lesional *Staphylococcus* and correlated with decreased IFN signaling, inflammatory gene expression, and barrier dysfunction.

The study included 12 patients randomized to receive a week of topical treatment with either 2% mupirocin or petroleum jelly vehicle on a single, accessible cutaneous lupus erythematosus (CLE) lesion. While mupirocin decreased the lesional *Staphylococcus* burden, the relative abundance of other bacterial genera colonizing CLE lesions was unaltered by mupirocin treatment. Microbial profiling of nasal swabs demonstrated that topical skin application of mupirocin to CLE lesions also resulted in a significant decrease of *Staphylococcus* carriage in the nares.

After topical mupirocin treatment, the investigators identified 173 differentially expressed genes in CLE lesions. Mupirocin treatment, but not vehicle control, decreased

the expression of genes involved in IFN signaling. Mupirocin treatment also up-regulated the expression of key skin barrier pathways and down-regulated pathways involved in skin mitosis and cell division. The Type I IFN-related gene changes in skin treated with mupirocin correlated with decreased monocytes and activated dendritic cells.

The authors conclude that a topical antibiotic could reduce *Staphylococcus* colonization and decrease lupus skin inflammation and type I IFN responses. A medication targeting *S. aureus* on the skin may thus benefit CLE as a primary treatment or adjunct therapy. They call for more research to better understand the CLE lesional factors influencing colonization by staphylococcal species.

Journal Club

A monthly feature designed to facilitate discussion on research methods in rheumatology.

Association of Therapies for Axial Spondyloarthritis on the Risk of Hip and Spine Fractures

Driscoll et al, *Arthritis Rheumatol.* 2025;77:577–685

Among people with axial spondyloarthritis (axSpA), risk of vertebral fracture is doubled, and risk of non-vertebral fracture is increased by 10%. This increased risk is thought to be due to local bone remodeling in the spine and systemic inflammation. While TNF inhibitors (TNFi) are effective at controlling axSpA symptoms, their effects on fracture risk are not known. To address this knowledge gap, Driscoll et al assessed the impact of TNFi and nonbiologic conventional synthetic disease-modifying antirheumatic drugs (csDMARDs) on hip and spine fractures in patients with axSpA, relative to patients receiving nonsteroidal anti-inflammatory drugs (NSAIDs).

This study applied a nested case-control study design to data on adults with axSpA from the Merative MarketScan Database (2006–2021). A case-control design was chosen because of the relative rarity of the outcome (hip or spine fracture) and to allow use of all fracture cases in the data set. Hip and spine fractures were defined by ICD-9 or ICD-10 diagnosis or procedure codes. For each patient with fracture (cases), up to 10 controls without fracture were selected. Medication exposure (TNFi, csDMARDs, NSAIDs [referent], or none) was assessed hierarchically for association with risk of hip or spine fracture using unconditional logistic regression

with confounder adjustment. The study included 1,229 patients with fracture and 12,290 controls. Individuals receiving TNFi had 29% lower odds of fracture compared to those receiving NSAIDs (odds ratio [OR] 0.71, 95% confidence interval [CI] 0.59–0.85), accounting for age, sex, and diagnosis year. Results were similar in the fully adjusted model (OR 0.75, 95% CI 0.62–0.91) and when stratified by sex.

Questions

1. What are the strengths and weaknesses of using claims data to study risk of fractures? Would such a study have been feasible using other types of data (e.g., electronic health records, registry)?
2. How did the choice of the referent group (NSAIDs) impact interpretation of the results? How might results have changed if the referent group was no medication?
3. How might confounding by indication affect the results of this study? What if individuals with more severe axSpA were more likely to be treated with a TNFi? What if more frail individuals were less likely to be treated with a TNFi?

Arthritis & Rheumatology

An Official Journal of the American College of Rheumatology
www.arthritisrheum.org and wileyonlinelibrary.com

Editor

Daniel H. Solomon, MD, MPH, *Boston*

Deputy Editors

Richard J. Bucala, MD, PhD, *New Haven*

Mariana J. Kaplan, MD, *Bethesda*

Peter A. Nigrovic, MD, *Boston*

Co-Editors

Karen H. Costenbader, MD, MPH, *Boston*

David T. Felson, MD, MPH, *Boston*

Richard F. Loeser Jr., MD, *Chapel Hill*

Journal Publications Committee

Chair - Betty Tsao, PhD, *Charleston*

Member - ARP Liaison

Cynthia Crowson, PhD, *Stewartville*

Members

Elana Bernstein, MD, MSc, *New York*

Krati Chauhan, MD, PhD, *Burlington*

Daniel B. Horton, MD, MSCE, *New Brunswick*

Suraj Rajasimhan, PharmD

Faria Latif Sami, MD, *Birmingham*

Himanshu Vashistha, PhD, MBA, *Great Neck*

Editorial Staff

Susan Case, *Vice President, Strategic Marketing,*

Communications and Publishing, Maryland

Maggie Parry, *Director, Quality and Production, Georgia*

Brian T. Robinson, *Director, Digital Content, Pennsylvania*

Chris Reynolds, *Product Manager, Georgia*

Christy Austin, *Publishing Coordinator, Washington*

Laura Bolte, *Managing Editor, North Carolina*

Associate Editors

Marta Alarcón-Riquelme, MD, PhD, *Granada*

Neil Basu, MD, PhD, *Glasgow*

Edward M. Behrens, MD, *Philadelphia*

Bryce Binstadt, MD, PhD, *Minneapolis*

Nunzio Bottini, MD, PhD, *San Diego*

John Carrino, MD, MPH, *New York*

Andrew Cope, MD, PhD, *London*

Adam P. Croft, MBChB, PhD, MRCP,

Birmingham

Nicola Dalbeth, MD, FRACP, *Auckland*

Chad Deal, MD, *Cleveland*

Brian M. Feldman, MD, FRCPC, MSc, *Toronto*

Richard A. Furie, MD, *Great Neck*

J. Michelle Kahlenberg, MD, PhD,
Ann Arbor

Yvonne Lee, MD, MMSc, *Chicago*

Katherine Liao, MD, MPH, *Boston*

Bing Lu, MD, DrPH, *Boston*

Stephen P. Messier, PhD,

Winston-Salem

Rachel E. Miller, PhD, *Chicago*

Janet E. Pope, MD, MPH, *FRCPC,*

London, Ontario

Lisa G. Rider, MD, *Bethesda*

Christopher T. Ritchlin, MD, MPH,

Rochester

William Robinson, MD, PhD, *Stanford*

Amr Sawalha, MD, *Pittsburgh*

Carla R. Scanzello, MD, PhD,

Philadelphia

Georg Schett, MD, *Erlangen*

Ami A. Shah, MD, MHS, *Baltimore*

Sakae Tanaka, MD, PhD, *Tokyo*

Maria Trojanowska, PhD, *Boston*

Edith M. Williams, PhD, MS, *Rochester*

Advisory Editors

Ayaz Aghayev, MD, *Boston*

Joshua F. Baker, MD, MSCE,
Philadelphia

Bonnie Bermas, MD, *Dallas*

Jamie Collins, PhD, *Boston*

Kristen Demoruelle, MD, PhD, *Denver*

Christopher Denton, PhD, FRCP, *London*

Anisha Dua, MD, MPH, *Chicago*

John FitzGerald, MD, *Los Angeles*

Lauren Henderson, MD, MMSc, *Boston*

Monique Hinchcliff, MD, MS, *New Haven*

Hui-Chen Hsu, PhD, *Birmingham*

Mohit Kapoor, PhD, *Toronto*

Seoyoung Kim, MD, ScD, MSCE, *Boston*

Vasileios Kytтарыs, MD, *Boston*

Carl D. Langefeld, PhD, *Winston-Salem*

Christian Lood, PhD, *Seattle*

Dennis McGonagle, FRCPI, PhD, *Leeds*

Julie Paik, MD, MHS, *Baltimore*

Julie Zikherman, MD, *San Francisco*

AMERICAN COLLEGE OF RHEUMATOLOGY

Carol Langford, MD, MHS, *Cleveland*, **President**

William Harvey, MD, MSc, *Boston*, **President-Elect**

Anne Bass, MD, *New York*, **Treasurer**

Angus Worthing, MD, *Washington, DC*, **Secretary**

Steven Echard, IOM, CAE, *Atlanta*, **Executive Vice-President**

© 2025 American College of Rheumatology. All rights reserved, including rights for text and data mining and training of artificial technologies or similar technologies. No part of this publication may be reproduced, stored or transmitted in any form or by any means without the prior permission in writing from the copyright holder. Authorization to copy items for internal and personal use is granted by the copyright holder for libraries and other users registered with their local Reproduction Rights Organization (RRO), e.g. Copyright Clearance Center (CCC), 222 Rosewood Drive, Danvers, MA 01923, USA (www.copyright.com), provided the appropriate fee is paid directly to the RRO. This consent does not extend to other kinds of copying or use such as copying for general distribution, for advertising or promotional purposes, for creating new collective works, for resale, or for artificial intelligence tools or technologies. Special requests should be addressed to: permissions@wiley.com.

Access Policy: Subject to restrictions on certain backfiles, access to the online version of this issue is available to all registered Wiley Online Library users 12 months after publication. Subscribers and eligible users at subscribing institutions have immediate access in accordance with the relevant subscription type. Please go to online@wiley.com for details.

The views and recommendations expressed in articles, letters, and other communications published in Arthritis & Rheumatology are those of the authors and do not necessarily reflect the opinions of the editors, publisher, or American College of Rheumatology. The publisher and the American College of Rheumatology do not investigate the information contained in the classified advertisements in this journal and assume no responsibility concerning them. Further, the publisher and the American College of Rheumatology do not guarantee, warrant, or endorse any product or service advertised in this journal.

Cover design: Todd Machen

© This journal is printed on acid-free paper.

Arthritis & Rheumatology

An Official Journal of the American College of Rheumatology
www.arthritisrheum.org and wileyonlinelibrary.com

VOLUME 77 • June 2025 • NO. 6

In This Issue	A25
Journal Club	A26
Clinical Connections	A27
Special Articles	
Editorial: Revisiting the Synovium as a Structural Correlate of Pain in Osteoarthritis <i>Rachel E. Miller and Richard F. Loeser</i>	629
Expert Perspectives on Clinical Challenges: Management of Relapses in Giant Cell Arteritis <i>Marco A. Alba, Sebastian Unizony, Kenneth J. Warrington, Giuseppe Murgia, Sergio Prieto-González, Carlo Salvarani, Eric L. Matteson, and Tanaz A. Kermani</i>	632
Rheumatoid Arthritis	
Endogenous Retroelement Activation is Implicated in Interferon- α Production and Anti-Cyclic Citrullinated Peptide Autoantibody Generation in Early Rheumatoid Arthritis <i>Faye A. H. Cooles, Gemma Vidal Pedrola, Najib Naamane, Arthur G. Pratt, Ben Barron-Millar, Amy E. Anderson, Catharien M. U. Hilkens, John Casement, Vincent Bondet, Darragh Duffy, Fan Zhang, Ruchi Shukla, and John D. Isaacs</i>	646
Brief Report: Changes in Descending Pain Modulation During Anti-Tumor Necrosis Factor Therapy: A Prospective Study in Rheumatoid Arthritis and Spondyloarthritis <i>Anne-Priscille Trouvin, Arielle Simunek, Joël Coste, Terkia Medkour, Alice Combier, Lucile Poiroux, François Vidal, Sandrine Carvès, Didier Bouhassira, and Serge Perrot</i>	658
Osteoarthritis	
Association of Synovial Innate Immune Exhaustion With Worse Pain in Knee Osteoarthritis <i>Holly T. Philpott, Trevor B. Birmingham, Garth Blackler, J. Daniel Klapak, Alexander J. Knights, Easton C. Farrell, Benoit Fiset, Logan A. Walsh, J. Robert Giffin, Edward M. Vasarhelyi, Steven J. MacDonald, Brent A. Lanting, Tristan Maerz, and C. Thomas Appleton, on behalf of the WOREO Knee Study Group</i>	664
Spondyloarthritis	
Association of Therapies for Axial Spondyloarthritis on the Risk of Hip and Spine Fractures <i>Devin Driscoll, Navya George, Christine Peloquin, S. Reza Jafarzadeh, Jean W. Liew, and Maureen Dubreuil</i>	677
Psoriatic Arthritis	
Derivation of a Multivariable Psoriatic Arthritis Risk Estimation Tool (PRESTO): A Step Towards Prevention <i>Lihi Eder, Ker-Ai Lee, Vinod Chandran, Jessica Widdifield, Aaron M. Drucker, Christopher Ritchlin, Cheryl F. Rosen, Richard J. Cook, and Dafna D. Gladman</i>	686
Systemic Lupus Erythematosus	
Outcome of Patients With Lupus Nephritis Treated With an Anti-CD40 Monoclonal Antibody According to Kidney Biopsy Features <i>Martina Uzzo, Helmut Schumacher, Juergen Steffgen, Simone Deutschel, David Jayne, and Ingeborg Bajema</i>	696
Topical Mupirocin Treatment Reduces Interferon and Myeloid Signatures in Cutaneous Lupus Erythematosus Lesions Through Targeting of <i>Staphylococcus</i> Species <i>Lisa Abernathy-Close, Joseph Mears, Allison C. Billi, Sirisha Sirobhushanam, Celine Berthier, Annie Lu, Zeran Zhang, Amy Hurst, Johann E. Gudjonsson, and J. Michelle Kahlenberg</i>	705
Atherosclerotic Plaque Progression and Incident Cardiovascular Events in a 10-Year Prospective Study of Patients With Systemic Lupus Erythematosus: The Impact of Persistent Cardiovascular Risk Factor Target Attainment and Sustained DORIS Remission <i>Nikolaos Papazoglou, Petros P. Sfrikakis, and Maria G. Tektonidou</i>	716

Systemic Sclerosis

Cross-Phenotype Genome-Wide Association Study on the Shared Genetic Susceptibility to Systemic Sclerosis and Primary Biliary Cholangitis

Yiming Luo, Atlas Khan, Lili Liu, Cue Hyunkyu Lee, Gabriel J. Perreault, Sydney F. Pomenti, Pravitt Gourh, Krzysztof Kiryluk, and Elana J. Bernstein. 727

Brief Report: Disturbed Spatial WNT Activation—A Potential Driver of the Reticularized Skin Phenotype in Systemic Sclerosis

Sara Chenguiti Fakhouri, Honglin Zhu, Yi-Nan Li, Moritz Ronicke, Aleix Rius Rigau, Clara Dees, Laura Konstantinidis, Ralf Schmid, Alexandru-Emil Matei, Markus Eckstein, Carol Geppert, Ingo Ludolph, Alexander Kreuter, Michael Sticherling, Carola Berking, Raymund E. Horsch, Georg Schett, Jörg H. W. Distler, and Christina Bergmann. 740

Myositis

Genetic Architecture of Idiopathic Inflammatory Myopathies From Meta-Analyses

Catherine Zhu, Younghun Han, Jinyoung Byun, Xiangjun Xiao, Simon Rothwell, Frederick W. Miller, Ingrid E. Lundberg, Peter K. Gregersen, Jiri Vencovsky, Vikram R. Shaw, Neil McHugh, Vidya Limaye, Albert Selva-O'Callaghan, Michael G. Hanna, Pedro M. Machado, Lauren M. Pachman, Ann M. Reed, Lisa G. Rider, Øyvind Molberg, Olivier Benveniste, Timothy Radstake, Andrea Doria, Jan L. De Bleecker, Boel De Paepe, Britta Maurer, William E. Ollier, Leonid Padyukov, Lucy R. Wedderburn, Hector Chinoy, Janine A. Lamb, and Christopher I. Amos, for the Myositis Genetics Consortium 750

Efficacy and Safety of Subcutaneous Abatacept Plus Standard Treatment for Active Idiopathic Inflammatory Myopathy: Phase 3 Randomized Controlled Trial

Rohit Aggarwal, Ingrid E. Lundberg, Yeong-Wook Song, Aziz Shaibani, Victoria P. Werth, and Michael A. Maldonado 765

Letter

Balancing Weight Reduction Benefits and Risks: Implications for Serum Urate Management.

Comment on the Article by Fukui et al

Pei Liu, Yongqiang Sun, Kun Zhao, and Peijian Tong 777

Reply

Sho Fukui, Masato Okada, and Daniel H. Solomon 778

The Oral Microbiota in Persons at Risk for Rheumatoid Arthritis: Follow-Up Data for the Article

by Kroese et al

Johanna M. Kroese, Bernd W. Brandt, Mark J. Buijs, Wim Crielaard, Frank Lobbezoo, Bruno G. Loos, Laurette van Boheemen, Dirkjan van Schaardenburg, Egija Zaura, and Catherine M.C. Volgenant. 778

Short-Term Risk of Cardiovascular Events in People Newly Diagnosed With Gout: Comment

on the Article by Cipolletta et al

Zichang Liu, Yanwei Zhu, and Hui Zhao 780

Reply

Edoardo Cipolletta, Laila J. Tata, and Abhishek Abhishek 781

Enhancing Knee Osteoarthritis Prediction: Comment on the Article by Li et al

Qin Guo, Hui Li, and Chengshan Guo 782

Reply

Shengfa Li and Changhai Ding. 783

Cover image: The figure on the cover (from Chenguiti Fakhouri et al; pages 740–749) depicts the trichrome staining of fibrotic skin tissue from the forearm of a systemic sclerosis (SSc) patient. This image illustrates the “reticularization phenomenon” that is further characterized in the article in SSc: flattening of rete ridges, loss of dermal papillae and increased parallelism of collagen fibers usually observed in the reticular part of the dermis. Skin papillae are central for proper skin function as they contain nerve endings and capillaries.

EDITORIAL

Revisiting the Synovium as a Structural Correlate of Pain in Osteoarthritis

Rachel E. Miller¹  and Richard F. Loeser² 

Osteoarthritis (OA) pain is a major contributor to the burden of chronic pain worldwide due to the prevalence of OA as well as the limited effective treatment options. Over the last two decades, much has been revealed about the structural correlates of OA pain through imaging studies such as magnetic resonance imaging (MRI) and musculoskeletal ultrasound. Evidence of inflammation such as synovitis/effusion have consistently been associated with disease progression, pain severity, fluctuations of pain, development of pain sensitization, and worsening of pain sensitization.¹ As such, synovitis remains of interest as an interventional target; however, there is a need to improve our mechanistic understanding of how joint inflammation produces OA pain in order to identify specific molecular targets.² Although we appreciate that cells such as macrophages and fibroblasts within the synovium of patients with OA contribute to disease pathology, the recent rapid development and application of transcriptomic technologies has given us a much more detailed understanding of the different states these cells can assume and of the molecular profiles associated with each of these cell states. Philpott et al³ provided a new set of spatial transcriptomics, spatial proteomics, and single-cell RNA sequencing data collected from OA synovial samples at the time of joint replacement surgery from patients with severe pain compared to patients with mild to moderate pain.

Philpott et al³ show through spatial transcriptomics that a higher proportion of macrophages is present in the subintima in patients with worse pain. This is consistent with previous work using single-photon-emission computed tomography imaging combined with high-resolution computed tomography (SPECT/CT), which demonstrated that the quantity of activated (folate receptor- β -expressing) macrophages in the knee was associated with OA pain.⁴ In addition, another study used RNA sequencing to uncover two different populations of patients with OA, one with more inflammatory-like macrophages that were characterized by

a cell proliferation signature, and another with more classical OA macrophages that displayed a signature suggesting aberrant tissue repair. However, correlations with pain were not performed.⁵ One of the markers of these classical OA macrophages, HTRA1, was also up-regulated in the spatial transcriptomics data of patients with more pain in the study by Philpott et al.³

Additionally, Philpott et al³ provided evidence in patients with more severe pain for a reduction in immune cell diversity, an increase in synovial proteins associated with “immune exhaustion,” and a reduction in cell surface markers of myeloid and T lymphocytes, immune signaling, and cell growth and survival suggesting a dysfunction in innate immunity. Consistent with this dysfunctional state, macrophages taken from these patients had a decreased capacity to phagocytose particles in vitro. Synovial samples from patients with more pain also had increased perivascular edema as determined by histopathology. The presence of severe perivascular edema appears to be a relatively rare event, previously reported to be present in only 10.7% of this cohort⁶, and therefore, further investigation into the association of this histologic feature with pain in other cohorts and in preclinical models seems warranted. Overall, the findings by Philpott et al³ support the idea that the macrophages in these patients with high pain in this cohort have impaired function that contributes to increased synovial damage.

The spatial profiling work by Philpott et al³ also demonstrated that genes involved in mitochondrial stress response and regulation of processes such as angiogenesis and neurite outgrowth were increased in patients with more pain. Single-cell RNA sequencing supported the concept that both myeloid cells and fibroblasts are producing factors that could contribute to angiogenesis and nerve growth. Two other recent studies also reported synovial fibroblast RNA sequencing profiles that suggested production of factors supporting sensory neuron outgrowth.^{7,8} In the first study, RNA sequencing was performed on

Supported by the National Institute of Arthritis and Musculoskeletal and Skin Diseases, NIH (grant R01-AR-077019 to Dr Miller), and the National Institute of Aging, NIH (grant R01-AG-044034 to Dr Loeser).

¹Rachel E. Miller, PhD: Rush University Medical Center, Chicago, Illinois; ²Richard F. Loeser, MD: University of North Carolina at Chapel Hill.

Author disclosures are available at <https://onlinelibrary.wiley.com/doi/10.1002/art.43086>.

Address correspondence via email to Rachel E. Miller, PhD, at Rachel_Miller@rush.edu.

Submitted for publication December 4, 2024; accepted in revised form December 9, 2024.

OA synovium taken from painful versus nonpainful sites within the same patient at the time of elective knee arthroscopy or arthroplasty, and functional pathway analysis revealed that synovial tissue taken from painful sites promoted fibrosis, inflammation, and the growth and activity of neurons.⁸ Single-cell RNA sequencing demonstrated that there was a fibroblast subset present in samples taken from painful synovial sites in patients with early OA with a gene signature supporting the formation and development of neurites. Application of conditioned medium from these painful fibroblasts indeed stimulated neurite outgrowth more than nonpainful fibroblast-conditioned medium.⁸ In the second study, a machine learning approach was used to identify 815 genes associated with pain in synovial samples taken from patients with rheumatoid arthritis with low levels of inflammation present at the time of joint arthroplasty.⁷ They found that these genes were associated with neuronal development, and one factor in particular, netrin-4, was tested and found to support sensory neuron sprouting.⁷ Philpott et al³ also reported increased netrin-4 expression in the subintima of patients with more pain.

The ability of patients to distinguish pain at sites with differing amounts of synovitis⁸ implies that these sites have altered neuronal input at the level of the joint—that is, either an increase in the numbers of nerves innervating and/or sensitization of these nerves as a result of increased exposure to inflammatory stimuli. In preclinical models of OA, localized sprouting of nerves in the medial synovium has been observed to be an early event in three different mouse models with OA.⁹ Although these observations used traditional coronal sectioning of mouse joints, tissue clearing and lightsheet imaging should soon allow us to also understand the distribution of nerves throughout the synovium in these preclinical models.¹⁰ In addition, although MRI has given us the ability to understand spatially where sites of synovitis occur in three dimensions, innervation patterns in the healthy human joint as well as in painful and nonpainful sites of the synovium in humans with OA still need to be elucidated. The currently limited available reports do not provide a clear assessment of whether nerve fiber density in the human synovium changes with synovitis levels or with symptom severity.

The response of sensory nerves to secreted factors in the local synovial environment is also a potentially targetable contribution to OA pain—in their work, Philpott et al³ showed that conditioned medium from synovial cells taken from patients with more pain caused higher levels of neuronal stress, as measured through cleaved caspase-3 expression, compared to medium from patients with less pain. Additionally, many factors identified in the analyses as up-regulated in the myeloid cells or fibroblasts of patients with higher pain levels have previously been shown to have the ability to signal to both nonneuronal cells as well as to sensory neurons. For example, OA synovial cells have previously been shown to be a source of nerve growth factor

(NGF),¹¹ a neurotrophic factor with a strong association with OA pain,¹² and the NGF signaling pathway was identified here as up-regulated in myeloid cells of patients with more pain.³ In addition, the chemokine CCL2 was found to be up-regulated in the myeloid cells of patients with more pain,³ and preclinical studies across several laboratories have demonstrated a role for this pathway in OA pain.^{13–15} The large amounts of data being generated by this³ and other OA cohorts will be a valuable resource for researchers to interrogate as they search for new targets linked to pain that are locally produced in the joint.

In conclusion, Philpott et al³ demonstrated that in late-stage knee OA, examination of the molecular and cellular makeup of the synovium could distinguish patients with severe pain from those with mild to moderate pain suggesting the time is right for reconsidering synovial targets for OA pain.

AUTHOR CONTRIBUTIONS

All authors contributed to at least one of the following manuscript preparation roles: conceptualization AND/OR methodology, software, investigation, formal analysis, data curation, visualization, and validation AND drafting or reviewing/editing the final draft. As corresponding author, Dr Miller confirms that all authors have provided the final approval of the version to be published, and takes responsibility for the affirmations regarding article submission (eg, not under consideration by another journal), the integrity of the data presented, and the statements regarding compliance with institutional review board/Declaration of Helsinki requirements.

REFERENCES

1. Neogi T. Structural correlates of pain in osteoarthritis. *Clin Exp Rheumatol* 2017;35(Suppl 107):75–78.
2. Mathiessen A, Conaghan PG. Synovitis in osteoarthritis: current understanding with therapeutic implications. *Arthritis Res Ther* 2017; 19(1):18.
3. Philpott HT, Birmingham TB, Blackler G, et al. Association of synovial innate immune exhaustion with worse pain in knee osteoarthritis. *Arthritis Rheumatol* 2025;77(6):664–676.
4. Kraus VB, McDaniel G, Huebner JL, et al. Direct in vivo evidence of activated macrophages in human osteoarthritis. *Osteoarthritis Cartilage* 2016;24(9):1613–1621.
5. Wood MJ, Leckenby A, Reynolds G, et al. Macrophage proliferation distinguishes 2 subgroups of knee osteoarthritis patients. *JCI Insight* 2019;4(2):e125325.
6. Philpott HT, Birmingham TB, Carter MM, et al. Association between synovial tissue damage and pain in late-stage knee osteoarthritis: a cross-sectional study. *Osteoarthritis Cartilage* 2024;32(11): 1503–1512.
7. Bai Z, Bartelo N, Aslam M, et al. Synovial fibroblast gene expression is associated with sensory nerve growth and pain in rheumatoid arthritis. *Sci Transl Med* 2024;16(742):eadk3506.
8. Nanus DE, Badoume A, Wijesinghe SN, et al. Synovial tissue from sites of joint pain in knee osteoarthritis patients exhibits a differential phenotype with distinct fibroblast subsets. *EBioMedicine* 2021;72: 103618.
9. Obeidat AM, Ishihara S, Li J, et al. Intra-articular sprouting of nociceptors accompanies progressive osteoarthritis: comparative evidence in four murine models. *Front Neuroanat* 2024;18:1429124.

10. Ko FC, Fullam S, Lee H, et al. Clearing-enabled light sheet microscopy as a novel method for three-dimensional mapping of the sensory innervation of the mouse knee. *J Orthop Res* Published online November 15, 2024. <https://doi.org/10.1002/jor.26016>
11. Stoppiello LA, Mapp PI, Wilson D, et al. Structural associations of symptomatic knee osteoarthritis. *Arthritis Rheumatol* 2014;66(11): 3018–3027.
12. Lane NE, Schnitzer TJ, Birbara CA, et al. Tanezumab for the treatment of pain from osteoarthritis of the knee. *N Engl J Med* 2010;363(16): 1521–1531.
13. Longobardi L, Temple JD, Tagliafierro L, et al. Role of the C-C chemokine receptor-2 in a murine model of injury-induced osteoarthritis. *Osteoarthritis Cartilage* 2017;25(6):914–925.
14. Miller RE, Tran PB, Das R, et al. CCR2 chemokine receptor signaling mediates pain in experimental osteoarthritis. *Proc Natl Acad Sci U S A* 2012;109(50):20602–20607.
15. Miotla Zarebska J, Chanalaris A, Driscoll C, et al. CCL2 and CCR2 regulate pain-related behaviour and early gene expression in post-traumatic murine osteoarthritis but contribute little to chondropathy. *Osteoarthritis Cartilage* 2017;25(3):406–412.

EXPERT PERSPECTIVES ON CLINICAL CHALLENGES

Management of Relapses in Giant Cell Arteritis

Marco A. Alba,¹ Sebastian Unizony,² Kenneth J. Warrington,³ Giuseppe Murgia,⁴ Sergio Prieto-González,⁴ Carlo Salvarani,⁵ Eric L. Matteson,³ and Tanaz A. Kermani⁶

Giant cell arteritis (GCA) is a relapsing large vessel vasculitis with risk of serious ischemic manifestations, including vision loss and vascular damage in the form of large artery stenosis, aneurysms, and dissections. Approximately 50% of patients treated with glucocorticoid (GC) monotherapy and 30% of patients receiving adjunctive therapy with tocilizumab experience disease relapses, often during the first 2 years after diagnosis. Although most relapses in GCA do not involve life- or organ-threatening presentations and can be controlled successfully, frequent relapses may lead to increased prescription of GC and consequent treatment-related morbidity, in addition to risk of further vascular damage. Emerging data suggest that persistent disease activity may lead to increased vascular morbidity. Additionally, although tocilizumab decreases the frequency of relapses, more than 50% of patients relapse after discontinuation of therapy. Therefore, although interleukin-6 blockade suppresses disease activity, it does not restore tolerance. In this article, we discuss the practical diagnosis and management of GCA relapses from an expert perspective. Current treatment options for GCA relapses, including those recommended by international guidelines, and novel potential therapies are reviewed.

Introduction

An 83-year-old woman presented with a 3-week history of new temporal headache, scalp tenderness, jaw claudication, fever, malaise, unintentional weight loss of 3.62 kg, cervical pain, and bilateral shoulder stiffness. She denied any visual symptoms. On examination, she had a painful, pulseless enlarged right temporal artery (TA). Vascular examination was normal without bruits or pulse loss. Laboratory tests were notable for a hemoglobin of 10 mg/dL, platelet count of 650,000 per mm, C-reactive protein (CRP) of 8.8 mg/dL, and erythrocyte sedimentation rate (ESR) of 110 mm/hr. Biopsy specimen of the right TA confirmed giant cell arteritis (GCA). High-dose glucocorticoid (GC) treatment was initiated with prednisone 60 mg/day with complete resolution of her symptoms. [¹⁸F]-fluorodeoxyglucose (FDG) positron emission computed tomography (PET/CT), performed 2 days after initiation of high-dose GCs, showed no abnormal uptake (Figure 1).

One year later, while receiving prednisone 5 mg daily, she reported a 2-week history of polymyalgia rheumatica (PMR)

symptoms, along with recurrence of daily headache and fever. Laboratory results were notable for new elevated ESR and CRP levels. PET/CT results were obtained and demonstrated avid FDG uptake in the ascending and descending aorta (Figure 1), consistent with a relapse of GCA.

Background. GCA is a granulomatous large vessel (LV) vasculitis that predominantly affects the aorta and its major branches.¹ This is the most common vasculitis in patients aged ≥50 years in North America and Europe, with an estimated pooled annual incidence and prevalence of 10 cases per 100,000 and 52 cases per 100,000 persons aged ≥50 years, respectively.²

The signs and symptoms of GCA depend on the pattern of arterial inflammation (cranial vs extracranial) and the intensity of the systemic inflammatory response and may include constitutional symptoms, cranial symptoms (headache, jaw claudication, and scalp tenderness), and visual changes (eg, amaurosis fugax, diplopia, and permanent visual loss; Table 1).^{3–7} Vertebrobasilar stroke (1.5%–7.5% of patients) and tongue or scalp necrosis

¹Marco A. Alba, MD: Hospital Universitari Mútua Terrassa, Terrassa, Spain; ²Sebastian Unizony, MD: Massachusetts General Hospital, Harvard Medical School, Boston; ³Kenneth J. Warrington, MD, Eric L. Matteson, MD: Mayo Clinic College of Medicine and Science, Rochester, Minnesota; ⁴Giuseppe Murgia, MD, Sergio Prieto-González, MD: Hospital Clínic Barcelona, University of Barcelona, Barcelona, Spain; ⁵Carlo Salvarani, MD: Azienda USL-IRCCS di Reggio Emilia, Università di Modena e Reggio Emilia, Reggio Emilia, Italy; ⁶Tanaz A. Kermani, MD: University of California, Los Angeles.

Author disclosures are available at <https://onlinelibrary.wiley.com/doi/10.1002/art.43098>.

Address correspondence via email to Tanaz A. Kermani, MD, at tkermani@mednet.ucla.edu.

Submitted for publication September 15, 2024; accepted in revised form December 10, 2024.

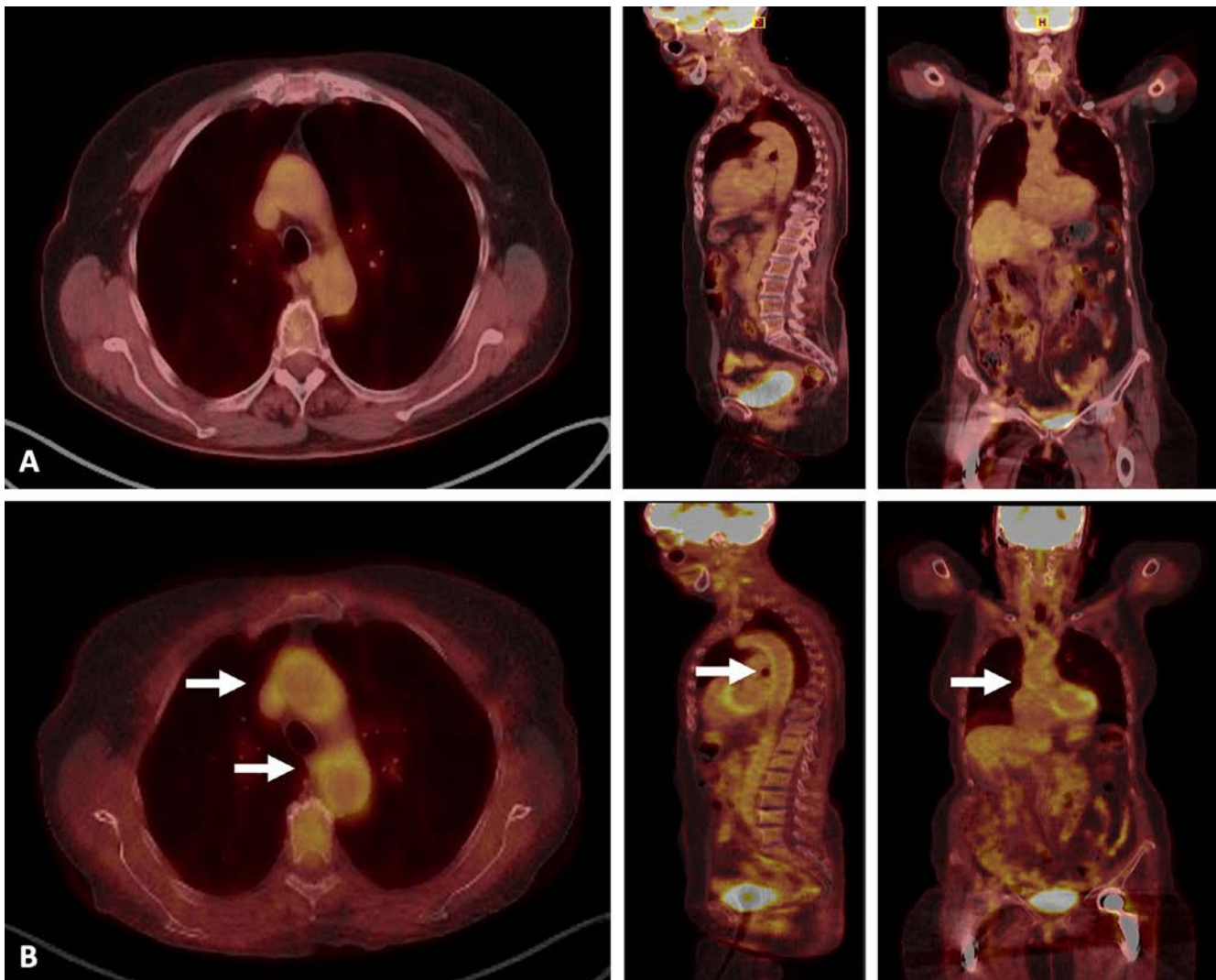


Figure 1. Large vessel vasculitis relapse in a patient with GCA. Images show an 83-year-old woman with biopsy-proven GCA, whose disease onset was characterized by a three-week history of headache, scalp tenderness, jaw claudication, and constitutional symptoms. (A) Initial FDG PET/CT performed two days after the start of high-dose glucocorticoids (60 mg/day prednisone) showed no abnormal vascular or musculoskeletal uptake. (B) One year after diagnosis, the patient relapsed with daily headache, polymyalgia rheumatica symptoms, fever, and elevated acute-phase reactants. PET/CT demonstrates avid uptake of FDG in the ascending and descending aorta (arrows) as well as in the carotid arteries. Axial, sagittal, and coronal views are presented. FDG, [^{18}F]-fluorodeoxyglucose; GCA, giant cell arteritis; PET/CT, positron emission computed tomography.

(<1%) are rare ischemic complications.^{4,8,9} Approximately 40% to 60% of patients present with concurrent symptoms of PMR, a related inflammatory disease characterized by aching and morning stiffness of shoulder and pelvic girdle.^{3–7}

At diagnosis, involvement of the aorta and its major proximal branches (especially the subclavian and axillary arteries) is detected in 20% to 67% of patients by computed tomography angiography, 60% by magnetic angiography, and 83% by PET/CT.^{4,6,10–12} Although LV involvement is frequently identified by imaging techniques, signs and symptoms related to them, for example, arm claudication (1%–16%), leg claudication (4%–6%), arterial bruits (4%–21%), pulse abnormalities (3%–25%),

and asymmetric blood pressure readings (3%–20%), are uncommon.^{4,6,10–13}

The spectrum of GCA encompasses phenotypes categorized according to the predominance of cranial or LV involvement (extracranial disease), with over 80% of patients having some cranial manifestation.^{6,13} Isolated LV involvement (no cranial features) was estimated at 12% in a large-international cohort.¹³ Overlapping manifestations may exist in a significant proportion of patients.^{6,13} Patients with a predominance of cranial manifestations are usually older and have a higher prevalence of cranial ischemia (eg, headache, jaw claudication, and scalp tenderness), in addition to increased ocular involvement (eg, amaurosis fugax)

Table 1. Frequency of clinical and laboratory characteristics of patients with giant cell arteritis at presentation and during relapse*

	Diagnosis	Relapse
Constitutional symptoms (%)	51–68	8.2–50
Fever	9–42	8.2
Weight loss	26–50	
Malaise	40–50	20
Polymyalgia rheumatica (%)	21–60	13–65
Cranial manifestations (%)		19–68
Headache	32–85	13–62
Scalp tenderness	13–44	7.8–32
Jaw claudication	22–51	13–44
Abnormal temporal artery (decreased/absent pulse, tenderness, or nodular, cord-like)	15–80	
Visual abnormalities (%)		
Amaurosis fugax	5–18	
Permanent visual loss	4–14	1–3.3 (GC monotherapy) 0–1 (TCZ)
Large-vessel involvement detected by imaging techniques (%)	20–83	34–75
Symptomatic large vessel involvement (%)	25–37	0–12.5 (severe aortic involvement: 4.5–7.7)
Limb claudication ^a	1–16	
Large artery bruits ^b	4–21	
Pulse abnormalities	3–25	
Laboratory findings (%)		
Patients with elevated ESR	68–100	Variable according to definition and/or use of TCZ
Patients with elevated CRP	91–100	Variable according to definition and/or use of TCZ
Patients with anemia	13–55	22

* CRP, C-reactive protein; ESR, erythrocyte sedimentation rate; GC, glucocorticoids; Hb, hemoglobin; LV, large vessel; SD, standard deviation; TCZ, tocilizumab.

^a Approximately 50% in patients with GCA with predominant LV vasculitis.

^b Approximately 30% in patients with GCA and LV vasculitis.

and TA abnormalities.^{6,13} Patients with GCA and LV involvement (LV GCA) tend to be younger at disease onset, have a high burden of upper extremity vascular abnormalities, may exhibit thoracic pain due to aortitis or aortic dissection, and usually show constitutional symptoms and PMR.^{6,13} Cranial symptoms are less common in LV GCA.

Given the risk of irreversible vision loss from arteritic ischemic optic neuropathy, prompt initiation of GC is important once the diagnosis is suspected, even while awaiting confirmatory testing. The majority of patients with GCA experience a substantial symptomatic improvement after initiation of high-dose GC. Although GC induce rapid disease remission and improvement in symptoms, GC monotherapy is associated with relapses in approximately 45% of patients, requiring an increase in GC doses with risk of GC-related adverse effects (AE).^{14–23} Other potential complications associated with repeated relapses and persistent disease activity may include GCA-related vascular damage. Additionally, studies have found that extracranial LV involvement is associated with increased risk of relapses, cardiovascular disease, and death.^{6,11,12,16,24–27} A recent PET/CT study found that in addition to the intensity and extent of initial aortic inflammation, ongoing LV inflammation contributes to thoracic aortic aneurysm formation.²⁸ Tocilizumab (TCZ), an interleukin-6 (IL-6) antagonist, is an efficacious GC-sparing therapy.²⁹ However, treatment with TCZ usually results in prompt normalization of acute-phase reactants used to assess disease activity, even if inflammatory disease activity has not been fully suppressed. Additionally, relapses are

frequent after discontinuation of therapy with TCZ.^{30–34} Given the clinical importance and high frequency of relapses in GCA, in this paper, we provide clinicians with a practical and comprehensive approach to the diagnosis and management of GCA relapses.

Approach to diagnosis and management. *Diagnosis and classification of relapses.* The spectrum of the clinical features observed as part of GCA relapses are similar to those observed in patients during disease presentation (Table 1).¹⁷ However, manifestations may be less severe or blunted by GC therapy and are accompanied by less prominent laboratory abnormalities than at initial diagnosis. Patients may relapse with the same clinical features originally presented at vasculitis onset, although new manifestations, as in the described case with LV involvement, can also develop.¹⁷ Importantly, severe ischemic manifestations (eg, vision loss) or symptomatic aortic structural complications (eg, aortic dissection) are rare during GCA relapses, occurring in approximately 2.5% of patients and accounting for 3% to 7.8% of all relapses.^{15,35}

The diagnosis of a relapse relies on the reappearance of GCA-related manifestations following a period of clinical remission. It also requires consideration and exclusion of alternate causes for the patient's symptoms and clinical findings. Headache (13%–62%) and PMR (13%–65%) are the most common symptoms in patients with relapsing GCA on treatment with GC or TCZ therapy (Table 1).^{17,36–41} Constitutional symptoms may

be observed in approximately 30% to 50% of patients. Severe neuro-ophthalmic ischemic manifestations are uncommon during disease relapses.^{15,17,36–41} Although recurrent visual symptoms have been reported in 0% to 10% of patients,^{42–44} the incidence of new irreversible sight loss is 1% to 3.3% in patients treated with GC monotherapy and <1% in those receiving TCZ.^{35–37,39–41,44–46} Similarly, symptomatic LV involvement is a rare feature after treatment initiation, with frequencies between 0% to 12.5%.^{15,17,36–41}

In patients treated with GC monotherapy, the recurrence of clinical manifestations is usually accompanied by abnormal laboratory results, particularly elevated levels of ESR and CRP.^{36–41} An increase in acute-phase reactants may precede clinical manifestations. However, ESR and CRP are nonspecific, and its increase in the absence of symptoms should also prompt evaluation for other causes, like infections. Escalation of treatment is not advised in a patient who is otherwise doing well clinically based solely on increases in ESR and CRP, although more close monitoring may be warranted.⁴⁷ In cases of uncertainty, LV imaging to evaluate for LV disease may be helpful.⁴⁸ ESR and CRP levels may vary according to relapse characteristics. For example, higher elevations are observed in patients with cranial manifestations in comparison with isolated PMR.^{39,40} ESR and CRP are of limited value for monitoring disease activity in patients receiving TCZ, which blunts the IL-6-mediated acute-phase response. In addition to clinical and laboratory evaluation, vascular imaging techniques, such as PET/CT or magnetic resonance imaging angiography, may also be useful in evaluating for relapses during TCZ treatment and in patients with LV disease.⁴⁸ Although symptomatic LV involvement is uncommon during relapses, LV imaging abnormalities may be uncovered in 34% to 75% of patients who are relapsing with LV GCA.^{14,41,49} Given the absence of typical cranial symptoms, the subset of patients with extracranial GCA may require monitoring with imaging as part of disease activity assessment. However, at present, the significance of findings like vessel wall edema, vessel wall thickening, or FDG uptake on PET, which may persist in patients with LV vasculitis, are unclear.^{50,51} As a result, treatment may not need to be escalated in a patient in clinical remission without findings of anatomic progression (new lesions, for example).

For treatment purposes, it is helpful to classify relapses as major or minor, depending on the severity of organ involvement.⁵² Major relapses include severe ischemic complications (eg, permanent loss of vision, amaurosis fugax, jaw claudication, stroke, and limb claudication) or active LV inflammation leading to arterial aneurysms, stenosis, or dissections (Figure 2).⁵² Relapses not fulfilling these criteria are categorized as minor (eg, headache, isolated PMR, or systemic symptoms).⁵²

Can we predict patients at risk for relapses? Relapses may occur at any time during the course of GCA, although they tend to develop mostly during the first 2 years after diagnosis and are rare after the fifth year.¹⁷ Unfortunately, there is no clinical,

laboratory, or imaging biomarker that can accurately predict a relapsing course in GCA.^{36–40}

In patients with GCA treated with GC monotherapy, variables at disease onset that were more frequent in patients with relapses compared with those that achieved sustained remission include female sex,^{12,16,38,53} LV involvement,^{6,12,16,24} and an intense systemic inflammatory response (encompassed by fever, anemia, thrombocytosis, and highly elevated ESR and CRP).^{37–41,54} Increased arterial FDG uptake detected by PET,²⁴ GC monotherapy, and a rapid decrease in GC dose and/or a short duration of GC therapy (especially before 12 months) has also been identified as factors associated with GCA relapses.^{14,16,17,41} In patients receiving TCZ, an initial prednisone dose <30 mg/day, cranial manifestations, and worse patient-reported outcomes (quantified by the Functional Assessment of Chronic Illness Therapy [FACIT]–Fatigue and Short Form 36 [SF-36] Physical Component Summary scores) were factors associated to refractory and relapsing disease.^{30,32,53}

Given the absence of useful predictors in clinical practice, a relevant aspect of the management of patients with GCA is to frequently reassess disease activity by monitoring clinical, laboratory, and, if indicated, imaging parameters. Although both the American College of Rheumatology/Vasculitis Foundation (ACR/VF) guidelines and EULAR recommend long-term follow-up of patients, the optimal frequency or duration have not been established.^{47,52} ACR/VF guidelines recommend considering factors such as the duration of remission, areas affected by vasculitis, risk of progression, treatment status, and the reliability of the patient to report new symptoms.⁴⁷ EULAR recommendations suggest routine follow-up every 1 to 3 months for the first year and every 3 to 6 months thereafter.⁵² Patients should be counseled to contact the physician for prompt evaluation in case of new symptoms. Assessments should include history, physical examination, and laboratory evaluations.⁴⁷ In the case of patients with extracranial involvement, imaging at regular intervals (6–12 months unless in long-term remission) may be considered, even in patients in apparent clinical remission, to assess for the development of new lesions or progression of pre-existing structural damage. However, no consensus agreement exists on this regard, and the decision should be individualized based on patient factors such as areas affected, treatment, disease activity, and risk of complications.⁴⁸ Because aortic aneurysms are a late complication of GCA, all patients should be monitored even after discontinuation of therapy.^{52,55} There is currently no consensus on the imaging modalities or frequency of screening for aneurysms in GCA. Given the increased risk of ascending thoracic aneurysms, echocardiography might be a useful screening tool.

What factors may influence the treatment of relapses in patients with GCA? A number of clinical factors may influence the treatment of relapses, such as the manifestations of the relapse, the dose of prednisone at relapse, patient comorbidities, rate of GC taper, non-GC treatment at the time of relapse, and

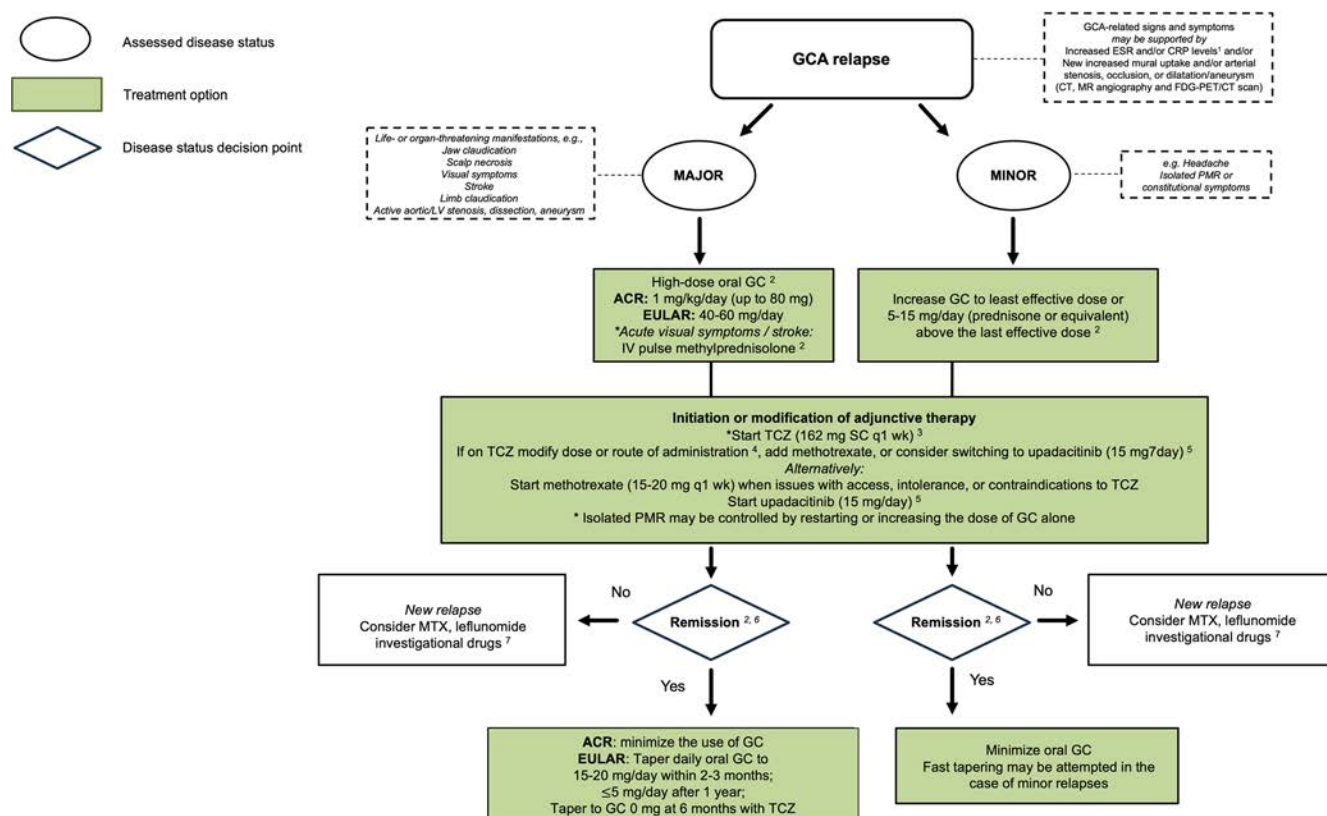


Figure 2. Suggested management algorithm for patients with giant cell arteritis relapses.¹ The use of ESR and CRP is unsuitable in patients receiving TCZ because this drug is able to suppress their synthesis.² Recommendations by the 2021 ACR/Vasculitis Foundation Guideline for the Management of Giant Cell Arteritis and Takayasu Arteritis⁴² and 2018 update of the EULAR recommendations for the management of large vessel vasculitis.⁵² TCZ is particularly recommended for relapses of cranial symptoms or relapses occurring in patients under moderate-to-high doses of GC.⁴ For example, if a patient relapses while on TCZ administered SQ, switch administration to intravenous injections. Change of dose and frequency may also be attempted (eg, from every other week increase to weekly injections).⁵ Based on the results of the Study to Evaluate the Safety and Efficacy of Upadacitinib in Participants With Giant Cell Arteritis, a phase 3, multicenter, randomized, double-blind, placebo-controlled study (published in abstract form). This treatment is not currently approved by regulatory agencies for GCA and should be considered investigational.⁶ Dose and duration of oral GC therapy can be variable depending on a patient's manifestations and comorbidities, toxicity related to GC use, number of flares, and the patient's preferences.⁷ Entry into an investigational trial may also be an option for patients with refractory disease. Alternatively, consider other therapeutic options under active investigation (eg, secukinumab) with published data showing potential efficacy. ACR, American College of Rheumatology; CRP, C-reactive protein; CT, computed tomography; ESR, erythrocyte sedimentation rate; FDG, [¹⁸F]-fluorodeoxyglucose; GC, glucocorticoid; GCA, giant cell arteritis; IV, intravenous; LV, large vessel; MR, magnetic resonance; MTX, methotrexate; PET, positron emission tomography; PMR, polymyalgia rheumatica; SC, subcutaneous; TCZ, tocilizumab. Color figure can be viewed in the online issue, which is available at <http://onlinelibrary.wiley.com/doi/10.1002/art.43098/abstract>.

type and management of previous relapses. The most important factor is the severity of the relapse and organs affected because that influences management. A major relapse that results in severe ischemic manifestations such as stroke, neuro-ophthalmic complications, or inflammation leading to structural damage warrants treatment with high doses of GC for reinduction, whereas a minor relapse or relapse of PMR may be managed by increasing the GC to the previous effective dose.⁵²

A rapid GC taper in the absence of adjunctive therapy may also result in relapses.^{29,56} In the clinical trial of TCZ in GCA (GiACTA), there were two placebo arms: one with a rapid 26-week GC taper (50 patients, 46% newly diagnosed) and another with a 52-week GC taper (51 patients; 45% newly diagnosed).²⁹ The proportion of patients with relapses was 68% in

the 26-week GC placebo group and 49% in the 52-week GC placebo group.²⁹ Additionally, the cumulative GC dose at the end of the study were similar in both placebo arms (3.3 g in the 26-week arm and 3.8 g in the 52-week arm), likely reflecting relapses that required an increase in GC therapy in the 26-week placebo arm.²⁹ Thus, if a patient is on GC monotherapy, it may be prudent to consider a more gradual taper.⁵² If a relapse occurs after discontinuation of TCZ, restarting the medication is beneficial, although in some patients, GC may be temporarily required.^{32,52,57}

Suggested algorithm for management of relapses in GCA. The management of relapses begins with the confirmation of an increase in disease activity followed by the assessment of the severity of the relapse (Figure 2). In the case of a major relapse (ie, with ischemic manifestations), high-dose GC is warranted

given their rapid onset of action, and addition of adjunctive therapy should be considered.^{47,52} The choice of GC-sparing therapy may be influenced by the patient's comorbidities, cost, or availability of the treatment, but the strongest evidence is for TCZ.²⁹ In some cases, the addition of methotrexate (MTX) may be considered.^{47,52} In patients who are already on adjunctive therapy, optimizing the dose if possible is recommended.^{47,52} In GiACTA, the weekly dose of TCZ was more efficacious than an every-other-week dose in patients with relapsing disease.²⁹ Although we have limited data, adding a conventional immunosuppressive therapy like MTX to TCZ may also be considered in select cases.⁵⁸ Based on the results of a large phase 3 randomized controlled trial (currently only available in abstract form), switching from TCZ to upadacitinib (UPA) 15 mg daily (selective JAK1 inhibitor) may also be considered, if appropriate.⁵⁹ If the patient is already on adjunctive treatment with MTX, optimizing the dose or switching to TCZ (unless there are contraindications) may be helpful.⁵² For minor relapses, increasing GC to the last effective dose is reasonable. In patients with frequent relapses or those at risk for GC toxicity, even in cases of minor relapses, adjunctive therapy should be considered and discussed with the patient. In patients with relapsing disease despite the above strategies or with contraindications to the treatments above, investigational therapies may need to be considered.

Once remission has been achieved, GC should be gradually tapered because long-term prescription is associated with significant toxicity. Despite their widespread prescription, the optimal pace of tapering, dose, and duration of GC therapy during the maintenance phase remain unknown and need to be individualized for each patient based on the clinical course, comorbidities, GC-related AE, and patient's values and preferences.^{47,52} A small proof-of-concept study of 30 patients with GCA (50% with relapsing disease) treated with an 8-week GC taper (starting dose 20–60 mg) and TCZ 162 mg weekly showed sustained remission⁶⁰ in 77% at week 52. Even though no vision loss was observed in this study, the number of patients studied was small, and additional studies comparing different GC regimens are needed before short tapers can be recommended.⁶⁰

As for duration of adjunctive therapy, multiple studies have found relapses in nearly half the patients after discontinuation of treatment with TCZ.^{30,31,33,34,57} The data suggest that although it is efficacious as a GC-sparing therapy, a subset of patients will have relapsing disease and may require long-term therapy with TCZ. In general, we favor gradually lowering the dose of TCZ, which can be accomplished by increasing the frequency of treatment rather than abrupt discontinuation of therapy. Patients with historically relapsing disease, significant vascular damage, or LV disease may benefit from longer duration of treatment, although additional data are needed.

Our patient was diagnosed with a major relapse. Prednisone was increased to 40 mg/day, and subcutaneous (SQ) TCZ 162 mg weekly was initiated. She improved rapidly following GC

administration. Headache and PMR symptoms resolved promptly, fever subsided quickly, and ESR and CRP normalized 1 week after the initiation of treatment. She remained in long-term remission on TCZ with discontinuation of prednisone after 6 months.

Evidence. *GCs for relapsing disease.* GCs are considered the initial measure to regain disease control during GCA relapses due to their potent anti-inflammatory and immunosuppressive effect. Although high-quality data regarding the optimal GC dose for a disease relapse are scarce (Table 2), recent guidelines endorsed by the ACR/VF, the EULAR, and the Pan American League of Associations for Rheumatology (PANLAR) recommend the reinstitution or escalation of high-dose GC in the case of major relapses.^{47,52,61} In the rare case in which a patient relapses with vision loss or ischemic stroke attributable to GCA, intravenous methylprednisolone should be considered.^{47,52,61} For patients experiencing minor relapses, an increase in daily prednisone to either the last effective dose or 5 to 15 mg/day above this dose is recommended.^{47,52} Data supporting the above are from population-based studies.^{37,39,54,62,63}

Although the optimal GC taper has not been studied prospectively, current EULAR recommendations suggest tapering GC to 15 to 20 mg/day within 2 to 3 months with a goal of ≤5 mg by the end of 1 year.⁵² The ACR/VF and the PANLAR recommendations emphasized minimizing the prescription of GC as much as possible but without establishing a therapy regimen.^{47,61} In patients on treatment with TCZ, the 26-week GC taper outlined in the GiACTA study may be considered.^{29,60}

Adjunctive therapy for relapsing disease. GC therapy, although effective at alleviating symptoms and inflammation, is also associated with significant AE.^{19,20} Although adjunctive therapy is beneficial in cases of relapses, it is unclear whether all newly diagnosed patients need adjunctive therapy.

TCZ. Two prospective randomized clinical trials (RCTs) demonstrated efficacy of TCZ in patients with new and relapsing GCA (Table 3).^{29,64} This includes a phase 2 clinical trial evaluating intravenous 8 mg/kg TCZ every 4 weeks along with a standardized GC taper and a large, multicenter, phase 3 trial evaluating SQ TCZ with standardized GC taper.^{29,64} In GiACTA, patients were randomized to placebo with a 26-week prednisone taper, placebo with a 52-week prednisone taper, 162 mg SQ TCZ every other week with a 26-week prednisone taper, or 162 mg SQ TCZ weekly with a 26-week prednisone taper.²⁹ The primary end point of sustained GC-free remission at week 52 was met in 56% of patients in the TCZ-weekly arm, 53% in the TCZ-every-other-week arm, 14% in placebo-26-week prednisone taper and 18% in placebo-52-week prednisone taper.²⁹ Relapses were observed in 23% in the weekly TCZ arm and 26% in the TCZ-every-other-week compared with 68% in the placebo group and 26-week prednisone arm and 49% in the placebo group and 52-week prednisone arm.²⁹ Patients treated with TCZ also

Table 2. Studies evaluating glucocorticoid therapy in giant cell arteritis*

Treatment	Reference	Study design	Patient population	Intervention	Outcomes
Induction	Hunder et al ⁹⁵	RCT	New disease	Alternate-day dosing vs daily GC administration	Remission at 4 weeks achieved in 80% treated with daily GC vs 30% on those receiving alternate-day dosing
	Kyle and Hazleman ⁹⁶	Prospective	New disease	Prednisone 40 mg (high dose) vs 20 mg (low dose) for 4 weeks	Relapse 20% in the high-dose GC group vs 40% in the low-dose GC group
Comparison of IV GC vs oral GC	Chevalet et al ⁹⁷	RCT	New GCA without cranial ischemia	Single IV pulse methylprednisolone (240 mg) vs placebo, followed by oral prednisone (0.7 mg/kg/day)	No GC-sparing effect or steroid-related side effects with IV GC
	Mazlumzadeh et al ⁹⁸	RCT	New GCA without cranial ischemia	IV methylprednisolone (15/mg/kg) vs placebo, followed by prednisone 40 mg/day	Apparent GC-sparing effect. 71% of patients were in remission at week 36 in the IV methylprednisolone vs 15% in the oral group
	Trives-Folguera et al ⁹⁹	Retrospective	Not reported	IV methylprednisolone pulses vs oral GC	Relapse rate did not differ according to initial therapy (20% in IV GC group vs 19% in oral GC group)
	Hayreh et al ¹⁰⁰	Retrospective	New GCA with visual involvement	IV GC vs oral GC	Visual improvement in only 7% of patients treated with IV GC vs 5% in oral GC
	Chan et al ¹⁰¹	Retrospective	New GCA with visual loss	IV GC vs oral GC	Improved visual acuity in 40% of patients with IV GC vs 13% with oral GC
Maintenance	Stone et al ²⁹	RCT (phase 3)	New or relapsing disease	26-week GC taper vs 52-week GC taper	Relapse 68% in the placebo group with the 26-week taper vs 49% in the 52-week taper

* The CORTODOSE study, a phase 3, prospective multicenter randomized clinical trial is currently comparing two GC-tapering schedules (28 vs 52 weeks, NCT04012905). GC, glucocorticoid; GCA, giant cell arteritis; IV, intravenous; RCT, randomized clinical trial.

showed clinically meaningful improvement in health-related quality of life measures, including SF-36 and FACIT-Fatigue.²⁹

A subsequent analysis of GiACTA, which included long-term follow-up at 3 years, showed treatment with TCZ was beneficial in newly diagnosed patients as well as those with relapsing disease, including a longer median time to first relapse in both groups and lower risk of relapse in patients with new and relapsing disease treated with the weekly TCZ.⁶⁵ Several studies have also evaluated the effects of TCZ on PET activity with improvement while on TCZ.^{66–69}

At present, it remains unclear whether all newly diagnosed patients need to be started on TCZ because a subset of patients are able to taper without relapses while on GC monotherapy. There are differing perspectives in the guidelines from ACR/VF who recommend TCZ in all patients with GCA, including those with newly diagnosed disease, and EULAR who recommend TCZ in patients with relapsing or refractory disease.^{47,52} Patients with newly diagnosed disease at risk for GC-related AE and those with LV disease may also benefit from early initiation of TCZ.^{70,71} In the case of relapsing disease, both ACR/VF and EULAR

recommend adjunctive immunosuppression with TCZ with consideration for MTX in select circumstances.^{47,52}

The optimal duration of treatment with TCZ also remains to be determined, with frequent relapses approaching 50% at 2 years after discontinuation of therapy, even after treatment for over 1 year.^{30,31,33,34,57} In the phase 2 study evaluating TCZ, relapses were observed in 8 of 17 patients (47%) in clinical remission at week 52 after discontinuation of treatment (mean duration 6 months from stopping treatment to relapse).³⁰ In the GiACTA trial, at the end of 52 weeks, patients entered a 104-week open-label arm in which they could continue or discontinue treatment with GC, TCZ, or MTX at the discretion of the investigator.³³ Although data are limited given the design, only 42% of patients in the TCZ group remained in clinical remission off GC and TCZ³³ at week 52. Another small study evaluated a gradual decrease in the frequency of TCZ from every week for 1 year to every other week for 1 year before discontinuation of therapy and found a relapse rate of 26% at 6 months, but long-term follow-up is not available.³⁴ While in GiACTA, the weekly dosing was more effective than the every-other-week dosing at

Table 3. Prospective studies demonstrating efficacy of adjunctive immunosuppression in giant cell arteritis*

Treatment	Reference	Study design	Patient population	Intervention	Outcomes	Current or upcoming studies ^a
TCZ	Villiger et al ⁶⁴	RCT	New or relapsing disease	IV TCZ 8 mg/kg every 4 weeks vs placebo, standardized GC taper	Higher proportion in remission at prednisone dose of 0.1 mg/kg/day at week 12 in TCZ arm	TCZ vs MTX (NCT03892785)
	Stone et al ²⁹	RCT (phase 3)	New or relapsing disease	SQ TCZ 162 mg every week or every other week vs placebo, standardized GC taper	Sustained GC-free remission at week 52 higher in both TCZ groups, lower cumulative GC doses in TCZ	MTX after TCZ for induction (NCT05623592)
MTX	Jover et al ⁷³	RCT	New diagnosis	MTX 10 mg/week vs placebo, standardized GC taper	Fewer relapses in group on MTX, fewer proportion with multiple relapses on MTX, lower cumulative GC with MTX	TCZ vs MTX (NCT03892785), MTX after TCZ for induction (NCT05623592)
	Spiera et al ⁷⁴	RCT	New diagnosis	MTX 7.5 mg/week vs placebo, GC taper per treating physician	No difference in cumulative GC doses or number of weeks to discontinue GC	
	Hoffman et al ⁷⁵	RCT	New diagnosis	MTX 15 mg/week vs placebo, standardized GC taper	Treatment failure (relapses) similar in both groups	
	Mahr et al ⁷⁶	Meta-analysis	Three clinical trials of MTX	MTX vs placebo	MTX lowered risk of relapse, reduced cumulative GC	
LEF	Kramaric et al ⁷⁹	OLT	New diagnosis	LEF 10 mg added to GC at week 12 vs GC monotherapy, standardized GC taper	Fewer relapses in LEF vs GC monotherapy	None presently
ABA	Langford et al ⁸²	RCT (phase 2)	New or relapsing disease	IV ABA 10 mg/kg days 1, 15, and 29 and week 8. Patients in remission at week 12 randomized to continued ABA vs placebo, standardized GC taper	Higher proportion in ABA without relapses at week 52	Phase 3 RCT of ABA vs placebo (NCT04474847)
SEC	Venhoff et al ¹⁰²	RCT (phase 2)	New or relapsing disease	SEC 300 mg week 0, 1, 2, 3, and 4 and then every 4 weeks vs placebo, standardized GC taper	Higher proportion in sustained remission at week 28 and week 52 with SEC	SEC in newly diagnosed patients in remission (NCT05380453), phase 3 RCT of SEC vs placebo (NCT04930094)
Baricitinib	Koster et al ⁸⁴	OLT	Relapsing disease	Baricitinib 4 mg/day	93% in GC-free remission at week 52	
UPA ^b	Blockmans et al ⁵⁹	RCT (phase 3)	New or relapsing disease	UPA 7.5 mg/day or 15 mg/day vs placebo, standardized GC taper	Higher proportion on UPA 15 mg daily in sustained remission at week 52	RCT evaluating upadacitinib (NCT03725202), full results not available

* ABA, abatacept; GC, glucocorticoid; IV, intravenous; LEF, leflunomide; MTX, methotrexate; OLT, open-label trial; RCT, randomized controlled trial; SEC, secukinumab; SQ, subcutaneous; TCZ, tocilizumab; UPA upadacitinib.

^a Per clinicaltrials.gov.

^b Only available in abstract form.

preventing relapses in the subset of patients with relapsing disease; in retrospective studies, both doses appear efficacious.^{29,31,32,34,58}

In a multicenter observational study of 417 patients with GCA in prolonged remission, TCZ was decreased in 231 patients by spacing out SQ TCZ to 162 mg every other week (65% cases) or lowering the dose from 8 mg/kg every 4 weeks to 4 mg/kg every 4 weeks⁵⁸ (44%). After a median follow-up of 2 years, there were no differences in the relapse rates of patients on reduced-dose TCZ versus full-dose TCZ⁵⁸ (5.6% versus 10.4%, $P = 0.18$). A higher frequency of patients in the full dose group had severe infections⁵⁸ (19.9% versus 6.6% for reduced dose, $P = 0.01$). However, 23% to 26% of patients in this cohort were also on adjunctive immunosuppression with MTX making the effects of TCZ withdrawal difficult to assess.⁵⁸ The authors propose a gradual withdrawal of TCZ after 1 year of treatment and at least 6 months of remission rather than abrupt discontinuation of therapy.⁵⁸ In another study evaluating relapse risk after discontinuation of TCZ in 114 patients, neither the dose of TCZ prescribed nor duration of treatment with TCZ affected relapse risk, with >50% relapses at 12 months after discontinuation of treatment.³²

At present, we have no data to support that duration of treatment with TCZ impacts relapse rate after discontinuation or that gradually spacing out TCZ to discontinuation would be more efficacious. Several studies have shown frequent relapses after stopping TCZ.^{31,32,34,57,58,64,72} It may be judicious to leave some patients, particularly those with history of relapses or LV manifestations, on treatment long term. Whether other strategies including adjunctive therapies like MTX would allow long-term remission after discontinuation of TCZ remains to be seen. An RCT evaluating the benefit of adding MTX for continued remission maintenance after induction with TCZ and GC is planned (NCT05623592). Strategies evaluating de-escalation of treatment and factors that might predict which patients will be able to successfully discontinue treatment need further investigation.

UPA. The safety and efficacy of UPA, a selective JAK1 inhibitor, was evaluated in a large RCT, Study to Evaluate the Safety and Efficacy of Upadacitinib in Participants With Giant Cell Arteritis. Patients with new (70%) or relapsing (30%) disease were randomized to 7.5 mg/day UPA ($n = 107$) or 15 mg/day UPA ($n = 209$) along with a 26-week GC taper or placebo with a 52-week GC taper ($n = 112$).⁵⁹ The primary end point of sustained remission at week 52 was met in 46% in 15 mg UPA vs 29% on placebo ($P = 0.019$; results only available in abstract form). Cumulative GC doses were lower in the UPA group (1,615 mg vs 2,882 mg, $P < 0.001$) with improvement in patient-reported outcomes. Although 7.5 mg UPA showed numerically better efficacy compared with placebo, it did not reach statistical significance. AE, including herpes zoster, lymphopenia, anemia, and nonmelanoma skin cancer, were numerically higher with UPA. Major adverse cardiovascular events were not observed in the UPA group. Evaluation of the publication of the full results will be

important. The medication is currently not approved for GCA by any regulatory agency. Additionally, taking into consideration the average age of patients with GCA and the black-box warnings JAK inhibitors carry for risk of major cardiovascular events, thrombosis, and malignancy, caution will be needed with the prescription of UPA. We anticipate this will be an available option for GCA in the future and do not recommend it as first line, but if appropriate, it may be an option for patients who fail or do not tolerate TCZ. Like TCZ, it would be contraindicated in patients with diverticulitis. There should be a discussion with the patient regarding the safety profile of UPA, the need to actively monitor and control cardiovascular risk factors, and ensure appropriate vaccinations like varicella zoster and age- and sex-appropriate cancer screenings are up to date.

MTX. Whereas we consider MTX in patients with relapsing disease, the three RCTs evaluating MTX in GCA included only patients with newly diagnosed disease and with conflicting results (Table 3).^{73–75} A subsequent meta-analysis of these trials showed a modest benefit of MTX with fewer relapses and lower GC exposure in patients receiving MTX.⁷⁶ Observational data from clinical practice suggest a benefit of MTX on reducing GCA disease relapses and GC cumulative dose.⁷⁷ Despite inconclusive evidence, international guidelines suggest MTX as an option to relapsing disease in patients with contraindications or limited access to TCZ.^{47,52,61}

Although definitive evidence of the superiority of TCZ over MTX is lacking, in previous studies, TCZ showed a more substantial GC-sparing effect and a larger reduction in the risk of relapse. A phase 3 RCT comparing MTX and TCZ is currently underway (NCT03892785).

Leflunomide. Retrospective series suggest a benefit of leflunomide (LEF) in patients with newly diagnosed or refractory GCA (Table 3).^{54,78} A recent prospective open-label study evaluated LEF in patients with newly diagnosed GCA without contraindications to treatment and found a lower number of relapses in patients receiving LEF (15%) compared with GC monotherapy⁷⁹ (45%).

Options for patients who fail TCZ or have contraindications. Patients may relapse despite treatment with TCZ or have contraindications to TCZ. In these select circumstances, options include the addition of adjunctive immunosuppression like MTX to TCZ or consideration of other targeted therapies that are currently under investigation (Table 3). In GiACTA, stable doses of MTX could be initiated at screening, continued in the double-blind period, and reduced and/or discontinued at the investigator's discretion.²⁹ Thirty of 250 patients (12%) received adjunctive MTX; 10% of TCZ-treated patients and 15% in the placebo-arm had no clear benefit of MTX in outcomes of sustained remission, disease relapse rate, or GC-sparing effect, although the numbers were small.^{80,81} However, in a multicenter observational study of 134 patients, 38% received combination therapy, mainly MTX, with TCZ.⁵⁸ These patients were younger and had longer disease

duration and more LV disease than the 62% receiving TCZ alone.⁵⁸ The study found the prescription of combined therapy allowed for a longer duration of remission.⁵⁸

Based on our understanding of the pathogenesis of GCA, other adjunctive therapies are under investigation with promising results. To date, only small phase 2 studies have been published (Table 3). In cases in which patients have exhausted or have contraindications to available treatment options, the clinician may consider these options based on the data currently available. This so called “off-label” use should be discussed clearly with the patient along with the data and potential benefits. None of the medications discussed below are currently approved by regulatory agencies for the treatment of GCA.

Abatacept. A phase 2, double-blind, multicenter trial of 49 patients with GCA with newly diagnosed and relapsing disease evaluated abatacept (CTLA-4lg, a T cell modulator).⁸² All patients were treated with abatacept (10 mg/kg on day 1, 15, and 29 and week 8) in addition to a standardized prednisone taper.⁸² At 12 weeks, patients in remission ($n = 41$) were randomized to continue abatacept (10 mg/kg every 28 days) along with a continued prednisone taper or switched to placebo with a prednisone taper.⁸² The relapse-free survival at 12 months was 48% for the abatacept group compared with 31% for the placebo group ($P = 0.049$). Median duration of remission was also longer in the abatacept group compared with placebo (9.9 versus 3.9 months, $P = 0.023$).⁸² The ACR/VF expert panel considers abatacept as an alternative to TCZ when anti-IL-6 blockade is not effective and/or contraindicated.⁴⁷ A phase 3 study evaluating the efficacy of abatacept is underway (NCT04474847).

Secukinumab. In a multicenter, phase 2 randomized, double-blind, placebo-controlled trial, patients with new onset or relapsing GCA were randomized to secukinumab (monoclonal antibody to IL-17A) 300 mg injections on week 0, 1, 2, 3, and 4 and then every 4 weeks through week 48 ($n = 27$) or placebo ($n = 25$) and a standardized 26-week prednisolone taper.⁸³ The primary end point was the median proportion (Bayesian analysis) of patients with sustained remission until week 28.⁸³ A higher percentage of patients in the secukinumab group were able to maintain sustained remission compared with placebo at 28 weeks (70% versus 20%) and 52 weeks⁸³ (59% versus 8%). A phase 3 study is currently underway (NCT04930094).

JAK signal inhibitors. An open-label study of 15 patients who are relapsing with GCA evaluated 4 mg/day baricitinib (JAK1/JAK2 inhibitor) for 52 weeks.⁸⁴ One patient discontinued baricitinib after 4 weeks because of worsening renal function, but of the remaining 14 patients, only 1 (7%) relapsed by 52 weeks, with the remaining 13 patients achieving GC-free remission.⁸⁴ Four of 14 patients (29%) relapsed in the 12-week follow-up period following baricitinib discontinuation.⁸⁴ The clinical trial of UPA has been presented earlier in the article.

A recent real-world analysis⁸⁵ of patients who are relapsing with GCA that previously failed other therapies reported that treatment with baricitinib ($n = 15$), tofacitinib ($n = 10$), or UPA ($n = 10$) leads to complete remission in 46% of patients. Relapses and AE were reported in approximately 40% of patients.

Ustekinumab. Studies evaluating ustekinumab (IL-12/23 antagonist) yielded mixed results, with an open-label study in refractory GCA demonstrating GC-sparing effect whereas a prospective RCT evaluating patients with new and relapsing disease was terminated early after 7 of the 10 patients enrolled experienced a relapse.^{86,87}

Guselkumab. A phase 2 RCT evaluating guselkumab (IL-23 inhibitor) in patients with new and relapsing GCA was recently terminated after it failed to meet its primary end point, indicating this may not be an important pathway to target in the treatment of GCA (NCT04633447).

Mavrilimumab. Mavrilimumab (granulocyte-macrophage colony-stimulating factor antagonist) was evaluated in a phase 2 multicenter RCT for new or relapsing GCA with lower risk of relapse.⁸⁸ In this study, mavrilimumab alongside GC was superior to GC in achieving sustained remission⁸⁸ at week 26 (83% vs 50%). However, the medication is not available commercially and has not been approved by the Food and Drug Administration for any indication.

Prevention of treatment-related AEs. GC toxicity burden is high and frequent in patients with GCA.^{18–22} In population-based studies, approximately 90% of patients experienced at least one AE associated with GC treatment, with 60% sustaining two or more side effects.¹⁸ A major goal in GCA management is to minimize GC exposure.¹⁸ At diagnosis, patients should be evaluated for the presence of comorbidities that may increase GC toxicity, and during follow-up, reassessment of GC-associated AE should be performed regularly.

Osteoporosis. The incidence rate of osteoporosis and fractures is increased by 38% to 67% in patients with GCA.⁸⁹ According to the 2022 ACR guideline for the prevention and treatment of GC-induced osteoporosis, measures designed to prevent GC-associated bone loss are recommended for all patients receiving ≥ 2.5 mg/day of prednisone when its prescription is anticipated for ≥ 3 months.⁹⁰ This includes a balanced diet, calcium and vitamin D supplementation, and when indicated, pharmacotherapy.⁹⁰

Infections. Incidence of severe infections is increased in GCA.⁹¹ According to the most updated ACR guidelines,⁹² annual seasonal influenza and pneumococcal vaccinations as well as immunizations against herpes zoster and SARS-CoV-2 are recommended for all patients under immunosuppressive medication. In countries with high prevalence, screening and treatment of latent tuberculosis need to be performed in patients receiving high-dose GC or when TCZ is considered. Evidence on the use of *Pneumocystis jirovecii* prophylaxis in GCA is scarce,^{91,93} Although *P jirovecii* pneumonia is uncommon among patients

with GCA, it is associated with significant mortality rates^{91,93} (approximately 30%). Therefore, the decision to start preventive measures to mitigate the risk of *P jirovecii* pneumonia should be decided on an individual basis, particularly in patients receiving high-dose GC therapy (≥ 30 mg/day prednisone).

Discussion

Despite the availability of efficacious therapies like TCZ, relapses remain a significant challenge facing patients with GCA and the clinicians caring for them. Relapses expose patients to disease- and treatment-related morbidity. A better understanding of the risk factors of relapse may allow identification of patients who would benefit from early initiation of adjunctive therapies.

Although TCZ is effective at lowering the risk of relapses, at present, it is unknown which patients would most benefit from anti-IL-6 therapy. A large proportion of patients receiving TCZ relapse once therapy is discontinued, and therefore, the optimal duration of treatment and the subset of patients that might benefit from prolonged immunosuppression remain unknown. Also, the markers of inflammation that are often used in the assessment of patients are unhelpful due to the effect of TCZ receiving IL-6. As result, there is an unmet need for biomarkers that allow the diagnosis or prediction of relapses, especially while receiving treatment with TCZ, but also biomarkers of deep remission, which may allow de-escalation of immunosuppression.

It also remains poorly understood whether the different subsets of patients with GCA have different prognoses. In studies that reported the effect of GC and TCZ on vascular activity of patients with GCA, a significant improvement in vascular inflammation was usually observed after treatment initiation, although persistent vessel wall abnormalities were detected in 30% to 50% of patients.^{30,67–69,71,94} The long-term risks of persistent, often subclinical, vascular inflammation and the effect of TCZ or emerging therapies on long-term vascular complications need further investigation. We need treatments that allow sustained remission even after discontinuation of therapy, positively impacting patients' quality of life in addition to preventing vascular damage; new therapeutic options are under investigation.

The long-term consequences and real-life impact that a relapsing course has on the outcomes of patients with GCA remain underexamined. Increased disease-related vascular morbidity and GC-associated AE (particularly infections, bone fractures, and cardiovascular complications) are potential complications that may be associated with frequent relapses.

Conclusions

As with many autoimmune rheumatic diseases, there is currently no cure for GCA. The goals of therapy are to control the disease, minimize relapses, prevent vascular damage, and minimize side effects of therapy. Although the increased prescription of

TCZ has mitigated the relapse rate in GCA while on therapy, patients still remain at risk of disease and treatment AE. Relapses continue to represent an unmet need for patients with GCA. Although never subjected to evaluation in RCTs, GC remain the cornerstone of the management of GCA relapses, which includes increasing the GC dose and adding a disease-modifying agent, particularly in the presence of severe manifestations and frequent relapses. The great challenge in the management of GCA is to find the balance among the relapse risk of the inflammatory activity, prevention of vascular complications, iatrogenic effects of GC therapy or adjunctive therapies, and the well-being of patients.

Author Contributions

All authors contributed to at least one of the following manuscript preparation roles: conceptualization AND/OR methodology, software, investigation, formal analysis, data curation, visualization, and validation AND drafting or reviewing/editing the final draft. As corresponding author, Dr Kermani confirms that all authors have provided the final approval of the version to be published, and takes responsibility for the affirmations regarding article submission (eg, not under consideration by another journal), the integrity of the data presented, and the statements regarding compliance with institutional review board/Declaration of Helsinki requirements.

REFERENCES




- Jennette JC, Falk RJ, Bacon PA, et al. 2012 revised International Chapel Hill Consensus Conference nomenclature of vasculitides. *Arthritis Rheum* 2013;65(1):1–11.
- Li KJ, Semenov D, Turk M, et al. A meta-analysis of the epidemiology of giant cell arteritis across time and space. *Arthritis Res Ther* 2021; 23(1):82.
- Putman MS, Gribbons KB, Ponte C, et al. Clinicopathologic associations in a large international cohort of patients with giant cell arteritis. *Arthritis Care Res (Hoboken)* 2022;74(6):1013–1018.
- Garvey TD, Koster MJ, Crowson CS, et al. Incidence, survival, and diagnostic trends in GCA across seven decades in a North American population-based cohort. *Semin Arthritis Rheum* 2021;51(6):1193–1199.
- Gonzalez-Gay MA, Barros S, Lopez-Diaz MJ, et al. Giant cell arteritis: disease patterns of clinical presentation in a series of 240 patients. *Medicine (Baltimore)* 2005;84(5):269–276.
- Muratore F, Kermani TA, Crowson CS, et al. Large-vessel giant cell arteritis: a cohort study. *Rheumatology (Oxford)* 2015;54(3):463–470.
- Calamia KT, Hunder GG. Clinical manifestations of giant cell (temporal) arteritis. *Clin Rheum Dis* 1980;6(2):389–403.
- Gonzalez-Gay MA, Vazquez-Rodriguez TR, Gomez-Acebo I, et al. Strokes at time of disease diagnosis in a series of 287 patients with biopsy-proven giant cell arteritis. *Medicine (Baltimore)* 2009;88(4): 227–235.
- Alba MA, Cid MC. Scalp necrosis in giant cell arteritis. *Mayo Clin Proc* 2014;89(10):e99.
- Blockmans D, de Ceuninck L, Vanderschueren S, et al. Repetitive 18F-fluorodeoxyglucose positron emission tomography in giant cell arteritis: a prospective study of 35 patients. *Arthritis Rheum* 2006; 55(1):131–137.
- Prieto-González S, Arguis P, García-Martínez A, et al. Large vessel involvement in biopsy-proven giant cell arteritis: prospective study

- in 40 newly diagnosed patients using CT angiography. *Ann Rheum Dis* 2012;71(7):1170–1176.
12. de Mornac D, Espitia O, Neel A, et al. Large-vessel involvement is predictive of multiple relapses in giant cell arteritis. *Ther Adv Musculoskelet Dis* 2021;13:1759720X211009029.
 13. Gribbons KB, Ponte C, Craven A, et al. Diagnostic assessment strategies and disease subsets in giant cell arteritis: data from an international observational cohort. *Arthritis Rheumatol* 2020;72(4):667–676.
 14. Mainbourg S, Addario A, Samson M, et al. Prevalence of giant cell arteritis relapse in patients treated with glucocorticoids: a meta-analysis. *Arthritis Care Res (Hoboken)* 2020;72(6):838–849.
 15. Aussedat M, Lobbes H, Samson M, et al. Epidemiology of major relapse in giant cell arteritis: a study-level meta-analysis. *Autoimmun Rev* 2022;21(1):102930.
 16. Moreel L, Betrains A, Molenberghs G, et al. Epidemiology and predictors of relapse in giant cell arteritis: a systematic review and meta-analysis. *Joint Bone Spine* 2023;90(1):105494.
 17. Alba MA, Kermani TA, Unizony S, et al. Relapses in giant cell arteritis: updated review for clinical practice. *Autoimmun Rev* 2024;23(6):103580.
 18. Proven A, Gabriel SE, Orces C, et al. Glucocorticoid therapy in giant cell arteritis: duration and adverse outcomes. *Arthritis Rheum* 2003;49(5):703–708.
 19. Wilson JC, Sarsour K, Collinson N, et al. Serious adverse effects associated with glucocorticoid therapy in patients with giant cell arteritis (GCA): a nested case-control analysis. *Semin Arthritis Rheum* 2017;46(6):819–827.
 20. de Boysson H, Barakat C, Dumont A, et al. Tolerance of glucocorticoids in giant cell arteritis: a study of patient-reported adverse events. *Rheumatology (Oxford)* 2022;61(9):3567–3575.
 21. Perrineau S, Ghesquière T, Charles P, et al; French Vasculitis Study Group (FVSG). A French cohort of patients with giant cell arteritis: glucocorticoid treatment and its associated side effects. *Clin Exp Rheumatol* 2021;39 Suppl 129(2):155–160.
 22. Wu J, Keeley A, Mallen C, et al. Incidence of infections associated with oral glucocorticoid dose in people diagnosed with polymyalgia rheumatica or giant cell arteritis: a cohort study in England. *CMAJ* 2019;191(25):E680–E688.
 23. Therkildsen P, Nielsen BD, de Thurah A, et al. All-cause and cause-specific mortality in patients with giant cell arteritis: a nationwide, population-based cohort study. *Rheumatology (Oxford)* 2022;61(3):1195–1203.
 24. Grayson PC, Alehashemi S, Bagheri AA, et al. 18 F-fluorodeoxyglucose-positron emission tomography as an imaging biomarker in a prospective, longitudinal cohort of patients with large vessel vasculitis. *Arthritis Rheumatol* 2018;70(3):439–449.
 25. Guédon AF, Froger C, Agard C, et al. Identifying giant cell arteritis patients with higher risk of relapse and vascular events: a cluster analysis. *QJM*. 2024;hcae105.
 26. Elfishawi MM, Kaymakci MS, J Achenbach S, et al. Reappraisal of large artery involvement in giant cell arteritis: a population-based cohort over 70 years. *RMD Open* 2024;10(1):10.
 27. Aouba A, Gonzalez Chiappe S, Eb M, et al. Mortality causes and trends associated with giant cell arteritis: analysis of the French national death certificate database (1980–2011). *Rheumatology (Oxford)* 2018;57(6):1047–1055.
 28. Blockmans D, Moreel L, Betrains A, et al. Association between vascular FDG uptake during follow-up and the development of thoracic aortic aneurysms in giant cell arteritis. *Front Med (Lausanne)* 2024;11:1384533.
 29. Stone JH, Tuckwell K, Dimonaco S, et al. Trial of tocilizumab in giant-cell arteritis. *N Engl J Med* 2017;377(4):317–328.
 30. Adler S, Reichenbach S, Gloor A, et al. Risk of relapse after discontinuation of tocilizumab therapy in giant cell arteritis. *Rheumatology (Oxford)* 2019;58(9):1639–1643.
 31. Matza MA, Dagincourt N, Mohan SV, et al. Outcomes during and after long-term tocilizumab treatment in patients with giant cell arteritis. *RMD Open* 2023;9(2):9.
 32. Samec MJ, Rakholiya J, Langenfeld H, et al. Relapse risk and safety of long-term tocilizumab use among patients with giant cell arteritis: a single-enterprise cohort study. *J Rheumatol* 2023;50(10):1310–1317.
 33. Stone JH, Han J, Aringer M, et al; GiACTA investigators. Long-term effect of tocilizumab in patients with giant cell arteritis: open-label extension phase of the Giant Cell Arteritis Actemra (GiACTA) trial. *Lancet Rheumatol* 2021;3(5):e328–e336.
 34. Tomelleri A, Campochiaro C, Farina N, et al. Effectiveness of a two-year tapered course of tocilizumab in patients with giant cell arteritis: a single-centre prospective study. *Semin Arthritis Rheum* 2023;59:152174.
 35. Lozachmeur N, Dumont A, Deshayes S, et al. Frequency and characteristics of severe relapse in giant cell arteritis. *Rheumatology (Oxford)* Published online March 18, 2024. <https://doi.org/10.1093/rheumatology/keae174>
 36. Kermani TA, Warrington KJ, Cuthbertson D, et al; Vasculitis Clinical Research Consortium. Disease relapses among patients with giant cell arteritis: a prospective, longitudinal cohort study. *J Rheumatol* 2015;42(7):1213–1217.
 37. Martínez-Lado L, Calviño-Díaz C, Piñeiro A, et al. Relapses and recurrences in giant cell arteritis: a population-based study of patients with biopsy-proven disease from northwestern Spain. *Medicine (Baltimore)* 2011;90(3):186–193.
 38. Labarca C, Koster MJ, Crowson CS, et al. Predictors of relapse and treatment outcomes in biopsy-proven giant cell arteritis: a retrospective cohort study. *Rheumatology (Oxford)* 2016;55(2):347–356.
 39. Restuccia G, Boiardi L, Cavazza A, et al. Flares in biopsy-proven giant cell arteritis in northern Italy: characteristics and predictors in a long-term follow-up study. *Medicine (Baltimore)* 2016;95(19):e3524.
 40. Alba MA, García-Martínez A, Prieto-González S, et al. Relapses in patients with giant cell arteritis: prevalence, characteristics, and associated clinical findings in a longitudinally followed cohort of 106 patients. *Medicine (Baltimore)* 2014;93(5):194–201.
 41. Muratore F, Boiardi L, Restuccia G, et al. Relapses and long-term remission in large vessel giant cell arteritis in northern Italy: characteristics and predictors in a long-term follow-up study. *Semin Arthritis Rheum* 2020;50(4):549–558.
 42. Chan CC, Paine M, O'day J. Predictors of recurrent ischemic optic neuropathy in giant cell arteritis. *J Neuroophthalmol* 2005;25(1):14–17.
 43. Hayreh SS, Zimmerman B. Management of giant cell arteritis. Our 27-year clinical study: new light on old controversies. *Ophthalmologica* 2003;217(4):239–259.
 44. Unizony S, McCulley TJ, Spiera R, et al. Clinical outcomes of patients with giant cell arteritis treated with tocilizumab in real-world clinical practice: decreased incidence of new visual manifestations. *Arthritis Res Ther* 2021;23(1):8.
 45. Aiello PD, Trautmann JC, McPhee TJ, et al. Visual prognosis in giant cell arteritis. *Ophthalmology* 1993;100(4):550–555.
 46. Hachulla E, Boivin V, Pasturel-Michon U, et al. Prognostic factors and long-term evolution in a cohort of 133 patients with giant cell arteritis. *Clin Exp Rheumatol* 2001;19(2):171–176.
 47. Maz M, Chung SA, Abril A, et al. 2021 American College of Rheumatology/Vasculitis Foundation Guideline for the management of giant cell arteritis and Takayasu arteritis. *Arthritis Rheumatol* 2021;73(8):1349–1365.

48. Dejaco C, Ramiro S, Bond M, et al. EULAR recommendations for the use of imaging in large vessel vasculitis in clinical practice: 2023 update. *Ann Rheum Dis* 2024;83(6):741–751.
49. Kermani TA, Diab S, Sreih AG, et al; Vasculitis Clinical Research Consortium. Arterial lesions in giant cell arteritis: a longitudinal study. *Semin Arthritis Rheum* 2019;48(4):707–713.
50. Bosch P, Bond M, Dejaco C, et al. Imaging in diagnosis, monitoring and outcome prediction of large vessel vasculitis: a systematic literature review and meta-analysis informing the 2023 update of the EULAR recommendations. *RMD Open* 2023;9(3):9.
51. Reichenbach S, Adler S, Bonel H, et al. Magnetic resonance angiography in giant cell arteritis: results of a randomized controlled trial of tocilizumab in giant cell arteritis. *Rheumatology (Oxford)* 2018;57(6):982–986.
52. Hellmich B, Agueda A, Monti S, et al. 2018 update of the EULAR recommendations for the management of large vessel vasculitis. *Ann Rheum Dis* 2020;79(1):19–30.
53. Unizony SH, Bao M, Han J, et al. Treatment failure in giant cell arteritis. *Ann Rheum Dis* 2021;80(11):1467–1474.
54. Hocevar A, Rotar Z, Jese R, et al. Do early diagnosis and glucocorticoid treatment decrease the risk of permanent visual loss and early relapses in giant cell arteritis: a prospective longitudinal study. *Medicine (Baltimore)* 2016;95(14):e3210.
55. García-Martínez A, Arguis P, Prieto-González S, et al. Prospective long term follow-up of a cohort of patients with giant cell arteritis screened for aortic structural damage (aneurysm or dilatation). *Ann Rheum Dis* 2014;73(10):1826–1832.
56. Mensch N, Hemmig AK, Aschwanden M, et al. Rapid glucocorticoid tapering regimen in patients with giant cell arteritis: a single centre cohort study. *RMD Open* 2023;9(3):9.
57. Quick V, Abusalameh M, Ahmed S, et al. Relapse after cessation of weekly tocilizumab for giant cell arteritis: a multicentre service evaluation in England. *Rheumatology (Oxford)* Published online November 11, 2023. <https://doi.org/10.1093/rheumatology/kead604>
58. Calderón-Goercke M, Castañeda S, Aldasoro V, et al; Tocilizumab in Giant Cell Arteritis Spanish Collaborative Group. Tocilizumab in refractory giant cell arteritis. Monotherapy versus combined therapy with conventional immunosuppressive drugs. Observational multicenter study of 134 patients. *Semin Arthritis Rheum* 2021;51(2):387–394.
59. Blockmans D, Penn SK, Setty A, et al. Efficacy and safety of upadacitinib in patients with giant cell arteritis (SELECT-GCA): a double-blind, randomized controlled phase 3 trial [abstract]. *Ann Rheum Dis* 2024;83:232–233.
60. Unizony S, Matza MA, Jarvie A, et al. Treatment for giant cell arteritis with 8 weeks of prednisone in combination with tocilizumab: a single-arm, open-label, proof-of-concept study. *Lancet Rheumatol* 2023;5(12):e736–e742.
61. Scolnik M, Brance ML, Fernández-Ávila DG, et al; Pan American League of Associations for Rheumatology (PANLAR). Pan American League of Associations for Rheumatology guidelines for the treatment of giant cell arteritis. *Lancet Rheumatol* 2022;4(12):e864–e872.
62. Les I, Pijoán JI, Rodríguez-Álvarez R, et al. Effectiveness and safety of medium-dose prednisone in giant cell arteritis: a retrospective cohort study of 103 patients. *Clin Exp Rheumatol* 2015;33(2 Suppl 89):S-90–S-97.
63. Felten L, Leuchten N, Aringer M. Glucocorticoid dosing and relapses in giant cell arteritis—a single centre cohort study. *Rheumatology (Oxford)* 2022;61(5):1997–2005.
64. Villiger PM, Adler S, Kuchen S, et al. Tocilizumab for induction and maintenance of remission in giant cell arteritis: a phase 2, randomised, double-blind, placebo-controlled trial. *Lancet* 2016;387(10031):1921–1927.
65. Stone JH, Spotswood H, Unizony SH, et al. New-onset versus relapsing giant cell arteritis treated with tocilizumab: 3-year results from a randomized controlled trial and extension. *Rheumatology (Oxford)* 2022;61(7):2915–2922.
66. Muratore F, Marvisi C, Cassone G, et al. Treatment of giant cell arteritis with ultra-short glucocorticoids and tocilizumab: the role of imaging in a prospective observational study. *Rheumatology (Oxford)* 2024;63(1):64–71.
67. Quinn KA, Dashora H, Novakovich E, et al. Use of 18F-fluorodeoxyglucose positron emission tomography to monitor tocilizumab effect on vascular inflammation in giant cell arteritis. *Rheumatology (Oxford)* 2021;60(9):4384–4389.
68. Prieto Peña D, Martínez-Rodríguez I, Atienza-Mateo B, et al. Evidence for uncoupling of clinical and 18-FDG activity of PET/CT scan improvement in tocilizumab-treated patients with large-vessel giant cell arteritis. *Clin Exp Rheumatol* 2021;39(2 Suppl 129):69–75.
69. Sebastian A, Kayani A, Prieto-Pena D, et al. Efficacy and safety of tocilizumab in giant cell arteritis: a single centre NHS experience using imaging (ultrasound and PET-CT) as a diagnostic and monitoring tool. *RMD Open* 2020;6(3):6.
70. Martín-Gutiérrez A, Loricera J, Narváez J, et al; Tocilizumab in Giant Cell Arteritis Spanish Collaborative Group. Effectiveness of tocilizumab in aortitis and aneurysms associated with giant cell arteritis. *Eur J Intern Med* 2024;129:78–86.
71. Schönau V, Roth J, Tascilar K, et al. Resolution of vascular inflammation in patients with new-onset giant cell arteritis: data from the RIGA study. *Rheumatology (Oxford)* 2021;60(8):3851–3861.
72. Stone JH, Han J, Aringer M, et al; GiACTA investigators. Long-term effect of tocilizumab in patients with giant cell arteritis: open-label extension phase of the Giant Cell Arteritis Actemra (GiACTA) trial. *Lancet Rheumatol* 2021;3(5):e328–e336.
73. Jover JA, Hernández-García C, Morado IC, et al. Combined treatment of giant-cell arteritis with methotrexate and prednisone. a randomized, double-blind, placebo-controlled trial. *Ann Intern Med* 2001;134(2):106–114.
74. Spiera RF, Mitnick HJ, Kupersmith M, et al. A prospective, double-blind, randomized, placebo controlled trial of methotrexate in the treatment of giant cell arteritis (GCA). *Clin Exp Rheumatol* 2001;19(5):495–501.
75. Hoffman GS, Cid MC, Hellmann DB, et al; International Network for the Study of Systemic Vasculitides. A multicenter, randomized, double-blind, placebo-controlled trial of adjuvant methotrexate treatment for giant cell arteritis. *Arthritis Rheum* 2002;46(5):1309–1318.
76. Mahr AD, Jover JA, Spiera RF, et al. Adjunctive methotrexate for treatment of giant cell arteritis: an individual patient data meta-analysis. *Arthritis Rheum* 2007;56(8):2789–2797.
77. Koster MJ, Yeruva K, Crowson CS, et al. Efficacy of methotrexate in real-world management of giant cell arteritis: a case-control study. *J Rheumatol* 2019;46(5):501–508.
78. Das S, Goswami RP, Sinha D, et al. Efficacy of leflunomide as a steroid-sparing agent in treatment of Indian giant cell arteritis patients: a 2-year follow-up study. *Int J Rheum Dis* 2022;25(6):650–658.
79. Kramarič J, Rotar Ž, Tomšič M, et al. Performance of leflunomide as a steroid-sparing agent in giant cell arteritis: a single-center, open-label study. *Front Med (Lausanne)* 2022;9:1069013.
80. Stone JH, Han J, Mohan S. Efficacy of adjunctive methotrexate in patients with giant cell arteritis treated with tocilizumab plus prednisone tapering: subanalysis of a phase 3 trial [abstract]. *Arthritis Rheumatol* 2020;72(Suppl 10). <https://acrabstracts.org/abstract/efficacy-of-adjunctive-methotrexate-in-patients-with-giant-cell-arteritis->

- [treated-with-tocilizumab-plus-prednisone-tapering-subanalysis-of-a-phase-3-trial/](#)
81. Mohan S, Han J, Stone JH. Efficacy of adjunctive methotrexate in patients with giant cell arteritis treated with tocilizumab plus prednisone tapering: subanalysis of the GiACTA trial [abstract]. *Ann Rheum Dis* 2020;79(Suppl 1):693.
 82. Langford CA, Cuthbertson D, Ytterberg SR, et al; Vasculitis Clinical Research Consortium. A randomized, double-blind trial of abatacept (CTLA-4lg) for the treatment of giant cell arteritis. *Arthritis Rheumatol* 2017;69(4):837–845.
 83. Venhoff N, Schmidt WA, Bergner R, et al. Safety and efficacy of secukinumab in patients with giant cell arteritis (TiTAIn): a randomised, double-blind, placebo-controlled, phase 2 trial. *Lancet Rheumatol* 2023;5(6):e341–e350.
 84. Koster MJ, Crowson CS, Giblon RE, et al. Baricitinib for relapsing giant cell arteritis: a prospective open-label 52-week pilot study. *Ann Rheum Dis* 2022;81(6):861–867.
 85. Loricera J, Tofade T, Prieto-Peña D, et al. Effectiveness of Janus kinase inhibitors in relapsing giant cell arteritis in real-world clinical practice and review of the literature. *Arthritis Res Ther* 2024; 26(1):116.
 86. Matza MA, Fernandes AD, Stone JH, et al. Ustekinumab for the treatment of giant cell arteritis. *Arthritis Care Res (Hoboken)* 2021; 73(6):893–897.
 87. Conway R, O'Neill L, Gallagher P, et al. Ustekinumab for refractory giant cell arteritis: a prospective 52-week trial. *Semin Arthritis Rheum* 2018;48(3):523–528.
 88. Cid MC, Unizony SH, Blockmans D, et al; KPL-301-C001 Investigators. Efficacy and safety of mavrilimumab in giant cell arteritis: a phase 2, randomised, double-blind, placebo-controlled trial. *Ann Rheum Dis* 2022;81(5):653–661.
 89. Paskins Z, Whittle R, Sultan AA, et al. Risk of fracture among patients with polymyalgia rheumatica and giant cell arteritis: a population-based study. *BMC Med* 2018;16(1):4.
 90. Humphrey MB, Russell L, Danila MI, et al. 2022 American College of Rheumatology guideline for the prevention and treatment of glucocorticoid-induced osteoporosis. *Arthritis Rheumatol* 2023; 75(12):2088–2102.
 91. Tedeschi SK, Jin Y, Vine S, et al. Giant cell arteritis treatment patterns and rates of serious infections. *Clin Exp Rheumatol* 2022; 40(4):826–833.
 92. Bass AR, Chakravarty E, Akl EA, et al. 2022 American College of Rheumatology guideline for vaccinations in patients with rheumatic and musculoskeletal diseases. *Arthritis Care Res (Hoboken)* 2023; 75(3):449–464.
 93. Kermani TA, Ytterberg SR, Warrington KJ. *Pneumocystis jiroveci* pneumonia in giant cell arteritis: a case series. *Arthritis Care Res (Hoboken)* 2011;63(5):761–765.
 94. Quinn KA, Ahlman MA, Alessi HD, et al. Association of 18 F-fluorodeoxyglucose-positron emission tomography activity with angiographic progression of disease in large vessel vasculitis. *Arthritis Rheumatol* 2023;75(1):98–107.
 95. Hunder GG, Sheps SG, Allen GL, et al. Daily and alternate-day corticosteroid regimens in treatment of giant cell arteritis: comparison in a prospective study. *Ann Intern Med* 1975;82(5):613–618.
 96. Kyle V, Hazleman BL. Treatment of polymyalgia rheumatica and giant cell arteritis. I. Steroid regimens in the first two months. *Ann Rheum Dis* 1989;48(8):658–661.
 97. Chevalet P, Barrier JH, Pottier P, et al. A randomized, multicenter, controlled trial using intravenous pulses of methylprednisolone in the initial treatment of simple forms of giant cell arteritis: a one year followup study of 164 patients. *J Rheumatol* 2000;27(6): 1484–1491.
 98. Mazlumzadeh M, Hunder GG, Easley KA, et al. Treatment of giant cell arteritis using induction therapy with high-dose glucocorticoids: a double-blind, placebo-controlled, randomized prospective clinical trial. *Arthritis Rheum* 2006;54(10):3310–3318.
 99. Trives-Folguera L, Molina-Collada J, López K, et al. Oral or pulse glucocorticoid use at the onset of giant cell arteritis and its influence on the risk of relapse: a retrospective study. *Rheumatol Int* 2023;43(7): 1333–1340.
 100. Hayreh SS, Zimmerman B, Kardon RH. Visual improvement with corticosteroid therapy in giant cell arteritis. Report of a large study and review of literature. *Acta Ophthalmol Scand* 2002;80(4): 355–367.
 101. Chan CC, Paine M, O'Day J. Steroid management in giant cell arteritis. *Br J Ophthalmol* 2001;85(9):1061–1064.
 102. Venhoff N, Schmidt WA, Lamprecht P, et al. Efficacy and safety of secukinumab in patients with giant cell arteritis: study protocol for a randomized, parallel group, double-blind, placebo-controlled phase II trial. *Trials* 2021;22(1):543.

Endogenous Retroelement Activation is Implicated in Interferon- α Production and Anti-Cyclic Citrullinated Peptide Autoantibody Generation in Early Rheumatoid Arthritis

Faye A. H. Cooles,¹  Gemma Vidal Pedrola,¹ Najib Naamane,¹ Arthur G. Pratt,²  Ben Barron-Millar,¹ Amy E. Anderson,¹  Catharien M. U. Hilken,¹ John Casement,¹ Vincent Bondet,³ Darragh Duffy,³ Fan Zhang,⁴ Ruchi Shukla,⁵ and John D. Isaacs²

Objective. Endogenous retroelements (EREs) stimulate type 1 interferon (IFN-I) production but have not been explored as potential interferonogenic triggers in rheumatoid arthritis (RA). We investigated ERE expression in early RA (eRA), a period in which IFN-I levels are increased.

Methods. ERE expression (long terminal repeat [LTR] 5, long interspersed nuclear element 1 [LINE-1], and short interspersed nuclear element [SINE]) in disease-modifying treatment-naïve eRA whole-blood and bulk synovial tissue samples was examined by reverse transcription–polymerase chain reaction and NanoString alongside IFN- α activity. Circulating lymphocyte subsets, including B cell subsets, from patients with eRA and early psoriatic arthritis (ePsA) were flow cytometrically sorted and similarly examined. Existing established RA and osteoarthritis (OA) synovial single-cell sequencing data were reinterrogated to identify repeat elements, and associations were explored.

Results. There was significant coexpression of all ERE classes and *IFNA* in eRA synovial tissue samples ($n = 22$, $P < 0.0001$) and significant positive associations between whole-blood LINE-1 expression ($n = 56$) and circulating IFN- α protein ($P = 0.018$) and anti-cyclic citrullinated peptide (anti-CCP) titers ($P < 0.0001$). ERE expression was highest in circulating eRA B cells, particularly naïve B cells compared with ePsA, with possible ERE regulation by SAM and HD Domain Containing Deoxynucleoside Triphosphate Triphosphohydrolase 1 transcription (SAMDH1) implicated and associations with *IFNA* again observed. Finally, in established RA synovium, LTRs, particularly human endogenous retroviral sequence K (HERVK), were most increased in RA compared with OA, in which, for all synovial subsets (monocytes, B cells, T cells, and fibroblasts), ERE expression associated with increased IFN-I signaling ($P < 0.001$).

Conclusion. Peripheral blood and synovial ERE expression is examined for the first time in eRA, highlighting both a potential causal relationship between ERE and IFN-I production and an intriguing association with anti-CCP autoantibodies. This suggests EREs may contribute to RA pathophysiology with implications for future novel therapeutic strategies.

The views expressed herein are those of the authors and not necessarily represent those of the National Health Service, the NIHR, or the Department of Health.

Supported by The Medical Research Council, Academy of Medical Sciences, JGW Patterson Foundation, and British Society of Rheumatology. Experimental work at Newcastle University was additionally supported by the Medical Research Council in collaboration with GlaxoSmithKline (grant MR/S50239X/1). Newcastle researchers received infrastructural support via the NIHR Newcastle Biomedical Research Centre (BRC), a partnership between Newcastle Hospitals NHS Foundation Trust and Newcastle University, funded by the National Institute for Health and Care Research (NIHR), and the Research into Inflammatory Arthritis Centre Versus Arthritis (grant 22072).

¹Faye A. H. Cooles, MBChB (Hons), PhD, Gemma Vidal Pedrola, PhD, Najib Naamane, MA, Ben Barron-Millar, PhD, Amy E. Anderson PhD, Catharien M. U. Hilken, PhD, John Casement, PhD: Newcastle University, Newcastle

upon Tyne, United Kingdom; ²Arthur G. Pratt, MBChB, PhD, John D. Isaacs, MBBS, PhD: Newcastle University and Newcastle Hospitals NHS Foundation Trust, Newcastle upon Tyne, United Kingdom; ³Vincent Bondet, PhD, Darragh Duffy, PhD: Institut Pasteur, Université Paris Cité, Paris, France; ⁴Fan Zhang, PhD: Harvard Medical School, Boston, Massachusetts; ⁵Ruchi Shukla, PhD: Newcastle University and Northumbria University, Newcastle upon Tyne, United Kingdom.

Additional supplementary information cited in this article can be found online in the Supporting Information section (<https://acrjournals.onlinelibrary.wiley.com/doi/10.1002/art.43083>).

Author disclosures are available at <https://onlinelibrary.wiley.com/doi/10.1002/art.43083>.

Address correspondence via email to Faye A. H. Cooles, MBChB (Hons), PhD, at faye.cooles@ncl.ac.uk.

Submitted for publication May 14, 2024; accepted in revised form November 25, 2024.

INTRODUCTION

Type 1 interferons (IFN-I) have pleiotropic effects on the immune system and prime cellular responses to effectively clear, typically viral, infection.¹ In this context, widespread cellular activation is desirable, but in the absence of infection, IFN-I-associated increased cellular priming or activation can be inappropriate.² Excess IFN- α can promote a breach of tolerance in autoantibody producing B cells as well as facilitate more effective presentation of antigen, potentially of self-components.³ We have previously demonstrated increased IFN-I signaling and serum IFN- α levels in early rheumatoid arthritis (eRA) with negative prognostic implications on initial disease control and clinical outcomes.^{4,5} An elevated interferon gene signature (IGS) also increases the likelihood of progression to RA in at risk populations, such as those with anti-cyclic citrullinated peptide (anti-CCP)-positive arthralgia.^{6,7} However, it remains unknown what drives this IFN-I release in eRA.

Endogenous retrotransposons or retroelements (EREs) are sequences of DNA derived from ancient transposable elements, such as retroviruses, that have been historically incorporated into the genome.⁸ Although the majority are inactive, some have retained transcriptional activity, and their replication cycle and organization is similar to exogenous retroviruses, such as HIV.⁸ EREs as a group can be subdivided into endogenous retroviruses (ERVs), often detected as long terminal repeats (LTRs), long interspersed nuclear element 1 (LINE-1), and short interspersed nuclear elements (SINEs), most commonly “Alu.” Some EREs, such as ERVs, can replicate, generating a strand of messenger RNA (mRNA) and, subsequently, a double-stranded RNA product, which then inserts into a unique region of the genome, often separate from the area of origin; depending on the site of insertion, this potentially disrupts protein coding regions.^{8,9} This process of active retrotransposition results in the accumulation of cytosolic DNA, which triggers an interferon regulatory factor 3 (IRF3)-dependent innate immune response, including the release of IFN-I.^{10–12} Indeed, single mutations in human genes that regulate retroelement replication, such as *TREX1* or *SAMHD1*, cause type 1 interferonopathies such as Aicardi-Goutières syndrome (AGS).¹³

The potential for an association between EREs and IFN-I production in autoimmunity is increasingly appreciated.^{10–14} In diseases in which IFN-I are known to play a pathogenic role, such as systemic lupus erythematosus or primary Sjögren's disease, there is evidence of increased LINE-1 activity in disease relevant tissue associated with increased local IFN- α production.¹⁴ Although established RA synovium was shown to overexpress LINE-1 nearly two decades ago,¹⁵ interferon response gene profiles within the IGS vary between autoimmune diseases, potentially implicating disparate interferonogenic triggers.¹⁶ This highlights the need to examine for any association between EREs and IFN-I in RA specifically. Furthermore, some ERVs retain their

ability to produce viral protein, and ERV viral protein products have been detected in the peripheral circulation of patients with RA and linked to autoantibody generation.^{17–20}

To date, EREs have not been examined in RA in relation to IFN-I production or in eRA, a period in which IFN-I signaling, and autoantibody generation, is important.^{4,5} We therefore explored ERE expression in whole-blood, circulating lymphocyte subsets and synovial tissue samples from treatment-naïve patients with eRA and hypothesized a potential association between ERE activity and (1) IFN-I generation and/or (2) autoantibody generation.

METHODS

Patient cohorts. Glucocorticoid and disease-modifying antirheumatic drug-naïve patients attending Newcastle upon Tyne Hospitals were enrolled for this study from the Northeast Early Arthritis Cohort at the point of diagnosis of either RA (with reference to 2010 American College of Rheumatology/EULAR RA classification criteria; patients with eRA) or psoriatic arthritis (early psoriatic arthritis [ePsA]), which constituted a non-RA early inflammatory arthritis control group with the same disease duration.²¹ Contemporaneous clinical parameters were recorded, including disease activity scores (Disease Activity Score-28 using the erythrocyte sedimentation rate [ESR]), Igs (IgG, IgA, and IgM), markers of inflammation (C reactive protein [CRP] and ESR), and serological status, (rheumatoid factor [RF] and anti-CCP titers).

IGS and serum cytokines. Serum samples were spun and frozen within four hours of blood draw, undergoing no more than one freeze-thaw cycle before measurement of IFN γ , interleukin 6 (IL-6), IL-12p70, tumor necrosis factor α (TNF α), IL-1 β , IL-2, IL-13, IL-4, and IL-10 by MSD technology (Meso Scale Discovery) as per manufacturers' instructions. Serum IFN α was measured using the digital Simoa platform as described.⁴ Serum IFN monoclonal antibodies (specific for all IFN α subtypes) were isolated from patients with autoimmune polyendocrinopathy-candidiasis-ectodermal dystrophy (APECED)²² and provided to author DD by ImmunoCore under a material transfer agreement (MTA). The IGS was generated from whole-blood RNA, as described previously, by the mean expression of five interferon response genes (IRGs) *MxA*, *IFI6*, *OAS1*, *ISG15*, and *IFI44L*.⁵

Flow cytometric cell sorting. For all samples, peripheral blood mononuclear cells (PBMCs) were isolated from whole blood using density centrifugation and underwent immediate flow cytometric sorting. Plasmacytoid dendritic cells (pDCs), conventional CD1c⁺ DCs, CD4⁺ T cells, CD8⁺ T cells, CD19⁺ B cells, and CD14⁺ monocytes were sorted as previously described,²³ and B cell subsets including naïve B cells (CD19⁺IgD⁺CD27⁻), memory B cells (CD19⁺IgD⁻CD27⁺), CD5⁺ B cells (CD19⁺CD5⁺), and age-associated B cells (ABCs) (CD19⁺CD11c⁺CD21⁻) were

flow cytometrically sorted from PBMCs from both patients with eRA and ePsA, as previously described.²⁴

Endogenous retroelement quantification. *Whole-blood and circulating lymphocytes.* Whole-blood RNA was isolated using the Tempus Spin Isolation Kit (Tempus, Thermo Fisher Scientific) and treated with TurboDNase (Ambion) to remove any contaminating genomic DNA (gDNA). The absence of gDNA was confirmed by *HBP1* polymerase chain reaction (PCR) and gel electrophoresis (Supplementary File 1). RNA was reverse-transcribed to complementary DNA (cDNA) using Superscript II (Thermo Fisher Scientific) and gene specific primers for LINE-1 (L1) and housekeeper TATA box binding protein (TBP) as previously described,²⁵ (Supplementary File 2). Reverse transcription PCR (RT-PCR) using SYBR Green Master Mix (Thermo Fisher Scientific) was performed using specific primers for L1-5' untranslated region (UTR) and *TBP* (Supplementary File 1). cDNA generation using L1-specific primers close to 3' end and quantitative PCR using primers targeting 5'UTR of L1 enhanced the detection of authentic full-length L1 transcriptions. Consensus sequences from across L1 subtypes were used in the primers to maximize relevant transcription identification. Subsequent expression was displayed as a ratio of a biologic control (HEK293T cell line ERE expression) to minimize any batch effects.

Sorted cell subsets were processed as previously described.^{23,24} In brief, the contemporaneous lymphocyte subsets had RNA isolated using Qiagen RNeasy Plus Micro Kits, which was then applied to a gDNA Eliminator spin column (both Qiagen) as per the manufacturer's instructions. For the B cell subsets, 15,000 cells were sorted into RF10 (RPMI 1640 culture medium containing 10% fetal calf serum; both Sigma-Aldrich). After sorting, the cells were pelleted and lysed in RNeasy Lysis Buffer (Qiagen). Either 50 ng of RNA or the lysate from 15,000 cells, respectively, was loaded onto a NanoString nCounter Human immunology V2 Panel chip (NanoString Technologies Inc), including customized probes against SINE Alu element AluYa5, LTR5, and LINE-1 5'UTR (L1-5'UTR) (Supplementary File 3), and run according to manufacturer's instructions. Again, consensus sequences from these three ERE families were used in the probes based on the authors' previous work,²⁵ extended to meet NanoString capture probe criteria.

Synovial tissue. Synovial biopsy specimens of wrist or knee joints were retrieved as described²⁶ using a 16-gauge Quick-Core Biopsy Needle (Cook Medical) or Temno Biopsy Needle (Carefusion/Becton Dickinson) from consenting individuals before the commencement of immunomodulatory therapy, including systemic glucocorticoids. Tissue was paraffin-embedded as previously described, approximately 24 hours after collection, into 10% neutral buffered formalin.²⁷ Total RNA was extracted from curls taken from formalin-fixed paraffin-embedded (FFPE) blocks using the RNeasy FFPE kit and quality-assessed by Qubit fluorometric

quantitation according to the manufacturers' instructions. Samples that passed quality control (25 ng) for transcriptional profiling employed the nCounter PanCancer Immune profiling codeset panel, modified to include the probes for EREs, as previously mentioned (Supplementary File 3).

In silico analysis of established RA and osteoarthritis synovial tissue single-cell sequencing data sets.

RepEnrich is a computational method that allows for the analysis of repetitive elements in any organism with a reference genome available that has repetitive element annotation.²⁸ This platform was applied to freely available established RA and osteoarthritis (OA) synovial tissue single-cell data (<https://immunogenomics.io/ampra>) from the Accelerating Medicines Partnership Rheumatoid Arthritis and Systemic Lupus Erythematosus Consortium.²⁸ Full analysis details are in Supplementary File 4, and cohort demographic data are available from the study by Zhang et al.²⁹ Comparison between synovial cell subsets was performed using the cellular clustering described in the study by Zhang et al.²⁹

Statistical analysis. GraphPad Prism (V.5.0; GraphPad Software) and R Core Team (2020) software were used. Univariate generalized linear models, Mann-Whitney U-tests, one-way analysis of variance (ANOVA) (with Tukey's post hoc analysis), and Wilcoxon-signed rank tests were performed, employing a significance threshold in which $\alpha = 5\%$. Lymphocyte and B cell subsets NanoString nCounter data analysis was performed in R (v4.2.1), as described previously.^{23,24} Synovium data were processed similarly, as outlined in Supplementary File 5.

Data availability statement and ethics statement.

The data are available for the purposes of academic research on reasonable request to the corresponding author. For the early disease data, all patients provided written, informed consent to participate in the study, which was approved by the Northeast – Newcastle and North Tyneside 2 Research Ethics Committee (12/NE/0251). For established RA and OA data, consent was obtained as previously outlined.²⁹

RESULTS

Patient cohorts. The whole-blood LINE-1 analysis cohort included 56 patients with eRA. Simultaneous B cell, T cell, DC, and monocyte cell-specific retroelement expression was obtained from eight patients with rheumatoid factor-positive and anti-CCP-positive (double seropositive) eRA. B cell subset expression was assessed between double-seropositive patients with eRA and ePsA ($n = 4$ each) matched for age and sex, with comparable levels of inflammation (CRP and ESR). The synovial tissue cohort comprised 22 patients with eRA. Full demographic and clinical data are shown for all the cohorts in Table 1.

Table 1. Demographic data of patients and controls*

Cohort	Whole blood eRA (n = 56)	Circulating lymphocyte subsets eRA (n = 8)	Circulating B cell subsets		Bulk synovial tissue eRA (n = 22)
			eRA (n = 4)	ePsA (n = 4)	
Age, median (range), yr	58 (30–87)	56 (49–64)	62 (63–78)	62 (60–80)	63 (41–78)
Sex ratio, M:F	1:1.8	3:1	1:1	1:1	1:1
Seropositive (either anti-CCP or RF), n (%)	43 (77)	8 (100)	4 (100)	0	14 (64)
CRP, median (range)	8 (4–114)	7 (4–56)	9 (4–127)	7 (4–167)	22 (4–62)
DAS-28-ESR, median (range)	4.3 (1.3–7.6)	3.71 (1.63–6.18)	4.47 (1.33–8.53)	n/a	4.74 (2.47–7)

* Anti-CCP, anti-citrullinated peptide; CRP, C-reactive protein; DAS-28-ESR, Disease Activity Score-28 using the erythrocyte sedimentation rate; ePsA, early psoriatic arthritis; eRA, early rheumatoid arthritis; F, female; M, male; n/a, not applicable; RF, rheumatoid factor.

eRA synovial and peripheral blood endogenous retroelement expression and IFN- α . In eRA whole-synovial tissue samples, hierarchical clustering of coexpression correlations of all available genes demonstrated clustering of *IFNA* and retroelements (Figure 1A). A heatmap of the correlations between genes within the ERE cluster is shown in Supplementary File 6. Pathway analysis (Kyoto Encyclopedia of Genes and Genomes [KEGG] pathway database) of the ERE cluster implicated enrichment of JAK-STAT signaling ($P = 0.004$), primarily due to the association with IFN-I, an enrichment also seen in gene ontology (GO) terms ($P = 2.71 \times 10^{-6}$) (Supplementary File 6). *IFNA* transcripts (*IFNA1*, *IFNA2*, *IFNA7*, *IFNA8*, and *IFNA17*) significantly positively associated with all classes of ERE (Figure 1B) but was strongest for LTR5: *IFNA17*, $R = 0.91$, Pearson correlation coefficient, Benjamini Hochberg False Discovery Rate (BH) adjusted $P = 4.68 \times 10^{-9}$. A similar significant association between ERE activity and *IFNA* was reported in patients who were either anti-CCP positive ($n = 13$) or anti-CCP negative ($n = 22$), for example, LTR5 and *IFNA17* were $R = 0.92$ vs 0.88 , respectively.

There was no significant association with ERE expression and any other cytokine transcript including IFN γ , IL-6, IL-12 p70, TNF α , IL-1 β , IL-2, IL-13, IL-4 and IL-10 (data not shown). In eRA whole-blood samples, there was a significant positive association between LINE-1 transcript expression and circulating IFN- α protein, $P = 0.018$ (Figure 1C). This was not seen with any of the other circulating cytokines measured: IFN γ , IL-6, IL-12 p70, TNF α , IL-1 β , IL-2, IL-13, IL-4, and IL-10, $P > 0.05$ for all, data not shown. There was no significant association between the whole-blood IGS and LINE-1 transcription expression (Figure 1D), despite a positive trend ($P = 0.06$) between the IGS and circulating IFN- α (data not shown). Finally, whole-blood LINE-1 expression did not correlate with age or sex (Supplementary File 7).

eRA whole-blood LINE-1 expression and correlation with anti-CCPtiter. There was a significant positive association between anti-CCP titers (International Units [IU]) and LINE-1 (L1-5'UTR, linear regression, $P < 0.0001$, $R^2 = 0.38$), which was not seen for RF titers (Figure 2A and B). Expression did not appear to reflect global B cell function because there was no association between circulating Ig levels IgM, IgG, or IgA

and whole-blood LINE-1 (linear regression, $P > 0.4$ for all) (Figure 2C). Smoking is implicated in both anti-CCP generation and ERE activity^{30,31}; however, there was no significant difference in whole-blood LINE-1 expression between cohorts based on smoking status ($P > 0.05$, ANOVA) (Figure 2D). There was also no significant association between LINE-1 expression and disease activity (Disease Activity Score-28), or its components including, tender joint count (TJC), swollen joint count (SJC), visual analogue scale (VAS), CRP, and ESR (data not shown).

ERE expression in circulating eRA B cells, particularly naïve subsets, and associations with increased *IFNA* transcription. LTR5, LINE-1, and AluYa5 expression was compared between lymphocyte subsets (B cells, pDCs, CD1c⁺ DCs, CD14⁺ monocytes, CD8⁺, and CD4⁺ T cells) from eight patients with double-seropositive eRA. ERE expression was significantly increased in B cells compared with other lymphocyte subsets (Figure 3A). ERE activity in the B cell compartment was examined further comparing ABCs, naïve, memory and CD5⁺ B cells in eRA, with patients with ePsA as disease controls. There was a trend toward increased expression of ERE in patients with eRA in all subsets, which became highly significant for naïve B cells (Figure 3B).

When grouping together and pooling all the B cell subset transcriptomic data from our eRA cohort, ERE significantly associated with *IFNA* transcription (Figure 3C and D). Hierarchical clustering of coexpression correlations of all available genes further demonstrated clustering of *IFNA* and EREs (Supplementary File 8). Clusters were visually defined, and a heatmap of the correlations between the genes within the ERE cluster is shown in Supplementary File 9. Pathway analysis of this cluster in eRA alone demonstrated limited terms achieving significance; however, when examining pooled ePsA and eRA data, increased ERE expression was associated with enrichment of KEGG pathways relating to viral infection as well as phosphatidylinositol 3-kinase/protein kinase B (PI3K/Akt) signaling, and GO terms were enriched for lymphocyte activation involved in immune response ($P = 0.0005$) (Supplementary File 9).

Furthermore, in eRA, there was significantly increased *IFNA2* transcript in naïve and CD5 B cells compared with memory B

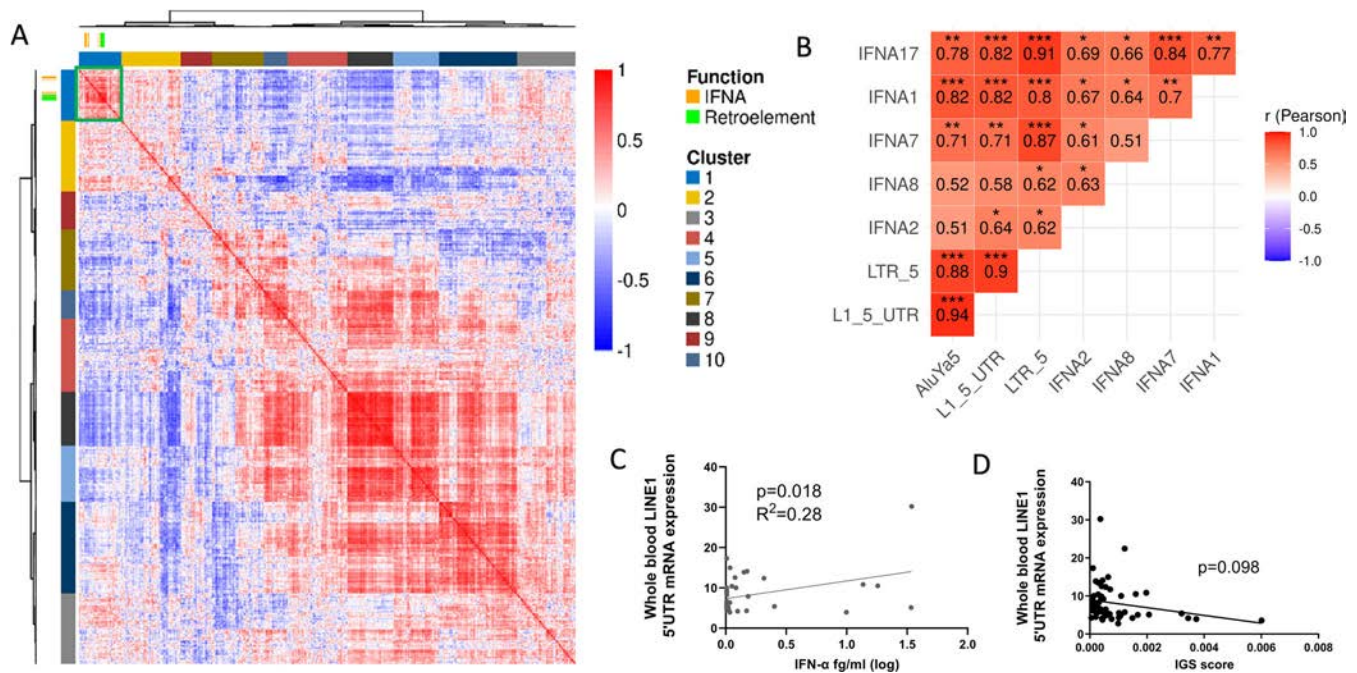


Figure 1. (A) Hierarchical clustering of early RA bulk synovial tissue gene expression correlations. Rows and columns depict genes, and the color bar represents the Pearson's coefficient (r) of their pairwise gene expression correlation. Dendrograms show hierarchical clustering of the genes by their expression correlation patterns. *IFNA* and EREs are highlighted by individual gene markers and the locations of their correlations by the green box. (B) Heatmap of correlation profiles between early RA bulk synovial *IFN* transcription and ERE classes. Significant (Benjamini Hochberg False Discovery Rate adjusted P value < 0.05) correlations are highlighted, $*P < 0.05$, $**P < 0.01$, $***P < 0.001$. (C) Whole-blood L1–5'UTR expression was analyzed in patients with early RA and shown in arbitrary units in relation to expression in HEK293T. Linear regression of early RA whole blood (L1–5'UTR) and circulating IFN- α protein level, $n = 42$, and (D) whole-blood IGS, $n = 56$, is shown. AluYa5, Alu element Ya5; ERE, endogenous retroelement; IFN, interferon; IGS, interferon gene signature; L1–5'UTR; LINE-1 5'UTR; LINE-1, long interspersed nuclear element 1; LTR, long terminal repeat; mRNA, messenger RNA; RA, rheumatoid arthritis; UTR, untranslated region.

cells, a pattern not seen in ePsA (Figure 3E), and, when comparing directly between eRA and ePsA, there was a trend toward higher expression of *IFNA2* in eRA-naïve B cells than in ePsA-naïve B cells, although this was not significant (Supplementary File 10). Finally, to explore potential signaling pathways, we examined associations between EREs and key innate immune sensors, retinoic acid-inducible gene I (RIG-I), melanoma differentiation-associated protein 5 (MDA5), Toll-like receptor 7 (TLR7), cyclic GMP-AMP synthase (cGAS), and TLR9 in the pooled lymphocyte subsets. A significant positive association was only seen between RIG-I and LTR5 ($R^2 = 0.64$, $P < 0.05$) (Supplementary File 11).

SAMHD1 is implicated in eRA peripheral blood B cell retroelement replication. We examined expression of key enzymes involved in ERE activation in circulating B cells. SAM and HD Domain Containing Deoxynucleoside Triphosphate Triphosphohydrolase 1 (SAMHD1) transcript, an enzyme limiting retroelement replication,³² was significantly reduced in eRA B cells when compared with all other circulating lymphocytes ($P < 0.001$) (Figure 4A). Furthermore, eRA expression of SAMHD1 inversely correlated with ERE transcript expression examined

across all lymphocyte subsets (Figure 4B and Supplementary File 12). SAMHD1 expression was significantly reduced ($P < 0.01$) in eRA-naïve B cells compared to ABCs, and a trend was noted for reduced expression compared with memory and CD5⁺ B cells. This pattern was not seen in ePsA controls (Figure 4C). Finally, SAMHD1 was uniquely and significantly reduced in eRA-naïve B cells ($P < 0.005$) compared with ePsA-naïve B cells (Figure 4D). Ribonuclease H degrades RNA in RNA/DNA hybrids and expression of one of its key components, Ribonuclease H2 subunit A (RNASEH2A), was similar across all lymphocyte subsets and did not correlate with ERE expression. Conversely, three prime repair exonuclease 1 (TREX1), another key enzyme negatively regulating ERE expression, varied by cell subset, with the lowest expression being in T cells. There was an inverse association between TREX1 and ERE expression in eRA pooled lymphocytes, but expression in B cell subsets between eRA and ePsA cohorts was comparable (all in Supplementary File 13). Bulk synovial expression of ERE in the patients with eRA did not associate with *SAMHD1*, *TREX1*, or *RNASEH2* and, in neither circulating eRA lymphocyte subsets nor synovial tissue did *DNMT1*, *DNMT3A*, or *DNMT3B* (DNA methyltransferase enzymes,

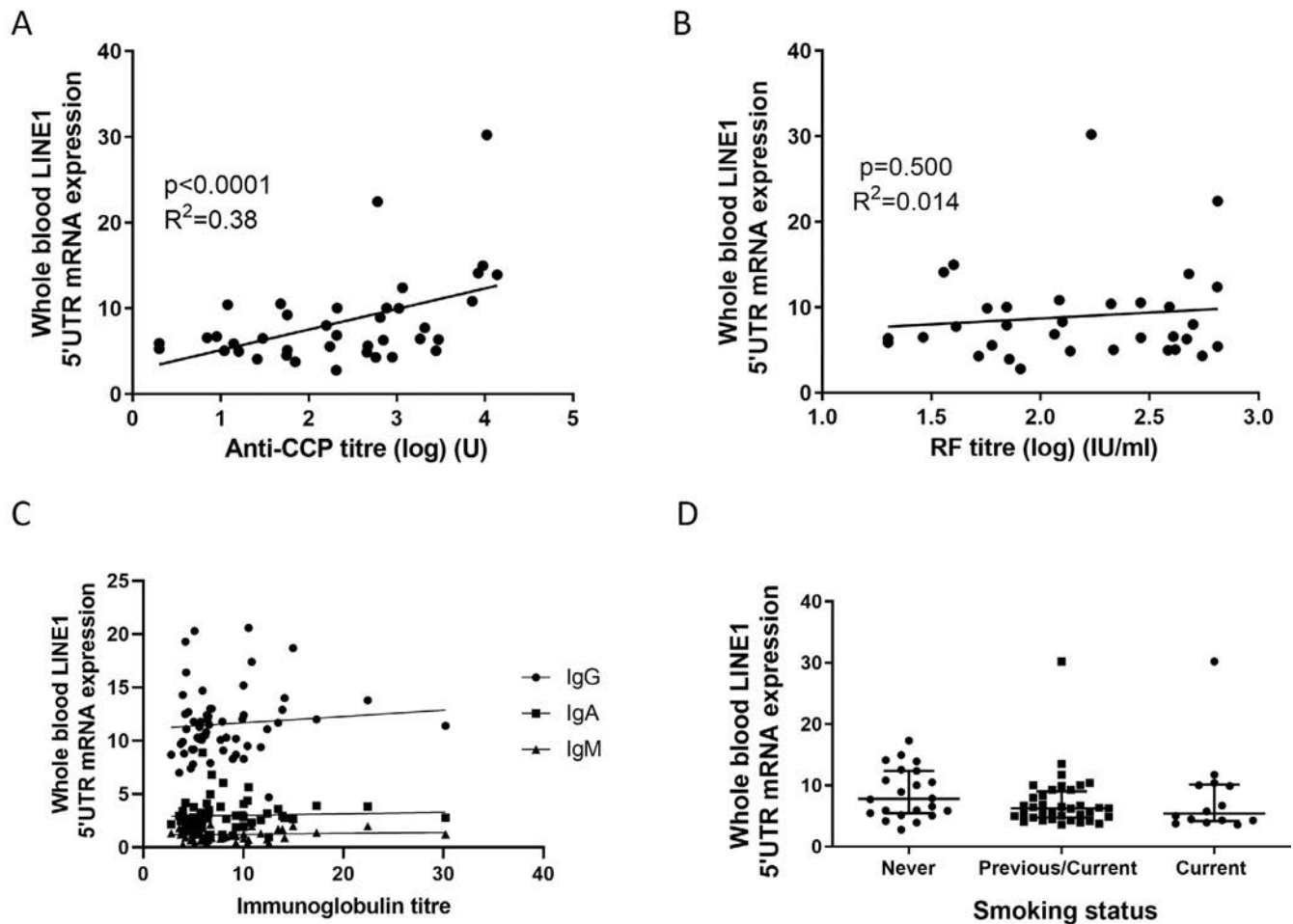


Figure 2. Whole-blood L1–5'UTR expression was analyzed in patients with early RA ($n = 56$) and is shown in arbitrary units in relation to expression in HEK293T cells. (A and B) Linear regression between patients with early RA ($n = 39$) anti-CCP titres or RF titres ($n = 34$) and whole-blood L1–5'UTR expression. (C) Linear regression between L1–5'UTR expression and circulating IgG (IgA, IgM, and IgG) in patients with early RA ($n = 56$), $P > 0.05$ for all. (D) Comparison of L1–5'UTR expression between patients with early RA based on smoking status: never, previous/current, and current. Anti-CCP, anti-cyclic citrullinated peptide; L1–5'UTR; LINE-1 5'UTR; LINE-1, long interspersed nuclear element 1; mRNA, messenger RNA; RA, rheumatoid arthritis; RF, rheumatoid factor.

important in the epigenetic regulation of EREs) associate with ERE expression.

ERE in RA synovial cell subsets and IFN-I signaling.

Given differences in ERE expression observed in peripheral blood subsets, but strong correlation profiles between eRA bulk synovial IFN transcription and ERE classes (Figure 1), we wished to examine synovial tissue in more detail. Synovial single-cell transcriptomic data from patients with established RA and OA was grouped into B cells, fibroblasts, monocytes, and T cells as previously described²⁹ and reinterrogated for repeat element expression. This generated multiple individual ERE expression counts that could be grouped into classes, such as LTR. Examination of these individual ERE expression counts, when grouped into classes, demonstrated that in all RA synovial cell subsets, at a single-cell level, LTR was proportionally the most highly

expressed class (Figure 5A). Individual ERE expression counts were compared between OA and RA, and the proportion of all individual ERE expression counts within each class that were comparatively either reduced or increased in RA for each cell subset were demonstrated (Figure 5B and Supplementary File 14). In RA, the majority of ERE expression counts within the LTR class were increased for all synovial cellular subsets, whereas counts in the LINE and SINE classes were predominantly decreased. Individual ERE fold changes are shown in Supplementary Data S1.

Given that the LTRs were most widely increased in RA, we examined this class in more detail. LTRs consist of ERV families—ERV1, ERVK, ERVL, and)(ERVL—mammalian-apparent LTR retrotransposons [MaLR])—and individual ERE counts within these family clusters were compared between RA and OA. Individual ERE expression counts increased in RA B cells were compared with OA B cells for each ERV family and is shown

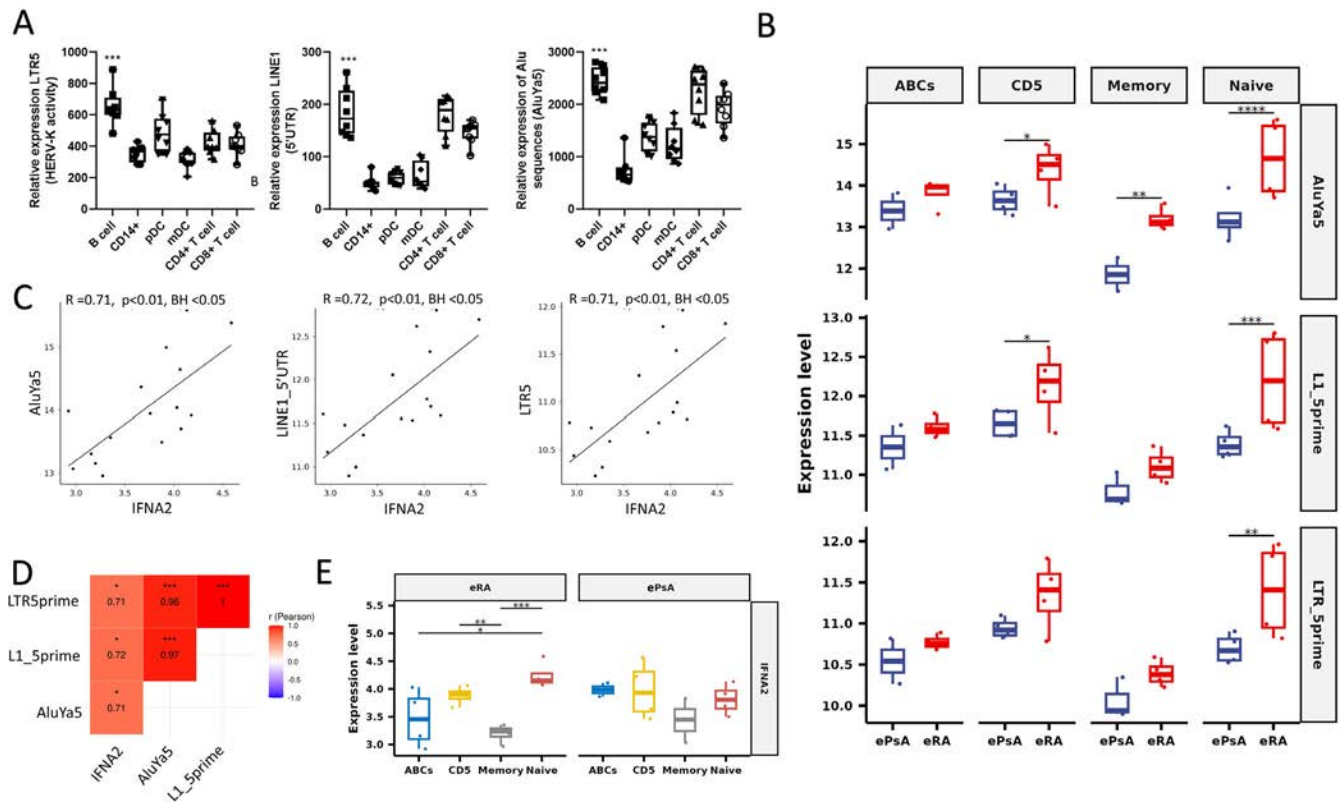


Figure 3. (A) Circulating lymphocyte (CD19⁺ B cells, CD14, pDCs, conventional mDCs, CD4, and CD8) retroelement (endogenous retroelements) expression (LTR5, LINE-1 [L1-5'UTR], AluYa5) in eRA (n = 8). Data are presented as box and whisker plots, in which the horizontal line represent the median value, the box represents upper and lower quartiles, and the whiskers represent ranges. Kruskal-Wallis test, BH adjusted. (B) Expression of all retroelement classes in B cell subsets, age ABCs (CD19⁺CD11c⁺CD21⁺), CD5⁺ B cells (CD19⁺CD5⁺), memory B cells (CD19⁺IgD⁺CD27⁺), and naïve B cells (CD19⁺IgD⁺CD27⁺) from patients with eRA and early disease controls (ePsA), Wald test. (C) Pearson correlation coefficient of *IFNA2* and SINE (AluYa5), LINE-1 (L1_5prime), and LTR5 (LTR_5prime) expression from eRA cells, $P < 0.01$, BH adjusted. (D) Heatmap of correlation profiles between *IFN* transcription and retroelement classes in pooled eRA B cell subsets. Significant (BH adjusted P value < 0.05) correlations are highlighted. (E) Comparison of *IFNA2* expression across B cell subsets in eRA and ePsA, paired t tests. * $P < 0.05$, ** $P < 0.01$, *** $P < 0.001$. ABC, associated B cell; AluYa5, Alu element Ya5; BH, Benjamini Hochberg False Discovery Rate; CD4, CD4⁺ T cells; CD14, CD14⁺ monocyte; ePsA, early psoriatic arthritis; eRA, early rheumatoid arthritis; IFN, interferon; L1-5'UTR; LINE-1, long interspersed nuclear element 1; LTR, long terminal repeat; mDC, conventional CD1c⁺ DC; mRNA, messenger RNA; pDC, plasmacytoid dendritic cell; SINE, short interspersed nuclear element; UTR, untranslated region.

in Figure 5C. When comparing the comparative increased counts (Log2Fold) in RA versus OA among the ERV families, overall expression was greatest in the ERVK family (Kruskal-Wallis test, BH adjusted $P < 0.0006$) (Figure 5C).

For all ERV families, hierarchical clustering of correlations between gene expression and ERE expression counts was performed. In all cell subsets, there was a positive correlation between IFN-I response genes (*IFI44L*, *OAS1*, *IFI6*, *ISG15*, and *Mx1*) and LTR expression grouped by ERV family. All correlations met statistical significance with BH adjusted $P < 0.001$. Figure 5D depicts B cell correlations (see Supplementary File 15 for remaining synovial cell subsets). *IFNA* counts were too low for comparable analysis to be performed in all cellular subsets. Pathway analysis of the top 20 pathways correlating with LTR repeats across cell subsets demonstrated enrichment of viral response

(SARS-CoV-2), antigen processing pathways, and antimicrobial humoral response in B cells (Figure 5E).

DISCUSSION

We examined EREs for the first time in drug-naïve eRA and demonstrated that EREs are transcriptionally active in both whole-blood and synovial tissue samples, with variable expression across circulating lymphocyte subsets. Expression was the highest in B cells, particularly naïve B cells, which was not seen in ePsA. We demonstrate for the first time in RA that ERE activity in blood and synovial tissue associates with increased IFN- α at both the transcription and protein levels. We also saw a positive association between ERE and CCP titers, which was absent for

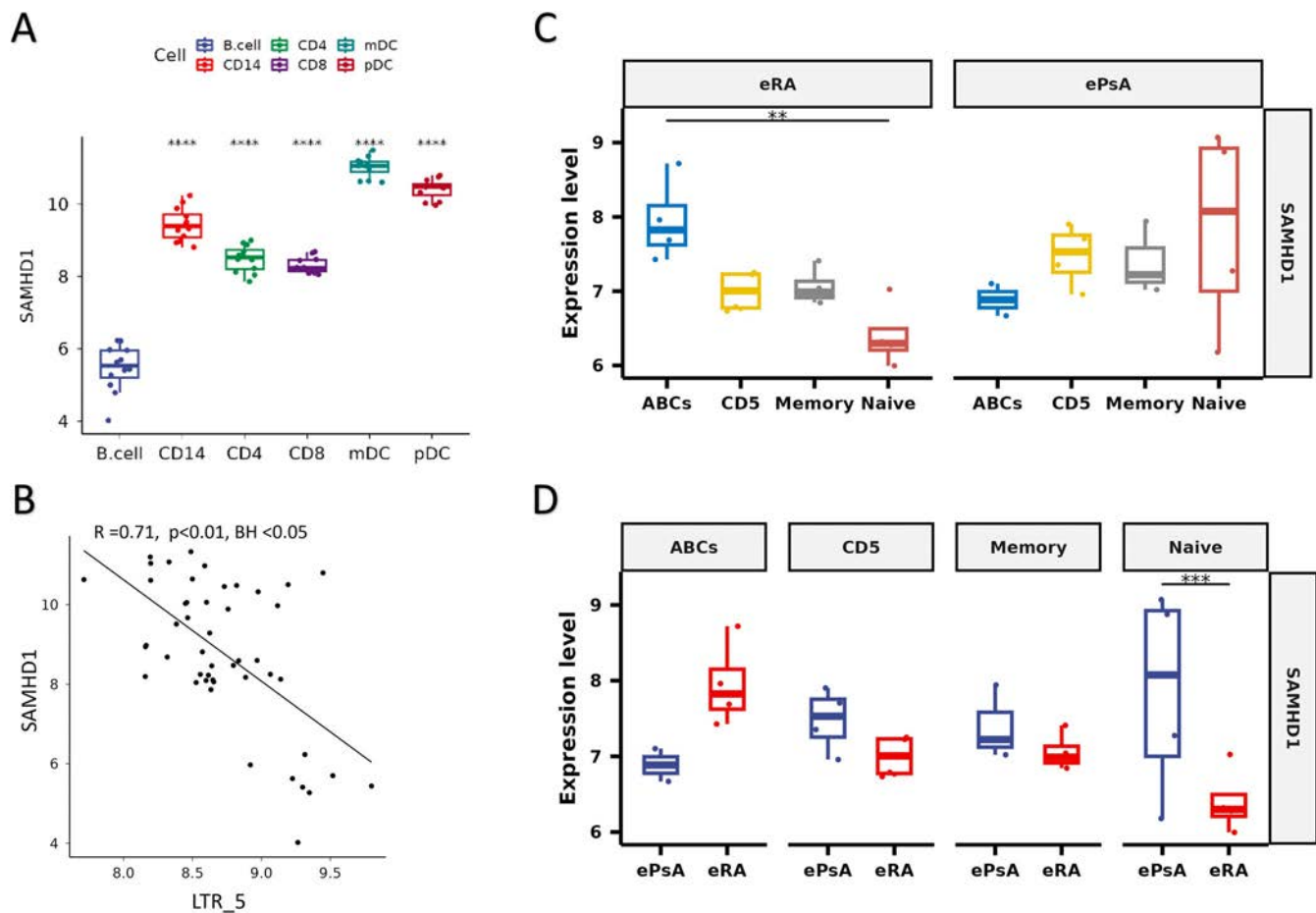


Figure 4. (A) Expression of *SAMHD1* as determined by Nanostring Technology in peripheral blood lymphocyte subsets (CD19⁺ B cells, CD14⁺ monocytes [CD14], CD4⁺ T-cells [CD4], CD8⁺ T-cells [CD8], conventional CD1c⁺ DCs [mDCs] and plasmacytoid dendritic cells [pDCs]) from patients with eRA (n = 8), with B cells used as a reference in pairwise paired t tests. (B) Pearson's correlation coefficient of *SAMHD1* and LTR5 in these same circulating lymphocytes grouped and pooled together, BH adjusted $P < 0.0001$. (C) *SAMHD1* expression, determined by Nanostring Technologies, was examined in age-associated B cells (ABCs, CD19⁺CD11c⁺CD21⁻), CD5⁺ B cells (CD19⁺CD5⁺), memory B cells (CD19⁺IgD⁻CD27⁻), and naïve B cells (CD19⁺IgD⁺CD27⁻) from patients with eRA and patients with ePsA. Differences in *SAMHD1* expression was examined within disease cohort and (D) between disease cohorts. Wald test with BH adjusted and raw P values are shown for 3C and 3D, respectively. $^{**}P < 0.01$, $^{***}P < 0.001$. Apparent discrepancies in values on Y columns between panels A, C, and D reflect technical variation in assay reference ranges. ABC, age associated B cell; BH, Benjamini Hochberg False Discovery Rate; CD4, CD4⁺ T cells; CD14, CD14⁺ monocyte; ePsA, early psoriatic arthritis; eRA, early rheumatoid arthritis; LTR, long terminal repeat; mDC, conventional CD1c⁺ DC; pDC, plasmacytoid dendritic cell; SAMHD1, SAM and HD Domain Containing Deoxynucleoside Triphosphate Triphosphohydrolase 1. Color figure can be viewed in the online issue, which is available at <http://onlinelibrary.wiley.com/doi/10.1002/art.43083/abstract>.

RF. Cumulatively, these data offer intriguing insights into a potential role for EREs in RA pathophysiology.

In bulk synovial tissue samples, from both patients with seropositive and seronegative eRA, we identified a significant positive association between *IFNA* transcription and ERE expression, particularly noted with LTR5. LTR5 expression denotes ERVK (HML-2, Human MMTV-like, group 2) activity,³³ which has been recently integrated into the human genome, and multiple copies possess potential biologic activity.³⁴ Indeed, some of the most compelling evidence of the involvement of EREs in RA has implicated this ERV. It has been detected in the plasma of patients with RA, with higher levels associating with active disease.³⁵ Although ERVK transcripts have previously been detected in established RA blood and synovial tissue samples,^{35,36} this is the first time they

have been demonstrated in early disease and in association with IFN- α upregulation. Furthermore, when reanalyzing an independent, established RA synovial tissue single-cell RNA-sequencing (scSeq) data set in the public domain, we observed ERVK to be the most up-regulated subtype when compared with other ERVs. In contrast to eRA bulk synovial tissue analyses, we could find no direct association between ERE expression and *IFNA* transcript in scSeq data from major cellular subsets, including B cells, fibroblasts, monocytes, and T cells, in established RA, although there was evidence of increased downstream IFN-I signaling. We previously showed circulating IFN- α declines during the first 6 months after RA diagnosis,⁴ potentially explaining this difference from eRA, although the influence of distinct cellular composition and/or sampling technique cannot be excluded. ERVs also induce

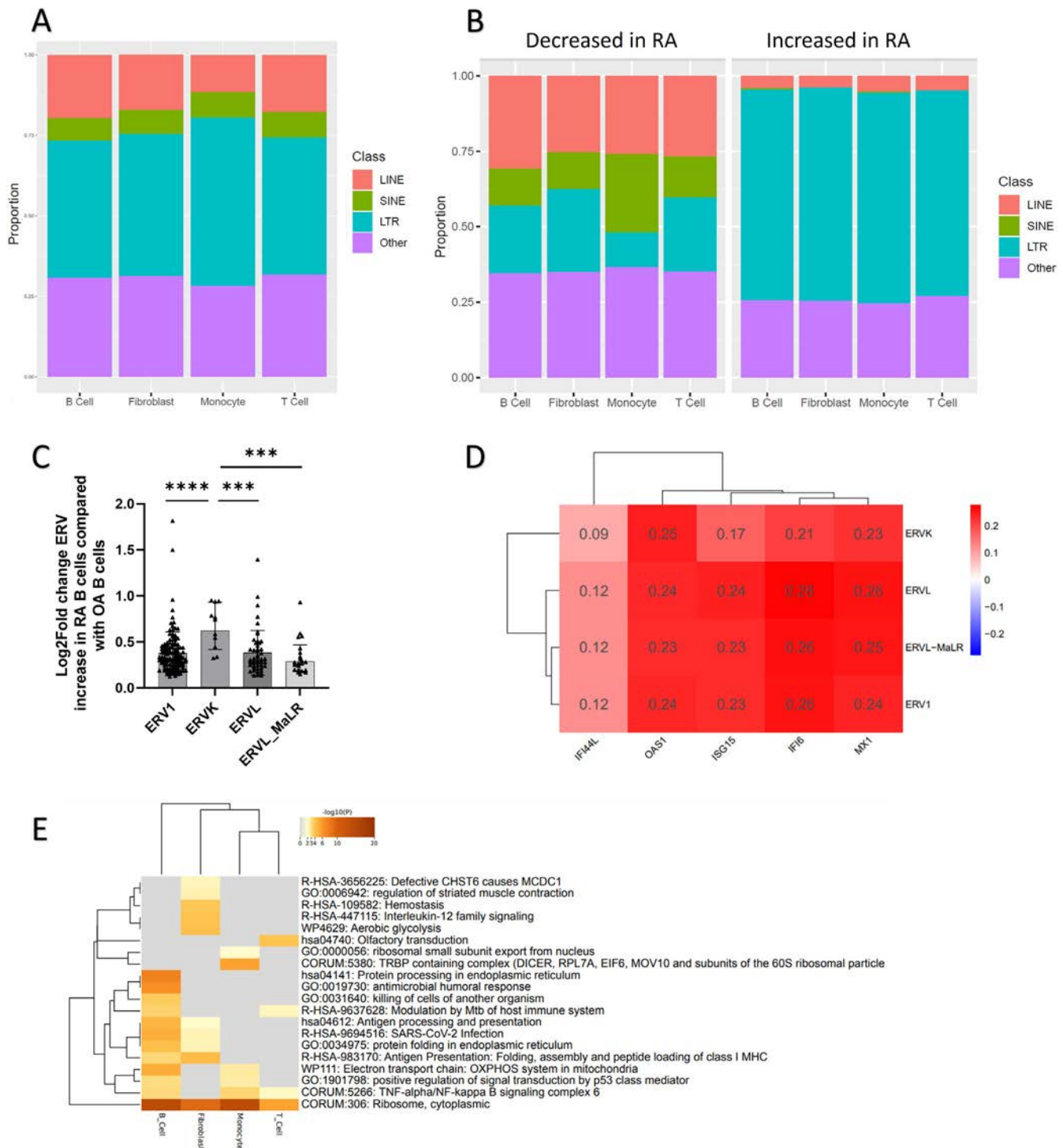


Figure 5. RepEnrich was applied to synovial scSeq data from established RA and OA controls, and repeat element enrichment/ERE were identified. Cellular clusters included monocytes, fibroblasts, T cells, and B cells. (A) The proportion of scSeq repeat element/ERE expression, grouped by ERE class, in each cell subset in established RA synovial tissue. (B) Proportion of individual EREs, grouped by class, with either increased or reduced expression in RA versus OA. (C) The LTR class is divided into ERV1, ERVK, ERV, and ERV_MaLR families, with individual ERE expression counts within each family. Depiction of increased differential expression (Log2FoldChange) in RA compared with OA of each individual ERE count within each ERV family. This is compared between the individual ERV families, Kruskal-Wallis, BH adjusted $P = 0.0006$, and individual Mann-Whitney U-tests. (D) Hierarchical clustering of correlations between gene expression of interferon response genes and repeat element enrichment counts in RA B cells. Pearson's correlation coefficients depicted. All correlations were significant, BH $P < 0.001$. (E) MetaScope pathway analysis of all genes with a correlation of ≥ 0.4 with LTR repeat elements in each of the individual cell subsets. The top 20 pathways are depicted. **** $P < 0.0001$, *** $P < 0.005$. BH, Benjamini Hochberg False Discovery Rate; ERE, endogenous retroelements; ERV, endogenous retrovirus; LINE, long interspersed nuclear element; LTR, long terminal repeat; MaLR, mammalian-apparent LTR retrotransposons; OA, osteoarthritis; RA, rheumatoid arthritis; scSeq, single-cell RNA-sequencing; SINE, short interspersed nuclear element.

TNF α ,³⁷ which induces IRG expression independently of IFN-I in RA synovial fibroblasts,³⁸ an association we also identified in our pathway analysis, and this process may become dominant in established disease. Nonetheless, the clear association of ERE expression in RA synovial tissue with both *IFNA* transcription and IFN-I signaling mirrors what is seen elsewhere in systemic autoimmunity,¹⁴ as well as organ-specific autoimmunity, such as type 1 diabetes, and warrants further exploration.

Circulating immune cell subsets and their activation may contribute to, or reflect, tissue-specific processes. Notably, eRA synovial fluid IFN- α levels are comparable to those in the circulation.⁴ In eRA, we demonstrated positive associations between EREs and circulating B cell *IFNA* transcript levels as well as between whole-blood *LINE1* activity and circulating IFN- α protein levels, the latter, again, in both seropositive and seronegative patients. The double-stranded RNA sensor RIG-I was potentially implicated in ERE sensing by these data, consistent with our previously reported association between RIG-I and circulating IFN- α levels in eRA.⁴ An association between *IFNA* transcription and whole-blood retrotransposon activity has recently been reported in other autoimmune diseases,³⁹ but our demonstration of an association with IFN- α protein reinforces potential biologic relevance in RA. Similar to other autoimmune diseases,³⁹ we did not find a significant association between ERE activity and downstream IFN-I signaling, although we noted a trend toward an inverse association with the IGS. This apparent discrepancy may arise because many IRGs are potent LINE-1–negative regulators.⁴⁰ Thus, examining upstream IFN- α protein levels, as we did here, may be optimal when delineating associations between IFN- α and EREs.

This is the first time all major classes of EREs have been simultaneously examined in circulating lymphocyte subsets, wherein we found the highest ERE expression in B cells, particularly naïve B cells. Although background inflammation levels could affect ERE activity,²⁰ expression levels were increased in RA B cell subsets compared with patients with ePsA matched for inflammation. Furthermore, ERE expression in eRA whole-blood samples, although associated with circulating IFN- α levels, was independent of other circulating inflammatory cytokines. In keeping with this differential ERE expression, there was increased *IFNA* transcription in RA-naïve B cells. Single-cell analysis of RA circulating B cell subsets previously demonstrated increased sensitivity to IFN- α and increased *IFNA* transcripts in RA-naïve B cells, resulting in increased basal activation and proliferation.⁴¹ The role of IFN- α in B cell function and the pathophysiology of autoimmunity has been well established, whereby it can enhance B cell proliferation, activation, and autoantibody production.³ Pretreatment with IFN- α also enhances pathologic B cell proliferative responses and plasmablast differentiation.⁴² This potentially associates EREs to known RA pathophysiologic processes via enhanced IFN-I signaling.

Indeed, EREs may also be implicated in B cell–driven autoimmunity independently of IFN- α , via antibody responses to cell

components associated with ERE nucleic acid, allowing molecular mimicry and cross activation to occur.^{17,43} Overlap between rheumatic disease–associated autoantibodies, including anti-Ro60 and RF, have been linked to ERE activity.^{19,20,44} We also showed a significant positive association between whole-blood LINE-1 activity and anti-CCP titers, but not RF. Pathway analysis suggested a positive correlation between synovial B cell EREs and antigen processing and presentation. Antibodies against human ERVK *env*, as well as against its citrullinated form, have been detected in established RA, are increased in anti-citrullinated protein antibody (ACPA)–positive patients, and positively correlate with anti-CCP titers.⁴⁵ These data suggest EREs may contribute to citrullinated antigen detected by ACPA and cumulatively hint at a role for EREs in promoting autoantibody generation in RA.

Variation in circulating B cell ERE expression was associated with a reciprocal decrease in *SAMHD1*. This enzyme depletes intracellular deoxynucleoside triphosphate (dNTP) pools, thus limiting ERE replication, and its deficiency has been implicated in interferonopathies.⁴⁶ *SAMHD1* expression can vary between cell subsets,⁴⁷ with lower levels previously reported in B cells.⁴⁸ In B cells, *SAMHD1* is increased in G1 cell cycle phases, wherein it can enhance the development of high affinity antibodies.⁴⁹ Naïve B cells, in phase G0, theoretically therefore would have lower levels of *SAMHD1* and thus increased ERE expression, as we demonstrated. We also saw enrichment of PI3K/Akt signaling in B cells, and in AGS, this pathway has been implicated in linking *SAMHD1* deficiency to increased IFN-I response.⁵⁰ *SAMHD1* is classed as an IFN response gene, and the reduced expression in naïve B cells may appear paradoxical given the increased IFN- α reported. However, in some primary human cells, *SAMHD1* levels did not change following IFN- α exposure and, in reality, this relationship is likely to be more nuanced.^{47,51} Finally, *SAMHD1* expression levels do not necessarily correlate with its deoxynucleoside triphosphohydrolase (dNTPase) activity and cellular dNTP availability⁴⁷; nevertheless, the reciprocal variability in expression levels between ERE expression and *SAMHD1* are suggestive that an association may exist.

There are recognized differences among gene expression changes, pathways, upstream regulators, and cellular functional states between synovium and peripheral blood in RA.⁵² Indeed, we did not see any link between *SAMHD1* expression and synovial ERE expression. We hypothesize that other retrotransposon regulatory mechanisms may be more relevant in synovial tissue, such as epigenetic silencing,^{14,53} with promoter methylation having been shown to affect LINE1 activity in autoimmune diseases.^{14,39} Although we did not explore these mechanisms in detail, we did not see any difference between retrotransposon activity and DNA methyltransferase 1 (DNMT1), DNMT3A, or DNMT3B expression, known epigenetic modifiers of ERE activity.³⁹ This may reflect the sample size but may also suggest

other mechanisms are dominant, such as SAMHD1 in B cells, or even differential expression in the recently described human silencing hub (HUSH) complex, a known gatekeeper of ERE-induced IFN-I expression.⁵³ These provide promising avenues for future research.

Study limitations include the theoretical nonspecific detection of EREs present within other transcripts. However, primer design and cDNA generation were optimized to detect full-length transcripts to minimize this possibility. For some analyses, particularly those relating to B cell subsets, patient numbers were limited, with large variation reported. This likely reflects the heterogeneity inherent in RA populations, and future studies focusing primarily on cellular subsets of interest, such as B cells, will allow analysis of larger cohorts and inclusion of seronegative patients, an aspect currently lacking in our work. Finally, longitudinal studies will also help inform any differences between early and established RA and how ERE activity may change with time or in response to treatment.

In conclusion, we examine for the first time ERE activity in eRA and present potentially important associations between ERE activity and IFN-I, B cell function, and autoantibody generation. Within this context, it is intriguing that antiretroviral drugs highly active antiretroviral therapy (HAART) have ameliorated symptoms in RA.⁵⁴ Further work is needed to comprehensively explore the putative pathogenic involvement of EREs in eRA. This will allow greater understanding of RA pathophysiology and potentially provide new therapeutic targets.

ACKNOWLEDGMENTS

The authors wish to thank Professors Stefan Siebert and Iain McInnes (University of Glasgow), Drs Shaun Flint and Katherine Nevin (GSK), and Professor Soumya Raychaudhuri (Harvard Medical School) for their contributions.

AUTHOR CONTRIBUTIONS

All authors contributed to at least one of the following manuscript preparation roles: conceptualization AND/OR methodology, software, investigation, formal analysis, data curation, visualization, and validation AND drafting or reviewing/editing the final draft. As corresponding author, Dr Cooles confirms that all authors have provided the final approval of the version to be published, and takes responsibility for the affirmations regarding article submission (eg, not under consideration by another journal), the integrity of the data presented, and the statements regarding compliance with institutional review board/Declaration of Helsinki requirements.



REFERENCES

- Walter MR. The role of structure in the biology of interferon signaling. *Front Immunol* 2020;11:606489.
- Fernandez-Ruiz R, Niewold TB. Type I Interferons in autoimmunity. *J Invest Dermatol* 2022;142(3 Pt B):793–803.
- Kiefer K, Oropallo MA, Cancro MP, et al. Role of type I interferons in the activation of autoreactive B cells. *Immunol Cell Biol* 2012;90(5):498–504.
- Cooles FAH, Tarn J, Lendrem DW, et al; RA-MAP Consortium. Interferon- α -mediated therapeutic resistance in early rheumatoid arthritis implicates epigenetic reprogramming. *Ann Rheum Dis* 2022;81(9):1214–1223.
- Cooles FAH, Anderson AE, Lendrem DW, et al. The interferon gene signature is increased in patients with early treatment-naïve rheumatoid arthritis and predicts a poorer response to initial therapy. *J Allergy Clin Immunol* 2018;141(1):445–448.e4.
- Lübbbers J, Brink M, van de Stadt LA, et al. The type I IFN signature as a biomarker of preclinical rheumatoid arthritis. *Ann Rheum Dis* 2013;72(5):776–780.
- Macías-Segura N, Castañeda-Delgado JE, Bastian Y, et al. Transcriptional signature associated with early rheumatoid arthritis and healthy individuals at high risk to develop the disease. *PLoS One* 2018;13(3):e0194205.
- Volkman HE, Stetson DB. The enemy within: endogenous retroelements and autoimmune disease. *Nat Immunol* 2014;15(5):415–422.
- Richardson SR, Doucet AJ, Kopera HC, et al. The influence of LINE-1 and SINE retrotransposons on mammalian genomes. *Microbiol Spectr* 2015;3(2):Mdna3-0061-2014.
- De Cecco M, Ito T, Petrashen AP, et al. L1 drives IFN in senescent cells and promotes age-associated inflammation. *Nature* 2019;566(7742):73–78.
- Mustelin T, Ukadike KC. How retroviruses and retrotransposons in our genome may contribute to autoimmunity in rheumatological conditions. *Front Immunol* 2020;11:593891.
- Zhao K, Du J, Peng Y, et al. LINE1 contributes to autoimmunity through both RIG-I- and MDA5-mediated RNA sensing pathways. *J Autoimmun* 2018;90:105–115.
- Lee-Kirsch MA, Wolf C, Günther C. Aicardi-Goutières syndrome: a model disease for systemic autoimmunity. *Clin Exp Immunol* 2014;175(1):17–24.
- Mavragani CP, Sagalovskiy I, Guo Q, et al. Expression of long interspersed nuclear element 1 retroelements and induction of type I interferon in patients with systemic autoimmune disease. *Arthritis Rheumatol* 2016;68(11):2686–2696.
- Ali M, Veale DJ, Reece RJ, et al. Overexpression of transcripts containing LINE-1 in the synovia of patients with rheumatoid arthritis. *Ann Rheum Dis* 2003;62(7):663–666.
- de Jong TD, Vosslander S, Mantel E, et al. Physiological evidence for diversification of IFN α - and IFN β -mediated response programs in different autoimmune diseases. *Arthritis Res Ther* 2016;18(1):49.
- Tugnet N, Rylance P, Roden D, et al. Human endogenous retroviruses (HERVs) and autoimmune rheumatic disease: is there a link? *Open Rheumatol J* 2013;7(1):13–21.
- Nakagawa K, Brusic V, McColl G, et al. Direct evidence for the expression of multiple endogenous retroviruses in the synovial compartment in rheumatoid arthritis. *Arthritis Rheum* 1997;40(4):627–638.
- Nelson PN, Roden D, Nevill A, et al. Rheumatoid arthritis is associated with IgG antibodies to human endogenous retrovirus gag matrix: a potential pathogenic mechanism of disease? *J Rheumatol* 2014;41(10):1952–1960.
- Freimanis G, Hooley P, Ejtehadi HD, et al. A role for human endogenous retrovirus-K (HML-2) in rheumatoid arthritis: investigating mechanisms of pathogenesis. *Clin Exp Immunol* 2010;160(3):340–347.
- Aletaha D, Neogi T, Silman AJ, et al. Rheumatoid arthritis classification criteria: an American College of Rheumatology/European League Against Rheumatism collaborative initiative. *Annals of the Rheumatic Diseases* 2010;69:1580–1588.
- Meyer S, Woodward M, Hertel C, et al; APECED patient collaborative. AIRE-deficient patients harbor unique high-affinity disease-ameliorating autoantibodies. *Cell* 2016;166(3):582–595.

23. Cooles FAH, Anderson AE, Skelton A, et al. Phenotypic and transcriptomic analysis of peripheral blood plasmacytoid and conventional dendritic cells in early drug naïve rheumatoid arthritis. *Front Immunol* 2018;9:755.
24. Vidal-Pedrola G, Naamane N, Cameron JA, et al. Characterization of age-associated B cells in early drug-naïve rheumatoid arthritis patients. *Immunology* 2023;168(4):640–653.
25. Shukla R, Upton KR, Munoz-Lopez M, et al. Endogenous retrotransposition activates oncogenic pathways in hepatocellular carcinoma. *Cell* 2013;153(1):101–111.
26. Kelly S, Humby F, Filer A, et al. Ultrasound-guided synovial biopsy: a safe, well-tolerated and reliable technique for obtaining high-quality synovial tissue from both large and small joints in early arthritis patients. *Ann Rheum Dis* 2015;74(3):611–617.
27. Maney NJ, Lemos H, Barron-Millar B, et al. Pim kinases as therapeutic targets in early rheumatoid arthritis. *Arthritis Rheumatol* 2021;73(10):1820–1830.
28. Criscione SW, Zhang Y, Thompson W, et al. Transcriptional landscape of repetitive elements in normal and cancer human cells. *BMC Genomics* 2014;15(1):583.
29. Zhang F, Wei K, Slowikowski K, et al; Accelerating Medicines Partnership Rheumatoid Arthritis and Systemic Lupus Erythematosus (AMP RA/SLE) Consortium. Defining inflammatory cell states in rheumatoid arthritis joint synovial tissues by integrating single-cell transcriptomics and mass cytometry. *Nat Immunol* 2019;20(7):928–942.
30. Kawano H, Saeki H, Kitao H, et al. Chromosomal instability associated with global DNA hypomethylation is associated with the initiation and progression of esophageal squamous cell carcinoma. *Ann Surg Oncol* 2014;21(S4)(suppl 4):S696–S702.
31. Linn-Rasker SP, van der Helm-van Mil AHM, van Gaalen FA, et al. Smoking is a risk factor for anti-CCP antibodies only in rheumatoid arthritis patients who carry HLA-DRB1 shared epitope alleles. *Ann Rheum Dis* 2006;65(3):366–371.
32. Gramberg T, Kahle T, Bloch N, et al. Restriction of diverse retroviruses by SAMHD1. *Retrovirology* 2013;10(1):26.
33. Grow EJ, Flynn RA, Chavez SL, et al. Intrinsic retroviral reactivation in human preimplantation embryos and pluripotent cells. *Nature* 2015;522(7555):221–225.
34. Mao J, Zhang Q, Cong YS. Human endogenous retroviruses in development and disease. *Comput Struct Biotechnol J* 2021;19:5978–5986.
35. Reynier F, Verjat T, Turrel F, et al. Increase in human endogenous retrovirus HERV-K (HML-2) viral load in active rheumatoid arthritis. *Scand J Immunol* 2009;70(3):295–299.
36. Ehlhardt S, Seifert M, Schneider J, et al. Human endogenous retrovirus HERV-K(HML-2) Rec expression and transcriptional activities in normal and rheumatoid arthritis synovia. *J Rheumatol* 2006;33(1):16–23.
37. Saresella M, Rolland A, Marventano I, et al. Multiple sclerosis-associated retroviral agent (MSRV)-stimulated cytokine production in patients with relapsing-remitting multiple sclerosis. *Mult Scler* 2009;15(4):443–447.
38. Bonelli M, Dalwigk K, Platzer A, et al. IRF1 is critical for the TNF-driven interferon response in rheumatoid fibroblast-like synoviocytes: JAKinibs suppress the interferon response in RA-FLSs. *Exp Mol Med* 2019;51(7):1–11.
39. Kuriyama Y, Shimizu A, Kanai S, et al. Coordination of retrotransposons and type I interferon with distinct interferon pathways in dermatomyositis, systemic lupus erythematosus and autoimmune blistering disease. *Sci Rep* 2021;11(1):23146.
40. Zhao X, Zhao Y, Du J, et al. The interplay among HIV, LINE-1, and the interferon signaling system. *Front Immunol* 2021;12:732775.
41. Han L, Tu S, Shen P, et al. A comprehensive transcriptomic analysis of alternate interferon signaling pathways in peripheral blood mononuclear cells in rheumatoid arthritis. *Aging (Albany NY)* 2021;13(16):20511–20533.
42. Akita K, Yasaka K, Shirai T, et al. Interferon α enhances B cell activation associated with FOXM1 induction: potential novel therapeutic strategy for targeting the plasmablasts of systemic lupus erythematosus. *Front Immunol* 2021;11:498703.
43. Trela M, Nelson PN, Rylance PB. The role of molecular mimicry and other factors in the association of human endogenous retroviruses and autoimmunity. *APMIS* 2016;124(1–2):88–104.
44. Hung T, Pratt GA, Sundararaman B, et al. The Ro60 autoantigen binds endogenous retroelements and regulates inflammatory gene expression. *Science* 2015;350(6259):455–459.
45. Wang X, Hefton A, Ni K, et al. Autoantibodies against unmodified and citrullinated human endogenous retrovirus K envelope protein in patients with rheumatoid arthritis. *J Rheumatol* 2022;49(1):26–35.
46. White TE, Brandariz-Nuñez A, Martinez-Lopez A, et al. A SAMHD1 mutation associated with Aicardi-Goutières syndrome uncouples the ability of SAMHD1 to restrict HIV-1 from its ability to downmodulate type I interferon in humans. *Hum Mutat* 2017;38(6):658–668.
47. Coggins SA, Mahboubi B, Schinazi RF, Kim B et al. SAMHD1 functions and human diseases. *Viruses* 2020;12(4):382.
48. Schmidt S, Schenkova K, Adam T, et al. SAMHD1's protein expression profile in humans. *J Leukoc Biol* 2015;98(1):5–14.
49. Thientosapol ES, Bosnjak D, Durack T, et al. SAMHD1 enhances immunoglobulin hypermutation by promoting transversion mutation. *Proc Natl Acad Sci USA* 2018;115(19):4921–4926.
50. Oh C, Ryoo J, Park K, et al. A central role for PI3K-AKT signaling pathway in linking SAMHD1-deficiency to the type I interferon signature. *Sci Rep* 2018;8(1):84.
51. Li M, Zhang D, Zhu M, et al. Roles of SAMHD1 in antiviral defense, autoimmunity and cancer. *Rev Med Virol* 2017;27(4):e1931.
52. Lee EJ, Lilja S, Li X, et al. Bulk and single cell transcriptomic data indicate that a dichotomy between inflammatory pathways in peripheral blood and arthritic joints complicates biomarker discovery. *Cytokine* 2020;127:154960.
53. Tunbak H, Enriquez-Gasca R, Tie CHC, et al. The HUSH complex is a gatekeeper of type I interferon through epigenetic regulation of LINE-1s. *Nat Commun* 2020;11(1):5387.
54. Chen JW, Deng GS, Zhang WS, et al. Case report: safety and efficacy of adalimumab in treating difficult-to-treat rheumatoid arthritis in a human immunodeficiency virus-positive patient, one year follow-up. *Front Immunol* 2022;13:942642.

BRIEF REPORT

Changes in Descending Pain Modulation During Anti-Tumor Necrosis Factor Therapy: A Prospective Study in Rheumatoid Arthritis and Spondyloarthritis

Anne-Priscille Trouvin,¹  Arielle Simunek,² Joël Coste,² Terkia Medkour,¹ Alice Combier,³ Lucile Poiroux,³ François Vidal,⁴ Sandrine Carvès,²  Didier Bouhassira,⁵ and Serge Perrot¹

Objective. In rheumatoid arthritis (RA) and spondyloarthritis (SpA), managing persistent pain remains challenging. Little is known regarding impaired pain pathways in these patients and the impact of biologic disease-modifying anti-rheumatic drugs (bDMARDs). The objective of the Rheumatism Pain Inhibitory Descending Pathways study was to assess pain thresholds and descending pain modulation in patients with active RA or SpA following introduction of a tumor necrosis factor inhibitor (TNFi).

Methods. Patients with active disease (50 with RA and 50 with SpA) naive to bDMARDs or targeted synthetic DMARDs and starting a TNFi were included. Patients were observed for six months after TNFi initiation with clinical, psychological, and pain assessment. At all visits, participants underwent quantitative sensory testing with heat and cold pain thresholds and descending inhibition by conditioned pain modulation (CPM). Descending pain control (CPM effect) was assessed as the change in heat pain threshold (°C) following a conditioning stimulus.

Results. Of the 100 patients (59 women, mean \pm SD age 45.8 ± 14.6 years), 74 completed the six-month follow-up. Thermal pain thresholds did not significantly change during follow-up. CPM effect improved significantly during follow-up (mean \pm SD $0.25 \pm 2.57^\circ\text{C}$ at baseline and $2.96 \pm 2.50^\circ\text{C}$ at six months; $P < 0.001$). At the end of follow-up, the mean CPM effect was significantly higher in patients without significant pain compared with patients with persistent pain (>3 of 10 on the Brief Pain Inventory) (mean \pm SD $3.25 \pm 2.68^\circ\text{C}$ vs $2.47 \pm 2.11^\circ\text{C}$; $P = 0.04$) and in patients achieving remission or low disease activity compared with patients with active rheumatism (mean \pm SD $3.31 \pm 2.68^\circ\text{C}$ vs $2.18 \pm 1.87^\circ\text{C}$; $P = 0.01$).

Conclusion. In active inflammatory rheumatism, impaired descending pain modulation, but not thermal pain thresholds, is improved after TNFi treatment, suggesting a possible effect of TNFi on central pain modulation.

INTRODUCTION

One challenge in the care of chronic inflammatory rheumatism is persistent pain despite low disease activity and/or remission. Reducing joint pain is a primary treatment expectation for patients.¹ However, there is often a failure to adequately address this need for pain relief.² Remarkably, pain persists in up to one-third of patients who show a good therapeutic response.^{3,4}

Understanding the underlying mechanisms of this persistent pain is of significant clinical importance, as it suggests that its origins are not solely related to peripheral inflammatory processes. Changes in central pain processing may play a role in maintaining and/or amplifying pain independently of peripheral inflammation.⁵ Notably, central sensitization (CS), characterized by long-lasting increased responsiveness of the nociceptive systems and clinically associated with widespread hyperalgesia,

Supported by the EFIC-Grunenthal Grant (to Dr Trouvin) and the Cercle d'Etude de la Douleur en Rhumatologie (to Dr Trouvin).

¹Anne-Priscille Trouvin, MD, PhD, Terkia Medkour, PhD, Serge Perrot, MD, PhD: Le Groupe Hospitalier Universitaire Paris Centre Cochin and Université Paris Cité, Paris, France, and Inserm U987, Université de Versailles Saint Quentin, Paris-Saclay University, AP-HP, Ambroise Paré Hospital, Boulogne-Billancourt, France; ²Arielle Simunek, MD, Joël Coste, MD, PhD, Sandrine Carvès, MD: Le Groupe Hospitalier Universitaire Paris Centre Cochin and Université Paris Cité, Paris, France; ³Alice Combier, MD, Lucile Poiroux, MD: Le Groupe Hospitalier Universitaire Paris Centre Cochin, Paris, France; ⁴François Vidal, MD: Le Groupe Hospitalier Universitaire Paris-Saclay Ambroise Paré, Boulogne-Billancourt, France; ⁵Didier Bouhassira, MD, PhD: Inserm U987,

Université de Versailles Saint Quentin, Paris-Saclay University, AP-HP, Ambroise Paré Hospital, Boulogne-Billancourt, France.

Additional supplementary information cited in this article can be found online in the Supporting Information section (<https://acrjournals.onlinelibrary.wiley.com/doi/10.1002/art.43084>).

Author disclosures are available at <https://onlinelibrary.wiley.com/doi/10.1002/art.43084>.

Address correspondence via email to Anne-Priscille Trouvin, MD, PhD, at annepriscille.trouvin@aphp.fr.

Submitted for publication March 14, 2024; accepted in revised form December 3, 2024.

may have a major pathophysiologic role. Proposed mechanisms for CS include enhanced excitatory synaptic transmission in central nociceptive systems and/or alterations of endogenous pain modulation (such as decreased inhibition and/or increased facilitation) resulting in maladaptive plasticity in the spinal cord or brain.⁵ Clinical markers of CS are predominantly assessed through quantitative sensory testing (QST) and encompass a decrease in pain threshold and an increased effect of temporal summation of nociceptive stimuli. Alteration of endogenous pain modulation, specifically descending modulation, is typically evaluated using conditioned pain modulation (CPM) paradigms, which measure the modulatory effects (inhibition or facilitation) of a conditioning painful stimulus on a test stimulus applied to a distant body area.⁶

Our recent findings from the prospective Rheumatism Pain Inhibitory Descending Pathways (RAPID) study, which included patients with active rheumatoid arthritis (RA) or spondyloarthritis (SpA), revealed a significant impairment in inhibitory CPM effect, compared to controls, before initiation of biologic disease-modifying antirheumatic drug (bDMARD) treatment.⁷ These results, in line with previous studies that demonstrated alterations in CPM in patients with RA and other markers of CS^{8,9} highlight the specific role for central mechanisms in the pathophysiology of chronic pain in these patients. However, CPM was not measured after treatment, so to date it is unknown whether CPM alterations are reversible, as this has been shown in other chronic pain conditions after treatments.¹⁰

In this study, we present the follow-up results of our RAPID study cohort, assessing descending pain modulation through CPM paradigms in patients with RA or SpA up to six months after initiating tumor necrosis factor inhibitor (TNFi) treatment. Our primary objective was to further investigate the changes in CPM over the course of the treatment and the correlations on the overall response to treatment and the persistence of pain post treatment.

PATIENTS AND METHODS

Study population. The RAPID study is a multicenter study that included patients with active RA or SpA before the administration of bDMARDs. The patients were recruited from two French university hospital rheumatology departments (Paris and Boulogne-Billancourt) from February 2019 to June 2021. The inclusion criteria were described previously in the study by Trouvin et al.⁷ Patients were included immediately before initiating a TNFi therapy for active articular disease and were observed for six months, with visits at three and six months. The study was reviewed and approved by the Sud-Est IV ethics committee under agreement number 2018-A00248-47. All participants provided written informed consent.

Clinical characteristics were systematically assessed before each visit (ie, at baseline, three months, and six months), before the QST session. The data collected included current

treatments, erythrocyte sedimentation rate (ESR), and C-reactive protein (CRP) level. Disease activity scores were calculated with the Disease Activity Score in 28 joints using the ESR (DAS28-ESR) for patients with RA or the Ankylosing Spondylitis Disease Activity Score using the CRP level (ASDAS-CRP) for patients with SpA. Pain, functional impact, and psychological impact were assessed using the Brief Pain Inventory (BPI), the Health Assessment Questionnaire score for patients with RA and the Bath Ankylosing Spondylitis Disease Activity Index/Bath Ankylosing Spondylitis Functional Index score for patients with SpA, the Insomnia Severity Index (ISI), the Hospital Anxiety Depression scale (HAD), and the Pain Catastrophizing Scale (PCS).

QST. Patients underwent QST and CPM testing at inclusion and at both follow-up visits after the initiation of the TNFi therapy by a single observer. Thermal (heat and cold) pain thresholds were assessed with the TSA II Neurosensory Analyzer. A contact Peltier thermode (30 × 30 mm) was applied to the skin over the dominant volar forearm. The baseline temperature of the thermode was adjusted to the patient's skin temperature. Thresholds were measured by the method of limits: stimuli of increasing or decreasing intensities were applied, and for each stimulus, the patients pressed a button that reversed the thermal stimulation as soon as the stimulation became painful. The interstimulus intervals used were 15–20 seconds for heat pain thresholds (HPTs) and 20–30 seconds for cold pain thresholds (CPTs). The maximum and minimum temperatures were set to 50°C for heat and 0°C for cold. The thermal rate of change was 2°C/s. Thresholds were calculated as the mean threshold recorded in three successive measures and are expressed as absolute thresholds (°C).

CPM. We used a CPM paradigm involving the application of test stimuli to the dominant upper limb and conditioning stimuli to the lower limb. The test stimulus was the HPT measured as described previously, and the conditioning stimulus was immersion of the nondominant foot in a bath of circulating cold water at 8°C (CORIO CD-900F Refrigerated/Heating Circulator) for one minute. As instructed, patients could withdraw their foot from the cold water bath if they felt the pain was unbearable during the immersion. Most patients withdrew their foot before the end of the one minute with verbal assessment of pain being unbearable. For patients going through the whole minute of immersion, oral pain assessment of the conditioning stimulus was made, and all patients rated pain at 8 of 10 or more. HPT was measured again, as described previously, immediately after conditioning. The CPM effect was calculated as the difference (expressed in °C) between HPT measured after and before the conditioning stimulus. A positive difference (ie, a higher HPT after conditioning than before conditioning) indicated activation of descending pain inhibition.

Statistical analysis. Given that the study was exploratory, there was no power calculation because, to our knowledge, no previous prospective studies on CPM permitted specific calculations, nor do standards regarding sample size.

Results are expressed as means \pm SDs for continuous variables or as frequencies and percentages for categorical variables. The primary outcome was the comparison of the CPM effect measured before and six months after TNFi initiation.

Longitudinal paired data were compared using a parametric test (if normal distribution) or nonparametric tests (if not normally distributed). Correlations between CPM and pain intensities using the BPI pain scales (pain right now, worst pain, least pain, and pain in general) were assessed by calculating Spearman's rank correlation coefficient.

The primary outcome (change in CPM) was considered regarding two disease end points with the following stratification: (1) disease activity at the end of follow-up, with patients achieving remission or low disease activity ($\text{DAS28} \leq 3.2$ or $\text{ASDAS} < 2.1$) compared to patients with residual activity, and (2) residual pain at the end of follow-up, with patients measuring pain intensity (using the BPI scale "pain in general") as ≤ 3 of 10 compared to patients with residual pain. Comparison of thermal QST and CPM between patients stratified by these two end points was performed using Student's *t*-test or the Mann-Whitney U test depending on the distribution of the data.

A multivariate analysis using two models to predict the achievement of each of the two end points: remission or low activity and pain ≤ 3 of 10. The variables integrated into the models were tested in three stages: (1) demographic variables package (age, sex, disease duration); (2) clinical data (disease duration, disease activity, worst pain, pain in general), questionnaires (positive Fibromyalgia Rapid Screening Tool questionnaire, positive Central Sensitization index questionnaire, HAD anxiety, HAD depression, ISI, PCS), and CPM upon inclusion package; and (3) the third package, with CPM at three months and patients' reported outcomes of efficacy and satisfaction. Regarding this absence of power calculation, the RAPID study might be underpowered for such hypothesis testing. Statistical analyses were performed using SAS version 9.4 software (SAS Institute Inc). The data supporting this article will be shared on reasonable request to the corresponding author.

RESULTS

Patients' characteristics and clinical effects of treatment. One hundred patients with active disease were included (50 with RA and 50 with SpA), 59 were women, and the mean \pm SD age was 45.8 ± 14.6 years. Baseline clinical characteristics and disease activity have been previously described.⁷ Because of the COVID-19 pandemic, only 87 patients from the initial cohort initiated bDMARD treatment with a TNFi (50 patients received etanercept, 33 received adalimumab, 2 received infliximab, and 2 received certolizumab).

Of the cohort, 74 patients completed the six-month follow-up (36 with RA and 38 with SpA) (Sup Material 1). At six months, remission was achieved by 20 patients with RA (55.6% of the patients with RA) and 12 patients with SpA (31.6% of the patients with SpA); low disease activity was achieved by 6 patients with RA (16.7% of the patients with RA) and 13 patients with SpA (34.2% of the patients with SpA); 8 patients with RA (22.2% of the patients with RA) had moderate activity; 12 patients with SpA (31.6% of the patients with SpA) had high disease activity; 2 patients with RA (5.5% of the patients with RA) had high disease activity; and 1 patient with SpA (2.6% of the patients with SpA) had very high disease activity. At the end of follow-up, the average pain intensity significantly decreased across the patient population (Table 1): 47 patients (63.5%) reported no significant residual pain (average daily pain intensity ≤ 3 of 10), whereas 27 (36.5%) reported persistent pain (average daily pain intensity > 3). The changes in other outcomes are summarized in Table 1, showing significant reductions in functional impact, HAD depression, PCS, and ISI scores at the six-month assessment.

Changes in CPM effect and in pain thresholds. The overall CPM effect exhibited a significant increase at three months (mean \pm SD $2.64 \pm 2.12^\circ\text{C}$; $P < 0.001$) compared to baseline values (mean \pm SD $0.25 \pm 2.57^\circ\text{C}$), and this effect was sustained at six months (mean \pm SD $2.96 \pm 2.50^\circ\text{C}$; $P < 0.001$) (Figure 1). At three months follow-up, the mean CPM effect in patients who achieved remission or low disease activity ($n = 42$) was not significantly different than the mean CPM effect in patients who still had an active disease ($n = 35$). The mean CPM effect in patients with no significant residual pain (BPI pain scale ≤ 3 of 10) ($n = 45$) was not significantly different from the mean CPM effect of patients with residual pain (BPI pain scale > 3 of 10) ($n = 32$). At the end of the six-month follow-up, the mean CPM effect in patients who achieved remission or low disease activity ($n = 51$) was significantly different from the mean CPM effect in patients who still had an active disease ($n = 23$) (mean \pm SD $3.31 \pm 2.68^\circ\text{C}$ vs $2.18 \pm 1.87^\circ\text{C}$, respectively; $P = 0.018$), and the mean CPM effect in patients with no significant residual pain (BPI pain scale ≤ 3 of 10) ($n = 47$) was significantly different from the mean CPM effect of patients with residual pain (BPI pain scale > 3 of 10) ($n = 27$) (mean \pm SD $3.25 \pm 2.68^\circ\text{C}$ vs $2.47 \pm 2.11^\circ\text{C}$, respectively; $P = 0.046$) (Sup Material 2).

The changes in CPM were significantly correlated with changes in pain intensity ratings (Table 2). This indicates that a higher increase in CPM was associated with a greater decrease in pain intensity. This is in line with the previous finding of a mean CPM effect significantly higher at six months in patients without significant residual pain compared to those patients with persistent pain. In contrast, the changes in CPM effect did not show any significant correlation with changes in disease activity scores (Table 2), with the changes in blood inflammatory biomarkers at three months (ESR: $r = 0.16$, $P = 0.21$; CRP: $r = -0.13$,

Table 1. Clinical characteristics of patients throughout follow-up*

	Inclusion (N = 100 patients; 50 with RA and 50 with SpA)	3 mo (n = 81 patients; 40 with RA and 41 with SpA)	6 mo (n = 74 patients; 36 with RA and 38 with SpA)	Comparison (baseline to 6 mo), <i>P</i>
Activity score				
Patients with RA: DAS28-ESR	4.97 ± 0.94	3.1 ± 1.3	2.5 ± 1.35	<0.0001
Patients with SpA: ASDAS-CRP	3.27 ± 0.86	1.9 ± 0.8	1.8 ± 0.89	<0.0001
Functional impact				
Patients with RA: HAQ (of 3)	1.1 ± 0.8	0.7 ± 0.8	0.6 ± 0.8	<0.0001
Patients with SpA: BASFI (of 10)	4.2 ± 2.6	2.5 ± 2.5	1.9 ± 1.9	<0.0001
Mean pain intensity in general (of 10)	5.7 ± 1.4	3.2 ± 2.3	2.9 ± 2.5	<0.0001
HAD anxiety (of 21)	8.5 ± 5.4	7.3 ± 4.7	7.6 ± 5	NS
HAD depression (of 21)	7.2 ± 4.5	5.7 ± 4.5	5.6 ± 4.2	0.0009
Insomnia Severity Index (of 28)	12.9 ± 7.1	10 ± 7.1	9.8 ± 7	<0.0001
Pain Catastrophizing Scale (of 52)	23.3 ± 13.9	17.5 ± 14.8	16.1 ± 14.5	<0.0001

* Data are expressed as the mean ± SD unless otherwise stated. ASDAS-CRP, Ankylosing Spondylitis Disease Activity Score using the C-reactive protein level; BASFI, Bath Ankylosing Spondylitis Functional Index; DAS28-ESR, Disease Activity Score in 28 joints using the erythrocyte sedimentation rate; HAQ, Health Assessment Questionnaire; HAD, Hospital Anxiety Depression Scale; NS, not significant; RA, rheumatoid arthritis; SpA, spondyloarthritis.

$P = 0.28$) and six months (ESR: $r = 0.1$, $P = 0.42$; CRP: $r = -0.02$, $P = 0.89$), or with any of the other functional and psychological scores. Finally, variation of the CPM effect over the six-month follow-up was not explained by any of the baseline parameters (Sup Material 3). For the multivariate analysis to predict the achievement of each of the two end points (remission or low activity and pain ≤ 3 of 10) for all two models, none of the baseline data, in particular CPM effect, were predictive of achieving remission or

low activity or absence of residual pain at the end of follow-up (Sup Material 4).

Thermal pain thresholds did not significantly change during the course of the treatment (Sup Material 5). There was no ceiling effect for the HPT. Maximal possible stimulation temperature was 50°C, and no patient ever reached this temperature as their HPT. In contrast, a few patients reached 0°C as their CPT. The mean ± SD HPT was 42.35 ± 3.68°C at baseline, 41.89 ± 3.65°C at

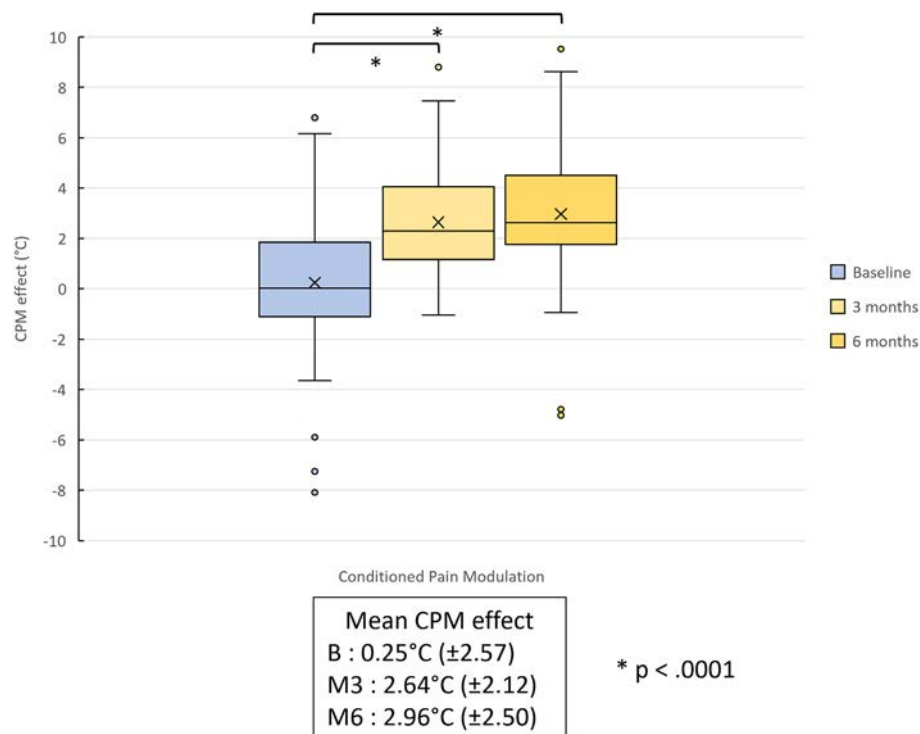


Figure 1. CPM effect evolution during follow-up. Box and whisker plots of CPM effect at baseline, three months' follow-up, and six months' follow-up. Box plots represent the upper quartile, lower quartile, the median (horizontal line), and the mean (X). Whiskers enclose 1.5 × the inter-quartile range. CPM, conditioned pain modulation.

Table 2. Spearman rank correlation coefficient between variation of CPM effect throughout follow-up and clinical and biologic variation during follow-up*

Variation of the considered data between baseline and 6 mo	Spearman rank correlation coefficient (r)	P value
Δ DAS28 (n = 36 patients)	-0.178	0.3
Δ ASDAS (n = 38 patients)	-0.33	0.4
Δ ESR (n = 74 patients)	0.105	0.42
Δ CRP (n = 74 patients)	-0.016	0.89
Δ HAQ (n = 36 patients)	0.00719	0.97
Δ BASFI (n = 38 patients)	-0.11211	0.5
Δ pain right now (n = 74 patients)	-0.39	0.0005
Δ worst pain (n = 74 patients)	-0.38	0.0007
Δ least pain (n = 74 patients)	-0.24	0.04
Δ pain in general (n = 74 patients)	-0.47	<0.0001
Δ HAD anxiety (n = 74 patients)	0.0341	0.77
Δ HAD depression (n = 74 patients)	-0.0886	0.45
Δ Insomnia Severity Index (n = 74 patients)	-0.1281	0.28
Δ Pain Catastrophizing Scale (n = 74 patients)	-0.0106	0.93

* Bold values indicate significant Spearman correlation. ASDAS, Ankylosing Spondylitis Disease Activity Score; BASFI, Bath Ankylosing Spondylitis Functional Index; CPM, conditioned pain modulation; CRP, C-reactive protein; DAS28, Disease Activity Score in 28 joints; ESR, erythrocyte sedimentation rate; HAD, Hospital Anxiety Depression Scale; HAQ, Health Assessment Questionnaire; Δ, variation.

three months, and $42.17 \pm 3.67^{\circ}\text{C}$ at six months. The mean \pm SD CPT was $13.11 \pm 10.04^{\circ}\text{C}$ at baseline, $13.47 \pm 9.31^{\circ}\text{C}$ at three months, and $12.86 \pm 9.45^{\circ}\text{C}$ at six months. At the end of follow-up, there was no significant difference between patients with and without persistent pain (HPT mean \pm SD: $42.26 \pm 3.74^{\circ}\text{C}$ vs $42.12 \pm 3.67^{\circ}\text{C}$, $P = 0.99$; CPT mean \pm SD: $13.04 \pm 9.54^{\circ}\text{C}$ vs $12.77 \pm 9.49^{\circ}\text{C}$, $P = 0.76$) or between patients in remission or with low disease activity and those with active disease (HPT mean \pm SD: $41.97 \pm 3.67^{\circ}\text{C}$ vs $42.63 \pm 3.71^{\circ}\text{C}$, $P = 0.43$; CPT mean \pm SD: $13.33 \pm 9.36^{\circ}\text{C}$ vs $11.83 \pm 9.76^{\circ}\text{C}$, $P = 0.54$). There was no significant difference in the variation of thermal thresholds between baseline and six months in patients with or without persistent pain or between patients in remission or with low disease activity and those with active disease (Sup Material 6).

DISCUSSION

The RAPID study was the first prospective study with repeated QST and CPM before and after bDMARD initiation. This study, in a homogenous group of patients with active disease at inclusion and naive to bDMARD demonstrates an improvement of descending modulation after TNFi initiation.

Impaired descending pain modulation and altered descending inhibitory controls have already been found in inflammatory rheumatic diseases.^{7,8} This alteration of descending modulation seems to be correlated with pain intensity in patients with active disease,⁷ and an inverse association of CPM with tender joint count was also highlighted by Lee et al.⁹ These modifications of

descending pain inhibition might be the counterpart of excessive TNF α . Descending inhibitory controls have not previously been assessed continuously before and after TNFi initiation, and the RAPID study shows modification of descending inhibitory controls after treatment introduction. Descending controls were not improved to the same level in patients with residual pain or with residual disease activity at the end of follow-up. Regarding the latter group, maintenance of altered CPM effect might be explained by persistent active disease and the presence of proinflammatory cytokines.^{5,7,9} We would like to stress that, as of today, there are very few insights regarding clinical significance of CPM variation. It is thought that a negative or null CPM effect becoming positive would indicate (re)appearance of descending inhibiting control; however, it is unknown if this is clinically significant for $+1^{\circ}\text{C}$ of CPM effect or $+3^{\circ}\text{C}$.

Modification of descending modulation contributes to CS; however, the influence of TNFi on the pain pathways is not totally understood. The role of TNFi in human pain pathways in rheumatic settings has barely been studied. In patients with RA, two studies using functional magnetic resonance imaging reported a rapid decrease in activity in brain structures of the pain matrix after one infliximab infusion¹¹ or certolizumab pegol injection.¹² This decrease in cerebral activity was observed as soon as 24 hours¹¹ to 3 days¹² after TNFi injection and preceded clinical response, which was only observed 28 days after treatment initiation.¹² Another study on patients with RA using imaging revealed a central action of TNFi; Cavanagh et al¹³ used single-photon emission computed tomography to measure the effect of adalimumab over the density and activity of the serotonin transporter (SERT) in the brain. Both SERT activity and density are increased by proinflammatory cytokines, and adalimumab infusion significantly decreased SERT density.

In the central nervous system, descending inhibitory controls are mainly modulated through the periaqueductal gray (PAG) and rostral ventromedial medulla.^{5,10} In these central structures, the descending inhibitory signal is mainly mediated by noradrenaline, serotonin, and opioids and potentially by other neurotransmitters, such as γ -aminobutyric acid (GABA).¹⁴ Rodent studies have shown a possible effect of TNF α on PAG neurons; Xu et al¹⁴ reported elevated TNF α levels in the PAG in rodents with neuropathic pain, and this correlated with an impaired GABAergic descending inhibitory system. In the study by Hess et al¹¹ on TNF α transgenic mice that developed inflammatory arthritis, they used functional magnetic resonance imaging to detect higher amplitudes and more widespread activation of the pain matrix. When infliximab was administered to the animals, the first changes in the pain matrix brain activation appeared as early as 24 hours after TNFi injection. The increased activity was totally reversed by TNFi, and the expanded activation was partially reversed. Moreover, a higher degree of connectivity in a cluster comprising the thalamus, PAG, and amygdala was observed in TNF transgenic mice compared with wild-type animals. TNF inhibition

resulted in a rapid but partial dissolution of this cluster.¹¹ TNFi are large molecules that cannot cross the blood–brain barrier, these results regarding their action on the pain have yet to be understood.

Regarding thermal QST, the thermal pain threshold did not significantly change during follow-up in our study. In inflammatory rheumatism, thermal pain thresholds might not be the most suitable QST modality. In other studies using this QST modality, most reported no difference in HPT or CPT in patients with RA or SpA¹⁵ compared to controls. Overall, these results question the use of thermal QST in patients with chronic inflammatory rheumatism. The choice of QST modality is still a matter of debate, and there is no consensus today regarding the appropriate measures to assess CS in chronic inflammatory rheumatism. A few patients had floor ceiling effect with the CPT, but this had no consequences regarding CPM assessment because all patients either withdrew their foot before the whole minute of conditioning or rated their pain as 8 of 10 or more.

The RAPID study has some limitations. There was no control group throughout the follow-up. All participants initiated a TNFi, preventing conclusion to a specific TNF inhibition effect. Finally, given the limited knowledge of the CPM effect in rheumatic disease, power calculation was not possible; therefore, negative results might be due to a possibly underpowered analysis. The prediction models finding only the CPM at three months as being predictive of remission or low disease activity achievement might be due to underpower, larger studies could test the hypothesis of CPM at baseline being predictive of treatment response.

The RAPID study demonstrated that altered inhibitory pain controls in active RA and SpA are improved after TNFi treatment. These results indicate the presence of different descending controls in patients with residual pain, and future studies should focus on exploring pain pathways in patients in remission or with low disease activity, as targeted treatments of the descending pain pathways may be of interest for these patients.

AUTHOR CONTRIBUTIONS

All authors contributed to at least one of the following manuscript preparation roles: conceptualization AND/OR methodology, software, investigation, formal analysis, data curation, visualization, and validation AND drafting or reviewing/editing the final draft. As corresponding author, Dr Trouvin confirms that all authors have provided the final approval of the version to be published and takes responsibility for the affirmations regarding article submission (eg, not under consideration by another journal), the integrity of the data presented, and the

statements regarding compliance with institutional review board/Declaration of Helsinki requirements.

REFERENCES

1. Taylor PC, Ancuta C, Nagy O, et al. Treatment satisfaction, patient preferences, and the impact of suboptimal disease control in a large international rheumatoid arthritis cohort: SENSE study. *Patient Prefer Adherence* 2021;15:359–373.
2. Radawski C, Genovese MC, Hauber B, et al. Patient perceptions of unmet medical need in rheumatoid arthritis: a cross-sectional survey in the USA. *Rheumatol Ther* 2019;6(3):461–471.
3. Svensson B, Forslind K, Andersson M. Unacceptable pain in the BARFOT inception cohort of patients with rheumatoid arthritis: a long-term study. *Scand J Rheumatol* 2020;49(5):371–378.
4. Strand V, Deodhar A, Alten R, et al. Pain and fatigue in patients with ankylosing spondylitis treated with tumor necrosis factor inhibitors: multinational real-world findings. *J Clin Rheumatol* 2021;27(8):e446–e455.
5. Zhang A, Lee YC. Mechanisms for joint pain in rheumatoid arthritis (RA): from cytokines to central sensitization. *Curr Osteoporos Rep* 2018;16(5):603–610.
6. Nir RR, Yarnitsky D. Conditioned pain modulation. *Curr Opin Support Palliat Care* 2015;9(2):131–137.
7. Trouvin AP, Simunek A, Coste J, et al. Mechanisms of chronic pain in inflammatory rheumatism: the role of descending modulation. *Pain* 2023;164(3):605–612.
8. Lee YC, Lu B, Edwards RR, et al. The role of sleep problems in central pain processing in rheumatoid arthritis. *Arthritis Rheum* 2013;65(1):59–68.
9. Lee YC, Bingham CO III, Edwards RR, et al. Association between pain sensitization and disease activity in patients with rheumatoid arthritis: a cross-sectional study. *Arthritis Care Res (Hoboken)* 2018;70(2):197–204.
10. Ramaswamy S, Wodehouse T. Conditioned pain modulation-A comprehensive review. *Neurophysiol Clin* 2021;51(3):197–208.
11. Hess A, Axmann R, Rech J, et al. Blockade of TNF- α rapidly inhibits pain responses in the central nervous system. *Proc Natl Acad Sci USA* 2011;108(9):3731–3736.
12. Rech J, Hess A, Finzel S, et al. Association of brain functional magnetic resonance activity with response to tumor necrosis factor inhibition in rheumatoid arthritis. *Arthritis Rheum* 2013;65(2):325–333.
13. Cavanagh J, Paterson C, McLean J, et al. Tumour necrosis factor blockade mediates altered serotonin transporter availability in rheumatoid arthritis: a clinical, proof-of-concept study. *Ann Rheum Dis* 2010;69(6):1251–1252.
14. Xu D, Zhao H, Gao H, et al. Participation of pro-inflammatory cytokines in neuropathic pain evoked by chemotherapeutic oxaliplatin via central GABAergic pathway. *Mol Pain* 2018;14:1744806918783535.
15. Trouvin AP, Attal N, Perrot S. Assessing central sensitization with quantitative sensory testing in inflammatory rheumatic diseases: a systematic review. *Joint Bone Spine* 2022;89(5):105399.

Association of Synovial Innate Immune Exhaustion With Worse Pain in Knee Osteoarthritis

Holly T. Philpott,¹ Trevor B. Birmingham,¹ Garth Blackler,² J. Daniel Klapak,² Alexander J. Knights,³ Easton C. Farrell,³ Benoit Fiset,⁴ Logan A. Walsh,⁴ J. Robert Giffin,¹ Edward M. Vasarhelyi,¹ Steven J. MacDonald,¹ Brent A. Lanting,¹ Tristan Maerz,³ and C. Thomas Appleton,¹ on behalf of the WOREO Knee Study Group

Objective. Uncontrolled pain remains a major clinical challenge in the management of knee osteoarthritis (OA), the most common disabling joint disease. Worse pain is associated with synovial innate immune cell infiltration (synovitis), but the role of innate immune-regulatory cells in pain is unknown. Our objective was to identify synovial innate immune cell subsets and pathophysiologic mechanisms associated with worse pain in patients with knee OA.

Methods. Synovial tissue biopsies from 122 patients with mild-to-severe knee OA pain (Knee Injury and OA Outcome Score [KOOS]) were analyzed to identify associations between synovial histopathology and worse pain. We then used spatial transcriptomics and proteomics of synovial tissue microenvironments (n = 32), followed by single-cell RNA sequencing (n = 8), to identify synovial cell composition and cell-cell communication networks in patients with more severe OA pain.

Results. Histopathological signs of synovial microvascular dysfunction and perivascular edema were associated with worse KOOS pain (−10.76; 95% confidence interval [CI] −18.90 to −2.61). Patients with worse pain had fewer immune-regulatory macrophages, expanded fibroblast subsets, and enrichment in neurovascular remodeling pathways. Synovial macrophages from patients with worse pain expressed markers of immune exhaustion and decreased phagocytic function (−19.42%; 95% CI −35.96 to −2.89) and their conditioned media increased neuronal cell stress in dorsal root ganglia.

Conclusion. Although synovitis increases during OA, our findings suggest that exhaustion, dysfunction, and loss of immune-regulatory macrophages is associated with worse pain and may be an important therapeutic target.

INTRODUCTION

Pain is a major clinical challenge in osteoarthritis (OA) and the main driver of disability and poor quality of life. Synovitis is associated with increased pain and OA disease progression.^{1–5} Although synovitis is an important and potentially modifiable contributor to knee OA pain and progression, we currently lack sufficient understanding of underlying mechanisms to define effective treatment targets.^{1,3,6}

The inflammatory mechanisms associated with OA are clearly different from those driving disease activity and progression in rheumatoid arthritis (RA). Whereas RA is an autoimmune disease with a major component involving the adaptive immune system, inflammation in OA is largely mediated by innate immune cells and mechanisms.^{7–11} Understanding the role of innate immune mechanisms in OA may yield important insights related to uncontrolled OA pain.

Supported in part by grants from the Academic Medical Organization of Southwestern Ontario, the Canadian Institutes of Health Research (CIHR), the Canada Research Chairs Program, and Western University's Bone and Joint Institute. Dr Philpott's work was supported by a Frederick Banting and Charles Best Doctoral Award from CIHR. Dr Knights' work was supported by a Pioneer Postdoctoral Fellowship from the University of Michigan and the National Institutes of Health (grant K99-AR-081894).

¹Holly T. Philpott, PhD, Trevor B. Birmingham, PT, PhD, J. Robert Giffin, MD, MBA, Edward M. Vasarhelyi, MD, MSc, Steven J. MacDonald, MD, Brent A. Lanting, MD, MSc, C. Thomas Appleton, MD, PhD: University of Western Ontario and London Health Sciences Centre-University Hospital, London, Ontario, Canada; ²Garth Blackler, BAT, J. Daniel Klapak, BAT: University of

Western Ontario, London, Ontario, Canada; ³Alexander J. Knights, PhD, Easton C. Farrell, MSE, Tristan Maerz, PhD: University of Michigan, Ann Arbor; ⁴Benoit Fiset, BSc, GrDip Bioinformatics, Logan A. Walsh, PhD: McGill University, Montreal, Quebec, Canada.

Additional supplementary information cited in this article can be found online in the Supporting Information section (<https://acrjournals.onlinelibrary.wiley.com/doi/10.1002/art.43089>).

Author disclosures and a graphical abstract are available online at <https://onlinelibrary.wiley.com/doi/10.1002/art.43089>.

Address correspondence via email to C. Thomas Appleton, MD, PhD, at tom.appleton@sjhc.london.on.ca.

Submitted for publication June 13, 2024; accepted in revised form December 10, 2024.

Macrophages dominate the synovial immune cell landscape in OA,^{12,13} increase nociception,¹⁴ and orchestrate neurovascular remodeling processes in other diseases.^{15–18} However, macrophage ablation does not prevent the development of OA,¹⁹ suggesting that certain populations of immune cells are important for joint homeostasis. Through crosstalk with other immune and nonimmune cells in synovial tissues, proinflammatory and/or regulatory macrophage subsets might be able to modify nociception in complex synovial microenvironments. Although whether synovial macrophage activation, function, and subsets are related to pain severity in OA is not well understood, high-throughput tools including single-cell RNA sequencing are beginning to reveal cellular and molecular profiles in OA synovial tissues,^{12,20} allowing us to investigate the relationship between synovial cell subsets and pain. For example, one study found that distinct fibroblast subtypes isolated from painful joint sites were associated with a neuroplastic profile (eg, neuronal cell survival and neurite outgrowth),²¹ although synovial immune cells were not studied and detailed molecular data linking synovial immune profiles to clinically relevant pain experiences is lacking.

In this study, we provide the first combined spatial transcriptomic and/or proteomic and single-cell RNA-sequencing analyses of synovial tissues focused on pain in OA. Our objective was to identify synovial macrophage subsets associated with worse pain in patients with knee OA and pathophysiologic mechanisms in synovial lining, sublining, and microvascular microenvironments.

MATERIALS AND METHODS

Study participants and subgroup selection.

Participants with symptomatic, radiographic late-stage knee OA (Kellgren-Lawrence [KL] grades 3 or 4),²² pain (ranging from mild to severe), and compromised function warranting total knee arthroplasty or high tibial osteotomy were included. All patients fulfilled the American College of Rheumatology classification criteria.²³ Patients who received joint injections within six months before surgery were not included. We recruited sequential patients scheduled for surgical intervention, which permitted collection of synchronized demographics, patient-reported measures of pain, and synovial histopathology data in this cross-sectional study. Participants provided written informed consent, and the cohort was approved by Western University's Research Ethics Board for Health Sciences Research Involving Human Subjects (number 109255) and complied with the Declaration of Helsinki. Reporting was aligned with Strengthening the Reporting of Observational Studies in Epidemiology guidelines.²⁴

A subgroup of 32 patients ($n = 16$ more pain; and $n = 16$ less pain) was selected from the cohort for spatial profiling using GeoMx from NanoString. The subgroup was selected first by splitting the cohort into upper (least pain) and lower (most pain) quartiles of Knee Injury and OA Outcome Score (KOOS) pain subscale score. Based on our regression analysis, we selected

patients with more severe pain and worse perivascular edema (more severe disease and tissue damage) and patients with less pain and less perivascular edema. Then, 16 patients with cores that provided adequate tissue to sample three different synovial tissue microenvironments of interest were selected from the upper and lower KOOS pain quartiles. A subgroup of eight patients ($n = 4$ more pain; $n = 4$ less pain) analyzed by spatial profiling were selected to also undergo single-cell sequencing.

Patient-reported outcome measures of pain.

Participants completed the KOOS Pain subscale (9 items: 0–100), in which lower scores indicate worse pain. The KOOS is valid and reliable for individuals with knee OA.^{25,26} A clinically important difference in KOOS is defined as a change in 8.0 to 10.0 points.²⁷

Synovial tissue histopathology. Synovial tissue biopsies were collected during surgery from the lateral suprapatellar recess. Serial sections (5- μ m thick) spanning a total of 500 μ m of tissue were stained with hematoxylin and eosin. Synovial tissue samples were graded, including two to five sections (at least 100 μ m apart) per patient, by assessing six features of synovial histopathology as previously described²⁸: (1) synovial lining thickness, (2) subsynovial infiltrate, (3) vascularization, (4) surface fibrin deposition, (5) fibrosis, and (6) perivascular edema. The grades for each tissue section per patient were averaged for each individual histopathological feature and then binned into the following categories: category 1 is none or normal (average grade < 0.5); category 2 is mild (average grade between 0.5 to 1.5); and category 3 is moderate or severe (average grade > 1.5).

Spatial profiling of gene and protein expression.

Three synovial tissue anatomic microenvironment regions of interest (ROIs) were defined as follows: (1) synovial lining, (2) subintima, and (3) microvessel. Therefore, 96 ROIs comprising three different synovial microenvironments from a total of 32 patients were analyzed using both whole-transcriptome spatial profiling and predefined protein panels in parallel. The synovial tissue microenvironment ROIs were selected using known morphologic markers, including nuclei (DAPI), CD68 (macrophages), CD45 (hematopoietic cells), and smooth muscle actin (microvessels). Each ROI included a minimum of 200 cells.

The GeoMX predefined protein profiling consisted of 132 targets across 11 panels: immune activation status, immune cell typing, pan-tumor, immuno-oncology drug target, cell death, MAPK signaling, phosphatidylinositol 3-kinase/protein kinase B signaling, myeloid, autophagy, neural cell profiling, and glial cell subtyping. A full list of protein targets can be found in Supplementary Protein Profiling Targets File. Full details regarding synovial tissue dissociation into single-cell suspension, single-cell RNA library preparation, and single-cell sequencing can be found in Supplementary Materials and Methods.

Analysis of single-cell sequencing data. Alignment was conducted to the GRCh38.p13 (2020-A), reference genome and filtering, barcoding, and unique molecular identifier counting were performed using Cell Ranger version 6.1.1 and the 10x Genomics recommended default parameters. All downstream processing and analysis steps on the feature-barcode matrixes were performed in the R package Seurat version 4.1.0. Full details on single-cell workflow can be found in Supplementary Materials and Methods.

Phagocytosis assay. Phagocytic index was measured in synovial macrophage isolated from a subset of patients reporting more pain ($n = 8$) and less pain ($n = 8$). We used the Phagocytosis Assay Kit (number 500290), according to the manufacturer's protocol (Caymen Chemical Company). Phagocytic index was defined as the number of CD68+ macrophages containing one or more phagocytosed fluorescein isothiocyanate+ beads as a proportion of total CD68+ macrophages. Full details can be found in Supplementary Materials and Methods.

Rat dorsal root ganglia explant stimulation. A total of 32 dorsal root ganglia (DRGs) harvested from 18-week-old naive male Sprague Dawley rats were stimulated for 72 hours with one of the following: (1) media conditioned by synovial cells with more pain ($n = 8$), (2) media conditioned by synovial cells from patients with less pain ($n = 8$), (3) lipopolysaccharide (LPS) (200 ng/mL; $n = 8$), or (4) unconditioned complete RPMI media (RPMI, 10% fetal bovine serum, and 1% penicillin/streptomycin; $n = 8$). LPS is a potent inflammatory mediator and has been used to induce pain sensitivity and neuroinflammation^{29–31} and affect neuronal cell morphology in preclinical studies^{31,32} and was therefore used as a positive control. DRG cell bodies were immunolabeled for cleaved caspase 3 (CC3), a marker of cell stress, and DRG-supporting cells were labeled with ionized calcium-binding adapter molecule 1 (Iba1), a marker of immune cell activation. Full details can be found in Supplementary Materials and Methods.

Statistical analyses. *Synovial histopathology and pain outcomes.* We fitted a series of multivariate linear regression models to evaluate the associations between features of synovial histopathology and patient-reported outcomes measures of pain (KOOS Pain subscale scores). Results were reported as unstandardized β -coefficients with 95% confidence intervals (CIs). Full details of statistical analyses can be found in Supplementary Materials and Methods.

GeoMX spatial profiling analysis. All analyses were completed in NanoString's GeoMX Analysis Suite (version 2.5.0.145). Differentially expressed genes or proteins were identified in each synovial microenvironment (lining, subintima, and microvessel) using linear mixed modeling while adjusting for patient identifier and body mass index (BMI) and with a

Benjamini-Hochberg correction to control for false discovery rate. Full details can be found in Supplementary Material and Methods.

Phagocytic index of synovial macrophages. Phagocytic index of synovial macrophages was compared between groups of patients with more pain ($n = 8$) and less pain ($n = 8$) using an unpaired t -test. Results are presented as means with 95% CIs.

CC3 and Iba1 quantification in cultured DRGs. Percentage of CC3+ cell bodies and Iba1+ supporting cells were compared between patients reporting more pain ($n = 8$) and less pain ($n = 8$) and the unconditioned negative control group ($n = 8$) or LPS-stimulated positive control group ($n = 8$) using unpaired one-tailed t -tests. Results are presented as mean with 95% CIs.

Data availability. All single-cell RNA-sequencing data and spatial profiling data are publicly available via the NCBI GEO using the accession numbers GSE248453, GSE248454, and GSE248455. Other data and analytic codes are available upon reasonable request.

RESULTS

Out of 125 participants screened for eligibility, synovial biopsy was obtained for 122 participants and included in the primary analysis. Study participant demographics and clinical characteristics are shown in Table 1 for the (1) total cohort, (2) spatial profiling, and (3) single-cell RNA-sequencing subgroups of patients with more versus less pain. Frequency of pain medication prescription is shown in Supplementary Table 1.

Association between worse pain and synovial tissue perivascular edema. Regression analyses were performed while controlling for confounding variables to determine which features of synovial histopathology are associated with worse pain. Perivascular edema was strongly associated with worse KOOS pain that was likely clinically meaningful (-10.76 ; 95% CI -18.90 to -2.61) (Table 2), suggesting that pain may be related to synovial microvascular dysfunction.

Spatial profiling analysis of synovial microenvironments. We next used spatial profiling of synovial lining, sublining, and microvascular compartments to identify pathophysiologic processes associated with worse OA pain. Subgroups of patients with severe pain or mild-to-moderate KOOS pain and perivascular edema scores were matched on sex, BMI, and radiographic joint damage (KL grade), providing 16 patients from each subgroup for spatial transcriptomic and proteomic analyses. The subgroups had similar demographics to the total cohort (Table 1). As expected, patients with worse pain had higher histopathological scores for perivascular edema, lower histopathological scores for immune infiltrate, and were younger compared with patients with less pain, in keeping with more severe OA disease. The means and distributions of sex,

Table 1. Patient demographics and clinical characteristics for total cohort and digital spatial profiling and single-cell RNA-sequencing subgroups*

Characteristics	Total cohort (n = 122)	Spatial profiling subgroups		scRNAseq subgroups	
		Less pain (n = 16)	More pain (n = 16)	Less pain (n = 4)	More pain (n = 4)
Age, mean \pm SD (range), years	67.1 \pm 8.5 (41–85)	73.1 \pm 5.1 (60–80)	65.4 \pm 7.5 (55–79)	74.5 \pm 5.5 (67–80)	64.8 \pm 4.7 (59–69)
Sex, n (%)					
Women	58 (47.5)	7 (43.8)	6 (37.5)	2 (50.0)	2 (50.0)
Men	64 (52.5)	9 (56.2)	10 (62.5)	2 (50.0)	2 (50.0)
BMI, mean \pm SD (range)	32.7 \pm 5.5 (21.1–47.2)	33.1 \pm 4.9 (24.8–40.3)	33.1 \pm 5.1 (25.9–47.2)	30.1 \pm 6.8 (24.8–40.0)	29.2 \pm 2.9 (25.9–32.7)
KL grade, n (%)					
Grade 3	48 (39.3)	8 (50.0)	8 (50.0)	0 (0.0)	2 (50.0)
Grade 4	74 (60.7)	8 (50.0)	8 (50.0)	4 (100.0)	2 (50.0)
KOOS Pain, mean \pm SD (range), 0–100	47.2 \pm 15.7 (0–89)	60.6 \pm 12.1 (42–89)	37.8 \pm 10.0 (19–53)	62.8 \pm 5.3 (56–67)	34.5 \pm 10.9 (19–44)
Histopathology, mean \pm SD (range)					
Lining thickness	0.8 \pm 0.8 (0–3)	1.0 \pm 0.8 (0–3)	0.9 \pm 1.0 (0–3)	0.8 \pm 1.0 (0–2)	0.8 \pm 1.0 (0–2)
Subsynovial infiltrate	1.1 \pm 0.8 (0–3)	1.8 \pm 0.9 (0–3)	0.9 \pm 0.6 (0–2)	2.3 \pm 1.0 (1–3)	1.0 \pm 0.0 (1–1)
Vascularization	2.0 \pm 0.9 (0–3)	1.7 \pm 1.0 (0–3)	2.7 \pm 0.5 (2–3)	2.3 \pm 1.0 (1–3)	2.3 \pm 0.5 (2–3)
Fibrin	0.9 \pm 0.4 (0–1)	0.9 \pm 0.3 (0–1)	0.9 \pm 0.3 (0–1)	1.0 \pm 0.0 (1–1)	0.8 \pm 0.5 (0–1)
Fibrosis	1.1 \pm 0.7 (0–3)	1.2 \pm 0.7 (0–3)	1.3 \pm 0.5 (0–3)	1.1 \pm 0.5 (1–2)	1.3 \pm 0.5 (1–2)
Perivascular edema	0.6 \pm 0.7 (0–3)	0.0 \pm 0.0 (0–0)	1.6 \pm 0.6 (0–3)	0.0 \pm 0.0 (0–0)	2.3 \pm 0.5 (2–3)

* Synovial histopathology scores are reported as the mean of median scores for each feature. Lower KOOS pain scores indicate worse pain. BMI, body mass index; KL, Kellgren-Lawrence; KOOS, Knee Injury and Osteoarthritis Outcome Score; scRNAseq, single-cell RNA sequencing.

KL grade, and BMI were similar among groups, indicating effective matching.

Representative images of the synovial microenvironment ROIs analyzed by spatial profiling as well as differential gene and protein expression of patients with more pain are shown in Figure 1. Genes involved in mitochondrial stress response and regulation of processes such as angiogenesis, vessel maintenance, wound healing, and neurite outgrowth were increased in patients with more pain, whereas genes involved in regulation of innate immune signaling were decreased. Proteins involved in immune exhaustion, cellular response to stress, apoptosis, and wound healing were increased in patients with worse pain, whereas cell surface markers of myeloid and T lymphocytes, immune signaling, and cell growth and survival were decreased, corresponding to diminished innate immune cell content and diversity. A full list of differentially expressed genes from each ROI can be found in Supplementary File - GeoMX DE Lists.

Enrichment of Reactome gene sets in patients with worse pain for each synovial microenvironment are shown in Supplementary Table 2. In the synovial lining, enriched gene sets include those related to neuronal development and maintenance, cell metabolism, and regulation of angiogenesis. In the sublining, enriched gene sets include extracellular matrix (ECM) reorganization and fibrosis, neuronal regulation, immune signaling, and cell metabolism. In the microvascular compartment, enriched gene sets include neuronal regulation, ECM organization, fibrosis, and enrichment of many proinflammatory Toll-like receptor (TLR) cascades. Together, these data show that the synovial

microenvironments from patients with more pain express signaling pathways related to neurovascular remodeling, immune signaling, and profibrotic processes.

Table 2. Multivariate linear regression model estimates for KOOS pain and histopathological features of synovial inflammation and damage (n = 122)*

Predictor: histopathology	β -coefficient	SE	95% CI
Lining thickness			
<0.5	Reference	Reference	Reference
0.5–1.5	1.55	3.11	–4.61 to 7.72
>1.5	–4.32	4.28	–12.79 to 4.16
Subsynovial infiltrate			
<0.5	Reference	Reference	Reference
0.5–1.5	–2.45	4.01	–10.39 to 5.50
>1.5	2.30	4.71	–7.03 to 11.63
Vascularization			
<0.5	Reference	Reference	Reference
0.5–1.5	3.05	6.33	–9.49 to 15.60
>1.5	–0.62	5.45	–11.41 to 10.18
Fibrin			
<0.5	Reference	Reference	Reference
0.5–1.5	3.06	5.20	–7.24 to 13.36
>1.5	–	–	–
Fibrosis			
<0.5	Reference	Reference	Reference
0.5–1.5	3.65	3.38	–3.05 to 10.35
>1.5	3.00	4.31	–5.54 to 11.55
Perivascular edema			
<0.5	Reference	Reference	Reference
0.5–1.5	–4.70	2.85	–10.35 to 0.95
>1.5	–10.76	4.11	–18.90 to –2.61

* Adjusting for age, sex, and body mass index. CI, confidence interval; KOOS, Knee Injury and Osteoarthritis Outcome Score.

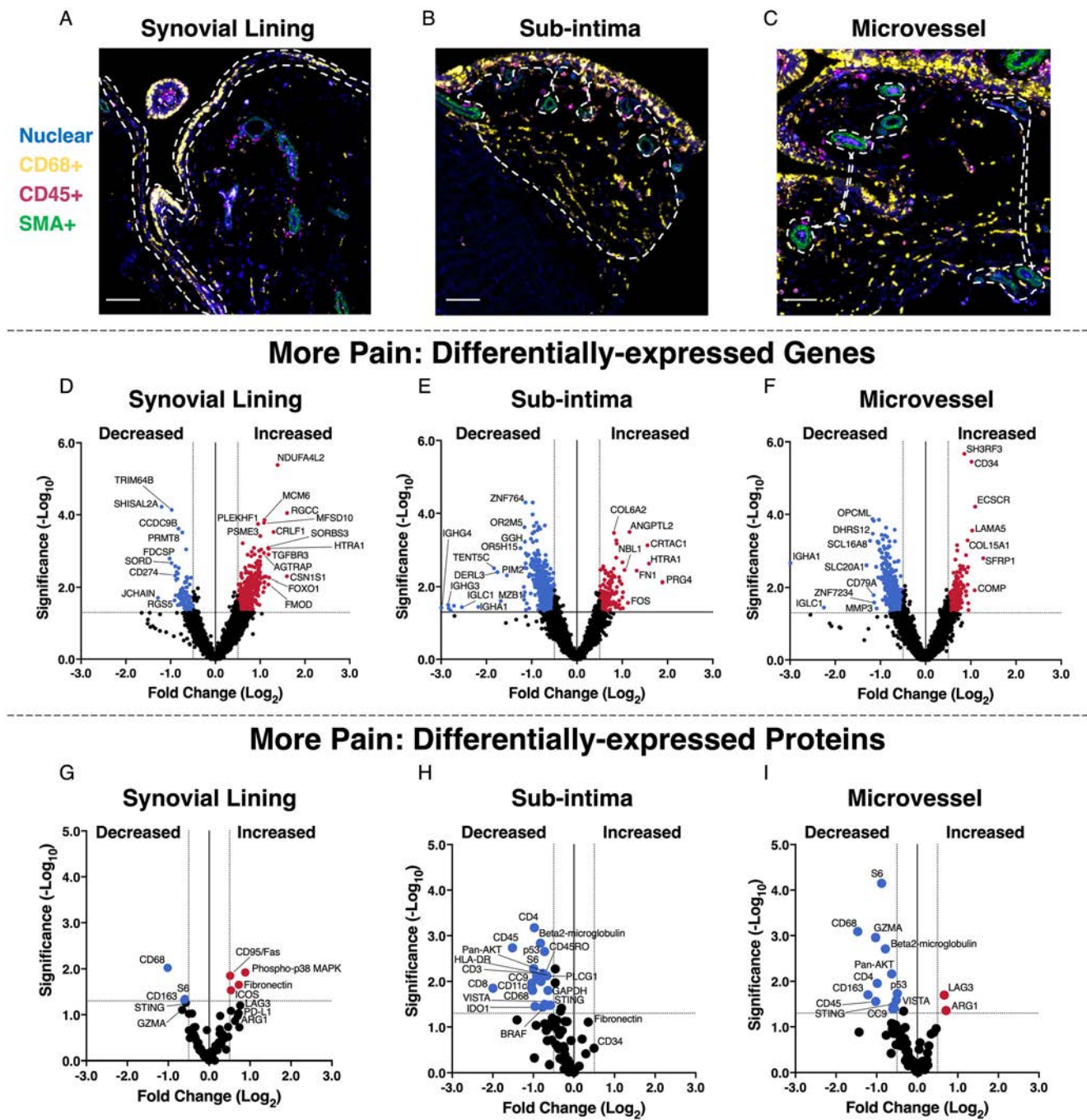


Figure 1. Spatial profiling of synovial lining, subintima, and microvessel microenvironments. (A–C) Representative images of the synovial microenvironment regions of interest. Immunofluorescence images from the spatial profiling analysis with morphology markers for CD68+ macrophages (yellow), CD45+ cells (magenta), SMA+ cells (green), and nuclear stain (blue). Representative synovial microenvironment regions of interest for (A) synovial lining, (B) subintima, and (C) microvessel are outlined with white, dashed lines. Scale bar = 100 μ m. Volcano plots displaying the top differentially expressed (increased vs decreased expression) (D–F) genes and (G–I) proteins for each synovial tissue microenvironment: synovial lining, subintima, and microvessel in patients with more pain (relative to less pain). Genes with increased expression in patients with more pain are represented by red dots, and genes with decreased expression in more pain are represented by blue dots. The y-axis represents the log₁₀ *P* value with cut-off set at 1.3 (*P* < 0.05), and the x-axis represents the log₂ fold change with cut-off set at 0.5. Differential gene expression (*n* = 16 per group) was derived by fitting linear mixed models while adjusting for patient ID and BMI and with a Benjamini-Hochberg correction to control for FDR. BMI, body mass index; CD45, hematopoietic cell marker; CD68, macrophage marker; FDR, false discovery rate; ID, identifier; SMA, smooth muscle actin vessel marker.

Cell deconvolution from spatial transcriptomics.

Because our gene expression data suggested that worse pain was associated with decreased innate and adaptive immune cells, we used deconvolution algorithms to estimate the proportion of each immune cell type present in each synovial microenvironment (Supplementary Figure 1). Patients with worse pain had a higher proportion of nonconventional and/or intermediate monocytes (mean difference 3.76%; 95% CI 0.53–6.99) in the synovial lining. In the subintima, there were higher proportions of macrophages (mean difference 8.16%; 95% CI 0.16–16.17) and fibroblasts (mean difference 11.2%; 95% CI 3.30–19.07) and lower proportions of plasma cells (mean difference –5.78%; 95% CI –10.52 to –1.04) and naive CD4+ T cells (mean difference –8.05%; 95% CI –13.15 to –2.96) and a similar trend for CD8+ memory T cells (mean difference –1.12%; 95% CI –2.3 to 0.07). In microvessels, there were higher proportions of fibroblasts (mean difference 8.53%; 95% CI 2.86–14.19) and endothelial cells (mean difference 7.73%; 95% CI 1.66–13.80) and lower proportions of CD8+ memory T cells (mean difference –2.32%; 95% CI –3.81 to –0.83) and neutrophils (mean difference –2.84%; 95% CI –4.66 to –1.02) and a similar trend for plasma cells (mean difference –2.79%; 95% CI –5.95 to 0.37). These data suggest that worse pain is associated with decreased immune cell diversity in synovial tissues.

Single-cell RNA-sequencing analysis. To investigate changes in immune cell profiles and crosstalk mechanisms associated with worse pain, we analyzed synovial cell profiles at the cellular level using single-cell RNA sequencing. The pain subgroups demonstrated similar demographics to the total cohort (see Table 1). Patients with more pain had higher histopathological scores for perivascular edema, a lower histopathological score for immune infiltrate, and were younger compared with patients with less pain.

We profiled a total of 14,522 synovial cells, comprising 15 distinct cell populations (Figure 2A), including myeloid and dendritic cells, lining and sublining fibroblasts, T cells, B cells, plasma cells, mast cells, endothelial cells, and mural cells. We observed large differences in the proportions of cell types between patients with worse pain compared with patients reporting less pain, especially in the myeloid and fibroblast subsets (Figure 2C). Patients reporting worse pain had fewer myeloid (–19.5%; 95% CI –32.3 to –6.8) and other immune cells but much higher proportions of lining (19.0%; 95% CI –7.9 to 45.9) and sublining (13.0%; 95% CI –5.3 to 31.4) fibroblasts, endothelial cells, and mural cell clusters (Supplementary Table 3). These data corroborate the spatial profiling findings and suggest that lower immune cell diversity and expansion of fibroblast subsets are important features in synovial tissues from patients experiencing worse pain.

Next, we conducted cell type-specific analyses to identify differences in myeloid cell and fibroblast (Figure 2D–K) subtypes and gene expression between patients reporting more versus

less pain. We identified four myeloid subtypes previously described by Huang et al, including transitional macrophages (T-MΦ, expressing both proinflammatory and immune-resolving genes), interferon-stimulated macrophages (IFNS-MΦ, expressing interferon-related genes), S100A8^{hi} macrophages (highly expressing S100A8; S100A8+), and immune-regulatory macrophages (IR-MΦ).²⁰ We also identified lining macrophages (expressing proteoglycan 4 [*PRG4*], secreted protein acidic and cysteine rich [*SPARC*], chloride intracellular channel 5 [*CLIC5*], and V-set and immunoglobulin containing 4 [*VSIG4*]), lymphatic vessel endothelial hyaluronan receptor 1 (LYVE1+) macrophages, dendritic cells, proliferating macrophages, mast cells, and a non-specific macrophage cluster we were unable to further classify. Strikingly, patients with worse pain had a reduction in all immune cell subtypes except the LYVE1+ macrophages, which were increased, and an almost complete absence of IFNS-MΦ and IR-MΦ (Figure 2E).

Similarly, we identified eight subtypes of fibroblasts, including lining fibroblasts (PRG4, CD55, and collagen type XXII α-1 chain), leucine-rich repeat containing 15 (LRRC15+) lining, senescent lining (calponin-1, cyclin-dependent kinase inhibitor 1A, regulator of G protein signaling 16, and G protein-coupled receptor 1), sublining progenitor (dipeptidylpeptidase 4, peptidase inhibitor 16, and CD34), perivascular sublining (midkine and ANGPT1), HLA-DRA^{hi}, intermediate fibroblasts (PRG4 and Thy-1 cell surface antigen), and a nonspecific fibroblast cluster that did not correspond to any previously reported fibroblast gene signatures (Figure 2F). LRCC15+ lining, senescent lining, and sublining progenitor fibroblasts were increased in patients with worse pain (Figure 2G).

To determine if myeloid and fibroblast subsets demonstrate different physiologic states between patients with worse pain versus less pain, we assessed differentially expressed genes between pain groups and performed gene set enrichment analysis (Figure 2H–K). Numerous processes related to neurovascular signaling and remodeling, proinflammatory innate immune signaling pathways, immune regulation, extracellular matrix remodeling, and cell stress and metabolism were positively enriched in myeloid cells (Figure 2I) and fibroblasts (Figure 2K) from patients with worse pain. Collectively, these results demonstrate that patients with worse pain exhibit striking reductions in immune and regulatory myeloid cell subsets and increases in senescent and sublining fibroblast subsets, in association with increased transcriptional signatures relevant to proalgesic, proinflammatory, neurovascular remodeling, and profibrotic processes.

Immune-stromal crosstalk profiles. Considering that myeloid and stromal cells are known to communicate in wound healing and other disease contexts, we hypothesized that crosstalk between immune and stromal cells may be dysregulated in patients with worse pain. Patients with more pain showed a lack

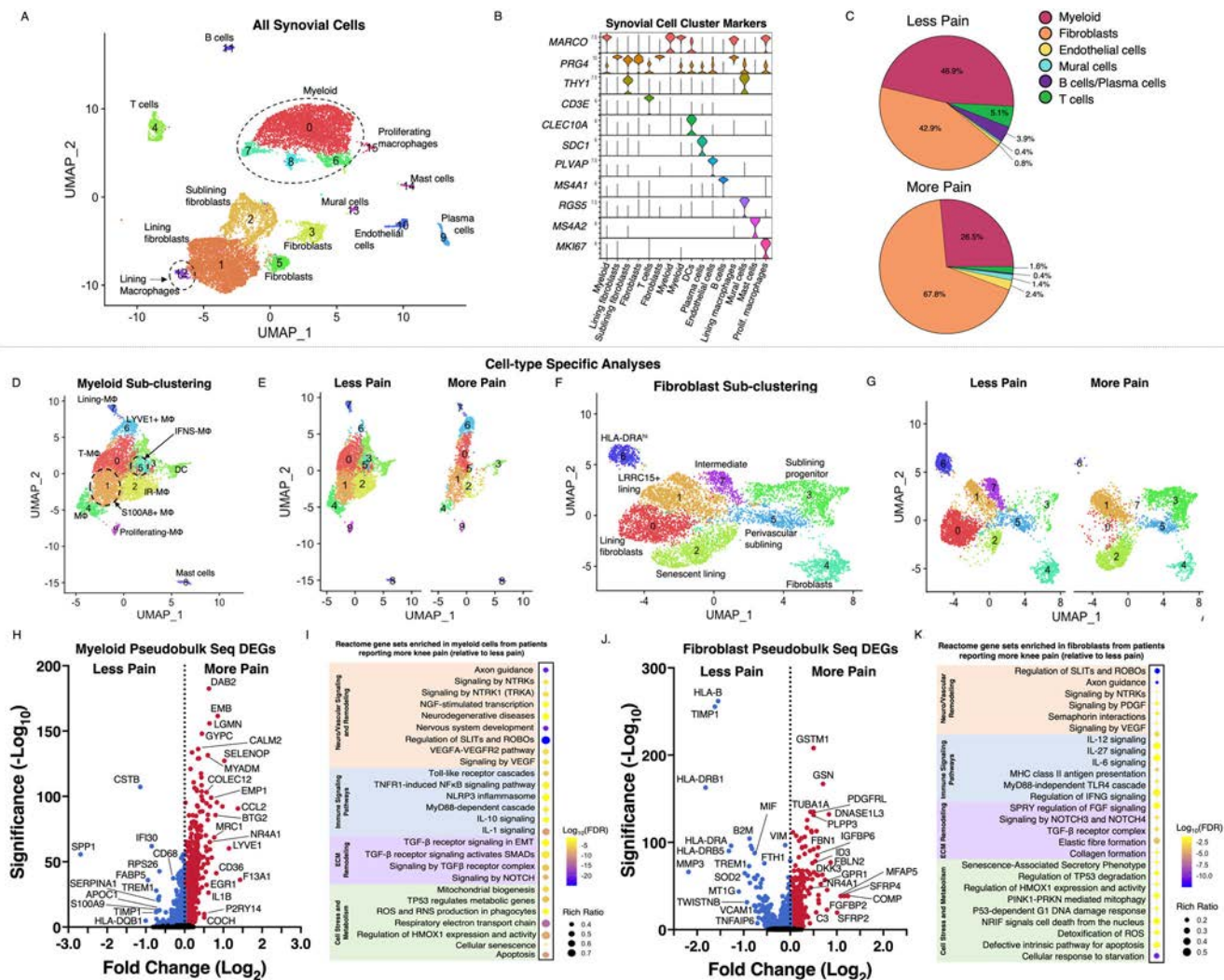


Figure 2. Single-cell transcriptomics of OA synovium from patients with more versus less pain. (A) UMAP plot of synovial cell clusters annotated by cell types. (B) Expression level of the selected marker(s) used for identification of each cluster. (C) Proportion of main cell types in patients reporting "less pain" (n = 4) and patients reporting "more pain" (n = 4). (D–K) Cell type-specific analyses for myeloid cells and fibroblasts. (D) Subclustering of myeloid cells plotted on UMAP and annotated by subtype: T-MΦ, IFN-γ-MΦ, IR-MΦ, and S100A8+ macrophages (S100A8^{hi}). (E) Myeloid subclustering UMAPs plotted by pain group. (F) Subclustering of fibroblast cells plotted on UMAP and annotated by subtype: lining fibroblasts, LRRC15+ lining, senescent lining, sublining progenitor, fibroblasts, perivascular sublining, HLA-DRA^{hi} fibroblasts, and intermediate fibroblasts. (G) Fibroblast subclustering UMAPs plotted separated by pain group. (H) Volcano plot of differentially expressed genes from myeloid pseudobulk analysis. (I) Bubble plot of Reactome gene sets enriched in myeloid cells from more pain relative to less pain. (J) Volcano plot of differentially expressed genes from fibroblast pseudobulk analysis. (K) Bubble plot of Reactome gene sets enriched in fibroblasts from more pain relative to less pain. DC, dendritic cell; DEG, differentially expressed gene; EMT, epithelial–mesenchymal transition; IFN-γ-MΦ, interferon-stimulated macrophage; IL, interleukin; IR-MΦ, immune-regulatory macrophage; LRRC15+, leucine-rich repeat containing 15; MHC, major histocompatibility complex; NGF, nerve growth factor; NTRK, neurotrophic tyrosine receptor kinase; OA, osteoarthritis; PDGF, platelet-derived growth factor; ROBO, roundabout homolog; SLIT, slit guidance ligand; RNS, reactive nitrogen species; ROS, reactive oxygen species; T-MΦ, transitional macrophage; TGF, transforming growth factor; TLR, Toll-like receptor; TNFR, tumor necrosis factor receptor; TRKA, tropomyosin-related kinase receptor A; UMAP, Uniform Manifold Approximation and Projection for Dimension Reduction; VEGFR, vascular endothelial growth factor receptor. Color figure can be viewed in the online issue, which is available at <http://onlinelibrary.wiley.com/doi/10.1002/art.43089/abstract>.

of semaphorin, heparan sulfate, ANGPTL, and vascular endothelial growth factor signaling and instead featured increases in PDGF, CD99, and visfatin crosstalk signaling mechanisms compared with patients with less pain (Supplementary Figure 2). These changes suggest that myeloid-fibroblast crosstalk involving vascular and neural regulatory signaling pathways in patients

with lower OA-related pain may be replaced by more pathologic fibrotic and dysregulated neurovascular physiology in patients experiencing worse pain. Although the reason for this change is not clear, it could relate to altered immune-regulatory cell function. Therefore, we further investigated the function of innate immune cells in synovial tissues.

Synovial macrophage function and innate immune exhaustion. The reduction in myeloid cell diversity in single-cell analyses combined with increased expression of immune exhaustion markers from spatial profiling analyses suggested that synovial macrophages may be dysfunctional or exhausted. To investigate whether worse pain is associated with synovial macrophages dysfunction, we measured phagocytic function of CD68+ synovial tissue macrophages in vitro following isolation from synovial tissues and recovery in monolayer culture. Synovial macrophages from patients with worse pain demonstrated a

lower phagocytic index (-19.42 ; 95% CI -35.96 to -2.89) compared with patients with less pain (Figure 3A and B). Functional annotation of the single-cell dataset showed that phagocytosis-related gene sets were expressed primarily by the T-M Φ and the IR-M Φ subsets of macrophages (Figure 3C) and that these subsets were reduced in patients with more pain (Figure 3D and 3E). Loss of phagocytic function in combination with increased expression of markers of exhaustion suggest that innate immune exhaustion in synovial macrophages occurs in patients with worse pain.

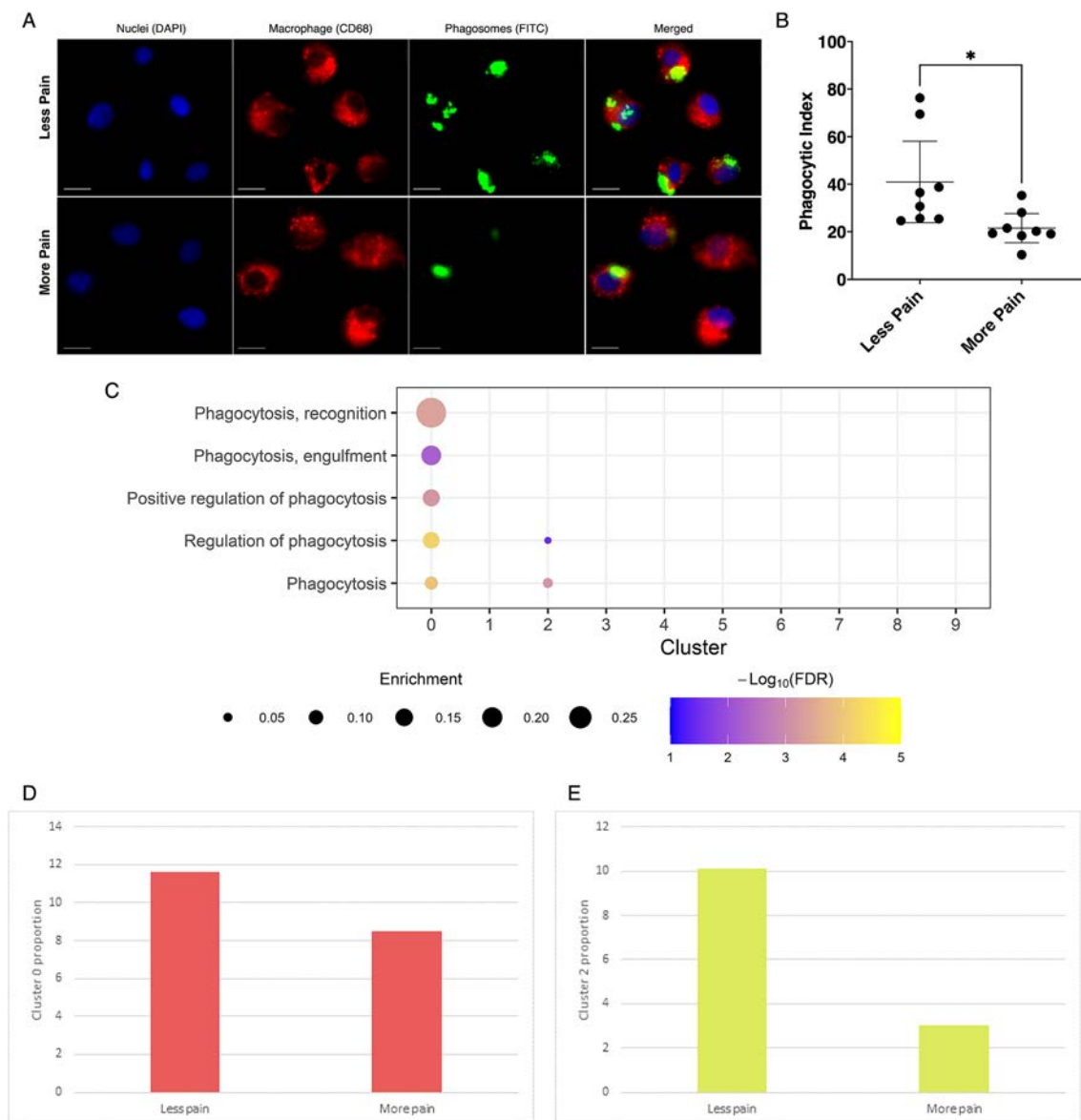


Figure 3. CD68+ macrophage phagocytic index among patients with more versus less pain. (A) Representative immunofluorescence images of CD68+ macrophages (red) and phagocytosing beads (green) from patients with more or less pain. (B) Dot plot displaying the individual measures of and mean \pm 95% CI phagocytic index for more pain ($n = 8$) and less pain ($n = 8$) groups. Phagocytic index is defined as the number of CD68+ macrophages with one or more phagocytosed beads out of the total number of CD68+ macrophages. An unpaired t -test was used to compare phagocytic index between groups. DAPI nuclear stain. Scale bar = 10 μ m. $*P < 0.05$. CD68, macrophage marker; CI, confidence interval; FDR, false discovery rate; FITC, fluorescein isothiocyanate latex bead marker. Color figure can be viewed in the online issue, which is available at <http://onlinelibrary.wiley.com/doi/10.1002/art.43089/abstract>.

DRG neuronal cell activation. Because synovial tissues from patients with worse pain contained dysfunctional macrophages and enrichment of neurovascular remodeling pathways, we investigated whether secreted factors from synovial cells influenced DRG neuronal cell activation (Figure 4) using organ cultures of rat lumbar DRGs. Media conditioned by synovial cells from patients with worse pain increased cleaved caspase-3 in neuronal cell bodies (13.72%; 95% CI 0.65–28.09) compared with unconditioned media (control), whereas DRGs stimulated with media conditioned by synovial cells from patients with less pain did not (Figure 4A–E). The percentage of Iba1+ supporting cells was similar among conditions (Figure 4A–D and F). Together, these findings suggest that synovial cells from patients with worse pain secrete factors that increase neuronal cell stress signals.

DISCUSSION

Synovitis measured by imaging is strongly associated with increased risk of pain and joint damage in OA. Although it is logical to assume that more inflammation is likely to worsen OA outcomes, we currently lack detailed information about the composition and cell-cell communication networks present in OA-related synovitis that are associated with worse OA pain. In this study, we combined spatial molecular profiling with single-cell RNA-sequencing analyses of synovial tissues to identify immunophenotypic and biologic mechanisms associated with worse pain in knee OA. Two major themes emerged in our findings. First, worse pain was associated with macrophage exhaustion, characterized by increased expression of cell exhaustion and cell stress markers, reduction in innate and adaptive immune cells, and impaired macrophage phagocytic function. Second, worse pain was also associated with increased expression of gene and protein markers and cell-cell communication pathways characteristic of neurovascular signaling and remodeling. This latter finding was strongly supported by a clinically meaningful association of pain with perivascular edema in synovial tissue histopathology. Further suggesting that worse pain outcomes in knee OA are linked to macrophage exhaustion and neurovascular remodeling, our ex vivo organ culture model of nociception in lumbar DRGs demonstrated that cells isolated from synovial tissues containing dysfunctional macrophages secrete factors that increase neuronal cell activation. These experiments therefore uncover an exciting and unexpected link to innate IR-M Φ , which may initially play protective roles but become dysfunctional or lost in patients with worse pain.

All patients included in this study had late-stage knee OA with severe enough symptoms to warrant surgical intervention. Despite this context, there was a very wide range of pain severity. This allowed us to strategically test associations of knee pain with synovial histopathology and identify pathophysiologic mechanisms associated with worse pain while controlling for potential

confounders. Synovial perivascular edema was associated with a clinically meaningful decrease (worse pain) in KOOS pain scores. Other histopathological signs of inflammation were not clearly associated with pain, which is likely because inflammation is a common feature among patients with active, symptomatic knee OA. Importantly, in other chronic diseases, perivascular edema indicates the transition from active inflammation to tissue damage.^{33,34} Accordingly, reducing or preventing synovial tissue damage might be an important treatment goal in OA. Moreover, these new findings implicate synovial microvascular dysfunction in OA pain experiences, which extends the published literature on angiogenic processes in OA.^{35–39}

Because single-cell sequencing and spatial profiling identified decreased innate and adaptive immune cells and suggested that innate immune cells, particularly macrophages, are dysfunctional in patients with more pain, we confirmed that synovial macrophages from patients with more pain have decreased phagocytic capacity. Impaired phagocytic function in synovial tissue macrophages would likely lead to poor clearance of tissue debris and cell turnover products in OA, which in turn could exacerbate proinflammatory and pain signaling through TLR and other DAMP-mediated mechanisms^{9,40} and drive synovial cell dysfunction. These results are well-aligned with a recent study in which we identified that synovial macrophages demonstrate impaired efferocytic capability, which can also be induced by exposure to OA synovial fluid from patients with worse pain and rescued by treatment with interleukin-4.⁴¹ Combined with our present findings, these data support the concept that the impaired synovial macrophage function may lead to poor tissue healing and worse pain but may be reversible.

Although innate immune synovial cell dysfunction has not previously been reported in the OA literature, existing knowledge from other disease contexts may help inform the potential role(s) of innate immune-regulatory cells in OA. Interestingly, we observed that a near-total lack of IR-M Φ in patients with worse pain was accompanied by expansion of LRCC15+ lining, senescent lining, and sublining progenitor fibroblasts. In the tumor microenvironment, LRCC15+ fibroblasts suppress tumor-infiltrating immune cells, thereby limiting their effector function.⁴² Accordingly, synovial macrophages might play a protective role in regulating and/or suppressing the expansion of pathologic fibroblast subsets in OA, whereas we found that synovial macrophages become exhausted in patients with more painful knee OA. Similarly, in RA, therapeutic enhancement of remission-maintaining (regulatory) macrophages in the synovium of patients with RA can aid in restoring synovial tissue homeostasis.⁴³ It is therefore possible that enhancing regulatory macrophages in OA might help to restore OA joint homeostasis. Underscoring the importance of macrophages to homeostasis, macrophages are also critically important for mitigating redox stress in tissues,⁴⁴ so macrophage exhaustion might also contribute to oxidative damage.

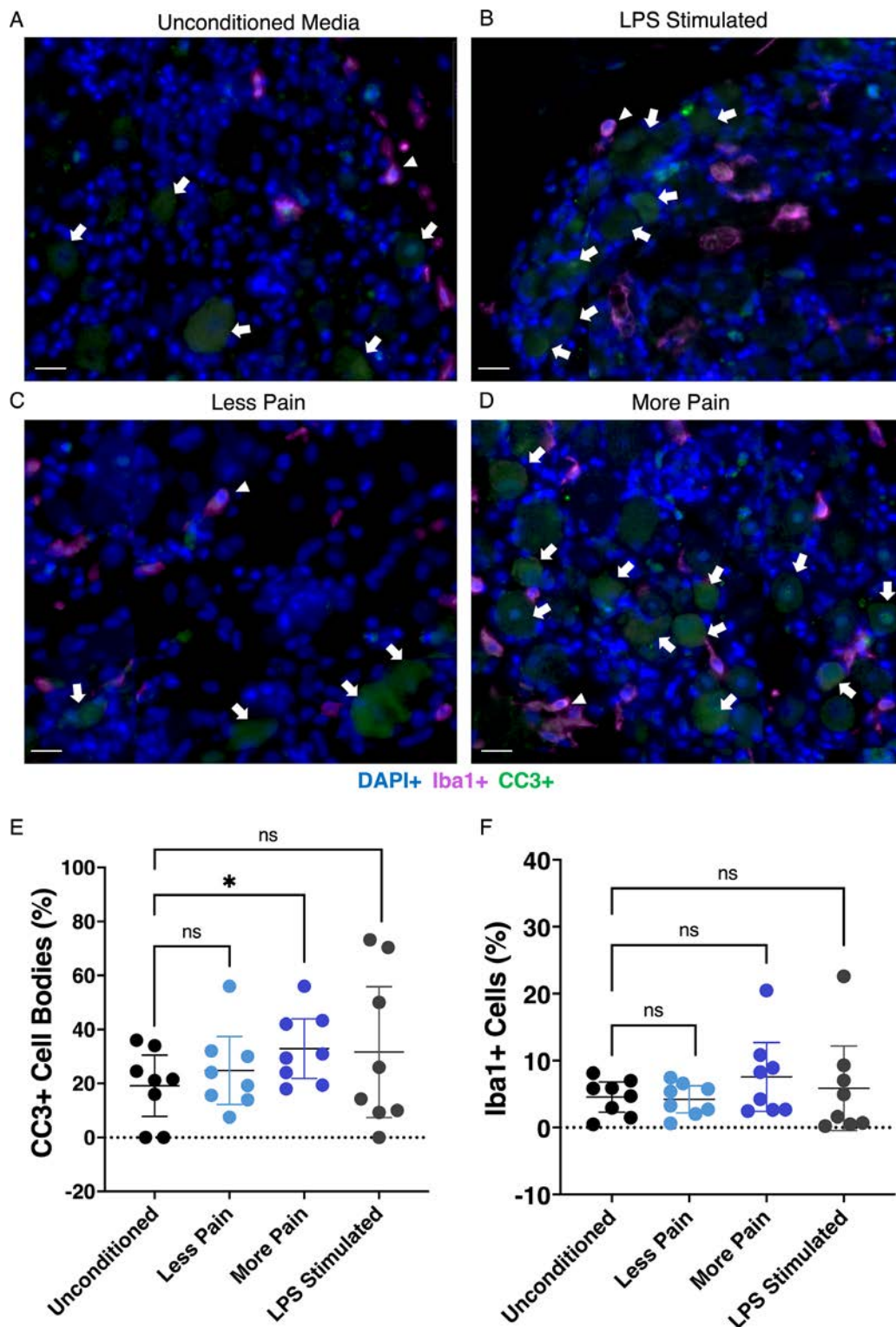


Figure 4. CC3 and Iba1 quantification in rat DRGs after stimulation with media conditioned by synovial cells from patients with more versus less pain. (A–D) Representative immunofluorescence images for each stimulation group ($n = 8$ per group). Groups are as follows: (A) unconditioned, (B) LPS stimulated, (C) less pain, and (D) more pain. Dot plots displaying the individual measures and mean \pm 95% CI of (E) CC3+ cell bodies (green) and (F) Iba1+ cells (magenta) per stimulation group. Unpaired t -tests were used to compare the percentage of positive cells between groups. White arrow and arrowhead indicate CC3+ cell bodies and Iba1+ cells, respectively. DAPI nuclear stain. Scale bar = 20 μm . * $P < 0.05$. CC3, cleaved caspase 3; CI, confidence interval; DRG, dorsal root ganglia; Iba1, ionized calcium-binding adapter molecule 1 activated microglia marker; LPS, lipopolysaccharide. Color figure can be viewed in the online issue, which is available at <http://onlinelibrary.wiley.com/doi/10.1002/art.43089/abstract>.

Neuronal and vascular remodeling is essential for joint homeostasis and wound healing.^{38,45} However, inappropriate neurovascular sprouting^{35,46,47} and microvascular dysfunction (ie, perivascular edema)^{28,48} occurs in OA joints, which we found were associated with worse pain. Our findings align with other recent studies that demonstrate neuroplastic transcriptomic profiles in the synovium.^{21,49} Nanus et al showed that factors secreted by synovial fibroblasts from patients with painful, early-stage OA joints promoted DRG neuronal cell survival and neurite outgrowth.²¹ Our findings support and extend upon this work, suggesting that neuronal plasticity pathways are driven by both fibroblasts and innate immune cells in patients with OA. Further, by demonstrating the ability of synovial cells to alter neuronal cell stress in vitro, these data also suggest that appropriate crosstalk among innate immune cells, fibroblasts, and sensory neurons may be required to prevent OA-related nociception. Understanding both pro- and antinociceptive crosstalk mechanisms should be a major priority for the field.

Our inferred cell-cell communication analysis provides some such insights. For example, myeloid cells participating in semaphorin and angiopoietin-like signaling may play key nociceptive roles in synovial tissues during OA. Semaphorin and angiopoietin-like signaling can regulate appropriate axon guidance, angiogenesis, and modulate immune cell function, inflammation, and metabolism during stressful states.^{50,51} Because myeloid and stromal cells are responsible for guiding angiogenic and neurogenic processes,^{18,52} loss of synovial myeloid cell diversity may shift the responsibility for carrying out these homeostatic functions to other synovial cell subtypes, contributing to inappropriate or dysfunctional neurovascular changes within the OA joint. Future longitudinal studies should investigate when and how synovial cell subpopulations are shifted or lost and whether restoring innate immune-regulatory function can improve neurovascular derangement and pain in OA. Additionally, immune-stromal crosstalk from patients with more pain was participating in visfatin signaling. Taken together with a recent study from Li and colleagues that identified common progenitors between synovium and fat pad in the joint,⁵³ this suggests there may be a role in adipose transformation of synovial cells in the more-pain context and should be explored further.

Limitations of our study include the cross-sectional design, precluding us from drawing conclusions about a causal relationship between synovial pathophysiology and the progression of knee OA pain. However, we expect that a causal relationship is likely based on similar findings in preclinical OA models. Furthermore, patients with worse pain in our study were younger with worse tissue damage, implying they had experienced faster disease and pain progression. Although neuronal cells were not represented in our cell-cell communication analysis, our in vitro findings validated that synovial cells from patients with worse pain can transactivate DRGs in culture, as predicted by our single-cell transcriptomic findings.

In conclusion, worse knee pain in OA is associated with macrophage exhaustion and microvascular dysfunction. Our findings suggest that different synovial cell subsets play opposing roles in OA-related pain. In particular, regulatory macrophage dysfunction and expanded senescent lining and sublining fibroblasts are exciting candidate mediators of OA-related pain pathophysiology. Because the synovium is critical for maintaining joint health and homeostasis, innate immune cell exhaustion may be a novel treatment target for preventing the progression of pain and joint failure in OA.

ACKNOWLEDGMENTS

The authors would like to acknowledge all members of the Western Ontario Registry for Early OA (WOREO) Knee Study research team and the participants in the WOREO Knee Study.

AUTHOR CONTRIBUTIONS

All authors contributed to at least one of the following manuscript preparation roles: conceptualization AND/OR methodology, software, investigation, formal analysis, data curation, visualization, and validation AND drafting or reviewing/editing the final draft. As corresponding author, Dr Appleton confirms that all authors have provided the final approval of the version to be published and takes responsibility for the affirmations regarding article submission (eg, not under consideration by another journal), the integrity of the data presented, and the statements regarding compliance with institutional review board/Declaration of Helsinki requirements.



REFERENCES

- Hill CL, Hunter DJ, Niu J, et al. Synovitis detected on magnetic resonance imaging and its relation to pain and cartilage loss in knee osteoarthritis. *Ann Rheum Dis* 2007;66(12):1599–1603.
- Neogi T, Guermazi A, Roemer F, et al. Association of joint inflammation with pain sensitization in knee osteoarthritis: the Multicenter Osteoarthritis Study. *Arthritis Rheumatol* 2016;68(3):654–661.
- Baker K, Grainger A, Niu J, et al. Relation of synovitis to knee pain using contrast-enhanced MRIs. *Ann Rheum Dis* 2010;69(10):1779–1783.
- Oo WM, Linklater JM, Bennell KL, et al. Are OMERACT knee osteoarthritis ultrasound scores associated with pain severity, other symptoms, and radiographic and magnetic resonance imaging findings? *J Rheumatol* 2021;48(2):270–278.
- Sarmanova A, Hall M, Fernandes GS, et al. Association between ultrasound-detected synovitis and knee pain: a population-based case-control study with both cross-sectional and follow-up data. *Arthritis Res Ther* 2017;19(1):281.
- Felson DT, Niu J, Neogi T, et al; MOST Investigators Group. Synovitis and the risk of knee osteoarthritis: the MOST Study. *Osteoarthritis Cartilage* 2016;24(3):458–464.
- Wang Q, Rozelle AL, Lepus CM, et al. Identification of a central role for complement in osteoarthritis. *Nat Med* 2011;17(12):1674–1679.
- Blom AB, van Lent PL, Libregts S, et al. Crucial role of macrophages in matrix metalloproteinase-mediated cartilage destruction during experimental osteoarthritis: involvement of matrix metalloproteinase 3. *Arthritis Rheum* 2007;56(1):147–157.

9. Lees S, Golub SB, Last K, et al. Bioactivity in an aggrecan 32-mer fragment is mediated via toll-like receptor 2. *Arthritis Rheumatol* 2015;67(5):1240–1249.
10. Scanzello CRPAC, Plaas A, Crow MK. Innate immune system activation in osteoarthritis: is osteoarthritis a chronic wound? *Curr Opin Rheumatol* 2008;20(5):565–572.
11. Robinson WH, Lepus CM, Wang Q, et al. Low-grade inflammation as a key mediator of the pathogenesis of osteoarthritis. *Nat Rev Rheumatol* 2016;12(10):580–592.
12. Wood MJ, Leckenby A, Reynolds G, et al. Macrophage proliferation distinguishes 2 subgroups of knee osteoarthritis patients. *JCI Insight* 2019;4(2):e125325.
13. Benito MJ, Veale DJ, FitzGerald O, et al. Synovial tissue inflammation in early and late osteoarthritis. *Ann Rheum Dis* 2005;64(9):1263–1267.
14. Geraghty T, Winter DR, Miller RJ, et al. Neuroimmune interactions and osteoarthritis pain: focus on macrophages. *Pain Rep* 2021;6(1):e892.
15. Haywood L, McWilliams DF, Pearson CI, et al. Inflammation and angiogenesis in osteoarthritis. *Arthritis Rheum* 2003;48(8):2173–2177.
16. Var SR, Shetty AV, Grande AW, et al. Microglia and macrophages in neuroprotection, neurogenesis, and emerging therapies for stroke. *Cells* 2021;10(12):3555.
17. Wang R, Liu Y, Ye Q, et al. RNA sequencing reveals novel macrophage transcriptome favoring neurovascular plasticity after ischemic stroke. *J Cereb Blood Flow Metab* 2020;40(4):720–738.
18. Du Cheyne C, Tay H, De Spiegelaere W. The complex TIE between macrophages and angiogenesis. *Anat Histol Embryol* 2020;49(5):585–596.
19. Wu CL, McNeill J, Goon K, et al. Conditional macrophage depletion increases inflammation and does not inhibit the development of osteoarthritis in obese macrophage Fas-induced apoptosis-transgenic mice. *Arthritis Rheumatol* 2017;69(9):1772–1783.
20. Huang ZY, Luo ZY, Cai YR, et al. Single cell transcriptomics in human osteoarthritis synovium and in silico deconvoluted bulk RNA sequencing. *Osteoarthritis Cartilage* 2022;30(3):475–480.
21. Nanus DE, Badoume A, Wijesinghe SN, et al. Synovial tissue from sites of joint pain in knee osteoarthritis patients exhibits a differential phenotype with distinct fibroblast subsets. *EBioMedicine* 2021;72:103618.
22. Kellgren JH, Lawrence JS. Radiological assessment of osteoarthritis. *Ann Rheum Dis* 1957;16(4):494–502.
23. Altman R, Asch E, Bloch D, et al; Diagnostic and Therapeutic Criteria Committee of the American Rheumatism Association. Development of criteria for the classification and reporting of osteoarthritis. Classification of osteoarthritis of the knee. *Arthritis Rheum* 1986;29(8):1039–1049.
24. von Elm E, Altman DG, Egger M, et al; STROBE Initiative. The Strengthening the Reporting of Observational Studies in Epidemiology (STROBE) statement: guidelines for reporting observational studies. *J Clin Epidemiol* 2008;61(4):344–349.
25. Ruysen-Witrand A, Fernandez-Lopez CJ, Gossec L, et al. Psychometric properties of the OARSI/OMERACT osteoarthritis pain and functional impairment scales: ICOAP, KOOS-PS and HOOS-PS. *Clin Exp Rheumatol* 2011;29(2):231–237.
26. Mehta SP, Sankar A, Venkataramanan V, et al. Cross-cultural validation of the ICOAP and physical function short forms of the HOOS and KOOS in a multi-country study of patients with hip and knee osteoarthritis. *Osteoarthritis Cartilage* 2016;24(12):2077–2081.
27. Roos EM, Lohmander LS. The Knee Injury and Osteoarthritis Outcome Score (KOOS): from joint injury to osteoarthritis. *Health Qual Life Outcomes* 2003;1(1):64.
28. Minten MJM, Blom A, Snijders GF, et al. Exploring longitudinal associations of histologically assessed inflammation with symptoms and radiographic damage in knee osteoarthritis: combined results of three prospective cohort studies. *Osteoarthritis Cartilage* 2019;27:71–79.
29. Nürnberger F, Ott D, Claßen R, et al. Systemic lipopolysaccharide challenge induces inflammatory changes in rat dorsal root ganglia: an ex vivo study. *Int J Mol Sci* 2022;23(21):13124.
30. Hsieh C-T, Lee Y-J, Dai X, et al. Systemic lipopolysaccharide-induced pain sensitivity and spinal inflammation were reduced by minocycline in neonatal rats. *Int J Mol Sci* 2018;19(10):2947.
31. Park S-Y, Han J-S. Neuroprotective effect of Bcl-2 on lipopolysaccharide-induced neuroinflammation in cortical neural stem cells. *Int J Mol Sci* 2022;23(12):6399.
32. D'Angelo B, Astarita C, Boffo S, et al. LPS-induced inflammatory response triggers cell cycle reactivation in murine neuronal cells through retinoblastoma proteins induction. *Cell Cycle* 2017;16(24):2330–2336.
33. Bruni C, Frech T, Manetti M, et al. Vascular leaking, a pivotal and early pathogenetic event in systemic sclerosis: should the door be closed? *Front Immunol* 2018;9:2045.
34. Varga J, Trojanowska M, Kuwana M. Pathogenesis of systemic sclerosis: recent insights of molecular and cellular mechanisms and therapeutic opportunities. *J Scleroderma Relat Disord* 2017;2(3):137–152.
35. Walsh DA, Bonnet CS, Turner EL, et al. Angiogenesis in the synovium and at the osteochondral junction in osteoarthritis. *Osteoarthritis Cartilage* 2007;15(7):743–751.
36. Ashraf S, Mapp PI, Walsh DA. Contributions of angiogenesis to inflammation, joint damage, and pain in a rat model of osteoarthritis. *Arthritis Rheum* 2011;63(9):2700–2710.
37. Ashraf S, Wibberley H, Mapp PI, et al. Increased vascular penetration and nerve growth in the meniscus: a potential source of pain in osteoarthritis. *Ann Rheum Dis* 2011;70(3):523–529.
38. Mapp PI, Walsh DA. Mechanisms and targets of angiogenesis and nerve growth in osteoarthritis. *Nat Rev Rheumatol* 2012;8(7):390–398.
39. Bonnet CS, Walsh DA. Osteoarthritis, angiogenesis and inflammation. *Rheumatology (Oxford)* 2005;44(1):7–16.
40. Miller RE, Ishihara S, Tran PB, et al. An aggrecan fragment drives osteoarthritis pain through Toll-like receptor 2. *JCI Insight* 2018;3(6):e95704.
41. Del Sordo L, Blackler GB, Philpott HT, et al. Impaired efferocytosis by synovial macrophages in patients with knee osteoarthritis. *Arthritis Rheumatol* 2023;75(5):685–696.
42. Krishnamurthy AT, Shyer JA, Thai M, et al. LRRC15+ myofibroblasts dictate the stromal setpoint to suppress tumour immunity. *Nature* 2022;611(7934):148–154.
43. Alivernini S, MacDonald L, Elmesmari A, et al. Distinct synovial tissue macrophage subsets regulate inflammation and remission in rheumatoid arthritis. *Nat Med* 2020;26(8):1295–1306.
44. Ryan DG, O'Neill LAJ. Krebs cycle reborn in macrophage immunometabolism. *Annu Rev Immunol* 2020;38(1):289–313.
45. McDougall JJ. Osteoarthritis is a neurological disease - an hypothesis. *Osteoarthritis Cartilage* 2019;1(1-2):100005.
46. Obeidat AM, Miller RE, Miller RJ, et al. The nociceptive innervation of the normal and osteoarthritic mouse knee. *Osteoarthritis Cartilage* 2019;27(11):1669–1679.
47. Suri S, Gill SE, Massena de Camin S, et al. Neurovascular invasion at the osteochondral junction and in osteophytes in osteoarthritis. *Ann Rheum Dis* 2007;66(11):1423–1428.

48. Philpott HT, Carter MM, Birmingham TB, et al. Synovial tissue perivascular edema is associated with altered gait patterns in patients with knee osteoarthritis. *Osteoarthritis Cartilage* 2022;30(1):42–51.
49. Bratus-Neuenschwander A, Castro-Giner F, Frank-Bertoncelj M, et al. Pain-associated transcriptome changes in synovium of knee osteoarthritis patients. *Genes (Basel)* 2018;9(7):338.
50. Alto LT, Terman JR. Semaphorin signaling, methods and protocols. In: Terman JR, ed. *Semaphorin Signaling*. Springer; 2017:1–25.
51. Santulli G. Angiopoietin-like proteins: a comprehensive look. *Front Endocrinol (Lausanne)* 2014;5:4.
52. Zigmond RE, Echevarria FD. Macrophage biology in the peripheral nervous system after injury. *Prog Neurobiol* 2019;173:102–121.
53. Li J, Gui T, Yao L, et al. Synovium and infrapatellar fat pad share common mesenchymal progenitors and undergo coordinated changes in osteoarthritis. *J Bone Miner Res* 2024;39(2):161–176.

Association of Therapies for Axial Spondyloarthritis on the Risk of Hip and Spine Fractures

Devin Driscoll,¹ Navya George,¹ Christine Peloquin,¹ S. Reza Jafarzadeh,¹  Jean W. Liew,¹ and Maureen Dubreuil² 

Objective. People with axial spondyloarthritis (axSpA) have increased fracture risk relative to the general population, possibly related to chronic inflammation. We assessed the impact of treatment with receiving tumor necrosis factor inhibitors (TNFis) and nonbiologic conventional synthetic disease-modifying antirheumatic drugs (csDMARDs) on hip and spine fractures in patients with axSpA, relative to receiving nonsteroidal anti-inflammatory drugs (NSAIDs).

Methods. We conducted a nested case–control study using 2006 to 2021 data from the Merative MarketScan Database. We included adults 18 to 65 years old with at least one inpatient or at least two outpatient axSpA International Classification of Diseases, Ninth Revision (ICD-9), or International Classification of Diseases, Tenth Revision (ICD-10), diagnosis codes separated by at least seven days. The primary outcome was hip and/or spine fracture, defined by ICD-9 or ICD-10 diagnosis or procedure codes. For each patient with fracture (cases), we selected up to 10 controls without fracture. We evaluated medication exposure (TNFis, csDMARDs, NSAIDs [referent], or none) hierarchically using pharmacy claims and procedure codes. We assessed the relation of medication exposure with hip and spine fracture risk using unconditional logistic regression with confounder adjustment.

Results. Our main analysis included 13,519 individuals with axSpA, comprising 1,229 patients with fracture and 12,290 controls. Individuals receiving TNFis had 29% lower odds of fracture compared to those receiving NSAIDs (odds ratio [OR] 0.71, 95% confidence interval [CI] 0.59–0.85), accounting for age, sex, and diagnosis year. Results were similar in the fully adjusted model (OR 0.75, 95% CI 0.62–0.91) and when stratified by sex.

Conclusion. Using a large US insurance claims database, we found evidence for a protective effect of receiving TNFis on fracture risk in patients with axSpA underscoring a potential impact of TNFis in diminishing comorbidities linked with axSpA.

INTRODUCTION

Axial spondyloarthritis (axSpA) is an inflammatory arthritis of the spine with a prevalence of up to 1% among US adults.¹ In addition to spinal involvement, those affected may have inflammation of the eyes, skin, or bowel, and nearly half of patients with axSpA can have peripheral joint arthritis.^{1,2} Radiographic axSpA (r-axSpA; formerly known as ankylosis spondylitis) is a subtype of axSpA with structural damage in the sacroiliac joints seen on

conventional radiography,³ whereas nonradiographic axSpA (nr-axSpA) is a subtype of axSpA without structural damage on conventional radiography.³ Approximately half of individuals with axSpA have large-joint, lower-extremity involvement (hip or knee).⁴

Fracture is an outcome of concern in axSpA given its association with morbidity and mortality.^{5,6} Individuals with r-axSpA have been shown to have increased risk for fractures compared to the general population, accounting for age and sex.^{6–8} A

Supported by the National Institute of Arthritis and Musculoskeletal and Skin Diseases, NIH (grants R03-AR-076495 and P30-AR-072571). Dr Liew's work was supported by the Rheumatology Research Foundation (RRF) Investigator Award, a Spondyloarthritis Research and Treatment Network pilot grant, and the Spondylitis Association of American Jane Bruckel Early Career Investigator Award. Dr Dubreuil's work was supported by the RRF and the Boston University Clinical and Translational Science Institute.

¹Devin Driscoll, MD, Navya George, MD, Christine Peloquin, MPH, S. Reza Jafarzadeh, DVM, MPVM, PhD, Jean W. Liew, MD, MS: Boston University Chobanian and Avedisian School of Medicine, Boston, Massachusetts; ²Maureen Dubreuil, MD, MSc: Boston University Chobanian and Avedisian School of Medicine and Veterans Affairs Boston Healthcare System, Boston, Massachusetts.

Additional supplementary information cited in this article can be found online in the Supporting Information section (<https://acrjournals.onlinelibrary.wiley.com/doi/10.1002/art.43082>).

Author disclosures are available at <https://onlinelibrary.wiley.com/doi/10.1002/art.43082>.

[Correction added on 30 April 2025, after first online publication: The text "those with" was deleted from the Objective section of the article abstract.]

Address correspondence via email to Maureen Dubreuil, MD, MSc, at mdubreuil@bu.edu.

Submitted for publication May 20, 2024; accepted in revised form November 22, 2024.

2017 meta-analysis showed that the risk of vertebral fracture in individuals with r-axSpA was doubled, whereas the risk of all non-vertebral fractures was increased by 10%.⁷ The increased risk for vertebral fractures is thought to be due to local bone remodeling in the spine, causing some areas of excess bone formation and stiffness with other areas of decreased bone density. The increased risk for nonvertebral fractures is thought to be due to systemic inflammation.^{8–10}

Mainstays of axSpA treatment, as per clinical practice guidelines, recommend reception of nonsteroidal anti-inflammatory drugs (NSAIDs) as first-line treatment and then tumor necrosis factor inhibitors (TNFis) for those who have persistently elevated disease activity.^{11–13} The reception of conventional synthetic disease-modifying antirheumatic drugs (csDMARDs) is not recommended to treat axial inflammation but can be used for peripheral arthritis.^{11,12} Other therapies, such as receiving interleukin (IL)-17 inhibitors and JAK inhibitors, are currently recommended for patients with axSpA following a lack of response or contraindications to receiving TNFis.^{11,12}

There is a paucity of data on the effects of treatment, specifically receiving TNFis, on aspects of axSpA beyond spinal inflammation. A Spanish population-based cohort study in 2014 found that regular reception of NSAIDs greatly attenuated fracture risk in individuals with axSpA.¹⁴ This study, however, did not look at the association of receiving csDMARDs and TNFis on fracture risk in this population. There also have been no large-scale studies assessing the effect of receiving TNFis on fracture risk in patients with axSpA despite some smaller studies suggesting increased bone density with receiving TNFis among patients with r-axSpA.^{15,16} Therefore, the goal of this study was to determine the effect of treatment by receiving TNFis and csDMARDs on fractures in patients with axSpA using a nested case-control study design with the hypothesis that receiving TNFis reduces the risk of fractures, relative to receiving NSAIDs.

PATIENTS AND METHODS

Data source. We used data from the Merative MarketScan Database, which consists of medical and drug data from employers and health plans.¹⁷ It contains data for over 250 million individuals, including employees, their spouses, and dependents, who are covered by employer-sponsored private health insurance in the United States.¹⁷ Because this study involved the analysis of pre-existing, deidentified data, it was deemed exempt from requiring Boston University Medical Campus Institutional Review Board approval (H-39098).

Study population. Claims were used to identify individuals with axSpA ages 18 to 65 years old from January 1, 2006, to December 31, 2021. A start date of January 1, 2006, was chosen because this reflects the period of time in which TNFis became more widely prescribed to patients with axSpA and

were incorporated into international treatment guidelines.¹⁸ The end date of our study was December 31, 2021. axSpA (including both r-axSpA and nr-axSpA) was operationally defined as at least one inpatient claim with an axSpA International Classification of Diseases, Ninth Revision (ICD-9), or ICD-10, diagnosis code or at least two outpatient claims at least seven days apart with axSpA diagnosis codes.^{19,20} Such algorithms for identification of axSpA have previously been shown to have high positive predictive values (PPVs; 88%–100%), indicating their ability to correctly identify axSpA when the condition is present.

Study design and outcomes of interest. We conducted a nested case-control study (Figures 1 and 2). Study entry date (disease date) was either the date of the first axSpA inpatient claim or the date of the second axSpA outpatient claim. Included were individuals who were observed until fracture (outcome), 65 years of age, coverage end date, or study end date (December 31, 2021). Follow-up ended at 65 years of age because individuals become Medicare eligible at this age, and the data set did not include services or prescriptions billed to Medicare.

The primary outcome of interest was composite hip and/or spine fracture, and the secondary outcome was spine fracture. Outcome definitions were based upon the algorithm by Wright et al.²¹ Hip fracture was defined as at least one inpatient ICD-9 or ICD-10 diagnosis code in any billing position or at least one outpatient ICD-9 or ICD-10 diagnosis code in any position plus a Current Procedural Terminology procedure code. Spine fracture was defined as one inpatient or outpatient ICD-9 or ICD-10 diagnosis code in any position. We did not require outcomes to be incident because two-thirds of spine fractures are asymptomatic and are diagnosed incidentally.²²

For each patient with a fracture, we selected up to 10 controls without fracture.²³ The index date for patients with fracture was the date of the first fracture claim and for controls, the index date was a random date from the corresponding patient's fracture year. Included individuals needed to have a year of continuous enrollment before their index date. The outcome assessment period was from disease date until the end of the continuous enrollment period.

Exposure of interest. The exposure of interest was treatment by receiving axSpA medication class within six months before the index date, based on pharmacy and medical claims data. Categories of medication class included TNFis, csDMARDs, NSAIDs (reference group), and no medication reception. Within a given medication class, drug reception was defined as receiving at least one prescription within the six months before the index date. For patients who received drugs from multiple medication classes, exposure was classified by the highest hierarchical group used, with the rankings defined, in order, as TNFis, csDMARDs,

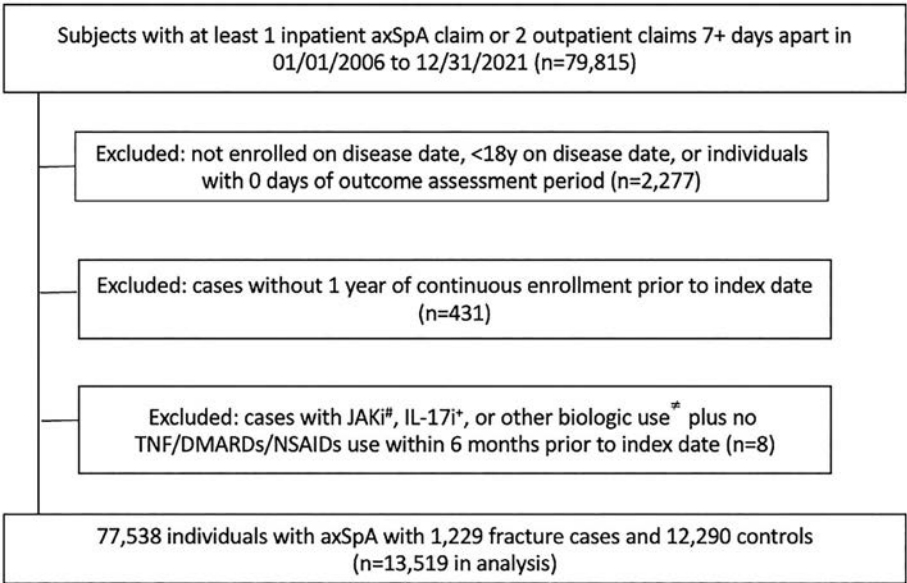


Figure 1. Selection of study population, patients with fracture (cases), and controls. axSpA, axial spondyloarthritis; DMARD, disease-modifying antirheumatic drug; IL-17i, interleukin-17 inhibitor; JAKi, JAK inhibitor; NSAID, nonsteroidal anti-inflammatory drug; TNF, tumor necrosis factor; y, years Sex/. [#]JAKis include abrocitinib, baricitinib, tofacitinib, and upadacitinib; ⁺IL-17is include ixekizumab and secukinumab; ^{*}≠ Other biologics include abatacept, anakinra, canakinumab, guselkumab, risankizumab, ustekinumab, sarilumab, and tocilizumab.

NSAIDs, no medication. JAK inhibitors and non-TNFi biologics (eg, IL-17 inhibitors) were not included in this study due to limited numbers of patients receiving them during this time period. We chose NSAIDs as the active comparator reference group given the treatment guidelines for axSpA recommend prescribing NSAIDs as the first-line therapy.^{11,12}

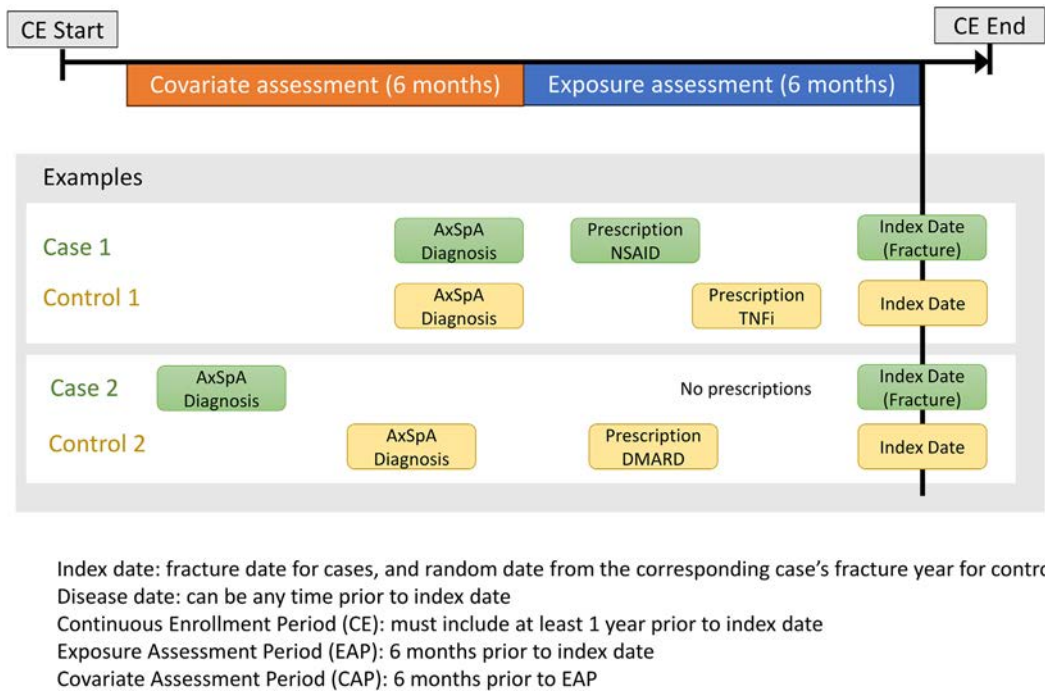


Figure 2. CE, EAP, and CAP in relation to index date and disease date. The index date is the fracture date for patients and the random date from the corresponding patient's fracture year for controls. The disease date can be any time before index date. The CE must include at least one year before the index date. The EAP is six months before the index date. The CAP is six months before the EAP. AxSpA, axial spondyloarthritis; DMARD, disease-modifying antirheumatic drug; NSAID, nonsteroidal anti-inflammatory drug; TNFi, tumor necrosis factor inhibitor.

Other covariates. Potential confounders for the relationship between axSpA medication class and fracture were identified a priori. Demographic confounders included age, sex, and diagnosis year for axSpA. Diagnosis year was included as a confounder because the year of axSpA diagnosis would influence medication choice and because previous research reported a temporal trend in fractures in individuals with axSpA.²⁴ Comorbidities associated with fracture risk included alcohol use disorder, body mass index (BMI), breast cancer, chronic kidney disease (CKD; stage 2 or higher), falls, inflammatory bowel disease, osteoporosis, prostate cancer, and tobacco use. Medication reception associated with fracture risk included receiving antiepileptic drugs, glucocorticoids, and osteoporosis medications (including antiresorptive and anabolic therapies). Surrogates of axSpA disease activity included erythrocyte sedimentation rate (ESR)/C-reactive protein (CRP) laboratory orders and health care use modeled as the number of primary care and rheumatology outpatient visits. Covariates were assessed within the six months before the exposure assessment period (covariate assessment period; Figure 2), except for age, BMI, and diagnosis year. Age was assessed on the index date, BMI was defined as the most recent value within the six months before the exposure assessment period and was a categorical variable (underweight, normal, overweight/obese, or missing data), and diagnosis year was modeled as a categorical variable defined as the four-year period during which an individual was diagnosed with axSpA (2006–2009, 2010–2013, 2014–2017, or 2018–2021).

Statistical analysis. We examined the odds of hip and/or spine fracture comparing axSpA medication class versus NSAID reception using unconditional logistic regression. Models were sequentially adjusted for age, sex, and diagnosis year in our minimally adjusted model, and all potential confounders were noted above in our fully adjusted model, which was our main analysis model. These analyses were conducted using SAS version 9.4. We did not match patients and controls because it is prohibitive in the case–control design and introduces confounding, rather than mitigating them, by the matching factor(s). Furthermore, matching in a case–control design limits inferences from the study to the matched sets, precluding the generalizability of inferences outside of the study sample.²⁵

To assess the robustness of our results, we performed the following sensitivity analyses: stratifying by sex, stratifying by fracture before disease date, and using csDMARDs as the reference group. When stratifying by sex, we omitted prostate cancer as a covariate for the female stratum. Because those with history of prior fracture are at heightened risk for recurrent fracture, we additionally examined potential effect modification by stratifying analyses based on history of prior hip or spine fracture. Given limited numbers, separate analysis for hip fracture alone was not conducted. These analyses were conducted using SAS, version 9.4.

The algorithm we used to capture fractures in administrative data was previously validated and noted to have a high PPV. However, due to its imperfect sensitivity, fractures may still be underdiagnosed. To formally assess how the imperfect sensitivity of the algorithm may have affected our effect measures, we performed a quantitative bias analysis for outcome misclassification. This estimated the odds ratio (OR) for the primary outcome if there was misclassification in detecting fractures by 10%, 20%, or 30%, corresponding to sensitivities of 90%, 80%, or 70%, respectively, while assuming 100% specificity (ie, that individuals without fractures are not diagnosed with fractures). These analyses were conducted using the R package *episensr*.²⁶

RESULTS

In the main analysis, we included 13,519 individuals with axSpA, comprising 1,229 patients with a hip or spine fracture and 12,290 controls (Figure 1; Table 1). The outcome of hip or spine fracture was present in 9.1% of the study sample (Figure 1). Among patients with fracture, the mean age was 53 years, with 38% being female. Compared to controls, patients with fracture had a higher frequency of fracture risk factors, including CKD, glucocorticoid reception, osteoporosis, receiving osteoporosis medications, and tobacco consumption but a lower frequency of ESR/CRP laboratory tests or rheumatology visits (Table 1).

Among patients with fracture, 25.1% received TNFis, 9.4% received csDMARDs, 17.9% received NSAIDs, and 47.6% did not receive any medication (Supplementary Table 1). After adjusting for age, sex, and diagnosis year, individuals receiving TNFis demonstrated 29% lower odds of fracture compared to those receiving NSAIDs (OR 0.71, 95% confidence interval [CI] 0.59–0.85; Figure 3; Supplementary Table 2). The result of the fully adjusted model was similar (OR 0.75, 95% CI 0.62–0.91; Figure 3). Individuals who received csDMARDs did not have a statistically significant lower odds of fracture compared to those who received NSAIDs in either the minimally or fully adjusted model (OR 0.96, 95% CI 0.76–1.23, and OR 0.93, 95% CI 0.72–1.19, respectively; Figure 3).

In sensitivity analyses, when comparing individuals who received TNFis to those who received csDMARDs as the reference group, there was a 26% decrease in odds of fracture when the model was minimally adjusted for age, sex, and diagnosis year (OR 0.74, 95% CI 0.58–0.92; Supplementary Table 3). Results were attenuated in the fully adjusted model (OR 0.81, 95% CI 0.64–1.02; Supplementary Table 3). With sex stratification, there were 462 patients with fracture (7.8%) among female patients, whereas there were 767 patients with fracture (10.1%) among the male patients (Supplementary Table 4). Female patients had higher frequencies of fracture risk factors compared to male patients. Female patients had decreased odds of fracture when receiving TNFis compared to receiving NSAIDs in the minimally

Table 1. Baseline demographics and clinical characteristics of the case-control sample of individuals with axSpA (main analysis)*

Characteristic	Patients with fracture, n (%)	Controls, n (%)
Total patients, n	1,229	12,290
Age, mean \pm SD, y	52.7 \pm 9.6	47.1 \pm 11.0
Year of axSpA diagnosis		
2006–2009	374 (30.4)	4,029 (32.8)
2010–2013	393 (32.0)	4,166 (33.9)
2014–2017	307 (25.0)	2,888 (23.5)
2018–2021	155 (12.6)	1,207 (9.8)
Female	462 (37.6)	5,464 (44.5)
Alcohol use disorder	23 (1.9)	69 (0.6)
BMI		
Underweight	0 (0.0)	12 (0.1)
Normal	12 (1.0)	83 (0.7)
Overweight/obese	139 (11.3)	1,064 (8.7)
Missing	1,078 (87.7)	11,131 (90.6)
Breast cancer	12 (1.0)	81 (0.7)
CKD	100 (8.1)	398 (3.2)
Falls	34 (2.8)	144 (1.2)
IBD	72 (5.9)	582 (4.7)
Osteoporosis	108 (8.8)	321 (2.6)
Prostate cancer	17 (1.4)	60 (0.5)
Tobacco use	80 (6.5)	391 (3.2)
Antiepileptic medication reception ^a	69 (5.6)	496 (4.0)
Glucocorticoid reception ^b	286 (23.3)	2,163 (17.6)
Osteoporosis medication reception ^c	67 (5.5)	225 (1.8)
ESR/CRP laboratory order	418 (34.0)	5,077 (41.3)
Primary care visit ^d	897 (73.0)	8,287 (67.4)
Rheumatology visit ^d	392 (31.9)	5,071 (41.3)

* axSpA, axial spondyloarthritis; BMI, body mass index; CKD, chronic kidney disease; CRP, C-reactive protein; ESR, erythrocyte sedimentation rate; IBD, inflammatory bowel disease.

^a Antiepileptic drugs are included in the supplementary materials.

^b Glucocorticoids are included in the supplementary materials.

^c Osteoporosis medications include alendronate, risedronate, etidronate, ibandronate, pamidronate, tiludronate, zoledronic acid, teriparatide, romosozumab, and denosumab.

^d Primary care and rheumatology visits were defined as the number of individuals with at least one visit that occurred any time within the covariate assessment period.

and fully adjusted model, similar to the main analysis (OR 0.73, 95% CI 0.52–1.01; fully adjusted Table 2). For male patients, minimally adjusted analysis revealed a 31% decrease (OR 0.69, 95% CI 0.55–0.87) in fracture odds for those receiving TNFis compared to receiving NSAIDs, and this significance persisted in the fully adjusted model (OR 0.77, 95% CI 0.60–0.99; Table 2).

When stratified by prior fracture history, there were 222 patients with fracture among those with history of prior fracture ($n = 330$), and 1,007 patients with fracture among those without a history of prior fracture ($n = 13,189$; Supplementary Table 4). Those with history of prior fracture had a higher frequency for fracture risk factors, including alcohol use disorder, CKD, falls, osteoporosis, reception of osteoporosis medication, and tobacco use. Those with a history of prior fracture had a lower frequency of ESR/CRP laboratory tests or rheumatology visits compared to those without a history of prior fracture. In the fully adjusted

analysis, among those with prior fracture, there was a trend toward reduced odds of fracture by 41% for those receiving TNFis compared to those receiving NSAIDs (OR 0.59, 95% CI 0.23–1.51; Table 3). Among those without a history of prior fracture, there was a trend toward reduced odds of fracture by 17% for those receiving TNFis compared to those receiving NSAIDs in the fully adjusted model (OR 0.83, 95% CI 0.67–1.03; Table 3). For the outcome limited to spine fracture ($n = 1,130$ patients with fracture and 11,300 controls; Supplementary Table 5), patients who received TNFis demonstrated a 27% decrease in odds for fracture compared to those who received NSAIDs after adjusting for age, sex, and diagnosis year (OR 0.73, 95% CI 0.61–0.89; Supplementary Table 6). This significant association persisted in the fully adjusted analysis (OR 0.81, 95% CI 0.66–0.99; Supplementary Table 6).

Results of the quantitative bias analysis, assuming a sizable 30% outcome misclassification (corresponding to 70% sensitivity of our algorithms for identifying fractures), showed that the OR for the primary outcome would be 0.62 (95% CI 0.51–0.74), similar to our observed crude OR of 0.63 for those receiving TNFis compared to those receiving NSAIDs. Results were similar when assuming 20% and 10% outcome misclassification. This confirms our assumption that regardless of the extent of misclassification in fractures due to the imperfect sensitivity of its algorithm, estimates of the OR remain unbiased due to the nondifferential nature of the outcome misclassification.

DISCUSSION

In our nested case-control study using data from a large US insurance claims database, we observed a protective association between TNFi reception and risk of hip and spine fractures among individuals with axSpA compared to those receiving NSAIDs. Although we found no discernible effect modification by sex, analyses stratified by history of prior fracture suggested a stronger protective effect for TNFi reception among those with a history of prior fracture. However, due to the limited sample size in each stratum, the clinical implications of this finding warrant further scrutiny. When specifically examining spine fractures, we identified a similar reduction in fracture odds among individuals with axSpA who received TNFis compared to those who received NSAIDs. Our data lend support for the reception of TNFi in the population with axSpA, suggesting a potential protective effect against future fractures.

Fracture constitutes a significant outcome in axSpA given its implications for morbidity and mortality and the heightened risk of both vertebral and nonvertebral fractures observed in individuals with axSpA compared to those without axSpA.^{5–7} Previous studies have reported fracture prevalence in individuals with axSpA ranging from 11% to 24.6%, whereas in our study, among a population of 77,538 individuals with axSpA, the frequency of fracture was 9.1%.²⁷ Sites of concern for fracture in individuals with

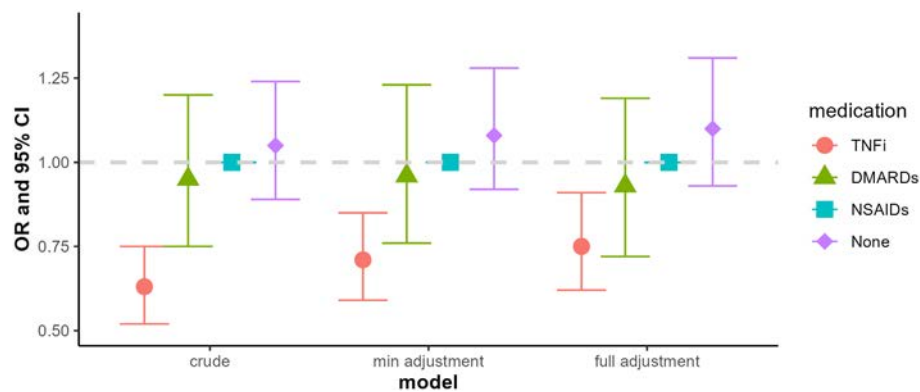


Figure 3. Odds of hip or spine fracture for crude, minimally, and fully adjusted analysis for receiving TNFis, csDMARDs, and no medication with NSAIDs as the referent. TNFis include etanercept, adalimumab, golimumab, certolizumab and infliximab. csDMARDs include apremilast, auranofin, azathioprine, chloroquine, cyclophosphamide, cyclosporine, gold sodium thiomalate, hydroxychloroquine, leflunomide, methotrexate, minocycline, mycophenolate, and sulfasalazine. The NSAID list is in the supplementary material. The minimally adjusted model is adjusted for age, sex, and diagnosis year. The fully adjusted model is adjusted for age, sex, disease year, alcohol use disorder, antiepileptic drug reception, body mass index, breast cancer, chronic kidney disease, falls, glucocorticoid reception, inflammatory bowel disease, osteoporosis, osteoporosis medication reception, prostate cancer, tobacco use, erythrocyte sedimentation rate/C-reactive protein laboratory orders, and number of outpatient visits (rheumatology and primary care). CI, confidence interval; csDMARD, conventional synthetic disease-modifying antirheumatic drug; DMARD, disease-modifying antirheumatic drug; NSAID, nonsteroidal anti-inflammatory drug; OR, odds ratio; TNFi, tumor necrosis factor inhibitor.

axSpA encompass both the spine and peripheral sites, including the hip and forearm. The risk for vertebral fracture in individuals with axSpA was found to be twice that of individuals without the disease, whereas the risk for hip or forearm fracture was observed to be elevated by 10% compared to those without axSpA.⁷ Despite the elevated risk of fractures in axSpA, there remains a paucity of literature investigating the impact of biologic therapies, particularly receiving TNFis, on fracture outcomes.

Randomized controlled trials are limited in their ability to study fracture outcomes due to the long duration of follow-up required.²⁸ Previous attempts to explore this relationship have been confined to small observational studies. For instance, van der Weijden et al²⁹ followed a cohort of 49 individuals with axSpA

who received TNFis for two years and noted an increase in bone mineral density (BMD) at the hip and spine during this period but with a concomitant rise in vertebral fractures. Similarly, Maas et al³⁰ and Beek et al¹⁶ studied cohorts of 104 and 131 individuals with axSpA, respectively, who received TNFis for four years. These studies demonstrated the development of new vertebral fractures despite improvements in BMD. A possible explanation for this is the overestimation of BMD using traditional anteroposterior lumbar dual x-ray absorptiometry screening in patients with axSpA with longstanding disease and syndesmophyte formation. However, because TNFi reception therapy is expected to prevent further vertebral structural changes, any increase in BMD should not be attributed to additional syndesmophyte formation.³¹ A

Table 2. Results of multivariable analyses assessing the relation of medication class exposure with hip and spine fracture risk among individuals with axial spondyloarthritis stratified by sex*

Sex/Medication	Patient with fracture, n	Control, n	Crude OR (95% CI)	Adjusted for age, sex, disease year, OR (95% CI)	Fully adjusted, OR (95% CI) ^a
Female					
TNFis	111	1,725	0.69 (0.51–0.94)	0.75 (0.56–1.02)	0.73 (0.52–1.01)
csDMARDs	69	657	1.13 (0.81–1.59)	1.09 (0.77–1.54)	0.93 (0.65–1.34)
None	204	2,240	0.98 (0.75–1.29)	0.99 (0.76–1.31)	1.01 (0.76–1.35)
NSAIDs	78	842	1.0	1.0	1.0
Male					
TNFis	197	2,618	0.58 (0.47–0.73)	0.69 (0.55–0.87)	0.77 (0.60–0.99)
csDMARDs	47	426	0.86 (0.60–1.21)	0.82 (0.58–1.17)	0.87 (0.61–1.25)
None	381	2,680	1.10 (0.90–1.35)	1.14 (0.93–1.41)	1.15 (0.93–1.42)
NSAIDs	142	1,102	1.0	1.0	1.0

* CI, confidence interval; csDMARD, conventional synthetic disease-modifying antirheumatic drug; NSAID, nonsteroidal anti-inflammatory drug; OR, odds ratio; TNFi, tumor necrosis factor inhibitor.

^a The fully adjusted model was adjusted for age, sex, disease year, alcohol use disorder, antiepileptic drug reception, body mass index, breast cancer, chronic kidney disease, falls, glucocorticoid reception, inflammatory bowel disease, osteoporosis, osteoporosis medication reception, prostate cancer, tobacco use, erythrocyte sedimentation rate/C-reactive protein laboratory orders and number of outpatient visits (rheumatology and primary care).

Table 3. Results of multivariable analyses assessing the relation of medication class exposure with hip and spine fracture risk among individuals with axial spondyloarthritis stratified by history of prior fracture*

History	Patient with fracture, n	Control, n	Crude OR (95% CI)	Adjusted for age, sex, disease year, OR (95% CI)	Fully adjusted, OR (95% CI) ^a
Prior fracture					
TNFis	35	25	0.45 (0.21–0.96)	0.56 (0.25–1.24)	0.59 (0.23–1.51) ^b
csDMARDs	16	16	0.32 (0.13–0.78)	0.40 (0.15–1.02)	0.34 (0.12–1.01) ^b
None	121	51	0.76 (0.40–1.46)	0.79 (0.40–1.56)	0.74 (0.36–1.50) ^b
NSAIDs	50	16	1.0	1.0	1.0 ^b
No prior fracture					
TNFis	273	4,318	0.72 (0.59–0.88)	0.80 (0.66–0.98)	0.83 (0.67–1.03)
csDMARDs	100	1,067	1.06 (0.82–1.38)	1.08 (0.83–1.40)	1.04 (0.79–1.36)
None	464	4,869	1.08 (0.90–1.30)	1.11 (0.92–1.33)	1.13 (0.94–1.37)
NSAIDs	170	1,928	1.0	1.0	1.0

* BMI, body mass index; CI, confidence interval; csDMARD, conventional synthetic disease-modifying antirheumatic drug; NSAID, nonsteroidal anti-inflammatory drug; OR, odds ratio; TNFi, tumor necrosis factor inhibitor.

^a The fully adjusted model was adjusted for age, sex, disease year, alcohol use disorder, antiepileptic drug reception, BMI, breast cancer, chronic kidney disease, falls, glucocorticoid reception, inflammatory bowel disease, osteoporosis, osteoporosis medication reception, prostate cancer, tobacco use, erythrocyte sedimentation rate/C-reactive protein laboratory orders and number of outpatient visits (rheumatology and primary care).

^b BMI is not included given the missing data.

previous observational study of fracture incidence in patients with axSpA during the TNFi era showed an increase in fracture incidence rates over time rather than the decrease that would be expected with greater reception of TNFis in patients with axSpA; however, this finding may have been influenced by a trend toward increased detection of fracture over the study period.²⁴

There are several potential explanations for our finding of a protective effect of receiving TNFis on fracture risk in individuals with axSpA. This can be explained by TNFis reducing both disease progression in the axial spine and systemic inflammation. By slowing local bone remodeling within the axial spine with TNFi reception, both bone density and architecture may be preserved, thus lowering risk for vertebral fractures.^{15,32,33} Lower systemic inflammation can reduce bone turnover and the subsequent risk of osteoporosis and peripheral fractures.³⁴ Finally, improved disease control globally can lead to improvement in mobility and physical activity, indirectly improving health and reducing comorbidities that can be risk factors for fractures.³⁵ Our findings underscore the multifaceted benefits of TNFi reception therapy in patients with axSpA, extending beyond the management of axial symptoms to mitigate associated comorbidities, including fractures.

Although our study provides valuable insights, it is subject to several limitations. First, there may be potential misclassification for our cohort with axSpA, as well as for fracture outcomes, derived solely from diagnostic and procedure codes. However, we used published strategies to identify those with axSpA and fracture.^{19–21} Although the prior validation study reported good PPVs using their fracture identification algorithm, the performance of lack of these codes to identify controls without fractures is unknown because negative predictive values were not presented. Exposures may also be misclassified. We assessed medication exposures in the six

months preceding the outcome (for patients with axSpA), with the assumption that this was the main medication acting on fracture risk during that time period. We were not able to account for changing or switching exposures due to the case-control study design. Second, despite adjusting for demographic and comorbidity confounders, as well as using surrogates for disease activity such as laboratory orders for markers of inflammation and health care use, the potential for residual confounding remains. Notably, the administrative database analyzed in this study lacks detailed information on the level of disease activity, posing a limitation in fully adjusting for this variable in the analysis. Moreover, the level of missing data (>50%) for BMI, a known strong confounder for fracture risk, may introduce bias to our results. Additionally, the low frequencies observed for alcohol use disorder may indicate under-reporting or information bias, another source of missing data. Third, confounding by indication should be considered. Individuals with axSpA not receiving TNFis might have contraindications for biologic therapy that are also associated with increased risk of fracture. However, our results show that individuals with fractures exhibited more risk factors for fractures than controls. Despite this, our findings demonstrate a protective effect of TNFis. Thus, the observed protective effect of TNFis may potentially underestimate the true impact. Fourth, we used a case-control design for statistical efficiency due to low number of outcomes per exposure group. Compared to a cohort design, a case-control design precludes the ability to define exposure periods that would allow for conduct of a target trial emulation. Finally, we did not have adequate numbers of hip fractures to conduct analyses limited to hip fracture only.

Our study's strength lies in leveraging a substantial US database with comprehensive medical and drug records. We were able to identify a large cohort of over 70,000 individuals with

axSpA, allowing for the identification of a large number of patients with hip and spine fracture for analysis, surpassing the sample sizes used in previous studies. Our study demonstrates a protective effect of receiving TNFi on fracture risk in individuals with axSpA compared with receiving NSAIDs or csDMARDs. Future research investigating the impact of the timing of TNFi initiation and alternative axSpA treatment modalities, such as IL-17 inhibitors and JAK inhibitors, on fracture risk in patients with axSpA will further enhance our understanding of how fracture risk may be mitigated in this population.

ACKNOWLEDGMENTS

The authors acknowledge the Boston Musculoskeletal Clinical Research Collaboratory Research Accelerator group for their insightful comments on this manuscript. The authors thank Nene Okonu (Department of Biostatistics) for her help with the quantitative bias analysis.

AUTHOR CONTRIBUTIONS

All authors contributed to at least one of the following manuscript preparation roles: conceptualization AND/OR methodology, software, investigation, formal analysis, data curation, visualization, and validation AND drafting or reviewing/editing the final draft. As corresponding author, Dr Dubreuil confirms that all authors have provided the final approval of the version to be published, and takes responsibility for the affirmations regarding article submission (eg, not under consideration by another journal), the integrity of the data presented, and the statements regarding compliance with institutional review board/Declaration of Helsinki requirements.

REFERENCES

- Reveille JD, Weisman MH. The epidemiology of back pain, axial spondyloarthritis and HLA-B27 in the United States. *Am J Med Sci* 2013; 345:431–436.
- Taurog JD, Chhabra A, Colbert RA. Ankylosing spondylitis and axial spondyloarthritis. *N Engl J Med* 2016;374:2563–2574.
- van der Heijde D, Molto A, Ramiro S, et al. Goodbye to the term ‘ankylosing spondylitis’, hello ‘axial spondyloarthritis’: time to embrace the ASAS-defined nomenclature. *Ann Rheum Dis* 2024;83:547–549.
- López-Medina C, Molto A, Sieper J, et al. Prevalence and distribution of peripheral musculoskeletal manifestations in spondyloarthritis including psoriatic arthritis: results of the worldwide, cross-sectional ASAS-PerSpA study. *RMD Open* 2021;7:e001450.
- Wysham KD, Murray SG, Hills N, et al. Cervical spinal fracture and other diagnoses associated with mortality in hospitalized ankylosing spondylitis patients. *Arthritis Care Res (Hoboken)* 2017;69:271–277.
- Walsh JA, Song X, Kim G, et al. Evaluation of the comorbidity burden in patients with ankylosing spondylitis using a large US administrative claims data set. *Clin Rheumatol* 2018;37:1869–1878.
- Pray C, Feroz NI, Nigil Haroon N. Bone mineral density and fracture risk in ankylosing spondylitis: a meta-analysis. *Calcif Tissue Int* 2017; 101:182–192.
- Weiss RJ, Wick MC, Ackermann PW, et al. Increased fracture risk in patients with rheumatic disorders and other inflammatory diseases -- a case-control study with 53,108 patients with fracture. *J Rheumatol* 2010;37:2247–2250.
- Vosse D, Landewé R, van der Heijde D, et al. Ankylosing spondylitis and the risk of fracture: results from a large primary care-based nested case-control study. *Ann Rheum Dis* 2009;68:1839–1842.
- Davey-Ranasinghe N, Deodhar A. Osteoporosis and vertebral fractures in ankylosing spondylitis. *Curr Opin Rheumatol* 2013;25: 509–516.
- Ward MM, Deodhar A, Akl EA, et al. American College of Rheumatology/Spondylitis Association of America/Spondyloarthritis Research and Treatment Network 2015 recommendations for the treatment of ankylosing spondylitis and nonradiographic axial spondyloarthritis. *Arthritis Rheumatol* 2016;68:282–298.
- Ramiro S, Nikiphorou E, Sepriano A, et al. ASAS-EULAR recommendations for the management of axial spondyloarthritis: 2022 update. *Ann Rheum Dis* 2023;82:19–34.
- Bautista-Molano W, Fernández-Ávila DG, Brance ML, et al. Pan American League of Associations for rheumatology recommendations for the management of axial spondyloarthritis. *Nat Rev Rheumatol* 2023;19:724–737.
- Muñoz-Ortego J, Vestergaard P, Rubio JB, et al. Ankylosing spondylitis is associated with an increased risk of vertebral and nonvertebral clinical fractures: a population-based cohort study. *J Bone Miner Res* 2014;29:1770–1776.
- Haroon NN, Sriganthan J, Al Ghanim N, et al. Effect of TNF-alpha inhibitor treatment on bone mineral density in patients with ankylosing spondylitis: a systematic review and meta-analysis. *Semin Arthritis Rheum* 2014;44:155–161.
- Beek KJ, Rusman T, van der Weijden MAC, et al. Long-term treatment with TNF-alpha inhibitors improves bone mineral density but not vertebral fracture progression in ankylosing spondylitis. *J Bone Miner Res* 2019;34:1041–1048.
- Merative MarketScan Research Databases. Merative. Accessed January 06, 2025. <https://www.merative.com/documents/merative-marketscan-research-databases>
- Zochling J, van der Heijde D, Burgos-Vargas R, et al. ASAS/EULAR recommendations for the management of ankylosing spondylitis. *Ann Rheum Dis* 2006;65:442–452.
- Dubreuil M, Peloquin C, Zhang Y, et al. Validity of ankylosing spondylitis diagnoses in the health improvement network. *Pharmacoepidemiol Drug Saf* 2016;25:399–404.
- Singh JA, Holmgren AR, Krug H, et al. Accuracy of the diagnoses of spondylarthritides in Veterans Affairs medical center databases. *Arthritis Rheum* 2007;57:648–655.
- Wright NC, Daigle SG, Melton ME, et al. The design and validation of a new algorithm to identify incident fractures in administrative claims data. *J Bone Miner Res* 2019;34:1798–1807.
- McCarthy J, Davis A. Diagnosis and management of vertebral compression fractures. *Am Fam Physician* 2016;94:44–50.
- Taylor JM. Choosing the number of controls in a matched case-control study, some sample size, power and efficiency considerations. *Stat Med* 1986;5:29–36.
- Merjanah S, Liew JW, Bihn J, et al. Trends in fracture rates over two decades among veterans with ankylosing spondylitis. *Arthritis Care Res (Hoboken)* 2023;75:2481–2488.
- Pearce N. Analysis of matched case-control studies. *BMJ* 2016;352: i969.
- Fox MP, MacLehose RF, Lash TL. Applying Quantitative Bias Analysis to Epidemiologic Data. 2nd ed. Springer Cham; 2021;164–165:199–200. Statistics for Biology and Health. <https://link.springer.com/10.1007/978-3-030-82673-4>
- Ramírez J, Nieto-González JC, Curbelo Rodríguez R, et al. Prevalence and risk factors for osteoporosis and fractures in axial spondyloarthritis: a systematic review and meta-analysis. *Semin Arthritis Rheum* 2018;48:44–52.

28. Ashany D, Stein EM, Goto R, et al. The effect of TNF inhibition on bone density and fracture risk and of IL17 inhibition on radiographic progression and bone density in patients with axial spondyloarthritis: a systematic literature review. *Curr Rheumatol Rep* 2019;21:20.
29. van der Weijden MAC, van Denderen JC, Lems WF, et al. Etanercept increases bone mineral density in ankylosing spondylitis, but does not prevent vertebral fractures: results of a prospective observational cohort study. *J Rheumatol* 2016;43:758–764.
30. Maas F, Spoorenberg A, Brouwer E, et al. Radiographic vertebral fractures develop in patients with ankylosing spondylitis during 4 years of TNF- α blocking therapy. *Clin Exp Rheumatol* 2016;34:191–199.
31. Hinze AM, Louie GH. Osteoporosis management in ankylosing spondylitis. *Curr Treat Options Rheumatol* 2016;2:271–282.
32. Nigil Haroon N, Szabo E, Raboud JM, et al. Alterations of bone mineral density, bone microarchitecture and strength in patients with ankylosing spondylitis: a cross-sectional study using high-resolution peripheral quantitative computerized tomography and finite element analysis. *Arthritis Res Ther* 2015;17:377.
33. Briot K, Gossec L, Kolta S, et al. Prospective assessment of body weight, body composition, and bone density changes in patients with spondyloarthropathy receiving anti-tumor necrosis factor-alpha treatment. *J Rheumatol* 2008;35:855–861.
34. Arends S, Spoorenberg A, Houtman PM, et al. The effect of three years of TNF α blocking therapy on markers of bone turnover and their predictive value for treatment discontinuation in patients with ankylosing spondylitis: a prospective longitudinal observational cohort study. *Arthritis Res Ther* 2012;14:R98.
35. Braun J, McHugh N, Singh A, et al. Improvement in patient-reported outcomes for patients with ankylosing spondylitis treated with etanercept 50 mg once-weekly and 25 mg twice-weekly. *Rheumatol (Oxford)* 2007;46:999–1004.

Derivation of a Multivariable Psoriatic Arthritis Risk Estimation Tool (PRESTO): A Step Towards Prevention

Lihi Eder,¹ Ker-Ai Lee,² Vinod Chandran,³ Jessica Widdifield,⁴ Aaron M. Drucker,⁵ Christopher Ritchlin,⁶ Cheryl F. Rosen,³ Richard J. Cook,² and Dafna D. Gladman³

Objective. A simple, scalable tool that identifies psoriasis patients at high risk for developing psoriatic arthritis (PsA) could improve early diagnosis. We aimed to develop a risk prediction model for the development of PsA and to assess its performance among patients with psoriasis.

Methods. We analyzed data from a prospective cohort of psoriasis patients without PsA at enrollment. Participants were assessed annually by a rheumatologist for the development of PsA. Information about their demographics, psoriasis characteristics, comorbidities, medications, and musculoskeletal symptoms was used to develop prediction models for PsA. Penalized binary regression models were used for variable selection while adjusting for psoriasis duration. Risks of developing PsA over 1- and 5-year time periods were estimated. Model performance was assessed by the area under the curve (AUC) and calibration plots.

Results. Among 635 psoriasis patients, 51 and 71 developed PsA during the 1-year and 5-year follow-up periods, respectively. The risk of developing PsA within 1 year was associated with younger age, male sex, family history of psoriasis, back stiffness, nail pitting, joint stiffness, use of biologic medications, patient global health, and pain severity (AUC 72.3). The risk of developing PsA within 5 years was associated with morning stiffness, psoriatic nail lesion, psoriasis severity, fatigue, pain, and use of systemic nonbiologic medication or phototherapy (AUC 74.9). Calibration plots showed reasonable agreement between predicted and observed probabilities.

Conclusions. The development of PsA within clinically meaningful time frames can be predicted with reasonable accuracy for psoriasis patients using readily available clinical variables.

INTRODUCTION

Psoriatic arthritis (PsA) is an inflammatory musculoskeletal disease affecting up to a third of patients with psoriasis (1). Early diagnosis and treatment are critical to prevent or reduce the severity of adverse PsA-related outcomes (2). In approximately 75% of patients, the development of PsA follows the diagnosis of psoriasis (1). As such, patients with psoriasis serve as a high-risk population for PsA on whom early detection and prevention efforts can be focused. There is an essential need to optimize risk

prediction for PsA among patients with psoriasis, which should improve care delivery for high-risk patients. However, no such prediction tool currently exists. A simple, scalable tool that identifies patients with psoriasis who are at high risk for developing PsA will be an important step towards improving early detection enabling opportunities for early interventions, which may halt progression from psoriasis to PsA.

Recent research efforts are focused on revealing risk factors in psoriasis patients to identify individuals at increased risk for PsA. The most consistent evidence suggests that obesity, extensive psoriasis,

Supported by a New Investigator Grant from the Physician Services Incorporated (PSI) Foundation. Dr. Eder's work was supported by Canada Research Chair in Inflammatory Rheumatic Diseases (Tier 2). Dr. Chandran's work was supported by a Pfizer Chair Research Award, Rheumatology, University of Toronto. The Psoriatic Arthritis Program at Toronto Western Hospital is supported by the Krembil Foundation.

¹Lihi Eder, MD, PhD: Women's College Research Institute, Women's College Hospital, Toronto, Ontario, Canada, and Department of Medicine, University of Toronto, Toronto, Ontario, Canada; ²Ker-Ai Lee, MMath, Richard J. Cook, PhD: Department of Statistics and Actuarial Science, University of Waterloo, Waterloo, Ontario, Canada; ³Vinod Chandran, MBBS, MD, DM, PhD, Cheryl F. Rosen, MD, Dafna D. Gladman, MD: Department of Medicine, University of Toronto, and Schroder Arthritis Institute, Krembil Research Institute, Toronto Western Hospital, Toronto, Ontario, Canada; ⁴Jessica Widdifield,

PhD: Sunnybrook Research Institute, Sunnybrook Hospital, and Institute for Clinical Evaluative Sciences (ICES), and Institute of Health Policy, Management and Evaluation, University of Toronto, Toronto, Ontario, Canada; ⁵Aaron M. Drucker, MD, SCM: Women's College Research Institute, Women's College Hospital, and Department of Medicine, University of Toronto, and ICES, and Institute of Health Policy, Management and Evaluation, University of Toronto, Toronto, Ontario, Canada; ⁶Christopher Ritchlin, MD, MPH: Division of Rheumatology, University of Rochester, Rochester, New York.

Author disclosures and graphical abstract are available at <https://onlinelibrary.wiley.com/doi/10.1002/art.42661>.

Address correspondence via email to Lihi Eder MD, PhD, at lihi.eder@wchospital.ca.

Submitted for publication April 6, 2023; accepted in revised form June 14, 2023.

and psoriatic nail lesions predict the development of PsA among psoriasis patients (3–7). Other, less consistent risk factors include the location of psoriasis (intergluteal or scalp) (6), history of uveitis (4), comorbidities, such as thyroid disease and depression (4,8), and a recent history of physical trauma (9,10). In addition, the presence of nonspecific musculoskeletal symptoms, such as pain, fatigue, and stiffness, predicts the development of overt PsA among psoriasis patients (11,12). Although those individual risk factors for PsA are somewhat clinically useful, no unifying prediction tool currently exists.

Risk estimation using prediction tools plays an important role in shaping treatment plans, based on the ability of the risk score to accurately predict and stratify a patient's risk (13). A prognostic model for PsA could assist clinicians in identifying susceptible psoriasis patients for screening or interventional purposes and facilitate informed decision-making by both the treating physician and patient. Such a prediction tool would enable tailored management of individuals with psoriasis (eg, referral to rheumatology and close monitoring of high-risk individuals), which is expected to foster timely diagnosis of PsA, ultimately improving disease outcomes. The development of prediction tools for PsA was identified as a research priority by the American Academy of Dermatology and the Group for Research and Assessment of Psoriasis and PsA (14,15). In addition, the advent of novel immune-modulating therapies that target shared proinflammatory cytokines for psoriasis and PsA brings new opportunities for interventional studies aiming to prevent or delay the onset of PsA in susceptible psoriasis patients who do not yet have joint involvement. Thus, a prediction tool that identifies patients with psoriasis at high-risk for PsA will be an important first step in the development and testing of interventional strategies that may ultimately halt disease progression.

The objective of the study was to develop and internally validate a Psoriatic Arthritis Risk Estimation Tool (PRESTO) in patients with psoriasis.

PATIENTS AND METHODS

The Transparent Reporting of a multivariable prediction model for Individual Prognosis or Diagnosis framework guided the development of the methodology and reporting for this study (16).

Setting

The ongoing University of Toronto Psoriasis Cohort started in 2006 as a prospective longitudinal cohort study aiming to study risk factors for the development of PsA among patients with psoriasis. Patients enrolled in the cohort have a dermatologist-confirmed diagnosis of psoriasis. They are recruited mainly from dermatology clinics and phototherapy centers in the Greater Toronto Area but also from family medicine clinics and through advertisements in hospitals and local media. All patients are assessed prior to enrollment by a rheumatologist to exclude those with inflammatory arthritis in the past or at the time of assessment. Rheumatologists examine

the joints for the presence of tenderness, swelling and deformities, and signs of dactylitis, enthesitis, and tenosynovitis and evaluate the spine for restriction in movements. If definitive clinical findings of PsA are found, the patient is excluded from the study prior to enrollment. Imaging modalities, such as radiographs, MRI, or ultrasound, are performed only in cases of clinical doubt to investigate the nature of existing abnormalities. Patients with noninflammatory musculoskeletal conditions, such as osteoarthritis, are allowed to be enrolled. This process ensures that all study participants are free of clinical inflammatory arthritis at the time of enrollment. In this study, we used data from January 2006 to December 2019. We excluded patients without any follow-up study visits. The study was approved by the University Health Network Research Ethics Board. All patients signed an informed consent form.

Data collection

All study participants were reassessed annually by a rheumatologist who determined whether PsA had developed since the last study visit and to collect information on potential risk factors for PsA. Information was collected using standard protocols that record information about lifestyle habits, medical family history, musculoskeletal symptoms, comorbidities, medications, and skin examination findings. The presence of musculoskeletal symptoms was recorded by the rheumatologist at each visit. Physical examination included the evaluation of their height and weight, and skin assessment for psoriasis type, location, and activity (using psoriasis area and severity index [PASI]). The presence of psoriatic nail lesions was also documented. The rheumatologist also examined 66 and 68 joints for swelling and tenderness, respectively, and evaluated 18 enthesal sites for tenderness, and assessed for signs of dactylitis.

Musculoskeletal symptom severity was recorded using self-reported questionnaires. Stiffness level was measured on a 0- to 10-cm visual analogue scale. Pain level was measured on a numeric rating scale ranging from 0 (no pain) to 10 (severe pain). Current pain severity was also measured on a five-category Likert scale ranging from 1 = none to 5 = very severe. Fatigue was measured by functional assessment of chronic illness therapy-fatigue (FACIT-F), with lower scores indicating higher level of fatigue. The subject's self-reported global health status was measured on a five-category Likert scale ranging from 1 = very good to 5 = Very poor. Ability to function compared with 1 year ago was also assessed on a Likert scale ranging from 1 = much better to 5 = much worse. The presence of human leukocyte antigen (HLA)-B*27 allele was assessed. See Supplementary Information 1, available on the *Arthritis & Rheumatology* website at <http://onlinelibrary.wiley.com/doi/10.1002/art>, for detailed information on collection of study variables.

Case definition

A comprehensive assessment of symptoms and signs of PsA was performed at each study visit by a rheumatologist

experienced in assessing patients with PsA. The diagnosis of PsA was based on clinical findings, as described above. Imaging modalities were ordered only if clinically indicated to investigate abnormalities that may suggest PsA. The diagnosis of PsA was determined after reviewing the clinical, laboratory, and imaging data (if available). Information on HLA-B*27 status was not considered as part of the diagnostic process.

To address the issue of lost to follow-up, we contacted patients who failed to return for their yearly follow-up (missed two or more consecutive annual visits) to determine if they are alive and whether they have seen a physician for musculoskeletal symptoms. We also reviewed all relevant medical records from rheumatologists and other specialists outside of our research group to determine whether they received a new diagnosis of PsA.

Statistical analysis

We calculated descriptive statistics, including mean (SD) for continuous variables and frequencies (percentages) for categorical variables. Data on up to 10% of patient-reported outcome variables and body mass index (BMI) were missing. We used multiple imputation to handle missing data (via proc MI in SAS) based in predictive mean matching using full conditional specification; five complete data sets were generated by imputation.

The time at risk was the time from clinic entry to the development of PsA or, for those not developing PsA, to the earliest of the dates of death, moving out of province, or loss to follow-up. For the development of the PRESTO predictive tool, the risk of developing PsA was estimated over 1- and 5-year moving, overlapping time windows (see Supplementary Information 2, available on the *Arthritis & Rheumatology* website at <http://onlinelibrary.wiley.com/doi/10.1002/art>). That is, baseline covariates were used separately to predict the development of PsA within 1 and 5 years. Information on baseline covariates was updated in subsequent visits along with an update of the prediction windows. For the 5-year prediction model, this update often resulted in overlapping prediction windows. Thus, individual patients can contribute multiple observation windows with different index dates to the analysis, depending on their length of follow-up and number of visits. Based on our prior studies that showed an increase in nonspecific musculoskeletal symptoms closer to the time of diagnosis (11), we hypothesized that different variables would predict PsA at each of these two time windows. Therefore, we aimed to develop two separate prediction models to estimate the shorter- and longer- term PsA risk within two clinically meaningful time periods.

We selected 29 variables as potential predictors for the models based on existing literature on risk factors for the development of PsA in psoriasis patients. Additional guiding principles for the selection of potential predictors were availability of information in our cohort and their typical availability in routine clinical practice. The following time-varying covariates were considered as possible prognostic variables for PsA: age, sex, family history of

psoriasis, family history of PsA or ankylosing spondylitis, arthralgia, morning joint stiffness, heel pain, back pain, morning back stiffness, BMI, flexural psoriasis, pustular psoriasis, palmoplantar psoriasis, PASI score, psoriasis body surface area, psoriatic nail lesions, pitting, onycholysis, iritis, inflammatory bowel disease (IBD), joint stiffness severity, FACIT-F, patient global health, current pain severity, ability to function compared with 1 year ago, and pain level (numeric rating scale [NRS]), HLA-B*27, phototherapy or use of nonbiologic systemic therapy, and use of biologic therapy. Because of software limitations for the handling of multi-level categorical variables, all covariates measured on Likert scales were converted to binary variables (see Supplementary Information 1, available on the *Arthritis & Rheumatology* website at <http://onlinelibrary.wiley.com/doi/10.1002/art>).

To avoid sparse data situations arising from covariates with low frequencies, the baseline distribution of all potential binary predictors by PsA conversion status were examined using 2×2 contingency tables. Predictors with less than five cell counts for at least one of the imputed data sets were excluded from the analysis prior to fitting the regression models.

We fitted multivariable logistic regression models adjusting for covariates, the duration of psoriasis, and the log duration at risk to estimate the probability of developing PsA within each of 1-year and 5-year time windows from consecutive study visits. If an individual considered at risk of PsA did not develop PsA before their next study visit, the covariates were updated and used to predict PsA onset within the next future time window. Individuals not observed to develop PsA over the entire duration of follow-up gave censored conversion times.

The penalized regression method using weighted stacked objective function and least absolute shrinkage and selection operator penalty function for binary response with 5-fold cross-validation is used for variable selection and to minimize overfitting (17). Because we have five imputed data sets, and each imputed data set may lead to different sets of selected predictors, the stacked approach was applied to pool the objective functions across imputations. This is a way to pool the penalized regression estimates across imputed data sets. Because stacking five imputed data sets can be viewed as artificially increasing the sample size by five times, a weight is added to each subject to address the increase in sample size. We assign an observation weight of 1/5 to a visit that has some missing covariates; otherwise, the observation weight is 1. The models were internally validated by 5-fold cross-validation.

We assessed model performance using metrics for discrimination and calibration, including the area under the curve (AUC) and calibration plots, respectively. To calculate AUC and its confidence interval, we used Rubin's combining rule to aggregate estimates on five imputed data sets (18). Two hundred bootstrap samples were used, sampling individuals' entire courses, to obtain a nonparametric bootstrap standard error of the aggregate AUC. A priori, we considered an AUC of greater than 70% acceptable. We

calculated sensitivity and specificity for varying cutoff values for each model based on averages of five imputed data sets.

RESULTS

A total of 786 patients with psoriasis were screened. Of those, 84 patients were excluded because of the presence of PsA and other rheumatic conditions at baseline. A total of

702 patients with psoriasis without clinical evidence of musculoskeletal inflammatory disease enrolled in the Toronto Psoriasis Cohort were followed from January 1, 2006 to December 31, 2019. Of these patients, 67 patients were excluded from the analysis because they only had a single visit and did not contribute any follow-up data. Of 635 patients included in the analysis, 51 and 71 patients developed PsA within the 1-year and 5-year time windows, respectively (Table 1).

Table 1. Baseline characteristics of study participants*

	All participants (N = 635)	Participants with PsA in 1-year window (N = 51)	Participants with PsA in 5-year window (N = 71)
Age (years)	47.0 (13.5)	47.6 (11.7)	46.8 (12.4)
Sex: male	360 (56.7%)	31 (60.8%)	43 (60.6%)
Race and ethnicity			
White	483 (76.1%)	41 (80.4%)	53 (74.6%)
South Asian	45 (7.1%)	3 (5.9%)	6 (8.5%)
Chinese	28 (4.4%)	2 (3.9%)	3 (4.2%)
Filipino	18 (2.8%)	1 (2.0%)	2 (2.8%)
Middle Eastern	14 (2.2%)	0 (0.0%)	2 (2.8%)
Black	11 (1.7%)	1 (2.0%)	2 (2.8%)
Southeast Asian	11 (1.7%)	0 (0.0%)	0 (0.0%)
Other	25 (3.9%)	3 (5.9%)	3 (4.2%)
Psoriasis duration (years)	16.0 (14.3)	20.3 (16.2)	17.6 (15.1)
Family history of psoriasis	268 (42.2%)	24 (47.1%)	33 (46.5%)
Family history of PsA	24 (3.8%)	3 (5.9%)	3 (4.2%)
Arthralgia	165 (26.0%)	7 (13.7%)	15 (21.1%)
Morning stiffness	66 (10.4%)	4 (7.8%)	6 (8.5%)
Heel pain	10 (1.6%)	1 (2.0%)	2 (2.8%)
Back pain	275 (43.3%)	23 (45.1%)	32 (45.1%)
Back stiffness	52 (8.1%)	2 (3.9%)	3 (4.2%)
BMI	28.0 (5.9)	28.5 (5.6)	28.6 (5.7)
Flexural psoriasis	14 (2.2%)	2 (3.9%)	3 (4.2%)
Pustular psoriasis	12 (1.9%)	0 (0%)	1 (1.4%)
Palmoplantar psoriasis	27 (4.3%)	0 (0%)	2 (2.8%)
PASI score	5.3 (6.0)	6.0 (5.9)	6.5 (6.3)
BSA (%)	8.6 (11.7)	7.1 (5.8)	9.7 (9.8)
Nail lesions	303 (47.7%)	29 (56.9%)	42 (59.2%)
Pitting	231 (36.4%)	23 (45.1%)	33 (46.5%)
Onycholysis	200 (31.5%)	20 (39.2%)	31 (43.7%)
Iritis	4 (0.6%)	1 (2.0%)	1 (1.4%)
IBD	2 (0.3%)	0 (0%)	0 (0%)
Stiffness level (VAS in mm)	18.3 (34.9)	23.0 (29.4)	20.1 (27.0)
FACIT-F	44.7 (7.2)	41.5 (7.8)	41.1 (7.7)
HLA-B*27	22 (3.5%)	0 (0%)	2 (2.8%)
Use of nonbiologic systemic therapies or phototherapy for psoriasis ^a	447 (70.4%)	41 (80.4%)	58 (81.7%)
Use of systemic biologic therapies for psoriasis ^b	32 (5.0%)	2 (3.9%)	2 (2.8%)
Patient's global health: very good or good vs. fair/poor/very poor	365 (79.2%)	31 (79.5%)	35 (72.9%)
Current pain severity: Any level of pain ^c	223 (48.5%)	27 (69.2%)	33 (68.8%)
Ability to function compared with previous year: much better or somewhat better ^d	94 (20.5%)	12 (30.8%)	13 (27.1%)
Pain level (NRS, 0–10)	1.5 (2.2)	1.9 (2.2)	2.0 (2.3)

* BMI = body mass index; BSA = body surface area; FACIT-F = functional assessment of chronic illness therapy—fatigue; HLA = human leukocyte antigen; IBD = inflammatory bowel disease; IL = interleukin; NRS = numeric rating scale; PASI = psoriasis area and severity index; TNF = tumor necrosis factor; VAS = visual analogue scale.

^a Methotrexate, apremilast, cyclosporine, soriatane.

^b IL-17, IL-12/23, IL-23, or TNF inhibitors.

^c Current pain (Likert) very severe/severe/moderate/mild vs. none.

^d Ability to function compared with previous year: much better or somewhat better vs. about the same/somewhat worse/much worse.

Of the 29 prespecified potential predictors, the following predictors were excluded because of low prevalence: family history of PsA, heel pain, flexural psoriasis, pustular psoriasis, iritis, IBD, and HLA-B*27. Use of biologic systemic therapy was excluded only for the 5-year prediction model.

One-year prediction model

The following variables were selected for the 1-year prediction model: age, male sex, family history of psoriasis, morning back stiffness, nail pitting, stiffness level, use of biologic systemic medications, patient global health, and pain (any level vs. none). These variables were associated with a higher risk of developing PsA except for age and patients’ global health, which were associated with a reduced risk (see Figure 1A). The discriminatory ability of the model was acceptable with an AUC of 72.3% (95% confidence interval [95% CI] 65.5–79.1). Model calibration, qualitatively assessed by reviewing the calibration plot, was excellent with an almost perfect agreement between the observed versus predicted cases (Figure 2A and B). Sensitivity and specificity for various cutoff levels are shown in Figure 3.

Five-year prediction model

The following variables were selected for the 5-year prediction model: presence of morning joint stiffness, PASI, psoriatic nail

lesions, FACIT-F, use of nonbiologic systemic medications/phototherapy, and pain (any level vs. none). The discriminatory ability of the model was acceptable with an AUC of 74.9% (95% CI 69.3–80.5; Figure 1B). Model calibration showed reasonable agreement between observed versus predicted cases in the first to fourth lower quantiles of predicted probability but more substantial disagreement in the fifth quantile, with underestimation of the actual risk by the prediction model (Figure 2C and D). Sensitivity and specificity for various cutoff levels are shown in Figure 3.

DISCUSSION

We derived and internally validated a novel risk prediction tool for PsA: PRESTO. PRESTO estimates PsA risk within shorter and longer time horizons using easily collected information, including many variables that were previously reported as risk factors for PsA. PRESTO has demonstrated good model fit metrics, including discrimination and calibration, and its threshold could be adjusted depending on the purpose of its use (eg, higher sensitivity for screening, higher specificity for enrichment with high-risk patients for interventional studies). Accurate estimation of PsA risk using PRESTO among patients with psoriasis has important potential applications in clinical care, such as promoting early diagnosis and interventions to prevent progression from psoriasis to PsA.

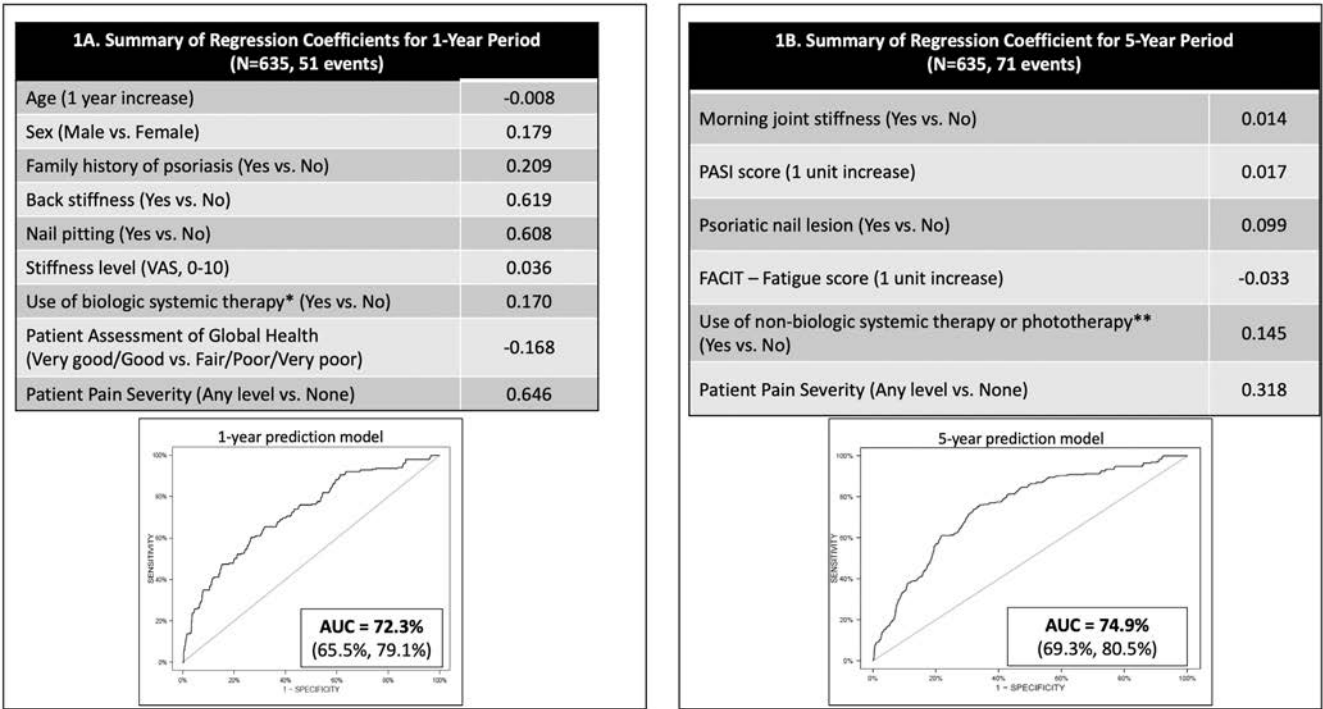


Figure 1. Prediction models for the development of PsA in psoriasis within 1-year period (A) and within 5-year period (B). Abbreviations: AUC = area under the curve; FACIT = functional assessment chronic illness therapy; PASI = psoriasis area and severity index; PsA = psoriatic arthritis; VAS = visual analogue scale. *Biologic systemic therapy includes current use of inhibitors of TNF, IL-17, IL-12/23 or IL-23. **Nonbiologic systemic therapies include current use of acitretin, apremilast, methotrexate, or cyclosporine.

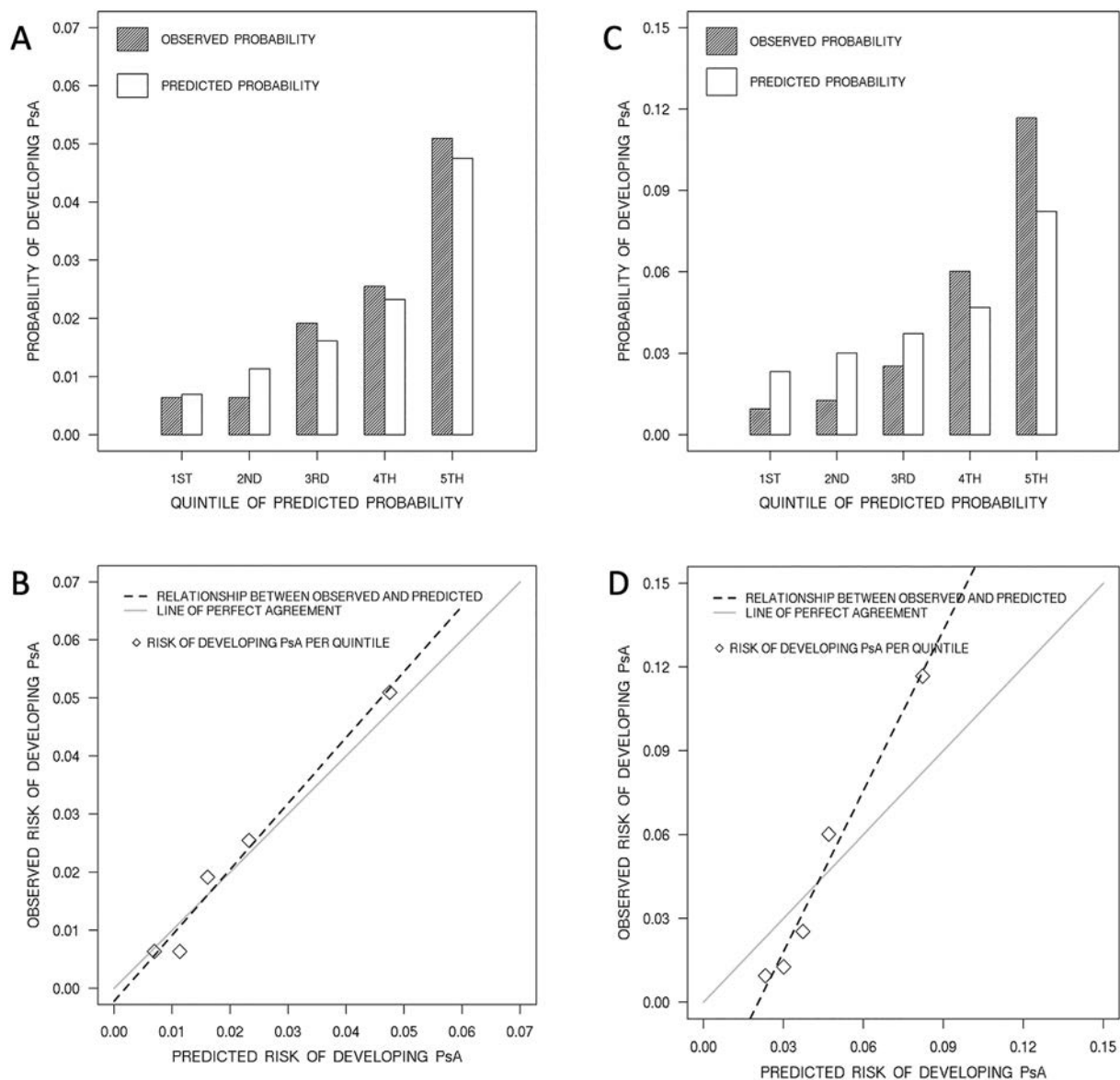


Figure 2. Calibration plots by quintile of predicted vs. observed probabilities for 1-year (A and B) and 5-year periods (C and D). Abbreviation: PsA = psoriatic arthritis.

PRESTO uses a mathematical model to estimate PsA risk. To facilitate its use, we developed a webpage with a PRESTO calculator (<http://sharpmindtill120.x10host.com/PRESTO-PsA>; see Supplementary Information 3, available on the *Arthritis & Rheumatology* website at <http://onlinelibrary.wiley.com/doi/10.1002/art>, for a calculator). We also created risk tables for various patient profiles (Figure 4). PRESTO builds upon existing literature on clinical risk factors for PsA. We purposely focused on assessing risk factors that are simple to measure in clinic setting via patient interview or physical examination. Our prediction tool includes many variables that have been previously associated with a higher risk of developing PsA, such as extensive psoriasis, psoriatic nail lesions, and nonspecific musculoskeletal symptoms (4,6,11,19,20). The inclusion of these

variables in PRESTO strengthens its face validity. Interestingly, several previously reported risk factors for PsA, such as HLA-B*27, family history of PsA, uveitis, and flexural psoriasis, were not included in the risk prediction model because of their scarcity in our cohort. This finding may be due to immortal time bias, which can complicate the development of risk prediction models for PsA. Genetic factors or their surrogates (eg, family history of PsA) are associated with the development of PsA concurrently or shortly after the onset of psoriasis (21). Thus, our population of patients with longstanding psoriasis may have been depleted of patients carrying these risk factors, rendering these factors less useful for prediction of PsA among patients with longstanding psoriasis who are commonly seen in dermatology clinics.

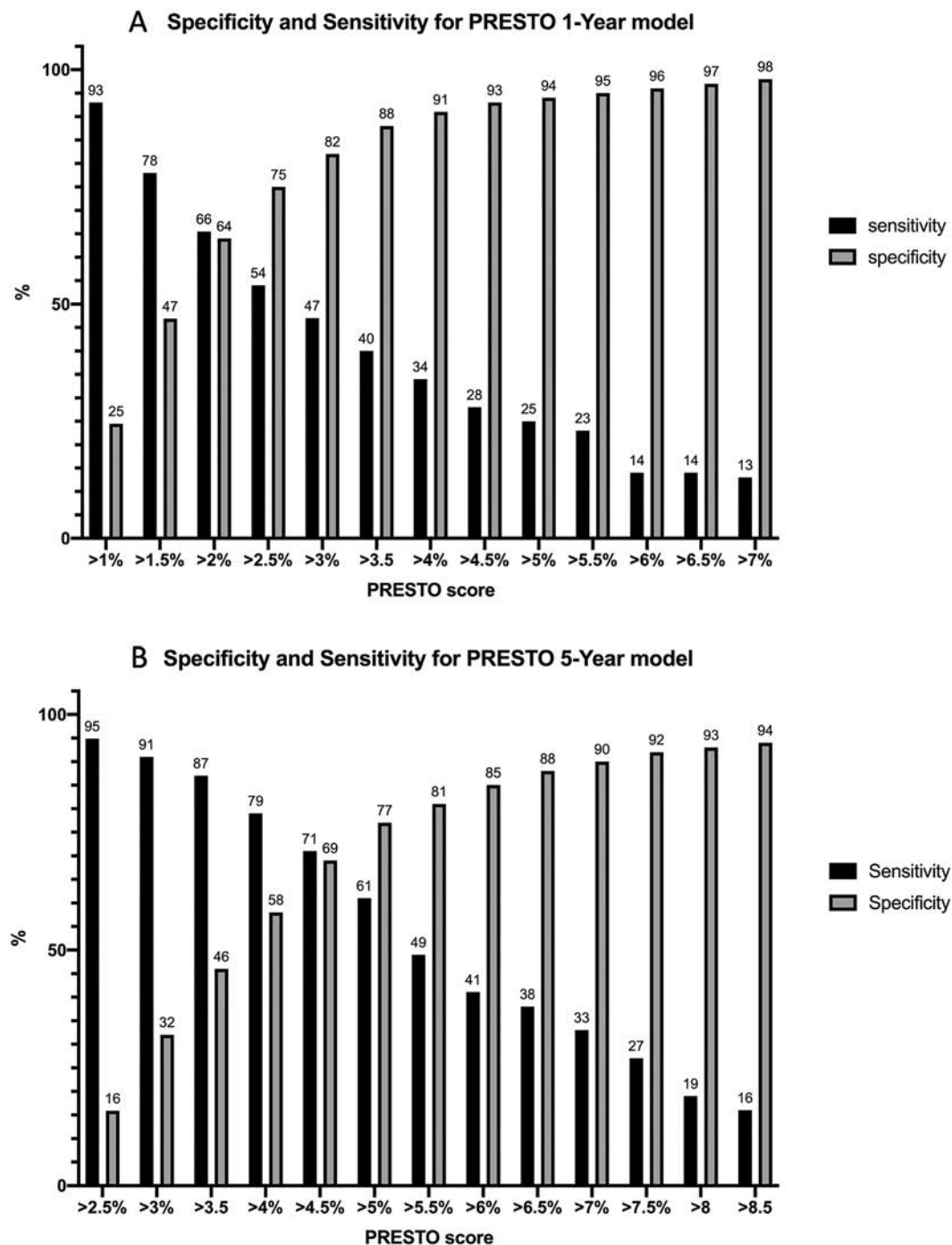


Figure 3. Sensitivity and Specificity of the model by selected cutoff point. **(A)** PRESTO score for 1 year window. **(B)** PRESTO score for 5-year window. The X axis in each graph depicts the probability of developing PsA for each model. The Y axis depicts the sensitivity and specificity (%) for each cut point. Abbreviations: PRESTO = Psoriatic Arthritis Risk Estimation Tool; PsA = psoriatic arthritis.

We have described a prodrome of nonspecific musculoskeletal symptoms occurring up to 5 years before the development of overt PsA (11,22). We found that the prevalence and severity of these symptoms increase closer to the diagnosis of PsA, which may lead to time-dependent effect sizes associated with these predictors. This result influenced our decision to develop two

separate prediction models, one for estimating the short-term risk (within 1 year) and the other for longer-term risk estimation (within 5 years). Indeed, the composition of the two risk models differ, although both include a combination of patient-reported musculoskeletal symptoms and psoriasis features and therapies. An important strength of our study is the availability of prospectively

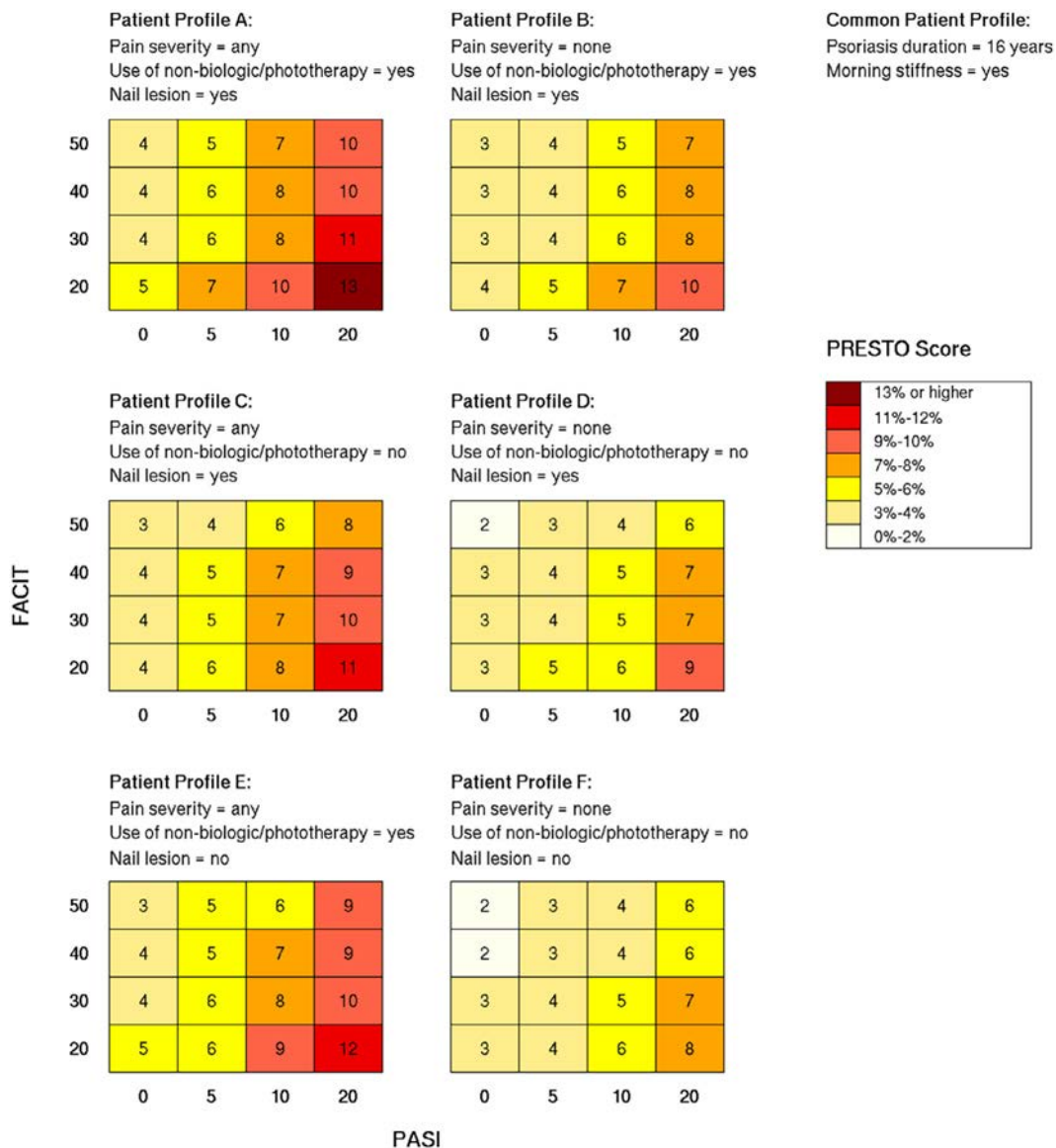


Figure 4. Estimated probability of developing PsA for six patient profiles based on the 5-year model. Abbreviations: FACIT = functional assessment of chronic illness therapy; PRESTO = Psoriatic Arthritis Risk Estimation Tool; PsA = psoriatic arthritis.

collected, time-varying information that estimated PsA risk within prespecified time frames, reflecting the dynamic nature of these factors in a real-life setting.

The relationship between the use of systemic therapies for psoriasis and future risk of PsA remains controversial. Use of biologic therapies and nonbiologic therapies or phototherapy were included in the 1-year and 5-year risk prediction models, respectively, both being associated with a higher risk of PsA. We showed that use of acitretin was associated with a higher risk of developing incident PsA among psoriasis patients (4). Similarly, Lindberg et al reported that use of systemic therapies or phototherapy was associated with an increased incidence rate of PsA among psoriasis patients (23). Studies that specifically assessed the question of whether use of biologic medications for psoriasis

lowers the risk of developing PsA, showed conflicting results (24–26). It is important to note that our study was not designed to assess whether the use of systemic therapy modifies PsA risk; thus, interpretation of the direction of association between medication use and PsA risk in the context of a multivariable prediction model should be performed with great caution. The use of systemic therapy as a variable in a prediction model can be viewed as a surrogate for psoriasis severity, which has been associated with a higher risk of developing PsA.

Screening for at-risk individuals is an important part of preventive medicine. The rationale is to identify disease during an early and preclinical stage. Early disease may be easier and less expensive to treat, which positions screening strategies as potentially sound investments for health care systems. Risk estimation

using prediction tools plays an important role in tailoring treatment plans to fit the patient's individual risk factors. The assessment of a patient's absolute risk is integral to the assessment of major prevention and treatment targets in various medical fields, such as cardiology (Framingham Risk Score). In rheumatology, risk prediction tools have been developed to estimate the risk of developing rheumatoid arthritis (RA) in high-risk populations, such as family members. They combine clinical, serologic, and genetic data to provide an absolute risk estimation of developing RA with generally good predictive ability (AUC of 0.70 to 0.85) (27,28). These tools have been implemented in clinical and research settings as educational tools for high-risk populations and for selection of high-risk individuals for prevention trials (29,30). In PsA, a strong rationale exists for using a risk prediction tool, possibly more so than in RA, given the easily identifiable target population of patients with psoriasis. Indeed, the Preventing Arthritis in a Multicentre Psoriasis At-Risk cohort trial (NCT05004727) is the first randomized controlled prevention trial, aimed to assess the efficacy of guselkumab versus placebo for reducing rate of progression from psoriasis to PsA. The study uses some clinical and ultrasound parameters to enrich features associated with high risk of PsA. Future studies could use the PRESTO score to accurately estimate PsA risk for enrichment of prevention trials with at-risk patients and to inform sample size calculation. With more treatment options for both psoriasis and PsA combined with a better understanding of PsA pathophysiology, prevention trials using either targeted therapies or nonpharmaceutical interventions become more relevant.

This study has several limitations. First, the relatively small sample size may have reduced the precision of the model and prevented the inclusion of previously reported risk factors that were present in only a few patients but may have had a strong effect size. The small sample size also prevented analysis by sex and race and ethnic group. Second, the generalizability of the study may be somewhat limited because most of the patients were recruited from dermatology clinics, leading to overrepresentation of moderate-severe psoriasis. Therefore, PRESTO will require an external validation to assess its performance in other populations of psoriasis patients with different characteristics. Thirdly, because of the study design, patients who developed PsA prior or concurrently to psoriasis were excluded. Therefore, our incident cases of PsA may overrepresent certain subtypes of PsA that are associated with longer duration between the onset of psoriasis and PsA.

In summary, we derived and internally validated a novel risk prediction tool for PsA in patients with psoriasis. PRESTO has good model performance and can provide estimated risk of developing PsA within shorter and longer time periods that are relevant for both clinical and research purposes. If further validated, we anticipate that PRESTO may facilitate efforts to improve early detection of at-risk populations enabling opportunities for early interventions that may halt progression to PsA.

REFERENCES

- Ritchlin CT, Colbert RA, Gladman DD. Psoriatic arthritis. *N Engl J Med* 2017;376:957–70.
- Haroon M, Gallagher P, FitzGerald O. Diagnostic delay of more than 6 months contributes to poor radiographic and functional outcome in psoriatic arthritis. *Ann Rheum Dis* 2015;74:1045–50.
- Scher JU, Ogdie A, Merola JF, et al. Preventing psoriatic arthritis: focusing on patients with psoriasis at increased risk of transition [review]. *Nat Rev Rheumatol* 2019;15:153–66.
- Eder L, Haddad A, Rosen CF, et al. The incidence and risk factors for psoriatic arthritis in patients with psoriasis: a prospective cohort study. *Arthritis Rheumatol* 2016;68:915–23.
- Love TJ, Zhu Y, Zhang Y, et al. Obesity and the risk of psoriatic arthritis: a population-based study. *Ann Rheum Dis* 2012;71:1273–7.
- Wilson FC, Icen M, Crowson CS, et al. Incidence and clinical predictors of psoriatic arthritis in patients with psoriasis: a population-based study. *Arthritis Rheum* 2009;61:233–9.
- Tey HL, Ee HL, Tan AS, et al. Risk factors associated with having psoriatic arthritis in patients with cutaneous psoriasis. *J Dermatol* 2010;37:426–30.
- Lewinson RT, Vallerand IA, Lowerison MW, et al. Depression is associated with an increased risk of psoriatic arthritis among patients with psoriasis: a population-based study. *J Invest Dermatol* 2017;137:828–35.
- Eder L, Law T, Chandran V, et al. Association between environmental factors and onset of psoriatic arthritis in patients with psoriasis. *Arthritis Care Res (Hoboken)* 2011;63:1091–7.
- Thorarensen SM, Lu N, Ogdie A, et al. Physical trauma recorded in primary care is associated with the onset of psoriatic arthritis among patients with psoriasis. *Ann Rheum Dis* 2017;76:521–5.
- Eder L, Polachek A, Rosen CF, et al. The development of psoriatic arthritis in patients with psoriasis is preceded by a period of nonspecific musculoskeletal symptoms: a prospective cohort study. *Arthritis Rheumatol* 2017;69:622–9.
- Faustini F, Simon D, Oliveira I, et al. Subclinical joint inflammation in patients with psoriasis without concomitant psoriatic arthritis: a cross-sectional and longitudinal analysis. *Ann Rheum Dis* 2016;75:2068–74.
- Moons KG, Royston P, Vergouwe Y, et al. Prognosis and prognostic research: what, why, and how? *BMJ* 2009;338:b375.
- Ryan C, Korman NJ, Gelfand JM, et al. Research gaps in psoriasis: opportunities for future studies. *J Am Acad Dermatol* 2014;70:146–67.
- Jadon DR, Chandran V, Stober C, et al. Proceedings of the 2017 GRAPPA Collaborative Research Network Meeting. *J Rheumatol Suppl* 2018;94:54–61.
- Collins GS, Reitsma JB, Altman DG, et al. Transparent Reporting of a multivariable prediction model for Individual Prognosis or Diagnosis (TRIPOD): the TRIPOD Statement. *Ann Intern Med* 2015;162:55–63.
- Du J, Boss J, Han P, et al. Variable selection with multiply-imputed datasets: choosing between stacked and grouped methods. *J Comput Graph Stat* 2022;21:1063–75.
- Cho H, Matthews GJ, Harel O. Confidence intervals for the area under the receiver operating characteristic curve in the presence of ignorable missing data [review]. *Int Stat Rev* 2019;87:152–77.
- Ogdie A, Harrison RW, McLean RR, et al. Prospective cohort study of psoriatic arthritis risk in patients with psoriasis in a real-world psoriasis registry. *J Am Acad Dermatol* 2022;87:1303–11.
- Ogdie A, Shin DB, Love TJ, et al. Body surface area affected by psoriasis and the risk for psoriatic arthritis: a prospective population-based cohort study. *Rheumatology (Oxford)* 2022;61:1877–84.

21. FitzGerald O, Haroon M, Giles JT, et al. Concepts of pathogenesis in psoriatic arthritis: genotype determines clinical phenotype. *Arthritis Res Ther* 2015;17:115.
22. Eder L, Tu K, Rosen CF, et al. Health care utilization for musculoskeletal issues during the prediagnosis period in psoriatic arthritis: a population-based study. *Arthritis Care Res (Hoboken)* 2021;73:680–6.
23. Lindberg I, Lilja M, Geale K, et al. Incidence of psoriatic arthritis in patients with skin psoriasis and associated risk factors: a retrospective population-based cohort study in Swedish routine clinical care. *Acta Derm Venereol* 2020;100:adv00324.
24. Meer E, Merola JF, Fitzsimmons R, et al. Does biologic therapy impact the development of PsA among patients with psoriasis? *Ann Rheum Dis* 2022;81:80–6.
25. Felquer ML, LoGiudice L, Galimberti ML, et al. Treating the skin with biologics in patients with psoriasis decreases the incidence of psoriatic arthritis. *Ann Rheum Dis* 2022;81:74–9.
26. Gisondi P, Bellinato F, Targher G, et al. Biological disease-modifying antirheumatic drugs may mitigate the risk of psoriatic arthritis in patients with chronic plaque psoriasis. *Ann Rheum Dis* 2022;81:68–73.
27. Karlson EW, Ding B, Keenan BT, et al. Association of environmental and genetic factors and gene–environment interactions with risk of developing rheumatoid arthritis. *Arthritis Care Res (Hoboken)* 2013;65:1147–56.
28. Van de Stadt LA, Witte BI, Bos WH, et al. A prediction rule for the development of arthritis in seropositive arthralgia patients. *Ann Rheum Dis* 2013;72:1920–6.
29. Prado MG, Iversen MD, Yu Z, et al. Effectiveness of a web-based personalized rheumatoid arthritis risk tool with or without a health educator for knowledge of rheumatoid arthritis risk factors. *Arthritis Care Res (Hoboken)* 2018;70:1421–30.
30. Sparks JA, Iversen MD, Kroouze RM, et al. Personalized Risk Estimator for Rheumatoid Arthritis (PRE-RA) Family Study: rationale and design for a randomized controlled trial evaluating rheumatoid arthritis risk education to first-degree relatives. *Contemp Clin Trials* 2014;39:145–57.

Outcome of Patients With Lupus Nephritis Treated With an Anti-CD40 Monoclonal Antibody According to Kidney Biopsy Features

Martina Uzzo,¹  Helmut Schumacher,² Juergen Steffgen,³ Simone Deutschel,⁴ David Jayne,⁵ 
and Ingeborg Bajema⁶

Objective. A phase 2 trial tested different doses of the anti-CD40 monoclonal antibody BI 655064 as an add-on therapy to the standard of care in patients with class III or IV lupus nephritis (LN) with active disease. A post hoc analysis showed a potential benefit of the higher tested doses (180 and 240 mg) versus a low dose (120 mg) or placebo. We investigated whether the treatment effect of BI 655064 on kidney outcomes may be modified by the presence of glomerular monocytes, a target for this drug with a well-known role in LN pathogenesis.

Methods. One hundred one renal biopsies of patients with LN enrolled in the BI 655064 trial were scored centrally. The estimated glomerular filtration rate (eGFR), spot urine protein/urine creatinine ratio (UP/UC), and complete renal response (CRR) were evaluated over 52 weeks. Patients were divided according to a “better” or “worse” performance than the average of all patients in the cohort, predicted by a mixed model for repeated measurements. Logistic regression models adjusted for potential confounders were used to assess the association between different treatment doses and outcomes according to the presence or absence of monocytes.

Results. A higher BI 655064 dose (180 or 240 mg) was associated with better outcomes of UP/UC and CRR when glomerular monocytes were present in kidney biopsy samples (odds ratio [OR] 3.66 [95% confidence interval (CI) 1.09–12.3], $P = 0.04$; OR 4.58 [95% CI 1.24–16.9], $P = 0.02$). A trend toward improved eGFR was also observed in these patients (at 52 weeks, $P = 0.08$).

Conclusion. In LN kidney biopsy samples with glomerular monocytes, high-dose BI 655064 treatment improved proteinuria at 52 weeks and resulted in a higher CRR compared to biopsy samples without glomerular monocytes. Histologic features may guide the choice of treatment for individual patients with LN.

INTRODUCTION

Lupus nephritis (LN) is a common and serious manifestation of systemic lupus erythematosus (SLE). About one-third of patients with SLE develop LN within five years from disease onset, and kidney involvement is responsible for an increase in SLE-related mortality and morbidity.^{1,2} Particularly, kidney biopsy samples identified as International Society of Nephrology/Renal Pathology Society (ISN/RPS) class III or IV LN are associated with a worse renal outcome, causing irreversible kidney damage.^{3–5}

A deeper insight into the pathogenesis of the disease and the introduction of new treatment options changed LN management over the last decades^{4,6–8}; however, the risk of end-stage kidney disease (ESKD) in LN is still 5% to 30% at 10 years.^{2,9,10} A recent randomized, double-blind, placebo-controlled, phase 2 trial tested different doses of the anti-CD40 monoclonal antibody BI 655064 as an add-on therapy to standard of care (SoC) (mycophenolate mofetil plus glucocorticoids) in LN patients with active renal disease (protein level in urine >1 g/day) and ISN/RPS 2003 class III or IV LN at kidney biopsy.¹¹

Presented in part at the European Renal Association Congress 2023 and as a poster at the American Society of Nephrology Kidney Week 2023.

Supported by Boehringer Ingelheim.

¹Martina Uzzo, MD: University of Milano-Bicocca, Monza, Italy, and University of Groningen, University Medical Center, Groningen, The Netherlands; ²Helmut Schumacher, PhD: Statistical Consultant, Ingelheim, Germany; ³Juergen Steffgen, MD, PhD: Boehringer Ingelheim International, Biberach, Germany; ⁴Simone Deutschel, MSc: Boehringer Ingelheim RCV, Vienna, Austria; ⁵David Jayne, MD: University of Cambridge, Cambridge, United Kingdom; ⁶Ingeborg Bajema, MD, PhD: University of Groningen, University Medical Center, Groningen, The Netherlands.

Additional supplementary information cited in this article can be found online in the Supporting Information section (<https://acrjournals.onlinelibrary.wiley.com/doi/10.1002/art.43076>).

Author disclosures are available at <https://onlinelibrary.wiley.com/doi/10.1002/art.43076>.

Address correspondence via email to Martina Uzzo, MD, at m.uzzo@campus.unimib.it.

Submitted for publication April 5, 2024; accepted in revised form November 22, 2024.

The pathway leading to both physiologic and pathologic antibody production requires lymphocyte activation through paired costimulatory signals, such as CD40–CD40L. CD40 is a transmembrane receptor belonging to the tumor necrosis factor superfamily, expressed on antigen-presenting cells (APCs). CD40–CD40L interaction plays a key role in LN pathogenesis, and, in patients with SLE, CD40L is overexpressed in various cell types, such as B and T cells, monocytes, and dendritic cells. Moreover, the infiltration of monocytes in glomeruli affected by LN is a CD40–CD40L mediated process.^{4,12}

In 2003, a trial tested the efficacy of BG9588, a humanized anti-CD40L antibody, in patients with class III or IV LN; although serologic markers improved, a higher incidence of thrombotic events occurred in the treatment cohort, and the trial was suspended.¹³ Two mutations in the fragment crystallizable domain prevented complement and platelet activation in the second-generation anti-CD40 antibody BI 655064. Although the BI 655064 phase 2 trial failed to demonstrate a dose–response relationship for complete renal response (CRR) at 52 weeks (a composite outcome based on proteinuria and the estimated glomerular filtration rate [eGFR]), a post hoc analysis showed a benefit of the higher tested doses (180 and 240 mg) versus a low dose (120 mg) and placebo.¹¹

We investigated whether the add-on therapy with BI 655064 would be of particular benefit for certain patients with a specific biopsy profile. For this study, we focused on monocytes: APCs that have a physiologic constitutive expression of CD40 on their cell membranes, are easily recognizable using light microscopy, and have a well-known role in LN pathogenesis. The objective of our study was to examine whether high-dose treatment with BI 655064 showed a higher efficacy on renal outcomes, namely proteinuria and eGFR, in patients with a particular kidney biopsy profile, thereby focusing in more detail on monocytes.

MATERIALS AND METHODS

Patients and study design. We collected kidney biopsy samples from patients with LN, classified according to the ISN/RPS LN classification in a central review, who were enrolled in the phase 2 BI 655064 trial.¹¹ The study was conducted in accordance with the principles of the Declaration of Helsinki and under the guidance of The Strengthening the Reporting of Observational Studies in Epidemiology cohort reporting guidelines.¹⁴

Patients. The multicentric, randomized, double-blind, placebo-controlled, phase 2 trial evaluated the effect of the anti-CD40 monoclonal antibody BI 655064 on CRR in patients with active LN for 52 weeks.¹¹ Patients were randomized to receive a dose of 120, 180, or 240 mg of BI 655064 or placebo in a 1:1:2:2 ratio. Patients in both the placebo and the BI 655064 arms were treated with the SoC of LN. Patients between 18 and 70 years of age with an American College of Rheumatology

criteria-based diagnosis of SLE¹⁵ and biopsy-proven LN were enrolled. Active renal disease was defined by a Spot urine protein/urine creatinine ratio (UP/UC) ≥ 1 at screening. Patients who received immunosuppressive induction therapy during the six months before screening were excluded. Induction therapy for LN with SoC started within six weeks before randomization was allowed.

Renal biopsies. Patients with kidney biopsy samples identified as ISN/RPS 2003 class III or IV LN were included, and the coexistence of class V was allowed.⁵ Kidney biopsies had to be performed within three months before screening. From the initial trial cohort ($n = 121$), we received all but four kidney biopsy samples ($n = 117$). After central evaluation, we included 101 biopsy samples in the study, distributed across the control and treatment groups as per previous randomization. Supplemental Figure 1 shows the biopsy sample selection process.

Renal biopsy assessment. Kidney biopsy samples were received at Pathan Laboratories in Rotterdam, the Netherlands, between February 1, 2020, and September 15, 2022, for central evaluation. Original glass slides of all biopsy samples were provided and checked for quality. Hematoxylin and eosin, periodic acid–Schiff, and periodic acid methenamine silver stains were provided. Immunofluorescence and electron microscopy findings were provided from the original reports, and whether they were consistent with a diagnosis of LN was checked. Each biopsy sample was evaluated by an experienced pathologist (IB), who was unaware of the actual treatment arm. Agreement between the eventual classes as defined by the local laboratory and the central evaluation was determined. Biopsy samples were evaluated according to a previously established scoring form that consisted of two parts: part 1 contained general data, such as ISN/RPS 2003 LN classification; part 2 contained detailed histologic parameters scored for each glomerulus separately (Supplemental Table 1). Inflammatory cells in glomeruli were first scored as either absent or present, irrespective of their exact location in the glomerular tuft. Subtypes (lymphocytes, monocytes, neutrophil granulocytes, eosinophilic granulocytes) were scored as positive in a single glomerulus if there were at least three cells of a subtype present. The presence or absence of inflammatory cells was evaluated through direct count using light microscopy. Immunostaining was not available.

Clinical data. Baseline demographic and clinical data were provided by the BI 655064 phase 2 trial team. Clinical measurements consisted of the eGFR (Chronic Kidney Disease Epidemiology Collaboration equation [CDK-EPI]) and spot UP/UC at baseline and weeks 1, 2, 4, 6, 8, 12, 16, 21, 26, 30, 35, 40, 46, and 52. Twenty-four-hour urine was collected at baseline and weeks 26 and 52.

Outcome measures. In a first step, we investigated the association between biopsy sample features and kidney outcomes. Among the biopsy sample features detailed in Supplemental Table 1 (part 2), those occurring in fewer than 10 patients were excluded. Kidney outcomes were CRR at the last available visit, spot UP/UC, and eGFR in the overall cohort. CRR was defined as both a urine protein level <0.5 g/g creatinine (derived using spot urine collections) and either an eGFR (CDK-EPI) ≥ 90 mL/min/1.73 m² or a $<20\%$ decrease from baseline if the eGFR was <90 mL/min/1.73 m².

In a second step, all biopsy sample features that appeared to be related to clinical outcome in the first step were entered into one multivariable model. Through a routine model selection procedure, biopsy sample features predictive of clinical outcome were identified.

Finally, because monocytes express CD40, which is the target of BI 655064, we investigated whether high-dose treatment with BI 655064 (180 and 240 mg) was beneficial when monocytes were present in the biopsy sample. The model used for this analysis was adjusted for all the predictors identified in the multivariable model of the second step.

Data analysis. Categorical data are presented as percentages, and continuous data are presented as means with SDs or medians with interquartile ranges, as appropriate. Because the distribution of UP/UC is known to be skewed, data were log-transformed before analysis. Interrater agreement between central and local biopsy LN classification was tested using McNemar's test and quantified using the kappa coefficient.

Regarding clinical outcome measures, patients were divided in "better" or "worse" performers, indicative of their outcome in comparison to the average performance of all patients in the cohort for CRR. Patients who met the response criteria belonged to the "better" group, and those with no response belonged to

the "worse" group. For UP/UC and eGFR, the performance was evaluated through a mixed model for repeated measurements, including all available measurements adjusting for baseline. Better or worse performers were assessed depending on whether the last observed value of an individual patient was higher or lower than the value predicted by the model at the respective visit; in this way, all patients with at least one follow-up measurement were included in the analysis. For each histopathologic feature, we tested whether the biopsy values were differently distributed between the "better" and "worse" groups using the chi-square test for categorical data and the Wilcoxon rank sum test for count data. Features with a P value <0.1 were entered into a logistic regression model with outcome (better or worse) as a response, and a model selection procedure was used to identify the best multivariable model for the prediction of clinical outcome based on biopsy parameters. We applied the forward selection method with a P value of 0.2 for inclusion into the model. The final model (also logistic regression) included as main factors the presence or absence of monocytes, treatment (placebo or 120 mg of BI 655064 vs 180 and 240 mg of BI 655064), and the respective interaction and was adjusted for the biopsy sample features previously identified as potentially predictive. Results are expressed as odds ratios (ORs) with two-sided 95% confidence intervals (CIs) in the two strata. Two-sided P values <0.05 were considered significant. Analyses were performed using SAS statistical software version 9.4 (SAS Institute Inc). The data underlying this article will be shared on reasonable request to the corresponding author.

RESULTS

Patient selection and characteristics of the study population. Patient selection is reported in Figure 1. The 101 eligible patients were divided into four groups according to therapy,

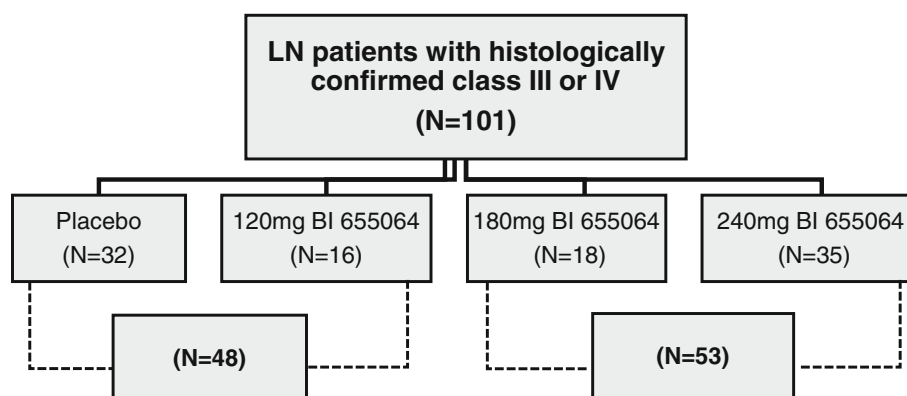


Figure 1. Patient selection chart. According to the International Society of Nephrology/Renal Pathology Society 2003 classification, patients with class III or IV LN were included, and the coexistence of class V was allowed. A cohort of 101 patients was eligible for the study (see text for further details). Patients had been previously randomized in four groups, as per the BI 655064 phase 2 trial protocol (2:1:1:2): 32 patients were in the placebo arm, 16 were in the 120-mg BI 655064 arm, 18 were in the 180-mg BI 655064 arm, and 35 were in the 240-mg BI 655064 arm. For analytical purposes, we combined patients belonging to the placebo and the low-dose 120-mg BI 655064 groups (48 patients) as well as those in the high-dose 180- and 240-mg BI 655064 groups (53 patients). LN, lupus nephritis.

Table 1. Baseline characteristics of a cohort of patients with ISN/RPS class III and class IV LN*

	Total	Treatment			
		Placebo	BI 655064 (120 mg)	BI 655064 (180 mg)	BI 655064 (240mg)
Number of patients	101	32	16	18	35
Age at screening, mean (SD), y	34.3 (10.1)	32.8 (8.5)	36.2 (12.0)	34.9 (10.0)	34.6 (10.8)
Female sex, n (%)	89 (88)	31 (97)	11 (69)	16 (89)	31 (89)
Time since diagnosis, n (%)					
<24 mo	52 (52)	18 (56)	7 (44)	9 (50)	18 (51)
≥24 mo	49 (49)	14 (44)	9 (56)	9 (50)	17 (49)
eGFR (CDK-EPI), mean (SD), mL/min/1.73 m ²	90.3 (29.5)	88.3 (27.4)	88.1 (32.4)	99.9 (22.2)	88.3 (33.2)
UP/UC (spot urine), median (IQR), g/g	2.8 (1.4–4.6)	2.6 (1.0–3.9)	4.2 (1.5–8.7)	3.0 (2.2–4.3)	2.7 (1.1–3.9)
SLEDAI score, mean (SD)	11.0 (5.5)	10.9 (5.4)	11.0 (5.7)	10.6 (6.5)	11.4 (5.2)
ISN/RPS 2003 LN classification (central evaluation), n (%)					
III	32 (32)	14 (44)	5 (31)	4 (22)	9 (26)
IV	69 (68)	18 (56)	11 (69)	14 (78)	26 (74)

* Data are from the control arm and the different BI 655064 dose groups. For analytical purposes, we combined the placebo and the 120-mg BI 655064 treatment groups and the 180- and 240-mg BI 655064 treatment groups. Baseline characteristics refer to the time of screening. Continuous variables are reported as mean (SD) or median (IQR), and categorical variables are reported as n (%). CDK-EPI, Chronic Kidney Disease Epidemiology Collaboration formula; eGFR, estimated glomerular filtration rate; IQR, interquartile range; ISN, International Society of Nephrology; LN, lupus nephritis; RPS, Renal Pathology Society; SLEDAI, Systemic Lupus Erythematosus Disease Activity Index; UP/UC, urine protein/urine creatinine ratio.

as per previous randomization (2:1:1:2): 32 patients were in the placebo arm, 16 were in the 120-mg BI 655064 arm, 18 were in the 180-mg BI 655064 arm, and 35 were in the 240-mg BI 655064 arm.

The clinical and demographic characteristics of the total cohort and the different treatment groups are shown in Table 1. The mean age of patients enrolled in the total cohort was 34.3 (SD 10.1) years, and there was an expected female predominance (88%). Of the 101 patients enrolled, 49 (49%) were

diagnosed with SLE more than 24 months before screening. The mean eGFR (CDK-EPI) at screening in the total cohort was 90.3 (SD 29.5) mL/min/1.73 m², and the median UP/UC was 2.4 (interquartile range 1.4–4.5). The mean Systemic Lupus Erythematosus Disease Activity Index score at baseline was 11.0 (SD 5.5).

The mean number of glomeruli in the overall cohort was 18.6 (SD 11.7). There was a higher prevalence of the ISN/RPS class IV SLE renal biopsy results compared to class III (68% vs 32%, respectively).⁵ A moderate agreement between local and central

Table 2. Baseline characteristics of a cohort of patients with ISN/RPS class III and class IV LN*

	Total	Treatment		P value ^a
		Placebo and BI 655064 (120 mg)	BI 655064 (180 mg) and BI 655064 (240 mg)	
Number of patients	101	48	53	–
Age at screening, mean (SD), y	34.3 (10.1)	33.9 (9.8)	34.7 (10.4)	0.71
Female sex, n (%)	89 (88)	42 (88)	47 (89)	0.85
Time since diagnosis, n (%)				0.91
<24 mo	52 (52)	25 (52)	27 (51)	–
≥24 mo	49 (49)	23 (48)	26 (49)	–
eGFR (CDK-EPI), mean (SD), mL/min/1.73 m ²	90.3 (29.5)	88.2 (28.8)	92.2 (30.2)	0.50
UP/UC (spot urine), median (IQR), g/g	2.8 (1.4–4.6)	2.9 (1.1–5.4)	2.7 (1.6–4.1)	0.70
SLEDAI score, mean (SD)	11.0 (5.5)	11.0 (5.4)	11.1 (5.6)	0.90
ISN/RPS 2003 LN classification (central evaluation), n (%)				0.10
III	32 (32)	19 (40)	13 (25)	–
IV	69 (68)	29 (60)	40 (76)	–

* Data are from the combined placebo and 120-mg BI 655064 treatment groups compared to the combined 180- and 240-mg BI 655064 treatment groups. Baseline characteristics refer to the time of screening. Continuous variables are reported as mean (SD) or median (IQR), and categorical variables are reported as n (%). CDK-EPI, Chronic Kidney Disease Epidemiology Collaboration formula; eGFR, estimated glomerular filtration rate; IQR, interquartile range; ISN, International Society of Nephrology; LN, lupus nephritis; RPS, Renal Pathology Society; SLEDAI, Systemic Lupus Erythematosus Disease Activity Index; UP/UC, urine protein/urine creatinine ratio.

^a P < 0.05.

assessment of ISN/RPS classes in LN was shown (simple κ coefficient 0.48, 95% CI 0.29–0.67). A total of 54 (53.5%) patients had a biopsy sample with monocytes present, whereas 47 (46.5%) did not.

For this analysis, we combined patients belonging to the placebo and the low-dose 120-mg BI 655064 groups as well as those in the high-dose 180- and 240-mg BI 655064 groups: altogether, there were 48 and 53 patients, respectively. Data of the two combined groups are reported in Table 2. Clinical and demographic features at baseline were similar in the two combined groups. Furthermore, class III and IV were about equally distributed.

Histologic and clinical parameters association.

Patients were classified in two groups according to a better or

worse performance. At the end of treatment (52 weeks), 78 (77%) and 82 (81%) patients had available UP/UC and eGFR measurement, respectively. We tested the association between histologic parameters and better or worse renal outcomes in the overall cohort; the main results are shown in Table 3 (biopsy sample features that were not statistically significant at the univariate analysis are not reported in Table 3). The presence or absence of monocytes in the glomerular tuft was tested too; no association with a better or worse outcome was shown in the overall cohort, irrespective of treatment. The presence of karyorrhexis was associated with a better outcome in terms of UP/UC (OR 2.88 [95% CI 1.06–7.83], $P = 0.04$). The presence of endocapillary hypercellularity in more than 50% of glomeruli was associated with a better outcome in terms of eGFR when compared to biopsy samples with endocapillary hypercellularity in less than 20% of glomeruli

Table 3. Univariable and multivariable analysis of correlation between findings in renal biopsy and outcomes in the total population*

	Univariable analysis ^a	Multivariable analysis ^b	
	P^c	OR (95% CI) ^d	P^c
UP/UC, g/g			
LN class (IV vs III)	0.02	–	–
Ischemic cells	0.07	–	–
Interstitial fibrosis	0.03		0.18
$\geq 5\%$ vs $< 5\%$		0.50 (0.19–1.30)	–
$\geq 25\%$ vs $< 5\%$		0.34 (0.08–1.50)	–
Lymphocytes	0.04	–	–
Glomerular monocytes	0.09	–	–
Crescents, extracapillary proliferation	0.09	–	–
Karyorrhexis	0.02	2.88 (1.06–7.83)	0.04
Pseudothrombi	0.03	2.38 (0.83–6.81)	0.10
eGFR (CDK-EPI), mL/min/1.73 m ²			
Infiltration	0.09	–	–
Infiltration neutrophils	0.06	5.08 (0.53–48.4)	0.16
LN class (IV vs III)	0.04	–	–
Endocapillary hypercellularity	0.006		0.009
$\geq 20\%$ vs $< 20\%$		1.38 (0.40–4.76)	
$\geq 50\%$ vs $< 20\%$		4.57 (1.38–15.1)	
Endothelial swelling	0.007	–	–
Influx of inflammatory cells	0.03	–	–
Lymphocytes	0.02	–	–
Synechia/adhesion	0.07	–	–
Pseudothrombi	0.04	–	–
CRR at last available visit			
Interstitial fibrosis	0.019		0.043
$\geq 5\%$ vs $< 5\%$		0.39 (0.15–1.65)	
$\geq 25\%$ vs $< 5\%$		0.23 (0.06–0.95)	
Reabsorption droplets	0.029	2.94 (0.99–8.76)	0.05
Ischemic cells	0.023	–	–
Pseudothrombi	0.024	2.97 (1.02–8.65)	0.05

* All the collected biopsy features occurring in at least 10 patients were entered in an univariable analysis (Supplemental Table 1, part 2). Parameters with a P value < 0.1 in the univariable analyses were entered into a multivariable logistic regression model, and a routine model selection procedure (with $P < 0.2$) was used to identify parameters predictive for outcome in the overall cohort. Biopsy features with a P value ≥ 0.1 at the univariable analysis were not reported in this table. CDK-EPI, Chronic Kidney Disease Epidemiology Collaboration formula; CI, confidence interval; CRR, complete renal response; eGFR, estimated glomerular filtration rate; LN, lupus nephritis; OR, odds ratio; UP/UC, urine protein/urine creatinine ratio.

^a Chi-square or Wilcoxon test; only parameters with a P value < 0.1 are presented.

^b Logistic regression; only parameters with a P value < 0.2 are presented.

^c $P < 0.05$.

^d For “better” outcome.

Table 4. Treatment effect related to the presence of monocytes*

BI 655064 (180 and 240 mg) vs placebo/BI 655064 (120 mg)	Presence of monocytes (n = 54)		Absence of monocytes (n = 47)	
	OR (95% CI) ^a	P ^b	OR (95% CI) ^a	P ^b
UP/UC, g/g				
Adjusted analysis ^c	3.66 (1.09–12.3)	0.04	1.36 (0.39–4.72)	0.63
Unadjusted analysis	3.89 (1.25–12.1)	0.02	1.28 (0.40–4.12)	0.42
eGFR (CDK-EPI), mL/min/1.73 m ²				
Adjusted analysis ^c	2.41 (0.73–7.98)	0.15	0.69 (0.19–2.48)	0.57
Unadjusted analysis	2.62 (0.85–7.97)	0.09	1.08 (0.34–3.41)	0.89
CRR at last available visit				
Adjusted analysis ^c	4.58 (1.24–16.9)	0.02	0.77 (0.20–2.98)	0.71
Unadjusted analysis	3.33 (1.09–10.2)	0.02	1.29 (0.39–4.24)	0.68

* The effect of high-dose treatment (BI 655064 180 mg plus BI 655064 240 mg) vs low-dose treatment or no treatment (placebo plus BI 655064 120 mg) on outcomes was evaluated according to the presence or absence of monocytes in kidney biopsy samples. A total of 54 (53.5%) biopsy samples contained monocytes, whereas 47 (46.5%) did not. The model was adjusted for all the significant predictors previously entered in the multivariable regression model on the overall cohort. The results of both the adjusted and unadjusted analyses are reported. Features occurring in fewer than 10 patients were excluded. CDK-EPI, Chronic Kidney Disease Epidemiology Collaboration formula; CI, confidence interval; CRR, complete renal response; eGFR, estimated glomerular filtration rate; OR, odds ratio; UP/UC urine protein/urine creatinine ratio.

^a For “better” outcome.

^b $P < 0.05$.

^c The model was adjusted for all the significant predictors previously identified in the multivariable analysis: interstitial fibrosis, karyorrhexis, pseudothrombi for UP/UC, infiltration granulocytes, endocapillary hypercellularity for eGFR, interstitial fibrosis, reabsorption droplets, and pseudothrombi for CRR.

(OR 4.57 [95% CI 1.38–15.1], $P = 0.01$ in global trend test). Finally, the association between clinical and histologic parameters was evaluated according to CRR at the last available visit: interstitial fibrosis in more than 25% of the biopsy sample was predictive of negative outcome when compared to biopsy samples with interstitial fibrosis in less than 5% of the sample (OR 0.23 [95% CI 0.06–0.95], $P = 0.04$ in global trend test). Furthermore, the presence of pseudothrombi was associated with a better outcome (OR 2.97 [95% CI 1.02–8.65], $P = 0.05$).

Treatment efficacy according to the presence of monocytes. Table 4 describes the effect of high-dose BI 655064 versus low-dose BI 655064 or placebo according to the presence or absence of monocytes in the kidney biopsy sample. Dose-dependent treatment efficacy was compared in the two groups after adjustment for the previously identified potential confounders (interstitial fibrosis, karyorrhexis, pseudothrombi for UP/UC, infiltration of granulocytes, endocapillary hypercellularity for eGFR, interstitial fibrosis, reabsorption droplets, and pseudothrombi for CRR). A higher treatment dose was associated with a better UP/UC outcome and a higher CRR in kidney biopsy samples containing glomerular monocytes (OR 3.66 [95% CI 1.09–12.3], $P = 0.04$; OR 4.58 [95% CI 1.24–16.9], $P = 0.02$, respectively). In contrast, a higher treatment dose was not predictive of the outcomes in kidney biopsy samples without glomerular monocytes.

The UP/UC mean profile over time, adjusted for the previously identified variables, is shown in Figure 2A and B. When we evaluated kidney biopsy samples containing glomerular monocytes, the UP/UC mean profile over time differed in the high-dose and

low-dose and placebo groups, reaching statistical significance at the end of follow-up (at 52 weeks, $P = 0.057$) (Figure 2A). In contrast, the UP/UC trend over time was similar in the two treatment groups when we evaluated biopsy samples without glomerular monocytes (at 52 weeks, $P = 0.92$) (Figure 2B).

The same process was used to evaluate the effect of high-dose treatment with BI 655064 on eGFR. No substantial association with the outcome was shown, neither with presence nor with absence of monocytes in kidney biopsy samples (Table 4). However, when we evaluated the eGFR mean profile over time, after adjusting for the previously identified confounders, a benefit of the higher doses in patients with monocytes in kidney biopsy samples was suggested at the end of follow-up (at 52 weeks, $P = 0.075$) (Figure 2C). Similarly to UP/UC, the eGFR trend over time did not diverge in the two treatment groups when we evaluated biopsy samples without glomerular monocytes (at 52 weeks, $P = 0.9830$) (Figure 2D).

DISCUSSION

In this post hoc analysis of the BI 655064 phase 2 trial, we showed that if glomerular monocytes were present in LN kidney biopsy samples, high-dose treatment with anti-CD40 monoclonal antibody improved the reduction of proteinuria at 52 weeks and led to a higher CRR than if monocytes were absent. Our study used a novel approach to investigate the relationship between specific features in kidney biopsy samples and treatment outcomes, suggesting that specific renal biopsy sample characteristics could direct the choice of treatment for individual patients with LN.

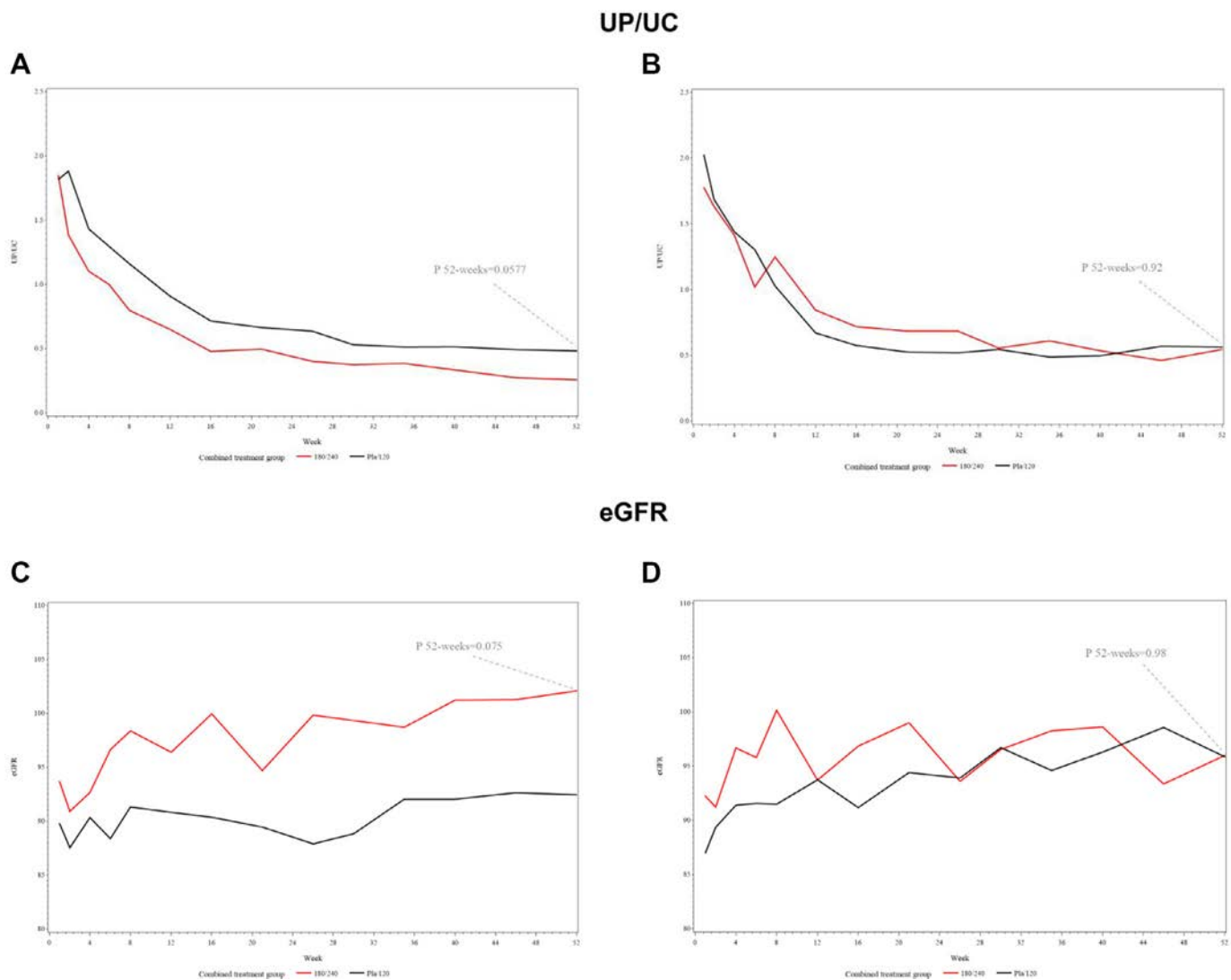


Figure 2. The impact of different treatment doses on UP/UC and eGFR mean profiles over 52 weeks in patients with (A and C) and without (B and D) monocytes in kidney biopsy samples. UP/UC and eGFR mean profile over 52 weeks were adjusted for the previously identified variables (interstitial fibrosis, karyorrhexis, pseudothrombi for UP/UC, infiltration of granulocytes, and endocapillary hypercellularity for eGFR). When we evaluated kidney biopsy samples containing glomerular monocytes, the UP/UC mean profile over 52 weeks differed in the high-dose (180 and 240 mg) and low-dose (120 mg) and placebo groups, reaching statistical significance at the end of follow-up (at 52 weeks, $P = 0.057$) (A). In contrast, the UP/UC trend over 52 weeks was similar in the two treatment groups when we evaluated biopsy samples with no glomerular monocytes (at 52 weeks, $P = 0.92$) (B). When we evaluated kidney biopsy samples containing glomerular monocytes, the eGFR mean profile over 52 weeks differed in the high-dose and low-dose and placebo groups. Despite the lack of statistical significance, the trend suggested a benefit of the higher doses at the end of follow-up (at 52 weeks, $P = 0.075$) (C). In contrast, the eGFR trend at 52 weeks was similar in the two treatment groups when we evaluated biopsy samples with no glomerular monocytes (at 52 weeks, $P = 0.98$) (D). eGFR, estimated glomerular filtration rate; UP/UC, spot urine protein/urine creatinine ratio.

The presence or absence of glomerular monocytes may guide the choice of anti-CD40 treatment use in future decision trees, resulting in selection of the most appropriate therapy for the most suitable patient.

Monocytes play a fundamental biologic role in LN and immune-complex glomerulonephritis, leading to kidney inflammation with different mechanisms: they mediate glomerular inflammation by patrolling and engaging other effectors, such as neutrophils, leading to further tissue injury; they may damage kidney tissue by

differentiating into macrophages producing proinflammatory cytokines^{16,17}; they can also act as APCs, presenting antigens intravascularly within glomerular capillaries.¹⁸

The infiltration of monocytes in glomeruli affected by LN is a CD40–CD40L mediated process.^{4,12} Up-regulation of CD40 on mesangial cells and endothelial cells leads to an increased production of monocyte chemoattractant protein 1 and adhesion molecules, facilitating monocyte adhesion and migration into the glomeruli.^{19–21} Previous studies revealed an up-regulated

expression of CD40 on immune and nonimmune cells in kidney biopsy samples of patients with proliferative LN; particularly, a single-cell RNA sequencing technique detected higher CD40 expression on B cells and macrophages of patients with class III and IV LN compared to healthy controls.^{19,22–24} Because CD40 is constitutively expressed on monocytes, these cells may be a particular target of anti-CD40 antibodies.²⁵

In 2004, Ruth et al²⁶ demonstrated the requirement for CD40–CD40L in delayed-type hypersensitivity crescentic glomerulonephritis, suggesting CD40 as a therapeutic target in humans. Perper et al²⁷ developed a chimeric anti-mouse CD40 antagonist monoclonal antibody and evaluated its ability to alleviate murine lupus. Their results showed reduced proteinuria and kidney inflammation, characterized by less CD3-positive T cells.²⁷ In addition to local effects, CD40 overexpression in patients with SLE was demonstrated in circulating cells.²⁸ Ideally, we would have liked to do immunohistochemical staining to evaluate all of the cells expressing CD40 in the glomeruli; however, unstained biopsy slides were not available, and we relied on morphologic details.

In the overall cohort, the presence or absence of monocytes in the glomerular tuft was not associated with the outcome. It was only in our more detailed analysis that we found that glomerular monocytes were modifying the effect of BI 655064 treatment on kidney outcomes, namely proteinuria and CRR. Proteinuria is a determinant of renal response in SLE clinical practice and trials because it is a risk factor for ESKD.^{6,29–32} In this analysis, the presence of monocytes in kidney biopsy samples of patients with LN was predictive of lower proteinuria and a higher CRR at 52 weeks. Although no significant effect was shown in terms of eGFR, the mean eGFR profiles of the two treatment groups diverged over time, showing a potential benefit of the higher doses in patients with monocytes in their kidney biopsy samples. The lack of statistical significance may be explained by the small sample size and original inclusion criteria: patients with an eGFR <30 mL/min/1.73 m² were excluded from the trial, and active renal disease was defined on a proteinuria-based cutoff (protein level in urine \geq 1.0 g/day or UP/UC \geq 1).¹¹ The baseline eGFR in the overall cohort was almost normal, and the time of follow-up was relatively short (52 weeks). We did not expect important changes based on eGFR, which may fail to reveal substantial parenchymal damage for a long time.

We acknowledge that our study has limitations. Although justified by the results of the phase 2 BI 655064 trial,¹¹ which demonstrated a beneficial effect of the higher doses of BI 655064 (180 and 240 mg) on kidney outcomes and showed that the low dose was so low that it had no effect at all, we mixed the placebo with the low-dose drug arm and compared it with the higher doses. All histopathological features were evaluated by a blinded experienced renal pathologist (IB), with no second opinion. The presence or absence of glomerular monocytes was evaluated through direct count using light microscopy.

Immunohistochemical staining could not be performed because of the lack of unstained tissue.

Through a novel reliable statistical approach, we investigated the predictive role of histologic features on renal outcomes in the overall cohort. The association of pseudothrombi, karyorrhexis, and endocapillary hypercellularity with a positive outcome was indicative of active disease, with a high burden of immunologic activity in the kidney, which is supposed to respond better to therapy when treated effectively. In line with previous studies,³³ reabsorption droplets may be indicative of a compensatory mechanism to adjust for protein loss, which could be related to the better outcome in terms of CRR.

In conclusion, the quest for the ideal LN regimen is going toward a more personalized patient-centered approach, looking for new therapies as well as subgroups of patients who would respond better to specific therapeutic regimens. Our study deals with this line of research, showing for the first time that the effect of a new specific therapy (BI 655064) could be predicted by the presence of some of its target cells in the kidney biopsy sample. Further studies are needed to confirm our results in bigger cohorts and to identify patterns of predictive features in the renal biopsy sample, making it possible to identify patients who are more suitable for one drug than another and directing the clinicians toward a patient-centered treatment approach.

AUTHOR CONTRIBUTIONS

All authors contributed to at least one of the following manuscript preparation roles: conceptualization AND/OR methodology, software, investigation, formal analysis, data curation, visualization, and validation AND drafting or reviewing/editing the final draft. As corresponding author, Dr Uzzo confirms that all authors have provided the final approval of the version to be published and takes responsibility for the affirmations regarding article submission (eg, not under consideration by another journal), the integrity of the data presented, and the statements regarding compliance with institutional review board/Declaration of Helsinki requirements.

ROLE OF THE STUDY SPONSOR


The study was supported and funded by Boehringer Ingelheim.

REFERENCES

1. Mok CC, Tang SSK. Incidence and predictors of renal disease in Chinese patients with systemic lupus erythematosus. *Am J Med* 2004; 117(10):791–795.
2. Mok CC. Towards new avenues in the management of lupus glomerulonephritis. *Nat Rev Rheumatol* 2016;12(4):221–234.
3. Hahn BH, McMahon MA, Wilkinson A, et al; American College of Rheumatology. American College of Rheumatology guidelines for screening, treatment, and management of lupus nephritis. *Arthritis Care Res (Hoboken)* 2012;64(6):797–808.
4. Ramanujam M, Steffgen J, Visvanathan S, et al. Phoenix from the flames: rediscovering the role of the CD40–CD40L pathway in systemic lupus erythematosus and lupus nephritis. *Autoimmun Rev* 2020;19(11):102668.

5. Bajema IM, Wilhelmus S, Alpers CE, et al. Revision of the International Society of Nephrology/Renal Pathology Society classification for lupus nephritis: clarification of definitions, and modified National Institutes of Health activity and chronicity indices. *Kidney Int* 2018;93(4):789–796.
6. Fanouriakis A, Kostopoulou M, Cheema K, et al. 2019 Update of the Joint European League Against Rheumatism and European Renal Association-European Dialysis and Transplant Association (EULAR/ERA-EDTA) recommendations for the management of lupus nephritis. *Ann Rheum Dis* 2020;79(6):713–723.
7. Furie R, Rovin BH, Houssiau F, et al. Two-year, randomized, controlled trial of belimumab in lupus nephritis. *N Engl J Med* 2020; 383(12):1117–1128.
8. Rovin BH, Solomons N, Pendergraft WF III, et al; AURA-LV Study Group. A randomized, controlled double-blind study comparing the efficacy and safety of dose-ranging voclosporin with placebo in achieving remission in patients with active lupus nephritis. *Kidney Int* 2019;95(1):219–231.
9. Mok CC, Kwok RCL, Yip PSF. Effect of renal disease on the standardized mortality ratio and life expectancy of patients with systemic lupus erythematosus. *Arthritis Rheum* 2013;65(8):2154–2160.
10. Parikh SV, Almaani S, Brodsky S, et al. Update on lupus nephritis: core curriculum 2020. *Am J Kidney Dis* 2020;76(2):265–281.
11. Jayne DR, Steffgen J, Romero-Diaz J, et al. Clinical and biomarker responses to BL 655064, an antagonistic anti-CD40 antibody, in patients with active lupus nephritis: a randomized, double-blind, placebo-controlled, phase II trial. *Arthritis Rheumatol* 2023;75(11): 1983–1993.
12. Fang T, Li B, Li M, et al. Engineered cell membrane vesicles expressing CD40 alleviate systemic lupus nephritis by intervening B cell activation. *Small Methods* 2023;7(3):e2200925.
13. Boumpas DT, Furie R, Manzi S, et al; BG9588 Lupus Nephritis Trial Group. A short course of BG9588 (anti-CD40 ligand antibody) improves serologic activity and decreases hematuria in patients with proliferative lupus glomerulonephritis. *Arthritis Rheum* 2003;48(3): 719–727.
14. von Elm E, Altman DG, Egger M, et al; STROBE Initiative. Strengthening the Reporting of Observational Studies in Epidemiology (STROBE) statement: guidelines for reporting observational studies. *BMJ* 2007; 335(7624):806–808.
15. Aringer M, Costenbader K, Daikh D, et al. 2019 European League Against Rheumatism/American College of Rheumatology Classification Criteria for Systemic Lupus Erythematosus. *Arthritis Rheumatol*. 2019;71(9):1400–1412.
16. Finsterbusch M, Hall P, Li A, et al. Patrolling monocytes promote intravascular neutrophil activation and glomerular injury in the acutely inflamed glomerulus. *Proc Natl Acad Sci USA* 2016;113(35):E5172–E5181.
17. Turner-Stokes T, Garcia Diaz A, Pinheiro D, et al. Live Imaging of monocyte subsets in immune complex-mediated glomerulonephritis reveals distinct phenotypes and effector functions. *J Am Soc Nephrol* 2020;31(11):2523–2542.
18. Westhorpe CLV, Norman MU, Hall P, et al. Effector CD4⁺ T cells recognize intravascular antigen presented by patrolling monocytes. *Nat Commun* 2018;9(1):747.
19. Yellin MJ, D'Agati V, Parkinson G, et al. Immunohistologic analysis of renal CD40 and CD40L expression in lupus nephritis and other glomerulonephritides. *Arthritis Rheum* 1997;40(1):124–134.
20. Delmas Y, Viallard JF, Solanilla A, et al. Activation of mesangial cells by platelets in systemic lupus erythematosus via a CD154-dependent induction of CD40. *Kidney Int* 2005;68(5):2068–2078.
21. Wagrowska-Danilewicz M, Stasikowska O, Danilewicz M. Correlative insights into immunoexpression of monocyte chemoattractant protein-1, transforming growth factor beta-1 and CD68+ cells in lupus nephritis. *Pol J Pathol* 2005;56(3):115–120.
22. Pamfil C, Makowska Z, De Groof A, et al. Intrarenal activation of adaptive immune effectors is associated with tubular damage and impaired renal function in lupus nephritis. *Ann Rheum Dis* 2018;77(12):1782–1789.
23. Uhm WS, Na K, Song GW, et al. Cytokine balance in kidney tissue from lupus nephritis patients. *Rheumatology (Oxford)* 2003;42(8): 935–938.
24. Arazi A, Rao DA, Berthier CC, et al; Accelerating Medicines Partnership in SLE network. The immune cell landscape in kidneys of patients with lupus nephritis. *Nat Immunol* 2019;20(7):902–914.
25. Laman JD, Molloy M, Noelle RJ. Switching off autoimmunity. *Science* 2024;385(6711):827–829.
26. Ruth AJ, Kitching AR, Li M, et al. An IL-12-independent role for CD40-CD154 in mediating effector responses: studies in cell-mediated glomerulonephritis and dermal delayed-type hypersensitivity. *J Immunol* 2004;173(1):136–144.
27. Perper SJ, Westmoreland SV, Karman J, et al. Treatment with a CD40 antagonist antibody reverses severe proteinuria and loss of saliva production and restores glomerular morphology in murine systemic lupus erythematosus. *J Immunol* 2019;203(1):58–75.
28. Menard LC, Habte S, Gonsiorek W, et al. B cells from African American lupus patients exhibit an activated phenotype. *JCI Insight* 2016; 1(9):e87310.
29. Gomez Mendez LM, Cascino MD, Katsumoto TR, et al. Outcome of participants with nephrotic syndrome in combined clinical trials of lupus nephritis. *Lupus Sci Med* 2019;6(1):e000308.
30. Malvar A, Pirruccio P, Alberton V, et al. Histologic versus clinical remission in proliferative lupus nephritis. *Nephrol Dial Transplant* 2017; 32(8):1338–1344.
31. Zickert A, Sundelin B, Svenungsson E, et al. Role of early repeated renal biopsies in lupus nephritis. *Lupus Sci Med* 2014;1(1):e000018.
32. Parodis I, Adamichou C, Aydin S, et al. Per-protocol repeat kidney biopsy portends relapse and long-term outcome in incident cases of proliferative lupus nephritis. *Rheumatology (Oxford)* 2020;59(11): 3424–3434.
33. Rodríguez-Almaraz E, Gutiérrez-Solís E, Rabadán E, et al. Something new about prognostic factors for lupus nephritis? A systematic review. *Lupus* 2021;30(14):2256–2267.

Topical Mupirocin Treatment Reduces Interferon and Myeloid Signatures in Cutaneous Lupus Erythematosus Lesions Through Targeting of *Staphylococcus* Species

Lisa Abernathy-Close, Joseph Mears, Allison C. Billi, Sirisha Sirobhushanam, Celine Berthier, Annie Lu, Zeran Zhang, Amy Hurst, Johann E. Gudjonsson, and J. Michelle Kahlenberg 

Objective. Cutaneous lupus erythematosus (CLE) is an inflammatory skin manifestation of systemic lupus erythematosus. Type I interferons (IFNs) promote inflammatory responses and are elevated in CLE lesions. We recently reported that CLE lesions are frequently colonized with *Staphylococcus aureus*. Here, we follow up via a proof-of-concept study to investigate whether type I IFN and inflammatory gene signatures in CLE lesions can be modulated with mupirocin, a topical antibiotic treatment against *S aureus*-mediated skin infections.

Methods. Participants with active CLE lesions (n = 12) were recruited and randomized into a week of topical treatment with either 2% mupirocin or petroleum jelly vehicle. Paired samples were collected before and after seven days of treatment to assess microbial lesional skin responses. Microbial samples from nares and lesional skin were used to determine baseline and posttreatment *Staphylococcus* abundance and microbial community profiles by 16S ribosomal RNA gene sequencing. Inflammatory responses were evaluated by bulk RNA sequencing of lesional skin biopsies.

Results. We identified 173 differentially expressed genes in CLE lesions after topical mupirocin treatment. Decreased lesional *Staphylococcus* burden correlated with decreased IFN pathway signaling and inflammatory gene expression and barrier dysfunction. Interestingly, mupirocin treatment lowered skin monocyte levels, and this mupirocin-associated depletion of monocytes correlated with decreased inflammatory gene expression.

Conclusion. Mupirocin treatment decreased lesional *Staphylococcus*, and this correlated with decreased IFN signaling and inflammatory gene expression. This study suggests a topical antibiotic could be employed to decrease lupus skin inflammation and type I IFN responses by reducing *Staphylococcus* colonization.

INTRODUCTION

Systemic lupus erythematosus (SLE) is a severe autoimmune disease with pleiotropic manifestations, including disfiguring skin disease, nephritis, and an increased risk of mortality.¹ A total of 70% of patients with SLE experience specific cutaneous eruptions grouped under the category of cutaneous lupus erythematosus (CLE).^{2,3} CLE can also exist in the absence of SLE. No US Food and Drug Administration–approved therapies

specifically for CLE exist, and CLE can be difficult to treat, leading to use of treatments with difficult side effects or immunosuppressive features.⁴ Thus, there is a critical need to uncover effective and less toxic therapies to improve patient outcomes.

Activation of interferon (IFN) signaling in the skin drives chemokine production which recruits monocytes and T cells to skin lesions and promotes the inflammatory process.^{5–7} Recent trials that block type I IFN signaling have identified type I IFNs as a central contributor to cutaneous inflammation in lupus skin⁸;

Supported by the NIH (grant K08-AR-078251 to Dr Billi, P30-AR-075043 to Dr Gudjonsson, and R01-AR-071384 and K24-AR-076975 to Dr Kahlenberg), and A. Alfred Taubman Medical Research Institute (Wexner Emerging Scholar funds to Dr Billi and Taubman Institute Innovative Program Award to Drs Gudjonsson and Kahlenberg). Dr Abernathy-Close's work was supported by the Michigan Institute for Clinical and Health Research (grants 5T32-AR-070843, UL1-TR-002240, and K12-TR-004374). Mr Mears's work was supported by the University of Michigan Medical Scientist Training Program (grant T32-GM-007863). Dr. Kahlenberg's work was supported by the Doris Duke Charitable Foundation (Physician Scientist Development Award).

Lisa Abernathy-Close, PhD, Joseph Mears, BS, Allison C. Billi, MD, PhD, Sirisha Sirobhushanam, PhD, Celine Berthier, PhD, Annie Lu, Zeran Zhang, BS, Amy Hurst, BS, Johann E. Gudjonsson, MD, PhD, J. Michelle Kahlenberg, MD, PhD: University of Michigan, Ann Arbor.

Dr Abernathy-Close, Mr Mears, and Dr Billi contributed equally to this work.

Additional supplementary information cited in this article can be found online in the Supporting Information section (<https://acrjournals.onlinelibrary.wiley.com/doi/10.1002/art.43079>).

Author disclosures and graphical abstract are available at <https://onlinelibrary.wiley.com/doi/10.1002/art.43079>.

[Correction added on 28 January 2025, after first online publication: In the article title, *Staphyloccal* was changed to *Staphylococcus*.]

Address correspondence via email to J. Michelle Kahlenberg, MD, PhD, at mkahlenb@med.umich.edu.

Submitted for publication August 22, 2024; accepted in revised form November 26, 2024.

however, global type I IFN blockade increased the rates of herpes zoster and influenza infections. Cutaneous production of type I IFNs in CLE may occur by several mechanisms, including secretion by invading inflammatory cells⁹ and epidermal production.^{10–12} Cytosolic nucleic acid sensors, such as the cGAS/stimulator of type I IFN gene pathway, also contribute to type I IFN up-regulation in SLE.^{13–15}

Human data support a link between *Staphylococcus aureus* and SLE. *S. aureus* is the most frequent cause of bacteremia in lupus patients, implying clinically significant exposure.¹⁶ Colonization data support increased intestinal and nasal carriage of *S. aureus* in patients with lupus.¹⁷ Importantly, *S. aureus* nasal carriage may be associated with risk of disease flare and development of lupus nephritis.¹⁸ We and others have recently reported that CLE lesions are frequently colonized by *S. aureus*.^{19,20} Furthermore, type I IFNs contribute to barrier disruption, leading to increased *S. aureus* adherence in SLE versus healthy control keratinocytes.¹⁹ *S. aureus* is also known to produce mediators that can induce inflammatory signaling and type I IFN production. Therefore, we hypothesized that *Staphylococcus* colonization contributes to a feed forward loop in which type I IFNs permit colonization and colonization increases IFN production. We thus tested this in patients with SLE by disrupting *S. aureus* colonization with topical antibiotic application.

MATERIALS AND METHODS

Study design and patients. Twelve patients with SLE with active CLE lesions were recruited from the Michigan Lupus Cohort for this study. Patients were randomly assigned to receive topical 2% mupirocin treatment (equivalent to 0.2 mM) or a vehicle control (petroleum jelly) three times per day for seven days. Lupus is a female-biased disease with a 9:1 female to male ratio. Our study sought to identify patients with SLE with active skin disease and did not discriminate based on sex. As a result, we had 1 male and 11 female patients in the study, in accordance with predicted ratios (See Supplemental Table 1). This study was approved by the University of Michigan Institutional Review Board, and all patients were provided with written informed consent.

CLE lesion analysis. This study was not designed to measure treatment effect. However, we did score the pre- and posttreatment CLE lesions for scale (0–2 points) and erythema (0–3 points) based on the Cutaneous Lupus Erythematosus Disease Activity and Severity Index measures for disease activity.²¹ Scoring was performed by JMK in an anonymized method using photographs obtained of designated lesions at the day 0 and day 7 research visits.

Bulk RNA sequencing and gene expression analysis.

Skin biopsies were flash-frozen and stored at -80°C until processing. RNA was isolated using Qiagen RNeasy kits. Libraries were generated with the assistance of the University of Michigan Advanced Genomics Core, and RNA sequencing was performed

on NovaSeq 6000. Samples passing quality controls were mapped and analyzed on a transcript level using the tuxedo suite (tophat/cufflinks/cuffdiff). Further analyses including batch correction based on grouped samples, principal component analysis, variance stabilizing transformation (VST) normalization, and differential gene expression were conducted using the DESeq2 package.

Fast gene set enrichment analysis. Starting with 34,839 genes tested for differential gene expression analysis, removal of genes with null adjusted *P* values and mapping hgnc gene symbols to entrez gene identifiers resulted in 15,109 genes remaining for gene set enrichment analysis. These genes were sorted according to *t*-statistic, and the fgsea package (v1.16.0) was used to run gene set enrichment analysis on the Reactome pathways with a maximum size of 500 genes, resulting in 185 pathways with Bonferroni-corrected $P < 0.05/2,341$.²² A similar process with differential gene expression analysis comparing petroleum jelly-treated samples with baseline yielded 11 pathways with Bonferroni-corrected $P < 0.05/2,341$.

Pathway gene score calculations. Genes from the relevant pathway (IFN signaling, dectin-1 signaling, and keratinization) were extracted from the Reactome pathways in the fgsea package, resulting in 118, 68, and 60 genes, respectively. Scores were calculated by taking the VST-normalized expression of each gene and subtracting the mean of that gene's expression across all mupirocin- or vehicle-treated samples before dividing by the SD of the VST-normalized expression of that gene in the same samples. Scores for each individual gene were then summed across all genes in the pathway.

Quantitative polymerase chain reaction of keratinocytes treated with mupirocin or *S. aureus*. The immortalized human keratinocyte cell line (N/TERTs)²³ was used to evaluate type I IFN epidermal responses to mupirocin and *S. aureus*. Keratinocytes were treated in vitro with 0.1 mM or 0.2 mM mupirocin or 10^7 CFU of *S. aureus* strain USA300 or vehicle as previously described for 24 hours.^{11,19,24} RNA was isolated from keratinocytes and converted to complementary DNA (cDNA) (iScript cDNA Synthesis Kit, BioRad), and quantitative real-time reverse transcriptase polymerase chain reaction (PCR) was performed using SyBR Green PCR Master Mix (Applied Biosystems, Thermo Fisher Scientific) and 7900HT Fast Real-Time PCR system (Applied Biosystems) with the support of the University of Michigan Advanced Genomics Core. Primers used for quantification of gene expression are as follows (all listed 5'→3'): *IFNK* GTGGCTTGAGATCCTTATGGGT (forward), CAGATTTTGCCAGGTGACTCTT (reverse); *IFNB* GCTTGATT-CCTACAAAGAAGCA (forward) and TAGATGGTCAATGCGGCGTA (reverse), *MX1* TACCAGGACTACGAGATTG (forward), TGCCAGGAAGGTCTATTAG (reverse).

16S ribosomal RNA gene sequencing and analysis.

Microbes colonizing CLE lesions were profiled with 16S ribosomal RNA (rRNA) gene sequencing. One skin lesion per patient was swabbed before treatment (day 0) and immediately following one week of treatment (day 7). Genomic DNA was extracted from lesional swab samples using MagAttract PowerMicrobiome kit (Qiagen), and the V4 hypervariable region of the 16S rRNA gene was amplified as previously described.²⁵ Libraries were cleaned and normalized and underwent quality control before a library was prepared for sequencing by the Illumina MiSeq platform using paired end reads, and sequences were processed using mothur (v.1.44.1).^{25,26} Operational taxonomic units were curated and converted to relative abundance. Shannon diversity index was used to show microbial community diversity changes in CLE lesions after treatment with topical mupirocin or vehicle control.

Digital cytometry. CIBERSORTx was used to infer the abundance of various immune cell types using bulk skin transcripts generated from CLE lesions.²⁷ A matrix of bulk gene expression for all 24 samples was given to the CIBERSORTx web interface, and the impute cell fractions function was run mapping to the LM22 database, which contains 547 genes from 22 human hematopoietic cell phenotypes.

Correlation analysis. Pearson correlation coefficient analysis was performed to measure the strength and direction of the relationship between *Staphylococcus* abundance and CLE lesional skin signaling pathways. Correlations between mupirocin-induced changes in skin monocyte levels and cutaneous gene expression were also evaluated.

Immunofluorescence. Immunofluorescence staining of frozen tissue sections from CLE lesions was performed to probe for monocytes. CLE lesional biopsies embedded in OCT media were sectioned and stained with anti-CD14 antibody (B365.1 [B-A8], Invitrogen) and mounted with ProLong Gold Antifade medium containing DAPI (Invitrogen). CD14⁺ cells present before and after mupirocin treatment in a representative CLE lesion were quantified using ImageJ software (National Institutes of Health) and normalized to total cell number. Cells with nuclei too dense to enumerate were excluded.

Statistical analyses. Statistical analyses of pre- and post-treatment comparisons between *Staphylococcus* abundance or changes in monocyte levels generated using a one-tailed paired *t*-test (for normally distributed data) or Wilcoxon signed-rank test (for nonparametric data) with GraphPad Prism software version 10.0.3 unless otherwise noted; $P < 0.05$ was considered statistically significant. The Shapiro-Wilk test was used to test for normal distribution. The Pearson correlation coefficient was calculated to measure correlations, and statistically significant relationships were determined by $P < 0.05$.

Study approval and Data Sharing. The study was reviewed and approved by the University of Michigan Institutional Review Boards of the University of Michigan Medical School under approval number HUM00136167. All patients underwent written, informed consent according to the Declaration of Helsinki. Clinical data information can be found in Supplemental Table 1. Sequence data from this study will be deposited in the GEO database and will be accessed using the accession code 14173587.

RESULTS

Mupirocin treatment reverses lupus-associated cutaneous gene expression.

Patients with SLE with active CLE lesions were randomly assigned to either 2% mupirocin or petroleum jelly as a vehicle control. A single, accessible lesion was selected by investigators for treatment (CLE subtype listed in Supplemental Table 1). Lesions were assessed after seven days of topical treatment. No significant change in lesion erythema or scale was noted for either petroleum jelly or mupirocin-treated lesions (Supplemental Table 2). Skin biopsies were collected from the target lesion, and RNA sequencing was performed. Principle component analysis of these data revealed transcriptional differences between pre- and posttreatment samples in participants randomized to 2% mupirocin, whereas no such differences were observed in participants randomized to receive vehicle (Figure 1A). We observed 173 genes differentially expressed between paired pretreatment samples and mupirocin-treated lesions (Supplemental Table 3); importantly, vehicle treatment induced no significant gene expression changes (Figure 1B). Differential gene set enrichment analysis revealed 617 pathways that were significantly altered in lesional skin after mupirocin treatment. Examination of the top 20 pathways showing greatest effect sizes revealed that mupirocin decreased the expression of genes involved in IFN signaling and active cellular division in CLE lesions, whereas genes involved in epithelial barrier function and lipid metabolism were up-regulated (Figure 1C). In contrast, only 11 pathways were detected to be significantly modulated in CLE lesions treated with vehicle alone, and these responses were characterized by up-regulated homeostatic mitochondrial signaling pathways involved in metabolism and down-regulation of genes involved in smooth muscle contraction (Figure 1D).

As *S. aureus* has been reported to promote type I IFN production,²⁸ we then tested the ability of *S. aureus* to induce keratinocyte relevant IFN genes in human keratinocytes.²³ Indeed, treatment with heat-killed *S. aureus* significantly up-regulated the type I IFN genes *IFNB* ($P < 0.0001$) and *IFNK* ($P = 0.0067$) and the IFN-stimulated gene *MX1* ($P < 0.0001$), whereas mupirocin alone had no effect on *IFNB*, *IFNK*, or *MX1* gene expression (Figure 2). Taken together, these data show that *S. aureus* induces type I IFN production and that mupirocin treatment of CLE lesions

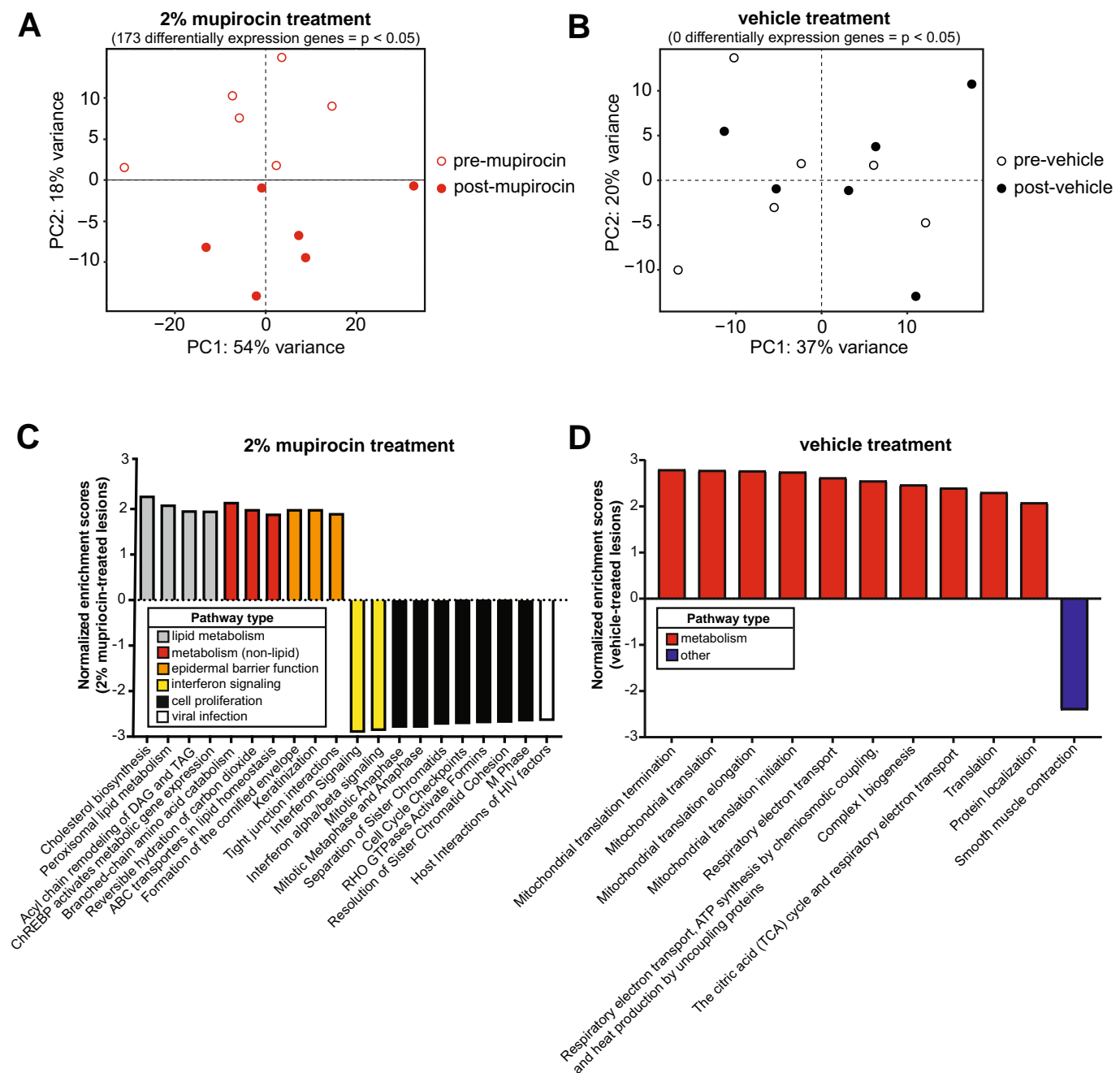


Figure 1. Mupirocin modifies skin gene expression in cutaneous lupus erythematosus lesions. PC analysis plots of (A) mupirocin-treated samples ($n = 6$) and (B) controls ($n = 6$). (C) Normalized gene enrichment scores calculated by fast gene set enrichment analysis (fgsea) showing the top 10 up-regulated and down-regulated pathways following mupirocin treatment, from a total of 185 pathways that were statistically significant by a Bonferroni-corrected $P < 0.05/2,341$. Petrolatum jelly (vehicle) treatment for 7 days specifically modulates homeostatic mitochondrial pathways and genes involved in smooth muscle contraction. (D) All 11 significantly up-regulated and down-regulated pathways associated with petrolatum jelly vehicle control treatment are shown (Bonferroni-corrected $P < 0.05$). PC, principle component.

represses IFN signatures, likely through killing of bacteria sensitive to mupirocin and not through direct effects on keratinocytes.

Mupirocin treatment lowers *Staphylococcus* burden on CLE lesional skin. We next determined the impact of mupirocin or vehicle treatment on the microbial diversity and

abundance of *Staphylococcus* on CLE lesions. Before treatment, the targeted lesion was swabbed, and a second swab was collected in the same location after one week of vehicle or mupirocin treatment. Paired nasal swabs were also collected. *Staphylococcus* abundance and cutaneous and nasal microbial diversity were assessed before and after topical treatment of the active CLE

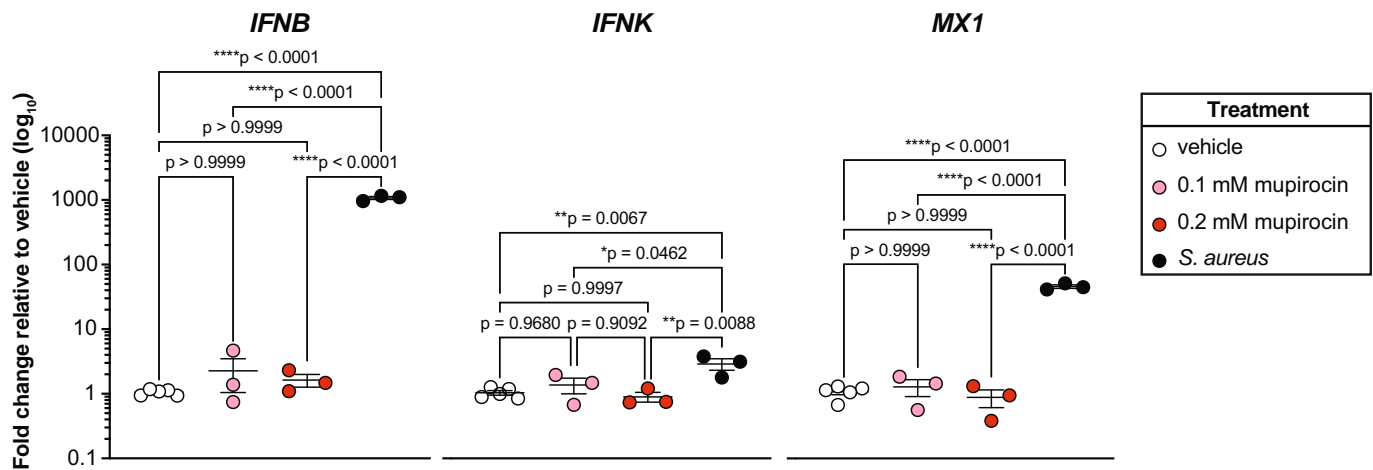


Figure 2. *Staphylococcus aureus* stimulates type I IFN responses in keratinocytes. Keratinocytes were incubated with 0.1 mM or 0.2 mM mupirocin (1% or 2%, respectively), live *S aureus* (10^7 colony-forming units), or vehicle for 24 hours and quantitative polymerase chain reaction was performed to evaluate induction of IFN-stimulated genes encoding IFN- κ , IFN- β , and MX1. Each dot represents the average of technical triplicates. Data were analyzed by one-way analysis of variance. * $P < 0.05$; ** $P < 0.05$; **** $P < 0.0001$. IFN, interferon.

lesion. CLE lesional skin and nasal swab samples were assayed by 16S rRNA sequencing. The relative abundance of bacterial genera colonizing CLE lesions were largely unaltered by mupirocin treatment, with the exception of *Staphylococcus*, whereas vehicle treatment did not significantly change lesional microbiota composition (Figure 3A depicts the pre- and posttreatment mean alpha diversities of each patient; intraindividual diversity is shown in Supplemental Figure 1A). Mupirocin reduced *Staphylococcus* burden on CLE lesions ($P = 0.0352$; Figure 3B) without altering overall microbial diversity ($P = 0.2812$; Figure 3C) or levels of other Gram-positive bacteria, such as species within the *Streptococcus* genus ($P = 0.1095$; Supplemental Figure 1B). Taken together, these data demonstrate compliance with topical therapy and the desired specificity of *S aureus* as the target microbe for treatment.

Microbial profiling of nasal swabs demonstrated that topical skin application of mupirocin to CLE lesions also resulted in a significant decrease of *Staphylococcus* carriage in the nares ($P = 0.0165$; Supplemental Figure 2B), suggesting possible transfer of mupirocin by participants to the nares as well. As expected, no change was observed in the alpha diversity of microbes detected in nasal samples from participants receiving either treatment (Supplemental Figure 2C).

Staphylococcus burden on CLE lesions correlates with cutaneous inflammation and barrier dysfunction.

Gene enrichment analysis was performed on CLE lesions to evaluate treatment-induced changes and determine whether they are associated with abundance in *Staphylococcus* species. Mupirocin treatment, but not vehicle control, resulted in decreased expression of genes involved in IFN signaling, the predominant dysregulated pathway in CLE lesions²⁹ (Figure 4A left panel; Supplemental Table 3). Similarly, mupirocin treatment also

resulted in reduced expression of genes associated with signaling of dectin-1 (Figure 4A, center panel), a receptor expressed on monocytes, macrophages, and dendritic cells, all important cell populations in CLE lesions.^{30,31} Genes involved in keratinization were enriched in CLE lesions after topical mupirocin (Figure 4A right). Critically, a reduction in *Staphylococcus* abundance was associated with decreased IFN and dectin-1 signaling and improved keratinization pathway scores (Figure 4B). No relationship was observed between the relative abundance of *Staphylococcus* nasal colonization of patients with CLE and alterations in these lesional skin pathways (Supplemental Figure 3A). Similarly, there was no relationship noted between *Staphylococcus* abundance and IFN or dectin-1 signaling before treatment (Supplemental Figure 3B). These data indicate that mupirocin reduces CLE lesional *Staphylococcus* colonization burden, and this reduction correlates with reduced signaling in CLE-associated IFN and dectin-1 signaling.

Mupirocin treatment lowers skin monocyte and activated dendritic cell levels in CLE lesions.

Given that we consistently observed a reduction in signaling pathways commonly associated with immune cells following 2% mupirocin treatment, we then used CIBERSORTx to deconvolute the RNA sequencing data into predicted cell populations impacted by treatment. Mupirocin treatment specifically reduced genes predicted to represent monocyte contributions to CLE lesions ($P = 0.0104$; Figure 5A upper panels), whereas significant shifts in other major immune cell populations were not observed after seven days of application (Figure 5B). We then validated this using immunofluorescent staining against the monocyte marker CD14. In vivo comparison in a single patient revealed a five-percentage point decrease in the proportion of lesional cells expressing the

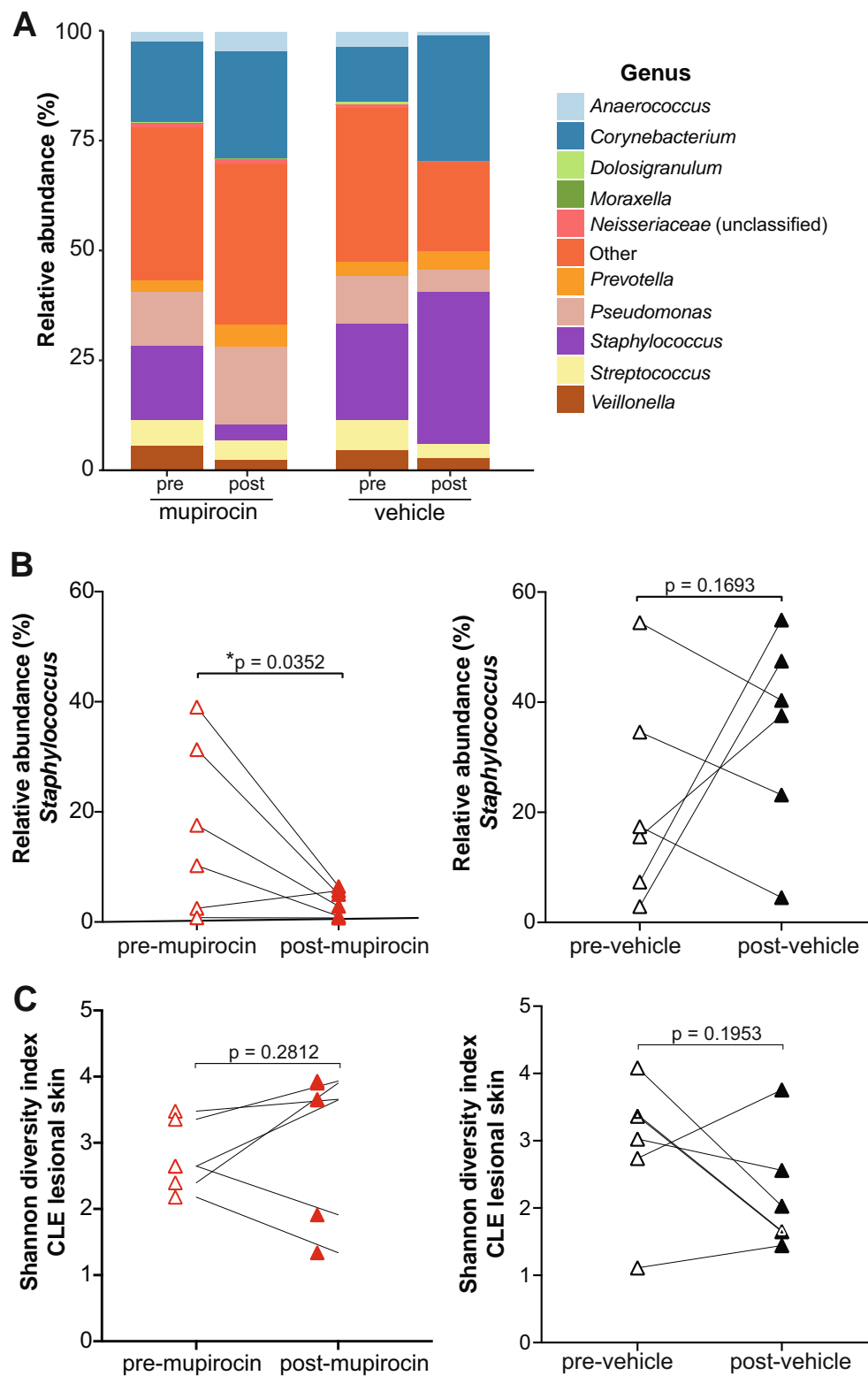


Figure 3. Mupirocin treatment of CLE lesions reduces *Staphylococcus* burden without altering overall skin microbial diversity. (A) Relative abundances of bacterial taxa by treatment group from lesional skin and nares ($n = 6$ per treatment). (B) Relative abundance plots of *Staphylococcus* and (C) Shannon diversity of bacteria colonizing CLE lesions pre- and posttreatment. Data were analyzed by one-tailed paired t -test ($n = 6$ per treatment condition). * $P < 0.05$. CLE, cutaneous lupus erythematosus.

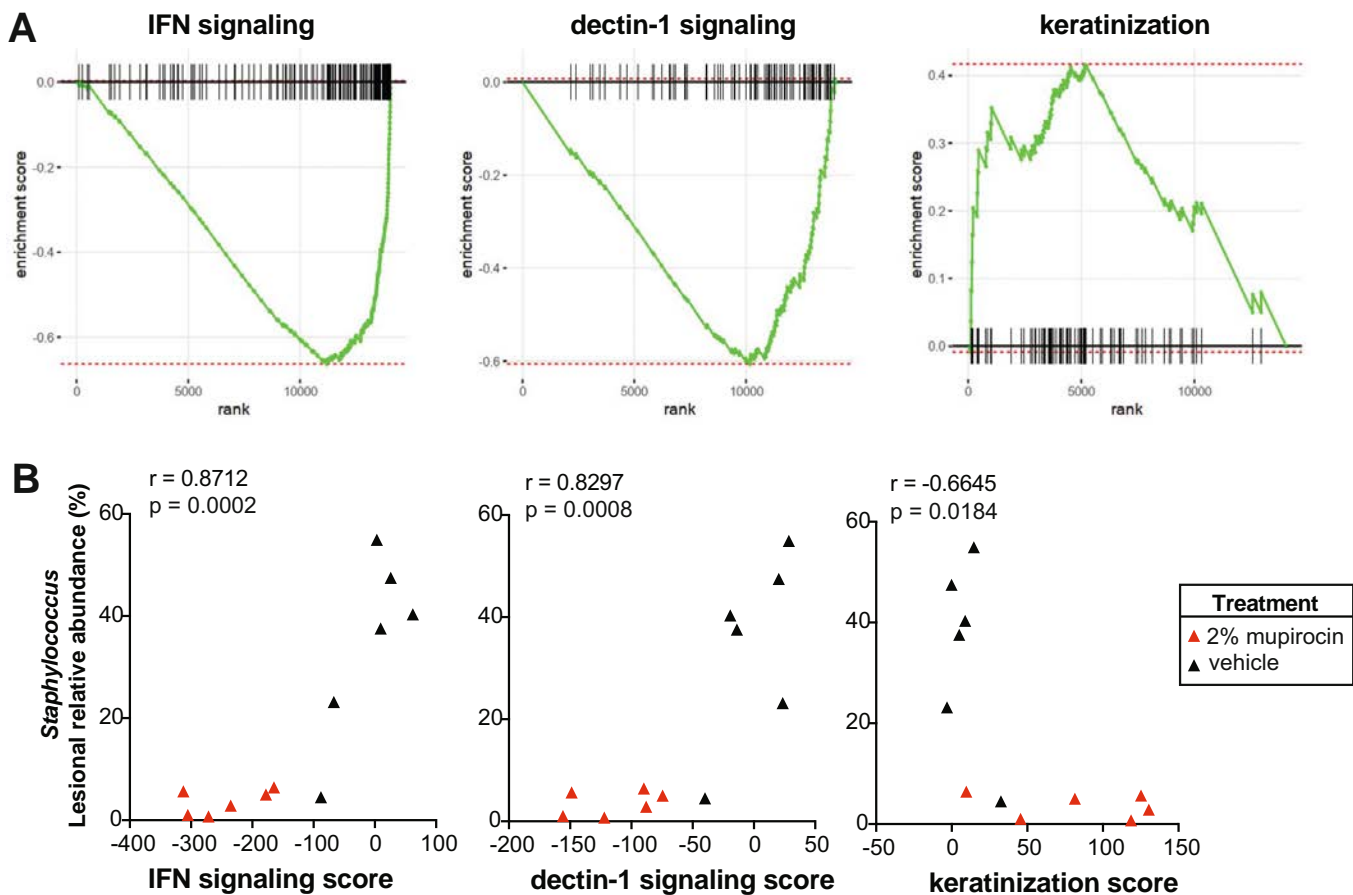


Figure 4. Mupirocin treatment modulates skin signaling pathways, and this correlates with *Staphylococcus* levels. (A) Relevant enrichment scores calculated for cutaneous lupus erythematosus lesions treated with mupirocin as determined by gene set enrichment analysis. (B) The relationship between *Staphylococcus* relative abundance and IFN signaling, dectin-1 signaling, or keratinization pathway scores after treatment was measured using the Pearson correlation coefficient ($n = 6$ samples per treatment). IFN, interferon.

monocyte marker CD14 after mupirocin treatment (Supplemental Figure 4). Genes predicted to represent activated dendritic cells in CLE lesions were also significantly decreased by mupirocin treatment ($P = 0.0443$; Figure 5A lower panels). These data show topical mupirocin treatment is associated with a reduction of monocytes and activated dendritic cells in CLE lesions.

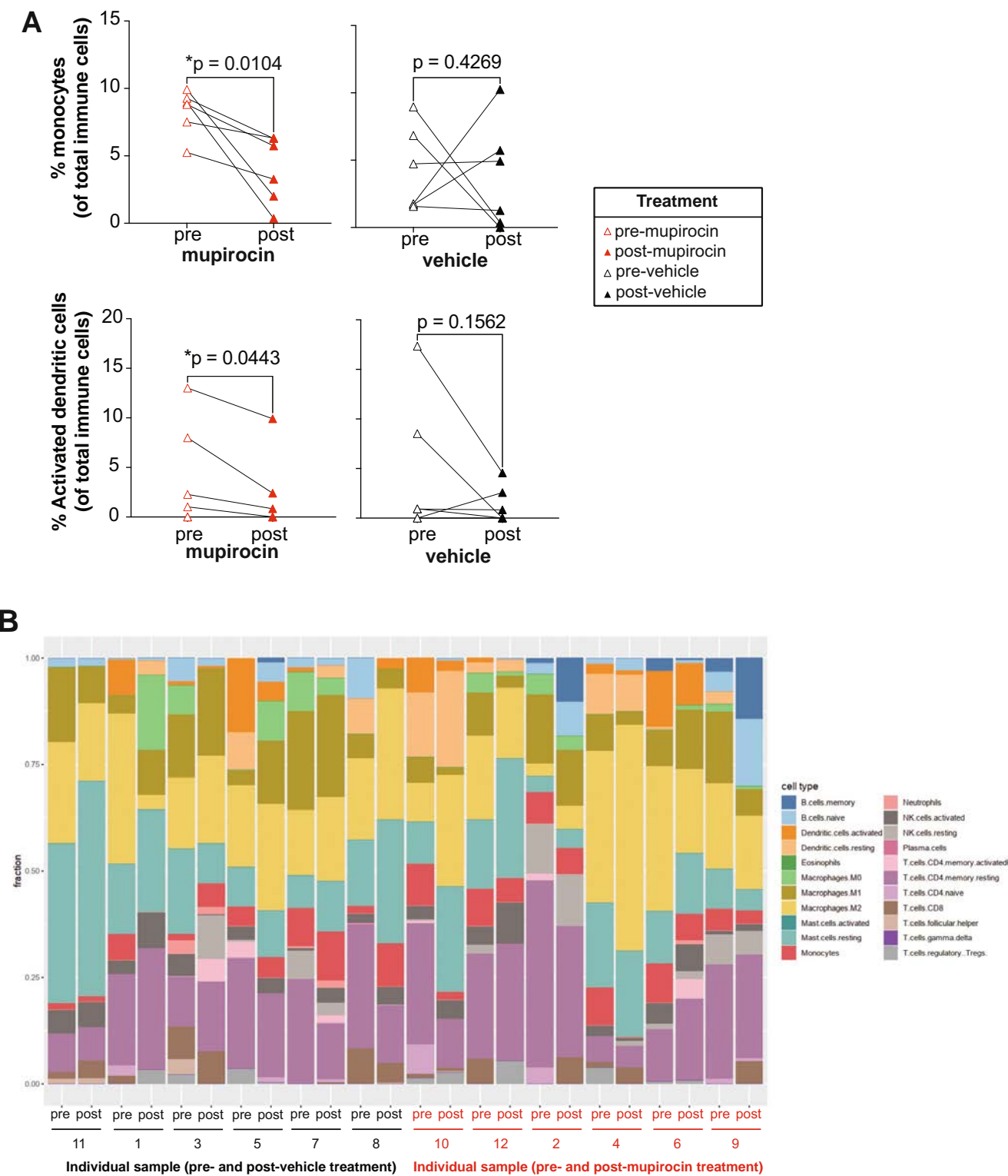
Mupirocin-associated loss of monocytes and activated dendritic cells correlates with decreased expression of genes involved in cutaneous inflammation and skin homeostasis. We then correlated predicted monocyte and activated dendritic cell abundance based on digital cytometry with all genes differentially expressed after mupirocin treatment. Of 174 differentially expressed genes, 7 genes were significantly associated with a change in monocytes, and 4 genes were significantly associated with a change in activated dendritic cells (Table 1). Reduced monocyte scores were associated with diminished expression of *PLSCR1*, a gene encoding the IFN-inducible protein phospholipid scramblase 1 (*PLSCR1*) ($r = 0.8368$; $P = 0.0380$) associated with lipid metabolism.

CASP7 and *PLEKHA4* expression also decreased with larger reductions in monocyte scores. Decreased activated dendritic cell scores were associated with several type I IFN-responsive dendritic cell genes including *AQP7* ($r = 0.4956$; $P = 0.3174$), *CILP* ($r = 0.4078$; $P = 0.4222$), *IFIT3* ($r = 0.2020$; $P = 0.7011$), and *THY1* ($r = 0.1122$; $P = 0.8323$). No relationship was observed between predicted gene expression in vehicle-treated CLE lesions and monocyte or activated dendritic cell scores (Supplemental Figure 5).

Taken together, our data indicate that reductions in *Staphylococcus* burden on cutaneous lupus lesions result in decreased IFN signaling and a reduction in innate inflammatory cell infiltrates.

DISCUSSION

S aureus is a dynamic colonizer of 30% of the US population³² and has been shown to promote SLE-like autoimmune inflammation.³³ Patients with SLE have a distinct skin microbiota compared with healthy controls,³⁴ and recent studies have reported increased *S aureus* colonization on CLE lesions, which



is facilitated by the high type I IFN environment of SLE skin.^{19,20} Here, we have now shown that elimination of *S aureus* through the use of a topical antibiotic provides a targeted reduction in

staphylococcal burden and attenuates the inflammatory signature within CLE lesions, including a reduction in type I IFN and innate immune signaling profiles and an increase in skin barrier genes.

Table 1. Mupirocin-induced monocyte and activated DC depletion is associated with the expression of 11 genes in cutaneous lupus erythematosus lesions*

Differentially expressed gene	Pearson correlation (<i>r</i>)	<i>P</i> value
<i>Δmonocytes</i>		
<i>IGLV3-19</i>	0.9885	0.0002
<i>TEAD4</i>	0.9722	0.0011
<i>PLEKHA4</i>	0.96	0.0024
<i>CASP7</i>	0.8997	0.0146
<i>AP001528.3</i>	0.8733	0.023
<i>PLSCR1</i>	0.8363	0.038
<i>DDX21</i>	-0.8399	0.0364
<i>Δactivated DCs</i>		
<i>AQP7</i>	-0.8307	0.0406
<i>CILP</i>	-0.8750	0.0225
<i>IFIT3</i>	-0.8985	0.0149
<i>THY1</i>	-0.8699	0.0243

* Significant correlations between the change in predicted monocyte and activated DC scores and differentially expressed genes observed after mupirocin treatment are shown. Relationships were measured by Pearson correlation coefficient. All statistically significant correlations of the 173 differentially expressed genes from Supplemental Table 3 are shown. DC, dendritic cell.

The links between SLE and *S aureus* have been suggested for more than a decade. Prolonged exposure to *S aureus* via repeated injection of *S aureus* proteins induces development of lupus-like disease in wild-type mice.³⁵ Colonization of murine bladder catheters with *S aureus* results in sterile inflammatory cell infiltration of organs as diverse as the kidney and lung in the absence of bacteremia.³⁶ Intriguingly, recent data have suggested that penetration of the epidermis by *S aureus* regularly occurs, even in normal skin,³⁷ and this is exaggerated in the presence of dysfunctional or absent skin barrier proteins, such as filaggrin.³⁸ This suggests that ongoing colonization may provide exposure to *S aureus* inflammatory triggers. Intriguingly, known CLE triggers such as UV light³⁹ and smoking⁴⁰ also have negative effects on skin barrier function.^{41,42}

Further study on the relationship between CLE triggers and *S aureus* colonization is warranted. Similarly, understanding CLE lesional factors influencing colonization by (or selection for) staphylococcal species may be required to develop precise and effective CLE-specific treatments.

Topical mupirocin treatment up-regulated the expression of key skin barrier pathways. This effect cannot be sufficiently explained by moisturization from treatment as use of petrolatum as a vehicle did not modify skin barrier gene expression. This is in contrast to a previous report in which treatment with petrolatum for 48 hours resulted in up-regulation of barrier genes and antimicrobial peptides.⁴³ This discrepancy may be related to differences in treatment protocol as we used petroleum jelly applied twice daily with nonocclusive bandages for 7 days, whereas the study by Czarnowicki et al used Finn chambers for full occlusion for 48 hours followed by 24 hours of no treatment before biopsy.⁴³

Petrolatum also did not result in major shifts in microbial composition in our study.

Treatment with mupirocin resulted in down-regulation of pathways involved in mitosis and cell division. This could reflect normalization of keratinocyte proliferation. The presence of epidermal scale is considered an indicator of disease in CLE. Discoid lupus erythematosus lesions in particular show hyperproliferation and abnormal differentiation of keratinocytes, manifesting clinically as hyperkeratosis and follicular plugging from keratin.⁴⁴ Here, treatment with mupirocin resulted in down-regulation of pathways involved in mitosis and cell division and increased keratinization, which could reflect normalization of keratinocyte maturation. Thus, mupirocin treatment may offer benefit in this regard. Longer-term studies are needed to assess the clinical response.

Type I IFN-related gene changes were observed to be correlated with decreased monocytes and activated dendritic cells after mupirocin treatment. PLSCR1 is an IFN-inducible phospholipid scramblase family member known to be involved in immune responses and antiviral activity.⁴⁵ Monocytes in patients with SLE have enhanced *PLSCR1* gene expression.⁴⁶ PLSCRs are important for lipid metabolism and contribute to inflammation, which is also modulated by mupirocin treatment. PLSCR1 negatively regulates Fc receptor-mediated phagocytosis during macrophage differentiation from precursors such as monocytes.⁴⁷ Furthermore, PLSCR1 may play a role in the antiviral response of IFN by amplifying and enhancing the IFN response through increased expression of select subset of potent antiviral genes.⁴⁸ Similarly, we also found repression of IFN-activated genes associated with an activated epidermal dendritic cell signature (*AQP7*, *CILP*, *IFIT3*, *THY1*).⁴⁹ Thus, mupirocin treatment may promote a switch from interferonogenic to tolerogenic myeloid phenotypes in the skin.

Thus, the data reported here raise the question of whether mupirocin, or other medications that target *S aureus* on the skin, could benefit CLE either as a primary treatment or as an adjunct therapy. A case report of lupus profundus showed benefit of mupirocin in combination with hydroxychloroquine and prednisone, but the effects of mupirocin alone were not assessed.⁵⁰ Typically, few side effects from mupirocin use are reported; however, the risk of antibacterial resistance remains a concern, with up to 80% resistance reported in countries where mupirocin is available over the counter.⁵¹ Thus, application of mupirocin in clinical practice would likely need defined periods of use and a strong risk-to-benefit ratio. Larger trials with clinical response datapoints are needed to understand whether mupirocin should be incorporated into clinical practice.

Limitations to our study include the low number of study participants and the short time frame of treatment. We did not see a change in clinical phenotype of the lesions; however, one week of treatment is unlikely to provide significant clinical change given drugs with successful track record for CLE, such as anifrolumab,

can take up to 12 weeks to show improvement in lesions.⁵² In addition, secondary to a tragic freezer accident that left us with only one paired pre- and postmupirocin biopsy sample available for confirmatory immunostaining, we were limited in our ability to validate the changes identified by RNA sequencing. These limitations notwithstanding, this study showed that in addition to direct antimicrobial properties, mupirocin improved CLE lesional inflammatory phenotypes. Lowering the burden of *Staphylococcus* was associated with reductions in IFN signaling and decreased monocyte infiltration. Thus, targeting staphylococcal skin colonization is an approach worth additional consideration and study for optimal management of CLE flares.

AUTHOR CONTRIBUTIONS

All authors contributed to at least one of the following manuscript preparation roles: conceptualization AND/OR methodology, software, investigation, formal analysis, data curation, visualization, and validation AND drafting or reviewing/editing the final draft. As corresponding author, Dr Kahlenberg confirms that all authors have provided the final approval of the version to be published, and takes responsibility for the affirmations regarding article submission (eg, not under consideration by another journal), the integrity of the data presented, and the statements regarding compliance with institutional review board/Declaration of Helsinki requirements.

REFERENCES

- Gómez-Puerta JA, Barbaiya M, Guan H, et al. Racial/ethnic variation in all-cause mortality among United States Medicaid recipients with systemic lupus erythematosus: a Hispanic and Asian paradox. *Arthritis Rheumatol* 2015;67(3):752–760.
- Klein RS, Morganroth PA, Werth VP. Cutaneous lupus and the cutaneous lupus erythematosus disease area and severity index instrument. *Rheum Dis Clin North Am* 2010;36(1):33–51.
- Mikita N, Ikeda T, Ishiguro M, et al. Recent advances in cytokines in cutaneous and systemic lupus erythematosus. *J Dermatol* 2011;38(9):839–849.
- Reich A, Werth VP, Furukawa F, et al. Treatment of cutaneous lupus erythematosus: current practice variations. *Lupus* 2016;25(9):964–972.
- Masek-Hammerman K, Peeva E, Ahmad A, et al. Monoclonal antibody against macrophage colony-stimulating factor suppresses circulating monocytes and tissue macrophage function but does not alter cell infiltration/activation in cutaneous lesions or clinical outcomes in patients with cutaneous lupus erythematosus. *Clin Exp Immunol* 2016;183(2):258–270.
- Kemp MG, Lindsey-Boltz LA, Sancar A. UV light potentiates STING (stimulator of interferon genes)-dependent innate immune signaling through deregulation of ULK1 (Unc51-like Kinase 1). *J Biol Chem* 2015;290(19):12184–12194.
- Ekholm L, Kahlenberg JM, Barbasso Helmers S, et al. Dysfunction of endothelial progenitor cells is associated with the type I IFN pathway in patients with polymyositis and dermatomyositis. *Rheumatology (Oxford)* 2016;55(11):1987–1992.
- Furie R, Khamashta M, Merrill JT, et al; CD1013 Study Investigators. Anifrolumab, an anti-interferon- α receptor monoclonal antibody, in moderate-to-severe systemic lupus erythematosus. *Arthritis Rheumatol* 2017;69(2):376–386.
- Vermi W, Lonardi S, Morassi M, et al. Cutaneous distribution of plasmacytoid dendritic cells in lupus erythematosus. Selective tropism at the site of epithelial apoptotic damage. *Immunobiology* 2009;214(9–10):877–886.
- Stannard JN, Reed TJ, Myers E, et al. Lupus skin is primed for IL-6 inflammatory responses through a keratinocyte-mediated autocrine type I interferon loop. *J Invest Dermatol* 2017;137(1):115–122.
- Sarkar MK, Hile GA, Tsoi LC, et al. Photosensitivity and type I IFN responses in cutaneous lupus are driven by epidermal-derived interferon kappa. *Ann Rheum Dis* 2018;77(11):1653–1664.
- Psarras A, Alase A, Antanaviciute A, et al. Functionally impaired plasmacytoid dendritic cells and non-haematopoietic sources of type I interferon characterize human autoimmunity. *Nat Commun* 2020;11(1):6149.
- Jeremiah N, Neven B, Gentili M, et al. Inherited STING-activating mutation underlies a familial inflammatory syndrome with lupus-like manifestations. *J Clin Invest* 2014;124(12):5516–5520.
- Liu Y, Jesus AA, Marrero B, et al. Activated STING in a vascular and pulmonary syndrome. *N Engl J Med* 2014;371(6):507–518.
- Günther C, Kind B, Reijns MA, et al. Defective removal of ribonucleotides from DNA promotes systemic autoimmunity. *J Clin Invest* 2015;125(1):413–424.
- Chen MJ, Tseng HM, Huang YL, et al. Long-term outcome and short-term survival of patients with systemic lupus erythematosus after bacteraemia episodes: 6-yr follow-up. *Rheumatology (Oxford)* 2008;47(9):1352–1357.
- Gul'neva Mlu, Romanov VA, Shilkina NP. Intestinal microecology in some systemic connective tissue diseases. In Russian. *Zh Mikrobiol Epidemiol Immunobiol* 2007;4(4):38–41.
- Conti F, Ceccarelli F, Iaianni G, et al. Association between *Staphylococcus aureus* nasal carriage and disease phenotype in patients affected by systemic lupus erythematosus. *Arthritis Res Ther* 2016;18(1):177.
- Sirobhushanam S, Parsa N, Reed TJ, et al. *Staphylococcus aureus* colonization is increased on lupus skin lesions and is promoted by IFN-mediated barrier disruption. *J Invest Dermatol* 2020;140(5):1066–1074.e4.
- Huang C, Yi X, Long H, et al. Disordered cutaneous microbiota in systemic lupus erythematosus. *J Autoimmun* 2020;108:102391.
- Krathen MS, Dunham J, Gaines E, et al. The Cutaneous Lupus Erythematosus Disease Activity and Severity Index: expansion for rheumatology and dermatology. *Arthritis Rheum* 2008;59(3):338–344.
- Korotkevich G, Sukhov V, Sergushichev A. 2019. Fast gene set enrichment analysis. *bioRxiv*. Preprint posted online February 1, 2021. <https://doi.org/10.1101/060012>.
- Dickson MA, Hahn WC, Ino Y, et al. Human keratinocytes that express hTERT and also bypass a p16(INK4a)-enforced mechanism that limits life span become immortal yet retain normal growth and differentiation characteristics. *Mol Cell Biol* 2000;20(4):1436–1447.
- Twilley D, Reva O, Meyer D, et al. Mupirocin promotes wound healing by stimulating growth factor production and proliferation of human keratinocytes. *Front Pharmacol* 2022;13:862112.
- Kozich JJ, Westcott SL, Baxter NT, et al. Development of a dual-index sequencing strategy and curation pipeline for analyzing amplicon sequence data on the MiSeq Illumina sequencing platform. *Appl Environ Microbiol* 2013;79(17):5112–5120.
- Schloss PD, Westcott SL, Ryabin T, et al. Introducing mothur: open-source, platform-independent, community-supported software for describing and comparing microbial communities. *Appl Environ Microbiol* 2009;75(23):7537–7541.
- Newman AM, Steen CB, Liu CL, et al. Determining cell type abundance and expression from bulk tissues with digital cytometry. *Nat Biotechnol* 2019;37(7):773–782.

28. Scumpia PO, Botten GA, Norman JS, et al. Opposing roles of Toll-like receptor and cytosolic DNA-STING signaling pathways for *Staphylococcus aureus* cutaneous host defense. *PLoS Pathog* 2017;13(7):e1006496.
29. Psarras A, Wittmann M, Vital EM. Emerging concepts of type I interferons in SLE pathogenesis and therapy. *Nat Rev Rheumatol* 2022;18(10):575–590.
30. Billi AC, Ma F, Plazyo O, et al. Nonlesional lupus skin contributes to inflammatory education of myeloid cells and primes for cutaneous inflammation. *Sci Transl Med* 2022;14(642):eabn2263.
31. Chen KL, Patel J, Zeidi M, et al. Myeloid dendritic cells are major producers of IFN- β in dermatomyositis and may contribute to hydroxy-chloroquine refractoriness. *J Invest Dermatol* 2021;141(8):1906–1914.e2.
32. Kuehnert MJ, Kruszon-Moran D, Hill HA, et al. Prevalence of *Staphylococcus aureus* nasal colonization in the United States, 2001–2002. *J Infect Dis* 2006;193(2):172–179.
33. Terui H, Yamasaki K, Wada-Irimada M, et al. *Staphylococcus aureus* skin colonization promotes SLE-like autoimmune inflammation via neutrophil activation and the IL-23/IL-17 axis. *Sci Immunol* 2022;7(76):eabm9811.
34. Zhou HY, Cao NW, Guo B, et al. Systemic lupus erythematosus patients have a distinct structural and functional skin microbiota compared with controls. *Lupus* 2021;30(10):1553–1564.
35. Chowdhary VR, Tilahun AY, Clark CR, et al. Chronic exposure to staphylococcal superantigen elicits a systemic inflammatory disease mimicking lupus. *J Immunol* 2012;189(4):2054–2062.
36. Chung JW, Greenwood-Quaintance KE, Karau MJ, et al. Superantigens produced by catheter-associated *Staphylococcus aureus* elicit systemic inflammatory disease in the absence of bacteremia. *J Leukoc Biol* 2015;98(2):271–281.
37. Nakatsuji T, Chiang HI, Jiang SB, et al. The microbiome extends to subepidermal compartments of normal skin. *Nat Commun* 2013;4(1):1431.
38. Nakatsuji T, Chen TH, Two AM, et al. *Staphylococcus aureus* exploits epidermal barrier defects in atopic dermatitis to trigger cytokine expression. *J Invest Dermatol* 2016;136(11):2192–2200.
39. Klein B, Kunz M. Current concepts of photosensitivity in cutaneous lupus erythematosus. *Front Med (Lausanne)* 2022;9:939594.
40. Piette EW, Foering KP, Chang AY, et al. Impact of smoking in cutaneous lupus erythematosus. *Arch Dermatol* 2012;148(3):317–322.
41. Hergesell K, Paraskevopoulou A, Opálka L, et al. The effect of long-term cigarette smoking on selected skin barrier proteins and lipids. *Sci Rep* 2023;13(1):11572.
42. Biniek K, Levi K, Dauskardt RH. Solar UV radiation reduces the barrier function of human skin. *Proc Natl Acad Sci USA* 2012;109(42):17111–17116.
43. Czarnowicki T, Malajian D, Khattri S, et al. Petrolatum: barrier repair and antimicrobial responses underlying this “inert” moisturizer. *J Allergy Clin Immunol* 2016;137(4):1091–1102.e7.
44. de Jong EM, van Erp PE, Ruiter DJ, et al. Immunohistochemical detection of proliferation and differentiation in discoid lupus erythematosus. *J Am Acad Dermatol* 1991;25(6 Pt 1):1032–1038.
45. Dal Col J, Lamberti MJ, Nigro A, et al. Phospholipid scramblase 1: a protein with multiple functions via multiple molecular interactors. *Cell Commun Signal* 2022;20(1):78.
46. Suzuki E, Amengual O, Atsumi T, et al. Increased expression of phospholipid scramblase 1 in monocytes from patients with systemic lupus erythematosus. *J Rheumatol* 2010;37(8):1639–1645.
47. Herate C, Ramdani G, Grant NJ, et al. Phospholipid scramblase 1 modulates FcR-mediated phagocytosis in differentiated macrophages. *PLoS One* 2016;11(1):e0145617.
48. Dong B, Zhou Q, Zhao J, et al. Phospholipid scramblase 1 potentiates the antiviral activity of interferon. *J Virol* 2004;78(17):8983–8993.
49. Hara-Chikuma M, Sugiyama Y, Kabashima K, et al. Involvement of aquaporin-7 in the cutaneous primary immune response through modulation of antigen uptake and migration in dendritic cells. *FASEB J* 2012;26(1):211–218.
50. Sutedja E, Widjaya MRH, Dharmadji HP, et al. Lupus erythematosus profundus with multiple overlying cutaneous ulcerations: a rare case. *Clin Cosmet Investig Dermatol* 2023;16:2721–2726.
51. Dallo M, Patel K, Hebert AA. Topical antibiotic treatment in dermatology. *Antibiotics (Basel)* 2023;12(2):12.
52. Morand EF, Furie R, Tanaka Y, et al; TULIP-2 Trial Investigators. Trial of anifrolumab in active systemic lupus erythematosus. *N Engl J Med* 2020;382(3):211–221.

Atherosclerotic Plaque Progression and Incident Cardiovascular Events in a 10-Year Prospective Study of Patients With Systemic Lupus Erythematosus: The Impact of Persistent Cardiovascular Risk Factor Target Attainment and Sustained DORIS Remission

Nikolaos Papazoglou,  Petros P. Sfikakis,  and Maria G. Tektonidou 

Objective. Cardiovascular disease (CVD) is a leading cause of death in individuals with systemic lupus erythematosus (SLE). We assessed atherosclerotic plaque progression and incident cardiovascular events in patients with SLE over a 10-year follow-up.

Methods. We prospectively analyzed 738 carotid ultrasound measurements (413 in patients with SLE and 325 in age/sex-matched healthy controls [HCs]) to assess new plaque development from baseline to 3-, 7-, and 10-year follow-up. Multivariate mixed-effects Poisson regression models examined potential predictors of plaque progression, including patient characteristics, Systemic Coronary Risk Evaluation, traditional cardiovascular risk factor (CVRF) target attainment, Definition of Remission in SLE (DORIS), medications, and persistent triple anti-phospholipid antibody (aPL) positivity during follow-up. Ten-year incident cardiovascular events were recorded, and univariate Cox regression analysis assessed potential associations.

Results. Patients with SLE had a 2.3-fold higher risk of carotid plaque progression than HCs (incidence rate ratio [IRR] 2.26, $P = 0.002$). Plaque progression risk in patients with SLE was reduced by 32% (IRR 0.68, $P = 0.004$) per each sustainedly attained CVRF target during follow-up, including blood pressure, lipids, smoking, body weight, and physical activity. DORIS achievement $\geq 75\%$ of follow-up was associated with a 43% decrease in atherosclerosis progression risk (IRR 0.57, $P = 0.033$). Ten-year risk of incident cardiovascular events was higher in individuals with SLE than HCs (eight versus one event, permutation-based log-rank $P = 0.036$) and was associated with persistent triple aPL positivity.

Conclusion. Patients with SLE experience a 2.3-fold higher 10-year atherosclerosis progression risk than HCs, mitigated by sustained CVRF control and prolonged clinical remission. Persistent triple aPL positivity is associated with increased incidence of CVD events.

INTRODUCTION

Systemic lupus erythematosus (SLE) is a systemic autoimmune disorder with an increased risk of premature atherosclerosis and cardiovascular disease (CVD) events.^{1–4} Despite advances in management, patients with SLE still bear a substantial death risk, primarily due to CVD complications, although the majority of patients are young adult women.⁵ Large cohort studies and systematic literature reviews have revealed a two to five

times greater risk of CVD events in patients with SLE than in the general population, which is disproportionately magnified among younger individuals.^{6–10}

Subclinical atherosclerosis, recognized as an independent predictor of CVD events, is more prevalent and progresses more rapidly in patients with SLE than in the general population or other high CVD risk disorders.^{1,11} Few prospective studies examining the progression of atherosclerotic plaques in a three- to five-year follow-up period showed a two- to three-fold heightened risk for

Nikolaos Papazoglou, MD, Petros P. Sfikakis, MD, Maria G. Tektonidou, MD: Rheumatology Unit, First Department of Propaedeutic Internal Medicine, Joint Academic Rheumatology Program, School of Medicine, National and Kapodistrian University of Athens, Athens, Greece.

Additional supplementary information cited in this article can be found online in the Supporting Information section (<https://acrjournals.onlinelibrary.wiley.com/doi/10.1002/art.43097>).

Author disclosures are available at <https://onlinelibrary.wiley.com/doi/10.1002/art.43097>.

Address correspondence via email to Maria G. Tektonidou, MD, at mtektonidou@med.uoa.gr.

Submitted for publication August 4, 2024; accepted in revised form December 13, 2024.

new plaque development in patients with SLE versus age- and sex-matched healthy controls (HCs).^{11,12} However, there is no evidence about plaque progression and incident CVD events in patients with SLE compared to HCs during a 10-year follow-up.

Both traditional cardiovascular risk factors (CVRFs) and SLE-related parameters, including disease activity, disease duration, lupus nephritis, glucocorticoids, and anti-phospholipid antibodies (aPLs), have been identified as major predictors of clinical and subclinical CVD in patients with SLE.^{1,13} The 2022 EULAR recommendations for cardiovascular risk management in individuals with rheumatic and musculoskeletal disorders including SLE and antiphospholipid syndrome (APS), highlighted meticulous assessment and control of modifiable CVRFs, along with minimal disease activity.¹⁴ Traditional CVRF target attainment, as defined by the 2016 European Society of Cardiology (ESC) guidelines based on 10-year CVD risk classification,¹⁵ can reduce CVD events in the general population. The impact of sustained traditional CVRF control and clinical remission in reducing the risk of accelerated atherosclerosis in individuals with SLE has not been previously evaluated in a 10-year timeframe.

Herein, we aimed to assess the progression of subclinical atherosclerosis and the development of cardiovascular events in patients with SLE versus age- and sex-matched HCs over a 10-year follow-up period. We investigated determinants of atherosclerotic plaque progression, including disease-related and traditional CVRFs, CVRF target attainment, and different durations of Lupus Low Disease Activity State (LLDAS)¹⁶ and sustained Definition of Remission in SLE (DORIS).¹⁷

PATIENTS AND METHODS

Study design and population. This is a 10-year vascular ultrasound follow-up study of patients fulfilling the 2012 classification criteria for SLE¹⁸ and HCs initially examined at our cardiovascular research laboratory in 2012 to 2013. At baseline assessment, 115 patients with SLE and 115 age- and sex-matched HCs without prior atherosclerotic CVD (ASCVD), active malignancy, pregnancy, or diabetes mellitus (DM) underwent a carotid ultrasound assessment. ASCVD included acute myocardial infarction, acute coronary syndrome, coronary or other arterial revascularization procedures, stroke, transient ischemic attack, aortic aneurysm, and peripheral artery disease.

After the baseline evaluation, all participants were invited for a 3-, 7-, and 10-year ultrasound evaluation of new carotid plaque development. Incident CVD events were also assessed during follow-up. Follow-up duration was defined as the time between the baseline assessment and the first CVD event, death, or loss to follow-up, whichever occurred first. For those who missed a 10-year carotid ultrasound but had completed a 10-year follow-up visit, incident CVD events were recorded from their medical files. All participants gave written informed consent according to the Declaration of Helsinki principles, and our study received

approval from our hospital's institutional review board (Laiko General Hospital Scientific Council number 16506).

Recorded parameters. *CVRFs.* We recorded the traditional CVRFs at baseline and at 3-, 7-, and 10-year follow-up visits: systolic and diastolic blood pressure, smoking (current status and pack-years), lipid profile (total cholesterol, low-density lipoprotein [LDL] cholesterol, high-density lipoprotein [HDL] cholesterol, and triglycerides), estimated glomerular filtration rate (eGFR), physical activity in weekly exercise minutes, family history of coronary artery disease, body mass index (BMI; weight/height²), waist circumference, and CVD-related medications (anti-hypertensives, lipid-lowering agents, antiplatelets, and antidiabetic drugs for patients diagnosed with DM during follow-up). We assessed individuals' CVD risk using the ESC-endorsed Systemic Coronary Risk Evaluation (SCORE) prediction tool,¹⁹ which estimates the 10-year risk of fatal CVD in individuals 40 to 69 years old with no previous ASCVD or type II DM.

Individuals aged <40 years were classified as "low risk" unless a modifier was present. We evaluated the CVRF target attainment based on individual CVD risk classified by the SCORE (low-moderate, high, and very high) and additional CVD risk modifiers (Supplementary Table 1) following the 2016 ESC guidelines¹⁵: systolic blood pressure <140 mm Hg and diastolic blood pressure <90 mm Hg; LDL <115 mg/dL in patients who were at low-moderate risk without CVD events (primary prevention), LDL <100 mg/dL or a reduction of at least 50% if the baseline LDL is between 100 and 200 mg/dL in patients who were at high risk without CVD events (primary prevention), and LDL <70 mg/dL or a reduction of at least 50% if the baseline LDL is between 70 and 135 mg/dL in patients classified as having very high CVD risk based on SCORE and CVD risk modifiers (primary prevention) or after the development of CVD events during the follow-up (secondary prevention); no target HDL, but >40 mg/dL in men and >45 mg/dL in women indicate lower risk; no target triglycerides, but <150 mg/dL indicates lower risk; no current smoking; BMI 20–25 kg/m² and waist circumference ≤94 cm in men and ≤80 cm in women; and ≥150 minutes per week of moderate aerobic physical activity (30 minutes for 5 days per week) or 75 minutes per week of vigorous aerobic physical activity (15 minutes for 5 days per week) or a combination thereof. In incident CVD event analysis, apart from SCORE, we also included the SCORE2 risk prediction model²⁰ endorsed by the 2021 ESC guidelines,²¹ which incorporates LDL, HDL, and triglycerides in addition to SCORE parameters. SCORE2 estimates both nonfatal myocardial infarction or stroke risk and the cardiovascular death risk, providing a more comprehensive evaluation.

SLE-related features. Laboratory tests were performed semi-annually, including complete blood count, erythrocyte sedimentation rate, serum creatinine, urinalysis, anti-double-stranded DNA antibodies, and C3 and C4 levels. The aPLs, including IgG and IgM anti-cardiolipin antibodies (aCLs) and anti-beta-2

glycoprotein I antibodies, and lupus anticoagulant (LA) were considered positive according to the Sydney APS classification criteria.²² Persistent triple aPL positivity was defined as positivity of all three aPLs at all four timepoints throughout follow-up (baseline and 3-, 7-, and 10-year follow-up).

The Systemic Lupus Erythematosus Disease Activity Index 2000 (SLEDAI-2K),²³ Physician Global Assessment (PGA; scale 0–3), Systemic Lupus International Collaborating Clinics (SLICC) American College of Rheumatology Damage Index,²⁴ LLDAS, and DORIS remission measures were assessed semiannually. LLDAS was defined as SLEDAI-2K ≤ 4 without significant organ involvement, absence of new disease activity, PGA ≤ 1 , prednisone dosage ≤ 7.5 mg/day, and standard maintenance doses of immunosuppressives and/or biologics.¹⁶ For clinical remission, we used the DORIS definition: clinical SLEDAI-2K score of 0, PGA < 0.5 , prednisolone dosage ≤ 5 mg/day, and stable antimalarials, immunosuppressives, and/or biologics.¹⁷ At each semiannual assessment during 10-year follow-up, LLDAS and DORIS were considered attained if their criteria were fulfilled over the preceding six-month period. For the initial years of our study, we retrospectively applied the LLDAS and DORIS criteria from medical files until 2016, when these definitions were introduced.^{16,25} LLDAS achievement throughout 100% (LLDAS100), 75% (LLDAS75), and 50% (LLDAS50) of the follow-up period, and DORIS remission achievement throughout 100% (DORIS100), 75% (DORIS75), and 50% (DORIS50) of the follow-up period were also assessed. Disease-related medications were recorded at the baseline, and follow-up ultrasound assessments: cumulative dose of glucocorticoids (sum of dose before the baseline examination and during the 10-year follow-up), consistent reception of hydroxychloroquine (over the entire follow-up period), immunosuppressives (cyclophosphamide, azathioprine, mycophenolate mofetil, cyclosporine, methotrexate, leflunomide), and biologics (rituximab, belimumab).

Vascular ultrasound. All ultrasonographic assessments were conducted in our cardiovascular research laboratory by the same blinded, experienced operator. Healthy participants were recruited through flyers in the local community. Atherosclerotic plaques were assessed using a 14.0-MHz multifrequency linear array probe on a high-resolution ultrasound machine (Vivid 7 Pro; GE HealthCare). Measurements were performed bilaterally in the near and far walls of the common carotid artery, carotid bulb, and internal carotid artery. According to Mannheim consensus,²⁶ plaques were defined as focal structures encroaching ≥ 0.5 mm into the lumen or $\geq 50\%$ compared with the surrounding intima-media thickness of the adjacent vascular wall or demonstrating an intima-media thickness ≥ 1.5 mm.

Statistical analysis. Qualitative variables were presented as frequencies and percentages and quantitative variables as median (interquartile range). The Shapiro–Wilk test was applied

to assess the normality of data distributions. To evaluate differences between groups, we employed the Mann–Whitney U test for quantitative variables and the Pearson's chi-square or Fisher's exact tests for qualitative variables. To assess carotid plaque progression during 10-year follow-up in patients with SLE versus HC individuals, and within the group with SLE, we applied multivariate mixed-effects Poisson regression models with a random intercept to account for the within-person repeated measurements. Models were adjusted for the timepoints of carotid ultrasound measurements (as a qualitative covariate with three levels: 3, 7, and 10 years) and CVRFs. To account for the time needed for carotid plaque development between different vascular ultrasound measurements, the natural logarithm (ln) of the difference between two consecutive measurement times was used as an offset. Regarding missing ultrasound data, we examined the differences in baseline characteristics among individuals followed over the study period and those lost to follow-up. We also examined the differential impact of CVRF target attainment on carotid plaque progression between patients with SLE and HCs using multivariable Poisson mixed-effects regression models, which additionally included the interaction of patients with SLE and HCs with the sum of CVRF targets. Due to 21.8%, 31.3%, 18.5%, 18.5%, and 18.5% missing data over different follow-up timepoints (3, 7, or 10 years) for blood pressure, LDL cholesterol, smoking status, body weight, and physical activity, respectively, in the HC group, we employed multiple imputation by chained equations²⁷ and conducted the analysis following Rubin's rules.²⁸

In the group with SLE, models included patients' age, the sum of sustainedly attained CVRF targets during follow-up for blood pressure, LDL, smoking, body weight, and physical activity, as per the 2016 ESC guidelines,¹⁵ DORIS75 ($\geq 75\%$ of follow-up), and medications (antihypertensives, lipid-lowering agents, and antiplatelets) at baseline. For patients for whom CVRF-related medication reception differed significantly between baseline and 10-year assessments, we controlled for their reception at 100% and $\geq 75\%$ of follow-up. For LDL target, considering the 2019 American College of Cardiology/American Heart Association guidelines,²⁹ which included inflammatory disorders among ASCVD risk enhancers, and the 2021 ESC guidelines,²¹ which stated that inflammatory conditions should be treated as in high-risk groups in the general population, we conducted a sensitivity analysis using the following LDL level goals: LDL < 100 mg/dL for patients with SLE without CVD events (high risk/primary prevention) and < 70 mg/dL for those developing CVD events during the 10-year follow-up (very high risk/secondary prevention).

We further assessed the 10-year incidence of CVD events using a permutation-based log-rank test to compare patients with SLE versus HCs, and we performed a univariate Cox regression analysis of CVD events to identify potential associations in the cohort with SLE. Covariates included in all analyses were selected either based on significant associations in the univariate analyses or were predetermined as clinically significant based on the

relevant literature.^{1,11–13,30–34} Statistical analyses were performed using STATA (version 12.0; College Station) and R (version 4.3.1; R Core Team, 2023).

Data availability. Individual participant data from this study can be obtained from the corresponding author after deidentification upon reasonable request. Requests should be directed to mtektionidou@gmail.com or mtektionidou@med.uoa.gr.

RESULTS

After a baseline vascular ultrasound assessment of 230 individuals (115 patients with SLE and 115 age- and sex-matched HCs), data from 205 of 230 participants (89.1%; 111 patients with SLE and 94 HCs) were included in our analysis involving 738 carotid ultrasound measurements (413 from patients with SLE and 325 from HCs) at four timepoints (baseline and 3-, 7-, and 10-year follow-up; Supplementary Figure 1, flowchart). Baseline characteristics of patients with SLE and HCs are presented in Table 1. All individuals were White Europeans, representing local demographic characteristics. At baseline, patients with SLE had a higher prevalence of pack-years smoking; antihypertensive, antiplatelet, and anticoagulant treatment reception; and carotid

plaque presence compared to HCs. Eight individuals (three patients with SLE and five HCs) were diagnosed and started receiving antidiabetic drugs during follow-up, maintaining good control (median hemoglobin A1c 6.6). CVRF-related medication reception at baseline and 10-year follow-up is shown in Supplementary Table 2. Each attained CVRF target per assessment and the sum of attained targets per assessment and throughout follow-up in the cohort with SLE are presented in Supplementary Table 3.

Disease-related parameters are shown in Table 2. In total, 85 of 111 patients (76.6%) maintained LLDAS $\geq 75\%$ of their follow-up duration, whereas 53 of 111 patients (47.7%) achieved DORIS remission status $\geq 75\%$ of follow-up. LLDAS and DORIS criteria at each semiannual assessment, along with annual SLICC scores, are displayed in Supplementary Tables 4 and 5, respectively. A total of 31 patients (27.9%) had a history of lupus nephritis at baseline, and 6 experienced a renal flare during the 10-year follow-up. No new patients with lupus nephritis were observed. At baseline, 34.2% of patients were aPL positive and 18.0% had coexistent APS. During follow-up, 25.2% had persistent aPL positivity and 4.5% had persistent triple aPL positivity. A total of 25 individuals (10.9%) were lost to follow-up (4 patients with SLE and 21 HCs). Their baseline CVRF characteristics did not differ

Table 1. Baseline demographic characteristics, cardiovascular risk parameters, and medications in the entire cohort*

Characteristic	Overall (n = 205)	SLE (n = 111)	Healthy controls (n = 94)	P value
White participants, n (%)	205 (100)	111 (100)	94 (100)	NA
Age, y	43.0 (35.1–53.0)	43.0 (36.0–52.0)	43.0 (34.5–52.8)	0.683
Female, n (%)	187 (91.2)	101 (91.0)	86 (91.5)	0.900
Systolic blood pressure, mm Hg	118.0 (110.0–128.0)	116.0 (109.0–124.0)	120.0 (111.0–133.8)	0.075
Diastolic blood pressure, mm Hg	72.5 (66.0–79.0)	71.0 (66.0–75.2)	76.0 (66.2–84.0)	0.014
Smoking, pack-years	1.4 (0.0–16.0)	6.0 (0.0–20.0)	0.0 (0.0–12.9)	<0.001
Smoking current, n (%)	76 (37.1)	45 (40.5)	31 (33.0)	0.264
Family history of CAD, n (%)	27 (13.2)	16 (14.4)	11 (11.7)	0.567
Total cholesterol, mg/dL	198.0 (175.0–226.0)	188.5 (170.8–223.8)	200.0 (181.0–228.0)	0.070
LDL, mg/dL	115.0 (96.0–137.0)	107.5 (92.0–132.5)	121.0 (101.0–139.0)	0.027
HDL, mg/dL	59.5 (49.0–70.0)	59.0 (49.0–71.2)	60.0 (48.0–67.0)	0.662
Triglycerides, mg/dL	86.0 (64.0–126.0)	93.0 (63.0–125.2)	79.0 (65.0–129.0)	0.645
BMI, kg/m ²	24.4 (21.5–28.1)	24.6 (21.3–28.4)	24.2 (21.8–28.0)	0.801
eGFR, mL/min/1.73 m ²	111 (102–117)	111 (102–116)	110 (101–117)	0.894
Exercise, min/wk	90.0 (0.0–210.0)	60.0 (0.0–210.0)	90.0 (0.0–210.0)	0.527
Antihypertensives, n (%)	56 (27.3)	40 (36.0)	16 (17.0)	0.002
Lipid-lowering agents, n (%)	17 (8.3)	10 (9.0)	7 (7.4)	0.686
Antiplatelets, n (%)	34 (16.6)	34 (30.6)	0 (0.0)	<0.001
Anticoagulants, n (%)	28 (13.7)	26 (23.4)	2 (2.1)	<0.001
Antidiabetic drugs, n (%) ^a	8 (3.9)	3 (2.7)	5 (5.3)	0.474
HbA1c, % ^a	6.6 (6.4–6.8)	6.6 (6.5–6.6)	6.7 (6.2–6.9)	0.764
SCORE	0.1 (0.0–0.6)	0.1 (0.0–0.7)	0.1 (0.0–0.5)	0.582
SCORE2	1.2 (0.0–3.1)	1.2 (0.0–3.1)	1.2 (0.0–3.2)	0.926

* Baseline demographic characteristics, cardiovascular risk parameters, and medications refer to baseline unless stated otherwise. Values represent median (interquartile range) unless alternately specified. SCORE: prediction of 10-year fatal cardiovascular disease corresponding to the 2016 ESC guidelines in low-risk countries. SCORE2: prediction of both the 10-year nonfatal myocardial infarction or stroke risk and 10-year cardiovascular death risk corresponding to the 2021 ESC guidelines in moderate-risk countries. P values represent differences between patients with SLE and controls at baseline assessment unless stated otherwise. P-values in bold indicate statistically significant differences ($P < 0.05$). BMI, body mass index; CAD, coronary artery disease; eGFR, estimated glomerular filtration rate; ESC, European Society of Cardiology; HbA1c, hemoglobin A1c; HDL, high-density lipoprotein; LDL, low-density lipoprotein; NA, not applicable; SCORE, Systemic Coronary Risk Evaluation; SLE, systemic lupus erythematosus.

^a The antidiabetic drugs and HbA1c values at 10-year follow-up among participants diagnosed with diabetes mellitus between baseline and 10-year follow-up were evaluated: three patients with SLE and five healthy controls.

Table 2. Disease-related characteristics in patients with SLE*

Characteristic	SLE (n = 111), n (%)
Disease duration, median (IQR), y	7.0 (1.5–14.0)
Cumulative prednisone dose, median (IQR), g ^a	12.6 (2.8–27.5)
Prednisone daily dose during follow-up, median (IQR), mg	0.3 (0.0–4.4)
Consistent hydroxychloroquine reception ^b	60 (54.1)
Immunosuppressive reception at baseline	44 (39.6)
SLEDAI-2K at baseline, median (IQR)	0.0 (0.0–4.0)
SLICC at baseline, median (IQR)	0.0 (0.0–1.0)
LLDAS50	97 (87.4)
LLDAS75	85 (76.6)
LLDAS100	43 (38.7)
DORIS50	76 (68.5)
DORIS75	53 (47.7)
DORIS100	25 (22.5)
Antiphospholipid syndrome at baseline	20 (18.0)
aPL positivity at baseline	38 (34.2)
Persistent aPL positivity	28 (25.2)
Persistently high aPL titers	13 (11.7)
Persistent triple aPL positivity	5 (4.5)
Persistent LA positivity	6 (5.4)
Persistent aCL (IgM or IgG) positivity	21 (18.9)
Persistent anti-β2 GPI (IgM or IgG) positivity	20 (18.0)
History of major SLE manifestations at baseline	
Lupus nephritis	31 (27.9)
Central nervous system involvement	12 (10.8)
Pericarditis	20 (18.0)
Pleuritis	12 (10.8)
Alopecia	13 (11.7)
Severe cytopenia	8 (7.2)
Pneumonitis	1 (0.9)

* Clinical characteristics and medications refer to baseline unless stated otherwise. anti-β2 GPI: anti-beta-2 glycoprotein I antibody; aCL, anti-cardiolipin antibody; aPL, anti-phospholipid antibody; DORIS, Definition of Remission in SLE; DORIS50, DORIS remission achievement ≥50% of the follow-up period; DORIS75, DORIS remission achievement ≥75% of the follow-up period; DORIS100, DORIS remission achievement throughout 100% of the follow-up period; IQR, interquartile range; LA, lupus anticoagulant; LLDAS, Lupus Low Disease Activity State; LLDAS50, LLDAS achievement ≥50% of the follow-up period; LLDAS75, LLDAS achievement ≥75% of the follow-up period; LLDAS100, LLDAS achievement throughout 100% of the follow-up period; SLE, systemic lupus erythematosus; SLEDAI-2K, Systemic Lupus Erythematosus Disease Activity Index 2000; SLICC, Systemic Lupus International Collaborating Clinics.

^a Cumulative prednisone exposure was evaluated before the baseline examination and during the 10-year follow-up.

^b Consistent hydroxychloroquine reception refers to 100% reception throughout the follow-up period.

from those of study participants, except for higher systolic blood pressure and BMI in the excluded individuals (Supplementary Table 6).

Carotid plaque progression in patients with SLE versus controls. Carotid plaque presence was significantly higher in patients with SLE versus HC individuals at all carotid

ultrasound timepoints (Table 3). Univariate analysis of plaque progression in patients with SLE versus HCs is presented in Supplementary Table 7. In Table 4, multivariate analysis model 4A revealed a 2.3-fold higher risk of plaque progression in patients with SLE versus controls (incidence rate ratio [IRR] 2.26, 95% confidence interval [CI] 1.34–3.81, $P = 0.002$) after controlling for baseline SCORE; eGFR; antihypertensive, lipid-lowering, and antiplatelet agents; and the number of carotid plaques at baseline. Based on this model, the expected 10-year evolution of the number of carotid plaques in patients with SLE versus HCs is shown in Figure 1A. In model 4B, which includes CVRFs not incorporated in SCORE, the incidence rate for carotid plaque progression remained significantly higher in patients with SLE versus HCs (IRR 2.20, 95% CI 1.33–3.64, $P = 0.002$), adjusting for age, smoking, eGFR, medications, and the number of carotid plaques at baseline. Because antihypertensive and lipid-lowering agent reception was higher at 10-year follow-up compared to baseline assessment ($P < 0.001$ for both; Supplementary Table 2), we also adjusted for their reception at 100% and ≥75% of follow-up; carotid plaque progression remained significantly higher in patients with SLE versus HCs (Table 4, models C, D, E, and F).

Multivariable analysis showed that sustained CVRF target attainment was significantly associated with reduced carotid plaque progression risk among patients with SLE. A protective but not statistically significant effect was observed in the HC group (Supplementary Table 8, models A, B, and C). The interaction of patients with SLE and HCs with the sum of CVRF targets did not reach statistical significance (for interaction, $P > 0.692$ in all models), suggesting a beneficial effect of CVRF target attainment in both groups.

Carotid plaque progression among patients with SLE.

A significant increase in plaque prevalence was observed from baseline to 3-, 7-, and 10-year follow-up among patients with SLE (21.6%, 31.2%, 42.9%, and 54.7%, respectively, $P < 0.001$; Table 3). Univariate analysis of CVRFs and disease-related variables for carotid plaque progression in the cohort with SLE is presented in Supplementary Table 9. In multivariate analysis, plaque progression risk was reduced by 32% for each CVRF sustainedly on target (IRR 0.68, 95% CI 0.53–0.89, $P = 0.004$) after controlling for age and reception of antihypertensives, lipid-lowering agents, and antiplatelets at baseline (Table 5, model A). Figure 1B shows the expected 10-year evolution of the number of carotid plaques in patients with SLE with varying numbers of CVRF targets sustainedly attained during the 10-year follow-up. A prolonged remission status, ≥75% of follow-up (DORIS75), was associated with a 43% decrease in atherosclerosis progression risk (IRR 0.57, 95% CI 0.34–0.95, $P = 0.033$; Table 5, model A). Figure 1C shows the expected 10-year evolution of the number of carotid plaques in patients with DORIS remission ≥75% of follow-up versus those without. Sensitivity analysis of carotid

Table 3. Carotid plaque presence and number of plaques in patients with SLE and HCs*

Characteristic	Baseline			3-Year follow-up			7-Year follow-up			10-Year follow-up		
	Patients with SLE (n = 111)	HCs (n = 94)	<i>P</i> value ^a	Patients with SLE (n = 109)	HCs (n = 91)	<i>P</i> value ^a	Patients with SLE (n = 98)	HCs (n = 69)	<i>P</i> value ^a	Patients with SLE (n = 95)	HCs (n = 71)	<i>P</i> value ^a
Carotid plaque presence, n (%)	24 (21.6)	7 (7.4)	0.005	34 (31.2)	10 (11.0)	0.001	42 (42.9)	9 (13.0)	<0.001	52 (54.7)	21 (29.6)	0.001
Number of carotid plaques, median (IQR)	0 (0–0)	0 (0–0)	0.004	0 (0–1)	0 (0–0)	<0.001	0 (0–2)	0 (0–0)	<0.001	1 (0–2)	0 (0–1)	<0.001

* Carotid plaque presence and the number of plaques in patients with SLE and HCs at baseline and follow-up assessments. The total numbers of individuals for each timepoint correspond to participants with carotid ultrasound measurements at baseline and 3-, 7-, and 10-year assessments (Supplementary Figure 1, flowchart). HC, healthy control; IQR, interquartile range; SLE, systemic lupus erythematosus.

^a *P* values represent the difference in carotid plaque presence and in the number of plaques in patients with SLE versus HCs at different assessments (baseline and 3, 7, and 10 years). *P* values in bold indicate statistically significant differences ($P < 0.05$).

plaque progression in patients with SLE using revised LDL cutoffs showed similar results (Supplementary Table 10).

Because lipid-lowering agent reception in patients with SLE was significantly higher at 10-year follow-up compared to baseline ($P < 0.001$; Supplementary Table 2), further adjustment for their reception at 100% and $\geq 75\%$ of follow-up was made; sustained CVRF control and DORIS remission $\geq 75\%$ of follow-up remained significantly correlated with lower plaque progression risk (Table 5, models B and C). Although achieving LLDAS throughout the entire follow-up (LLDAS100) was associated with reduced plaque progression in univariate analysis, this association was not significant in multivariate analysis (Supplementary Table 11).

Cardiovascular events in patients with SLE versus controls. During the 10-year follow-up, eight CVD events occurred in patients with SLE (two sudden cardiac deaths due to cardiac arrest, two acute coronary syndromes, two transient ischemic attacks, and two peripheral artery disease events) versus one CVD event (transient ischemic attack) among HCs. The incidence of CVD events was significantly higher in patients with SLE than HC individuals (permutation-based log-rank $P = 0.036$).

Cardiovascular events among patients with SLE. In exploratory univariate Cox regression analysis of incident CVD events, persistent aCL, LA, and triple aPL positivity over the 10-year follow-up, and antiplatelet reception at baseline, were associated with CVD events in patients with SLE (Supplementary Table 12), but these results should be interpreted with caution due to wide CIs. Baseline SCORE2 had a marginal statistical significance (hazard ratio [HR] 1.17, 95% CI 1.00–1.36, $P = 0.048$), whereas SCORE showed a trend toward significance for CVD events (HR 1.26, 95% CI 0.99–1.60, $P = 0.050$). However, in seven of eight patients who developed CVD events, the estimated 10-year risk of developing CVD according to both SCORE and SCORE2 predictions at baseline was low to moderate. The incorporation of carotid ultrasound at baseline

assessment enhanced the ability to predict the 10-year risk for CVD events from 12.5% (using only SCORE/SCORE2) to 37.5%, representing a three-fold increase in the detection rate (Supplementary Table 13). Given that disease activity is a major predictor of CVD events in patients with SLE,¹⁴ we examined the impact of DORIS75 in multivariate models (Supplementary Table 14). No association was found, but the low statistical power to perform a multivariate analysis given the low CVD event rates should be considered.

DISCUSSION

This study examines, for the first time to our knowledge, the progression of carotid atherosclerotic plaques in patients with SLE versus age- and sex-matched HCs over four serial timepoints in a 10-year follow-up period and the impact of sustained CVRF control and clinical remission. We found a 2.3-fold increased risk of new atherosclerotic plaques in patients with SLE versus HC individuals, mitigated by sustained CVRF target attainment and prolonged disease remission. We also observed a significantly higher incidence of CVD events in patients with SLE versus HCs, associated with persistent aCL, LA, and triple aPL positivity.

Only sporadic longitudinal studies have examined atherosclerotic plaque progression in patients with SLE versus HCs.^{11,12,31} In a previous three-year follow-up study from our group, the risk of plaque progression in patients with SLE (including both men and women) was significantly higher in patients with SLE (OR 2.81) than age- and sex-matched HCs but not in patients with rheumatoid arthritis versus HCs.¹¹ A five-year follow-up study showed a two-fold increased risk for plaque progression in women with SLE versus controls, associated with larger waist circumference and no reception of hydroxychloroquine.¹² In another study of White British women with SLE with a median five-year follow-up, new plaques were developed in 26% of patients.³⁰

Guidelines for CVD prevention in the general population defined specific treatment goals for each of CVRFs and

Table 4. Multivariate mixed-effects Poisson regression models of carotid plaque progression in patients with SLE versus healthy controls*

Characteristic	IRR (95% CI)	P value
Model A (including SCORE)		
Patients with SLE vs healthy controls	2.26 (1.34–3.81)	0.002
Antihypertensives	1.02 (0.61–1.71)	0.938
Lipid-lowering agents	1.64 (0.77–3.48)	0.198
Antiplatelets	0.99 (0.55–1.78)	0.971
SCORE	1.16 (0.96–1.42)	0.132
eGFR	0.80 (0.63–1.01)	0.059
Number of carotid plaques	0.88 (0.60–1.29)	0.520
Model B		
Patients with SLE vs healthy controls	2.20 (1.33–3.64)	0.002
Age, y	1.06 (1.03–1.08)	<0.001
Smoking	2.12 (1.36–3.30)	<0.001
Antihypertensives	1.05 (0.64–1.73)	0.851
Lipid-lowering agents	1.21 (0.60–2.41)	0.594
Antiplatelets	1.16 (0.67–2.02)	0.601
eGFR	0.84 (0.67–1.05)	0.128
Number of carotid plaques	0.71 (0.50–1.02)	0.064
Model C (including SCORE)		
Patients with SLE vs healthy controls	2.25 (1.32–3.82)	0.003
Antihypertensive reception $\geq 75\%$ of the follow-up period	1.18 (0.73–1.91)	0.744
Lipid-lowering agent reception $\geq 75\%$ of the follow-up period	1.10 (0.63–1.91)	0.744
Antiplatelets	1.00 (0.56–1.82)	0.982
SCORE	1.21 (1.02–1.45)	0.034
eGFR	0.82 (0.65–1.04)	0.106
Number of carotid plaques	0.87 (0.59–1.26)	0.455
Model D		
Patients with SLE vs healthy controls	2.22 (1.33–3.71)	0.002
Age, y	1.06 (1.04–1.09)	<0.001
Smoking	2.08 (1.33–3.23)	0.001
Antihypertensive reception $\geq 75\%$ of the follow-up period	0.93 (0.59–1.47)	0.754
Lipid-lowering agent reception $\geq 75\%$ of the follow-up period	0.95 (0.56–1.61)	0.855
Antiplatelets	1.15 (0.66–2.02)	0.620
eGFR	0.85 (0.68–1.06)	0.160
Number of carotid plaques	0.74 (0.52–1.04)	0.081
Model E (including SCORE)		
Patients with SLE vs healthy controls	2.32 (1.37–3.93)	0.002
Antihypertensive reception 100% of the follow-up period	0.97 (0.55–1.72)	0.916
Lipid-lowering agent reception 100% of the follow-up period	1.26 (0.77–3.48)	0.606
Antiplatelets	0.98 (0.54–1.78)	0.957
SCORE	1.22 (1.02–1.47)	0.032
eGFR	0.81 (0.63–1.01)	0.088
Number of carotid plaques	0.89 (0.61–1.30)	0.541
Model F		
Patients with SLE vs healthy controls	2.19 (1.32–3.63)	0.002
Age, y	1.06 (1.04–1.09)	<0.001
Smoking	2.06 (1.33–3.20)	<0.001
Antihypertensive reception 100% of the follow-up period	1.02 (0.59–1.76)	0.944
Lipid-lowering agent reception 100% of the follow-up period	0.79 (0.35–1.81)	0.578
Antiplatelets	1.18 (0.55–1.78)	0.553
eGFR	0.87 (0.69–1.09)	0.232
Number of carotid plaques	0.73 (0.60–1.29)	0.079

* Variables refer to baseline assessment unless specified otherwise. All models are also adjusted for the timepoints of carotid ultrasound measurements (as a qualitative covariate). SCORE prediction of 10-year fatal cardiovascular disease corresponding to the 2016 European Society of Cardiology guidelines in low-risk countries. *P*-values in bold indicate statistically significant variables ($P < 0.05$). CI, confidence interval; eGFR, estimated glomerular filtration rate; IRR, incidence rate ratio; SCORE, Systemic Coronary Risk Evaluation; SLE, systemic lupus erythematosus.

highlighted the importance of their attainment.¹⁵ Importantly, a suboptimal CVRF control was recently shown in a multicenter cross-sectional study of 3,401 patients with SLE from

24 countries and across 4 continents.³⁵ Although previous publications identified hypertension,³⁶ dyslipidemia,³⁶ increased waist circumference,¹² and SCORE¹¹ as predictors of intima-media

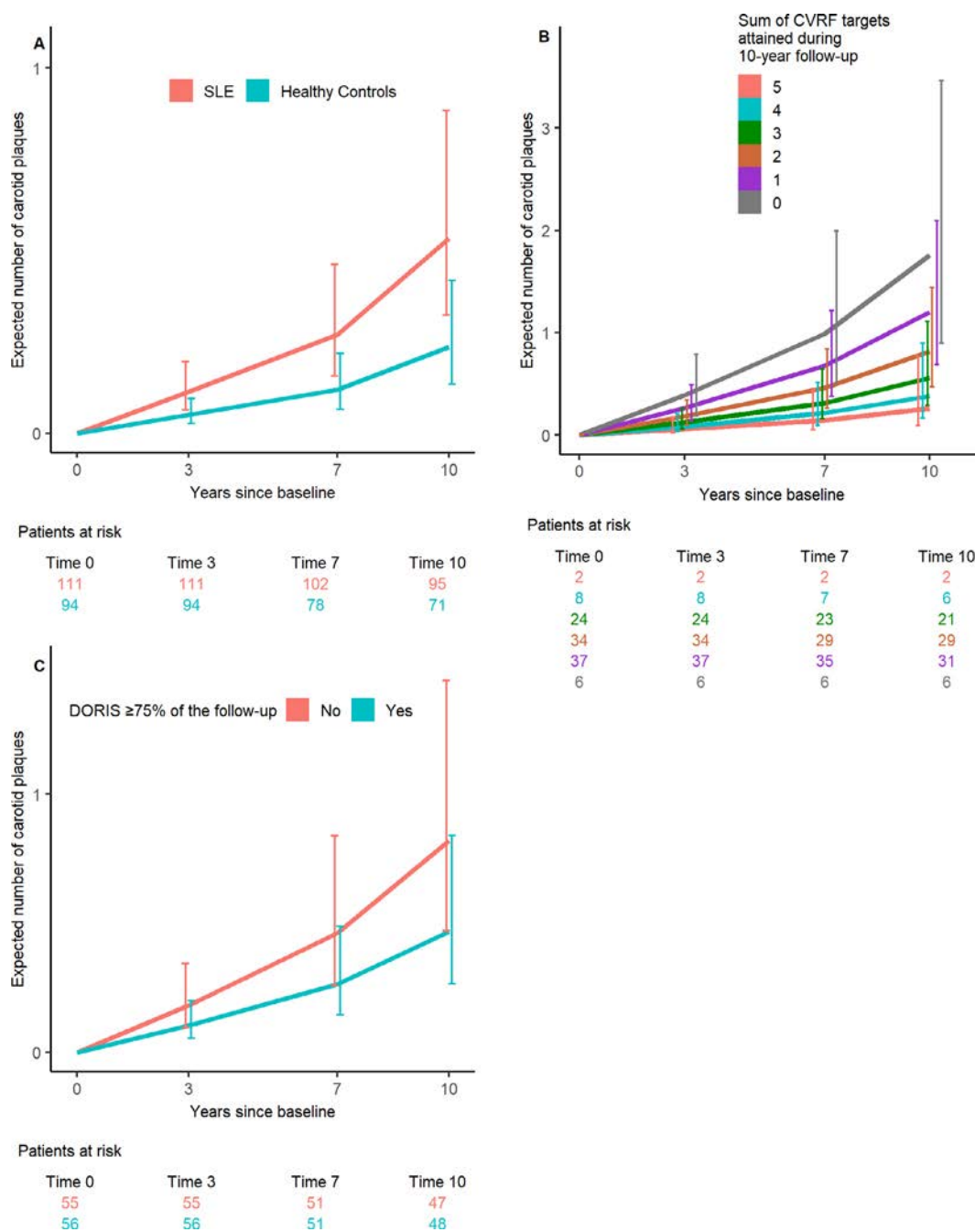


Figure 1. Expected 10-year evolution of the number of carotid plaques (A) for typical patients with SLE and healthy controls (HCs), (B) for typical individuals with SLE with varying numbers of cardiovascular risk factor (CVRF) targets sustainedly attained, and (C) for typical individuals with SLE with versus without DORIS remission for $\geq 75\%$ of follow-up. (A) Typical individuals are patients with SLE or HCs with baseline characteristic values (included in multivariate model 4A of plaque progression in patients with SLE vs HCs) set at the median for quantitative and at the mode for qualitative variables: no use of antihypertensives, lipid-lowering agents or antiplatelets, Systemic Coronary Risk Evaluation 0.1, estimated glomerular filtration rate 111 mL/minutes/1.73 m², and no carotid plaques. (B) Typical individuals with SLE are patients with baseline characteristic values (included in multivariate model 5A of plaque progression in patients with SLE) set at the median for quantitative and at the mode for qualitative variables: 43 years old; no reception of antihypertensives, lipid-lowering agents, or antiplatelets; and no DORIS remission $\geq 75\%$ of follow-up. (C) Typical individuals with SLE are patients with baseline characteristic values (included in multivariate model 5A) set at the median for quantitative and at the mode for qualitative variables: 43 years old; no reception of antihypertensives, lipid-lowering agents, or antiplatelets; and two CVRF targets sustainedly attained during the follow-up. DORIS, Definition of Remission in SLE; SLE, systemic lupus erythematosus.

Table 5. Multivariate mixed-effects Poisson regression analysis of carotid plaque progression in patients with SLE*

Characteristic	IRR (95% CI)	P value
Model A		
Age, y	1.03 (1.01–1.06)	0.010
Antihypertensives	0.64 (0.37–1.09)	0.100
Lipid-lowering agents	1.11 (0.50–2.46)	0.800
Antiplatelets	0.89 (0.51–1.55)	0.671
Sum of CVRF targets consistently attained throughout the follow-up period	0.68 (0.53–0.89)	0.004
DORIS75	0.57 (0.34–0.95)	0.033
Model B		
Age, y	1.04 (1.02–1.06)	0.001
Antihypertensives	0.70 (0.41–1.19)	0.187
Lipid-lowering agent reception $\geq 75\%$ of the follow-up period	0.66 (0.36–1.20)	0.174
Antiplatelets	0.82 (0.47–1.44)	0.482
Sum of CVRF targets consistently attained throughout the follow-up period	0.67 (0.51–0.87)	0.003
DORIS75	0.56 (0.33–0.94)	0.028
Model C		
Age, y	1.04 (1.01–1.07)	0.002
Antihypertensives	0.68 (0.40–1.16)	0.158
Lipid-lowering agent reception 100% of the follow-up period	0.60 (0.23–1.59)	0.306
Antiplatelets	0.87 (0.50–1.51)	0.616
Sum of CVRF targets consistently attained throughout the follow-up period	0.67 (0.52–0.88)	0.003
DORIS75	0.57 (0.34–0.96)	0.035

* Variables refer to baseline assessment unless specified otherwise. CVRF targets attained throughout the follow-up period represented targets consistently attained by the last follow-up assessment (at 3, 7, or 10 years) according to the 2016 European Society of Cardiology guidelines concerning blood pressure, low-density lipoprotein, smoking, body weight (body mass index and waist circumference), and physical activity. All models are also adjusted for the timepoints of carotid ultrasound measurements (as a qualitative covariate). P-values in bold indicate statistically significant variables ($P < 0.05$). CI, confidence interval; CVRF, cardiovascular risk factor; DORIS75, Definition of Remission in SLE remission achievement $\geq 75\%$ of the follow-up period; IRR, incidence rate ratio; SLE, systemic lupus erythematosus.

thickness or plaque acceleration in patients with SLE, no previous study examined the enduring impact of sustained CVRF target attainment on preventing plaque progression in a long-term follow-up. Although LDL and BMI attainment rates were almost double at each timepoint separately, sustained CVRF target attainment over the entire follow-up was only 22.5%, 23.4%, and 18.0% for LDL, body weight, and physical activity, respectively. The lower sustained target rates emphasize the need for consistent efforts to manage CVRFs in patients with SLE by encouraging lifestyle changes including healthy diet, regular exercise, and early initiation of lipid-lowering medications after appropriate CVD risk stratification.¹⁴

Regarding disease-related predictors of plaque progression in patients with SLE, previous studies were mainly focused on the baseline disease activity status overlooking the dynamic nature of disease activity over time.^{12,30} Our study uniquely tracks

multiple durations of LLDAS and DORIS throughout the entire follow-up period. The 2022 EULAR recommendations for CVD risk management in rheumatic diseases state that low disease activity should be maintained in patients with SLE to also reduce cardiovascular risk.¹⁴ Interestingly, our results showed that none of the examined LLDAS durations (LLDAS50, LLDAS75, or LLDAS100) prevented plaque progression in multivariate analysis. In contrast, maintaining DORIS $\geq 75\%$ of follow-up correlated with a 43% reduction in plaque progression risk. These findings support the importance of prioritizing a sustained remission rather than a low disease activity state for the prevention of atherosclerosis development and progression in patients with SLE.

We also examined incident CVD events during the 10-year follow-up in association with disease-related risk factors, the ESC-endorsed risk prediction tools SCORE/SCORE2, and CVRF targets. CVD events in patients with SLE are linked to both traditional CVRFs and disease-related features.^{32,33} We found that persistent aCL, LA, and triple aPL positivity were associated with incident CVD events in patients with SLE in univariate analysis. Positive aPLs have been described as independent predictors of subsequent CVD events in patients with SLE,^{14,37} but the impact of persistent triple aPL positivity in multiple measures over a 10-year follow-up is described for the first time. Two events in the group with SLE occurred in patients with positive aPLs who were subsequently diagnosed with APS. The distinction between atherothrombotic events attributable to APS and those due to atherosclerosis remains unclear. Evidence has also shown that aPL-mediated oxidative stress, endothelial dysfunction, and the oxidized LDL/ β_2 glycoprotein I complex-induced differentiation of macrophages to foam cells promote atherogenesis.³⁸ Although the results of our analysis reached statistical significance, they should be validated by multivariate analyses in larger prospective studies with higher incidence rates.

Although long-term hydroxychloroquine exposure has been associated with reduced CVD risk in patients with SLE,³⁴ consistent hydroxychloroquine reception was not found to protect against plaque progression or CVD events in our cohort, possibly due to its reception by most patients throughout follow-up. Glucocorticoid reception, although a well-established predictor of CVD events,³⁹ was not correlated with atherosclerosis progression or CVD event occurrence in our study, probably due to low doses received (median daily prednisone dose 0.3 mg). Lack of associations between the above medications and incident CVD events may also be explained by their small numbers.

Regarding the generic CVD risk prediction tools, although there was a marginally significant association between SCORE2 and CVD events and a trend toward significance between SCORE and CVD events in univariate analysis, both tools had limitations in their predictive ability. Median baseline SCORE2 (1.2%) failed to predict seven of eight CVD events, and SCORE (0.1%) did not predict any of the two CVD deaths in the cohort with SLE. This observation aligns with recent studies, including those conducted by our

group, suggesting that generic CVD prediction tools, such as Framingham and SCORE, may underestimate CVD risk in patients with SLE.^{40–42} However, data from various cohorts have shown that SCORE may perform better than Framingham in predicting plaque progression, the extent and severity of coronary artery disease, and CVD deaths.^{41,43,44} In the present study, the incorporation of baseline carotid ultrasound resulted in a three-fold increase in detection rate compared to generic SCORE/SCORE2 tools, suggesting its additive role in CVD risk assessment.

The strengths of the study include the following assessments for the first time: (a) 10-year atherosclerotic plaque progression in patients with SLE versus age- and sex-matched HC individuals, (b) predictive role of the sustained target attainment for each CVRF as defined by the ESC and two generic prediction scores, and (c) impact of LLDAS and DORIS at multiple time periods (50%, 75%, and 100% of the entire follow-up time) given that disease activity fluctuates over time and the assessment at only one time-point would lead to underestimations. All ultrasound examinations, from baseline to the last assessment, were performed by the same blinded assessor who has performed >2,000 ultrasounds in our cardiovascular research laboratory since 2010.^{11,31} There was a relatively small loss to follow-up (10.9%) considering the duration of follow-up (10 years) that was more pronounced in the HC group, reflecting the challenges of long-term evaluations in healthy populations. We also assessed for the first time the impact of persistent triple aPL positivity on incident CVD events. A limitation of the study is the lack of statistical power to perform a multivariate analysis of incident CVD events for all potential predictors due to low event rates; however, these rates are similar to those reported in recent prospective studies.^{45,46} Additionally, our cohort consisted solely of White Europeans, limiting the generalizability of our findings to more ethnically diverse populations. Given that aPLs have been associated with CVD events in the general population,^{47,48} lack of testing for aPL positivity in HCs might be an additional limitation.

Our findings showed that sustained CVRF control and prolonged clinical remission can substantially reduce atherosclerosis progression risk in patients with SLE, highlighting the need for consistent efforts to achieve both targets in this young adult population at high risk. Additionally, persistent triple aPL positivity was associated with incident CVD events, supporting the importance of their early identification and appropriate management.¹⁴ Further research should validate these findings in larger and more diverse cohorts with SLE.

ACKNOWLEDGMENT

We thank our ultrasonographic assessor, Mr George Konstantonis, for performing all ultrasonographic assessments during this study.

AUTHOR CONTRIBUTIONS

All authors contributed to at least one of the following manuscript preparation roles: conceptualization AND/OR methodology, software,


investigation, formal analysis, data curation, visualization, and validation AND drafting or reviewing/editing the final draft. As corresponding author, Dr Tektonidou confirms that all authors have provided the final approval of the version to be published and takes responsibility for the affirmations regarding article submission (eg, not under consideration by another journal), the integrity of the data presented, and the statements regarding compliance with institutional review board/Declaration of Helsinki requirements.

REFERENCES

1. Wu GC, Liu HR, Leng RX, et al. Subclinical atherosclerosis in patients with systemic lupus erythematosus: a systemic review and meta-analysis. *Autoimmun Rev* 2016;15:22–37.
2. Henrot P, Foret J, Barnetche T, et al. Assessment of subclinical atherosclerosis in systemic lupus erythematosus: a systematic review and meta-analysis. *Joint Bone Spine* 2018;85:155–163.
3. Tektonidou MG, Wang Z, Ward MM. Brief report: trends in hospitalizations due to acute coronary syndromes and stroke in patients with systemic lupus erythematosus, 1996 to 2012. *Arthritis Rheumatol* 2016;68:2680–2685.
4. Yazdany J, Pooley N, Langham J, et al. Systemic lupus erythematosus; stroke and myocardial infarction risk: a systematic review and meta-analysis. *RMD Open* 2020;6:e001247.
5. Tektonidou MG, Lewandowski LB, Hu J, et al. Survival in adults and children with systemic lupus erythematosus: a systematic review and Bayesian meta-analysis of studies from 1950 to 2016. *Ann Rheum Dis* 2017;76:2009–2016.
6. Schoenfeld SR, Kasturi S, Costenbader KH. The epidemiology of atherosclerotic cardiovascular disease among patients with SLE: a systematic review. *Semin Arthritis Rheum* 2013;43:77–95.
7. Bello N, Meyers KJ, Workman J, et al. Cardiovascular events and risk in patients with systemic lupus erythematosus: systematic literature review and meta-analysis. *Lupus* 2023;32:325–341.
8. Gu MM, Wang XP, Cheng QY, et al. A meta-analysis of cardiovascular events in systemic lupus erythematosus. *Immunol Invest* 2019;48:505–520.
9. Yafasova A, Fosbøl EL, Schou M, et al. Long-term cardiovascular outcomes in systemic lupus erythematosus. *J Am Coll Cardiol* 2021;77:1717–1727.
10. Lim SY, Bae EH, Han KD, et al. Systemic lupus erythematosus is a risk factor for cardiovascular disease: a nationwide, population-based study in Korea. *Lupus* 2018;27:2050–2056.
11. Krawvariti E, Konstantonis G, Sfikakis PP, et al. Progression of subclinical atherosclerosis in systemic lupus erythematosus versus rheumatoid arthritis: the impact of low disease activity. *Rheumatology* 2018;57:2158–2166.
12. Lertratanakul A, Sun J, Wu PW, et al. Risk factors for changes in carotid intima media thickness and plaque over 5 years in women with systemic lupus erythematosus. *Lupus Sci Med* 2021;8:e000548.
13. Tselios K, Sheane BJ, Gladman DD, et al. Optimal monitoring for coronary heart disease risk in patients with systemic lupus erythematosus: a systematic review. *J Rheumatol* 2016;43:54–65.
14. Drosos GC, Vedder D, Houben E, et al. EULAR recommendations for cardiovascular risk management in rheumatic and musculoskeletal diseases, including systemic lupus erythematosus and antiphospholipid syndrome. *Ann Rheum Dis* 2022;81:768–779.
15. Piepoli MF, Hoes AW, Agewall S, et al. 2016 European guidelines on cardiovascular disease prevention in clinical practice. *Eur Heart J* 2016;37:2315–2381.
16. Franklyn K, Lau CS, Navarra SV, et al. Definition and initial validation of a Lupus Low Disease Activity State (LLDAS). *Ann Rheum Dis* 2016;75:1615–1621.

17. van Vollenhoven RF, Bertsias G, Doria A, et al. 2021 DORIS Definition of Remission in SLE: final recommendations from an international task force. *Lupus Sci Med* 2021;8:e000538.
18. Petri M, Orbai AM, Alarcón GS, et al. Derivation and validation of the Systemic Lupus International Collaborating Clinics classification criteria for systemic lupus erythematosus. *Arthritis Rheum* 2012;64:2677–2686.
19. Conroy R. Estimation of ten-year risk of fatal cardiovascular disease in Europe: the SCORE project. *Eur Heart J* 2003;24:987–1003.
20. Hageman S, Pennells L, Ojeda F, et al. SCORE2 risk prediction algorithms: new models to estimate 10-year risk of cardiovascular disease in Europe. *Eur Heart J* 2021;42:2439–2454.
21. Visseren FLJ, Mach F, Smulders YM, et al. 2021 ESC guidelines on cardiovascular disease prevention in clinical practice. *Eur Heart J* 2021;42:3227–3337.
22. Miyakis S, Lockshin MD, Atsumi T, et al. International consensus statement on an update of the classification criteria for definite antiphospholipid syndrome (APS). *J Thromb Haemost* 2006;4:295–306.
23. Gladman DD, Ibañez D, Urowitz MB. Systemic Lupus Erythematosus Disease Activity Index 2000. *J Rheumatol* 2002;29:288–291.
24. Gladman D, Ginzler E, Goldsmith C, et al. The development and initial validation of the Systemic Lupus International Collaborating Clinics/American College of Rheumatology Damage Index for systemic lupus erythematosus. *Arthritis Rheum* 1996;39:363–369.
25. van Vollenhoven R, Voskuyl A, Bertsias G, et al. A framework for remission in SLE: consensus findings from a large international task force on definitions of remission in SLE (DORIS). *Ann Rheum Dis* 2017;76:554–561.
26. Touboul PJ, Hennerici MG, Meairs S, et al. Mannheim carotid intima-media thickness and plaque consensus (2004–2006–2011). *Cerebrovasc Dis* 2012;34:290–296.
27. van Buuren S. Multiple imputation of discrete and continuous data by fully conditional specification. *Stat Methods Med Res* 2007;16:219–242.
28. Rubin DB. *Multiple Imputation for Nonresponse in Surveys*. Wiley; 1987.
29. Arnett DK, Blumenthal RS, Albert MA, et al. 2019 ACC/AHA guideline on the primary prevention of cardiovascular disease: a report of the American College of Cardiology/American Heart Association Task Force on Clinical Practice Guidelines. *Circulation* 2019;140:e596–e646.
30. Haque S, Skeoch S, Rakieh C, et al. Progression of subclinical and clinical cardiovascular disease in a UK SLE cohort: the role of classic and SLE-related factors. *Lupus Sci Med* 2018;5:e000267.
31. Papazoglou N, Kravvariti E, Konstantonis G, et al. The impact of traditional cardiovascular risk factor control on 7-year follow-up atherosclerosis progression in systemic lupus erythematosus. *Rheumatology (Oxford)* 2024;63:50–57.
32. Ballocca F, D'Ascenzo F, Moretti C, et al. Predictors of cardiovascular events in patients with systemic lupus erythematosus (SLE): a systematic review and meta-analysis. *Eur J Prev Cardiol* 2015;22:1435–1441.
33. Katayama Y, Yanai R, Itaya T, et al. Risk factors for cardiovascular diseases in patients with systemic lupus erythematosus: an umbrella review. *Clin Rheumatol* 2023;42:2931–2941.
34. Fasano S, Pierro L, Pantano I, et al. Longterm hydroxychloroquine therapy and low-dose aspirin may have an additive effectiveness in the primary prevention of cardiovascular events in patients with systemic lupus erythematosus. *J Rheumatol* 2017;44:1032–1038.
35. Bolla E, Semb AG, Kerola AM, et al. Prevalence and target attainment of traditional cardiovascular risk factors in patients with systemic lupus erythematosus: a cross-sectional study including 3401 individuals from 24 countries. *Lancet Rheumatol* 2024;6:e447–e459.
36. Ajeganova S, Gustafsson T, Lindberg L, et al. Similar progression of carotid intima-media thickness in 7-year surveillance of patients with mild SLE and controls, but this progression is still promoted by dyslipidaemia, lower HDL levels, hypertension, history of lupus nephritis and a higher prednisolone usage in patients. *Lupus Sci Med* 2020;7:e000362.
37. Tektonidou MG, Laskari K, Panagiotakos DB, et al. Risk factors for thrombosis and primary thrombosis prevention in patients with systemic lupus erythematosus with or without antiphospholipid antibodies. *Arthritis Care Res (Hoboken)* 2009;61:29–36.
38. Tektonidou MG. Cardiovascular disease risk in antiphospholipid syndrome: thrombo-inflammation and atherothrombosis. *J Autoimmun* 2022;128:102813.
39. Ugarte-Gil MF, Mak A, Leong J, et al. Impact of glucocorticoids on the incidence of lupus-related major organ damage: a systematic literature review and meta-regression analysis of longitudinal observational studies. *Lupus Sci Med* 2021;8:e000590.
40. Drosos GC, Konstantonis G, Sfikakis PP, et al. Underperformance of clinical risk scores in identifying vascular ultrasound-based high cardiovascular risk in systemic lupus erythematosus. *Eur J Prev Cardiol* 2021;28:346–352.
41. Panopoulos S, Drosos GC, Konstantonis G, et al. Generic and disease-adapted cardiovascular risk scores as predictors of atherosclerosis progression in SLE. *Lupus Sci Med* 2023;10:e000864.
42. Gustafsson JT, Simard JF, Gunnarsson I, et al. Risk factors for cardiovascular mortality in patients with systemic lupus erythematosus, a prospective cohort study. *Arthritis Res Ther* 2012;14:R46.
43. Gunaydin ZY, Karagoz A, Bektas O, et al. Comparison of the Framingham risk and score models in predicting the presence and severity of coronary artery disease considering SYNTAX score. *Anatol J Cardiol* 2016;16:412–428.
44. Marchant I, Boissel JP, Kassai B, et al. SCORE should be preferred to Framingham to predict cardiovascular death in French population. *Eur J Cardiovasc Prev Rehabil* 2009;16:609–615.
45. Urowitz MB, Gladman DD, Farewell V, et al. Accrual of atherosclerotic vascular events in a multicenter inception systemic lupus erythematosus cohort. *Arthritis Rheumatol* 2020;72:1734–1740.
46. Urowitz MB, Su J, Gladman DD. Atherosclerotic vascular events in systemic lupus erythematosus: an evolving story. *J Rheumatol* 2020;47:66–71.
47. Vaarala O, Mänttari M, Manninen V, et al. Anti-cardiolipin antibodies and risk of myocardial infarction in a prospective cohort of middle-aged men. *Circulation* 1995;91:23–27.
48. Zuo Y, Navaz S, Liang W, et al. Prevalence of antiphospholipid antibodies and association with incident cardiovascular events. *JAMA Netw Open* 2023;6:e236530.

Cross-Phenotype Genome-Wide Association Study on the Shared Genetic Susceptibility to Systemic Sclerosis and Primary Biliary Cholangitis

Yiming Luo,¹ Atlas Khan,¹ Lili Liu,¹ Cue Hyunkyu Lee,¹ Gabriel J. Perreault,¹ Sydney F. Pomenti,¹ Pravitt Gourh,²  Krzysztof Kiryluk,¹ and Elana J. Bernstein¹

Objective. An increased risk of primary biliary cholangitis (PBC) has been reported in patients with systemic sclerosis (SSc). Our study aims to investigate the shared genetic susceptibility between the two disorders and to define candidate causal genes using cross-phenotype genome-wide association study (GWAS) meta-analysis.

Methods. We performed cross-phenotype GWAS meta-analysis and Bayesian colocalization analysis for patients with SSc and patients with PBC. We performed both genome-wide and locus-based analysis, including tissue and pathway enrichment analyses, fine-mapping, Bayesian colocalization analyses with expression quantitative trait loci and protein quantitative trait loci (pQTL) datasets, and phenome-wide association studies. Finally, we used an integrative approach to prioritize candidate causal genes from the novel loci.

Results. We detected a strong genetic correlation between SSc and PBC (global genetic correlation = 0.84, $P = 1.7 \times 10^{-6}$). In the cross-phenotype GWAS meta-analysis, we identified 44 nonhuman leukocyte antigens loci that reached genome-wide significance ($P < 5 \times 10^{-8}$). Evidence of shared causal variants between patients with SSc and patients with PBC was found for nine loci, five of which were novel. Integrating multiple sources of evidence, we prioritized *CD40*, *ERAP1*, *PLD4*, *SPPL3*, and *CCDC113* as novel candidate causal genes. The *CD40* risk locus colocalized with trans-pQTLs of multiple plasma proteins involved in B cell function.

Conclusion. Our study supports a strong shared genetic susceptibility between SSc and PBC. Using cross-phenotype analyses, we have prioritized several novel candidate causal genes and pathways for these disorders.

INTRODUCTION

Systemic sclerosis (SSc) is a multisystem autoimmune disease characterized by a complex interplay of fibrosis, vasculopathy, and inflammation. Unlike in other systemic autoimmune rheumatic diseases, the therapeutic response to immunosuppressive medications for patients with SSc is organ dependent. Certain organ involvement, including gastrointestinal tract fibrosis,

has not been found to be responsive to immunosuppressive therapy.¹

Primary biliary cholangitis (PBC) is an autoimmune liver disease characterized by the inflammation of the intrahepatic bile ducts, leading to liver fibrosis. Similar to the gastrointestinal involvement of SSc, the efficacy of immunosuppressive therapies for patients with PBC have not yet been established.² The prevalence of PBC in patients with SSc is 2% to 2.5%, substantially

Presented previously at the 2023 ACR Convergence: Luo Y, Khan A, Perreault G, et al. Shared genetic susceptibility between systemic sclerosis and primary biliary cholangitis: analyses from genome-wide association studies [abstract]. *Arthritis Rheumatol* 2023;75(Suppl 9). <https://acrabstracts.org/abstract/shared-genetic-susceptibility-between-systemic-sclerosis-and-primary-biliary-cholangitis-analyses-from-genome-wide-association-studies/>

Dr Luo's work was supported by the Rheumatology Research Foundation (Scientist Development Award). Dr Liu's work was supported by the National Institute of Diabetes and Digestive and Kidney Diseases, NIH (grant 1K01-DK-137031). Dr Lee's work was supported by the National Human Genome Research Institute, NIH (grant 1K99-HG-013546-01). Dr Bernstein's work was supported by the National Institute of Arthritis and Musculoskeletal and Skin Diseases, NIH (grant K23-AR-075112); the National Heart, Lung, and Blood Institute, NIH (grant R01-HL-164758); and the Department of Defense (grant W81XWH2210163).

¹Yiming Luo, MD, MHS, Atlas Khan, PhD, Lili Liu, PhD, Cue Hyunkyu Lee, PhD, Gabriel J. Perreault, MD, Sydney F. Pomenti, MD, Krzysztof Kiryluk, MD, MSc, Elana J. Bernstein, MD, MSc: Columbia University Irving Medical Center, New York City, New York; ²Pravitt Gourh, MD: National Institute of Arthritis and Musculoskeletal and Skin Diseases, NIH, Bethesda, Maryland.

Drs Kiryluk and Bernstein contributed equally to this work.

Additional supplementary information cited in this article can be found online in the Supporting Information section (<https://acrjournals.onlinelibrary.wiley.com/doi/10.1002/art.43081>).

Author disclosures are available at <https://onlinelibrary.wiley.com/doi/10.1002/art.43081>.

Address correspondence via email to Elana J. Bernstein, MD, MSc, at ejb2153@cumc.columbia.edu.

Submitted for publication July 23, 2024; accepted in revised form December 3, 2024.

higher than its prevalence of 0.4% in the general population.^{3,4} Thus, there is likely an overlap of etiopathogenesis between SSc and PBC.

Genome-wide association studies (GWAS) have been conducted in both patients with SSc and patients with PBC, identifying numerous genomic loci associated with these two disorders.^{5,6} Cross-phenotype GWAS analytic approaches that leverage existing GWAS summary statistics have emerged as a powerful new strategy for identifying shared mechanisms and novel risk loci.⁷ We used this approach to systematically assess overlapping susceptibility and identify novel candidate causal genes that contribute to the common etiopathogenesis of the two disorders.

METHODS

Study design and GWAS summary statistics. An overview of the study design is shown in Figure 1. We obtained summary statistics of patients with SSc and patients with PBC from their recent GWAS meta-analyses. The GWAS for patients with SSc was comprised of 26,679 individuals (9,095 patients and 17,584 controls),⁵ whereas the GWAS for patients with PBC was comprised of 24,510 individuals (8,021 patients and 16,489 controls).⁶ For comparison, we also obtained GWAS summary statistics for rheumatoid arthritis (RA)⁸ and systemic lupus erythematosus (SLE)⁹ because both are prevalent in patients with SSc. We also obtained GWAS summary statistics from expression quantitative trait locus (eQTL) datasets, including the eQTLGen, Genotype-Tissue Expression (GTEx, for skin, liver, and lung) and Correlated Expression and Disease Association Research (CEDAR), as well as plasma proteomics quantitative trait locus (pQTL) datasets from the UK Biobank.^{10–13} The GWAS summary statistics were harmonized using reference data from the 1000 Genome Project (phase 3) and underwent quality control with MungeSumstats.^{14,15} The included GWAS datasets are summarized in Supplementary Table 1.

Genetic correlation analysis. To quantify the degree of shared genetic susceptibility, we used linkage disequilibrium score regression (LDSC) to estimate the global genetic correlation (r_g), excluding the HLA region, among each phenotype pair (SSc, PBC, RA, and SLE).^{16,17} A Bonferroni-corrected P = of 8.3×10^{-3} was used as the significance threshold.

Cross-phenotype GWAS meta-analysis. We performed a cross-phenotype GWAS meta-analysis to identify pleiotropic loci shared between patients with SSc and patients with PBC. We combined the summary statistics of patients with SSc and patients with PBC using the fixed-effect model with effect size estimates and standard errors using METAL.¹⁸ Genomic control correction was applied to the summary statistics of each phenotype before the meta-analysis.¹⁹ After the meta-analysis, we

excluded single nucleotide polymorphisms (SNPs) in the HLA region or with evidence of heterogeneity ($_{het}$; $P_{het} < 0.05$). We used WANNVAR to annotate the lead SNPs of the significant loci.²⁰ We defined novel loci as those that were significant in the cross-phenotype meta-analysis but not significant in either SSc or PBC input for GWAS. The definitions of loci, lead SNPs, independent significant SNPs, and candidate SNPs are provided in the Supplementary Note. The loci were named based on the annotation of the lead SNPs from WANNVAR, which relies on the distance to nearby genes.²⁰

The fixed-effect model is limited in examining SNPs with heterogeneity of effects. Therefore, we performed a sensitivity analysis using the pleiotropic locus exploration and interpretation using optimal test (PLEIO) method.²¹ PLEIO is designed for cross-phenotype meta-analysis and can account for heritability, genetic correlation, and sample overlap. There is no established method for extrapolating Z-scores from PLEIO statistics. Therefore, we used the fixed-effect model statistics for subsequent analyses.

Tissue and pathway enrichment analyses. We used two methods to prioritize the pathways and tissues that contribute to the pleiotropy in patients with SSc and patients with PBC: multi-marker analysis of genomic annotation (MAGMA) and data-driven expression prioritized integration for complex traits (DEPICT).^{22–24} MAGMA and DEPICT perform enrichment analyses at pathway and tissue levels but use different approaches to associate loci with genes. MAGMA annotates SNPs based on their locations relative to genic regions (transcription start and stop sites ± 10 kb window). DEPICT prioritizes genes in a locus if genes in different loci have similar predicted functions. We reported the Bonferroni-corrected P values.

eQTL and chromatin interaction mapping. We used functional mapping and annotation²³ to perform eQTL and chromatin interaction mapping for candidate SNPs in each locus. For eQTL mapping, we focused on tissues and cells relevant to patients with SSc or patients with PBC, including skin, lung, liver, blood, and immune cells. We reported candidate SNPs with significant eQTLs (false discovery rate [FDR] < 0.05). For chromatin interaction mapping, we used high-throughput chromosome conformation capture (Hi-C) data from lung, liver, GM12878 (lymphoblastoid cell line), and IMR90 (lung fibroblast cell line). We reported genes linked to significant Hi-C element-promoter pairs (FDR $< 1 \times 10^{-6}$) in which candidate SNPs overlapped with these elements.

Colocalization between patients with SSc and patients with PBC. We performed Bayesian colocalization analyses between patients with SSc and patients with PBC in loci that are significant in the cross-phenotype meta-analysis with the fixed-effect model. Bayesian colocalization analyses infer the probability that a single genetic variant is causal to both traits

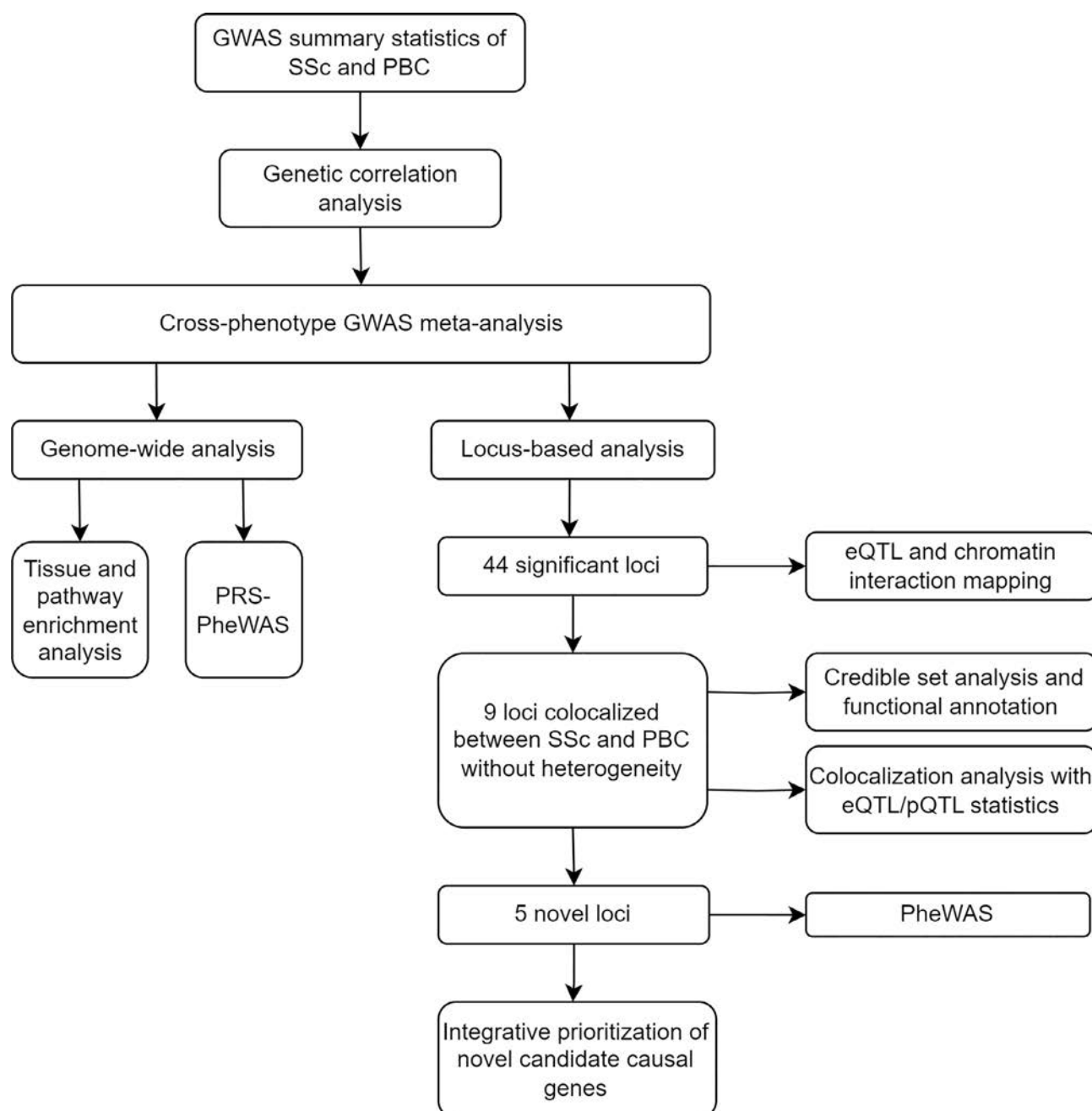


Figure 1. Flowchart for the overview of the study. We performed multiple cross-phenotype GWAS analyses to identify the shared genetic susceptibility between patients with SSc and patients with PBC. Additionally, we also performed a single-center retrospective chart review to evaluate the prevalence of PBC, including potentially undiagnosed individuals, in patients with SSc. eQTL, expression quantitative trait loci; GWAS, genome-wide association study; PBC, primary biliary cholangitis; PheWAS, phenome-wide association study; pQTL, protein quantitative trait loci; PRS, polygenic risk score; SSc, systemic sclerosis.

of interest in patients with SSc and patients with PBC. We performed colocalization using the wakefield method from the R package coloc.²⁵ For loci with independent signals in the conditional analysis ($P < 5 \times 10^{-8}$), we performed additional Bayesian colocalization analyses using statistics from the conditional analyses. Evidence of colocalization was defined as at least one signal with a posterior probability of hypothesis four that there is one variant causal to both traits (PP4) above 70%.

Fine-mapping and credible set analyses. We prioritized significant loci from the fixed-effect cross-phenotype meta-analysis that met the following criteria for statistical fine-mapping: (1) lead SNPs without evidence of heterogeneity ($P_{\text{het}} \geq 0.05$); (2) significant in the fixed-effect cross-phenotype meta-analysis; and (3) colocalized between patients with SSc and patients with PBC. We calculated the 99% credible sets using causal robust mapping method with annotations (CARMA).²⁶ CARMA is a novel

Bayesian model for fine-mapping that can better account for the uneven measurement of SNPs in each GWAS study of a meta-analysis, as well as the discrepancies between summary statistics and linkage disequilibrium (LD) data from external reference panels. A 99% credible set represents the smallest set of SNPs with the probability of including the causal variant exceeding 99%. This approach allows us to narrow down the list of potential causal SNPs within each locus. We incorporated functional annotation into CARMA using the prior causal probabilities based on the meta-analysis of 15 UK Biobank traits from polygenic functionally-informed fine-mapping (PolyFun). We annotated SNPs in the credible sets using data from the registry of candidate cis-regulatory elements from the Encyclopedia of DNA Elements (ENCODE) Project.²⁷

Colocalization between meta-analysis statistics and eQTL or pQTL datasets. For the loci showing colocalization between patients with SSc and patients with PBC without heterogeneity, we performed Bayesian colocalization analyses between the SSc–PBC meta-analysis statistics and eQTL or pQTL datasets. This approach aimed to infer causal transcripts or proteins associated with the shared genomic signals in patients with SSc and patients with PBC. For the eQTL Bayesian colocalization analyses, we included relevant tissues and cells, including blood, skin, lung, liver, and immune cells. We first screened genes using SNPs in the 99% credible set of a locus to query the eQTL databases. Next, we selected genes with significant eQTL signals for the Bayesian colocalization analyses. For loci that colocalized with a cis-pQTL signal, we performed additional Bayesian colocalization analyses between the meta-analysis statistics and trans-pQTLs measured at that locus to investigate the downstream effects of the candidate causal gene. A colocalization probability (PP4) above 70% was used as the significance threshold and 50% as the suggestive threshold.

Phenome-wide association studies. We performed phenome-wide association studies (PheWAS) for the lead SNP for each novel locus that colocalized between patients with SSc and patients with PBC. The PheWAS was performed within three biobanks: the Electronic Medical Records and Genomics III (eMERGE-III), All of Us, and the UK Biobank. Meta-PheWAS statistics were then calculated by fixed-effect meta-analysis of PheWAS results across the three biobanks.^{28–30} The details of the genotyping methods, imputation, quality control, ancestry inference, covariate adjustment, and phenotype identification were described in our previous studies.^{31–33}

To further explore pleiotropic associations, we performed meta-PheWAS analyses on the polygenic risk scores (PRS) of the cross-phenotype meta-analysis (PRS–meta-PheWAS). We used PRS continuous shrinkage, a method based on high-dimensional Bayesian regression, to generate the weights for PRS.³⁴ The HLA region was excluded. We set the Bonferroni-

corrected statistical significance threshold for phenome-wide significance at $P = 2.75 \times 10^{-5}$ (0.05 of 1,817 phecodes tested). Lastly, we manually queried the top SNPs using PheWAS results from the Open Targets Genetics webpage,^{35,36} which includes data from the GWAS Catalog, UK Biobank, and FinnGen. We designated the effect allele as the GWAS risk allele in SSc–PBC cross-phenotype analysis.

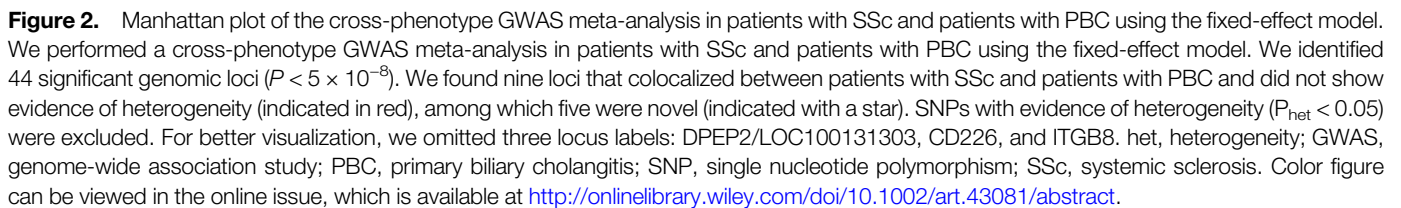
Integrative prioritization of novel candidate causal genes. For each novel locus, we prioritized the candidate causal gene using a consensus-based approach, selecting the gene with the highest number of supporting evidence across nine predictors: (1) genes most proximal to the lead SNP at the locus, (2) genes colocalizing with the locus in the examined cis-eQTL datasets, (3) genes colocalizing with the locus in the examined cis-pQTL datasets, (4) genes with a nonsynonymous coding variant in the credible set, (5) genes prioritized by MAGMA (FDR q value < 0.05),²² (6) genes prioritized by DEPICT (FDR q value < 0.05),²⁴ (7) genes receiving the top score from the variant-to-gene pipeline on the Open Targets Genetics webpage^{35,36} using the fine-mapped SNPs (posterior inclusion probability [PIP] $> 10\%$), (8) genes whose predicted regulatory elements from the ENCODE-rE2G model³⁷ intersected with the fine-mapped SNPs (PIP $> 10\%$), and (9) genes prioritized by the large language model GPT-4, which was recently suggested as a systematic way to mine literature for candidate causal gene prioritization (input described in the Supplementary Note).³⁸ We prioritized the genes with the highest priority scores within each locus.

Patients or the public were not involved in the design, or conduct, or reporting, or dissemination plans of our research. The cross-phenotype meta-analysis summary statistics are available under reasonable request to the corresponding author.

RESULTS

Global genetic correlation. There was a strong global genetic correlation between patients with SSc and patients with PBC ($r_g = 0.84$, $P = 1.7 \times 10^{-5}$), in which the effect estimate is comparable to the genetic correlation between patients with SSc and patients with SLE ($r_g = 0.84$, $P = 1.6 \times 10^{-15}$). The pairwise comparison of global genetic correlation in patients with SSc, patients with PBC, patients with RA, and patients with SLE is shown in Supplementary Figure 1.

Cross-phenotype GWAS meta-analysis. We performed a cross-phenotype meta-analysis for SSc and PBC using the fixed-effect model. The Manhattan plot is shown in Figure 2. There were 44 non-HLA loci that reached genome-wide significance ($P < 5 \times 10^{-8}$, Supplementary Table 2). The genomic inflation factor (λ) was 1.065, and the LDSC intercept was 1.010 (SE 0.012). In 16 out of the 44 significant loci (36%), there was evidence of heterogeneity in the lead SNPs ($P_{\text{het}} < 0.05$). However,



Given the high proportion of loci with evidence of heterogeneity, we performed another cross-phenotype meta-analysis between SSc and PBC using PLEIO as a sensitivity analysis. There were 58 non-HLA loci that reached genome-wide significance ($P < 5 \times 10^{-8}$, Supplementary Table 3). The genomic inflation factor (λ) was 1.091. Forty-one of the 44 loci (93%) that were significant in the fixed-effect model were also significant in PLEIO. Regarding the novel loci, five out of the seven (71%) identified in the fixed-effect model were also significant in PLEIO. The two novel loci that were only significant in the fixed-effect model, *CD40* and *AHNAK2*, had P values of 7.37×10^{-8} and 3.37×10^{-7} in PLEIO. Two novel loci, *NDFIP1* and *PPHLN1*, were significant only in PLEIO but not in the fixed-effect model. However, the evidence for the association of these loci with SSc was insufficient (lead SNP P values 3.93×10^{-2} and 1.33×10^{-2} , respectively). Thus, no further analyses were performed for these loci.

spleen ($P = 1.21 \times 10^{-6}$), whole blood ($P = 1.59 \times 10^{-6}$), Epstein-Barr virus-transformed lymphocytes ($P = 4.16 \times 10^{-4}$), lung ($P = 2.81 \times 10^{-3}$), and terminal ileum ($P = 4.63 \times 10^{-3}$) (Figure 3A, Supplementary Table 4). Concurrently, the DEPICT method significantly enriched 20 tissues and cells, most related to the immune system or respiratory tract. The top-ranked tissues and cells were mononuclear leukocytes ($P = 2.95 \times 10^{-5}$), oropharynx ($P = 3.80 \times 10^{-5}$), palatine tonsil ($P = 3.80 \times 10^{-5}$), and synovial fluid ($P = 2.63 \times 10^{-4}$) (Figure 3B, Supplementary Table 5).

eQTL and chromatin interaction mapping. We identified a total of 1,604 candidate SNPs from the 44 significant loci. These SNPs were mapped to 521 genes from eQTL and

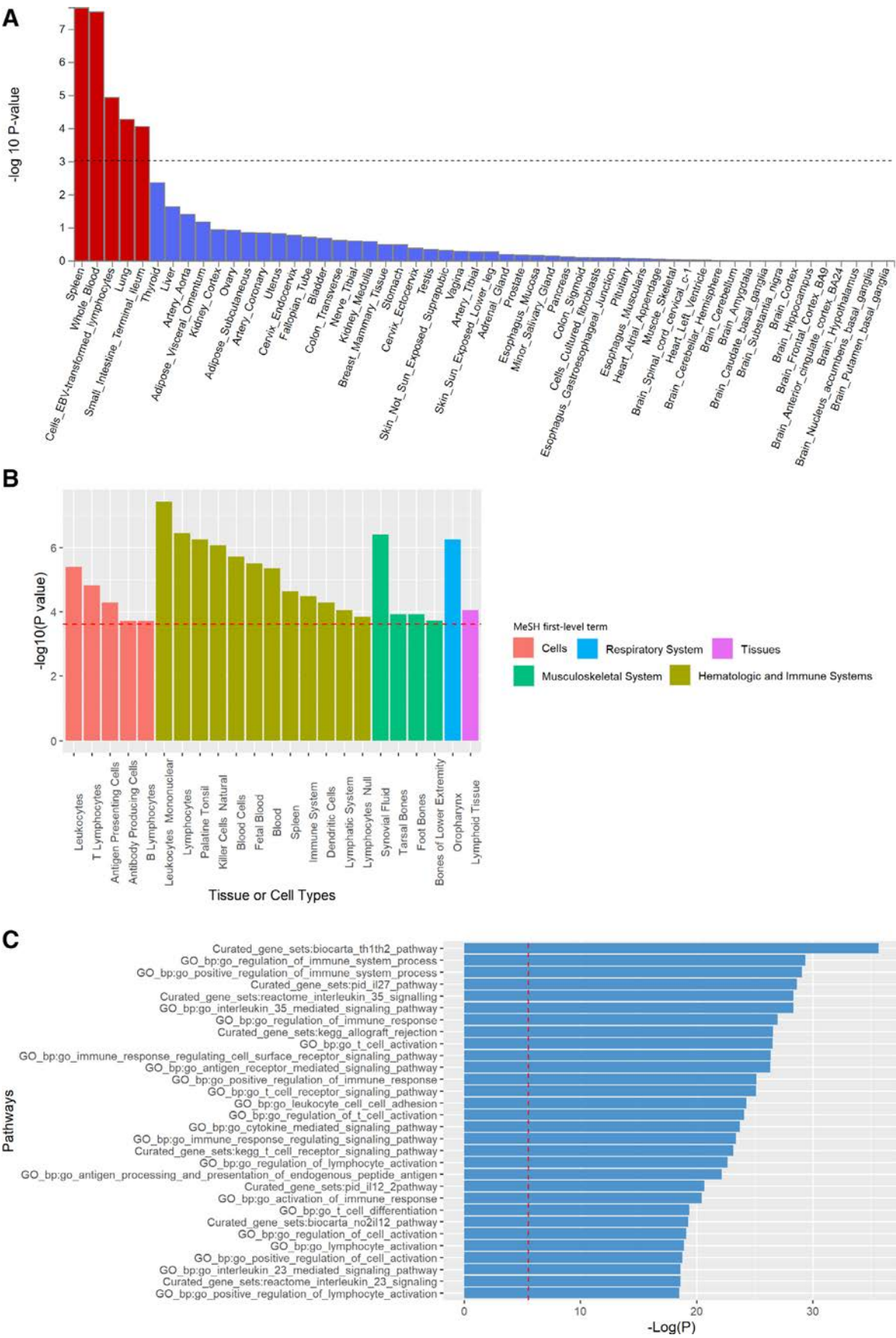


(Figure legend continues on next page.)

367 genes from Hi-C. Notably, 126 genes were concordant, appearing in both the eQTL and Hi-C analyses (Supplementary Table 8). Comprehensive results from the eQTL and chromatin interaction mapping are provided in Supplementary Tables 9 and 10, respectively.

Colocalization between SSc and PBC. Because of LD, significant SNPs within genomic loci may not necessarily be causal for the associated trait. Therefore, we conducted Bayesian colocalization analyses to determine whether there was at least one shared causal variant between SSc and PBC in loci significant in the cross-phenotype meta-analysis. We identified nine loci that colocalized between SSc and PBC ($PP4 > 70\%$) and did not have evidence of heterogeneity ($P_{het} \geq 0.05$), as detailed in Table 1 and Supplementary Figure 2. Notably, five were novel: *CSNK2A2/CCDC113*, *SPPL3*, *CAST/ERAP1*, *AHNAK2*, and *CD40*.

Fine-mapping and credible set analyses. We performed fine-mapping and generated 99% credible sets for the nine loci that were significant in the cross-phenotype meta-analysis, showed no evidence of heterogeneity, and colocalized between SSc and PBC. These analyses yielded 118 SNPs from 10 credible sets across the nine significant loci. Notably, none of the credible sets contained nonsynonymous coding variants. In seven of the nine loci (78%), at least one SNP from the corresponding credible set was located within a cis-regulatory element. Supplementary Table 11 summarizes the credible SNP sets for each locus.

Colocalization with tissue- and immune cell-specific cis-eQTL. In the nine loci that were significant in cross-phenotype meta-analysis without evidence of heterogeneity and colocalized with SSc and PBC, we further performed colocalization between SSc–PBC meta-analysis statistics and eQTL statistics in blood, skin, lung, liver and immune cells. In seven of the nine loci, the SSc–PBC meta-analysis statistics colocalized with at least one transcript in the examined eQTL statistics ($PP4 > 50\%$), prioritizing candidate causal genes at these loci (Figure 4, Supplementary Table 12). The eQTL colocalized transcripts were *IRF5*, *TNPO3*, *ANP32B*, *IL12RB1*, *ERAP1*, *ERAP2*, *SPPL3*, *AKT1*, *PLD4*, *LINC00638*, and *CD40*.

Colocalization with plasma cis- and trans-pQTL.

Across the nine loci mentioned above, only the *IL12RB1* and *CD40* loci encode secreted proteins previously assessed in blood pQTL datasets. These plasma proteins include interleukin 12 receptor subunit beta 1 (*IL12RB1*) and CD40, respectively. The SSc–PBC meta-analysis statistics colocalized with cis-pQTL for CD40 protein levels ($PP4 = 98\%$) but not with *IL12RB1* protein levels ($PP4 = 0.4\%$). The SSc–PBC risk allele was associated with lower plasma CD40 levels. Moreover, the SSc–PBC risk alleles at the CD40 locus colocalized in trans to reduced *BAFF* levels ($PP4 = 99\%$) and increased levels of *CD40L* ($PP4 = 99\%$), *FCER2* ($PP4 = 99\%$), *CD22* ($PP4 = 99\%$), *TRAF2* ($PP4 = 97\%$), *FCLR1* ($PP4 = 99\%$), and *TCL1A* ($PP4 = 99\%$).

PheWAS. We performed a meta-PheWAS for the five novel loci that colocalized between patients with SSc and patients with PBC. Three novel loci had significant associations with at least one phecode (Supplementary Figure 3). Rs10083496-G (*ANNAK2* locus) was associated with SLE (odds ratio [OR] = 1.12, $P = 2.05 \times 10^{-7}$). Rs4810485-T (*CD40* locus) was associated with non-Hodgkins lymphoma (OR = 1.11, $P = 1.38 \times 10^{-6}$) and anxiety disorders (OR = 1.04, $P = 2.86 \times 10^{-6}$).

We subsequently performed an additional meta-PheWAS analysis to evaluate phenotypic associations of a genome-wide PRS based on the SSc–PBC meta-analysis statistics, excluding the HLA region (SSc–PBC PRS). We identified a total of 134 significant associations, the majority of which were related to immune dysregulation. As expected, SSc (OR = 1.78, $P = 9.19 \times 10^{-30}$) and PBC (OR = 3.01, $P = 5.55 \times 10^{-86}$) were top-ranked in their effect estimates associated with the SSc–PBC PRS, confirming that the PRS captures the risk for both diseases in the external datasets. Moreover, the PRS was associated with systemic autoimmune rheumatic diseases including RA (OR = 1.24, $P = 2.16 \times 10^{-55}$), SLE (OR = 1.75, $P = 3.34 \times 10^{-64}$), sicca syndrome (OR = 1.58, $P = 9.46 \times 10^{-43}$), polyarteritis nodosa and allied conditions (OR = 1.18, $P = 6.72 \times 10^{-10}$), as well as with nonrheumatic autoimmune diseases including hypothyroidism (OR = 1.12, $P = 4.42 \times 10^{-55}$), multiple sclerosis (OR = 1.30, $P = 1.15 \times 10^{-23}$), inflammatory bowel disease and other gastroenteritis and colitis (OR = 1.14, $P = 3.23 \times 10^{-21}$), and idiopathic fibrosing alveolitis (OR = 1.19, $P = 2.00 \times 10^{-8}$) (Supplementary Figure 4 and Supplementary Table 13).

(Figure legend continued from previous page.)

Figure 3. Tissue and pathway enrichment analyses. (A) Tissue enrichment analysis using MAGMA-prioritized tissues related to the immune system (spleen, whole blood, and EBV-transformed lymphocytes), respiratory system (lung), and digestive system (terminal ileum). (B) Tissue enrichment analysis using DEPICT prioritized multiple tissues and cells related to the immune system, respiratory system, and musculoskeletal system. (C) Significant enrichment of multiple immune-related pathways associated with patients with SSc and patients with PBC using MAGMA. DEPICT, data-driven expression prioritized integration for complex traits; EBV, Epstein-Barr virus; GO, gene ontology; MAGMA, multi-marker analysis of genomic annotation; MeSH, medical subject headings; PBC, primary biliary cholangitis; SSc, systemic sclerosis. Color figure can be viewed in the online issue, which is available at <http://onlinelibrary.wiley.com/doi/10.1002/art.43081/abstract>.

Table 1. Genomic loci significant in the cross-phenotype GWAS, colocalized between patients with SSc and patients with PBC and do not have evidence of heterogeneity*

Locus	Lead SNP	CHR	BP	A1	A2	FE OR	FE <i>P</i> value	PLEIO <i>P</i> value	Colocalization PP4, %	Novel loci
<i>TNPO3</i>	rs17338998	7	128618559	T	C	1.52	2.37×10^{-40}	4.16×10^{-73}	98	No
<i>CSNK2A2/CCDC113</i>	rs2731783	16	58253460	A	G	1.15	7.79×10^{-11}	1.50×10^{-9}	96	Yes
<i>IL12RB1</i>	rs2305743	19	18193191	A	G	0.86	1.95×10^{-14}	7.42×10^{-14}	96	No
<i>LOC100506023</i>	rs2022449	1	173238736	T	G	1.12	1.69×10^{-10}	2.82×10^{-9}	92	No
<i>SPPL3</i>	rs551125	12	121203427	C	T	0.91	1.65×10^{-9}	2.59×10^{-8}	91	Yes
<i>CAST/ERAP1</i>	rs27524	5	96101944	A	G	0.9	4.89×10^{-10}	6.04×10^{-9}	85	Yes
<i>HEMGN/ANP32B</i>	rs4743150	9	100740124	T	C	0.88	8.29×10^{-11}	2.80×10^{-10}	85	No
<i>AHNAK2</i>	rs10083496	14	105402786	G	A	1.09	2.56×10^{-8}	7.37×10^{-8}	80	Yes
<i>CD40</i>	rs4810485	20	44747947	T	G	1.13	1.44×10^{-8}	7.37×10^{-8}	73	Yes

* A1, effect allele; A2, noneffect allele; BP, base pair; CHR, chromosome; FE, fixed-effect model; GWAS, genome-wide association study; OR, odds ratio; PBC, primary biliary cholangitis; PLEIO, pleiotropic locus exploration and interpretation using optimal test; PP4, posterior probability of hypothesis four that there is one variant causal to both traits; SNP, single nucleotide polymorphism; SSc, systemic sclerosis.

Additionally, we manually queried the top SNP from the novel loci using PheWAS results from the Open Targets Genetics webpage. Rs4810485-T (*CD40* locus) was associated with multiple autoimmune disorders, including RA (OR = 0.85, $P = 5.7 \times 10^{-9}$), inflammatory bowel disease (OR = 1.08,

$P = 4.6 \times 10^{-10}$), and multiple sclerosis (OR = 1.08, $P = 1.8 \times 10^{-5}$). Rs27524-G (*CAST/ERAP1* locus) was associated with ankylosing spondylitis (OR = 0.84, $P = 5.4 \times 10^{-7}$), iridocyclitis (OR = 0.88, $P = 6.9 \times 10^{-8}$), and psoriasis (OR = 0.85, $P = 1.6 \times 10^{-6}$).

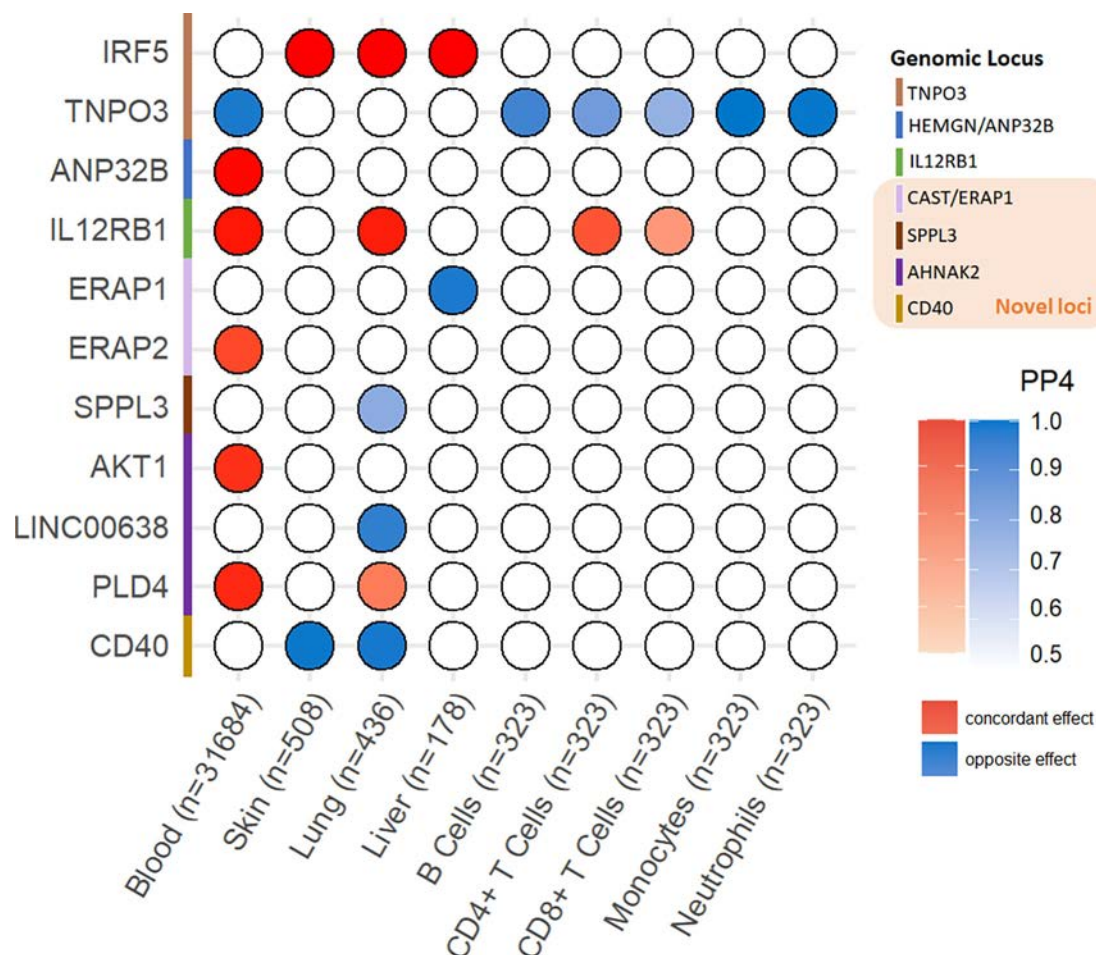


Figure 4. Bayesian colocalization analysis with eQTL in blood, skin, lung, liver, and immune cells. Out of the nine loci that were significant in the fixed-model cross-phenotype meta-analysis, showed no evidence of heterogeneity, and were colocalized between patients with SSc and patients with PBC, seven colocalized with expressed genes in at least one of the examined tissues. eQTL, expression quantitative trait loci; PBC, primary biliary cholangitis; PP4, posterior probability of hypothesis four that there is one variant causal to both traits; SSc, systemic sclerosis.

Locus	Lead SNP	Candidate gene	Nesrest gene	Cis-eQTL colocalization	Cis-pQTL colocalization	Nonsynonymous coding variant	MAGMA	DEPICT	V2G	ENCODE-rE2G	LLM	Number of supporting predictors
CD40	rs4810485	CD40										8
		MMP9										2
		CDH22										1
		NCOA5										1
		SLC12A5										1
		WFDC10A										1
		CTSA										1
ERAP1 /CAST	rs27524	ERAP1										6
		ERAP2										3
		LNPEP										1
		CAST										1
AHNAK2	rs10083496	PLD4										5
		AHNAK2										3
		AKT1										2
		CLBA1										2
		CDCA4										2
		CEP170B										1
		GPR132										1
SPPL3	rs551125	SPPL3										4
		OASL										2
		ACADS										1
		HNF1A										1
		P2RX7										1
CCDC113 /CSNK2A2	rs2731783	CCDC113										3
		CSNK2A2										2
		ZBTB42										1
		MMP15										1
		NDRG4										1

Figure 5. Integrative prioritization of novel candidate causal genes. We prioritized five novel candidate causal genes based on a consensus-based approach integrating nine predictors: *CD40*, *ERAP1*, *PLD4*, *SPPL3*, and *CCDC113*. DEPICT, data-driven expression prioritized integration for complex traits; ENCODE, Encyclopedia of DNA Elements; eQTL, expression quantitative trait loci; LLM, large language model; MAGMA, multi-marker analysis of genomic annotation; pQTL, protein quantitative trait loci; SNP, single nucleotide polymorphism; V2G, variant-to-gene. Color figure can be viewed in the online issue, which is available at <http://onlinelibrary.wiley.com/doi/10.1002/art.43081/abstract>.

Integrative prioritization of novel candidate causal genes. We prioritized five candidate causal genes from the novel loci using a scoring approach that integrates nine in silico annotation methods (Figure 5; MAGMA, DEPICT, and ENCODE-rE2G results in Supplementary Table 14–16; GPT-4 output described in the Supplementary Note). *CD40* received the highest priority score of 8, meeting all criteria except for credible sets containing a nonsynonymous coding variant. *ERAP1* received a priority score of 6, followed by *PLD4* with a score of 5. *SPPL3* and *CCDC113* received priority scores of 4 and 3, respectively.

DISCUSSION

Our study demonstrates a strong genetic correlation between patients with SSc and patients with PBC, with the correlation effect estimate comparable to that between patients with SSc and patients with SLE. The prevalence of PBC in patients with SSc was 2% to 2.5%, lower than the 8.4% to 14.7% prevalence of SLE in patients with SSc.^{3,4,39–41} Nevertheless, the prevalence of PBC in the general population, ranging from 19 to 402 per million people, was also much lower than that of SLE, which ranges from 200 to 1,500 per million people.^{42–46} Consequently, compared to the general population, the relative risk of PBC and SLE in patients with SSc likely mirrors their genetic correlation. Hence, our genetic correlation results, corroborated by the extent of phenotypic overlaps, support the existence of shared genetic susceptibilities and biologic mechanisms between patients with SSc and patients with PBC.

We identified 44 significant non-HLA genomic loci in the fixed-model cross-phenotype GWAS meta-analysis. The robustness of our meta-analysis was supported by the PRS–meta-PheWAS analysis. In this analysis, using independent external datasets, SSc and PBC ranked among the top hits associated with the PRS, derived from our SSc–PBC meta-analysis statistics. Moreover, the SSc–PBC PRS demonstrated associations with a broad spectrum of autoimmune disorders, highlighting that the shared genetic susceptibilities between patients with SSc and patients with PBC captured by our cross-phenotype meta-analysis represent pleiotropic genomic regions.

We identified five novel loci that were significant in the cross-phenotype GWAS meta-analysis and colocalized between SSc and PBC: *CSNK2A2/CCDC113*, *SPPL3*, *CAST/ERAP1*, *AHNAK2*, and *CD40*. Three of the five loci were independently confirmed in a GWAS in another population: *CD40* and *AHNAK2* loci were significant in a recent SSc GWAS meta-analysis that included the Japanese population,⁴⁷ and the *CSNK2A2/CCDC113* locus was significant in a PBC GWAS from the Chinese population.⁴⁸ Moreover, we found that the lead SNP in the *CD40*, *AHNAK2*, and *CAST/ERAP1* loci was associated with other autoimmune disorders in PheWAS. The pleiotropic effects observed at these loci underscore their potential role in promoting

autoimmunity. We subsequently prioritized five novel candidate causal genes in patients with SSc and patients with PBC using a consensus-based approach from nine predictors: *CD40*, *ERAP1*, *PLD4*, *SPPL3*, and *CCDC113*.

At the *CD40* locus, the SSc–PBC meta-analysis statistics colocalized with not only the reduced transcript but also reduced plasma protein levels of CD40. And the lead SNP, rs4810485, which has the highest PIP in the credible set at 44.2%, has been experimentally validated to reduce CD40 expression.⁴⁹ Such associations with reduced CD40 expression have also been observed in other autoimmune diseases, including inflammatory bowel disease and multiple sclerosis, as well as malignancy in our PheWAS analysis.^{50,51} This seems paradoxical given the established role of CD40 in promoting autoimmunity.⁵² However, CD40 deficiency, a rare monogenic disorder caused by bi-allelic loss of function variants in *CD40*, is characterized not only by humoral immunodeficiency but also by malignancy and autoimmunity, including sclerosing cholangitis and colitis.⁵³ Thus, a causal relationship between reduced *CD40* expression because of polymorphisms and an increased risk of autoimmunity and malignancy is biologically plausible, mimicking the phenotypic manifestations of its monogenic disease counterpart. Interestingly, at the *CD40* locus, the SSc–PBC meta-analysis statistics also colocalized with increased levels of multiple plasma proteins involved in B cell functions, including *CD40L*, *FCER2*, *CD22*, *TRAF2*, and *TCL1A*. This suggests a potential compensatory response. Soluble CD40L (sCD40L), the circulating form measured in the proteomics assay, is the ligand of *CD40*, which also binds to other receptors on endothelial cells and promotes vascular pathology.⁵⁴ Elevated sCD40L levels have been found in patients with SSc and are associated with its vascular manifestations.⁵⁵ Overall, the complex B cell dysregulation mediating genetically determined reduced *CD40* expression in patients with SSc warrants further investigation.

The novel candidate causal genes prioritized in our study likely contribute to SSc and PBC development through immune dysregulation in patients. Phospholipase D4 (PLD4) is predominantly expressed in multiple immune cells including B cells, monocytes, and dendritic cells.^{56,57} PLD4+ B cells are expanded in patients with SSc and likely autoreactive B cells undergoing toll-like receptor stimulation.⁵⁸ PLD4 also facilitates kidney fibrosis by modulating innate and adaptive immune responses resulting in transforming growth factor β (TGF β) signaling activation.⁵⁹ Endoplasmic reticulum aminopeptidase 1 (ERAP1) is a multifunctional enzyme regulating immune responses.⁶⁰ The SSc–PBC meta-analysis statistics colocalized with reduced ERAP1 expression. B cells lacking ERAP1 exhibit impaired proliferation and increased activation and costimulatory markers.⁶¹ Reduced signal peptide peptidase-like 3 (SPPL3), the effect direction associated with SSc and PBC, leads to diminished immunosurveillance from CD8+ T cells and natural killer cells. Both SSc and PBC are associated with elevated cancer risk, with recent findings

indicating that SSc carries a higher burden of somatic mutations and genomic instability.^{62–65} The function of *CCDC113* is poorly understood, but it has been found to promote cancer development via the TGF β signaling pathway.⁶⁶

The HLA class II region stands out as the strongest genetic association in both patients with SSc and patients with PBC, offering insights into their potential shared mechanisms. Across multiple populations, SSc has been robustly associated with the HLA-DRB1*11:04, HLA-DQB1*02:02, and HLA-DPB1*13:01 alleles.^{67,68} In patients with PBC, the HLA-DRB1*08:01, HLA-DQA1*04:01, and HLA-DQB1*04:02 haplotype has been consistently confirmed across different populations.^{69–71} Notably, HLA-DRB1*11:04 exhibits opposite effects in patients with SSc versus patients with PBC, increasing the risk of SSc but protecting against PBC.⁷⁰ Molecular mimicry has been proposed as a potential common mechanism driving HLA class II-mediated autoimmunity, including in patients with SSc and patients with PBC.^{67,69} Additionally, the peptide-binding groove of disease-associated HLA class II molecules might possess structural features that favor the binding of specific self-peptides, thereby shaping the autoreactive T cell repertoire.⁶⁹ Despite its importance, the HLA region was excluded from our genetic correlation analysis and cross-phenotype GWAS because of challenges from outlier effect, complex LD structures, and population stratification.

Our study has several limitations. First, we used summary statistics from published GWAS meta-analyses and were unable to perform standardized quality control with individual-level genotype data. Nevertheless, the GWAS studies included in our study were recent, comprised of large sample sizes from multiple cohorts, and led by international experts. Second, our study was performed in European ancestries; thus, our results may not be generalizable to other populations. Third, the sample size of patients with SSc and patients with PBC in our external datasets was limited, which precluded us from performing a replication GWAS to validate the newly discovered loci. Instead, we conducted a PRS–meta-PheWAS analysis to confirm that the PRS derived from our SSc–PBC meta-analysis captures the overall genetic risk of SSc and PBC in independent electronic health record (EHR)-based datasets. Fourth, the sample size of GTEx and CEDAR was smaller than that of eQTLGen, which could limit statistical power in our eQTL Bayesian colocalization analyses for the relevant tissues and cells. Fifth, our study evaluated the likelihood of causality for each candidate gene using diverse methods and selected genes with the highest number of supporting predictors for each locus. Although this approach is employed in recent studies,^{32,72} it assumes equal weight for all predictors and does not account for potential differences in their performance. Sixth, we were unable to examine population structure because individual-level genotype data were not available to us, although most of the GWAS data used in our study come from individuals of European ancestry. Finally, for our meta-PheWAS

analyses, the diagnoses in the EHR-based datasets rely on administrative codes, which may have nonrandom missingness and low sensitivity for phenotype detection.⁷³

In conclusion, our study revealed a strong genetic correlation between patients with SSc and patients with PBC and provided insights into their shared genetic susceptibility. We prioritized five novel genes that were potentially involved in the common causal mechanisms between SSc and PBC. These discoveries prioritize therapeutic targets for both patients with SSc and patients with PBC. Moreover, our study advocates for heightened awareness among rheumatologists about the possibility of concurrent PBC in patients with SSc.

AUTHOR CONTRIBUTIONS

All authors contributed to at least one of the following manuscript preparation roles: conceptualization AND/OR methodology, software, investigation, formal analysis, data curation, visualization, and validation AND drafting or reviewing/editing the final draft. As corresponding author, Dr Bernstein confirms that all authors have provided the final approval of the version to be published, and takes responsibility for the affirmations regarding article submission (eg, not under consideration by another journal), the integrity of the data presented, and the statements regarding compliance with institutional review board/Declaration of Helsinki requirements.

REFERENCES

- McMahan ZH, Kulkarni S, Chen J, et al. Systemic sclerosis gastrointestinal dysmotility: risk factors, pathophysiology, diagnosis and management. *Nat Rev Rheumatol* 2023;19(3):166–181.
- Lindor KD, Bowlus CL, Boyer J, et al. Primary biliary cholangitis: 2018 practice guidance from the American Association for the Study of Liver Diseases. *Hepatology* 2019;69(1):394–419.
- Rigamonti C, Shand LM, Feudjo M, et al. Clinical features and prognosis of primary biliary cirrhosis associated with systemic sclerosis. *Gut* 2006;55(3):388–394.
- Assassi S, Fritzler MJ, Arnett FC, et al. Primary biliary cirrhosis (PBC), PBC autoantibodies, and hepatic parameter abnormalities in a large population of systemic sclerosis patients. *J Rheumatol* 2009;36(10):2250–2256.
- López-Isaac E, Acosta-Herrera M, Kerick M, et al; European Scleroderma Group; Australian Scleroderma Interest Group (ASIG). GWAS for systemic sclerosis identifies multiple risk loci and highlights fibrotic and vasculopathy pathways. *Nat Commun* 2019;10(1):4955.
- Cordell HJ, Fryett JJ, Ueno K, et al; PBC Consortia; Canadian PBC Consortium; Chinese PBC Consortium; Italian PBC Study Group; Japan-PBC-GWAS Consortium; US PBC Consortium; UK-PBC Consortium. An international genome-wide meta-analysis of primary biliary cholangitis: novel risk loci and candidate drugs. *J Hepatol* 2021;75(3):572–581.
- Ellinghaus D, Jostins L, Spain SL, et al; International IBD Genetics Consortium (IBDGC); International Genetics of Ankylosing Spondylitis Consortium (IGAS); International PSC Study Group (IPSCSG); Genetic Analysis of Psoriasis Consortium (GAPC); Psoriasis Association Genetics Extension (PAGE). Analysis of five chronic inflammatory diseases identifies 27 new associations and highlights disease-specific patterns at shared loci. *Nat Genet* 2016;48(5):510–518.
- Ishigaki K, Sakaue S, Terao C, et al; BioBank Japan Project. Multi-ancestry genome-wide association analyses identify novel genetic

- mechanisms in rheumatoid arthritis. *Nat Genet* 2022;54(11):1640–1651.
9. Benthall J, Morris DL, Graham DSC, et al. Genetic association analyses implicate aberrant regulation of innate and adaptive immunity genes in the pathogenesis of systemic lupus erythematosus. *Nat Genet* 2015;47(12):1457–1464.
 10. Vösa U, Claringbould A, Westra HJ, et al; BIOS Consortium; i2QTL Consortium. Large-scale cis- and trans-eQTL analyses identify thousands of genetic loci and polygenic scores that regulate blood gene expression. *Nat Genet* 2021;53(9):1300–1310.
 11. Momozawa Y, Dmitrieva J, Théâtre E, et al; International IBD Genetics Consortium. IBD risk loci are enriched in multigenic regulatory modules encompassing putative causative genes. *Nat Commun* 2018; 9(1):2427.
 12. GTEx Consortium. The GTEx Consortium atlas of genetic regulatory effects across human tissues. *Science* 2020;369(6509):1318–1330.
 13. Sun BB, Chiou J, Traylor M, et al; Alnylam Human Genetics; AstraZeneca Genomics Initiative; Biogen Biobank Team; Bristol Myers Squibb; Genentech Human Genetics; GlaxoSmithKline Genomic Sciences; Pfizer Integrative Biology; Population Analytics of Janssen Data Sciences; Regeneron Genetics Center. Plasma proteomic associations with genetics and health in the UK Biobank. *Nature* 2023; 622(7982):329–338.
 14. Auton A, Brooks LD, Durbin RM, et al; 1000 Genomes Project Consortium. A global reference for human genetic variation. *Nature* 2015;526(7571):68–74.
 15. Murphy AE, Schilder BM, Skene NG. MungeSumstats: a Bioconductor package for the standardization and quality control of many GWAS summary statistics. *Bioinformatics* 2021;37(23):4593–4596.
 16. Bulik-Sullivan B, Finucane HK, Anttila V, et al; ReproGen Consortium; Psychiatric Genomics Consortium; Genetic Consortium for Anorexia Nervosa of the Wellcome Trust Case Control Consortium 3. An atlas of genetic correlations across human diseases and traits. *Nat Genet* 2015;47(11):1236–1241.
 17. Bulik-Sullivan BK, Loh PR, Finucane HK, et al; Schizophrenia Working Group of the Psychiatric Genomics Consortium. LD Score regression distinguishes confounding from polygenicity in genome-wide association studies. *Nat Genet* 2015;47(3):291–295.
 18. Willer CJ, Li Y, Abecasis GR. METAL: fast and efficient meta-analysis of genomewide association scans. *Bioinformatics* 2010;26(17): 2190–2191.
 19. Devlin B, Roeder K. Genomic control for association studies. *Biometrics* 1999;55(4):997–1004.
 20. Chang X, Wang K. wANNOVAR: annotating genetic variants for personal genomes via the web. *J Med Genet* 2012;49(7):433–436.
 21. Lee CH, Shi H, Pasaniuc B, et al. PLEIO: a method to map and interpret pleiotropic loci with GWAS summary statistics. *Am J Hum Genet* 2021;108(1):36–48.
 22. de Leeuw CA, Mooij JM, Heskes T, et al. MAGMA: generalized gene-set analysis of GWAS data. *PLoS Comput Biol* 2015;11(4):e1004219.
 23. Watanabe K, Taskesen E, van Bochoven A, et al. Functional mapping and annotation of genetic associations with FUMA. *Nat Commun* 2017;8(1):1826.
 24. Pers TH, Karjalainen JM, Chan Y, et al; Genetic Investigation of ANthropometric Traits (GIANT) Consortium. Biological interpretation of genome-wide association studies using predicted gene functions. *Nat Commun* 2015;6(1):5890.
 25. Wallace C. A more accurate method for colocalisation analysis allowing for multiple causal variants. *PLoS Genet* 2021;17(9):e1009440.
 26. Yang Z, Wang C, Liu L, et al. CARMA is a new Bayesian model for fine-mapping in genome-wide association meta-analyses. *Nat Genet* 2023;55(6):1057–1065.
 27. Moore JE, Purcaro MJ, Pratt HE, et al; ENCODE Project Consortium. Expanded encyclopaedias of DNA elements in the human and mouse genomes. *Nature* 2020;583(7818):699–710.
 28. Gottesman O, Kuivaniemi H, Tromp G, et al; eMERGE Network. The Electronic Medical Records and Genomics (eMERGE) Network: past, present, and future. *Genet Med* 2013;15(10):761–771.
 29. All of Us Research Program Investigators. The “All of Us” Research Program. *N Engl J Med* 2019;381(7):668–676.
 30. Bycroft C, Freeman C, Petkova D, et al. The UK Biobank resource with deep phenotyping and genomic data. *Nature* 2018;562(7726): 203–209.
 31. Liu L, Khan A, Sanchez-Rodriguez E, et al. Genetic regulation of serum IgA levels and susceptibility to common immune, infectious, kidney, and cardio-metabolic traits. *Nat Commun* 2022;13(1):6859.
 32. Kiryluk K, Sanchez-Rodriguez E, Zhou XJ, et al. Genome-wide association analyses define pathogenic signaling pathways and prioritize drug targets for IgA nephropathy. *Nat Genet* 2023;55(7):1091–1105.
 33. Khan A, Shang N, Nestor JG, et al. Polygenic risk affects the penetrance of monogenic kidney disease. *Nat Commun* 2023;14(1):8318.
 34. Ge T, Chen CY, Ni Y, et al. Polygenic prediction via Bayesian regression and continuous shrinkage priors. *Nat Commun* 2019;10(1):1776.
 35. Open Targets Genetics. Open Targets Genetics database search engine. Updated October 12, 2022. Accessed May 1, 2024. <https://genetics.opentargets.org>
 36. Ghoussaini M, Mountjoy E, Carmona M, et al. Open Targets Genetics: systematic identification of trait-associated genes using large-scale genetics and functional genomics. *Nucleic Acids Res* 2021;49(D1): D1311–D1320.
 37. Gschwind AR, Mualim KS, Karbalayghareh A, et al. An encyclopedia of enhancer-gene regulatory interactions in the human genome. *bioRxiv Preprint* posted online November 13, 2023. <https://doi.org/10.1101/2023.11.09.563812>
 38. Shringarpure SS, Wang W, Karagounis S, et al. Large language models identify causal genes in complex trait GWAS. *medRxiv Preprint* posted online May 31, 2024. <https://doi.org/10.1101/2024.05.30.24308179>
 39. Pakozdi A, Nihtyanova S, Moinezhadeh P, et al. Clinical and serological hallmarks of systemic sclerosis overlap syndromes. *J Rheumatol* 2011;38(11):2406–2409.
 40. Moinezhadeh P, Aberer E, Ahmadi-Simab K, et al; all participating DNSS centers. Disease progression in systemic sclerosis-overlap syndrome is significantly different from limited and diffuse cutaneous systemic sclerosis. *Ann Rheum Dis* 2015;74(4):730–737.
 41. Foocharoen C, Netwijtpan S, Mahakkanukrauh A, et al. Clinical characteristics of scleroderma overlap syndromes: comparisons with pure scleroderma. *Int J Rheum Dis* 2016;19(9):913–923.
 42. Kim WR, Lindor KD, Locke GR 3rd, et al. Epidemiology and natural history of primary biliary cirrhosis in a US community. *Gastroenterology* 2000;119(6):1631–1636.
 43. Sood S, Gow PJ, Christie JM, et al. Epidemiology of primary biliary cirrhosis in Victoria, Australia: high prevalence in migrant populations. *Gastroenterology* 2004;127(2):470–475.
 44. Tian J, Zhang D, Yao X, et al. Global epidemiology of systemic lupus erythematosus: a comprehensive systematic analysis and modelling study. *Ann Rheum Dis* 2023;82(3):351–356.
 45. Izmirly PM, Parton H, Wang L, et al. Prevalence of systemic lupus erythematosus in the United States: estimates from a meta-analysis of the Centers for Disease Control and Prevention National Lupus Registries. *Arthritis Rheumatol* 2021;73(6):991–996.
 46. Stojan G, Petri M. Epidemiology of systemic lupus erythematosus: an update. *Curr Opin Rheumatol* 2018;30(2):144–150.

47. Terao C, Ohmura K, Kawaguchi Y, et al. PLD4 as a novel susceptibility gene for systemic sclerosis in a Japanese population. *Arthritis Rheum* 2013;65(2):472–480.
48. Qiu F, Tang R, Zuo X, et al. A genome-wide association study identifies six novel risk loci for primary biliary cholangitis. *Nat Commun* 2017;8:14828.
49. Li G, Martínez-Bonet M, Wu D, et al. High-throughput identification of noncoding functional SNPs via type IIS enzyme restriction. *Nat Genet* 2018;50(8):1180–1188.
50. Liu JZ, van Sommeren S, Huang H, et al; International Multiple Sclerosis Genetics Consortium; International IBD Genetics Consortium. Association analyses identify 38 susceptibility loci for inflammatory bowel disease and highlight shared genetic risk across populations. *Nat Genet* 2015;47(9):979–986.
51. Patsopoulos NA, Baranzini SE, Santaniello A, et al; International Multiple Sclerosis Genetics Consortium. Multiple sclerosis genomic map implicates peripheral immune cells and microglia in susceptibility. *Science* 2019;365(6460):eaav7188.
52. Karnell JL, Rieder SA, Ettinger R, Kolbeck R. Targeting the CD40–CD40L pathway in autoimmune diseases: humoral immunity and beyond. *Adv Drug Deliv Rev* 2019;141:92–103.
53. Banday AZ, Nisar R, Patra PK, et al. Clinical and immunological features, genetic variants, and outcomes of patients with CD40 deficiency. *J Clin Immunol* 2023;44(1):17.
54. Michel NA, Zirikli A, Wolf D. CD40L and its receptors in atherothrombosis—an update. *Front Cardiovasc Med* 2017;4:40.
55. Allanore Y, Borderie D, Meune C, et al. Increased plasma soluble CD40 ligand concentrations in systemic sclerosis and association with pulmonary arterial hypertension and digital ulcers. *Ann Rheum Dis* 2005;64(3):481–483.
56. Schmiedel BJ, Singh D, Madrigal A, et al. Impact of genetic polymorphisms on human immune cell gene expression. *Cell* 2018;175(6):1701–1715.e16.
57. Monaco G, Lee B, Xu W, et al. RNA-seq signatures normalized by mRNA abundance allow absolute deconvolution of human immune cell types. *Cell Rep* 2019;26(6):1627–1640.e7.
58. Yasaka K, Yamazaki T, Sato H, et al. Phospholipase D4 as a signature of toll-like receptor 7 or 9 signaling is expressed on blastic T-bet + B cells in systemic lupus erythematosus. *Arthritis Res Ther* 2023;25(1):200.
59. Trivedi P, Kumar RK, Iyer A, et al. Targeting phospholipase D4 attenuates kidney fibrosis. *J Am Soc Nephrol* 2017;28(12):3579–3589.
60. Kochan G, Krojer T, Harvey D, et al. Crystal structures of the endoplasmic reticulum aminopeptidase-1 (ERAP1) reveal the molecular basis for N-terminal peptide trimming. *Proc Natl Acad Sci USA* 2011;108(19):7745–7750.
61. O'Connell P, Blake MK, Godbehere S, et al. Absence of ERAP1 in B cells increases susceptibility to central nervous system autoimmunity, alters B cell biology, and mechanistically explains genetic associations between ERAP1 and multiple sclerosis. *J Immunol* 2021;207(12):2952–2965.
62. Onishi A, Sugiyama D, Kumagai S, et al. Cancer incidence in systemic sclerosis: meta-analysis of population-based cohort studies. *Arthritis Rheum* 2013;65(7):1913–1921.
63. Liang Y, Yang Z, Zhong R. Primary biliary cirrhosis and cancer risk: a systematic review and meta-analysis. *Hepatology* 2012;56(4):1409–1417.
64. Ricard L, Hirsch P, Largeaud L, et al; MINHEMON (French network of dysimmune disorders associated with hemopathies). Clonal haematopoiesis is increased in early onset in systemic sclerosis. *Rheumatology (Oxford)* 2020;59(11):3499–3504.
65. Gniadecki R, Iyer A, Hennessey D, et al. Genomic instability in early systemic sclerosis. *J Autoimmun* 2022;131:102847.
66. Hou C, Yang Y, Wang P, et al. CCDC113 promotes colorectal cancer tumorigenesis and metastasis via TGF- β signaling pathway. *Cell Death Dis* 2024;15(9):666.
67. Gourh P, Safran SA, Alexander T, et al. HLA and autoantibodies define scleroderma subtypes and risk in African and European Americans and suggest a role for molecular mimicry. *Proc Natl Acad Sci USA* 2020;117(1):552–562.
68. Acosta-Herrera M, Kerick M, López-Isac E, et al; International SSc Group; Australian Scleroderma Interest Group (ASIG). Comprehensive analysis of the major histocompatibility complex in systemic sclerosis identifies differential HLA associations by clinical and serological subtypes. *Ann Rheum Dis* 2021;80(8):1040–1047.
69. Mulinacci G, Palermo A, Gerussi A, et al. New insights on the role of human leukocyte antigen complex in primary biliary cholangitis. *Front Immunol* 2022;13:975115.
70. Liu JZ, Almarri MA, Gaffney DJ, et al; UK Primary Biliary Cirrhosis (PBC) Consortium; Wellcome Trust Case Control Consortium 3. Dense fine-mapping study identifies new susceptibility loci for primary biliary cirrhosis. *Nat Genet* 2012;44(10):1137–1141.
71. Invernizzi P, Selmi C, Poli F, et al; Italian PBC Genetic Study Group. Human leukocyte antigen polymorphisms in Italian primary biliary cirrhosis: a multicenter study of 664 patients and 1992 healthy controls. *Hepatology* 2008;48(6):1906–1912.
72. Aragam KG, Jiang T, Goel A, et al; Biobank Japan; EPIC-CVD; CARDIoGRAMplusC4D Consortium. Discovery and systematic characterization of risk variants and genes for coronary artery disease in over a million participants. *Nat Genet* 2022;54(12):1803–1815.
73. Gianfrancesco MA, Goldstein ND. A narrative review on the validity of electronic health record-based research in epidemiology. *BMC Med Res Methodol* 2021;21(1):234.

BRIEF REPORT

Disturbed Spatial WNT Activation—A Potential Driver of the Reticularized Skin Phenotype in Systemic Sclerosis

Sara Chenguiti Fakhouri,¹ Honglin Zhu,² Yi-Nan Li,³ Moritz Ronicke,⁴ Aleix Rius Rigau,⁵ Clara Dees,⁶ Laura Konstantinidis,⁷ Ralf Schmid,⁸ Alexandru-Emil Matei,⁹ Markus Eckstein,¹⁰ Carol Geppert,¹¹ Ingo Ludolph,¹² Alexander Kreuter,¹³ Michael Sticherling,¹⁴ Carola Berking,¹⁵ Raymund E. Horch,¹⁶ Georg Schett,¹⁷ Jörg H. W. Distler,¹⁸ and Christina Bergmann¹⁹

Objective. Little is known on the mechanisms necessary to maintain the physiologic adult human skin integrity. This study aims to quantitatively describe anatomic changes in systemic sclerosis (SSc)–skin compared with controls and investigate the underlying mechanisms.

Methods. Skin morphology was histologically assessed in 23 patients with SSc, 18 controls, and 15 patients with hypertrophic scars. Spatial WNT/ β -catenin-activation was analyzed by RNAscope and immunofluorescence staining. Enrichment of reticular marker genes in predefined fibroblast subpopulations was done using Gene Ontology (GO) enrichment and gene set enrichment analysis.

Results. SSc skin showed a decrease in number ($P < 0.0001/P = 0.0004$), area ($P < 0.0001$), and height ($P < 0.0001$) of papillae compared with controls and hypertrophic scars, respectively. The expression of papillary/reticular marker genes shifted toward a reticular expression profile in SSc. On the level of previously defined fibroblast populations, the increase of reticular marker genes was particularly pronounced in the PI16+ and SFRP4+ populations ($P < 0.0001$, respectively). Mechanistically, the expression of the WNT/ β -catenin target *AXIN2* and the number of fibroblasts with nuclear β -catenin-staining-pattern increased in the papillary compared with the reticular dermis in healthy skin. This polarization was lost in SSc with a two-fold increase in β -catenin-positive fibroblasts and *AXIN2*-expressing fibroblasts throughout the dermis ($P = 0.0095$). Enrichment of genes related to WNT/ β -catenin-regulation was found in the PI16+ population that also relocates from the reticular to the papillary dermis in SSc.

Conclusion. We demonstrate an association of the “reticularized” skin phenotype in SSc with a profound loss of physiologic spatial WNT/ β -catenin-activation. Rescuing the spatial WNT/ β -catenin-activation might help restore the physiologic skin organization in future therapeutic approaches of fibrosing disorders.

INTRODUCTION

Systemic sclerosis (SSc) is a chronic connective tissue disorder that results in progressive fibrotic tissue changes of the skin

and inner organs. The skin is affected in almost all patients starting from the distal extremities (sclerodactyly) expanding to the proximal parts of the body during the course of the disease.¹ Skin fibrosis is a major cause of daily life impairment,² and the extent

This work was completed in the context of the doctoral thesis of Sara Chenguiti Fakhouri.

Supported by the German Research Foundation (grants BE 7036/2-1 (C. Bergmann, BE 7036/5-1 (C Bergmann, DI 1537/17-1 (JHW Distler), DI 1537/20-1 (JHW Distler), DI 1537/22-1 (JHW Distler), and DI 1537/23-1 (JHW Distler), the SFB (Sonderforschungsbereiche) CRC (Collaborative Research Center) 1181 (project A01 and C01 (G Schett, JHW Distler), the NOTICE Clinician Scientist Program of the German Research Association (grant RA 2506/7-21 to Drs Ronicke, Berking, and Bergmann), the ELAN (Erlanger Anschubsfinanzierung) Erlangen (grant 21-11-09-1 to C Bergmann), the Clinician Scientist Program of IZKF (Interdisziplinäre Zentrum für Klinische Forschung) Erlangen (C Bergmann), and the Bundesministerium für Bildung und Forschung (iMMUNE_ACS program, project 01EO2105, C Bergmann).

¹Sara Chenguiti Fakhouri, MSc: Department of Internal Medicine 3 - Rheumatology and Clinical Immunology, Friedrich-Alexander-University (FAU) Erlangen-Nürnberg and Uniklinikum Erlangen, Erlangen, Germany, and Deutsches Zentrum Immuntherapie (DZI), FAU Erlangen-Nürnberg and

Uniklinikum Erlangen, Erlangen, Germany; ²Honglin Zhu, MD: Department of Rheumatology and Immunology, Xiangya Hospital, Central South University, Changsha, Hunan, People's Republic of China; ³Yi-Nan Li, PhD: Department of Rheumatology, University Hospital Düsseldorf, Medical Faculty of Heinrich Heine University, Düsseldorf, Germany, and Hiller Research Center, University Hospital Düsseldorf, Medical Faculty of Heinrich Heine University, Düsseldorf, Germany; ⁴Moritz Ronicke, MD: Deutsches Zentrum Immuntherapie (DZI), FAU Erlangen-Nürnberg and Uniklinikum Erlangen, Erlangen, Germany, and Department of Dermatology, Friedrich-Alexander-University (FAU) Erlangen-Nürnberg and Uniklinikum Erlangen, Erlangen, Germany; ⁵Aleix Rius Rigau, PhD: Department of Internal Medicine 3 - Rheumatology and Clinical Immunology, Friedrich-Alexander-University (FAU) Erlangen-Nürnberg and Uniklinikum Erlangen, Erlangen, Germany, and Deutsches Zentrum Immuntherapie (DZI), FAU Erlangen-Nürnberg and Uniklinikum Erlangen, Erlangen, Germany; ⁶Clara Dees, PhD: Department of Internal Medicine 3 - Rheumatology and Clinical Immunology, Friedrich-

of skin involvement is recognized as risk factor for the progression of organ fibrosis.³

Healthy human skin forms the interface between the body and the environment and is characterized by a polarized, layered structure including the epidermis, the papillary and reticular dermis and the subcutaneous fat tissue.⁴ The papillary dermis is composed of loose collagen bundles surrounding blood vessels and nerve endings, whereas the reticular dermis is characterized by coarse collagen bundles.⁵ This physiologic skin structure is disrupted in SSC: the deregulation of fibroblasts and increased differentiation into myofibroblasts results in the exaggerated deposition of collagen-rich extracellular matrix throughout the dermis along with morphologic changes such as flattening of the rete ridges and loss of functional intradermal structures and skin appendices.^{6,7} Previous studies have described a correlation between histologic changes such as the hyalinized collagen score and the extent of local skin involvement as assessed by the modified Rodan skin score.^{7,8}

The mechanisms that are required to maintain the physiologic layered organization of healthy skin are largely unknown. Evidence from rodent models of skin morphogenesis suggests that spatial activation of WNT/ β -catenin signaling at the cellular and tissue level plays a central role in three-dimensional skin patterning.⁹ WNT/ β -catenin signaling has been characterized as central profibrotic regulator in fibrosing disorders by several groups.^{10–15} Activation occurs by overexpression of certain WNT proteins and by reduced expression of the endogenous WNT antagonist DKK1 in the skin.¹³ However, the spatial resolution of WNT activators and antagonists in adult human skin has not been described. Moreover, the mechanisms that maintain the polarized structure

of the skin in adults have barely been elucidated. Here we aimed to characterize the histopathologic changes in SSC skin, investigate the spatial regulation of WNT/ β -catenin signaling in normal human skin compared with SSC skin, and correlate changes in spatial WNT/ β -catenin signaling with histopathological characteristics in SSC.

PATIENTS AND METHODS

Patients. Skin biopsies from 23 patients with SSC and 18 healthy volunteers were used. All patients with SSC fulfilled the 2013 American College of Rheumatology/EULAR criteria for SSC. Twenty-two patients had limited cutaneous SSC and 41 were classified as diffuse cutaneous SSC according to the LeRoy classification.¹⁶ Skin biopsies from patients with SSC were taken from involved skin on the forearm. In 18 patients with SSC, skin biopsies were additionally taken from a clinically noninvolved skin area at the back. Eighteen patients were female, and five were male. The median age of patients with SSC was 55 years (range 41–69 years), and the median disease duration was 5 years (range 1–12 years). Control skin samples from 18 healthy individuals who underwent either orthopedic or plastic surgery were included. In addition, 15 samples of patients with hypertrophic scars were analyzed. The diagnosis of hypertrophic scars was based on the clinical judgment of two experienced dermatologists in conjunction with the histopathologic findings. The collection of biology samples and their analysis in context with clinical information were approved by the ethics committee of the Medical Faculty of the University of Erlangen-Nuremberg. All patients and

Alexander-University (FAU) Erlangen-Nürnberg and Uniklinikum Erlangen, Erlangen, Germany, and Deutsches Zentrum Immuntherapie (DZI), FAU Erlangen-Nürnberg and Uniklinikum Erlangen, Erlangen, Germany; ⁷Laura Konstantinidis: Department of Internal Medicine 3 - Rheumatology and Clinical Immunology, Friedrich-Alexander-University (FAU) Erlangen-Nürnberg and Uniklinikum Erlangen, Erlangen, Germany, and Deutsches Zentrum Immuntherapie (DZI), FAU Erlangen-Nürnberg and Uniklinikum Erlangen, Erlangen, Germany; ⁸Rafael Schmid, PhD: Department of Plastic and Hand Surgery, Laboratory for Tissue Engineering and Regenerative Medicine, University Hospital Erlangen, Friedrich Alexander University Erlangen-Nürnberg FAU, Erlangen, Germany; ⁹Alexandru-Emil Matei, MD: Department of Rheumatology, University Hospital Düsseldorf, Medical Faculty of Heinrich Heine University, Düsseldorf, Germany, and Hiller Research Center, University Hospital Düsseldorf, Medical Faculty of Heinrich Heine University, Düsseldorf, Germany; Fraunhofer Institute for Translational Medicine and Pharmacology ITMP, and Fraunhofer Cluster of Excellence for Immune Mediated Diseases CIMD, Frankfurt am Main, Germany; ¹⁰Markus Eckstein, MD: Department of Pathology, Friedrich-Alexander-University (FAU) Erlangen-Nürnberg and Uniklinikum Erlangen, Erlangen, Germany; ¹¹Carol Geppert, MD: Department of Pathology, Friedrich-Alexander-University (FAU) Erlangen-Nürnberg and Uniklinikum Erlangen, Erlangen, Germany; ¹²Ingo Ludolph, MD: Department of Plastic and Hand Surgery, Laboratory for Tissue Engineering and Regenerative Medicine, University Hospital Erlangen, Friedrich Alexander University Erlangen-Nürnberg FAU, Erlangen, Germany; ¹³Alexander Kreuter, MD: Department of Dermatology, Venereology, and Allergology, HELIOS St. Elisabeth Hospital Oberhausen, Oberhausen, Germany; ¹⁴Michael Sticherling, MD: Deutsches Zentrum Immuntherapie (DZI), FAU Erlangen-Nürnberg and Uniklinikum Erlangen, Erlangen, Germany, and Department of Dermatology, Friedrich-Alexander-University (FAU) Erlangen-Nürnberg and Uniklinikum Erlangen, Erlangen,

Germany; ¹⁵Carola Berking, MD: Deutsches Zentrum Immuntherapie (DZI), FAU Erlangen-Nürnberg and Uniklinikum Erlangen, Erlangen, Germany, and Department of Dermatology, Friedrich-Alexander-University (FAU) Erlangen-Nürnberg and Uniklinikum Erlangen, Erlangen, Germany; ¹⁶Raymund E. Horch, MD: Department of Plastic and Hand Surgery, Laboratory for Tissue Engineering and Regenerative Medicine, University Hospital Erlangen, Friedrich Alexander University Erlangen-Nürnberg FAU, Erlangen, Germany; ¹⁷Georg Schett, MD: Department of Internal Medicine 3 - Rheumatology and Clinical Immunology, Friedrich-Alexander-University (FAU) Erlangen-Nürnberg and Uniklinikum Erlangen, Erlangen, Germany, and Deutsches Zentrum Immuntherapie (DZI), FAU Erlangen-Nürnberg and Uniklinikum Erlangen, Erlangen, Germany; ¹⁸Jörg H. W. Distler, MD: Department of Rheumatology, University Hospital Düsseldorf, Medical Faculty of Heinrich Heine University, Düsseldorf, Germany, and Hiller Research Center, University Hospital Düsseldorf, Medical Faculty of Heinrich Heine University, Düsseldorf, Germany; Fraunhofer Institute for Translational Medicine and Pharmacology ITMP, and Fraunhofer Cluster of Excellence for Immune Mediated Diseases CIMD, Frankfurt am Main, Germany; ¹⁹Christina Bergmann, MD: Department of Internal Medicine 3 - Rheumatology and Clinical Immunology, Friedrich-Alexander-University (FAU) Erlangen-Nürnberg and Uniklinikum Erlangen, Erlangen, Germany.

Additional supplementary information cited in this article can be found online in the Supporting Information section (<https://onlinelibrary.wiley.com/doi/10.1002/art.43094>).

Author disclosures are available at <https://onlinelibrary.wiley.com/doi/10.1002/art.43094>.

Address correspondence via email to Christina Bergmann, MD, at christina.bergmann@uk-erlangen.de.

Submitted for publication January 10, 2024; accepted in revised form December 5, 2024.

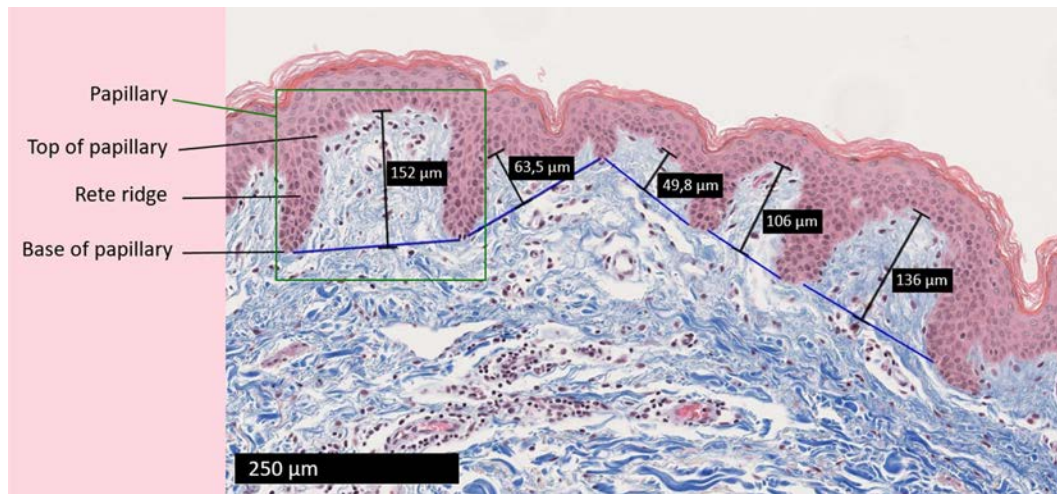


Figure 1. Visualization of papillary measurements.

control individuals signed an informed consent form approved by the local review board.

Histologic analyses. For visualization and quantification of dermal papillae, trichrome staining of the skin sections was used as described previously.^{17–19} Pictures were taken at 200-fold magnification with a Nanozoomer S60v2MD slide scanner (Hamamatsu Photonics). Papillae numbers per mm, papillae heights (defined as the distance between the base and the top of the papillae as demonstrated in Figure 1) and papillae areas were quantified at five different sites in one skin section from each patient in a blinded manner using the NDPView2 software (Hamamatsu Photonics).

Collagen fiber alignment (from 0° to 180°) and alignment coefficients were measured using Curvealign V4.0 Beta (MATLAB). Three regions of interest of 0.02 mm² were selected in the reticular dermis of each trichrome-stained skin section. The coefficient of alignment was calculated for all the collagen fibers within each region of interest using the Computed Tomography–Fiber analysis method according to the developer’s manual (<https://eliceirilab.org/software/curvealign/>). The alignment coefficient was calculated from zero (low parallelism between collagen fibers) to one (high parallelism between collagen fibers).

Immunofluorescence. Paraffin-embedded skin sections were fixed with 4% paraformaldehyde.²⁰ Epitope retrieval was performed using a heat-induced method; sections were incubated with preheated citrate buffer (10 mM sodium citrate, pH 6.0) and Tris-EDTA buffer (10 mM Tris, 1 mM EDTA, 0.05% Tween 20, pH 9.0). Sections were then blocked with phosphate buffered saline (PBS) supplemented with 2% Bovine serum albumin (BSA) and 5% horse serum. Primary antibodies were incubated overnight at 4°C. After washing, secondary antibodies

were incubated for an hour at room temperature. Next, the sections were counterstained with 4',6-diamidino-2-phenylindole (DAPI) (1:800, #sc-3598 Santa Cruz Biotechnology). Primary antibodies used were directed against β -catenin (1:250, #ab2365; abcam), prolyl-4-hydroxylase β (P4H β) (1:200, #ab2792; abcam), platelet derived growth factor α (PDGFR α) (1:200, #AF1062; R&D Systems), PI16 (1/200, #HPA043763; Atlas Antibodies), secreted frizzled related protein 4 (SFRP4, 1:20, 15328-1-AP, Protein-tech), Dickkopf-1 (1:100, #AF1096; R&D Systems), vimentin (1:1000, NBP1-97515; Novus Biologicals), Fibroblast activation protein α (FAP) (1:200, #AF3715; R&D Systems), CD90/Thy1 (1:250, #ab133350; abcam). Conjugated secondary antibodies (1:200, Alexa Fluor, Thermo Fisher Scientific) were used. Nuclei were stained with DAPI (1:800, #sc-3598, Santa Cruz Biotechnology). The staining was analyzed using a Nikon Eclipse 80i microscope (Nikon) and a BZ-X800 microscope (Keyence). Pictures were taken at 200-fold magnification. Borders of the papillary and reticular dermis were defined anatomically; we considered the superficial vascular plexus to be the limit between the papillary and reticular dermis.²¹ Thus, the papillary dermis was defined by the dermal-epidermal junction and the superficial vascular plexus. The reticular dermis was defined by the superficial vascular plexus and the beginning of the subcutis. Semiquantitative quantification of β -catenin-, FAP-, CD90-, PI16-, and SFRP4-positive cells in the papillary and reticular dermis was performed at three different sites of one skin section from each patient or control individual, in a blinded manner, using the Nikon NIS-Element software platform (Nikon). The β -catenin fluorescence intensity in the papillary and reticular dermis was quantified at seven different sites in one skin section from each patient or control using the ImageJ software (NIH, version 1.46).

RNAscope assay. Spatial transcriptional activation of the WNT/ β -catenin pathway was assessed through in situ

hybridization detection of *AXIN2* using an RNAscope Multiplex Fluorescent Kit V2 (Advanced Cell Diagnostics) combined with TSA Vivid Fluorophores (Bio-Techne) on paraffin-embedded, formalin-fixed skin sections according to the manufacturer's instructions. Briefly, formalin-fixed, paraffin-embedded skin sections are permeabilized to allow probe access to the target RNA. Probes are then hybridized to target RNA and labeled with fluorophores. Finally, the hybridization signal is amplified by sequentially binding amplifiers and labeled probes and nuclei were stained with DAPI. Quantification of *AXIN2*-positive cells in the papillary and reticular dermis was performed at three different sites of one skin section from each patient or control, in a blinded manner, using the Nikon NIS-Element software platform (Nikon). The *AXIN2* fluorescence intensity in the papillary and reticular dermis was quantified at four to seven different sites in one skin section from each patient or control using the ImageJ software (NIH, version 1.46).

Confocal microscopy and analysis. Confocal images of skin sections were acquired using a Leica Stellaris 8 confocal microscope (Leica Microsystems) at the Optical Imaging Center Erlangen. Pictures were taken at 630-fold magnification with a glycerol immersion lens and a resolution of 1024 × 1024 pixels. Stacks of images were acquired at 1 μm interval throughout the cells, in the papillary and the reticular dermis. The fluorescence intensity of the cytoplasmic and nuclear β -catenin was measured by creating a mask based on the fluorescent signal of the pan-fibroblast marker P4H β antibody (1:200, #ab2792; abcam) and DAPI (1:800, #sc-3598 Santa Cruz Biotechnology), respectively. To this end, the channel containing the DAPI nuclear marker was converted to a mask, which was applied to the β -catenin signal, and the fluorescence intensity analysis was performed by thresholding using the MorpholibJ plugin on the ImageJ software (NIH, version 1.46). The same procedure was conducted for cytoplasmic β -catenin with the pan-fibroblast marker P4H β signal.

Imaging mass cytometry staining and measurements. Imaging mass cytometry (IMC) was performed as described.²¹ The antibodies were acquired pre-conjugated (Standard Biotech) or in purified preparations. All the purified antibodies were first validated by standard immunofluorescence staining. Purified antibodies were consequently conjugated to lanthanide metals using the Maxpar X8 antibody labeling kit (Standard Biotech) following the manufacturer's instructions. The full panel was revalidated in IMC, and all antibodies were titrated in IMC. Paraffin-embedded skin sections (5 μm) were deparaffinized with xylene for 30 minutes and rehydrated in a graded series of alcohol (ethanol:deionized water 100:0, 100:0, 90:10, and 80:20 for 5 minutes each). For epitope retrieval, the slides were incubated for 30 minutes in preheated Tris-EDTA buffer (10 mM Tris base, 1 mM EDTA, and 0.05% Tween 20, pH 9). After the slides were cooled, they were blocked with 2% BSA

in PBS for one hour at room temperature. Samples were incubated overnight at 4°C with the antibody mix (in 0.5% BSA). Tissue samples were washed once in PBS-T (PBS and 0.2% Tween 20) and twice in PBS for five minutes each wash. DNA staining was performed with Iridium-Intercalator (125 μM) (Standard Biotech) 1/400 for five minutes at room temperature. Afterward, the samples were washed three times in PBS and once in deionized water for five minutes each. Finally, the tissue sections were dried and stored at room temperature.

The area to be ablated was chosen with a hematoxylin-eosin staining of a consecutive cut. The samples were acquired with the Hyperion Imaging System (Standard Biotech) coupled to a Helios mass cytometer (Standard Biotech) after daily calibration, tuning, and quality control. The laser ablation was done at a resolution of 1 μm^2 and a frequency of 200 Hz. All IMC data were stored as MCD and txt files.

IMC data analysis. First, the quality of the staining was checked with the software MCD viewer (Standard Biotech). The MCD files were converted to TIFF format and segmented into single cells using a publicly available analysis pipeline (<https://zenodo.org/record/3841961>). The single-cell data (mean expression of all pixels being the same cell and the spatial coordinates) were extracted as fcs and csv files, arcsinh normalized (cofactor 1), and rescaled between 0 and 1 with the R package Spectre.²¹ The populations of interest were selected by manual gating and spatial reference using the FlowJo software (fibroblasts were defined as Ecadherin-CD45-CD31-; afterward skin fibroblast subsets were selected: fibroblast FAP+CD90+, FAP+CD90-, FAP-CD90+.). The spatial representation of the different cell populations was done with the R package Cytomapper.^{22,23}

Gene set enrichment analyses. Gene set enrichment analyses (GSEA) were performed using the R packages clusterProfiler (3.18.0) and GSVA (V1.38.0). Reticular and papillary gene signature²⁴ scores in the Prospective Registry for Early Systemic Sclerosis (PRESS) cohort²⁵ (GSE130955) and the Genes versus Environment in Scleroderma Outcome Study (GENISOS) cohort (GSE58095)²⁶ were obtained through single-sample gene set enrichment analysis using gene lists from Solé-Boldo et al.²⁴ GSEA was used to analyze WNT3A-regulated gene signatures in relation to reticular and papillary marker genes,²⁴ the enrichment of reticular and papillary marker genes²⁴ in predefined fibroblast subsets,^{27,28} and the enrichment of WNT3A-regulated genes in the PI16+/- fibroblast population.

Statistical analysis. All data are presented as median with interquartile range with individual datapoints displayed as dots. Comparisons between experimental groups were analyzed with nonparametric Mann-Whitney-U-test using GraphPad Prism 8.3.0. In analysis including multiple tests, the *P* value of each test

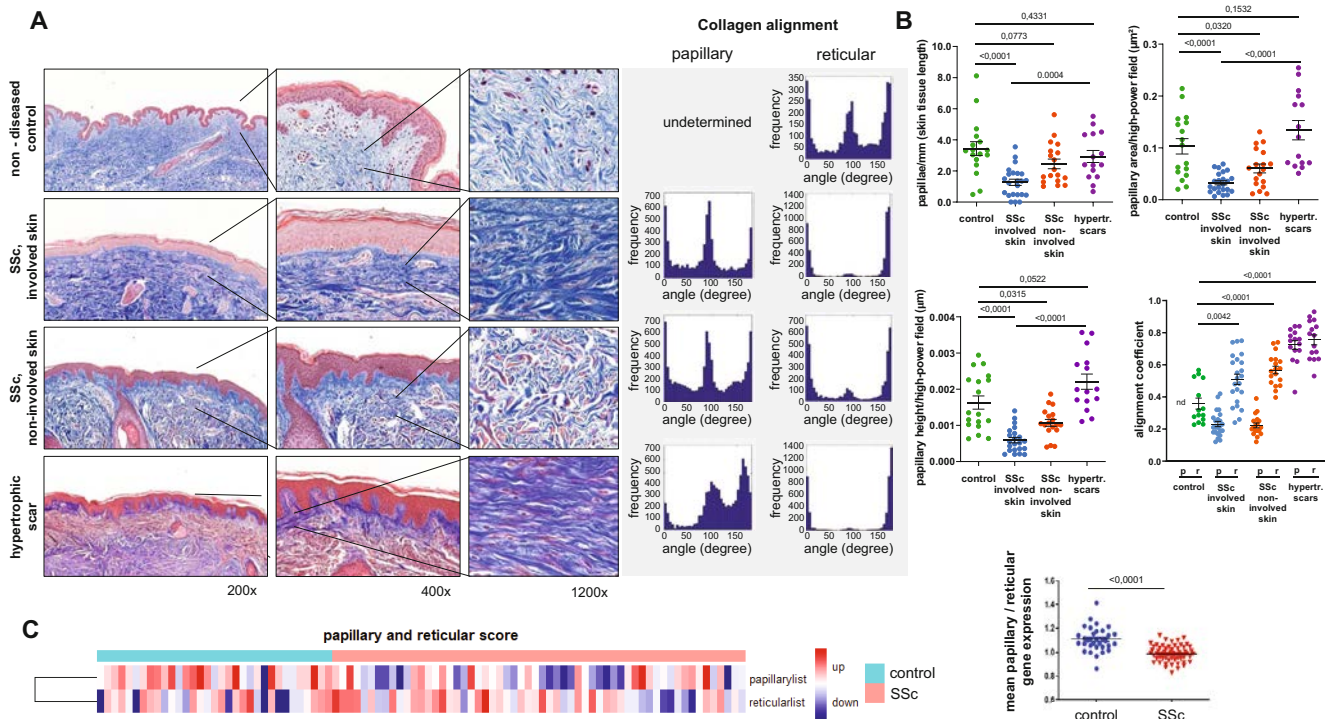


Figure 2. Morphology of the dermal papillae in SSc compared with nondiseased skin and hypertrophic scars. (A) Trichrome staining of skin sections of nondiseased control individuals ($n = 18$), involved (forearm) and noninvolved (back) skin of patients with SSc ($n = 23$), patients with hypertrophic scars ($n = 15$), and corresponding histograms representing collagen fiber orientation in angle frequency of individual collagen fibers. Representative images are shown at 200-, 400-, and 1,200-fold magnification. (B) Quantification of papillae/mm, papillary area/high-power field, papillary height/high-power field and collagen fiber alignment coefficient of skin sections of control individuals ($n = 18$), patients with SSc ($n = 23$), and patients with hypertrophic scars ($n = 15$) quantified from trichrome staining images. (C) Papillary and reticular gene scores in Prospective Registry for Early Systemic Sclerosis cohort (GSE130955) (Gene set list from Solé-Boldo et al²⁴). Data are presented as median \pm interquartile range. Statistical significance for each comparison was determined by Mann-Whitney U-test. $P < 0.0125$ was considered significant after Bonferroni correction. hypertr., hypertrophic; p, papillary; r, reticular; SSc, systemic sclerosis. Color figure can be viewed in the online issue, which is available at <http://onlinelibrary.wiley.com/doi/10.1002/art.43094/abstract>.

(p_i) was adjusted using the Bonferroni correction ($p_i = p/n$, n = number of tests, p = overall significance level).

RESULTS

Assessment of structural changes in fibrotic skin in SSc compared with nondiseased control skin and hypertrophic scars. Quantitative assessments of changes in the papillary dermis in SSc have not been described so far. Here, we analyzed the number of papillae per millimeter, papillae length, and area in trichrome-stained skin sections of healthy individuals, involved skin of patients with SSc (forearm), clinically noninvolved skin of patients with SSc (back), and of patients with hypertrophic scars as a second type of fibrosing skin disorder. In SSc-involved skin, dermal papillae were markedly decreased in number, area, and height compared with controls (Figure 2A and B).

Noninvolved SSc skin showed higher papillary content (papillae per mm, papillae length and papillae area) compared with clinically involved skin in SSc (Figure 2A and B), albeit below

the level of nondiseased controls. In contrast, number, area, and height of papillae in hypertrophic scars did not significantly differ from healthy controls, suggesting that papillary loss is a phenomenon specific to SSc rather than a general feature of fibrosing dermal disorders (Figure 2A and B). The papillae measurements including papillae number per mm, height, and area did not significantly differ between patients with limited cutaneous SSc (lcSSc) compared with diffuse cutaneous SSc (dcSSc) (Supplementary Figure 1).

As additional readout, we analyzed the orientation of collagen fibers using trichrome staining in skin sections of healthy donors, involved skin of patients with SSc, noninvolved skin of SSc, and hypertrophic scars. SSc skin and hypertrophic scar sections showed a higher alignment coefficient than healthy controls in the reticular dermis and a measurable alignment coefficient in the papillary dermis, consistent with the increased extracellular matrix deposition and the “reticularization” of the papillary dermis (Figure 2A and B). In healthy skin, the loose structure of the extracellular matrix in the papillary layer did not allow for a specific detection of individual collagen fibers and an alignment coefficient

could not be calculated. When comparing lcSSc and dcSSc skin sections, we measured similar levels of collagen alignment between the two subtypes, confirming a shared structural remodeling (Supplementary Figure 1).

To confirm these histologic observations with another approach, we compared published datasets of papillary and reticular marker genes²⁴ with differentially regulated genes in SSC compared with healthy controls described in the PRESS cohort.²⁵ Consistent with the morphologic changes, we observed that the expression of papillary versus reticular marker genes is shifted toward a reticular gene expression profile in SSC skin samples (Figure 2C). This is also reflected by the reduction of the ratio of mean papillary gene expression/mean reticular papillary gene expression in SSC compared with controls. Because the PRESS cohort mainly includes patients with early diffused disease and to confirm our results in another cohort dataset, we next analyzed the enrichment of papillary and reticular marker sets in a published dataset of the GENISOS cohort.²⁶ The GENISOS cohort includes patients with both lcSSc and dcSSc and with variable disease duration ranging from 0.5 to 20 years since the first onset of first non-Raynaud symptom. Analyzing the whole cohort, we observed a tendency of reduction of the papillary/reticular gene ratio, which was not significant (Supplementary Figure 2). Next, we analyzed patients with relatively low disease duration (≤ 4 years) and compared them with patients with a longer disease duration

(>4 years). Similar to our results obtained in the PRESS cohort, we observed a significant reduction of papillary/reticular marker genes in patients with less than or equal to four years disease duration. The majority of patients in this subgroup suffered from dcSSc, and no significant difference was observed between lcSSc and dcSSc. Reduction of the papillary/reticular score was less pronounced in patients with longer disease duration (>4 years) and was not statistically significant (Supplementary Figure 2).

Altered spatial activation of WNT signaling in SSC compared with healthy controls.

A tightly regulated spatial activation of WNT/ β -catenin signaling has recently been described as a core requirement for physiologic skin morphogenesis in mice.²⁹ Moreover, WNT/ β -catenin signaling has been described as a central profibrotic mediator.^{10,30} We thus analyzed whether a spatial WNT/ β -catenin activation is observed in adult healthy skin and might be perturbed in SSC. First, we analyzed whether WNT/ β -catenin-dependent target genes (GSE120106) are enriched in the papillary and in the reticular part of healthy skin.²⁴ We observed an enrichment of WNT3A-regulated genes in papillary healthy skin, and a tendency toward negative enrichment in reticular gene sets (Supplementary Figure 3A). In contrast to WNT3A-regulated genes, WNT5A-regulated gene signatures as markers of noncanonical WNT signaling did not show

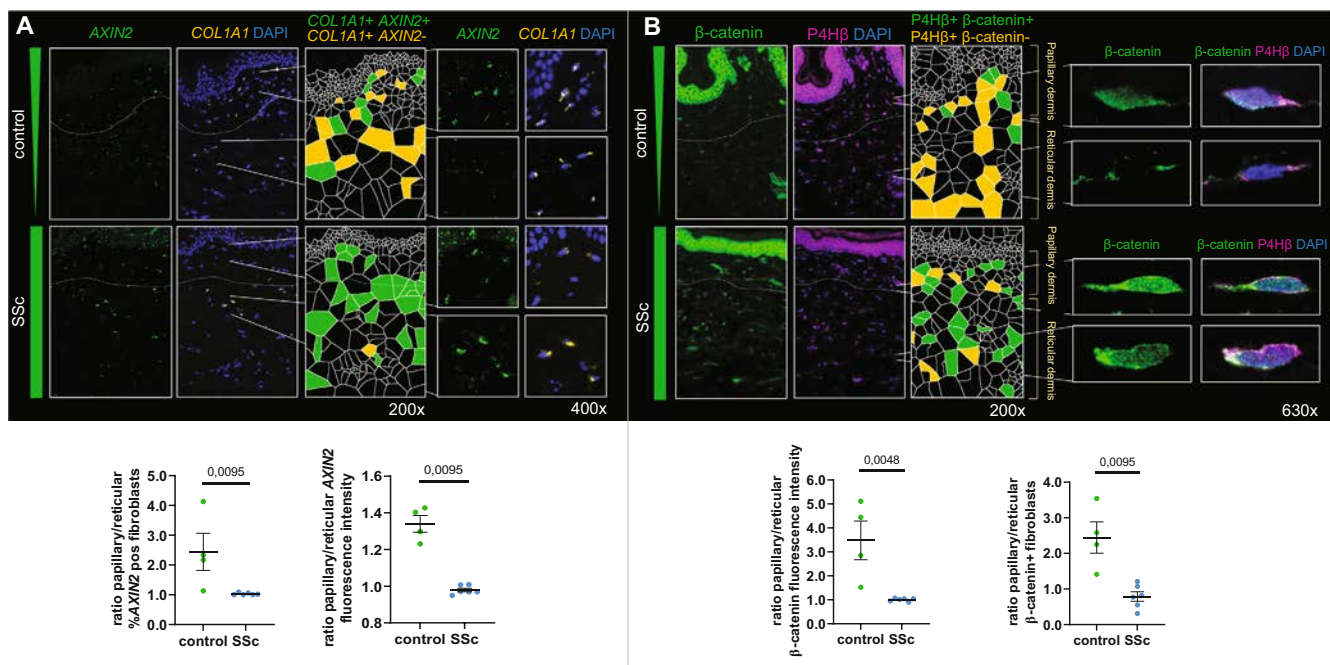


Figure 3. Spatial activation of WNT/ β -catenin signaling in healthy and SSC skin. (A) RNAscope in situ hybridization images of *COL1A1* (orange) and *AXIN2* (green) on skin sections of healthy individuals and patients with SSC. Representative images are shown at 200- and 400-fold magnification. Quantification is shown as bar graph. (B) Immunofluorescence staining and confocal immunofluorescence microscopy for β -catenin (green) and the pan-fibroblast marker P4H β (magenta) of papillary and reticular fibroblasts from nondiseased control individuals ($n = 4$) and patients with SSC ($n = 6$). Representative images are shown at 200- and 630-fold magnification. Data presented as median \pm interquartile range. Statistical significance was determined by Mann-Whitney U-test. $P < 0.05$ was considered significant. SSC, systemic sclerosis. Color figure can be viewed in the online issue, which is available at <http://onlinelibrary.wiley.com/doi/10.1002/art.43094/abstract>.

enrichment with neither papillary nor reticular marker gene lists (Supplementary Figure 3B), demonstrating that this enrichment is specific for WNT/ β -catenin signaling. To confirm the spatial transcriptional activity of WNT/ β -catenin signaling in human skin samples, we investigated the spatial expression of the WNT/ β -catenin target gene *AXIN2* using the RNAscope in situ hybridization technique (Figure 3A). As in previous studies,²⁵ *COL1A1* was used to identify dermal fibroblasts. Consistent with the bioinformatic analyses aforementioned, we observed significantly increased numbers of *AXIN2*, *COL1A1*-expressing cells in the papillary dermis compared with the reticular dermis in healthy skin. In contrast, in SSc skin, almost all *COL1A1*-expressing cells also expressed *AXIN2*, and a difference in the number of *AXIN2*, *COL1A1* positive cells between reticular and papillary cells was no longer detectable. The intensity of the *AXIN2* signal also demonstrated a loss of spatial expression gradients of *AXIN2* in SSc skin (Figure 3A). These results were confirmed on the protein level using immunofluorescence staining of *AXIN2* in combination with the pan-fibroblast marker P4H β , which showed a predominance of *AXIN2*-positive fibroblasts in the papillary dermis of control skin. This distribution was altered in SSc skin, and comparable levels of *AXIN2*-positive fibroblasts were measured in both the papillary and the reticular layer of the dermis, along with a general upregulation of *AXIN2* in SSc (Supplementary Figure 4).

To confirm these observations, we expanded the investigation of WNT/ β -catenin-regulated genes using cyclic in situ hybridization by COSMx as an additional more comprehensive spatial transcriptomic approach. This analysis revealed that the papillary to reticular ratio of several WNT-related genes, including *CTNNB1*, *FZD1*, *FZD5*, *FZD7*, *FZD8*, *VEGFC*, *WIF1*, *WNT11*, *WNT7B*, and *FGF18*,^{31–33} was found to be reduced in SSc skin fibroblasts compared with controls (Supplementary Figure 5). We also observed a tendency toward a decrease of the papillary to reticular ratio of noncanonical WNT-related genes in SSc skin, although this reduction was less pronounced compared with that seen with canonical WNT-related genes (Supplementary Figure 6).

Additionally, a distance profile analysis demonstrated that in healthy controls, fibroblasts expressing the WNT signature were located closer to the epidermis and predominantly in the papillary layer. In contrast, SSc skin showed that the WNT signature-expressing fibroblasts were more evenly distributed throughout the dermis, with similar cell densities observed in both the papillary and the reticular layer (Supplementary Figure 7). To a lesser extent, a similar distribution pattern was observed for noncanonical WNT-related genes, although the variation in localization was less pronounced (Supplementary Figure 8).

To analyze the spatial WNT activation by a complementary approach, we analyzed the spatial distribution of β -catenin expression in the skin by coimmunofluorescence staining for β -catenin and the pan-fibroblast marker P4H β (Figure 3B). In

healthy skin, fibroblasts with nuclear β -catenin expression were enriched in the papillary dermis by two-fold compared with the reticular dermis. In SSc skin, we observed an increase of β -catenin-positive fibroblasts throughout the dermis and a particular enrichment in the papillary layer was no longer detectable (Figure 2B), showing a general overexpression of β -catenin in SSc skin fibroblasts. In noninvolved SSc skin, the distribution of β -catenin-positive fibroblasts was similar to healthy skin (Supplementary Figure 9), confirming that the disruption of the spatial distribution is inherent to fibrotic skin changes. The distribution of β -catenin-positive fibroblasts was comparable between lcSSc and dcSSc skin sections, indicating a similar pattern of spatial alteration of WNT/ β -catenin signaling in both disease subtypes in involved skin (Supplementary Figure 10).

The physiologic regulation of WNT signaling relies on a controlled balance of several WNT agonists and antagonists.^{9–12,14,32–35} In fact, in addition to an upregulation of WNT agonists, WNT inhibitors have been shown to be reduced in SSc skin.^{14,36} We therefore analyzed the spatial distribution of the WNT antagonist DKK1 through coimmunofluorescence with the pan-fibroblast marker P4H β . Healthy control skin showed a predominance of DKK-positive fibroblasts in the reticular dermis. In SSc skin, we observed a significant downregulation of DKK throughout the dermis, with no differences of expression between the papillary and the reticular layer (Supplementary Figure 11).

Spatial distribution of fibroblast populations in SSc skin compared with controls.

A previous study in healthy skin identified enrichment of FAP⁺; CD90[−] fibroblasts in the papillary dermis, whereas FAP[−]; CD90⁺ fibroblasts were enriched in the reticular dermis.³⁷ Thus, we next analyzed whether the distribution of these two fibroblast populations in the papillary versus reticular dermis is perturbed in SSc. We observed an increase of both fibroblast populations in SSc compared with healthy controls. As analyzed by IMC and immunofluorescence, both FAP⁺; CD90[−] fibroblasts and FAP[−]; CD90⁺ fibroblasts were increased throughout the dermis, and particular enrichment of the FAP⁺; CD90[−] fibroblasts in the papillary dermis and FAP[−]; CD90⁺ fibroblasts in the reticular dermis was not detectable (Supplementary Figure 12).

On the transcriptomic level, fibroblast subpopulations have recently been identified based on single-cell RNA sequencing data.^{27,28} We analyzed whether an enrichment of reticular marker genes is found in these populations on the transcriptomic level (Figure 4A). We observed the most pronounced enrichment of reticular genes in the PI16⁺ and the SFRP4⁺ fibroblast subsets in SSc fibroblasts compared with control fibroblasts. Next, we analyzed whether the enrichment of reticular marker genes on the transcriptomic level is also associated with the spatial redistribution of these fibroblast populations in the dermis. As analyzed by immunofluorescence staining for PI16 and SFRP4 together with the pan-fibroblast marker P4H β , we observed an increased

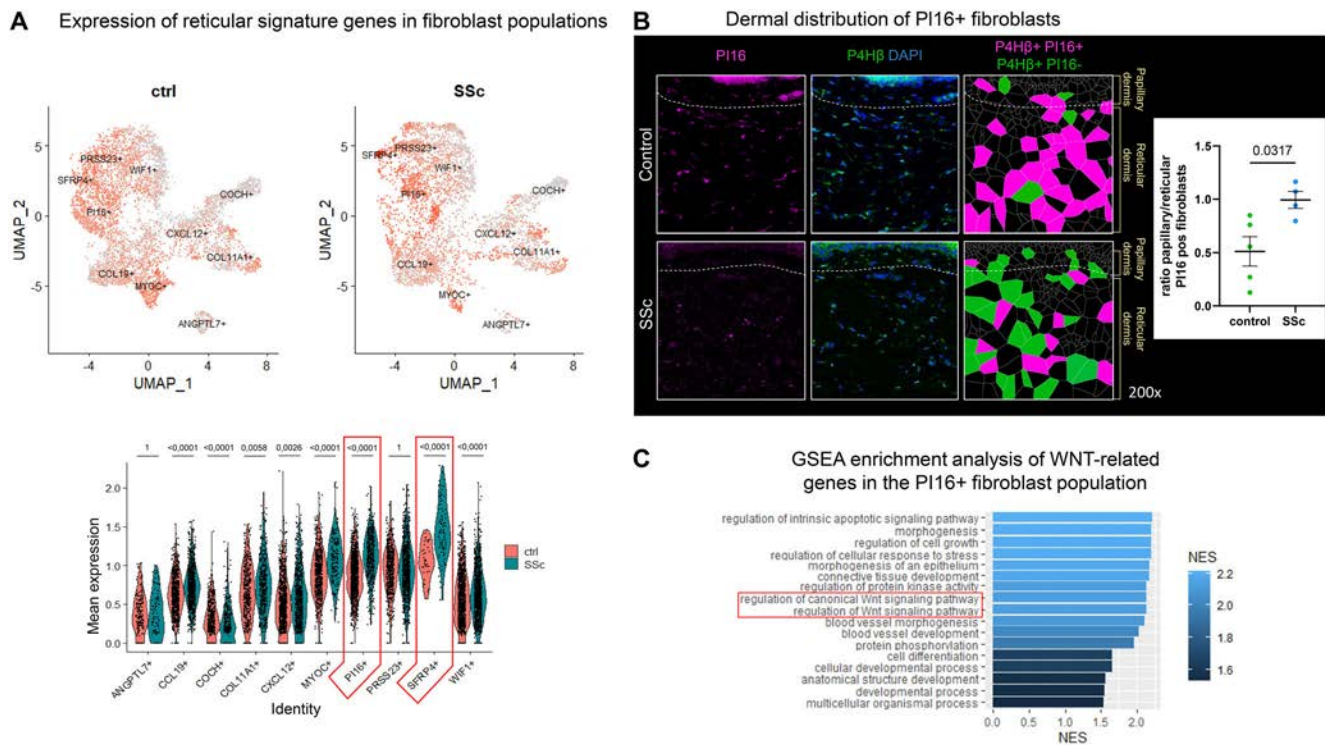


Figure 4. Analysis of fibroblast populations in relation to the papillary and reticular dermis in SSc compared with controls. (A) Mean expression of reticular marker genes in fibroblast populations defined based on small conditional RNA in SSc compared with control. Adjusted *P* values using the Bonferroni correction are shown. (B) Immunofluorescence staining for PI16 (magenta) and the pan-fibroblast marker *P4HB* (green) of nondiseased control individuals (*n* = 5) and patients with SSc (*n* = 4). Representative pictures are shown at 200-fold magnification. Data presented as median \pm interquartile range. Statistical significance was determined by Mann-Whitney U-test. *P* < 0.05 was considered significant. (C) NES of gene sets in a PI16-positive fibroblast cluster. ctrl, control; GSEA, gene set enrichment analysis; NES, normalized enrichment score; SSc, systemic sclerosis; UMAP, uniform manifold approximation and projection. Color figure can be viewed in the online issue, which is available at <http://onlinelibrary.wiley.com/doi/10.1002/art.43094/abstract>.

ratio of papillary versus reticular PI16+ fibroblasts in SSc skin compared with controls (Figure 4B). In noninvolved SSc skin, the distribution of PI16-positive fibroblasts was comparable with healthy skin (Supplementary Figure 13), indicating that these changes in spatial distribution are specific to fibrotic skin alterations. The ratio of SFRP4+ fibroblasts in the papillary versus reticular dermis did not differ in SSc samples compared with healthy controls (Supplementary Figure 14).

Having demonstrated that PI16+ fibroblasts are characterized by the enrichment of reticular marker genes on the transcriptomic level and anatomically relocate to the papillary dermis in SSc, we next analyzed whether PI16+ fibroblasts also show an increased activation of WNT/ β -catenin signaling. Using GSEA, we observed that gene sets associated with the regulation of WNT/ β -catenin signaling are enriched in the transcriptomic profile of the PI16+ fibroblast population (Figure 4C). Similar results were obtained using Gene Ontology term analysis (Supplementary Figure 15). Consistently, coimmunofluorescence staining of β -catenin and PI16 revealed an increase of β -catenin and PI16 colocalization levels in SSc skin compared with controls (Supplementary Figure 16). In summary, these results suggest that the PI16+ fibroblasts show a particular relocation to the papillary dermis in SSc and are associated with increased WNT/ β -catenin signaling.

DISCUSSION

Here we show for the first time that the physiologic gradient of WNT/ β -catenin signaling is perturbed in SSc skin along with anatomic changes of the papillary and reticular dermis and with changes in the spatial distribution of specific fibroblast subsets.

In human adult healthy skin, the activation of WNT/ β -catenin signaling is spatially distinct with increased activation of WNT/ β -catenin signaling in the papillary dermis compared with the reticular dermis. In contrast to healthy skin, the activation of WNT/ β -catenin signaling is exaggerated throughout the dermis in involved skin of patients with SSc, and the gradient of WNT/ β -catenin activation between the papillary and the reticular dermis is lost. This is paralleled by a reticular skin phenotype in SSc with reduced number, size, and height of dermal papillae and the predominance of a reticular gene expression profile. Of note, PI16+ fibroblasts show a particular enrichment for both reticular marker genes and genes related to the regulation of WNT/ β -catenin signaling and they are spatially enriched in the papillary dermis in SSc. These results suggest that PI16+ fibroblasts might contribute to the disruption of the skin layers in SSc.

Our findings could have potential implications for future therapeutic approaches. Dermal papillae contain sensitive skin

structures including vessels, nerve endings, mechanosensory corpuscles, hair bulbs, and skin adnexa. In addition, dermal papillae increase the skin surface and have a function in mechanotransduction themselves. Loss of the dermal papillae during fibrotic skin remodeling in SSc is thus not only associated with disrupted skin anatomy but also skin malfunction. Current state-of-the-art medications used to treat skin fibrosis mostly aim at reduction of progression of the fibrotic disease burden. Beyond that, future therapeutic approaches could aim at restoration of the normal skin structure in patients with SSc. This is further supported by a short-term clinical trial that showed that a topical WNT/ β -catenin inhibitor could promote fat tissue regeneration in SSc skin,³⁸ suggesting that local targeting of WNT/ β -catenin signaling may help to recover aspects of the physiologic tissue structure. The identification of dysregulated fibroblast populations that could specifically be targeted, whereas physiologic populations that remain unaffected might contribute to this approach. Based on our results, targeting PI16+ positive fibroblasts could be an interesting target; however, further functional experiments to better characterize this population would need to be performed as discussed in the following paragraph. Moreover, our results underline that the delicate balance of spatially distinct pathway modulation might be considered for restoring skin integrity in fibrosis disorders.

Our study has limitations. The human papillary skin structure is not sufficiently reflected in rodent skin models and advanced in vitro models showing a papillary dermis structure are not available at the time of the submission. Thus, functional experiments are limited and further studies to model the adult human dermal structure are needed to substantiate our findings.

ACKNOWLEDGMENT

Open Access funding enabled and organized by Projekt DEAL.

AUTHOR CONTRIBUTIONS

All authors contributed to at least one of the following manuscript preparation roles: conceptualization AND/OR methodology, software, investigation, formal analysis, data curation, visualization, and validation AND drafting or reviewing/editing the final draft. As corresponding author, Dr Bergmann confirms that all authors have provided the final approval of the version to be published, and takes responsibility for the affirmations regarding article submission (eg, not under consideration by another journal), the integrity of the data presented, and the statements regarding compliance with institutional review board/Declaration of Helsinki requirements.

REFERENCES

- Gabrielli A, Avvedimento EV, Krieg T. Scleroderma. *N Engl J Med* 2009;360:1989–2003.
- Decuman S, Smith V, Verhaeghe ST, Van Hecke A, De Keyser F. Work participation in patients with systemic sclerosis: a systematic review. *Clin Exp Rheumatol* 2014;32(6 suppl 86):S-206–S-213.
- Wu W, Jordan S, Graf N, et al; EUSTAR Collaborators. Progressive skin fibrosis is associated with a decline in lung function and worse survival in patients with diffuse cutaneous systemic sclerosis in the European Scleroderma Trials and Research (EUSTAR) cohort. *Ann Rheum Dis* 2019;78:648–656.
- Dyring-Andersen B, Løvendorf MB, Coscia F, et al. Spatially and cell-type resolved quantitative proteomic atlas of healthy human skin. *Nat Commun* 2020;11:5587.
- Kanidakis J. Anatomy, histology and immunohistochemistry of normal human skin. *Eur J Dermatol* 2002;12:390–399.
- Varga J, Abraham D. Systemic sclerosis: a prototypic multisystem fibrotic disorder. *J Clin Invest* 2007;117:557–567.
- Van Praet JT, Smith V, Haspelslagh M, Degryse N, Elewaut D, De Keyser F. Histopathological cutaneous alterations in systemic sclerosis: a clinicopathological study. *Arthritis Res Ther* 2011;13:R35.
- Montgomery H, O'Leary PA, Ragsdale WE, Jr. Dermatohistopathology of various types of scleroderma. *AMA Arch Derm* 1957;75:78–87.
- Matos I, Asare A, Levorse J, et al. Progenitors oppositely polarize WNT activators and inhibitors to orchestrate tissue development. *eLife* 2020;9:9.
- Akhmetshina A, Palumbo K, Dees C, et al. Activation of canonical Wnt signalling is required for TGF- β -mediated fibrosis. *Nat Commun* 2012;3:735.
- Beyer C, Reichert H, Akan H, et al. Blockade of canonical Wnt signalling ameliorates experimental dermal fibrosis. *Ann Rheum Dis* 2013;72:1255–1258.
- Beyer C, Schramm A, Akhmetshina A, et al. β -catenin is a central mediator of pro-fibrotic Wnt signaling in systemic sclerosis. *Ann Rheum Dis* 2012;71:761–767.
- Daoussis D, Tsamandas A, Antonopoulos I, et al. B cell depletion therapy upregulates Dkk-1 skin expression in patients with systemic sclerosis: association with enhanced resolution of skin fibrosis. *Arthritis Res Ther* 2016;18:118.
- Dees C, Schlottmann I, Funke R, et al. The Wnt antagonists DKK1 and SFRP1 are downregulated by promoter hypermethylation in systemic sclerosis. *Ann Rheum Dis* 2014;73:1232–1239.
- Wei J, Fang F, Lam AP, et al. Wnt/ β -catenin signaling is hyperactivated in systemic sclerosis and induces Smad-dependent fibrotic responses in mesenchymal cells. *Arthritis Rheum* 2012;64:2734–2745.
- LeRoy EC, Black C, Fleischmajer R, et al. Scleroderma (systemic sclerosis): classification, subsets and pathogenesis. *J Rheumatol* 1988;15:202–205.
- Bergmann C, Hallenberger L, Chenguiti Fakhouri S, et al. X-linked inhibitor of apoptosis protein (XIAP) inhibition in systemic sclerosis (SSc). *Ann Rheum Dis* 2021;80:1048–1056.
- Bergmann C, Brandt A, Merlevede B, et al. The histone demethylase Jumonji domain-containing protein 3 (JMJD3) regulates fibroblast activation in systemic sclerosis. *Ann Rheum Dis* 2018;77:150–158.
- Zehender A, Li YN, Lin NY, et al. TGF β promotes fibrosis by MYST1-dependent epigenetic regulation of autophagy. *Nat Commun* 2021;12:4404.
- Dees C, Pötter S, Zhang Y, et al. TGF- β -induced epigenetic deregulation of SOCS3 facilitates STAT3 signaling to promote fibrosis. *J Clin Invest* 2020;130:2347–2363.
- Ashhurst TM, Marsh-Wakefield F, Putri GH, et al. Integration, exploration, and analysis of high-dimensional single-cell cytometry data using Spectre. *Cytometry A* 2022;101:237–253.
- Eling N, Damond N, Hoch T, Bodenmiller B. Cytomapper: an R/Bioconductor package for visualization of highly multiplexed imaging data. *Bioinformatics* 2020;36:5706–5708.
- Györfi AH, Matei AE, Fuchs M, et al. Engrailed 1 coordinates cytoskeletal reorganization to induce myofibroblast differentiation. *J Exp Med* 2021;218:e20201916.

24. Solé-Boldo L, Raddatz G, Schütz S, et al. Single-cell transcriptomes of the human skin reveal age-related loss of fibroblast priming. *Commun Biol* 2020;3:188.
25. Skaug B, Khanna D, Swindell WR, et al. Global skin gene expression analysis of early diffuse cutaneous systemic sclerosis shows a prominent innate and adaptive inflammatory profile. *Ann Rheum Dis* 2020;79:379–386.
26. Assassi S, Sharif R, Lasky RE, et al; GENISOS Study Group. Predictors of interstitial lung disease in early systemic sclerosis: a prospective longitudinal study of the GENISOS cohort. *Arthritis Res Ther* 2010;12:R166.
27. Tabib T, Huang M, Morse N, et al. Myofibroblast transcriptome indicates SFRP2^{hi} fibroblast progenitors in systemic sclerosis skin. *Nat Commun* 2021;12:4384.
28. Zhu H, Luo H, Skaug B, et al. Fibroblast subpopulations in systemic sclerosis: functional implications of individual subpopulations and correlations with clinical features. *J Invest Dermatol* 2024;144:1251–1261.e13.
29. Fuchs E. Keratins and the skin. *Annu Rev Cell Dev Biol* 1995;11:123–153.
30. Wei J, Melichian D, Komura K, et al. Canonical Wnt signaling induces skin fibrosis and subcutaneous lipodystrophy: a novel mouse model for scleroderma? *Arthritis Rheum* 2011;63:1707–1717.
31. Ramakrishnan AB, Cadigan KM. Wnt target genes and where to find them. *F1000Res* 2017;6:746.
32. MacDonald BT, Tamai K, He X. Wnt/beta-catenin signaling: components, mechanisms, and diseases. *Dev Cell* 2009;17:9–26.
33. Nusse R, Clevers H. Wnt/beta-catenin signaling, disease, and emerging therapeutic modalities. *Cell* 2017;169:985–999.
34. Bergmann C, Distler JH. Canonical Wnt signaling in systemic sclerosis. *Lab Invest* 2016;96:151–155.
35. Dees C, Distler JH. Canonical Wnt signalling as a key regulator of fibrogenesis - implications for targeted therapies? *Exp Dermatol* 2013;22:710–713.
36. Henderson J, Pryzborski S, Stratton R, O'Reilly S. Wnt antagonist DKK-1 levels in systemic sclerosis are lower in skin but not in blood and are regulated by microRNA33a-3p. *Exp Dermatol* 2021;30:162–168.
37. Korosec A, Frech S, Gesslbauer B, et al. Lineage identity and location within the dermis determine the function of papillary and reticular fibroblasts in human skin. *J Invest Dermatol* 2019;139:342–351.
38. Lafyatis R, Mantero JC, Gordon J, et al. Inhibition of β -catenin signaling in the skin rescues cutaneous adipogenesis in systemic sclerosis: a randomized, double-blind, placebo-controlled trial of C-82. *J Invest Dermatol* 2017;137:2473–2483.

Genetic Architecture of Idiopathic Inflammatory Myopathies From Meta-Analyses

Catherine Zhu,¹ ID Younghun Han,¹ ID Jinyoung Byun,¹ ID Xiangjun Xiao,¹ Simon Rothwell,² ID Frederick W. Miller,³ ID Ingrid E. Lundberg,⁴ ID Peter K. Gregersen,⁵ ID Jiri Vencovsky,⁶ ID Vikram R. Shaw,¹ ID Neil McHugh,⁷ ID Vidya Limaye,⁸ ID Albert Selva-O'Callaghan,⁹ ID Michael G. Hanna,¹⁰ ID Pedro M. Machado,¹⁰ ID Lauren M. Pachman,¹¹ ID Ann M. Reed,¹² ID Lisa G. Rider,³ ID Øyvind Molberg,¹³ ID Olivier Benveniste,¹⁴ ID Timothy Radstake,¹⁵ ID Andrea Doria,¹⁶ ID Jan L. De Bleecker,¹⁷ ID Boel De Paepe,¹⁷ ID Britta Maurer,¹⁸ ID William E. Ollier,¹⁹ ID Leonid Padyukov,⁴ ID Lucy R. Wedderburn,²⁰ ID Hector Chinoy,²¹ ID Janine A. Lamb,² ID and Christopher I. Amos,¹ ID for the Myositis Genetics Consortium

Objective. Idiopathic inflammatory myopathies (IIMs, myositis) are rare systemic autoimmune disorders that lead to muscle inflammation, weakness, and extramuscular manifestations, with a strong genetic component influencing disease development and progression. Previous genome-wide association studies identified loci associated with IIMs. In this study, we imputed data from two prior genome-wide myositis studies and analyzed the largest myositis data set to date to identify novel risk loci and susceptibility genes associated with IIMs and its clinical subtypes.

Methods. We performed association analyses on 14,903 individuals (3,206 patients and 11,697 controls) with genotypes and imputed data from the Trans-Omics for Precision Medicine reference panel. Fine-mapping and expression quantitative trait locus colocalization analyses in myositis-relevant tissues indicated potential causal variants. Functional annotation and network analyses using the random walk with restart (RWR) algorithm explored underlying genetic networks and drug repurposing opportunities.

Results. Our analyses identified novel risk loci and susceptibility genes, such as *FCRLA*, *NFKB1*, *IRF4*, *DCAKD*, and *ATXN2* in overall IIMs; *NEMP2* in polymyositis; *ACBC11* in dermatomyositis; and *PSD3* in myositis with anti-histidyl-transfer RNA synthetase autoantibodies (anti-Jo-1). We also characterized effects of HLA region variants and the role of *C4*. Colocalization analyses suggested putative causal variants in *DCAKD* in skin and muscle, *HCP5* in lung, and *IRF4* in Epstein-Barr virus (EBV)-transformed lymphocytes, lung, and whole blood. RWR further prioritized additional candidate genes, including *APP*, *CD74*, *CIITA*, *NR1H4*, and *TXNIP*, for future investigation.

Conclusion. Our study uncovers novel genetic regions contributing to IIMs, advancing our understanding of myositis pathogenesis and offering new insights for future research.

INTRODUCTION

Idiopathic inflammatory myopathies (IIMs), characterized by chronic muscle weakness and muscle inflammation, are rare

heterogeneous autoimmune diseases.^{1,2} The underlying pathogenesis of myositis involves genetic components, which increase susceptibility to environmental insults and can confer an elevated risk of the disease.³

The opinions and assertions contained herein are those of the authors and do not necessarily represent those of the NIHR or the Department of Health and Social Care.

Partially supported by the Training in Precision Environmental Health Sciences Training Program (fellowship T32-ES-027801). This research was supported in part by the Intramural Research Program of the NIH. This research was supported by the NIHR Manchester Biomedical Research Centre (grant 203308), the NIHR Great Ormond Street Hospital Biomedical Research Centre (grant 18474), Myositis UK (grant 20380), Great Ormond Street Children's Charity (grant 20164), Versus Arthritis (grant 21593), and Medical Research Council (grant MR/n003322/1). Dr Lundberg's work was supported by the Swedish Research Council (grant 2020-01378), Region Stockholm Avtal om Läkarutbildning och Forskning (ALF project), the Swedish Rheumatism Association, and the King Gustaf V 80 Year Foundation. Dr Vencovsky's work was supported by the Czech Ministry of Health 00023728

(Institute of Rheumatology). Drs Han, Byun, Amos, and Wedderburn's work was supported by The Cure JM Foundation.

¹Catherine Zhu, MS, Younghun Han, PhD, Jinyoung Byun, PhD, Xiangjun Xiao, PhD, Vikram R. Shaw, MS, Christopher I. Amos, PhD: Baylor College of Medicine, Houston, Texas; ²Simon Rothwell, PhD, Janine A. Lamb, PhD: The University of Manchester, Manchester, United Kingdom; ³Frederick W. Miller MD, PhD, Lisa G. Rider, MD: National Institute of Environmental Health Sciences, NIH, Bethesda, Maryland; ⁴Ingrid E. Lundberg, MD, PhD, Leonid Padyukov MD, PhD: Karolinska Institutet and Karolinska University Hospital, Stockholm, Sweden; ⁵Peter K. Gregersen, MD: The Feinstein Institute, Manhasset, New York; ⁶Jiri Vencovsky, MD, DSc: Charles University, Prague, Czech Republic; ⁷Neil McHugh, MD: University of Bath, Bath, United Kingdom; ⁸Vidya Limaye, PhD: University of Adelaide, Adelaide, South Australia, Australia; ⁹Albert Selva-O'Callaghan, MD, PhD: Universitat Autònoma de Barcelona, Barcelona, Spain; ¹⁰Michael G. Hanna, MD, Pedro

Genome-wide association studies (GWAS) have emerged as powerful tools for elucidating the genetic basis of complex conditions, including myositis. Recent GWAS investigations have highlighted the involvement of genetic variants within the HLA region, contributing to the risk of myositis.⁴ Several alleles included in the 8.1 extended haplotype, which encompasses loci in class I, II, and III regions, have been associated not only with increased susceptibility to IIMs but also with other autoimmune disorders, such as rheumatoid arthritis, systemic lupus erythematosus, and Hashimoto thyroiditis in populations of European ancestry. Furthermore, variants in non-HLA loci, such as *PTPN22*, *STAT4*,⁵ *SDK2*, *LINC00924*, *NAB1*,⁶ and *C4A* deficiency,^{7,8} have been implicated in the pathogenesis of myositis; however, the lower number of patients and controls available in previous studies has limited novel discoveries and our ability to gain a comprehensive understanding of the genetic architecture of myositis.

To address these limitations and enhance our understanding of the underlying pathogenesis of myositis, we conducted meta-analyses, which combined two studies providing a total of 14,903 individuals of European descent, including 3,206 patients with myositis and 11,697 healthy controls. By integrating data from multiple cohorts, we confirmed known signals and discovered 10 novel associations for myositis and its clinical subtypes. Additional analysis with the complement *C4* system provided insights into the relative impacts of *HLA* and *C4* genes on disease susceptibility. Fine-mapping and expression quantitative trait locus (eQTL) colocalization suggested specific disease-associated genetic variants within the identified risk loci, highlighting their role in gene expression modulation in myositis-related tissues. We also constructed multiplex networks based on biologic pathways of susceptibility markers to explore potential risk candidate genes by using a random walk with restart (RWR) algorithm, which provided insights for hypothesis generation in future myositis research and offered potential avenues for targeted therapies and precision medicine approaches.

MATERIALS AND METHODS

Study populations. Samples from the Immunochip data set⁵ (7,486 controls, 2,688 patients) and an earlier GWAS

data set⁴ (4,712 controls, 1,710 patients) were obtained from the Myositis Genetics Consortium (MYOGEN).^{4–6} Subtypes of patients included in the overall analyses of the IIM group (total IIMs) were polymyositis (PM), dermatomyositis (DM), juvenile polymyositis, juvenile dermatomyositis (JDM), antisynthetase syndrome, inclusion body myositis (IBM), and necrotizing myopathy. Patients were selected based on the classification criteria in the previous studies.^{4–8} Analyses were performed on clinical subtypes comprising PM, DM, JDM, and myositis with anti-histidyl-transfer RNA synthetase autoantibodies (anti-Jo-1), which made up the largest numbers of subsets of patients.

Genotyping, quality control, and imputation. For each data set, samples without clinical information or misdiagnoses were excluded. The genotyping data were converted to GRCh38 positions using University of California, Santa Cruz's (UCSC) liftOver tool. Chromosome X was excluded from the analyses because of its absence in the GWAS data set. Single-nucleotide polymorphisms (SNPs) with a call rate <95% were removed. Individuals with >5% missing genotypes were excluded. Variants deviating from Hardy–Weinberg equilibrium (HWE) in controls ($P < 10^{-6}$) and in patients ($P < 10^{-10}$) were removed before imputation. Relatedness was checked using the KING-robust kinship estimator.⁹ Duplicates or related individuals (kinship > 0.12) within each data set were excluded to reduce correlations among participants. Principal components analysis (PCA) in the GWAS data set was performed using PLINK 1.9.¹⁰ In the Immunochip data set, PCA was calculated using ancestry inference using PCA and spatial analysis¹¹ based on the HapMap III reference panel (Supplementary Information). Outliers identified based on the PCA were removed from further analyses (Figures S1 and S2). In the meta-analyses, for closely related individuals between data sets (kinship > 0.15) and any duplicates between the two data sets, the data from the Immunochip data set were retained (Figure S1).

To expand the coverage of our investigation, genotypes from the arrays were imputed separately against the Trans-Omics for Precision Medicine reference panel.¹² SNPs located within 28 to 34 Mb on chromosome 6 were selected for HLA imputation against the multiethnic HLA reference panel (version 2.0 2022).¹³ Variants with imputation quality $r^2 < 0.6$, minor allele frequency

M. Machado, MD, PhD: University College London, London, United Kingdom; ¹¹Lauren M. Pachman, MD: Ann & Robert H. Lurie Children's Hospital of Chicago and Northwestern University Feinberg School of Medicine, Chicago, Illinois; ¹²Ann M. Reed, MD: Duke University, Durham, North Carolina; ¹³Øyvind Molberg, MD: Oslo University Hospital, Oslo, Norway; ¹⁴Olivier Benveniste, MD: Sorbonne Université, AP-HP, Myology Research Center UMR974, Pitié-Salpêtrière Hospital, Paris, France; ¹⁵Timothy Radstake, MD, PhD: University Medical Center Utrecht, Utrecht, The Netherlands; ¹⁶Andrea Doria, MD: University of Padova, Padova, Italy; ¹⁷Jan L. De Bleecker, MD, PhD, Boel De Paepe, PhD: Ghent University, Ghent, Belgium; ¹⁸Britta Maurer, MD: University Hospital, Bern, Switzerland; ¹⁹William E. Ollier, PhD: Manchester Metropolitan University, Manchester, United Kingdom; ²⁰Lucy R. Wedderburn, PhD: NIHR Biomedical Research Centre at Great Ormond Street Hospital, Centre for Adolescent Rheumatology Versus Arthritis, and University College London,

London, United Kingdom; ²¹Hector Chinoy, MD, PhD: NIHR Manchester Biomedical Research Centre, Manchester University NHS Foundation Trust and The University of Manchester, Manchester, United Kingdom, and Salford Royal Hospital, Northern Care Alliance NHS Foundation Trust and Manchester Academic Health Science Centre, Salford, United Kingdom.

Additional supplementary information cited in this article can be found online in the Supporting Information section (<https://acrjournals.onlinelibrary.wiley.com/doi/10.1002/art.43088>).

Author disclosures are available at <https://onlinelibrary.wiley.com/doi/10.1002/art.43088>.

Address correspondence via email to Catherine Zhu, MS, at catheriz@bcm.edu; Christopher Amos, Ph.D. at ciamos@salud.unm.edu

Submitted for publication March 12, 2024; accepted in revised form October 23, 2024.

(MAF) < 0.005, and postimputation HWE $P < 10^{-6}$ in controls were excluded from further analyses. C4 alleles were imputed against the European population from HapMap III, according to the impute4 protocol.¹⁴ The Supplementary Information provides further detail on data processing.

Statistical analyses. Association analyses were conducted on genotyped and imputed data from both controls and myositis patients, including the total myositis ($n=3,206$ patients); DM ($n = 1,131$ patients), JDM ($n = 645$ patients), PM ($n = 1,094$ patients) subtypes, and myositis with anti-Jo-1 ($n = 388$ patients) using SNPTTEST 2.5.6¹⁵ (-method expected), with adjustments for population variation based on the PCAs as described in the Supplementary Information. Inverse-variance fixed-effects meta-analyses and sex-stratified analyses for the total IIMs and subtypes were then performed using METASOFT.¹⁶ To identify independent and secondary signals, we implemented stepwise conditional and joint association (COJO) analyses using GCTA v1.94.¹⁷ Interaction analyses were performed to assess potential differences by sex and across subtypes, including PM, DM, and JDM. In the HLA region, meta-analyses were conducted on the genotyped and imputed HLA data. Additionally, C4 association analyses, along with COJO analyses of both C4 and HLA variants, were performed using R. Model details and parameters are provided in the Supplementary Information.

Fine-mapping and colocalization analyses. susieR is a Bayesian approach that evaluates multiple causal signals in a region simultaneously based on the Sum of Single Effects (SuSiE) regression framework. We identified 95% credible sets within the non-HLA region and 99% credible sets for the HLA region and subsequently computed the posterior inclusion probability (SNP.PIP) of causality. The colocalization analyses of meta-analyzed data and eQTL studies were performed using the coloc 5.2.1 R package.¹⁸ We selected eQTL studies of five myositis-associated tissue types from the Genotype-Tissue Expression v8,¹⁹ including Epstein-Barr virus (EBV)-transformed lymphocytes ($n = 147$), skin without sun exposure ($n = 517$), whole blood ($n = 670$), lung ($n = 515$), and skeletal muscle ($n = 706$) for 32 myositis-associated SNP signals. Specifically, we studied 60 analyses for the total IIM group, 25 for the PM group, 35 for the DM group, 15 for the JDM group, and 25 for the anti-Jo-1 group. Colocalization in specific tissue was considered when the posterior probability of shared causal variants in meta-analyzed myositis data and tissue-specific eQTL (PP.H4) exceeded 80%, with the identified variants residing in 90% credible sets. Details of the fine-mapping and colocalization analyses are described in the Supplementary Information.

Annotation and enrichment analyses. Significantly associated variants were annotated using ANNOVAR²⁰ based on the GRCh38 UCSC refGene and FAVOR.²¹ For intergenic variants, their corresponding nearest upstream and/or downstream

genes were reported. The RegulomeDB 2.2^{22,23} was used to annotate variants and assess potential regulatory impact. This database integrates information such as histone sequencing, DNase hypersensitivity footprints, transcription factor chromatin immunoprecipitation followed by sequencing (ChIP-seq), chromatin accessibility, and position weight matrix information (motif) to assign probability scores and rank the variants based on their likelihood of regulatory significance. The Gene Set Analysis Toolkit (WebGestaltR)²⁴ was used to perform functional enrichment. We report the results with false discovery rate (FDR) < 0.05.

RWR on multiplex networks. *RWR algorithm.* Network propagation has been widely applied in genetic analyses to prioritize potential genes based on biologic networks of risk markers.²⁵ RWR is a network propagation algorithm in which an iterative stimulate starts from seed nodes and traverses the network with a probability to move to adjacent nodes or back to the seed nodes. Upon reaching convergence, nodes are ranked based on their level of connection to the seed nodes (rank scores). Nodes with higher rank scores indicate stronger connections, suggesting their importance in the disease-related networks. In our study, genes or proteins represent nodes, and biologic interactions denote edges. We adapted the RWR algorithm on multiplex networks,²⁶ with the modifications detailed in the Supplementary Information. Disease genes reached suggestive significant threshold ($P = 1 \times 10^{-5}$) from the COJO analyses served as seed nodes, with $-\log_{10}(P)$ as the initial score. We used the default settings for the transition probability δ , the restart probability $1-\alpha$, and the restart probability of a given layer t . Multiplex network patterns were evaluated by permutation test. We reported the top 50 candidates with $P < 0.05$.

Construction of multiplex network. For the total IIMs and each clinical subgroup, we built their corresponding multiplex networks. Each layer of the multiplex network was composed of genes or proteins from the protein-protein interaction network, pathways from the KEGG databases, and coexpression RNA sequencing data. The multiplex network details are available in the Supplementary Information.

Data and code availability. The data, housed at Baylor College of Medicine, are part of the MYOGEN consortium and are available for collaboration through the network. Software, packages, and code used for the study can be found in the Supplementary Information.

RESULTS

The heritability of IIMs was estimated at 25% excluding the major histocompatibility complex (MHC) region and 59% when including it based on meta-analyzed GWAS and ImmunoChip data. This indicates a significant genetic component for myositis. To identify genetic risk factors, we performed analyses on total myositis and clinical subtypes, as detailed in Figure 1.

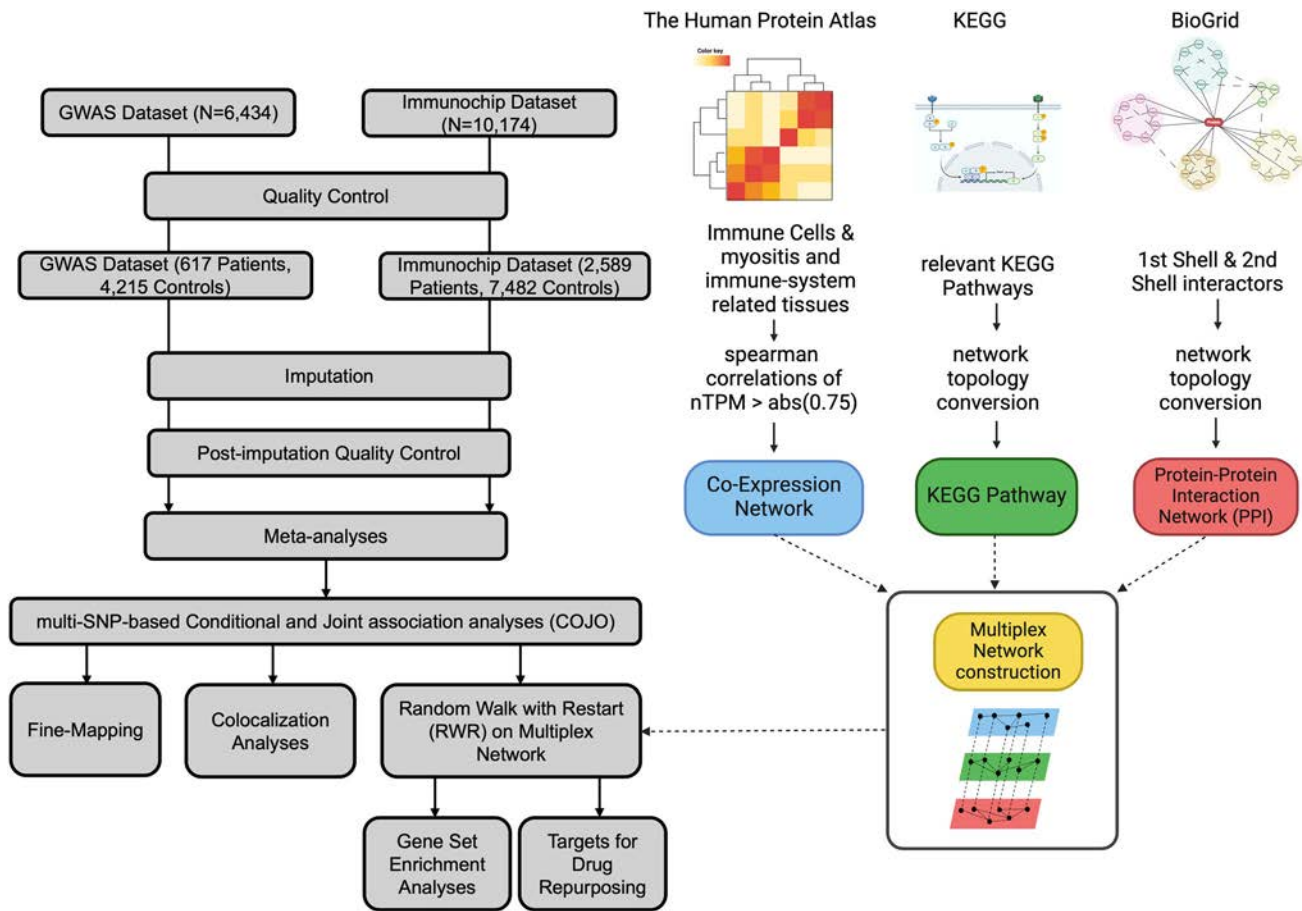


Figure 1. Overview of the study. Genotypes from GWAS and ImmunoChIP data sets are imputed after quality control. Meta-analyses are performed. Independent lead variants are then identified using multi-SNP-based COJO analyses on the results of meta-analyses. We also investigate credible sets of causal variants and prioritize additional candidate genes via RWR on multiplex networks. Each multiplex network integrates three different biological networks, including coexpression, KEGG pathway, and PPI. Leveraging the results of COJO analyses and RWR, we perform gene set enrichment analyses and explore potential drug repurposing opportunities. The figure was created with BioRender. GWAS, genome-wide association studies; nTPM, normalized transcripts per million; SNP, single-nucleotide polymorphism.

Novel risk loci in myositis and subtypes identified by meta-analyses.

We conducted meta-analyses for the total IIMs and subtypes to identify genome-wide significant signals. Many significant signals within risk loci are highly correlated because of linkage disequilibrium (LD), which complicates causal inference and functional interpretation. To elucidate the genetic pattern between correlated signals and distinguish independent variants that contribute to myositis, we employed a stepwise model that executed iterative COJO analyses. This approach captured the combined effects of multiple conditionally independent variants within a risk locus and allowed discoveries of additional novel variants (detail in Supplementary Information).

Our analyses showed that the majority of genome-wide significant signals ($P < 5 \times 10^{-8}$) are within the HLA region, confirming that HLA alleles are the strongest genetic risk factors for overall IIM and its subtypes. In addition, we identified several significant associations outside the HLA region (Figure 2, Table 1, Table S1).

In the total IIMs (Figure 2A), an intergenic variant near *HLA-DRB1/HLA-DQA1* (rs535777, $P = 3.78 \times 10^{-106}$, odds ratio [OR] 2.327) was the most significant signal within the HLA (Figures S3A and S4G). Outside the HLA region, we discovered novel variants within the total IIMs group and its subtypes and confirmed previously reported associations. *STAT4* (rs4853540, $P = 5.93 \times 10^{-9}$, OR 0.808) showed higher significance in our analysis compared to previous studies (Figure 3B and Figure S4B). We also identified a novel intronic locus in *NFKB1* (rs230514, $P = 3.86 \times 10^{-8}$, OR 1.185) (Figure 3C and Figure S4C). An independent signal rs12203592 in *IRF4* outside the HLA region on chromosome 6 was significant for total IIMs ($P = 8.41 \times 10^{-18}$, OR 1.439) (Figure 3D and Figure S4D). Several novel variants in the noncoding region showed genome-wide significant associations with myositis, including signals near *GJA1* and *HSF2* (rs7754730, $P = 1.47 \times 10^{-9}$, OR 1.189), *PINX1* (rs113538396, $P = 1.57 \times 10^{-10}$, OR 3.081), *ATXN2* (rs35350651, $P = 3.30 \times 10^{-9}$, OR 0.843), and *DCAKD*

Table 1. Conditionally independent variants that reach the genome-wide significance threshold from COJO analyses in the total IIMs, IIM subtypes, and myositis with anti-Jo-1 antibodies*

Group	Nearest gene	Lead SNP	CHR:POS	Function	Minor allele	Meta-analysis			Joint analysis				
						MAF	Effect size of minor alleles	SE of effect size	P	OR	Effect size	OR	P
Total IIMs	FCRLA (dist = 5024) ^a	rs6668534	1:161702205	intergenic	G	0.234	-0.192	0.035	5.39 × 10 ⁻⁸	0.826	-0.192	0.035	5.53 × 10 ⁻⁸
	STAT4	rs4853540	2:191052591	intronic	T	0.222	-0.213	0.037	5.93 × 10 ⁻⁹	0.808	-0.213	0.808	6.13 × 10 ⁻⁹
	NFKB1 ^a	rs230514	4:102550782	intronic	G	0.353	0.169	0.031	3.86 × 10 ⁻⁸	1.185	0.169	1.185	3.96 × 10 ⁻⁸
	IRF4 ^a	rs12203592	6:396321	intronic	T	0.157	0.364	0.042	8.41 × 10 ⁻¹⁸	1.439	0.364	1.439	9.97 × 10 ⁻¹⁸
	LINC01149 (dist = 5050); HCP5 (dist = 11157)	rs2516457	6:31452023	intergenic	A	0.466	-0.428	0.029	1.05 × 10 ⁻⁴⁷	0.652	-0.272	0.762	6.15 × 10 ⁻¹⁹
	TSBP1-AS1	rs1980496	6:32372293	ncRNA _{intronic}	T	0.398	0.397	0.030	2.71 × 10 ⁻⁴⁰	1.487	0.201	1.223	5.36 × 10 ⁻¹⁰
	HLA-DRB1 (dist = 20020); HLA-DQA1 (dist = 27550)	rs535777	6:32609856	intergenic	C	0.154	0.845	0.039	3.78 × 10 ⁻¹⁰⁶	2.327	0.691	1.996	2.89 × 10 ⁻⁵⁹
	HLA-DRB1 (dist = 37244); HLA-DQA1 (dist = 10322)	rs147774179	6:32627079	intergenic	G	0.049	0.313	0.060	1.83 × 10 ⁻⁷	1.367	0.448	1.565	1.50 × 10 ⁻¹³
	GJA1 (dist = 225016); HSF2 (dist = 724808)	rs7754730	6:121674743	intergenic	C	0.385	0.173	0.030	4.68 × 10 ⁻⁹	1.189	0.173	1.189	4.83 × 10 ⁻⁹
	PINX1 ^a	rs113538396	8:10777742	intronic	A	0.007	1.125	0.176	1.57 × 10 ⁻¹⁰	3.081	1.125	3.081	1.64 × 10 ⁻¹⁰
PM	ATXN2	rs35350651	12:111469627	intronic	AC	0.485	-0.171	0.029	3.30 × 10 ⁻⁹	0.843	-0.171	0.843	3.41 × 10 ⁻⁹
	DCAKD ^a	rs9898793	17:45038945	intronic	T	0.241	0.225	0.037	1.65 × 10 ⁻⁹	1.252	0.225	1.252	1.73 × 10 ⁻⁹
	PITPN2	rs2476601	1:113834946	exonic	A	0.101	0.407	0.066	5.70 × 10 ⁻¹⁰	1.503	0.407	1.503	5.90 × 10 ⁻¹⁰
	NEMP2 ^a	rs74925618	2:190513057	intronic	C	0.066	0.59	0.101	4.52 × 10 ⁻⁹	1.804	0.59	1.804	4.72 × 10 ⁻⁹
	PSORS1C3 (dist = 1826); HCG27 (dist = 9617)	rs28360059	6:31188143	intergenic	A	0.163	-0.573	0.072	1.63 × 10 ⁻¹⁵	0.564	-0.403	0.668	3.03 × 10 ⁻⁸
	MICA (dist = 25237); LINC01149 (dist = 1115)	rs3132473	6:31440552	intergenic	A	0.132	1.02	0.059	6.88 × 10 ⁻⁶⁸	2.772	0.893	2.443	6.79 × 10 ⁻⁴⁹
	HLA-DQB1 (dist = 2299); HLA-DQA2 (dist = 72435)	rs3135000	6:32668956	intergenic	A	0.472	0.496	0.046	1.41 × 10 ⁻²⁶	1.642	0.318	1.374	3.50 × 10 ⁻¹¹
	ABCB11 ^a	rs145940036	2:169006750	intronic	A	0.007	1.154	0.212	4.91 × 10 ⁻⁸	3.172	1.154	3.172	5.00 × 10 ⁻⁸
	IRF4 ^a	rs12203592	6:396321	intronic	T	0.154	0.386	0.064	1.69 × 10 ⁻⁹	1.471	0.386	1.471	1.77 × 10 ⁻⁹
	LINC01149 (dist = 5050); HCP5 (dist = 11157)	rs2516457	6:31452023	intergenic	A	0.476	-0.432	0.045	1.62 × 10 ⁻²¹	0.649	-0.286	0.752	1.86 × 10 ⁻⁹
DM	HCP5 (dist = 3152); HCG26 (dist = 2268)	rs3131617	6:31468961	intergenic	T	0.128	0.835	0.060	1.56 × 10 ⁻⁴⁴	2.306	0.556	1.743	2.74 × 10 ⁻¹⁷
	HLA-DRB5 (dist = 19601); HLA-DRB6 (dist = 2816)	rs371760589	6:32549887	intergenic	G	0.017	0.637	0.127	4.95 × 10 ⁻⁷	1.892	0.765	2.149	1.91 × 10 ⁻⁹
	HLA-DQB1	rs9274258	6:32663671	intronic	G	0.41	0.567	0.045	1.99 × 10 ⁻³⁶	1.762	0.451	1.57	2.64 × 10 ⁻²¹
	PINX1 ^a	rs113538396	8:10777742	intronic	A	0.006	1.353	0.232	5.22 × 10 ⁻⁹	3.868	1.353	3.868	5.35 × 10 ⁻⁹
	IRF4 ^a	rs12203592	6:396321	intronic	T	0.155	0.456	0.080	9.58 × 10 ⁻⁹	1.578	0.456	1.578	9.93 × 10 ⁻⁹
	HLA-DRA (dist = 20244); HLA-DRB5 (dist = 52063)	rs9268926	6:32465290	intergenic	G	0.191	0.273	0.068	6.72 × 10 ⁻⁵	1.314	0.403	1.496	7.90 × 10 ⁻⁹
	HLA-DRB5 (dist = 4802); HLA-DRB6 (dist = 17624)	rs1894553	6:32535089	intergenic	A	0.131	0.639	0.073	2.24 × 10 ⁻¹⁸	1.894	0.721	2.058	3.84 × 10 ⁻²²

(Continued)

Table 1. (Cont'd)

Group	Nearest gene	Lead SNP	CHR:POS	Function	Minor allele	Meta-analysis				Joint analysis		
						MAF	Effect size of minor alleles	SE of effect size	P	OR	Effect size	P
anti-Jo-1	HCP5 (dist = 205)	rs3132090	6:31462975	upstream	A	0.128	1.73	0.089	1.75×10^{-84}	5.643	1.017	1.99×10^{-20}
	HLA-DRA (dist = 8250);	rs9268791	6:32453296	intergenic	T	0.379	1.056	0.080	2.10×10^{-39}	2.874	0.916	6.26×10^{-24}
	HLA-DRB5 (dist = 64057)											
	HLA-DQA1 (dist = 14581); HLA-DQB1 (dist = 1205)	rs4713570	6:32658263	intergenic	T	0.258	0.967	0.076	1.65×10^{-37}	2.630	0.541	3.90×10^{-10}
	HLA-DQB1 (dist = 753)	rs9273370	6:32658715	downstream	G	0.408	-0.56	0.080	3.27×10^{-12}	0.571	-0.728	1.94×10^{-16}
	PSD3 ^a	rs6991531	8:18883152	intronic	C	0.012	1.442	0.247	5.01×10^{-9}	4.229	1.442	5.11×10^{-9}

* CHR:POS, chromosome and position in hg38; dist, distance; DM, dermatomyositis; IIMs, idiopathic inflammatory myopathies; JDM, juvenile dermatomyositis; MAF, minor allele frequency in combined patients and controls; ncRNA, non-coding RNA; OR, odds ratio; PM, polymyositis; SNP, single-nucleotide polymorphism.

^a Novel association outside HLA.

⁺ Near the genome-wide significance

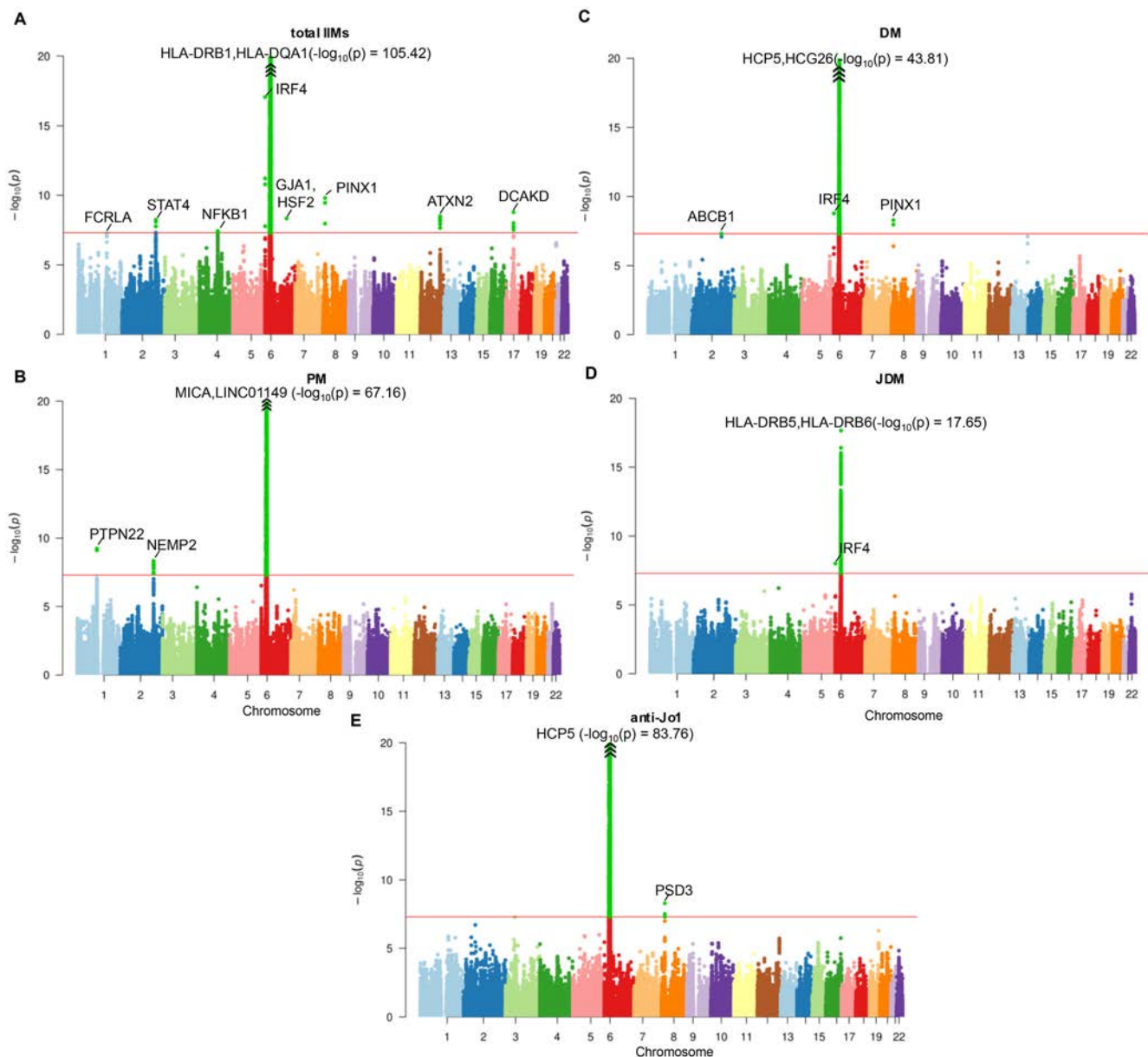


Figure 2. Manhattan plots of the total IIMs and subtypes of myositis. Signals reaching genome-wide significance level ($P = 5 \times 10^{-8}$, red line) are highlighted in green. The most significant signal at each risk locus is annotated. The locus at chromosome 6 is truncated at $-\log_{10}(P) = 20$. The arrow points to the most significant signal, with its P value in each plot. (A) Total IIMs: total myositis. (B) PM. (C) DM. (D) JDM. (E) Anti-Jo-1 autoantibody-positive myositis. DM, dermatomyositis; IIMs, idiopathic inflammatory myopathies; JDM, juvenile dermatomyositis; PM, polymyositis. Color figure can be viewed in the online issue, which is available at <http://onlinelibrary.wiley.com/doi/10.1002/art.43088/abstract>.

(rs9898793, $P = 1.65 \times 10^{-9}$, OR 1.252) (Figure 3E–H and Figure S4I–L). Near *FCRLA*, a novel intergenic locus (rs6668534, $P = 5.39 \times 10^{-8}$, OR 0.826) (Figure 3A and Figure S4A) was suggestively associated with total IIMs.

In analyses stratified by clinical subtypes, we identified some subset-specific and novel findings. In the PM subgroup (Figure 2B), we confirmed a previously identified risk variant of *PTPN22* (rs2476601, $P = 5.70 \times 10^{-10}$, OR 1.503) and identified a novel risk locus in *NEMP2* (rs74925618, $P = 4.52 \times 10^{-9}$, OR 1.804) (Figure 4A and Figure S5B). In the MHC region, the most

significant signal was an intergenic variant near *MICA/LINC01149* (rs1312473, $P = 6.88 \times 10^{-68}$, OR 2.772) (Figures S5D and S6). For DM (Figure 2C), the strongest signal came from *HCP5/HCG26* (rs3131617, $P = 1.56 \times 10^{-44}$, OR 2.306) (Figures S7D and S8A). Non-HLA intronic variants in *ABCB11* (rs145940036, $P = 4.91 \times 10^{-8}$, OR 3.172) and in *PINX1* (rs113538396, $P = 5.22 \times 10^{-9}$, OR 3.868) reached the genome-wide significance threshold in DM (Figure 4B and D and Figure S7A and G). Additionally, rs12203592 in *IRF4* was also significantly associated with both DM ($P = 1.69 \times 10^{-9}$, OR 1.471)

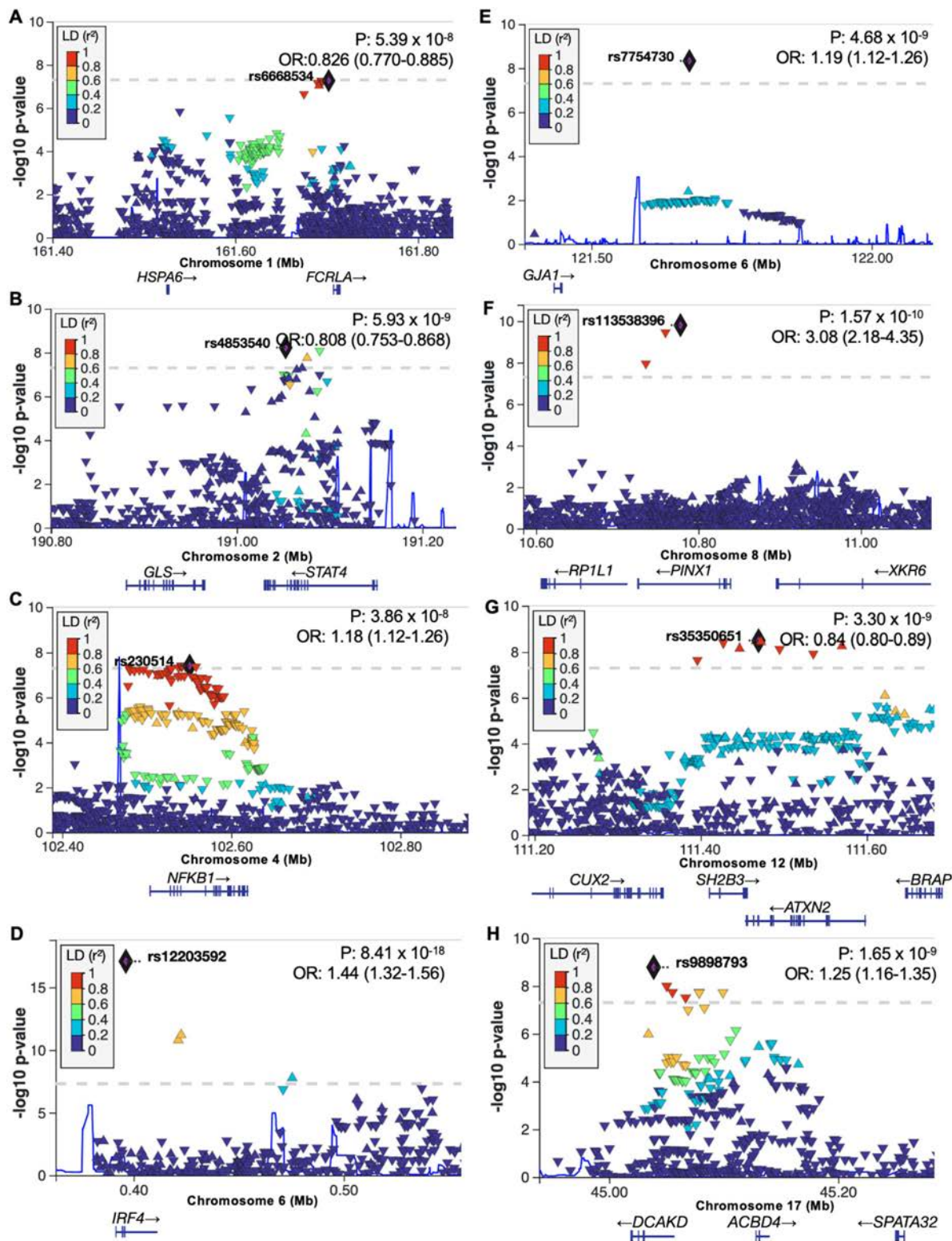


Figure 3. Regional plots of the most significant novel signals outside the HLA region in the total IIMs. The purple diamond indicates the index SNP. Variants imputed in both studies are represented by downward-pointing triangles, whereas those genotyped in at least one study are indicated by upward-pointing triangles. The color of each variant indicates the approximate value of the LD squared coefficient of correlation (r^2) between the index SNP and the corresponding variant. Index SNPs are (A) rs6668534 in *FCRLA* at chromosome 1; (B) rs4853540 in *STAT4* at chromosome 2; (C) rs230514 in *NFKB1* at chromosome 4; (D) rs12203592 in *IRF4* at chromosome 6; (E) rs7754730 in *GJA1* and *HSF2* at chromosome 6; (F) rs113538396 in *PINX1* at chromosome 8; (G) rs35350651 in *ATXN2* at chromosome 12; and (H) rs9898793 in *DCAKD* at chromosome 17. IIMs, idiopathic inflammatory myopathies; LD, linkage disequilibrium; OR, odds ratio; SNP, single-nucleotide polymorphism. Color figure can be viewed in the online issue, which is available at <http://onlinelibrary.wiley.com/doi/10.1002/art.43088/abstract>.

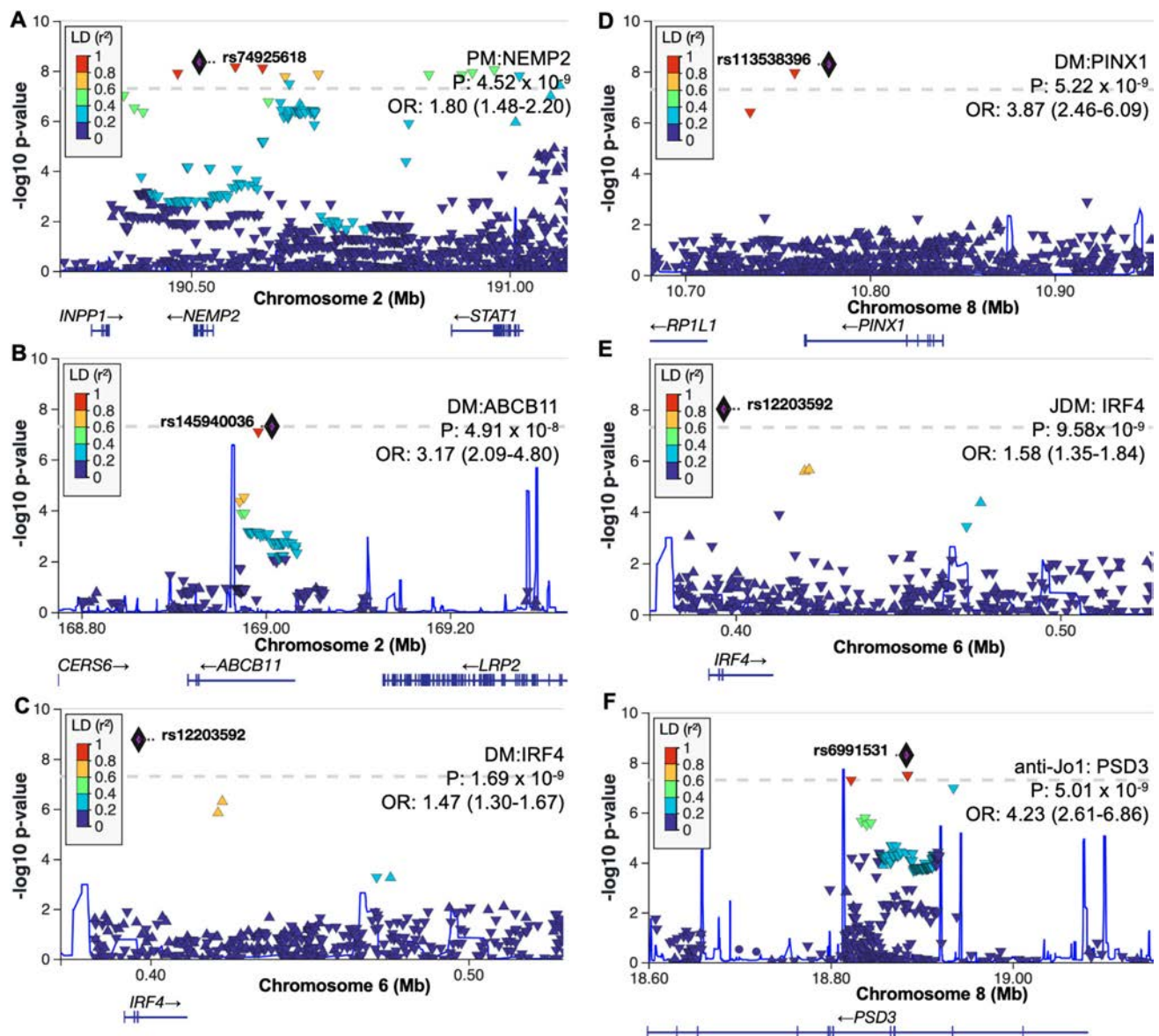


Figure 4. Regional plots of the most significant novel signals outside the HLA region in PM, DM, and myositis with anti-Jo-1. The purple diamond indicates the index SNP. Variants imputed in both studies are represented by downward-pointing triangles, whereas those genotyped in at least one study are indicated by upward-pointing triangles. The color of each variant corresponds to the approximate value of the LD squared coefficient of correlation (r^2) between the index SNP and a given variant. Index SNPs are (A) rs74925618 in *NEMP2* in PM; (B) rs145940036 in *ABCB11* in DM; (C) rs12203592 in *IRF4* in DM; (D) rs113538396 in *PINX1* in DM; (E) rs12203592 in *IRF4* in JDM; and (F) rs6991531 in *PSD3* in anti-Jo-1. DM, dermatomyositis; JDM, juvenile dermatomyositis; LD, linkage disequilibrium; OR, odds ratio; PM, polymyositis; SNP, single-nucleotide polymorphism. Color figure can be viewed in the online issue, which is available at <http://onlinelibrary.wiley.com/doi/10.1002/art.43088/abstract>.

and JDM ($P = 9.58 \times 10^{-9}$, OR 1.578) (Figure 4C and E). In JDM, the strongest signal observed was near *HLA-DRB5/HLA-DRB6* (rs1894553, $P = 2.24 \times 10^{-18}$, OR 1.894) at the HLA region (Figure 2D and Figures S7K and S9A).

In the anti-Jo-1 group, in addition to the strongest signal in *HCP5* (rs3132090, $P = 1.75 \times 10^{-84}$, OR 5.643) (Figure 2E and Figures S5F and S10A) located within the HLA region, a non-HLA risk locus in *PSD3* (rs6991531, $P = 5.01 \times 10^{-9}$, OR 4.229) was significantly associated with anti-Jo-1 myositis (Figure 4F and Figure S5J).

Sex-stratified analysis showed similar effect sizes in women and men, except a slightly stronger effect for *IRF4* in men. Formal analysis of sex interactions did not reveal significant differences in the identified signals between men and women, except for *IRF4* in the DM group, in which the effect was also marginally stronger in men (Tables S2 and S3). Pairwise interaction analyses among DM, JDM, and PM suggested that many of the identified variants have distinct effect sizes across subtypes and contribute to subtype-specific disease risk ($|Z_{\text{weighted}}| > 1.96$) (Table S4). The variant in *PTPN22* was significant in the interaction test across

different subtypes, with a larger effect or stronger association in PM compared to JDM and adult-onset DM, consistent with previous observations.²⁷ *IRF4* showed significant differences between JDM and other subtypes, with a higher OR in JDM compared to DM and total IIMs in the meta-analysis. This suggested that *IRF4* may play a more pivotal role in JDM, contributing to the significant interaction observed when comparing JDM with other subtypes. Variants in *ABCB11* and *PINX1* in the interaction tests between DM and JDM were not significant. The lack of significance may be due to low MAF of the variants, which could limit the power to detect associations and subtle differences in variant effects between subtypes.

Within the HLA region, an additional variant in the noncoding RNA locus in *TSBP1-AS1* ($P = 2.71 \times 10^{-40}$, conditional P [pC] = 9.06×10^{-9} , OR 1.487) was jointly significant within the HLA region in total IIMs (Table S5 and Figure S3) after conditioning on top signals. Variants that reached the suggestive threshold ($P = 1 \times 10^{-5}$) in autosomal regions of total IIMs and subtypes were reported (Table S6).

Roles of HLA variants and C4 as risk factors. To investigate the genetic architecture of myositis in the HLA region, we conducted HLA COJO analyses on the imputed HLA data. These analyses confirmed previously reported signals in the MHC class I and class II regions (Figure S11) and identified novel associations, such as *HLA-DRB1*16:01* ($pC = 1.57 \times 10^{-9}$) in the DM group after conditioning on the previously reported *HLA-B*08:01* allele. Additional HLA risk loci rs1265764 in *TSBP1-AS1* and rs116312062 in *HLA-DRB6* were also genome-wide significant (Table S7). The list of HLA alleles and HLA amino acids that reached the genome-wide significant threshold is shown in Table S8. We then further studied the MHC class III region, calculating the mean and SE of imputed dosages of C4 genes (*C4A*, *C4B*, *C4L*, and *C4S*) in both patients and controls. Patients showed lower levels of *C4A* and *C4L* compared to controls (Table S9). *C4A* and *C4L* were strongly correlated, as were *C4B* and *C4S* (Figure S12). Significant associations of *C4A* and *C4L* with myositis were found across total IIMs and subtypes (Table S10). Additionally, COJO analyses of HLA variants and C4 genes suggested that *HLA-DRB1*03:01* remained the strongest HLA risk allele in total IIMs, and *HLA-B*08:01* with rs116312062 were significant in PM and anti-Jo-1 groups. After accounting for effects from *C4A* or *C4L*, rs126574 and *HLA-DQA1*05:01* were no longer significant, suggesting these associations are due to LD with *C4A* or *C4L* (Table S11).

Credible sets of causal variants pinpointed by fine-mapping and eQTL colocalization analyses. Discoveries from the COJO analyses provided significant insights into the involvement of novel genetic risk loci in the underlying pathogenesis of myositis. To gain more perspective into the causal variants within the identified risk loci, we employed a Bayesian fine-mapping approach to identify candidates with potential direct

effects on disease phenotypes. The fine-mapping analyses yielded multiple 95% credible sets (99% for the HLA region), with each set containing a distinct group of variants with an assigned SNP.PIP of causality (Table S12). The SNP.PIP of each variant in a credible set indicates its likelihood of being causal within a specific risk locus. We reported candidate variant with the highest PIP in each credible set from the fine-mapping analyses (Table S13). Most of the highly probable causal variants were the lead variants detected from the COJO analyses. Fine-mapping identified rs535777 near *HLA-DRB1* as a top potential variant in causal credible sets for total IIMs and anti-Jo-1 in the HLA region. This variant confers a strong regulatory impact in the MHC class II region according to the RegulomeDB annotation (rank = 1b, probability = 1).

To assess the likelihood that genetic variants are causally related to disease phenotypes and gene expression in myositis-related tissues, we performed colocalization analyses and identified credible sets of variants (Table S14). The colocalization posterior probability of rs12203592 in the total IIMs, DM, and JDM indicated plausible shared causality in both the meta-analyzed myositis data and the expression level of *IRF4* in EBV-transformed lymphocytes (PP.H4 = 0.990, SNP.PIP = 1.000), lung (PP.H4 = 1.000, SNP.PIP = 1.000), and whole blood cells (PP.H4 = 1.000, SNP.PIP = 1.000) (Figure 5A). rs12950988 in *DCAKD* was the lead variant in the credible sets of total IIMs colocalization analysis in skeletal muscle (PP.H4 = 0.984, SNP.PIP = 0.928) and skin tissue (PP.H4 = 0.970, SNP.PIP = 0.428) (Figure 5B). We also observed colocalization of eQTLs for *HCP5* in lung tissue with both total myositis and DM. The most likely causal variants associated with these colocalization credible sets are rs3132090 for the *HCP5* eQTL with total myositis (PP.H4 = 0.902, SNP.PIP = 0.442) and rs3131618 for the *HCP5* eQTL with DM (PP.H4 = 0.945, SNP.PIP = 0.651) (Figure 5C).

Candidate genes and potential drug repurposing targets identified by RWR through biologic networks.

To provide more comprehensive insights into the genetic architecture of myositis and support future research, we performed network propagation with the RWR algorithm. This approach prioritizes candidate genes based on the functional connectivity of disease-associated genes within related biologic pathways. RWR on multiplex networks that integrate various biologic data sets (Table S15) enables robust and comprehensive analyses, capturing the global network topology while preserving individual network properties. Additional candidate genes were identified within each clinical group (Table S16 and Figure S13) based on their strength of connectivity to disease genes.

Notably, several genes belonging to nuclear transcription factor Y, including *NFYA*, *NFYB*, *NFYC*, *RFX*, and the transmembrane protein family, ranked as top candidates in the overall myositis group. *CIITA*, *APP*, and *CD74* were also the leading candidates across multiple groups. Gene set overrepresentation analyses of

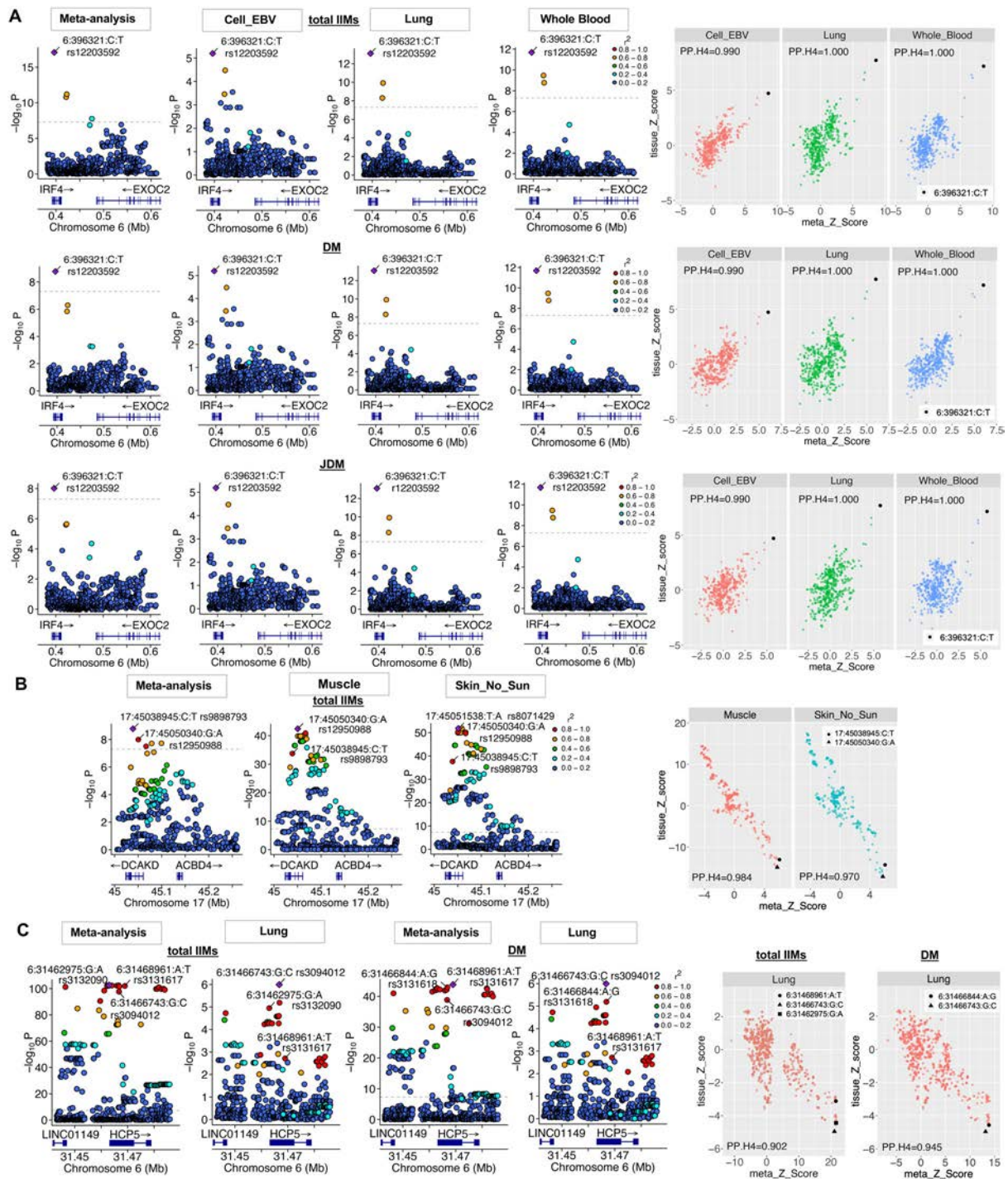


Figure 5. eQTL colocalization analyses within risk loci in significant tissues. Regional plots and plots of Z-score from eQTL studies versus meta-analyses of (A) *IRF4* in total IIMs, DM, and JDM. eQTL variants from ENSG00000137265.IRF4. circle (right panel): top variant in credible sets of meta-analyses, eQTL, and colocalization. (B) *DCAKD* in total IIMs. eQTL variants from ENSG00000172992.DCAKD. circle (right panel): top variant in credible sets of meta-analyses; triangle (right panel): top variant in credible sets of eQTL and colocalization. (C) *HCP5* in total IIMs and DM. eQTL variants from ENSG00000206337.HCP5. circle (right panel): top variant in credible sets of meta-analyses and DM colocalization; triangle (right panel): top variant in credible sets of eQTL; square (right panel): top variant in credible sets of total IIMs colocalization. Purple diamond: LD index. SNP.PP.H4: the probability of colocalization for the credible set. Only common variants between meta-analyses and eQTL are analyzed. DM, dermatomyositis; EBV, Epstein-Barr virus; eQTL, expression quantitative trait locus; IIMs, idiopathic inflammatory myopathies; JDM, juvenile dermatomyositis; LD, linkage disequilibrium; SNP, single-nucleotide polymorphism. Color figure can be viewed in the online issue, which is available at <http://onlinelibrary.wiley.com/doi/10.1002/art.43088/abstract>.

candidate and disease gene sets showed enrichment in immune-related processes and signaling pathways, prioritized for future investigation based on statistical significance (Figure S14). To explore the potential for drug repurposing in myositis, we also investigated if any disease (Table S6) and additional candidate genes (Table S16) from RWR were targets of drugs on the market according to the DrugBank database.²⁸ Potential treatments are listed in Table S17.

DISCUSSION

In our study, we explored the genetic architecture underlying myositis to gain a deeper insight into the genetic basis of IIMs. Our meta-analyses on 15,350 individuals of European descent identified novel genetic risk loci within and outside the HLA region in overall IIMs and subtypes.

In the total IIMs group, the OR of minor alleles in *FCRLA*, *STAT4*, and *ATXN2* suggested their protective effects against myositis. rs4853540 in *STAT4*, which targets the interferon regulatory factor 7 motif, may enhance transcription activity, as indicated by H3K4me1 and H3K27ac, in both T cells and B cells, suggesting its critical role in modulating immune responses (Figure S15A). rs35350651 within the 3'-untranslated region (3'-UTR) of *ATXN2* potentially regulates the highly conserved DNA-binding motif in the AT-rich interaction domain subfamily ARID3A, which is associated with autoimmune diseases^{29,30} and neuromuscular diseases, including diseases with similarities to IBM (eg, amyotrophic lateral sclerosis [ALS]),³¹ possibly through histone modification (Figure S15B). Future studies are needed to further understand mechanisms by which these variants may influence risk for IIMs development.

Through COJO analyses, rs12203592 in *IRF4*, genotyped in the ImmunoChip data set, was significant in the association study of the ImmunoChip data set and the meta-analyses of total, DM, and JDM groups, but not in the GWAS, where it was imputed. *IRF4* is associated with pigmentation, and its allele prevalence varies across European populations.³² Based on fine-mapping and colocalization analyses, rs12203592 might contribute to both the risk of myositis and gene expression levels in EBV-transformed lymphocytes, lung, and whole blood cells, but further studies in more homogeneous populations would be helpful. The novel genetic locus around *DCAKD*, rs9898793, with high posterior probability and in LD with the additional putative causal variant rs12950988, might modify regulatory elements, influencing *DCAKD* expression in skeletal muscle and skin tissue. rs3132090 near the *HCP5* locus was identified as the top variants in the colocalized credible sets for lung tissue in total myositis, and rs3131618 was the top variant in the colocalized credible sets in DM. Variants in the 3'-UTR proximal to the *HCP5* loci have been associated with myositis.³³ The novel variant rs3132090, upstream of the transcription start site of *HCP5*, may influence DNA-binding motifs in the TFAP2 members, including TFAP2A, TFAP2B, and TFAP2C, potentially modulating the expression of multiple targets (Figure S15C). Fine-mapping analyses also

identified rs535777, a putative causal variant with regulatory impacts on nuclear receptor NR1H3 and SIX1 in various immune cell types, such as CD4⁺ T cells (Figure S15D), which are related to autoimmune diseases and inflammatory processes.^{34,35}

When conducting stratified analysis based on clinical subtypes, we revealed distinct risk loci specifically associated with each subtype. In the PM group, rs74925618 in *NEMP2* was significant. *NEMP2* encodes a nuclear envelope integral membrane protein, suggesting a potential role in signaling pathways that might influence PM risk. *PINX1*, associated with total IIMs and DM, has also been linked to other autoimmune diseases in European ancestry.³⁶ In addition to subtype analyses, we investigated myositis with anti-Jo-1, the most common myositis-specific autoantibody. Despite the limited sample size in the anti-Jo-1 myositis group, rs3132090 near *HCP5* showed the strongest association among the subtype-specific signals. Outside the HLA region, *PSD3* had broader OR ranges, likely due to the small anti-Jo-1 sample size and low allele frequencies. Larger patient cohorts or combining with other anti-aminoacyl transfer-RNA-synthetases (anti-tRNA) autoantibodies could provide more compelling evidence for these novel signals. Certain subgroups, such as IBM, had insufficient sample sizes to support genetic analyses. Future studies with expanded cohorts are necessary to investigate these important but rarer subtypes. Another limitation of the study is the limited density of genotypes available in the arrays that we studied. In particular, three SNPs had limited support from nearby genotyped SNPs. The *PINX1* variant (rs113538396) was imputed in both data sets, and the *IRF4* (rs12203592) and *GJA1* (rs7754730) variants were genotyped only on the ImmunoChip data set. Further studies that directly genotype additional SNPs around these variants will help to validate these findings.

By exploring the impact of C4 located within the MHC class III region, we showed that patients had fewer copies of *C4A* and *C4L* than controls, with reduced copy numbers significantly associated with total IIMs and subtypes. These observations are consistent with previous studies linking lower copy number variations of *C4A* and *C4L* to increased risks of myositis and other autoimmune diseases.^{37,38}

The relative contributions of C4 isotypes and HLA variants as risk factors were also investigated, in addition to the analyses on HLA-imputed data. COJO analyses were performed, with copy numbers of each C4 isotype included as predictors to assess their impact on HLA associations. The strongest HLA alleles, *HLA-DRB1*03:01* in total IIMs and *HLA-B*08:01* in PM and anti-Jo-1, retained statistical significance, indicating their independence from C4 as risk factors in myositis. rs1265764 in *TSBP1-AS1*, which showed joint significance with other HLA variants in nearly all subtypes, was not significant after conditioning on C4, suggesting its dependence on C4.

To expand our understanding of the genetic network of myositis, we prioritized additional candidate genes based on the

biologic networks of risk markers using RWR. Several *RFX* genes, such as *RFX5*, ranked highly across groups. *RFX5* is evolutionary conservative, and its mutation can disrupt HLA expression, leading to immunodeficiency.³⁹ *CIITA* was also among the top candidates, playing an essential role in regulating transcriptional activity of the HLA class II promoter and, together with NFY and RFX, affecting the function of the immune system.^{40–42} *CD74* ranked at the top across multiple groups and has been previously suggested in animal models as a key regulator, binding to migration inhibitory factor, and a potential therapeutic target in alphavirus-induced myositis, in addition to its intracellular role in MHC class II antigen-presenting.⁴³ Another candidate, *APP*, is associated with neurodegenerative and neuroinflammatory conditions similar to IBM, such as ALS and multiple sclerosis.⁴⁴

NR1H4 (FXR) was one of the leading candidates in DM. Experiments have shown that overexpression of *NR1H4* inhibits expression of proinflammatory cytokine in inflammatory bowel diseases,⁴⁵ which are associated with DM and possibly share similar immunopathogenesis.⁴⁶ *TXNIP*, a top candidate in JDM, interacts with the NLRP3 inflammasome, which has been suggested to be associated with myositis.⁴⁷ The discoveries from RWR suggest new avenues for exploration and provide a foundation for future research hypothesis generation. Further investigations are helpful to understand the contribution and underlying pathogenicity of these candidate genes in myositis.

Because of the absence of standardized therapeutic guidelines for the treatment of IIM, the current therapeutic interventions for myositis are mainly guided by expert experience, case reports, and small clinical trials. Medications for myositis primarily consist of drugs that have received approval for other conditions and are used off-label in myositis.⁴⁸ To explore the potential for drug repurposing in myositis, we investigated if any disease and additional candidate genes from RWR were targets of drugs on the market. Current medications for myositis, such as human Ig and rituximab,⁴⁸ were confirmed in the analyses (Table S17). Antithymocyte Ig (rabbit) and valproic acid have also been investigated to treat certain autoimmune conditions.^{49,50} Other medications targeting the B lymphocyte antigen CD20, serine/threonine-protein kinase, and dipeptidyl peptidase 4 could also be considered for potential relevance to myositis treatment. Although our initial findings suggested possible opportunities for drug repurposing in myositis, further investigations and validations are necessary to provide more evidence, ultimately improving patient outcomes.

Overall, our study has identified novel genetic associations, providing valuable insights into the genetic architecture underlying myositis and its clinical subtypes. A limitation of our study is the variable spacing of SNP data across the genome. Because data were derived, in part, from the Immunochip data set, which focused on loci known to influence autoimmune conditions, there are regions where there are highly significant signals but for which further studies are needed to identify the most likely locus. Future

studies using denser genotyping or whole-genome sequencing would help to refine signals in these loci. Nevertheless, integrating results from the current GWAS studies not only contributes to our understanding of disease etiology but also helps guide future investigations and facilitate the development of more efficient and effective interventions and treatments for these complex autoimmune disorders.

ACKNOWLEDGMENTS

The authors thank Drs Michael Ombrello, Elaine Remmers, and Sandeep Agarwal for useful comments on the manuscript. Jan L. De Bleecker is a member of the European Reference Network for Neuromuscular Diseases. The authors acknowledge minimal usage of ChatGPT and Grammarly for checking spelling and grammar. Citation style was generated using Schiwheel.

AUTHOR CONTRIBUTIONS

All authors contributed to at least one of the following manuscript preparation roles: conceptualization AND/OR methodology, software, investigation, formal analysis, data curation, visualization, and validation AND drafting or reviewing/editing the final draft. As corresponding author, Ms Zhu and Dr. Amos, confirms that all authors have provided the final approval of the version to be published, and takes responsibility for the affirmations regarding article submission (eg, not under consideration by another journal), the integrity of the data presented, and the statements regarding compliance with institutional review board/Declaration of Helsinki requirements.





REFERENCES

1. Lundberg IE, de Visser M, Werth VP. Classification of myositis. *Nat Rev Rheumatol* 2018;14(5):269–278.
2. Rider LG, Miller FW. Deciphering the clinical presentations, pathogenesis, and treatment of the idiopathic inflammatory myopathies. *JAMA* 2011;305(2):183–190.
3. Lundberg IE, Fujimoto M, Vencovsky J, et al. Idiopathic inflammatory myopathies. *Nat Rev Dis Primers* 2021;7(1):86.
4. Miller FW, Chen W, O'Hanlon TP, et al; Myositis Genetics Consortium. Genome-wide association study identifies HLA 8.1 ancestral haplotype alleles as major genetic risk factors for myositis phenotypes. *Genes Immun* 2015;16(7):470–480.
5. Rothwell S, Cooper RG, Lundberg IE, et al; Myositis Genetics Consortium. Dense genotyping of immune-related loci in idiopathic inflammatory myopathies confirms HLA alleles as the strongest genetic risk factor and suggests different genetic background for major clinical subgroups. *Ann Rheum Dis* 2016;75(8):1558–1566.
6. Rothwell S, Amos CI, Miller FW, et al; Myositis Genetics Consortium. Identification of novel associations and localization of signals in idiopathic inflammatory myopathies using genome-wide imputation. *Arthritis Rheumatol* 2023;75(6):1021–1027.
7. Rose MR; ENMC IBM Working Group. 188th ENMC International Workshop: inclusion body myositis, 2–4 December 2011, Naarden, The Netherlands. *Neuromuscul Disord* 2013;23(12):1044–1055.
8. Hilton-Jones D, Miller A, Parton M, et al. Inclusion body myositis: MRC Centre for Neuromuscular Diseases, IBM workshop, London, 13 June 2008. *Neuromuscul Disord* 2010;20(2):142–147.
9. Manichaikul A, Mychaleckyj JC, Rich SS, et al. Robust relationship inference in genome-wide association studies. *Bioinformatics* 2010;26(22):2867–2873.

10. Purcell S, Neale B, Todd-Brown K, et al. PLINK: a tool set for whole-genome association and population-based linkage analyses. *Am J Hum Genet* 2007;81(3):559–575.
11. Byun J, Han Y, Gorlov IP, et al. Ancestry inference using principal component analysis and spatial analysis: a distance-based analysis to account for population substructure. *BMC Genomics* 2017;18(1):789.
12. Taliun D, Harris DN, Kessler MD, et al; NHLBI Trans-Omics for Precision Medicine (TOPMed) Consortium. Sequencing of 53,831 diverse genomes from the NHLBI TOPMed Program. *Nature* 2021;590(7845):290–299.
13. Luo Y, Kanai M, Choi W, et al; NHLBI Trans-Omics for Precision Medicine (TOPMed) Consortium. A high-resolution HLA reference panel capturing global population diversity enables multi-ancestry fine-mapping in HIV host response. *Nat Genet* 2021;53(10):1504–1516.
14. Sekar A, Bialas AR, de Rivera H, et al; Schizophrenia Working Group of the Psychiatric Genomics Consortium. Schizophrenia risk from complex variation of complement component 4. *Nature* 2016;530(7589):177–183.
15. Marchini J, Howie B. Genotype imputation for genome-wide association studies. *Nat Rev Genet* 2010;11(7):499–511.
16. Han B, Eskin E. Random-effects model aimed at discovering associations in meta-analysis of genome-wide association studies. *Am J Hum Genet* 2011;88(5):586–598.
17. Yang J, Ferreira T, Morris AP, et al; Genetic Investigation of ANthropometric Traits (GIANT) Consortium; DIAbetes Genetics Replication And Meta-analysis (DIAGRAM) Consortium. Conditional and joint multiple-SNP analysis of GWAS summary statistics identifies additional variants influencing complex traits. *Nat Genet* 2012;44(4):369–375.
18. Wallace C. A more accurate method for colocalisation analysis allowing for multiple causal variants. *PLoS Genet* 2021;17(9):e1009440.
19. Lonsdale J, Thomas J, Salvatore M, et al; GTEx Consortium. The Genotype-Tissue Expression (GTEx) project. *Nat Genet* 2013;45(6):580–585.
20. Wang K, Li M, Hakonarson H. ANNOVAR: functional annotation of genetic variants from high-throughput sequencing data. *Nucleic Acids Res* 2010;38(16):e164.
21. Zhou H, Arapoglou T, Li X, et al; NHGRI Genome Sequencing Program Variant Functional Annotation Working Group. FAVOR: functional annotation of variants online resource and annotator for variation across the human genome. *Nucleic Acids Res* 2023;51(D1):D1300–D1311.
22. Boyle AP, Hong EL, Hariharan M, et al. Annotation of functional variation in personal genomes using RegulomeDB. *Genome Res* 2012;22(9):1790–1797.
23. Dong S, Zhao N, Spragins E, et al. Annotating and prioritizing human non-coding variants with RegulomeDB v.2. *Nat Genet* 2023;55(5):724–726.
24. Liao Y, Wang J, Jaehnig EJ, et al. WebGestalt 2019: gene set analysis toolkit with revamped UIs and APIs. *Nucleic Acids Res* 2019;47(W1):W199–W205.
25. Cowen L, Ideker T, Raphael BJ, et al. Network propagation: a universal amplifier of genetic associations. *Nat Rev Genet* 2017;18(9):551–562.
26. Valdeolivas A, Tichit L, Navarro C, et al. Random walk with restart on multiplex and heterogeneous biological networks. *Bioinformatics* 2019;35(3):497–505.
27. Chinoy H, Platt H, Lamb JA, et al; UK Adult Onset Myositis Immunogenetic Collaboration and the Juvenile Dermatomyositis Research Group. The protein tyrosine phosphatase N22 gene is associated with juvenile and adult idiopathic inflammatory myopathy independent of the HLA 8.1 haplotype in British Caucasian patients. *Arthritis Rheum* 2008;58(10):3247–3254.
28. Wishart DS, Feunang YD, Guo AC, et al. DrugBank 5.0: a major update to the DrugBank database for 2018. *Nucleic Acids Res* 2018;46(D1):D1074–D1082.
29. Li Y, Li Z, Chen R, et al. A regulatory variant at 19p13.3 is associated with primary biliary cholangitis risk and ARID3A expression. *Nat Commun* 2023;14(1):1732.
30. Garton J, Barron MD, Ratliff ML, et al. New frontiers: ARID3a in SLE. *Cells* 2019;8(10):1136.
31. Van Daele SH, Moisse M, van Vugt JJFA, et al. Genetic variability in sporadic amyotrophic lateral sclerosis. *Brain* 2023;146(9):3760–3769.
32. Praetorius C, Grill C, Stacey SN, et al. A polymorphism in IRF4 affects human pigmentation through a tyrosinase-dependent MITF/TFAP2A pathway. *Cell* 2013;155(5):1022–1033.
33. Kulski JK. Long noncoding RNA HCP5, a hybrid HLA class I endogenous retroviral gene: structure, expression, and disease associations. *Cells* 2019;8(5):480.
34. Wang Z, Sadovnick AD, Traboulsee AL, et al. Nuclear receptor NR1H3 in familial multiple sclerosis. *Neuron* 2016;90(5):948–954.
35. Zhan H, Chen H, Tang Z, et al. SIX1 attenuates inflammation and rheumatoid arthritis by silencing MyD88-dependent TLR1/2 signaling. *Int Immunopharmacol* 2022;106:108613.
36. Gorlova OY, Li Y, Gorlov I, et al. Gene-level association analysis of systemic sclerosis: a comparison of African-Americans and White populations. *PLoS One* 2018;13(1):e0189498.
37. Zhou D, King EH, Rothwell S, et al; for MYOGEN Investigators. Low copy numbers of complement C4 and C4A deficiency are risk factors for myositis, its subgroups and autoantibodies. *Ann Rheum Dis* 2023;82(2):235–245.
38. Lundtoft C, Pucholt P, Martin M, et al; DISSECT Consortium; ImmunoArray Development Consortium. Complement C4 copy number variation is linked to SSA/Ro and SSB/La autoantibodies in systemic inflammatory autoimmune diseases. *Arthritis Rheumatol* 2022;74(8):1440–1450.
39. Sugiaman-Trapman D, Vitezic M, Jouhilahti EM, et al. Characterization of the human RFX transcription factor family by regulatory and target gene analysis. *BMC Genomics* 2018;19(1):181.
40. Reith W, Siegrist CA, Durand B, et al. Function of major histocompatibility complex class II promoters requires cooperative binding between factors RFX and NF-Y. *Proc Natl Acad Sci USA* 1994;91(2):554–558.
41. Ly LL, Yoshida H, Yamaguchi M. Nuclear transcription factor Y and its roles in cellular processes related to human disease. *Am J Cancer Res* 2013;3(4):339–346.
42. Sachini N, Papamatheakis J. NF-Y and the immune response: dissecting the complex regulation of MHC genes. *Biochim Biophys Acta Gene Regul Mech* 2017;1860(5):537–542.
43. Herrero LJ, Sheng KC, Jian P, et al. Macrophage migration inhibitory factor receptor CD74 mediates alphavirus-induced arthritis and myositis in murine models of alphavirus infection. *Arthritis Rheum* 2013;65(10):2724–2736.
44. Nguyen KV. β -Amyloid precursor protein (APP) and the human diseases. *AIMS Neurosci* 2019;6(4):273–281.
45. Gadaleta RM, van Erpecum KJ, Oldenburg B, et al. Farnesoid X receptor activation inhibits inflammation and preserves the intestinal barrier in inflammatory bowel disease. *Gut* 2011;60(4):463–472.
46. Sharif K, Ben-Shabat N, Mahagna M, et al. Inflammatory bowel diseases are associated with polymyositis and dermatomyositis-a

- retrospective cohort analysis. *Medicina (Kaunas)* 2022;58(12):1727.
47. Dubuisson N, Versele R, Davis-López de Carrizosa MA, et al. Walking down skeletal muscle lane: from inflammasome to disease. *Cells* 2021;10(11):3023.
48. Barsotti S, Lundberg IE. Current treatment for myositis. *Curr Treatm Opt Rheumatol* 2018;4(4):299–315.
49. Lytton SD, Denton CP, Nutzenberger AM. Treatment of autoimmune disease with rabbit anti-T lymphocyte globulin: clinical efficacy and potential mechanisms of action. *Ann N Y Acad Sci* 2007;1110(1):285–296.
50. Seet LF, Toh LZ, Finger SN, et al. Valproic acid exerts specific cellular and molecular anti-inflammatory effects in post-operative conjunctiva. *J Mol Med (Berl)* 2019;97(1):63–75.

Efficacy and Safety of Subcutaneous Abatacept Plus Standard Treatment for Active Idiopathic Inflammatory Myopathy: Phase 3 Randomized Controlled Trial

Rohit Aggarwal,¹  Ingrid E. Lundberg,²  Yeong-Wook Song,³  Aziz Shaibani,⁴ Victoria P. Werth,⁵ 
and Michael A. Maldonado⁶

Objective. Our objective was to evaluate the efficacy and safety of subcutaneous (SC) abatacept and standard of care (SOC) for the treatment of idiopathic inflammatory myopathy (IIM) over 52 weeks.

Methods. In this randomized, double-blind, placebo-controlled phase III trial, patients with treatment-refractory IIM received SC abatacept (at 125 mg weekly) with SOC (abatacept group) or a placebo with SOC (placebo group). A 24-week double-blind period was followed by an open-label period to assess outcomes from continued therapy with abatacept and initiation with abatacept (placebo-to-abatacept switch group) from 24 to 52 weeks. The primary end point was International Myositis Assessment and Clinical Studies definition of improvement (IMACS DOI) at week 24. Secondary efficacy and safety end points were assessed.

Results. Overall, 148 (double-blind) and 133 (open-label) patients were treated. Baseline demographics were well-balanced between treatment groups and disease subtypes. At 24 weeks, improvement per IMACS DOI was 56.0% for the abatacept group and 42.5% for the placebo group ($P = 0.083$); at 52 weeks, improvement was 69.8% (continued abatacept) and 69.0% (placebo-to-abatacept switch). The IMACS DOI rate at 24 weeks was greater in the nondermatomyositis (non-DM) group (abatacept: 57.1%; placebo: 32.3%; $P = 0.040$) than the DM group (abatacept: 55.0%; placebo: 50.0%; $P = 0.679$). The observed safety profile was similar in both groups.

Conclusion. The proportion of patients who met improvement criteria after 24 weeks was similar between abatacept and placebo groups. However, analysis by IIM subtype suggested there may be a sustained benefit of SC abatacept for patients with non-DM subtypes.

INTRODUCTION

Idiopathic inflammatory myopathy (IIM) comprises a group of chronic, systemic autoimmune inflammatory diseases of unknown etiology that primarily affect skeletal muscle with or without

cutaneous involvement and clinically manifest as muscle weakness with or without characteristic rashes.^{1,2} Other organs, such as the lungs, joints, vasculature, and gastrointestinal tract, are commonly involved.³ Polymyositis (PM), dermatomyositis (DM), antisynthetase syndrome, and immune-mediated necrotizing myopathy (IMNM)

[ClinicalTrials.gov](#) identifier: NCT02971683.

Results of this study were previously published in abstract form and presented at the Annual European Congress of Rheumatology of EULAR 2022 ([abstract number POS0839] Aggarwal R, Lundberg IE, Song YW, et al. Randomized, double-blind, placebo-controlled trial to evaluate efficacy and safety of SC abatacept in adults with active idiopathic inflammatory myopathy. *Ann Rheum Dis* 2022;81[suppl 1]:711; and American College of Rheumatology Convergence 2022; abstract number 2237 (<https://acrabstracts.org/abstract/randomized-placebo-controlled-trial-to-evaluate-efficacy-and-safety-of-subcutaneous-abatacept-in-adults-with-active-idiopathic-inflammatory-myopathy-results-of-the-24-week-double-blind-and-28-week-op/>)).

Supported by Bristol Myers Squibb.

Dr Aggarwal's work was supported by Boehringer Ingelheim, Bristol Myers Squibb, EMD Serono, and Q32. Dr Lundberg's work was supported by AstraZeneca. Dr Werth's work was supported by the NIH, the United States Department of Defense, The Veterans Association (VA Merit Review [BX005921]), Rome Pharmaceuticals, Ventus, Pfizer, Corbus, CSL Behring, Genentech/Roche, Argenx, Syntimmune, and Regeneron.

¹Rohit Aggarwal, MD: University of Pittsburgh, Pittsburgh, Pennsylvania; ²Ingrid E. Lundberg, MD: Karolinska Institutet and Karolinska University Hospital, Stockholm, Sweden; ³Yeong-Wook Song, MD: Seoul National University, Seoul, South Korea; ⁴Aziz Shaibani, MD: Nerve and Muscle Center of Texas, Houston, Texas; ⁵Victoria P. Werth, MD: Pennsylvania Medical School, Philadelphia, Pennsylvania; ⁶Michael A. Maldonado, MD: Immunology and Fibrosis Research and Development, Bristol Myers Squibb, Princeton, New Jersey.

Additional supplementary information cited in this article can be found online in the Supporting Information section (<http://onlinelibrary.wiley.com/doi/10.1002/art.43066>).

Author disclosures are available at <https://onlinelibrary.wiley.com/doi/10.1002/art.43066>.

Address correspondence via email to Rohit Aggarwal, MD, at aggarwalr@upmu.edu.

Submitted for publication October 18, 2023; accepted in revised form October 29, 2024.

are among the most common subtypes of IIM.^{2,4,5} Disease-specific autoantibodies can be detected in approximately 60% of patients with IIM and are highly specific for subtypes, possibly even predicting clinical and histologic features of the disease.⁶ The long-term effects of IIM can lead to significant physical disabilities, organ damage, and increased mortality.⁷

Treatment for most subtypes of IIM is anchored on the administration of systemic immunotherapies.^{8–10} Glucocorticoid treatment is commonly used as first-line therapy; however, because of the requirement of high doses and long-term administration, it is associated with significant side effects.¹¹ Additional therapies include conventional synthetic disease-modifying antirheumatic drugs, such as methotrexate or azathioprine, and gamma globulin.¹¹ The administration of novel targeted therapies has been reported, but there have been very few large, prospective, randomized controlled trials in this field.¹⁰ Given the paucity of available treatments, the toxicity of agents such as immunosuppressives, and the chronic, debilitating, and potentially life-threatening nature of the disease, there is a significant unmet need for safe and effective new therapies in IIM.

Up-regulation of multiple costimulatory molecules, such as CTLA-4 and CD28, have been identified in the muscle tissue of patients with IIM.^{12,13} Along with the expression of major histocompatibility complex molecules, this aberrant expression appears to impact normal immunoregulation in muscle and is associated with dysregulated T cell activity. Abatacept is a recombinant fusion protein consisting of the extracellular domain of human CTLA-4 and a fragment of the Fc domain of human Ig G1. Native CTLA-4 is a naturally occurring regulatory molecule that acts as a selective T cell costimulation modulator by binding to CD80 and CD86 on antigen-presenting cells. The CTLA-4 domain of abatacept blocks CD28 engagement with T cells, thereby inhibiting full activation of T cells.¹⁴ Abatacept has a well-established history of safety and efficacy in the treatment of autoimmune diseases, such as rheumatoid arthritis.^{15,16}

Multiple case reports and a small open-label controlled trial have suggested that abatacept may be effective for the treatment of patients with refractory IIM.^{17–22} The Abatacept Treatment in Polymyositis and Dermatomyositis study ([ClinicalTrials.gov](https://clinicaltrials.gov/ct2/show/study/NCT01315938): NCT01315938) demonstrated efficacy of intravenous abatacept in patients with DM and PM IIM subtypes.²³ In this “delayed-start” study, at the three-month time point after study start, 5 of 10 patients treated with abatacept were responders, compared with 1 of 7 patients treated with conventional background immunotherapies only. The current study evaluated the efficacy and safety of subcutaneous (SC) abatacept (at 125 mg weekly) in combination with standard treatment compared to placebo with standard treatment in patients with active refractory IIM.

PATIENTS AND METHODS

Study design. This was a randomized, double-blind, placebo-controlled phase III trial ([ClinicalTrials.gov](https://clinicaltrials.gov/ct2/show/study/NCT02971683): NCT02971683)

of SC abatacept for patients with active, treatment-refractory IIM (patients for whom standard immunosuppression did not work in the past). SC abatacept (at 125 mg once weekly) plus standard of care (SOC) was compared with SOC alone for patients with DM and non-DM IIM. The study was conducted from May 4, 2017, to February 8, 2021, at 58 clinical sites in 11 countries.

Here, we report data from the two main periods of the study (Figure S1). Candidate screening could last up to 28 days. The 24-week double-blind period began when patients were randomized (via automated interactive voice response system) in a 1:1 ratio to either abatacept (at 125 mg weekly) with SOC (abatacept group) or placebo with SOC (placebo group). Study drug administration was initiated at the time of randomization. At the discretion of the investigator, patients in either treatment group with worsening disease between weeks 12 and 24 were permitted to initiate rescue therapy if criteria for worsening disease were met. Worsening disease was defined as follows: (1) increase of ≥ 2 cm on visual analog scale (VAS) for physician global assessment of disease activity (PhGA), and either a $\geq 20\%$ worsening in Manual Muscle Test-8 (MMT-8) score or an increase of ≥ 2 cm on VAS for extramuscular global activity assessed on the Myositis Disease Activity Assessment Tool (MDAAT) compared with baseline; or (2) any three of the six International Myositis Assessment and Clinical Studies (IMACS) core set measures worsening by $\geq 30\%$ compared with baseline on two consecutive visits. IMACS definition of improvement (DOI) was based on six core measures (PhGA, patient global assessment of disease activity, MMT-8, Health Assessment Questionnaire-Disability Index [HAQ-DI], muscle enzyme levels, and extramuscular global disease activity as defined by MDAAT extramuscular global activity VAS).²⁴ Rescue therapy was given at the discretion of the clinician and included an increase in dose of current SOC therapy, addition of a new therapy or change in therapy. Rescue therapy was restricted to allowable concomitant medication per protocol: glucocorticoids alone, an immunosuppressant (methotrexate, azathioprine, mycophenolate, tacrolimus, or cyclosporine), or a combination of glucocorticoids and one of the listed immunosuppressants. Patients requiring rescue therapy remained anonymized to medication through week 24 and were able to enter the open-label period.

The open-label period consisted of an additional 28 weeks (weeks 24–52; Figure S1). At completion of the last double-blind visit, all patients in the placebo group were eligible to switch to SC abatacept (at 125 mg weekly) treatment in combination with SOC for the open-label period. The results summarized here for the open-label period are presented based on patients’ original treatment group assignments during the double-blind period (abatacept or placebo).

This study was conducted in accordance with the ethical principles originating in the Declaration of Helsinki. The study received appropriate approval by a central institutional review board (IRB)/independent ethics committee before initiation. Additionally, full board approval was obtained from the respective

governing IRBs and documentation of approval was submitted to the sponsor before initiating any study procedures. All patients or their legal representative provided written informed consent.

Consideration was given to the potential impact of the COVID-19 pandemic to study analyses and interpretations. Although the pandemic impacted key study visits for some participants, no adjustment to the analyses was considered necessary.

Study population. Patients with IIM including DM, PM, IMNM, juvenile myositis (JM), or overlap myositis subtypes were eligible for enrollment. Diagnosis was based on the Bohan and Peter classification criteria.²⁵ A diagnosis of DM required a confirmed characteristic rash. PM, IMNM, JM, or overlap myositis diagnoses had to be confirmed by previous muscle biopsy or a positive test for ≥ 1 myositis-specific autoantibody, available from either previous testing or testing at screening. Inclusion criteria were age ≥ 18 years, active treatment-refractory disease with muscle weakness, and taking background SOC (see Supplementary Methods).

Active IIM was determined by one of two approaches. Patient clinical history, clinical evaluation and testing (laboratories and studies) were reviewed by an independent expert adjudication committee who were asked to ascertain whether the patient had clearly active disease. Candidates could meet activity criteria without committee review if they met any one of these criteria: currently active myositis-associated rash, recent (within three months) muscle biopsy, magnetic resonance imaging, or electromyogram demonstrating active disease or creatine kinase more than five times the upper limit of normal (ULN) at screening. Patients were required to present with muscle weakness defined as an MMT-8 score ≤ 135 units at the time of screening. Additionally, eligibility required three of the six IMACS core set measures to be abnormal according to the following thresholds: MMT-8 ≤ 125 units; PhGA, or patient global assessment VAS ≥ 2 ; HAQ-DI ≥ 0.5 ; one or more muscle enzyme ≥ 1.3 times the ULN; or MDAAT extramuscular global activity VAS ≥ 2 . Overall eligibility of patients including diagnosis and disease activity was determined by an adjudication committee composed of IIM experts who evaluated patient medical records and adjudication forms submitted by study sites.

Patients were required to be started on SOC for IIM, defined as treatment with glucocorticoids and/or one of the following immunosuppressants: methotrexate, azathioprine, mycophenolate, tacrolimus, or cyclosporine. Dosages up to 30 mg/day of prednisone (or the equivalent) were allowed as SOC. Combinations of nonglucocorticoid immunosuppressants were not permitted during the double-blind period. Patients must have been taking the same medication(s) for IIM for 12 weeks before randomization (including a stable dosage for at least four weeks before randomization). Patients receiving azathioprine must have started at least 24 weeks before randomization (stable dosage for 12 weeks before randomization). SOC changes were not

allowed in the double-blind phase (except those required for toxicity or intolerance) but could be adjusted during the open-label period. Exclusion criteria are summarized in the Supplementary Methods; notably, patients with inclusion body myositis, severe muscle damage, severe pulmonary disease, and administration of rituximab and Ig within past six and three months, respectively, were excluded.

Patient and public involvement. Before completing the protocol, the research team engaged with both patients and patient advocacy groups for their input on the trial design using Bristol Myers Squibb's patient engagement group resources. Additionally, communications with patient advocacy groups occurred throughout the study regarding enrollment status. There was no patient or public involvement in the analysis or reporting of this study.

Study measures. *Efficacy.* The primary efficacy end point was achieving IMACS DOI, based on the six aforementioned core measures, at week 24 in patients who did not require rescue therapy. Achievement of IMACS DOI was defined as meeting the following criteria: (1) improvement of $\geq 20\%$ in any three IMACS core measures, (2) ≤ 2 IMACS core measure scores worsening by $\geq 25\%$, and (3) MMT-8 score worsening by $< 25\%$. All patients who discontinued study medication before week 24 and/or received rescue medication at any time during the 24-week double-blind period (defined as nonresponders) were considered as not achieving IMACS DOI for the primary analysis.

Secondary end points were mean changes at week 24 in Myositis Functional Index-2 using three proximal muscle groups (FI-3, calculated from FI-2 testing), HAQ-DI, extramuscular global disease activity, and Myositis Response Criteria (MRC) (with Total Improvement Score [TIS] of ≥ 20 as minimal improvement).^{26–28} TIS ranged from 0 to 100, and MRC categories were based on TIS and categorized per TIS thresholds for minimal, moderate, and major improvement (≥ 20 , ≥ 40 , and ≥ 60 points, respectively).

Exploratory end points included IMACS DOI, MRC TIS, mean changes in FI-3, HAQ-DI, and extramuscular global activity at week 52. The proportion of patients with minimal, moderate, and major improvement in disease by MRC score; mean changes in MMT-8, individual PhGA, and patient global assessment scores; and Cutaneous Dermatomyositis Disease Area and Severity Index (CDASI) activity and damage scores were assessed at weeks 24 and 52.²⁹

Safety. Adverse events (AEs), serious AEs (SAEs), and deaths were recorded. The safety analyses specified for the week 24 analysis were to be performed for the open-label period.

Statistical analyses. A sample size of 150 patients was planned based on the primary comparison of the proportion of patients with IMACS DOI at week 24 between the SC abatacept and the SC placebo groups on background SOC. With a 1:1

randomization, this would yield a power of approximately 90% to detect a treatment difference of 27% in the rate of IMACS DOI between the treatment groups based on a continuity corrected chi-square test. Analysis of the primary end point by IIM subtype (DM vs non-DM) was prespecified.

Efficacy end points were assessed in the intent-to-treat (ITT) population, which consisted of all patients randomly assigned and treated (with at least one dose of abatacept or placebo) in the double-blind period. Efficacy end points were assessed in the open-label abatacept population, which comprised all patients treated with at least one dose of abatacept during the open-label period. Safety end points were assessed in the as-treated population, which comprised all patients randomly assigned and treated in the double-blind period or the previously defined open-label abatacept population. Prespecified analyses by IIM subtype were performed and reported as overall, DM, and non-DM (PM and IMNM).

Double-blind period. For the primary end point, the proportion of patients meeting IMACS DOI at week 24 and not requiring rescue therapy was compared between the abatacept and placebo groups using a logistic regression model. Point estimates of the adjusted odds ratios (ORs) of the likelihood of achieving DOI and not requiring rescue therapy in the abatacept group compared with the placebo group were calculated with corresponding 95% confidence intervals (CIs) and *P* values. Secondary end points were assessed using a longitudinal (repeated measures) model. Adjusted means, standard errors, and 95% CIs for the adjusted mean difference between treatment groups were calculated. Primary end point data for 11 active participants were not available for week 24. The COVID-19 pandemic

impacted data collection for five patients who were unable to attend in-person site visits to complete study assessments because of pandemic-related restrictions; data were missing for other reasons for six additional patients. No adjustments to the prespecified analyses were considered necessary.

Open-label period. All patients who were treated during the open-label period were included in the open-label analysis, which was performed once all patients completed 52 weeks of study treatment. No formal statistical testing was conducted for any of the efficacy analyses. The open-label period analyses were based on the open-label-treated analysis population and are presented by patient treatment group during the double-blind period (abatacept or placebo). BMS policy on data sharing may be found at <https://www.bms.com/researchers-and-partners/independent-research/data-sharing-request-process.html>.

RESULTS

Patient disposition, demographics, and disease characteristics.

Overall, 202 patients were enrolled, 149 patients were randomly assigned (75 in the abatacept group and 73 in the placebo group; one patient was randomly assigned and not treated), and 134 patients (89.9%) completed the double-blind period and entered the open-label period (Figure 1). The overall rates of discontinuation were low: 6 patients (8.0%) and 8 patients (11.0%) in the double-blind period for the abatacept and placebo groups, respectively (Figure 1). Based on ITT analysis, these 14 patients were considered nonresponders for the primary end point. None of the enrolled patients

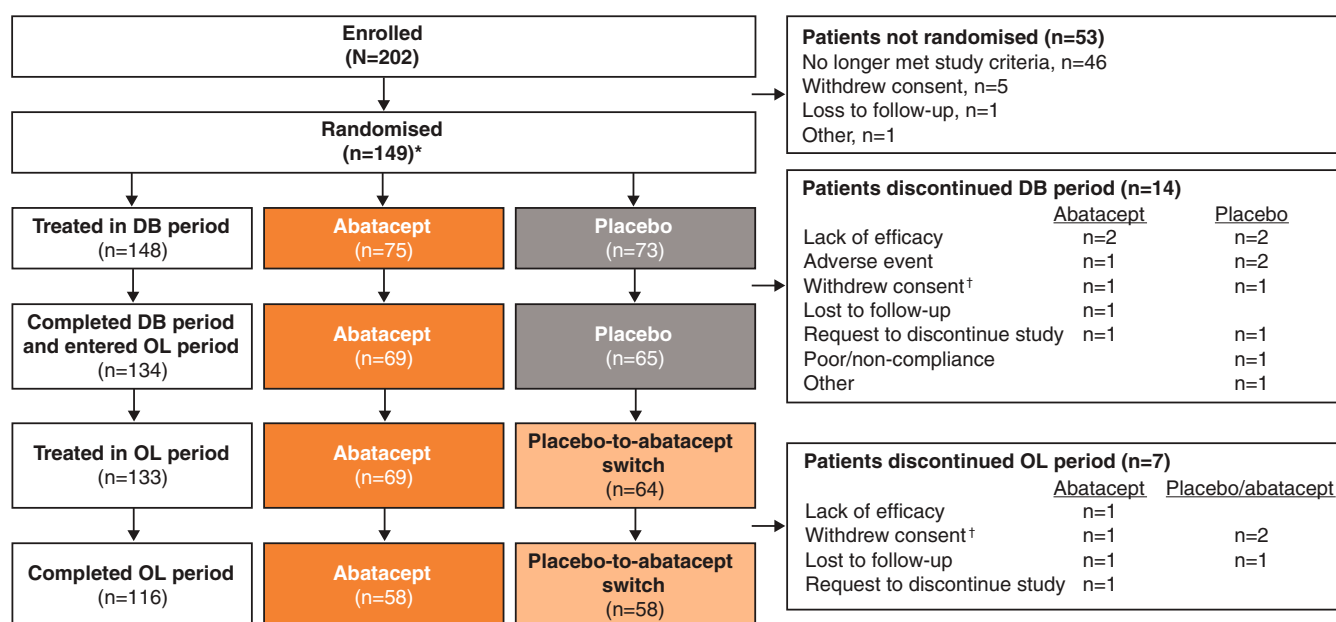


Figure 1. Patient disposition. *One patient was randomly assigned but not treated, leaving 148 randomly assigned and treated. [†]Includes patient request to discontinue treatment and patient withdrew consent. DB, double-blind; OL, open label. Color figure can be viewed in the online issue, which is available at <http://onlinelibrary.wiley.com/doi/10.1002/art.43066/abstract>.

had JM or overlap myositis; therefore, the IIM population only comprised patients with DM, PM, and IMNM.

The proportions of patients across treatment groups from each country included in the analysis were similar (Table S1). Baseline demographics and disease characteristics were similar across treatment groups (Table 1) and disease subtypes (Table S2) and were typical for this patient population. Overall, the mean age of patients was 48.7 (SD \pm 14.2) years, and the majority of patients were female (71.6%) and White (56.8%) (Table 1). Previous and concomitant use of glucocorticoids and immunosuppressants was comparable between treatment groups; concomitant glucocorticoid and an immunosuppressant agent were the most common SOC (Table S3). Overall, 55.4% of patients in both treatment groups had DM (Table 1); patients with PM and IMNM comprised the

remainder (abatacept: 25.3% and 21.3%; placebo: 34.2% and 8.2%, respectively). Patients had significant muscle weakness, with a mean MMT-8 score of 113.0 (SD \pm 18.1), and notable active disease indicated by a mean PhGA score of 5.4 (SD \pm 1.5). However, the mean extramuscular global activity VAS was low (2.6), and the skin disease activity score was moderate (mean CDASI activity score 15.5) for both groups. One patient in each treatment group met the criteria of worsening disease and received rescue therapy during the double-blind period; both patients were rescued with an increase in dose of current therapy and were considered as not achieving DOI for the primary objective analysis per the protocol.

Open-label period. A total of 133 patients were treated in the open-label period; 69 patients continued abatacept from the double-blind period, and 64 patients switched from a placebo to

Table 1. Baseline demographics and disease characteristics for patients with IIM during the double-blind period (week 24, intent-to-treat analysis population)*

Characteristic	Abatacept (n = 75)	Placebo (n = 73)	Total (N = 148)
Patients completed treatment, n (%)	69 (92.0)	65 (89.0)	134 (90.5)
Age, mean (SD), yr	49.3 (14.4)	48.1 (14.1)	48.7 (14.2)
Female, n (%)	52 (69.3)	54 (74.0)	106 (71.6)
Hispanic or Latino, n (%)	7 (9.3)	3 (4.1)	10 (6.8)
Not Hispanic or Latino, n (%)	19 (25.3)	19 (26.0)	38 (25.7)
Race, n (%)			
White	42 (56.0)	42 (57.5)	84 (56.8)
Black or African American	9 (12.0)	8 (11.0)	17 (11.5)
American Indian or Alaska Native	3 (4.0)	3 (4.1)	6 (4.1)
Asian	10 (13.3)	6 (8.2)	16 (10.8)
Japanese	11 (14.7)	10 (13.7)	21 (14.2)
Other	0	3 (4.1)	3 (2.0)
Unknown	0	1 (1.4)	1 (0.7)
Geographic region, n (%)			
North America	26 (34.7)	22 (30.1)	48 (32.4)
South America	18 (24.0)	26 (35.6)	44 (29.7)
Asia	20 (26.7)	16 (21.9)	36 (24.3)
Europe	11 (14.7)	9 (12.3)	20 (13.5)
Others	0 (0)	0 (0)	0 (0)
Disease duration, mean (SD), mo	61.8 (60.2)	58.3 (55.4)	60.1 (57.7)
IIM type, n (%)			
DM	40 (53.3)	42 (57.5)	82 (55.4)
PM	19 (25.3)	25 (34.2)	44 (29.7)
IMNM	16 (21.3)	6 (8.2)	22 (14.9)
Disease activity, mean (SD) ^a			
Physician global assessment of disease activity ^b	5.4 (1.6)	5.4 (1.5)	5.4 (1.5)
Patient global assessment of disease activity ^b	6.3 (2.1)	6.2 (2.2)	6.2 (2.2)
Extramuscular global activity ^b	2.4 (2.2)	2.7 (2.4)	2.6 (2.3)
MMT-8 score, mean (SD) ^a	115.1 (17.1)	110.8 (18.9)	113.0 (18.1)
HAQ-DI score, mean (SD) ^a	1.5 (0.7)	1.4 (0.7)	1.5 (0.7)
CDASI score, mean (SD)			
Activity	15.2 (15.1)	15.8 (13.9)	15.5 (14.4)
Damage	1.8 (3.5)	1.8 (2.9)	1.8 (3.2)
Muscle enzyme, mean (SD), CK (U/L) ^a	1,301.5 (1,844.0)	1,111.0 (2,024.5)	1,207.5 (1,930.9)
Concomitant medications of special interest, n (%)			
Systemic glucocorticoids	66 (88.0)	64 (87.7)	130 (87.8)
Immunosuppressive agents	56 (74.7)	54 (74.0)	110 (74.3)

* CDASI, Cutaneous Dermatomyositis Disease Area and Severity Index; CK, creatinine kinase; DM, dermatomyositis; HAQ-DI, Health Assessment Questionnaire-Disability Index; IIM, idiopathic inflammatory myopathy; IMNM, immune-mediated necrotizing myopathy; MMT-8, Manual Muscle Test-8; PM, polymyositis.

^a Core set measure.

^b 100-mm visual analog scale.

Table 2. Primary, secondary, and exploratory end points by treatment group and disease comparisons for the double-blind period (24 weeks, intent-to-treat analysis population)*

Outcome and IIM types	Abatacept (n = 75)	Placebo (n = 73)	Nominal <i>P</i> value or adjusted mean difference from placebo (95% CI) ^a
Primary end point: IMACS DOI without requiring rescue, n/m (%)			
All	42/75 (56.0)	31/73 (42.5)	0.083
DM	22/40 (55.0)	21/42 (50.0)	0.679
Non-DM	20/35 (57.1)	10/31 (32.3)	0.040
MRC (mean TIS), adjusted mean change from baseline (SE)			
All	40.8 (2.9), n = 62	37.2 (3.0), n = 58	3.6 (−2.9 to 10.1)
DM	46.0 (3.2), n = 31	43.6 (3.1), n = 35	2.5 (−6.5 to 11.4)
Non-DM	38.4 (3.2), n = 31	31.7 (3.6), n = 23	6.6 (−3.1 to 16.4)
Patients meeting MRC (TIS), n/m (%)			
All			
Moderate + major response	36/62 (58.1)	29/58 (50.0)	N/A
DM			
Moderate + major response	19/31 (61.3)	22/35 (62.9)	N/A
Non-DM			
Moderate + major response	17/31 (54.8)	7/23 (30.4)	N/A
FI-3, adjusted mean (SE) change from baseline			
All	4.1 (1.3), n = 59	1.2 (1.4), n = 58	2.9 (0 to 5.8)
DM	2.3 (1.6), n = 29	0.3 (1.4), n = 35	1.9 (−2.3 to 6.2)
Non-DM	3.2 (1.4), n = 30	−0.6 (1.5), n = 23	3.7 (−0.3 to 7.8)
HAQ-DI score, ^b adjusted mean (SE) change from baseline			
All	−0.3 (0.1), n = 66	−0.2 (0.1), n = 62	−0.1 (−0.3 to 0.0)
DM	−0.3 (0.1), n = 35	−0.2 (0.1), n = 37	−0.1 (−0.3 to 0.1)
Non-DM	−0.3 (0.1), n = 31	−0.1 (0.1), n = 25	−0.2 (−0.4 to 0.1)
Extramuscular global activity, ^b adjusted mean (SE) change from baseline			
All	−1.6 (0.2), n = 63	−1.4 (0.2), n = 60	−0.2 (−0.6 to 0.3)
DM	−1.9 (0.3), n = 32	−1.9 (0.3), n = 36	−0.1 (−0.8 to 0.7)
Non-DM	−1.1 (0.2), n = 31	−0.9 (0.2), n = 24	−0.2 (−0.8 to 0.3)
MMT-8 score, ^b adjusted mean (SE) change from baseline			
All	12.9 (1.9), n = 64	11.0 (2.0), n = 59	1.8 (−2.7 to 6.4)
DM	14.4 (2.2), n = 33	14.0 (2.1), n = 35	0.4 (−5.7 to 6.4)
Non-DM	12.1 (2.5), n = 31	7.8 (2.7), n = 24	4.3 (−3.0 to 11.7)
Physician global assessment of disease activity, ^{b,c} adjusted mean (SE) change from baseline			
All	−2.9 (0.3), n = 65	−2.7 (0.3), n = 62	−0.2 (−0.9 to 0.5)
DM	−2.8 (0.3), n = 34	−2.4 (0.3), n = 37	−0.4 (−1.2 to 0.5)
Non-DM	−2.4 (0.4), n = 31	−2.2 (0.5), n = 25	−0.1 (−1.4 to 1.2)
Patient global assessment of disease activity, ^{b,c} adjusted mean (SE) change from baseline			

(Continued)

Table 2. (Cont'd)

Outcome and IIM types	Abatacept (n = 75)	Placebo (n = 73)	Nominal <i>P</i> value or adjusted mean difference from placebo (95% CI) ^a
All	-1.4 (0.3), n = 66	-0.1 (0.3), n = 62	-0.4 (-1.1 to 0.4)
DM	-1.4 (0.3), n = 35	-1.4 (0.3), n = 37	-0.0 (-0.9 to 0.9)
Non-DM	-1.2 (0.4), n = 31	-0.3 (0.5), n = 25	-0.9 (-2.1 to 0.3)
CDASI score, adjusted mean (SE) change from baseline	n = 32	n = 34	-
Activity	-3.9 (2.8)	-4.4 (2.8)	0.5 (-2.7 to 3.7)
Damage	-0.2 (0.9)	-0.2 (0.9)	0.0 (-1.0 to 0.9)
Muscle enzyme, ^b CK (U/L), adjusted mean (SE) change from baseline			
All	-390.1 (142.3), n = 67	-63.1 (145.9), n = 61	-327.1 (-684.2 to 30.0)
DM	-270.5 (61.1), n = 35	-24.3 (59.4), n = 36	-246.1 (-413.9 to 78.3)
Non-DM	-475.8 (239.7), n = 32	-117.3 (264.9), n = 25	-358.5 (-1,074.6 to 357.6)

* CDASI, Cutaneous Dermatomyositis Disease Area and Severity Index; CI, confidence interval; CK, creatine kinase; DM, dermatomyositis; FI-3, Functional Index-2 using three proximal muscle groups; HAQ-DI, Health Assessment Questionnaire-Disability Index; IIM, idiopathic inflammatory myopathy; IMACS DOI, International Myositis Assessment and Clinical Studies definition of improvement; MMT-8, Manual Muscle Test-8; MRC, Myositis Response Criteria; N/A, not applicable; n/m, number of patients with response/number of patients in the analysis; TIS, Total Improvement Score.

^a Abatacept vs placebo.

^b Core set measure.

^c 100-mm visual analog scale.

abatacept. Approximately 95% of patients (n = 126) completed the open-label period. The overall rates of discontinuation in the open-label period were low: four patients (5.8%) and three patients (4.7%) in the abatacept and placebo-to-abatacept switch groups, respectively. Among the seven patients who discontinued the open-label period, the most common reasons for discontinuing included lack of efficacy, consent withdrawal, and loss to follow-up. The abatacept and placebo-to-abatacept switch treatment groups were well-balanced for the proportion of patients with DM (52.2% vs 60.9%, respectively) and PM (27.5% vs 31.3%, respectively). The baseline disease characteristics for patients in the open-label period did not differ significantly from those of patients in the double-blind period.

Primary and secondary efficacy end points. *Double-blind period.* The primary end point of proportion of patients meeting IMACS DOI at week 24 and not requiring rescue therapy was achieved by 56.0% of the abatacept group and 42.5% of the placebo group (adjusted OR 1.8, 95% CI 0.9–3.5; *P* = 0.083) (Table 2). No significant between-treatment differences were observed for the primary end point for patients with DM, but the non-DM (PM and IMNM) subtypes showed higher IMACS DOI rates in the abatacept group compared with placebo (57.1% vs 32.3%; *P* = 0.040) (Table 2). Only one patient in each treatment arm required rescue in the double-blind phase after meeting the criteria of worsening disease. Rates of achieving secondary end points, IMACS core measures, and FI-3 were numerically higher in the abatacept group compared with the placebo group; these treatment benefits were more notable for the non-DM (PM and IMNM) than the DM subtypes (Table 2, Table S4).

Overall, MRC categories of minimal, moderate and major improvement were comparable between the abatacept and placebo groups (Table 2). It is worth noting that the total number of patients for mean TIS and TIS categories was reduced from 75 to 62 patients in the abatacept group and from 73 to 58 patients in the placebo group because some core set measures were missed for some patients due to isolation and social distancing measures during the COVID-19 pandemic. Post hoc analysis for the MRC mean TIS category at week 24 showed greater improvement with abatacept versus placebo in the non-DM subtype (adjusted mean difference from placebo 6.6, 95% CI -3.1 to 16.4), whereas the difference in the DM subtype was not as pronounced (2.5, 95% CI -6.5 to 11.4; Figure 2).

Open-label period. In the open-label-treated analysis population at week 52, the proportion of patients achieving IMACS DOI at week 52 demonstrated a sustained benefit in continuing abatacept and an improvement when switching from a placebo to abatacept (proportion of patients achieving IMACS DOI: 69.8% [abatacept], 69.0% [placebo-to-abatacept switch]; Table 3, Figure S2A).

Similarly, MRC TIS continued to improve in both groups in the open-label period (Figures S3 and S2B). The proportion of patients in IMACS DOI and the MRC TIS over time in the abatacept and placebo groups with non-DM subtype are shown in Figures S2C and S2D. The proportion of patients without DM showing moderate-to-major response to abatacept was 54.8% at week 24 and 67.9% at week 52. For the placebo non-DM subtype, the proportion of patients showing moderate-to-major response was only 30.4%, which increased to 55.6% after

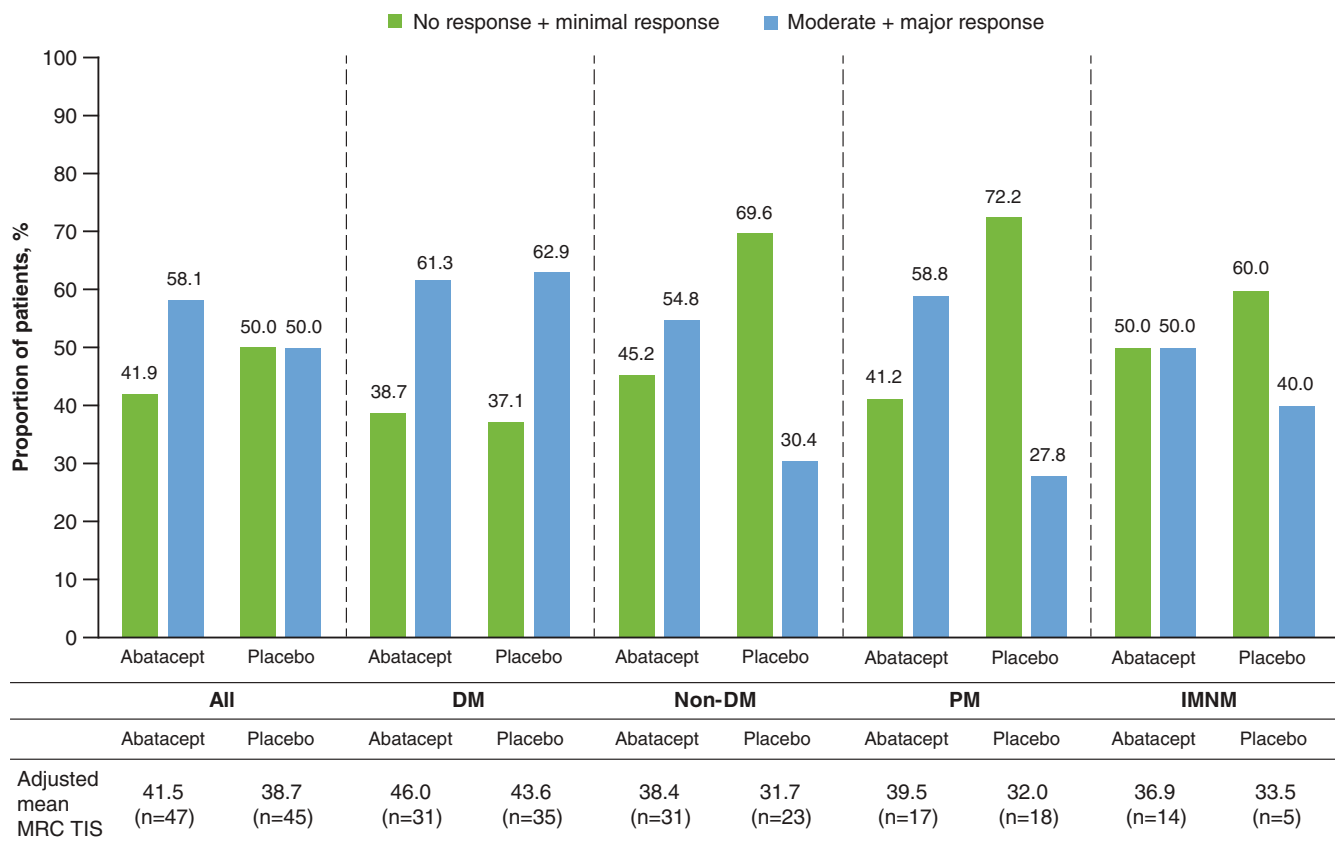


Figure 2. MRC at week 24 by TIS category (intent-to-treat analysis population). DM, dermatomyositis; IMNM, immune-mediated necrotizing myopathy; MRC, Myositis Response Criteria; PM, polymyositis; TIS, Total Improvement Score.

switching to abatacept in the open-label period. Other study end points also showed continued improvement, with a mean improvement from the baseline of 5.0 and 4.6 for FI-3 and −6.7 and −8.1 for CDASI in abatacept and placebo-to-abatacept switch groups, respectively, as well as −0.4 for HAQ-DI for both groups (Table 3).

Safety. Double-blind period. During the double-blind period, the observed safety end points were similar between the abatacept and placebo groups (Table 4) and consistent with the known safety profile of abatacept. The overall frequencies of AEs, SAEs, and AEs leading to discontinuation were comparable between the abatacept and placebo groups; four patients experienced SAEs in each treatment group.

Infections were reported in 25.3% of patients in the abatacept group and 42.5% of patients in the placebo group. Most of the reported infections were mild or moderate in intensity (17 patients [22.7%] in the abatacept group; 31 patients [42.4%] in the placebo group). No malignancies were reported in the abatacept or placebo groups. One death in the placebo arm was due to an unexplained acute respiratory event. No new safety concerns were identified during the double-blind period.

Open-label period. During the open-label period, the observed safety profile was consistent with that of the double-blind period and the known safety profile of abatacept (Table 4). SAEs were reported in 10 patients (14.5%) receiving abatacept and 4 patients (6.3%) in the placebo-to-abatacept switch group; most were considered unrelated to treatment. A total of four serious infections were reported, all of which were resolved, and the study drug was continued. COVID-19 was reported in one patient receiving abatacept, which led to a brief hospitalization. AEs were reported in 45 abatacept patients (65.2%) and 37 placebo-to-abatacept switch patients (57.8%). Infections were reported in 23 patients (33.3%) in the abatacept group and 17 patients (26.6%) in the placebo-to-abatacept switch group.

DISCUSSION

This was a large, multicenter, global, randomized controlled trial of 149 patients with IIM. The study failed to meet the primary objective of having an increase in the proportion of patients who met the improvement criteria (IMACS DOI) after 24 weeks of treatment with SC abatacept plus SOC compared with patients treated with placebo plus SOC. The observed responder rate in the treatment arm (56.0%) was very close to the rate expected

Table 3. Primary and secondary end points by treatment group and disease category in the open-label period (week 52, open-label-treated analysis population)*

End point and IIM type	Abatacept (n = 69)	Placebo-to-abatacept switch (n = 64)	Adjusted mean difference between groups (95% CI)
Patients with IMACS DOI without rescue medication, n/m (%)			
All	44/63 (69.8)	40/58 (69.0)	N/A
DM	25/35 (71.4)	27/39 (69.2)	N/A
Non-DM	19/28 (67.9)	13/19 (68.4)	N/A
Patients meeting MRC (TIS), n/m (%)			
All			
Moderate + major response	45/61 (73.8)	37/56 (66.1)	N/A
DM			
Moderate + major response	26/33 (78.8)	27/38 (71.1)	N/A
Non-DM			
Moderate + major response	19/28 (67.9)	10/18 (55.6)	N/A
FI-3, adjusted mean (SE) change from baseline			
All	5.0 (1.7), n = 55	4.6 (1.7), n = 56	0.4 (−3.7 to 4.5)
DM	3.3 (2.3), n = 30	4.9 (2.0), n = 38	−1.6 (−7.7 to 4.4)
Non-DM	4.3 (1.8), n = 25	2.1 (2.0), n = 18	2.2 (−3.2 to 7.6)
HAQ-DI score, ^a adjusted mean (SE) change from baseline			
All	−0.4 (0.1), n = 64	−0.4 (0.1), n = 59	−0.1 (−0.3 to 0.1)
DM	−0.4 (0.1), n = 35	−0.4 (0.1), n = 39	−0.1 (−0.3 to 0.1)
Non-DM	−0.4 (0.1), n = 29	−0.3 (0.1), n = 20	−0.1 (−0.4 to 0.2)
Extramuscular global activity, ^a adjusted mean (SE) change from baseline			
All	−1.7 (0.2), n = 62	−1.5 (0.2), n = 56	−0.2 (−0.7 to 0.3)
DM	−2.0 (0.3), n = 33	−1.9 (0.3), n = 38	−0.1 (−0.9 to 0.7)
Non-DM	−1.3 (0.2), n = 29	−1.0 (0.3), n = 18	−0.2 (−0.9 to 0.4)
MMT-8 score, ^a adjusted mean (SE) change from baseline			
All	14.1 (3.1), n = 63	15.8 (3.2), n = 58	−1.6 (−9.9 to 6.6)
DM	13.9 (4.5), n = 35	18.6 (4.3), n = 39	−4.7 (−17.2 to 7.8)
Non-DM	14.9 (2.6), n = 28	12.1 (3.1), n = 19	2.8 (−5.4 to 11.0)
Physician global assessment of disease activity, ^{a,b} adjusted mean (SE) change from baseline			
All	−3.7 (0.3), n = 64	−2.9 (0.3), n = 58	−0.7 (−1.4 to 0.0)
DM	−3.3 (0.3), n = 35	−2.7 (0.3), n = 39	−0.7 (−1.5 to 0.3)
Non-DM	−3.3 (0.4), n = 29	−2.4 (0.5), n = 19	−1.0 (−2.2 to 0.2)
Patient global assessment of disease activity, ^{a,b} adjusted mean (SE) change from baseline			
All	−2.2 (0.3), n = 64	−1.2 (0.3), n = 59	−1.0 (−1.8 to −0.2)
DM	−2.5 (0.4), n = 35	−1.5 (0.4), n = 39	−1.0 (−2.0 to 0.0)
Non-DM	−1.8 (0.4), n = 29	−0.9 (0.5), n = 20	−0.9 (−2.2 to 0.5)
CDASI overall score, adjusted mean (SE) change from baseline	n = 33	n = 36	
Activity	−6.7 (2.6)	−8.1 (2.5)	1.4 (−1.8 to 4.6)
Damage	0.5 (1.0)	−0.8 (1.0)	1.2 (0.0 to 2.4)
Muscle enzyme, ^a CK, adjusted mean (SE) change from baseline			
All	−566.3 (110.4), n = 63	−435.9 (114.7), n = 56	−130.3 (−415.2 to 154.5)
DM	−314.9 (59.3), n = 35	−174.6 (56.7), n = 38	−140.2 (−303.9 to 23.4)
Non-DM	−823.6 (215.6), n = 28	−636.9 (249.0), n = 18	−186.8 (−850.1 to 476.6)

* CDASI, Cutaneous Dermatomyositis Disease Area and Severity Index; CI, confidence interval; CK, creatine kinase; DM, dermatomyositis; FI-3, Functional Index-2 using three proximal muscle groups; HAQ-DI, Health Assessment Questionnaire-Disability Index; IIM, idiopathic inflammatory myopathy; IMACS DOI, International Myositis Assessment and Clinical Studies definition of improvement; MMT-8, Manual Muscle Test-8; MRC, Myositis Response Criteria; N/A, not applicable; n/m, number of patients meeting IMACS DOI/number of patients in the analysis; TIS, Total Improvement Score.

^a Core set measure.

^b 100-mm visual analog scale.

based on previous data. The response rate for the placebo group (42.5%), however, was higher than expected. Prespecified analysis by IIM subtype showed that the observed differences between

the abatacept and placebo arms were due to the patients with PM and IMNM. Patients who continued into the open-label period demonstrated continued benefit up to week 52 regardless of

Table 4. Safety summary of patients with idiopathic inflammatory myopathy during the double-blind (24 weeks, as-treated analysis population) and open-label periods (52 weeks, as-treated analysis population)*

End point	Double-blind period		Open-label period	
	Abatacept (n = 75)	Placebo (n = 73)	Abatacept (n = 69)	Placebo-to-abatacept switch (n = 64)
Deaths	0 (0)	1 (1.4)	0 (0)	0 (0)
Serious AEs	4 (5.3)	4 (5.5)	10 (14.5)	4 (6.3)
Related serious AEs	2 (2.7)	0 (0)	2 (2.9)	1 (1.6)
Discontinued due to serious AEs	0 (0)	2 (2.7)	0 (0)	0 (0)
AEs	52 (69.3)	56 (76.7)	45 (65.2)	37 (57.8)
Related AEs	15 (20.0)	18 (24.7)	9 (13.0)	4 (6.3)
Discontinued due to AEs	1 (1.3)	2 (2.7)	0 (0)	0 (0)
Infections and infestations	20 (26.7)	32 (43.8)	23 (33.3)	17 (26.6)
Upper respiratory tract infection	3 (4.0)	3 (4.1)	2 (2.9)	1 (1.6)
Urinary tract infection	4 (5.3)	1 (1.4)	2 (2.9)	1 (1.6)
Herpes zoster	1 (1.3)	3 (4.1)	3 (4.3)	0 (0)

* Values are the number (%). Serious AEs in the abatacept group: cellulitis, gastroenteritis, urinary tract infection, and renal failure; serious AEs in the placebo group: herpes zoster, vomiting, polymyositis, and acute respiratory failure. AE, adverse event.

original treatment group or IIM subtype. This was significant, given the patient population was notably weak with moderate-to-severe disease activity and did not respond to first-line therapy. Secondary efficacy end points showed a similar pattern.

Abatacept was generally well-tolerated and was relatively safe when added to concomitant background immunosuppressive drugs. No new safety concerns were identified. Comparable safety end points were observed between the abatacept and placebo groups during the double-blind and open-label periods.

This study enrolled patients with three types of IIM: DM, PM, and IMNM. PM is characterized by cellular infiltrate consisting of activated CD8⁺ T lymphocytes and macrophages found in the endomysium and in the perimysium.⁸ PM is often a diagnosis of exclusion and many patients previously diagnosed with PM are now considered to have antisynthetase syndrome or IMNM; patients with antisynthetase syndrome were not excluded in this study.³⁰ The more recently recognized IMNM is histologically characterized by myofiber necrosis with little or no inflammatory infiltrate.³⁰ IMNM is associated with antibodies against signal recognition particle and 3-hydroxy-3-methylglutaryl-coenzyme A reductase. Despite the clinical and histopathologic differences between subtypes of IIM, there is little evidence to guide the use of specific therapies in any given subtype, and treatment approaches are historically similar across subtypes.

The treatment of IIM subtypes has relied on the utilization of traditional immunosuppressants or immunomodulatory strategies.¹⁰ Therapeutic trials have not always been successful but have helped to improve study design and outcome measures.^{31–33} There is a significant unmet need for alternative, steroid-sparing therapies that are efficient, well-tolerated, and subtype specific. The recent successful study of intravenous immune globulin (Progress in Dermatomyositis [ProDERM] study) in patients with DM supports this argument.³⁴ Our study suggests that PM and IMNM subtypes may be more responsive to

treatment with abatacept than DM. In addition to monitoring other exploratory outcomes of physical activity, an additional analysis of biomarker samples, including myositis-specific and myositis-associated autoantibodies, may provide further insights.

The 2016 American College of Rheumatology/EULAR criteria have progressed study end points for clinical trials with the provision of a continuous TIS measure within MRC.^{35,36} This study design incorporated an escape protocol to identify patients whose symptoms worsened significantly during the double-blind period. Only two patients met the escape criteria and required rescue, suggesting future trial designs may be simplified. More specialized centers capable of identifying suitable patients and conducting these studies are needed. This will improve study recruitment and the reliability of study end points, including the predicted placebo response rate. Interventions that manage therapeutic expectations and improve patient ability to accurately report symptom severity have shown the most promise in reducing placebo response. It is worth assessing expectations of therapeutic benefit in clinical trials using these as covariables.³⁷

Studies of patients with IIM are challenging, as evidenced in this trial. High response rates of placebo patients meeting the improvement criteria continue to be an issue in IIM trials; possible explanations for this include concomitant background immunosuppressive therapy (especially relatively high doses of steroids), the subjective nature of various core set measures, and lack of expert centers and investigators required for a large clinical trial. The present study had a higher-than-expected placebo response rate seen in the DM, but not the non-DM, subtype. Moreover, our study suggests that the protocol for stabilizing background therapy before study entry, particularly surrounding the administration of systemic glucocorticoids, may have differential effects based on IIM subtype. As adjustments in concomitant background immunosuppressive therapy during the double-blind period only occurred in one patient in each treatment arm, this did not

contribute to differences seen between treatment arms and IIM subtypes. Studies that include multiple subtypes are conducted with the expectation that the novel therapy may help all subtypes based on preliminary data and to improve study feasibility. Because of the possibility that response rate may differ between subtypes, statistical plans should allow for prespecified analyses by subtype, as was done in this study.

This study had a few limitations. First, the patients described here had limited extramuscular disease at baseline, limiting the utility of this study to address improvement in nonmuscle organ systems. In the setting of such clinical variability, more significant disease manifestations, such as with interstitial lung disease, may not be suitable for study in this type of trial. Second, disturbances associated with the COVID-19 pandemic resulted in some missed core set measures for five patients because of isolation and social distancing measures, but data for 68 other patients were missing for other reasons. In addition, there were 14 patients who discontinued before 24 weeks in the double-blind period and were considered nonresponders for the primary end point. Although the missing data due to the pandemic alone are unlikely to have impacted interpretation of study results, the combined missing data for ~8% of study patients may have impacted the findings of this study.

This study failed to meet the primary end point, but analysis by IIM subtype suggested benefit of SC abatacept that was sustained up to one year of treatment when it was added to background therapy in patients with PM and IMNM. Therapy was well-tolerated with no new safety concerns identified in this IIM population.

ACKNOWLEDGMENTS

The study was executed by Sandra Overfield, Robin Scully, and Albert A. Thomas.

AUTHOR CONTRIBUTIONS

All authors were involved in drafting the article or revising it critically for important intellectual content, and all authors approved the final version to be published. Dr Aggarwal had full access to all of the data in the study and takes responsibility for the integrity of the data and the accuracy of the data analysis.

Study conception and design. Aggarwal, Lundberg, Werth, Maldonado.

Acquisition of data. Aggarwal, Lundberg, Song, Shaibani, Werth, Maldonado.

Analysis and interpretation of data. Aggarwal, Lundberg, Song, Shaibani, Werth, Maldonado.

ROLE OF THE STUDY SPONSOR

Professional medical writing by Candice Dcosta, MSc, and Joaquin Jaramillo, MD, and editorial assistance were provided by Caudex, a division of IPG Health Medical Communications, and were funded by Bristol Myers Squibb. Bristol Myers Squibb funded this study. Authors who are employees of Bristol Myers Squibb were involved in designing the study

and in the collection, analysis, or interpretation of the data. All authors, including those who were employees of the study sponsor, were involved in drafting/reviewing the manuscript and approved the final version for submission. Bristol Myers Squibb also approved the manuscript for submission.

REFERENCES

1. Miller FW. Classification of idiopathic inflammatory myopathies. In: Kagen L, ed. *The Inflammatory Myopathies*. Humana Press; 2009.
2. Lundberg IE, Tjälmlund A, Bottai M, et al; International Myositis Classification Criteria Project Consortium, the Euromyositis Register, and the Juvenile Dermatomyositis Cohort Biomarker Study and Repository (UK and Ireland). 2017 European League Against Rheumatism/American College of Rheumatology classification criteria for adult and juvenile idiopathic inflammatory myopathies and their major subgroups. *Arthritis Rheumatol* 2017;69(12):2271–2282.
3. Iaccarino L, Gatto M, Bettio S, et al. Overlap connective tissue disease syndromes. *Autoimmun Rev* 2013;12(3):363–373.
4. Baer AN. Differential diagnosis of idiopathic inflammatory myopathies. *Curr Rheumatol Rep* 2006;8(3):178–187.
5. Witt LJ, Curran JJ, Strek ME. The diagnosis and treatment of anti-synthetase syndrome. *Clin Pulm Med* 2016;23(5):218–226.
6. Betteridge Z, Tansley S, Shaddick G, et al; UKMyonet contributors. Frequency, mutual exclusivity and clinical associations of myositis autoantibodies in a combined European cohort of idiopathic inflammatory myopathy patients. *J Autoimmun* 2019;101:48–55.
7. Dobloug GC, Svensson J, Lundberg IE, et al. Mortality in idiopathic inflammatory myopathy: results from a Swedish nationwide population-based cohort study. *Ann Rheum Dis* 2018;77(1):40–47.
8. Dalakas MC, Hohlfield R. Polymyositis and dermatomyositis. *Lancet* 2003;362(9388):971–982.
9. Meyer A, Scirè CA, Talarico R, et al. Idiopathic inflammatory myopathies: state of the art on clinical practice guidelines [corrected]. *RMD Open* 2019;4(suppl 1):e000784.
10. Lundberg IE, Fujimoto M, Vencovsky J, et al. Idiopathic inflammatory myopathies. *Nat Rev Dis Primers* 2021;7(1):86.
11. Pipitone N, Salvarani C. Treatment of inflammatory myopathies. *Expert Rev Clin Immunol* 2018;14(7):607–621.
12. Nagaraju K, Raben N, Villalba ML, et al. Costimulatory markers in muscle of patients with idiopathic inflammatory myopathies and in cultured muscle cells. *Clin Immunol* 1999;92(2):161–169.
13. Behrens L, Kerschensteiner M, Misgeld T, et al. Human muscle cells express a functional costimulatory molecule distinct from B7.1 (CD80) and B7.2 (CD86) in vitro and in inflammatory lesions. *J Immunol* 1998;161(11):5943–5951.
14. Linsley PS, Nadler SG. The clinical utility of inhibiting CD28-mediated costimulation. *Immunol Rev* 2009;229(1):307–321.
15. Westhovens R, Kremer JM, Emery P, et al. Long-term safety and efficacy of abatacept in patients with rheumatoid arthritis and an inadequate response to methotrexate: a 7-year extended study. *Clin Exp Rheumatol* 2014;32(4):553–562.
16. Simon TA, Soule BP, Hochberg M, et al. Safety of abatacept versus placebo in rheumatoid arthritis: integrated data analysis of nine clinical trials. *ACR Open Rheumatol* 2019;1(4):251–257.
17. Kerola AM, Kauppi MJ. Abatacept as a successful therapy for myositis—a case-based review. *Clin Rheumatol* 2015;34(3):609–612.
18. Çağlayan M, Işık H, Oktayoglu P. A case of refractory polymyositis successfully treated with abatacept monotherapy. *Arch Rheumatol* 2020;35(4):618–622.

19. Rodziewicz M, Kiely P. The successful use of subcutaneous abatacept in refractory anti-human transcriptional intermediary factor 1-gamma dermatomyositis skin and oesophagopharyngeal disease. *Rheumatology (Oxford)* 2018;57(10):1866–1867.
20. Maeshima K, Kiyonaga Y, Imada C, et al. Successful treatment of refractory anti-signal recognition particle myopathy using abatacept. *Rheumatology (Oxford)* 2014;53(2):379–380.
21. Musuruana JL, Cavallasca JA. Abatacept for treatment of refractory polymyositis. *Joint Bone Spine* 2011;78(4):431–432.
22. Arabshahi B, Silverman RA, Jones OY, et al. Abatacept and sodium thiosulfate for treatment of recalcitrant juvenile dermatomyositis complicated by ulceration and calcinosis. *J Pediatr* 2012;160(3):520–522.
23. Tjärnlund A, Tang Q, Wick C, et al. Abatacept in the treatment of adult dermatomyositis and polymyositis: a randomised, phase IIb treatment delayed-start trial. *Ann Rheum Dis* 2018;77(1):55–62.
24. Rider LG, Giannini EH, Brunner HI, et al; International Myositis Assessment and Clinical Studies Group. International consensus on preliminary definitions of improvement in adult and juvenile myositis. *Arthritis Rheum* 2004;50(7):2281–2290.
25. Bohan A, Peter JB. Polymyositis and dermatomyositis (first of two parts). *N Engl J Med* 1975;292(7):344–347.
26. Rider LG, Werth VP, Huber AM, et al. Measures of adult and juvenile dermatomyositis, polymyositis, and inclusion body myositis: Physician and Patient/Parent Global Activity, Manual Muscle Testing (MMT), Health Assessment Questionnaire (HAQ)/Childhood Health Assessment Questionnaire (C-HAQ), Childhood Myositis Assessment Scale (CMAS), Myositis Disease Activity Assessment Tool (MDAAT), Disease Activity Score (DAS), Short Form 36 (SF-36), Child Health Questionnaire (CHQ), physician global damage, Myositis Damage Index (MDI), Quantitative Muscle Testing (QMT), Myositis Functional Index-2 (FI-2), Myositis Activities Profile (MAP), Inclusion Body Myositis Functional Rating Scale (IBMFRS), Cutaneous Dermatomyositis Disease Area and Severity Index (CDASI), Cutaneous Assessment Tool (CAT), Dermatomyositis Skin Severity Index (DSSI), Skindex, and Dermatology Life Quality Index (DLQI). *Arthritis Care Res (Hoboken)* 2011;63(0 11)(suppl 11):S118–S157.
27. Aggarwal R, Rider LG, Ruperto N, et al; International Myositis Assessment and Clinical Studies Group and the Paediatric Rheumatology International Trials Organisation. 2016 American College of Rheumatology/European League Against Rheumatism criteria for minimal, moderate, and major clinical response in adult dermatomyositis and polymyositis: An International Myositis Assessment and Clinical Studies Group/Paediatric Rheumatology International Trials Organisation Collaborative Initiative. *Arthritis Rheumatol* 2017;69(5):898–910.
28. Ernste FC, Chong C, Crowson CS, et al. Functional index-3: a valid and reliable functional outcome assessment measure in patients with dermatomyositis and polymyositis. *J Rheumatol* 2021;48(1):94–100.
29. Ahmed S, Chen KL, Werth VP. The validity and utility of the Cutaneous Disease Area and Severity Index (CDASI) as a clinical outcome instrument in dermatomyositis: a comprehensive review. *Semin Arthritis Rheum* 2020;50:458–462.
30. Selva-O'Callaghan A, Pinal-Fernandez I, Trallero-Araguás E, et al. Classification and management of adult inflammatory myopathies. *Lancet Neurol* 2018;17:816–828.
31. Schiftenbauer A, Garg M, Castro C, et al. A randomized, double-blind, placebo-controlled trial of infliximab in refractory polymyositis and dermatomyositis. *Semin Arthritis Rheum* 2018;47(6):858–864.
32. Oddis CV, Reed AM, Aggarwal R, et al; RIM Study Group. Rituximab in the treatment of refractory adult and juvenile dermatomyositis and adult polymyositis: a randomized, placebo-phase trial. *Arthritis Rheum* 2013;65(2):314–324.
33. Werth VP, Hejazi E, Pena SM, et al. Safety and efficacy of lenabasum, a cannabinoid receptor type 2 agonist, in patients with dermatomyositis with refractory skin disease: a randomized clinical trial. *J Invest Dermatol* 2022;142(10):2651–2659.e1.
34. Aggarwal R, Charles-Schoeman C, Schessl J, et al; ProDERM Trial Group. Trial of intravenous immune globulin in dermatomyositis. *N Engl J Med* 2022;387(14):1264–1278.
35. Rider LG, Aggarwal R, Machado PM, et al. Update on outcome assessment in myositis. *Nat Rev Rheumatol* 2018;14(5):303–318.
36. Aggarwal R, Rider LG, Ruperto N, et al; International Myositis Assessment and Clinical Studies Group and the Paediatric Rheumatology International Trials Organisation. 2016 American College of Rheumatology/European League Against Rheumatism Criteria for Minimal, Moderate, and Major Clinical Response in Adult Dermatomyositis and Polymyositis: An International Myositis Assessment and Clinical Studies Group/Paediatric Rheumatology International Trials Organisation Collaborative Initiative. *Arthritis Rheumatol* 2017;69(5):898–910.
37. Frisaldi E, Shaibani A, Benedetti F. Why we should assess patients' expectations in clinical trials. *Pain Ther* 2017;6(1):107–110.

LETTER

DOI 10.1002/art.43077

Balancing weight reduction benefits and risks: implications for serum urate management. Comment on the article by Fukui et al

To the Editor:

We read with interest the article by Fukui et al¹ in *Arthritis & Rheumatology* titled “Weight Reduction and Target Serum Urate Level: A Longitudinal Study of Annual Medical Examination,” which identified that small-weight reductions were associated with only small changes in serum urate (SU) levels. Some participants with hyperuricemia could achieve the target SU level with moderate to large weight reductions. We appreciate the study’s valuable contributions and suggest areas that need further exploration.

Firstly, we are intrigued by the impact of the rate and duration of weight loss on SU levels. Which approach, rapid or gradual weight reduction, is more effective for the long-term control of SU levels? How does the maintenance phase after weight loss affect SU levels in the long term? Additionally, the original text lacks detailed documentation of the causes of weight loss, hence, the interpretation of the impact of weight loss on SU levels may require greater caution. Furthermore, given that gout exhibits a certain familial aggregation, how does family history influence the effectiveness of weight loss? Are there certain genetic backgrounds for which the reduction in SU levels from weight management is more pronounced?

Secondly, from the perspective of socioeconomic factors, elements such as economic resources, social support, and educational levels may all influence an individual’s weight management strategies.^{2,3} However, this study appears to have overlooked the impact of these factors on weight loss and SU levels. Moreover, what role do psychologic factors play in weight management and SU level control?⁴ Do stress and emotional states affect the outcomes of weight management, thereby influencing SU levels? Whether the inclusion of psychosocial support in weight management programs is necessary to achieve a more comprehensive therapeutic effect warrants further investigation

Finally, is there a differential impact of sex hormone level fluctuations on SU levels in men and women during weight loss? Should future research explore the potential effects of sex hormone replacement therapy on uric acid levels, particularly among postmenopausal women?⁵ Furthermore, how can we balance

the potential benefits of weight reduction with its possible risks, such as nutritional deficiencies or the reduction of muscle mass? These questions warrant thoughtful consideration.

In conclusion, although the study by Fukui et al¹ provides valuable insights into the relationship between weight reduction and SU levels, it also highlights several critical areas for further investigation. Future research should delve into the nuances of weight loss strategies, the influence of socioeconomic and psychologic factors, and the role of sex hormones in uric acid management. Addressing these questions will enhance our understanding and improve clinical approaches to managing hyperuricemia effectively.

Author disclosures are available at <https://onlinelibrary.wiley.com/doi/10.1002/art.43077>.

Pei Liu, MD
Yongqiang Sun, MD
Sunjoint4002@126.com
Henan Luoyang Orthopedic Hospital (Henan Provincial Orthopedic Hospital)
Zhengzhou, Henan, China
Kun Zhao, MD
Shanghai Jiao Tong University Affiliated Sixth People’s Hospital South Campus
Shanghai, China
Peijian Tong, MD
The First Affiliated Hospital of Zhejiang Chinese Medical University
Hangzhou, Zhejiang, China

1. Fukui S, Okada M, Shinozaki T, et al. Weight reduction and target serum urate level: a longitudinal study of annual medical examination. *Arthritis Rheumatol* 2025;77(3):346–355.
2. Huang TT, Cawley JH, Ashe M, et al. Mobilisation of public support for policy actions to prevent obesity. *Lancet* 2015;385(9985):2422–2431.
3. Watson L, Belcher J, Nicholls E, et al. Latent class growth analysis of gout flare trajectories: a three-year prospective cohort study in primary care. *Arthritis Rheumatol* 2020;72(11):1928–1935.
4. Jafarzadeh SR, Neogi T, Stefanik JJ, et al. Mediating role of bone marrow lesions, synovitis, pain sensitization, and depressive symptoms on knee pain improvement following substantial weight loss. *Arthritis Rheumatol* 2020;72(3):420–427.
5. Karlsson T, Hadizadeh F, Rask-Andersen M, et al. Body mass index and the risk of rheumatic disease: linear and nonlinear mendelian randomization analyses. *Arthritis Rheumatol* 2023;75(11):2027–2035.

DOI 10.1002/art.43078

Reply


To the Editor:

We greatly appreciate valuable comments from Liu et al about our article on weight reduction and target serum urate (SU) levels using the Japanese annual health checkup database.¹ They suggested several essential topics that should be studied in future research.

First, the cause of weight loss is a meaningful discussion. Multiple versions of treatment are inevitable in observational studies examining the effect of weight change.² As we acknowledged in our article, our database has no specific information about the cause of weight loss. However, we tried to examine a more direct relationship between weight change and SU change by adjusting for dietary change and excluding patients with several conditions associated with weight loss, such as cardiovascular and kidney diseases and malignancies. Furthermore, it should also be noted that our primary analysis included a nonobese population. Both overweight and underweight are associated with overall death.³ Obviously, weight reduction recommendations should be personalized based on the overall health risks and benefits. We agree that the speed of weight reduction, family history of gout, and genetic interaction would be important in determining the association between weight reduction and SU. These are outside the scope of the present study, and our database does not include the information.

Second, we fully agree with their perspective on social support for weight reduction. As our study showed the potential effectiveness of weight reduction in SU management, health care providers should consider and integrate socioeconomic status and social support into their daily practice for better weight management and SU-level control.⁴ Socioeconomic status, as well as racial and sexual disparities, are also important in gout.^{5,6} Finally, we concur that an association of sexual hormone and its replacement therapy with SU level is a good topic that future research should investigate.

Dr Solomon's work was supported by the NIH grant AR-P3-0072577.

Sho Fukui, MD, MPH 
sfukui@bwh.harvard.edu
 Brigham and Women's Hospital and Harvard Medical School
 Boston, Massachusetts
 and St. Luke's International Hospital
 and Kyorin University School of Medicine
 Tokyo, Japan

Masato Okada, MD
 St. Luke's International Hospital
 Tokyo, Japan
 Daniel H. Solomon, MD, MPH
 Brigham and Women's Hospital and Harvard Medical School
 Boston, Massachusetts

1. Fukui S, Okada M, Shinozaki T, et al. Weight reduction and target serum urate level: a longitudinal study of annual medical examination. *Arthritis Rheumatol* 2025;77(3):346–355.
2. VanderWeele TJ, Hernán MA. Causal inference under multiple versions of treatment. *J Causal Inference* 2013;1(1):1–20.
3. Di Angelantonio E, Bhupathiraju SN, Wormser D, et al. Body-mass index and all-cause mortality: individual-participant-data meta-analysis of 239 prospective studies in four continents. *Lancet* 2016; 388(10046):776–786.
4. Elfhag K, Rössner S. Who succeeds in maintaining weight loss? A conceptual review of factors associated with weight loss maintenance and weight regain. *Obes Rev* 2005;6(1):67–85.
5. Hayward RA, Rathod T, Roddy E, et al. The association of gout with socioeconomic status in primary care: a cross-sectional observational study. *Rheumatology (Oxford)* 2013;52(11):2004–2008.
6. McCormick N, Lu N, Yokose C, et al. Racial and sex disparities in gout prevalence among US adults. *JAMA Netw Open* 2022;5(8):e2226804–e2226804.

DOI 10.1002/art.43090

The oral microbiota in persons at risk for rheumatoid arthritis: follow-up data for the article by Kroese et al

To the Editor

We would like to inform you about the follow-up results of our original study, of which the baseline results have been published in *Arthritis & Rheumatology*.¹ Because it has been suggested that rheumatoid arthritis (RA) may originate in the oral mucosa, our original study assessed the oral microbiota, using 16S ribosomal RNA gene amplicon sequencing, and periodontal condition in patients with early RA (n = 50) and individuals at risk of developing RA (patients with arthralgia positive for rheumatoid factor and/or anti-citrullinated protein antibody; n = 50) compared to healthy controls (n = 50).

For the periodontal variables—bleeding on probing, pocket probing depth, and periodontal inflamed surface area—no significant differences were found among the three groups. However, the baseline results showed a significant difference in the oral microbiota of stimulated saliva and tongue coating, with

Table 1. Comparison of baseline characteristics and periodontal variables between patients without arthritis and preclinical patients with arthritis, as determined by arthritis development during follow-up, within a group of individuals at risk of developing rheumatoid arthritis*

	Patients without arthritis (n = 33)	Preclinical patients with arthritis (n = 8)	P value
Age, mean (SD), yr	54.1 (7.0)	50.9 (10.4)	0.43 ^a
Female, n (%)	25 (76)	6 (75)	0.96 ^b
RF positive, n (%)	30 (91)	8 (100)	>0.99 ^c
ACPA positive, n (%)	15 (45)	6 (75)	0.24 ^c
Smoking, yes, n (%)	10 (30)	2 (25)	0.77 ^b
Periodontal assessment, median (IQR)			
BOP, percent	13.6 (6.5–32.7)	13.8 (10.6–30.2)	0.96 ^d
PPD (total six sites per tooth)	2.2 (2.0–2.5)	2.1 (2.0–2.4)	0.72 ^d
PISA, mm ²	195.7 (67.0–424.5)	174.8 (114.0–412.3)	>0.99 ^d

* ACPA, anti-citrullinated protein antibody; BOP, bleeding on probing; IQR, interquartile range; PISA, periodontal inflamed surface area; PPD, pocket probing depth; RF, rheumatoid factor.

^a Independent samples t-test.

^b Chi-square test.

^c Fisher's exact test.

^d Mann-Whitney U-test.

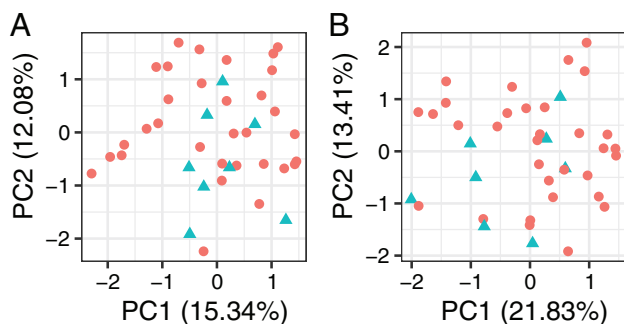


Figure 1. Principal components analysis plots, including the PC1 and PC2, displaying baseline microbial composition signatures of (A) stimulated saliva ($F = 1.12$; $P = 0.28$) and (B) tongue coating ($F = 1.26$; $P = 0.21$) of persons at risk for RA, stratified in patients without arthritis (red circles, $n = 32$; one sample for both sample types had too little sequencing output) and preclinical arthritis patients (cyan triangles, $n = 8$), as determined by RA development during follow-up. The F and P values were calculated using one-way permutational multivariate analysis of variance. The microbial compositions showed no significant differences in Shannon Diversity Index (saliva $P = 0.86$; tongue coating $P = 0.58$) or richness (saliva $P = 0.71$; tongue coating $P = 0.34$). For an extensive description of sample processing and data analysis methods, see the earlier publication on the baseline results.¹ PC, principal component; RA, rheumatoid arthritis.

the profiles of patients with early RA and at-risk individuals being characterized by a higher relative abundance of potentially pro-inflammatory bacterial species when compared to healthy controls, suggesting a possible association between oral bacteria and the onset of RA.

To further investigate this possible association, the group of at-risk individuals was observed over time with annual visits for three years or until RA onset (mean 33 [SD 15.5] months). With

this, we could monitor possible progression to RA and subsequently stratify the at-risk group into preclinical patients with arthritis and patients without arthritis. Follow-up data were available for 41 of the 50 at-risk individuals, of whom 8 individuals (19.5%) developed arthritis and were diagnosed with RA by their rheumatologist after a mean of 8 (SD 5.5) months following inclusion. When comparing the patients without arthritis with the preclinical patients with arthritis on baseline data, no differences were found, neither in baseline characteristics and periodontal variables (Table 1) nor in the oral microbial composition (Figure 1).

Thus, the follow-up results do not support our earlier suggestion of a possible association between the oral microbiota and the onset of RA. However, we strongly believe in the clinical significance of negative findings, and we find it of great importance to report these results to maximize scientific transparency and integrity.

An important limitation of our study is the low number of persons at risk for RA. We therefore argue that our results, although relevant for the research discussion on the topic, are as of yet not sufficient to dismiss a possible role of the oral microbiome in RA development. It is a topic of continuing interest,² and we suggest that future research on larger populations is needed for further clarification.

Author disclosures are available at <https://onlinelibrary.wiley.com/doi/10.1002/art.43090>.

Johanna M. Kroese, DDS, PhD

j.m.kroese@acta.nl

Bernd W. Brandt, PhD

Mark J. Buijs, BE

Wim Crielaard, PhD

Academic Center for Dentistry Amsterdam

University of Amsterdam and Vrije Universiteit Amsterdam

Amsterdam, The Netherlands
 Frank Lobbezoo, DDS, PhD
*Academic Center for Dentistry Amsterdam
 University of Amsterdam and Vrije Universiteit Amsterdam
 Amsterdam, The Netherlands and Malmö University
 Malmö, Sweden*
 Bruno G. Loos, DDS, MSc, PhD
*Academic Center for Dentistry Amsterdam
 University of Amsterdam and Vrije Universiteit Amsterdam
 Amsterdam, The Netherlands*
 Laurette van Boheemen, MD, PhD
 Dirkjan van Schaardenburg, MD, PhD
*Amsterdam Rheumatology and Immunology Center, Reade
 and Amsterdam University Medical Center
 Amsterdam, The Netherlands*
 Egija Zaura, DDS, PhD
 Catherine M.C. Volgenant, DDS, PhD
*Academic Center for Dentistry Amsterdam
 University of Amsterdam and Vrije Universiteit Amsterdam
 Amsterdam, The Netherlands*

1. Kroese JM, Brandt BW, Buijs MJ, et al. Differences in the oral microbiome in patients with early rheumatoid arthritis and individuals at risk of rheumatoid arthritis compared to healthy individuals. *Arthritis Rheumatol* 2021;73(11):1986–1993.
2. Juárez-Chairez MF, Cid-Gallegos MS, Jiménez-Martínez C, et al. The role of microbiota on rheumatoid arthritis onset. *Int J Rheum Dis* 2024;27(3):e15122.

DOI 10.1002/art.43091

Short-term risk of cardiovascular events in people newly diagnosed with gout: comment on the article by Cipolletta et al

To the Editor:

Gout is a common metabolic disease commonly associated with chronic inflammation, obesity, hypertension, and other cardiovascular risk factors. However, most of the existing studies have focused on the long-term cardiovascular risk in patients with gout, and fewer have assessed the risk of cardiovascular events in the short term after the first gout attack.^{1–3} It was with great interest that we read a recent paper by Cipolletta et al that examined the association between the first diagnosis of gout and short-term risk of cardiovascular events, thus filling a knowledge gap regarding the assessment of cardiovascular risk after an acute gout attack.⁴ In contrast to previous cohort and case-control studies, the study used a self-controlled case series (SCCS) methodology, which allows for a comparative intra-individual analysis and thus more accurately captures the direct impact of a first gout attack on cardiovascular events. In addition, the study

used large-scale national data and combined multiple data sources to provide greater assurance of the accuracy of the cardiovascular events in the study. The results of the study provide clinicians with a new perspective on risk management and underscore the importance of assessing cardiovascular risk at the time of initial gout diagnosis.

Limitations of this study should be further clarified. First, although SCCS methods can reduce individual fixed confounders, they do not adequately control for variables that change over time (eg, lifestyle, chronic disease progression, medication use). Particularly in diseases such as cardiovascular disease and gout, the dynamics of time-related factors such as obesity, blood pressure, and diabetes may significantly affect study results. Second, although the sensitivity analyses performed in the study address the issue of event dependence of exposure, they do not exclude the possibility that cardiovascular events themselves may influence gout flares. This bidirectional causality makes simple time series analysis insufficient to fully capture the complex interaction between the two. Third, although the study controlled for some confounders (eg, age, sex, medication prescription, and comorbidities), lifestyle factors such as diet, smoking, alcohol intake, and physical activity, which are strongly associated with cardiovascular events, were not adequately included in the analysis. Finally, patients with gout may be more likely to be detected as having cardiovascular disease due to increased frequency of medical visits for gouty attacks, and this “health-seeking behavior” may lead to an overestimation of cardiovascular events. Although negative controls were used in the study to assess this type of bias, the possibility of such bias could not be completely excluded.

Despite these limitations, this important study provides a compelling rationale for further prospective studies to better understand the interaction between gouty attacks and cardiovascular disease risk. Future research directions are obvious. First, the follow-up period should be extended to assess the incidence of cardiovascular disease in gout patients over 5, 10, or even more years to clarify the long-term risk. Second, future studies could include inflammatory markers (eg, interleukin [IL]-1 β , IL-6, tumor necrosis factor- α) or use genomic and metabolomic analyses to further define how the biological processes involved in a gouty attack contribute to cardiovascular events, thus providing a basis for personalized intervention strategies. Third, multinational multicenter studies can be conducted to include data from different ethnicities and regions to assess global differences in the association between gouty attacks and cardiovascular events, further enhancing the external validity and generalizability of the results. Finally, randomized controlled trials could be designed to assess whether intervention strategies (eg, anti-inflammatory therapy) can reduce the incidence of

cardiovascular events in gout patients. Such prospective studies could more directly validate the causal relationship between gout attacks and cardiovascular disease.

Author disclosures are available at <https://onlinelibrary.wiley.com/doi/10.1002/art.43091>.

Zichang Liu, MB
Yanwei Zhu, MM
Hui Zhao, MM
sqsyyzh@126.com
The First People's Hospital of Shangqiu
Henan, China

1. Mackenzie IS, Ford I, Nuki G, et al; FAST Study Group. Long-term cardiovascular safety of febuxostat compared with allopurinol in patients with gout (FAST): a multicentre, prospective, randomised, open-label, non-inferiority trial. *Lancet* 2020;396(10264):1745–1757.
2. Mouradjian MT, Plazak ME, Gale SE, et al. Pharmacologic management of gout in patients with cardiovascular disease and heart failure. *Am J Cardiovasc Drugs* 2020;20(5):431–445.
3. Pagidipati NJ, Clare RM, Keenan RT, et al. Association of gout with long-term cardiovascular outcomes among patients with obstructive coronary artery disease. *J Am Heart Assoc* 2018; 7(16):e009328.
4. Cipolletta E, Nakafero G, Richette P, et al. Short-term risk of cardiovascular events in people newly diagnosed with gout. *Arthritis Rheumatol* 2025; 77(2):202–211.

DOI 10.1002/art.43092

Reply

To the Editor:

We thank Dr Liu and colleagues for their interest in our study¹ and highlighting its provision of a new perspective on assessing risk management for cardiovascular risk at the time of initial gout evaluation. In our reply, we address the limitations they raise to further clarify the context of our study.

First, we agree with the authors that the self-controlled case-series analysis did not control for all variables that can change over time, such as lifestyle or medication use, which we discussed as a limitation in our original manuscript.¹ To minimize potential confounding due to time-varying covariates, we carried out a sensitivity analysis where we restricted the study period to around one year after the first gout diagnosis (Supplementary Tables S4 and S6 of our original manuscript).¹ We also carried out analyses stratifying patients by different major cardiovascular risk factors, including the use of some medications ascertained on or before the date of the first gout diagnosis (Supplementary Tables S5

and S7 of our original manuscript).¹ The consistency of an increased transient risk across these analyses provides some evidence of minimal effects of any residual confounding. In a self-controlled case-series analysis, patients contribute time to the study both before and after the exposure period, so true time-varying confounders need to change transiently in relation to the risk-exposure windows, which would not be the case with factors such as disease progression, obesity, or new diagnoses of diabetes raised by Liu et al.

Second, Liu et al raise that cardiovascular events themselves may influence gout flares and the potential bidirectional causality. As they noted, we checked a priori if event-dependent exposure could be an issue in our self-controlled case-series analysis as recommended.² We then performed two sensitivity analyses by considering an induction period and excluding gout flares with cardiovascular events recorded on the same date which showed results consistent with the main analysis (Supplementary Tables S4 and S6 of our original manuscript).¹


Third, Liu and colleagues raise the possibility of confounding by lifestyle factors such as diet, smoking, alcohol intake, and physical activity, which we fully acknowledge. Transient changes in these factors could have an impact on both gout flares and cardiovascular events. However, information recorded on these factors in the Clinical Practice Research Datalink is that ascertained during routine clinic appointments with the general practitioner. As such, these factors are incomplete for many patients, and timely information on their changes is not available at the level required for the analysis suggested by Liu et al.

Fourth, although the risk of residual confounding and unmeasurable biases cannot be completely ruled out from any observational research, the use of a negative control outcome greatly reduces the risk of a “health-seeking behavior” bias.³ As the authors have already pointed out, more robust evidence can only be drawn from randomized controlled trials and mechanistic observational studies.

We and others have reported an association between gout flares and cardiovascular events.^{4,5} Existing evidence from randomized controlled trials suggests that interventions to reduce vascular inflammation such as colchicine and canakinumab may reduce the risk of cardiovascular events in patients with coronary heart disease.^{6,7} Anti-inflammatory medications such as canakinumab have also shown to reduce the occurrence of flares in patients with gout and coexisting coronary heart disease.⁸ This provides further empirical evidence of the complex interplay between gout flares, inflammation, and cardiovascular events.

We again thank Dr Liu and colleagues for their interest in our work.

Author disclosures are available at <https://onlinelibrary.wiley.com/doi/10.1002/art.43092>.

Edoardo Cipolletta, MD 
msaec14@exmail.nottingham.ac.uk
 University of Nottingham,
 Nottingham, UK
 and Polytechnic University of Marche
 Ancona, Italy
 Laila J. Tata, PhD
 Abhishek Abhishek, PhD
 University of Nottingham
 Nottingham, UK

1. Cipolletta E, Nakafero G, Richette P, et al. Short-term risk of cardiovascular events in people newly diagnosed with gout. *Arthritis Rheumatol* 2024;art.42986.
2. Ghebremichael-Weldeselassie Y, Jabagi MJ, Botton J, et al. A modified self-controlled case series method for event-dependent exposures and high event-related mortality, with application to COVID-19 vaccine safety. *Stat Med* 2022;41(10):1735–1750.
3. Levintow SN, Nielson CM, Hernandez RK, et al. Pragmatic considerations for negative control outcome studies to guide non-randomized comparative analyses: a narrative review. *Pharmacoepidemiol Drug Saf* 2023;32(6):599–606.
4. Lopez D, Dwivedi G, Nossent J, et al. Risk of major adverse cardiovascular event following incident hospitalization for acute gout: a Western Australian population-level linked data study. *ACR Open Rheumatol* 2023;5(6):298–304.
5. Cipolletta E, Tata LJ, Nakafero G, et al. Association between gout flare and subsequent cardiovascular events among patients with gout. *JAMA* 2022;328(5):440–450.
6. Nidorf SM, Fiolet ATL, Mosterd A, et al; LoDoCo2 Trial Investigators. Colchicine in patients with chronic coronary disease. *N Engl J Med* 2020;383(19):1838–1847.
7. Ridker PM, Everett BM, Thuren T, et al; CANTOS Trial Group. Anti-inflammatory therapy with canakinumab for atherosclerotic disease. *N Engl J Med* 2017;377(12):1119–1131.
8. Solomon DH, Glynn RJ, MacFadyen JG, et al. Relationship of interleukin-1 β Blockade with incident gout and serum uric acid levels: exploratory analysis of a randomized controlled trial. *Ann Intern Med* 2018;169(8):535–542.

DOI 10.1002/art.43087

Enhancing knee osteoarthritis prediction: comment on the article by Li et al

To the Editor:

We appreciate the recent work by Li et al, demonstrating the potential of radiomic features for predicting knee osteoarthritis (KOA) progression and their clinical relevance.¹ However, there

are several aspects that could be further explored to improve the model's robustness and clinical applicability.

The study cohort had a significant gender imbalance, with the majority being women (67.3% in the development set and 70.6% in the test set) and particularly postmenopausal women, which may introduce bias in the model's predictions. Postmenopausal women experience hormonal changes that lead to bone metabolic alterations, reduced bone density, and microstructure degeneration, decreasing bone strength and resistance, and increasing fracture and joint damage risk. Reduced synovial fluid further diminishes joint lubrication, increasing cartilage wear and accelerating degeneration. Hormone decline also causes muscle atrophy, especially in thigh muscles supporting joints, reducing stability.² These changes collectively increase joint instability and fragility, accelerating KOA progression. If the model overlooks these factors, it may overestimate predictions for men or premenopausal women while underestimating risks for postmenopausal women. Therefore, conducting subgroup analyses for postmenopausal women, incorporating bone density, synovial fluid, and muscle mass changes, could improve the model's personalization and accuracy for high-risk groups.


The current model relies only on static magnetic resonance imaging (MRI) radiomic features, which may not fully capture early KOA progression. To enhance early prediction, additional key factors should be incorporated. Biomechanical data like gait analysis can provide insights into joint loading and stability because gait abnormalities often precede structural changes, making it a key predictor of early KOA changes.³ Lifestyle data, including exercise and diet, relates closely to early KOA progression, with healthy habits slowing degeneration and poor habits worsening it, thereby helping assess the impact of nonpharmacologic interventions. Psychological factors such as depression and anxiety increase pain sensitivity and exacerbate concerns, worsening KOA progression.⁴ Including psychological assessments can help identify high-risk patients for timely, personalized interventions. Finally, combining serum biomarkers with imaging data can detect early inflammation, differentiate KOA types, improve prediction accuracy, and guide targeted interventions like anti-inflammatory treatments.

Model interpretability is crucial for clinical application. Although the current model performs well in predictive accuracy, its black box nature can create trust issues that limit its use in clinical decision-making, especially when predictions influence treatment plans. Adding interpretable analysis helps clinicians understand the basis for predictions and facilitates better communication with patients, improving treatment adherence.⁵ Tools like Shapley additive explanations or local

interpretable model-agnostic explanations can clarify each radiomic feature's contribution, aiding radiologists and clinicians in focusing on key features like cartilage thickness or meniscus integrity. Additionally, heat maps overlaid on MRI scans visually highlight influential regions, helping patients understand their condition and increasing acceptance of treatment plans. In conclusion, subgroup analyses, inclusion of key factors, and enhanced model interpretability can greatly improve model accuracy, clinical adaptability, and ultimately deliver more personalized patient care.

Supported by the Medical and Health Research Project of Baoan District (number 2023JD250) and the Key Specialties in Clinical Medicine of the People's Hospital of Baoan Shenzhen (number 8).

Author disclosures are available at <https://onlinelibrary.wiley.com/doi/10.1002/art.43087>.

Qin Guo, MMed
Hui Li, MD 
chipperli@163.com
Chengshan Guo, MD
The Second Affiliated Hospital of Shenzhen University, The
People's Hospital of Baoan
Shenzhen, China

1. Li S, Cao P, Li J, et al. Integrating radiomics and neural networks for knee osteoarthritis incidence prediction. *Arthritis Rheumatol* 2024; 76(9):1377–1386.
2. Lu L, Tian L. Postmenopausal osteoporosis coexisting with sarcopenia: the role and mechanisms of estrogen. *J Endocrinol* 2023;259(1):e230116.
3. Diamond LE, Grant T, Uhlrich SD. Osteoarthritis year in review 2023: biomechanics. *Osteoarthritis Cartilage* 2024;32(2):138–147.
4. Hertel E, Arendt-Nielsen L, Olesen AE, et al. Quantitative sensory testing, psychological factors, and quality of life as predictors of current and future pain in patients with knee osteoarthritis. *Pain* 2024;165(8): 1719–1726.
5. Ali S, Akhlaq F, Imran AS, et al. The enlightening role of explainable artificial intelligence in medical & healthcare domains: a systematic literature review. *Comput Biol Med* 2023;166:107555.

DOI 10.1002/art.43085

Reply

To the Editor:

We appreciate the thoughtful feedback from Guo et al regarding our study on radiographic knee osteoarthritis (KOA) incidence prediction using magnetic resonance imaging (MRI) radiomic features and neural networks.¹ Their comments have highlighted important aspects related to model robustness,

cohort composition, and clinical applicability, and we are grateful for the opportunity to address their insights.

First, Guo et al raised an important point regarding the gender imbalance in our cohort, particularly the higher representation of postmenopausal women. This demographic focus was partly because the higher prevalence of KOA in this group reflected natural data availability. However, our baseline data revealed an intriguing outcome: the KOA incidence rates between postmenopausal women (age >55 years) and nonpostmenopausal women (age <55 years) in our study were not significantly different (50.6% vs 49.7%, $P = 0.848$) (Table 1). This lack of significant difference may suggest that other risk factors beyond menopause, such as genetic predisposition or lifestyle factors, could play an equally important role in KOA development, independent of menopausal status.^{2–4} Nonetheless, we agree that broader applicability would benefit from a more balanced cohort because hormonal and musculoskeletal differences significantly impact KOA progression.⁵ To address this in future studies, we plan to recruit a more diverse sample and conduct subgroup analyses to assess model performance across genders and age groups.

Second, we acknowledge the suggestion from Guo et al to incorporate additional biomechanical, lifestyle, and psychological factors into our model. Although we recognize these factors' relevance to KOA, our study focused primarily on the predictive power of static MRI-based radiomic features as a foundational approach. Adding biomechanical data such as gait analysis,⁶ lifestyle factors such as physical activity, and psychological assessments⁷ could indeed enhance predictive accuracy, especially in capturing early KOA changes. These multimodal data integrations are an exciting future direction, and we aim to investigate them in subsequent studies as data availability and technology permit.

Finally, regarding model interpretability, we agree that increasing transparency is crucial for clinical translation. Our model, as noted, operates with a black box nature that could limit its trust and usage in real-world decision-making. In future work, we plan to integrate explainability methods, such as Shapley additive explanations and local interpretable model-agnostic explanations, to better elucidate how specific radiomic features contribute to predictions.⁸ Additionally, using heatmaps to visualize influential regions on MRI images may help clinicians and patients understand the factors underlying risk assessments, thereby fostering greater acceptance and adherence to recommended interventions.

In conclusion, we thank Guo et al for their constructive comments. Their recommendations highlight critical areas for enhancing model accuracy, inclusivity, and interpretability that we aim to address in our ongoing research. We remain

Table 1. Baseline characteristics of the cohorts who were nonpostmenopause and postmenopause*

Characteristic	Nonpostmenopause (n = 170)	Postmenopause (n = 296)	P value
Age, mean \pm SD, y ^a	51.2 \pm 3.0	64.8 \pm 5.9	<0.001
BMI, mean \pm SD ^a	29.1 \pm 5.3	27.8 \pm 4.4	0.004
Knee injury, n (%) ^b	45 (26.5)	50 (16.9)	0.014
Treatment with NSAIDs, n (%) ^b	37 (21.8)	83 (28.0)	0.136
Treatment with glucosamine, n (%) ^b	61 (35.9)	109 (36.8)	0.876
Patients with KOA, n (%) ^b	86 (50.6)	147 (49.7)	0.848

* Bold text represents statistically significant *P* values. BMI, body mass index, KOA, knee osteoarthritis, NSAID, nonsteroidal anti-inflammatory drug.

^a Unpaired *t* tests are used for differences between means.

^b χ^2 tests are used for differences between proportions.

committed to advancing KOA predictive modeling to better serve diverse patient populations and improve clinical decision support.

Author disclosures are available at <https://onlinelibrary.wiley.com/doi/10.1002/art.43085>.

Shengfa Li, PhD 
*The Third People's Hospital of Chengdu,
 Affiliated Hospital of Southwest Jiaotong University,
 The Second Affiliated Chengdu Hospital of Chongqing Medical
 University
 Chengdu, China*
 Changhai Ding, PhD 
changhai.ding@utas.edu.au
*Zhujiang Hospital, Southern Medical University, Guangzhou,
 China and Menzies Institute for Medical Research,
 University of Tasmania
 Hobart, Tasmania, Australia*

- Li S, Cao P, Li J, et al. Integrating radiomics and neural networks for knee osteoarthritis incidence prediction. *Arthritis Rheumatol* 2024; 76(9):1377–1386.
- Evangelou E, Kerkhof HJ, Stykarsdottir U, et al. A meta-analysis of genome-wide association studies identifies novel variants associated with osteoarthritis of the hip. *Ann Rheum Dis* 2014;73(12):2130–2136.
- Spector TD, MacGregor AJ. Risk factors for osteoarthritis: genetics. *Osteoarthritis Cartilage* 2004;12 Suppl A:S39–S44.
- Hunter DJ, Bierma-Zeinstra S. Osteoarthritis. *Lancet* 2019;393(10182): 1745–1759.
- Lu L, Tian L. Postmenopausal osteoporosis coexisting with sarcopenia: the role and mechanisms of estrogen. *J Endocrinol* 2023;259(1): e230116.
- Diamond LE, Grant T, Uhlrich SD. Osteoarthritis year in review 2023: biomechanics. *Osteoarthritis Cartilage* 2024;32(2):138–147.
- Hertel E, Arendt-Nielsen L, Olesen AE, et al. Quantitative sensory testing, psychological factors, and quality of life as predictors of current and future pain in patients with knee osteoarthritis. *Pain* 2024;165(8): 1719–1726.
- Ali S, Akhlaq F, Imran AS, et al. The enlightening role of explainable artificial intelligence in medical & healthcare domains: a systematic literature review. *Comput Biol Med* 2023;166: 107555.